

ADSORPTION BEHAVIOUR OF DELTA-MANGANESE DIOXIDE IN RELATION
TO ITS USE AS A RESIN IN TRACE METAL SPECIATION STUDIES

By

SIMCHA STROES-GASCOYNE,
Landbouwkundig Ingenieur

A Thesis

Submitted to the School of Graduate Studies

in Partial Fulfilment of the Requirements

for the Degree

Doctor of Philosophy



McMaster University

April 1983

ADSORPTION OF COPPER ON DELTA-MANGANESE DIOXIDE

DOCTOR OF PHILOSOPHY (1983)
(Civil Engineering)

McMASTER UNIVERSITY
Hamilton, Ontario

TITLE: Adsorption Behaviour of Delta-Manganese Dioxide in
Relation to its Use as a Resin in Trace Metal Speciation
Studies.

AUTHOR: Simcha Stroes-Gascoyne, Landbouwkundig Ingenieur,
Agricultural University, Wageningen, The Netherlands.

SUPERVISORS: Professor James R. Kramer and
Professor William J. Snodgrass

NUMBER OF PAGES: xxi , 566

ABSTRACT

The accuracy of the $\delta\text{-MnO}_2$ method in determining Conditional Stability Constants (CSC's) for trace metal - organic complexes depends on the precise modeling of trace metal uptake by $\delta\text{-MnO}_2$. Accordingly, characteristics of $\delta\text{-MnO}_2$ and its adsorption behaviour for Cu were studied.

Laboratory preparation of $\delta\text{-MnO}_2$ is influenced by pH. A neutral redox process and an acid reduction of Mn^{7+} yield $\delta\text{-MnO}_2$, but an alkaline oxidation of Mn^{2+} does not produce $\delta\text{-MnO}_2$. Positive identification of MnO_x as $\delta\text{-MnO}_2$ includes confirmation of characteristics such as $x > 1.9$, an adsorption capacity (Γ_{max}) ≥ 0.25 mol Cu/mol MnO_2 , an amorphous XRD pattern, a specific TEM morphology and $1 < \text{pH}_{\text{zpc}} < 2$.

Natural and simulated aging of $\delta\text{-MnO}_2$ depends on temperature, pH and K content of the solid, and causes reduction of surface area and adsorption capacity by a factor 1.5 (natural) to 7 (simulated).

Adsorption of trace metals onto $\delta\text{-MnO}_2$ is described almost exclusively by a linearized Single Langmuir isotherm in the literature. This study found that Cu adsorption on $\delta\text{-MnO}_2$ deviates from Langmuir linearity at low surface coverages. Explanations include the existence of two adsorption sites (Double Langmuir model) and non-constant activity of surface groups. The Implicit Langmuir expression is derived from surface complexation theory to model the latter, and has the form :

$$\Gamma_{\text{ads}} = \Gamma_{\text{max}} \cdot \frac{\text{Cu}^{2+}}{\frac{(\text{H}^+)^n}{B} \cdot e^{\left(\frac{\Gamma_{\text{ads}}}{\Gamma_{\text{max}}} - 1\right)} + \text{Cu}^{2+}}$$

where Γ_{ads} (= mol Cu adsorbed / mol MnO_2) and the free Cu^{2+} concentration in solution are measured. Γ_{max} , B and n are the adsorption parameters.

This model predicts the observed deviation from linearity. The bindings

energy depends on the pH, the H^+/Cu^{2+} exchange ratio (n), the surface coverage ($\Gamma_{ads}/\Gamma_{max}$) and a constant B.

Adsorption isotherms were obtained over a pH range of 6 to 8.5, and a Cu_{total} range of 1 - 40 μM with glycine added to prevent precipitation of Cu. Adsorption results were fitted to Single, Double and Implicit Langmuir models, and compared. The Implicit Langmuir model describes Cu uptake by $\delta-MnO_2$ most accurately, and CSC's for Cu-NTA and Cu-glycine complexes were readily determined using this model.

^{14}C studies indicated that NTA, glycine and aspartic acid do not adsorb on $\delta-MnO_2$.

ACKNOWLEDGEMENTS

I would like to acknowledge the following persons for their assistance during the work described in this thesis :

Dr. James R. Kramer and Dr. William J. Snodgrass for their constantly offered support, encouragement and advice.

Dr. Alan A. Smith for his advice on the rules and regulations in the Civil Engineering Department.

The people in Lab. 413, for their most appreciated friendship which made the experimental part of this work a very pleasant undertaking : Jill Gleed, Bill Booty, Rick Playle, Ralph Jonassen, Andy Panko and June Olson.

Ota Mudroch for his adeptness with the Transmission Electron Microscope; without his efforts, part of this study would not have been possible.

Dr. C.M.G. van den Berg for leaving me his δ -MnO₂ samples, and for valuable help in the initial stages of this work.

Dr. D. Grundy for discussions on the structure of MnO₂.

Dr. D. Woods for lending me the Zeta-meter, and for his interest in this study.

Dr. Y.K. Chau for providing ¹⁴C-labelled NTA.

Dr. Brian Dempsey for valuable advice on "the horrible stuff", i.e. δ -MnO₂.

Stephen Goudey for assisting with liquid scintillation counting, and for his help with the autoclave experiments.

Jill Gleed for numerous A.A. analyses.

Frank Gibbs for DTA and TGA work.

Jake Karakostanoglou for his attempts to find Mn³⁺ in MnO₂ samples

with Electron Spin Resonance.

Bill Booty and Bill Snodgrass for help with computer work.

Jack Whorwood for printing the Electron Microscope photographs.

For the editing part of this thesis, I am indebted to the following persons :

Patricia Woodworth and Margareth Knox for accurate and speedy typing of the text.

Rogan Watson and Robyn Johnston for skillful drafting work.

Mel Gascoyne for typing of tables, references, appendices and proofreading. Robyn Johnston for proofreading.

The psychological and emotional side of writing and completing a Ph.D. thesis is hard to quantify. Many friends have contributed to this thesis in their own ways, by organizing canoeing trips, skiing tours, by throwing a party, but mostly by being friends in the true sense of the word.

I sincerely thank my parents for their unconditional emotional and financial support throughout my school- and university- years in Holland. My warmest thanks go to my husband, Mel Gascoyne, without whose constant emotional support, encouragement and optimism this thesis may have remained unfinished.

TABLE OF CONTENTS

	Page
CHAPTER 1 TRACE METAL INTERACTIONS WITH DISSOLVED ORGANICS AND PARTICULATE MATTER IN NATURAL WATERS	
1.1 Introduction	1
1.2 Origin of trace metals and their associations in natural waters	2
1.2.1 Dissolved inorganics	3
1.2.2 Dissolved organics	3
1.2.3 Importance of particulates in metal speciation	6
1.2.4 The combined influence on dissolved and particulate substances on trace metal speciation	13
1.3 Summary and research objectives	17
CHAPTER 2 PROCEDURES FOR THE DETERMINATION OF COMPLEXING CAPACITIES AND CONDITIONAL STABILITY CONSTANTS; OUTLINE OF RESEARCH	
2.1 Introduction	20
2.2 The concept of labile and non-labile trace metal-organic complexes and methods to measure complexing capacity	22
2.3 Methods for the determination of conditional stability constants of trace metal-organic complexes	28
2.3.1 Anodic Stripping Voltammetry (ASV)	28
2.3.2 Ion exchange methods (IE)	34
2.3.3 Ion specific electrode method (ISE)	35
2.3.4 Method of continuous variation (CV)	38
2.3.5 Potentiometric titration method (PT)	40
2.3.6 Gel filtration chromatography method (GFC)	42
2.3.7 Dialysis method (DI)	44
2.3.8 The δ -MnO ₂ method	46
2.4 Comparison between the δ -MnO ₂ method and the other procedures with respect to results for CSC's	50
2.5 Evaluation of the δ -MnO ₂ method as proposed by van den Berg (1979); Further formulation of research objectives	57
2.6 Summary	63
CHAPTER 3 NATURAL AND SYNTHETIC MANGANESE (IV) OXIDES	
3.1 Introduction	64
3.2 Formation and deposition of manganese oxides	65
3.2.1 Mn ²⁺ oxidation to MnO ₂ ; mechanisms and pathways	67
3.3 Description of the basic structure of some ubiquitous Mn(IV) oxides	73

	Page
3.4 δ -MnO ₂ and its related minerals	76
3.5 The preparation of δ -MnO ₂	87
3.5.1 The kinetics of the reaction between perman- ganate and manganous ions	88
3.6 Summary	94
CHAPTER 4. PREPARATION, CHARACTERIZATION AND AGING OF VARIOUS δ -MnO ₂ SAMPLES	
4.1 Introduction	101
4.2 Characteristics of and methods for characterizing δ -MnO ₂	103
4.2.1 Oxidation state of manganese in δ -MnO ₂	103
4.2.2 Surface area analysis	106
4.2.3 The pH of zero point of charge	107
4.2.4 X-ray diffraction (XRD) analysis	112
4.2.5 Electron microscopy	113
4.3 Preparation methods used in this study	115
4.4 Results and discussion of the comparative study	120
4.4.1 Oxidation states of the MnO ₂ 's	120
4.4.1.1 TGA results	123
4.4.2 Surface area determinations	126
4.4.3 The pH of zero point of charge	129
4.4.4 X-ray diffraction results	131
4.4.5 Transmission electron microscopy results	132
4.4.6 Discussion of the relationships between charac- teristics for δ -MnO ₂	138
4.4.6.1 Identification of δ -MnO ₂	138
4.4.6.2 The relationship between adsorption capacity and surface area	139
4.4.6.3 The correlation between adsorption capacity and percentages K and H ₂ O in the solid of MnO ₂ samples	142
4.4.6.4 The relationship between particle size, XRD patterns, oxidation state and H ₂ O content	146
4.4.6.5 The influence of pH of formation on the δ -MnO ₂ surface area	147
4.5 The influence of modifications of the neutral recipe on the oxidation state and morphology of δ -MnO ₂	148
4.6 Simulated aging study	154
4.7 Summary and conclusions	175

CHAPTER 5 ADSORPTION MODELS

5.1	Adsorption models for hydrous oxides	178
5.1.1	Introduction	178
5.1.2	Double Layer Theory	180
5.1.3	Adsorption models for inorganic cations	188
5.1.3.1	The Gouy-Chapman-Stern-Grahame model	190
5.1.3.2	The Adsorption-Hydrolysis model	192
5.1.3.3	The Ion-Solvent Interaction model (James and Healy model)	193
5.1.3.4	The Ion Exchange model	200
5.1.3.5	The Surface Complex Formation- or Site Binding- model	202
5.1.3.5.1	Constant Capacitance model	204
5.1.3.5.2	The Diffuse Layer model	205
5.1.3.5.3	Stern models	206
5.1.3.5.4	The Triple Layer model	207
5.1.3.5.5	Comparison of Surface Complex- ation or Site Binding models	212
5.1.4	Models for adsorption of anions and metal-ligand complexes	214
5.2	Adsorption models for trace metal adsorption on MnO_2	220
5.3	Development of a model for Cu adsorption on δ - MnO_2	244
5.3.1	Qualitative discussion of the influence of hypothesized surface- and double layer- config- urations on the surface charge of δ - MnO_2	244
5.3.2	Discussion of the influence of Cu^{2+} on the surface charge σ_0 of δ - MnO_2	250
5.3.3	Model development	258
5.4	Summary and conclusions	267

CHAPTER 6 EXPERIMENTAL PROCEDURES AND THEIR EVALUATION
(MASS BALANCES AND LIGAND ADSORPTION)

6.1	Introduction	269
6.2	Adsorption procedures	270
6.3	Difficulties associated with experimental procedures	273
6.3.1	Upper (and lower) limits of Cu addition	273
6.3.2	Ionic strength fluctuations	281
6.3.3	Mn release during Cu adsorption	282
6.3.3.1	Intermetallic interferences	283

	Page
6.3.4 Depression of Cu peaks during DPASV analysis	285
6.4 Mass balance for Cu	287
6.5 Mass balance for MnO ₂	296
6.6 Mass balance for glycine	297
6.7 Adsorption of other ligands	313
6.7.1 Aspartic acid	313
6.7.2 Adsorption of NTA	316
6.8 Example calculations for a calibration- and a titration experiment	316
6.9 Summary	323
CHAPTER 7 ADSORPTION BEHAVIOUR OF DIFFERENT δ-MnO ₂ SURFACES FOR Cu IN THE pH RANGE 6 TO 8.5	
7.1 Introduction	325
7.2 Adsorption isotherms obtained for a number of different δ-MnO ₂ surfaces	327
7.2.1 Comparison of the adsorption behaviour of a 'neutral', 'acid' and 'alkaline' δ-MnO ₂ surface	327
7.2.2 Comparison of the adsorption behaviour of three identically precipitated 'neutral' δ-MnO ₂ batches	329
7.2.3 Reproducibility of adsorption isotherms for 'neutrally' prepared δ-MnO ₂ 's at pH values in the range 6.0 to 8.5	335
7.2.4 Adsorption isotherms for various 'neutral' δ-MnO ₂ batches in the presence and absence of glycine	337
7.2.5 Comparison of adsorption isotherms for a neutral-ly and artificially aged δ-MnO ₂ surface	344
7.3 The fit of the adsorption results to three adsorption models; Statistical comparison of adsorption parameters and model fit	347
7.3.1 Introduction	347
7.3.2 The Single Langmuir model	348
7.3.3 The Double Langmuir model	363
7.3.4 The Implicit Langmuir model	367
7.3.5 Comparison of model fit for the Single-, Double-, and Implicit Langmuir models	374
7.3.6 Bindings energy variations and Kurbatov plots for the Implicit Langmuir model	375
7.4 Summary and conclusions	387

	Page
CHAPTER 8 USE OF THE IMPLICIT LANGMUIR MODEL IN THE CALCULATION OF CONDITIONAL STABILITY CONSTANTS	
8.1 Introduction	392
8.2 Results for NTA	392
8.2.1 Evaluation of values for NTA acidity and stability constants	393
8.2.2 Testcase: Titration of 2 μ M NTA at pH 7.5 using MnO ₂ III as resin	396
8.2.3 The possibility of 1:2 complex formation	409
8.2.4 Other results for NTA at pH 6 and 7	416
8.3 Determination of the conditional stability constant for glycine	423
8.4 The effect of the Cu/MnO ₂ ratio on the adsorption of Cu onto δ -MnO ₂ VIb at pH 6.0	429
8.5 Titrations of other amino acids	434
8.6 Summary and conclusions	442
CHAPTER 9 APPLICATIONS OF δ -MnO ₂ RESEARCH IN ENVIRONMENTAL ENGINEERING	
9.1 Introduction	446
9.2 Speciation studies : general	447
9.3 Speciation studies with emphasis on NTA and δ -MnO ₂	451
9.3.1 NTA, a case study	456
9.4 Radioactive (fuel) waste disposal	461
9.5 Environmental health studies	465
9.6 Summary	465
CHAPTER 10 SUMMARY, CONCLUSIONS AND RECOMMENDATIONS FOR FURTHER RESEARCH	
10.1 Context of research	467
10.2 The δ -MnO ₂ method	467
10.3 Structure, preparation and characterization of δ -MnO ₂	470
10.4 Adsorption theory	475
10.5 Adsorption of organics on the δ -MnO ₂ surface	476
10.6 Adsorption behaviour of various δ -MnO ₂ surfaces	477
10.7 Fitting of adsorption results to the Single-, Double- and Implicit Langmuir model	478

	Page
10.8 Determination of conditional stability constants for NTA and certain amino acids with the Implicit Langmuir model	480
10.9 Applications of δ -MnO ₂ research in the field of environmental engineering	481
10.10 Specific recommendations for further research	482
REFERENCES	485
APPENDIX I	512
APPENDIX II	518
APPENDIX III	519
APPENDIX IV	547
APPENDIX V	556
APPENDIX VI	565

LIST OF FIGURES

Figure		Page
2.1	Comparison of the effects of complexation between Cu and natural ligands on the Cu^{2+} concentration	55
2.2	Influence of known organic ligands on the free Cu^{2+} concentration	56
2.3	Comparison of the binding constant B for Cu adsorption on $\delta\text{-MnO}_2$, as obtained by van den Berg and in this work	59
2.4	Comparison of the adsorption capacity Γ_{max} for Cu adsorption on $\delta\text{-MnO}_2$, as obtained by van den Berg and in this work	60
3.1	Relationships between the various synthetic oxides of manganese, obtained under laboratory conditions	72
4.1	TGA analysis for various MnO_2 's	125
4.2	Adsorption isotherms for Cu on various MnO_2 's at pH 6.0, $I=0.01\text{N KNO}_3$	127
4.3	Electrophoretic mobility versus pH for MnO_2 's III and VIb	130
4.4	Electrophoretic mobility versus pH for MnO_2 VIIb	130
4.5	TEM appearance of $\delta\text{-MnO}_2$'s III, VIb and Xvc ('neutral')	134
4.6	TEM appearance of $\delta\text{-MnO}_2$ VIIb ('acid')	134
4.7	TEM appearance of $\delta\text{-MnO}_2$ VIIb ('alkaline')	135
4.8	TEM appearance of MnO_2 13 (van den Berg; naturally aged)	136
4.9	TEM appearance of MnO_2 XXV-A (artificially aged by heat treatment in autoclave)	136
4.10	TEM appearance of Baker- MnO_2 (commercial)	137
4.11	TEM appearance of Leco- MnO_2 (commercial)	137
4.12	Relationship between maximum adsorption capacity and %K in solid for various MnO_2 samples	144
4.13	Relationship between maximum adsorption capacity and % H_2O in solid for various MnO_2 samples	145
4.14	Relationship between pH and weight-%K in the $\delta\text{-MnO}_2$ samples prior to heat-induced aging	157
4.15	Relationship between pH and weight-%K in the $\delta\text{-MnO}_2$ samples after heat-induced aging	158

Figure		Page
4.16	TEM appearance of artificially aged MnO ₂ III	162
4.17	TEM appearance of artificially aged MnO ₂ VIIa	162
4.18	TEM appearance of artificially aged MnO ₂ VIIb	163
4.19	TEM appearance of artificially aged MnO ₂ XIa	163
4.20	TEM appearance of artificially aged MnO ₂ XI d	164
4.21	TEM appearance of artificially aged MnO ₂ XI e	164
4.22	TEM appearance of artificially aged MnO ₂ XIIIa	165
4.23	TEM appearance of artificially aged MnO ₂ XIIIc	165
4.24	TEM appearance of artificially aged MnO ₂ XIVb	166
4.25	TEM appearance of artificially aged MnO ₂ XVc	166
4.26	TEM appearance of artificially aged MnO ₂ XVIII	167
4.27	Morphological changes of δ -MnO ₂ upon heat treatment as a function of time	172
4.28	Suggested relationship between time and temperature for conversion of δ -MnO ₂ to cryptomelane	174
5.1	Charged surface and surrounding diffuse double layer	183
5.2	Change of potential (Ψ_x) with distance (x) to the surface	183
5.3	Qualitative relationship between colloid stability and thickness of the double layer	186
5.4	The Stern layer	186
5.5	Qualitative relation between charge and potential	189
5.6	Finite specific adsorption in the inner Helmholtz plane	189
5.7	Super equivalent adsorption resulting in sign reversal for the ζ potential	199
5.8	Possible locations for an adsorbed ion	199
5.9	Concepts of the electrical double layers in five surface complexation models	208
5.10	Ion exchange mechanism for trace metal adsorption on hydrous manganese dioxide	223
5.11	Langmuir plot of data for sorption of Co, Zn and Ca by 0.015g δ -MnO ₂ at pH 4	232
5.12	Langmuir adsorption isotherms for Zn adsorption at pH 7 for two γ -MnO ₂ 's with different specific surfaces	232
5.13	The δ -MnO ₂ surface at a pH below pH _{zpc}	247
5.14	The δ -MnO ₂ surface at pH _{zpc}	249
5.15	The δ -MnO ₂ surface at a pH above pH _{zpc}	251

Figure		Page
5.16	The δ -MnO ₂ surface at high pH	252
5.17	Surface charge of synthetic hematite (α -Fe ₂ O ₃) as a function of pH in the presence of four different concentrations of KCl	254
5.18	Surface- and Double-Layer-configuration of the δ -MnO ₂ surface for progressing Cu ²⁺ adsorption	256
5.19	Exchange of Na ⁺ for H ⁺ in the double layer of an AgI sol	254
5.20	Alternative possibilities for the adsorption of Cu ²⁺ ions on the δ -MnO ₂ surface	259
6.1	Typical example of the distribution of calibration points in the case of contamination at low concentrations and precipitation at high concentrations	276
6.2	Calibration of δ -MnO ₂ at pH's 7.0 and 7.5, illustrating CuO precipitation	280
6.3	Example calibration of MnO ₂ Xvc for Cu adsorption at pH 7.0, no organics present	319
6.4	Example titration 8.096 μ M NTA at pH 7.0 in the presence of MnO ₂ Xvc	322
7.1	Adsorption isotherms for three differently prepared δ -MnO ₂ batches, at pH 6.0, no glycine present	330
7.2	Adsorption isotherms for three differently prepared δ -MnO ₂ batches, at pH 6.0, 50 μ M glycine present	330
7.3	Adsorption isotherms for three differently prepared δ -MnO ₂ batches, at pH 7.0, 50 μ M glycine present	331
7.4	Adsorption isotherms for three differently prepared δ -MnO ₂ batches, at pH 8.0, 50 μ M glycine present	331
7.5	Adsorption isotherms for three identically prepared 'neutral' δ -MnO ₂ batches, at pH 6.0, no gly. present	333
7.6	Adsorption isotherms for three identically prepared 'neutral' δ -MnO ₂ batches, at pH 6.0, 50 μ M glycine present	333
7.7	Adsorption isotherms for three identically prepared 'neutral' δ -MnO ₂ batches, at pH 7.0, 50 μ M glycine present	334
7.8	Adsorption isotherms for three identically prepared 'neutral' δ -MnO ₂ batches, at pH 8.0, 50 μ M glycine present	334
7.9	Duplicate isotherms at pH 7.0, in the presence of 50 μ M glycine, for MnO ₂ III (App. III)	548
7.10	Duplicate isotherms at pH 7.5, in the presence of 50 μ M glycine, for MnO ₂ III	338
7.11	Duplicate isotherms at pH 8.5, in the presence of 50 μ M glycine, for MnO ₂ III (App. III)	548
7.12	Duplicate isotherms at pH 6.0, in the absence of 50 μ M glycine, for MnO ₂ VIb	338

Figure		Page
7.13	Duplicate isotherms at pH 6.0, in the presence of 50 μ M glycine, for MnO ₂ V1b (App.III)	550
7.14	Duplicate isotherms at pH 6.0, in the absence of 50 μ M glycine, for MnO ₂ XVc (App.III)	549
7.15	Duplicate isotherms at pH 7.0, in the absence of 50 μ M glycine, for MnO ₂ XVc (App.III)	549
7.16	Duplicate isotherms at pH 6.0, in the presence of 50 μ M glycine, for MnO ₂ XVc (App.III)	550
7.17	Duplicate isotherms at pH 7.0, in the presence of 50 μ M glycine, for MnO ₂ XVc (App.III)	551
7.18	Duplicate isotherms at pH 8.0, in the presence of four different amino acids, for MnO ₂ XVc	339
7.19	Isotherms in the presence, and absence, of glycine for MnO ₂ III, at pH 6.5	342
7.20	Isotherms in the presence, and absence, of glycine, for MnO ₂ V1b at pH 6.0 (120680) (App.III)	551
7.21	Isotherms in the presence, and absence, of glycine, for MnO ₂ V1b at pH 6.0 (290580) (App.III)	552
7.22	Isotherms in the presence, and absence, of glycine, for MnO ₂ V1b at pH 6.0 (210380)	342
7.23	Isotherms in the presence, and absence of organics (amino acids) at pH 6.0, for MnO ₂ XVc	343
7.24	Isotherms in the presence, and absence, of glycine, at pH 6.0, for MnO ₂ XVc (App.III)	552
7.25	Isotherms in the presence, and absence, of glycine, at pH 7.0, for MnO ₂ XVc (280681)	343
7.26	Isotherms in the presence, and absence, of glycine, at pH 7.0, for MnO ₂ XVc (210481,010381)(App.III)	553
7.27	Comparison of isotherms for a naturally and artificially aged 'neutral' δ -MnO ₂ , at pH 6.0, in the absence of glycine	346
7.28	Comparison of isotherms for a naturally and artificially aged 'neutral' δ -MnO ₂ , at pH 6.0, in the presence of 50 μ M glycine (App.III)	553
7.29	Comparison of isotherms for a naturally and artificially aged 'neutral' δ -MnO ₂ , at pH 7.0, in the presence of 50 μ M glycine (App.III)	554
7.30	Comparison of isotherms for a naturally and artificially aged 'neutral' δ -MnO ₂ , at pH 8.0, in the presence of 50 μ M glycine (App.III)	554
7.31	Isotherms in the presence, and absence, of glycine at pH 6.0, for MnO ₂ 13 (App.III)	555
7.32	Linearized Single Langmuir adsorption isotherms for three differently prepared δ -MnO ₂ batches at pH 6.0, no glycine present	352

Figure		Page
7.33	Linearized Single Langmuir isotherms for duplicate isotherms obtained for MnO ₂ III, at pH 7.5, in the presence of glycine	352
7.34	Linearized Single Langmuir isotherms for MnO ₂ VIb at pH 6.0, in the presence, and absence of gly.	353
7.35	Verification of the Implicit Langmuir model for MnO ₂ III, with new (1981) data for MnO ₂ III, at pH 6.5	371
7.36	Verification of the Implicit Langmuir model for MnO ₂ III with new (1981) data for MnO ₂ III, at pH 7.5	371
7.37	Verification of the Implicit Langmuir model for MnO ₂ III with new (1981) data for MnO ₂ III, at pH 8.5	372
7.38	Linearized Implicit Langmuir model for MnO ₂ VIIb ('alkaline') at pH 6.0	372
7.39	Linearized Implicit Langmuir model for MnO ₂ III ('neutral') at pH 7.5	373
7.40	Linearized Implicit Langmuir model for MnO ₂ VIb ('neutral') at pH 6.0	373
7.41	Kurbatov plot of the Implicit Langmuir model for MnO ₂ III	384
7.42	Kurbatov plot of the Implicit Langmuir model for MnO ₂ VIb	384
7.43	Kurbatov plot of the Implicit Langmuir model for MnO ₂ XVC	385
7.44	Kurbatov plot of the Implicit Langmuir model for MnO ₂ VIIb	385
7.45	Kurbatov plot of the Implicit Langmuir model for MnO ₂ VIIIb	386
7.46	Kurbatov plot of the Implicit Langmuir model for MnO ₂ 13	386
8.1	Titration of 2 μM NTA at pH 7.5	399
8.2	Titration of 4 μM NTA (and 40 μM glycine) at pH 8.0, using MnO ₂ XVC with Implicit Langmuir adsorption parameters	413
8.3	Titration of 8 μM NTA at pH 7	419
8.4	Titration of 4 μM NTA at pH 7	420
8.5	Titration of 8 μM NTA at pH 6	421
8.6	Adsorption isotherm for the titration of 40 μM Cu and 100 μM glycine with MnO ₂ VIb (7.5 - 120 μM) at pH 6.0	432
8.7	Linearized Single Langmuir isotherm for the titration of 40 μM Cu and 100 μM glycine with MnO ₂ VIb (7.5 - 120 μM) at pH 6.0	433

Figure		Page
8.8	Titration of 80 μ M aspartic acid in the presence of MnO_2 XVc at pH 8.0	437
8.9	Titration of 80 μ M alanine in the presence of MnO_2 XVc at pH 8.0	438
8.10	Titration of 80 μ M glutamic acid in the presence of MnO_2 XVc at pH 8.0	439
8.11	Summary of conditional stability constants for the Cu-NTA complex	445

LIST OF TABLES

Table		Page
1.1	Classification of particulate matter in natural waters	12
3.1	Crystallographic data for some Mn(IV) oxides	77
3.2	Partial nomenclature scheme for manganese oxide structures	87
3.3	Formation and various characteristics of 'artificial' δ -MnO ₂	96
4.1	Characteristics of various differently prepared (δ -) MnO ₂ surfaces	121
4.2	Calculated surface areas for MnO ₂ 's	128
4.3	Identification of δ -MnO ₂	140
4.4	Modifications of the neutral recipe	151
4.5	Oxidation state of the 'modified' neutral δ -MnO ₂ samples	153
4.6	The pH and K concentrations of the δ -MnO ₂ 's subjected to a simulated aging process by treatment in an autoclave	156
5.1	CFSE's of selected ions in an octahedral field	234
5.2	Adsorption of trace metals on δ -MnO ₂ ; Time required to reach equilibrium	238
5.3	Adsorption of trace metals on δ -MnO ₂ ; H ⁺ released per M ²⁺ adsorbed	241
6.1	Upper limits for Cu ²⁺ and Cu _{diss} to avoid CuO precipitation	278
6.2	Upper limits for Cu ²⁺ and Cu _{diss} concentrations to avoid Cu(OH) ₂ (s) formation, calculated with REDEQL 2	281
6.3	Peak depression of Cu during DPASV	286
6.4	Adsorbed, dissolved and total Cu concentrations of a typical calibration experiment, displaying mass balance irregularities	292
6.5	Typical Mn concentration variations during an adsorption experiment	298
6.6	Counting results for ¹⁴ C-labelled glycine adsorption experiments	
6.6a	Experiment 240781 - MnO ₂ XVC - pH 6.0 - 50 μ M ¹⁴ C-labelled glycine added	303
6.6b	Experiment 210681 - MnO ₂ XVC - pH 6.0 - 50 μ M ¹⁴ C-labelled glycine added	303
6.6c	Experiment 280681 - MnO ₂ XVC - pH 7.0 - 50 μ M ¹⁴ C-labelled glycine added	304
6.6d	Experiment 210781 - MnO ₂ 13 (van den Berg) - pH 6.0 - 50 μ M ¹⁴ C-labelled glycine added	304
6.6e	Experiment 210781 - MnO ₂ 13 (van den Berg) - pH 7.0 - 50 μ M ¹⁴ C-labelled glycine added	305

Table	Page	
6.6 cont.	6.6f Experiment 210781 - MnO ₂ 13 (van den Berg) - pH 8.0 - 50µM ¹⁴ C-labelled glycine added	305
6.7	Adsorption of ¹⁴ C-labelled glycine on glassware and filterpapers	308
6.8	Example calculation showing the influence of ¹⁴ C-labelled glycine adsorption on filtration equipment on the data for adsorption of ¹⁴ C-labelled glycine on MnO ₂	310
6.9	Adsorption of aspartic acid on MnO ₂	314
6.10	Adsorption behaviour of NTA on MnO ₂ at pH 6.0 and 7.0	317
6.11	Example calculation for a calibration experiment	318
6.12	Example calculation for a titration experiment	321
7.1	Experimental conditions for comparison study involving a 'neutral' δ-MnO ₂ (VIb), an 'alkaline' δ-MnO ₂ (VIIb) and an 'acid' δ-MnO ₂ (VIIIb)	332
7.2	Experimental conditions for comparison study involving the three 'neutral' δ-MnO ₂ surfaces, III, VIb and XVC	332
7.3	Experimental conditions for the study investigating reproducibility of isotherms for 'neutral' δ-MnO ₂ surfaces	336
7.4	Comparison of adsorption isotherms obtained for 'neutral' δ-MnO ₂ surfaces in the presence and absence of glycine	341
7.5	Experimental conditions for comparison study involving a naturally aged and an artificially aged 'neutral' δ-MnO ₂	345
7.6	Cu ₂ concentration ranges and linearized Single Langmuir adsorption parameters for duplicate isotherms obtained for the 'neutral' δ-MnO ₂ III surface at pH values 7.0 - 8.5	351
7.7	Comparison of linear and non-linear regression values of the adsorption parameters Γ _{max} and B	355
7.8	Comparison of non-linear regression values of the adsorption parameters Γ _{max} and B on the basis of a pooled t-test	360
7.9	Comparison of the Double Langmuir Regression parameters	365
7.10	Model parameters for the Implicit Langmuir model	370
7.11	Comparison of model fit by means of Residual Sums of Squares after regression	376
7.12	Comparison of model features for the Single-, Double- and Implicit Langmuir models	377
7.13	Comparison of bindings constants (pB values) for the Implicit Langmuir models, for various MnO ₂ 's involved in this study, at pH values of 6,7 and 8	379

Table		Page
7.14	Possible adsorption reactions for Cu on MnO ₂	380
8.1	Equilibrium constants for NTA (literature data)	394
8.2	Calculated equilibrium constants for NTA and Cu-NTA at I = 0.01 N KNO ₃	394
8.3	Calculation of Cu-species in the 2μM NTA experiment (using Single Langmuir parameters)	400
8.4	Recalculation of Cu-species in the 2μM NTA experiment (adjustment of CuOH ⁺ correction)	406
8.5	Recalculation of Cu-species in the 2μM NTA experiment (Cu(OH) ₂ correction)	406
8.6	Recalculation of Cu-species in the 2μM NTA titration (using Implicit Langmuir parameters)	408
8.7	Recalculation of Cu-species in the 2μM NTA titration (using Implicit Langmuir parameters and Cu(OH) ₂ correction)	408
8.8	Summary of titration results for NTA (2μM) at pH 7.5	410
8.9	Titration of 4μM NTA at pH 8.0	414
8.10	Values for L _t , L _s , K' _L and K' _S calculated by iterative method	415
8.11	Equilibrium constants for glycine and Cu-glycine	424
8.12	Titration of 40μM Cu and 72.6μM MnO ₂ VIB with glycine at pH 6.0	426
8.13	Calculation of K' _{Cu-gly} using Single Langmuir parameters	427
8.14	Calculation of K' _{Cu-gly} using Cu ²⁺ data measured by Cu electrode	427
8.15	Calculation of K' _{Cu-gly} using experimental data for Cu _{diss} and total glycine concentrations and the computer program REDEQL 2	428
8.16	Average values for K' _{Cu-gly} calculated from the same data set with different methods	428
8.17	Results for titration of 40μM Cu _t and 100μM glycine with MnO ₂ VIB at pH 6.0	431
8.18	Equilibrium constants for aspartic acid, alanine and glutamic acid, from REDEQL 2	431
8.19	Log K' _L and L _t values for 3 amino acids calculated via 3 different methods	441
9.1	Calculated concentrations of NTA for various aquatic environments	453
9.2	Degradation times for metal-NTA complexes	458

CHAPTER 1

TRACE METAL INTERACTIONS WITH DISSOLVED ORGANICS AND
PARTICULATE MATTER IN NATURAL WATERS1.1 Introduction

Trace metals such as Cu, Zn, Cd and Al exert varying degrees of toxicity to humans and to the entire eco-system. Present water quality standards are formulated in terms of total concentrations of trace metals, rather than in terms of the concentrations of individual metal species. However, it has been shown incontrovertibly during the past few decades that the chemical forms in which trace metals occur in natural waters, are far more significant with regard to biological toxicity, than are actual total metal concentrations. Free metal ions are generally the most toxic species. In order to determine this free ion, the character and strength of all possible metal associations in natural waters must be known as well as the influence of a changing environment upon these associations. For instance, the mobilizing influence of acidic precipitation upon metals in poorly buffered natural water systems is of great concern. The research described in this thesis is directed towards making a contribution to the eventual knowledge and understanding of the character and strength of associations of trace metals in natural aquatic systems.

1.2 Origin of Trace Metals and Their Associations in Natural Waters

Trace metals enter the environment through natural cycles and through man's activities. Chemical weathering of soils and rock is responsible for the major natural flux of trace metals to the aquatic system. Natural organic chelating agents can play an important role in the weathering process. Volcanism and tectonic activities can also be major release mechanisms of trace metals, albeit often localized.

Cultural causes of trace metals entering the aquatic environment include mining operations (i.e. weathering of waste rock, ore processing), a wide variety of industrial use of trace metals, the burning of fossil fuels and leaded gasoline (Leckie and James 1974).

The associations that have been described for metals in aquatic systems are (Florence 1977; Guy et al. 1975; Davis and Leckie 1978):

- a) Associations with dissolved material, including
 - i) inorganics: e.g. metal-anion complex formation such as soluble CuCO_3 , ZnSO_4 , CdCl^+ ,
 - and ii) organics: e.g. complexation of metals with dissolved organic compounds such as humics, aminoacids biological excretion products.
- b) Associations with particulates, including
 - i) inorganics: e.g. metal adsorption onto hydrous oxides such as $\text{Fe}(\text{OH})_3$, MnO_2 , SiO_2 ; metal-clay colloid ion exchange reactions; precipitation and coprecipitation reactions,
 - and ii) organics: e.g. metal adsorption onto humic colloids (coagulated humics), organic detrital

particles, algae, bacteria and organically coated particulates.

1.2.1 Dissolved Inorganics

Metal-inorganic anion complexes, such as soluble carbonates, sulphates, hydroxides, chlorides, phosphates and nitrates are relatively easy to assess. Acidity and equilibrium constants are available for most of these, although for some complexes, for instance $ZnCO_3$ and $Zn(OH)_2^0$, quite a discrepancy exists in the values of the constants reported in the literature (Bradford 1973; Zirino and Healy 1970; Zirino and Yamamoto 1972; Schindler 1967). In general, however, the various metal species and their concentrations in a particular inorganic system can be calculated from the characteristics of that system, such as pH, ionic strength, alkalinity, temperature, pressure and total concentrations of metals and inorganic ligands.

1.2.2 Dissolved Organics

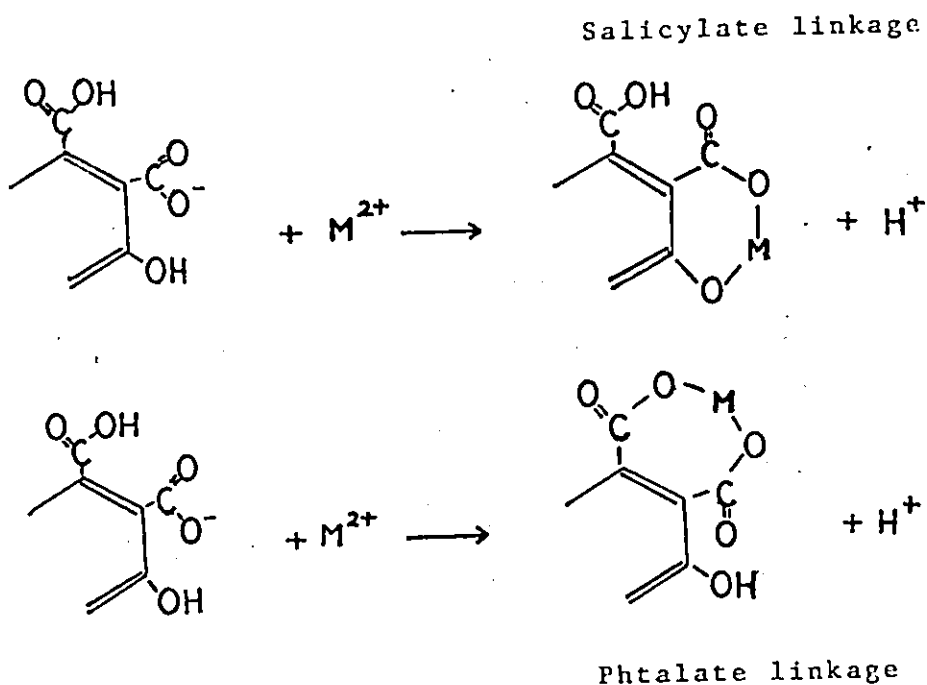
The calculation of metal speciation is relatively much more difficult for systems where dissolved organics are present, since the nature and molecular structure of these organics is usually not known. Significant concentrations of natural and synthetic complexing ligands are present in many aquatic systems as a result of natural runoff and human influences. Natural waterbodies carry organic material of soil origin, biological activities such as degradation and excretion processes, and anthropogenic inputs (for example waste water treatment plant effluent discharge and industrial organic inputs).

Humic compounds (humic acids, fulvic acids, humin) form a large part of the natural ligands. They are the end products of biological decay and polymerization in soils and sediments, are highly oxidized and chemically and biologically stable insofar that specific enzymes are required to break them down (Reuter and Perdue 1977). Extensive research has been carried out to reveal the structure of these organics (e.g. Schnitzer and Khan 1972; Schnitzer 1971; Gjessing 1976). Major components are phenolic, benzenecarboxylic and aliphatic acids. The presence of many oxygen containing functional groups can make these molecules highly reactive towards metal ions (Schnitzer and Hoffman 1967). Soil humics and water humics differ to a certain extent in the content of reactive carboxyl and phenolic groups.

The solubility of humic acids (as opposed to fulvic acids) is quite low in natural waters due to the fact that they are not, or only partly, ionized and contain many non-polar groups. On drying, humic acids form a very compact mass, impervious to gas molecules, but penetrable by water vapour due to swelling, which is for instance also a characteristic of the clay mineral montmorillonite. In the case of humic acids this situation changes on substitution of Na^+ for H^+ in its functional groups, and the resulting humates are colloiddally soluble in water, forming a very stable, negatively charged sol (Tschapek and Torres Sanchez 1978).

In natural waters, humic acids occur in dissolved, colloidal and possibly even in suspended form ($> 0.45 \mu\text{m}$) depending on pH, ionic strength etc. Humic acids, their colloids and particulates possess acidic functional groups which can bind metal ions. The amount of trace

metal taken up will be proportional but not necessarily equal to the number of available sites. Gaskill (1978) concludes that a variable fraction, anywhere from 0.1 to 90%, of potential complexing sites does indeed react, with most studies reporting values less than half the potential capacities. This implies a limiting complexing value, which may explain findings that adsorption of metal onto particulate humic material can be described by a Langmuir isotherm (Guy et al. 1975). The relative affinity of metal ions for humic acids reflects the ability of those ions to form complexes and/or chelates (e.g. $\text{Cu}^{2+} > \text{Zn}^{2+} > \text{Cd}^{2+} > \text{Ca}^{2+}$). Two possible linkages with ionized groups on humic materials are (Guy et al. 1975):



Manning and Ramamoorthy (1973) found that bidentate phthalate groups rather than salicylic acid-like bidentate groups were the principal chelators of fulvic acid. Since it was found that significant amounts of metal can be bound by humic material at pH's as low as 1.35, the most probable uptake mechanism can be described as a complexing process in which at least one proton is exchanged or no proton at all, or in which both processes occur simultaneously (Green and Manahan 1977).

Trace metal - dissolved organic complexation has received enormous attention in the recent literature. A number of techniques have been developed to measure complexing capacities and determine conditional stability constants. These techniques are applied with variable success. Model systems are often invoked to prove the method satisfactory. Chapter 2 discusses the better known techniques for determining complexing capacities and conditional stability constants.

1.2.3 Importance of Particulates in Metal Speciation

While most studies of metal speciation in natural waters have concentrated on the complexing influence of dissolved organic material, mechanisms of metal-interactions with particulate material may be equally important although they have received much less attention. Associations of trace metals with particulates and their subsequent settling enriches the metal content of sediments. The form in which these metals enter the sediment phase influences redistribution processes in the sediments; the degree to which metal-particulate interactions allow solubilization often controls the rate and extent in which they re-enter and recontaminate the water column (Rashid 1974; Pita and Hyne

1975; Nissenbaum and Swaine 1976; Ramamoorthy and Rust 1976; Green and Manahan 1977).

Particulates enter natural waters via runoff and discharge processes (erosion products, clay minerals etc.) and as a result of human activities (pollution) and atmospheric fallout. They form in situ by biological production, coagulation processes (humics), and precipitation reactions.

A particle in water is, by definition, a suspended as opposed to a dissolved entity with a certain ability to settle out, the rate of which can be related to size, density and shape. However, there is no reason to assume a size discontinuity among particulates in natural waters, from the order of Angstroms up through millimeters. An arbitrarily chosen, operationally defined boundary of $0.45 \mu\text{m}$ is generally accepted between dissolved and particulate phases. Some justification for the choice of this boundary is given by Lal (1977) for particulates in seawater: In the open ocean, $1-10 \mu\text{m}$ particles dominate; many of the larger particles have settled out of the water column by the time the currents can carry them to the open ocean. Particle size distribution in the oceans is usually satisfactorily described by the relation:

$$\frac{dN}{dr} = Ar^{-b} \quad (1.1)$$

$$\text{while } S \propto r^{-(b-3)} \quad (1.2)$$

$$M \propto r^{-(b-4)} \quad (1.3)$$

and $F \propto r^{-(b-6)}$

(1.4)

where: N = number of particulates

r = radius of particulates

S = total surface area of particulates

M = total mass of particulates

F = vertical mass flux of particulates across a layer

A = constant

b = determines the size-range of particles responsible for various processes; b is usually in the range of 4 to 5 for seawater.

Using these relationships, Lal (1977) calculates that the gravitational (or 'Stokes') settling process dominates settling of particulates $> 1 \mu\text{m}$ with densities $> 1.5 \text{ g.cm}^{-3}$ through distances of the order of 1 km with an eddy diffusivity of $1 \text{ cm}^2 \text{ sec}^{-1}$. Lal argues that particles $< 1 \mu\text{m}$ are usually not important in the open oceans since for particulates to be effective in bringing about chemical changes, the mass flux has to be appreciable and although S varies with r^{-1} or r^{-2} (b = 4 to 5), F varies with r or r^2 . Furthermore, small particles essentially follow the motion of water molecules if the eddy diffusivity is $\geq 1 \text{ cm}^2 \text{ sec}^{-1}$. With b in the range of 4 to 5, marine particles between 1 and $10 \mu\text{m}$ primarily contribute to trace element adsorption and transport downwards in the ocean. Thus for practical purposes, particles smaller than about $0.5 \mu\text{m}$ may be considered as in solution.

From the point of view of mass transport, the above argument has some validity for open ocean systems. In freshwaters, however, the percentage of very fine particulates is greater than in oceans and one can argue that mass transport downward depends on the total mass of the particulate phase rather than on the size distribution. From the point of view of chemical changes in speciation in natural waters, the boundary of 0.45 μm is probably meaningless. For example, many of the "soluble" trace metals in natural waters, "soluble" as defined by the 0.45 μm criterion, can be removed by stepwise ultrafiltration, using filters of increasingly smaller pore size (e.g. 0.4 - 0.01 μm).

Another argument against the 0.45 μm boundary is that often, very small "soluble" particles coagulate and/or they may become attached to larger particles or are coprecipitated. These processes cause "soluble" materials to settle out despite their size. On the other hand, dissolved organics may adsorb (with or without a trace metal as a link) on particulates, hence falling into the particulate classification.

These examples illustrate the questionable chemical significance of the 0.45 μm boundary. However, this criterion is widely used because from an analytical point of view it is convenient.

Conventional studies of natural water systems involve the collection of bulk samples of aquatic particulates followed by the determination of the average concentrations of pollutant species in the samples. While the utility of such measurements is beyond doubt, no information is obtained about the identities and amounts of pollutant

species that are concentrated in the microscopically small regions that form the particulate-water interface. Leachate and exchange studies (Keyser et al. 1978; Catanzaro 1976) indicate that many potentially toxic trace metals (and also pesticides) are highly enriched at the surface of many types of environmental particles. It is the surface of a particle that governs its heterogeneous reactivity towards solution species and it is also this surface that is directly accessible to extraction by aqueous leaching and exchange in the aquatic environment. A more surface chemistry oriented approach, involving analysis of individual surfaces, would provide valuable insight into the characteristics, reactivity and eventual impact of particulates on the environment. Such analyses are rapidly becoming more realistic due to the development of very advanced techniques.

Distinction is often made theoretically between organic and inorganic particulates but most often, particles are a mixture of organic and inorganic compositions. Analytically, one is restricted to determining percentages of organics and inorganics in the particulates of a bulk sample, since no satisfactory separation method of organic and inorganic particles exists.

Most organic analyses of river and lake waters are reported as total organic carbon concentrations (TOC). TOC can be subdivided into dissolved organic carbon (DOC, filtration) and particulate organic carbon (POC). Generally the DOC/POC ratio in lake waters varies from 6 to 10, with the lower ratio occurring in highly productive lakes (Reuter and Perdue 1977). Again, the DOC/POC ratio approach is governed by an operational definition of size but it has little chemical significance.

Further, TOC as the only measurement for the dissolved and dispersed phases in natural waters is not likely to provide important information with respect to the binding capacities of the fractions.

Table 1 classifies most substances, both dissolved and particulate, that can occur in natural waters, according to size, physical state, organic, inorganic, mixed and specifically man-made. The classification of inorganic particles by size is very well developed. This is due to the relative chemical stability of these particulates in natural systems as opposed to organic particulates which are subject to continuous decay. Physical states do overlap to a certain extent due to the character of definitions of these states (Folk 1974; Stumm 1977).

Almost all particles in aqueous systems have a surface charge, which may originate from dissociation of chemical groups fixed on the surfaces of particles, from adsorption of ions from the surrounding solution or from isomorphic substitution (see also Chapter 5). All possible uptake mechanisms of dissolved material onto particulates can be called sorption processes and the surface charge of particles plays a key role in these.

So far, most research considering the scavenging role of particulates with respect to trace metals has been restricted to relatively simple inorganic systems. Much work has been done on adsorption of metals onto hydrous oxides and clay minerals (Gadde and Laitinen 1974; Stumm et al. 1976; Bourg and Filby 1974). Adsorption processes have been satisfactorily described by Langmuir and Freundlich isotherms for hydrous metal oxides and clay minerals. A number of adsorption models has been developed to describe adsorption processes of metal ions.

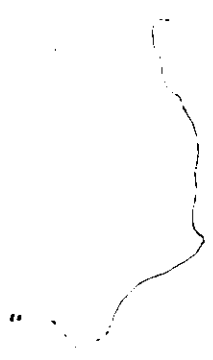
Table 1: Classification of 'particulate' matter in natural waters

partly composed from references: Folk 1974

Stumm 1977

___ well-established boundaries between classes

- - - - vague or overlapping boundaries



at hydrous oxide interfaces in terms of possible bindings mechanisms involved (Stumm et al. 1976). A detailed review of these models is given in Chapter 5.

1.2.4 The Combined Influence of Dissolved and Particulate Substances on Trace Metal Speciation

To date, most investigations of metal speciation have involved metal interactions with dissolved substances or with particulate materials and not both. The question arises whether data gathered from such single systems can be applied to a combined system of metals, dissolved substances and particulate materials or whether complex particulate-dissolved substance reactions occur which are not understood. An example of a more realistic system, in which the effects of both dissolved organics and particulates on metal speciation are combined, is that of Guy et al. (1975). Metal distributions were studied in a model system containing a hydrous metal oxide (MnO_2), a clay mineral (potassium bentonite) and colloidal humic acid as particulates, dissolved humic and tannic acid representing dissolved organic substances, and bicarbonate as a dissolved inorganic complex former. Results are reported in terms of the percentage distribution of metal over the particulate-, complexed- and free ion fractions. They conclude that their combination of these model-compounds into a synthetic representation of a natural water sample is in good agreement with the trends observed in natural waters.

Another method for evaluating trace metal interactions in natural waters are mathematical equilibrium models. During the last

15 years many computer simulation models have been developed (Nordstrom et al. 1979) in order to explain complex aquatic systems. For discrete packets of water, equilibrium situations are assumed as opposed to non-equilibrium kinetically controlled conditions. Only recently has metal adsorption onto particulates, in addition to dissolved complex formation, been included in this type of models. For example, the theoretical model of Vuceta and Morgan (1978) investigates the role of both complexation and adsorption on the speciation of trace metals in fresh waters as a function of pH, adsorbing surfaces, surface area and selected organic ligands. Calculations are performed using REDEQL2 (McDuff and Morel 1973) and adsorption is incorporated using the ion solvent interaction model (James and Healy 1972).

Evidence for the effects of adsorbed organics and/or trace metal-organic complexes on particle surfaces is rapidly accumulating. Chase (1979) studied the settling characteristics of organic-mineral aggregates (sediments) from lacustrine and marine environments. His experiments indicated that the presence of naturally occurring surface coatings, solution electrolytes and dissolved organic substances all caused settling behaviour of the aggregates to be inconsistent with Stokes law.

Neihof and Loeb (1972) conclude that it is quite possible that particulates in seawater are coated with adsorbed organics. No apparent correlation of mean electrophoretic mobilities with particulate size and/or morphology could be detected in seawater. Electrophoretic measurements made on model particulates (e.g. clay) normally exhibit +, 0 and - charges in the mobility range of 1.2 to $-1.5 \mu\text{m}$ after their equi-

libration with synthetic seawater (organic free). However, they all show negative mobilities, narrowed down to a range of -0.1 to -1.1 μm after equilibration with natural seawater. Dialysis experiments indicate that a high molecular weight component in seawater is involved in determining the charge on the particles. Adsorption of organics onto particulate surfaces can possibly include electrostatic, hydrogen and hydrophobic bonding. Furthermore, the cooperative nature of multiple bonding sites possible in macromolecules can result in very strong associations with particles that are not easily reversed (Neihof, and Loeb 1974; Loeb and Neihof 1975). Therefore, it is probable that seawater particulates are covered with organic films whose density is a function of available sites. Such organic covers give the particulates more uniform characteristics than their individual characteristics.

Hunter (1980) also performed electrophoretic mobility measurements and found that different, well characterized solid surfaces, upon exposure to seawater, become covered by a tenacious film of natural surface-active organic material, which dominates their subsequent surface chemistry. Hunter proposed that reliable thermodynamic entities (intrinsic equilibrium constants) can be calculated through detailed analysis of the electrophoretic measurements on suspended particles. Macromolecular species and hydrophobic humic material seem to be important contributors to the organic film on the particles while carboxylic acid and phenolic groups are responsible for the electrophoretic behaviour.

Only very recently has this phenomenon of particulates coated with organics been considered for freshwater model systems. Blutstein and Shaw (1981) studied the contribution of adsorption of Cu on parti-

culate matter, to the total Cu-binding capacity of lakewater. After removal of organic material adsorbed on particulate matter by ultraviolet (U.V.) irradiation, the adsorption capacity increased, indicating that adsorbed organic material inhibited Cu adsorption on the suspended particulates.

The experiments and model of Davis and Leckie (1978) investigated the effect of adsorbed organic ligands in trace metal uptake by hydrous oxides. Amorphous iron oxide was used as an adsorbing surface. Chloride and sulphate were representative of inorganic ligands, while several acids, all with more or less different adsorption behaviour, were used as organic ligands. They observed three major effects:

1. The presence of complexing ligands that do not adsorb on the surface decreases metal adsorption, because the ligand competes with the surface for the metal ion.
2. Trace metal adsorption can be significantly enhanced when a ligand is adsorbed with strongly complexing functional groups directed outward into the solution.
3. When a complexing ligand adsorbs on a hydrous oxide surface via its major complexing functional groups, metal adsorption on this surface will be reduced to a certain extent, depending on the amount of ligand adsorbed. The experimental results obtained with this model system provide convincing evidence that metal-ligand complexes can adsorb or alternatively that trace metals can be complexed by adsorbed ligands. At present there are no analytical methods capable of distinguishing between these two mechanisms.

Benjamin and Leckie (1981) present a semi-quantitative conceptual model for metal-ligand-surface interactions, during adsorption.

It considers the effects that complexation of trace metal ions with inorganic and organic ligands have on the completeness of the adsorption process. Complexed metal species are, according to their behaviour and their influence on the adsorption-process and -orientation, divided into 'metal-like' and 'ligand-like' species. 'Metal-like' adsorbed complexes are oriented in such a manner that the metal is closer to the surface, while 'ligand-like' adsorbed complexes are located with the ligand adjacent to the surface. Such a discrimination implies a qualitative different partitioning pattern of trace metals between solution and surface, particularly at low pH. This model has been applied (Benjamin and Leckie 1982) to a system in which the effect of complexation by Cl^- , SO_4 and S_2O_3 on the adsorption behaviour of Cd on oxide surfaces is investigated. Cd - Cl and Cd - SO_4 complexes are assumed to behave 'metal-like', while Cd - S_2O_3 complexes are assumed to be located in a 'ligand-like' position on the surface. The experimental results from this investigation are consistent with the developed model.

1.3 Summary and Research Objectives

A very considerable amount of study has been and is currently directed toward more precisely predicting the fate of trace metals in natural water systems.

A brief introduction to the possible trace-metal associations in natural water systems was presented here. Interactions with dissolved material can be divided into inorganic and organic associations, of which the latter are difficult to assess, due to the still largely unrevealed structure of natural organic material such as humics and

fulvics. The boundary between dissolved and particulate matter is arbitrary and from a chemical point of view meaningless. Primary interactions of trace metals with particulate matter are complicated by metal associations with soluble inorganic and organic ligands and by coatings on particles, composed of a film of organic material which can either have a positive or negative effect on the adsorption of trace metals. Furthermore, adsorption of metal-organic complexes onto particle surfaces is possible.

The primary research objective of the work presented in this thesis can be broadly formulated in terms of the intention to contribute to the clarification of interactions between trace metals and dissolved and particulate material in natural aquatic systems. The use of a well-established technique to determine trace metal - dissolved organic interactions (i.e. stability constants) would likely be most suitable to study trace metal associations. For reasons discussed in Chapter 2, the promising but relatively new δ -MnO₂-method (van den Berg 1979 a,b) was chosen. However, this method displayed some apparent weaknesses. Therefore an extensive, experimental evaluation was required to provide the δ -MnO₂-method with a solid basis on which reliable conclusions can be built regarding trace metal interactions in natural waters. Cu was used as a model-trace metal throughout the whole study. A more specific research objective can therefore be formulated in terms of the evaluation of the δ -MnO₂-method with respect to:

- the reproducibility and stability of δ -MnO₂ surface morphology;
- the reproducibility and stability of chemical reactivity of the δ -MnO₂ surface towards Cu;

- the specific adsorption behaviour of Cu with respect to $\delta\text{-MnO}_2$ under various pH conditions and Cu concentration ranges;
- the developing of a new adsorption model better suited to describe adsorption of Cu on the $\delta\text{-MnO}_2$ surface.

CHAPTER 2

PROCEDURES FOR THE DETERMINATION OF COMPLEXING CAPACITIES AND
CONDITIONAL STABILITY CONSTANTS; OUTLINE OF RESEARCH2.1 Introduction

During the last twenty years the interest and study of trace metal speciation in the aquatic environment has increased considerably. A significant problem encountered is an inability to measure the metal species as they are, without drastically altering their environment and equilibria. Although one can measure total metal concentrations quite accurately by Atomic Absorption Spectrophotometry, Atomic Fluorescence Spectrophotometry, Emission Spectroscopy, X-ray Fluorescence Spectrometry, etc. (Kopp 1977), discrimination between species is not possible with these techniques, except in special situations.

Polarography was invented around 1920. It was neglected for a long time but was revived in the sixties, mainly because of its capability to discriminate between metal species. The detection limit of conventional polarography is not low enough for most trace metal studies in natural waters. Modifications such as pulse polarography (P.P.), differential pulse polarography (DPP), anodic stripping voltammetry (ASV), pulse anodic stripping voltammetry (PASV) and differential pulse anodic stripping voltammetry (DPASV) have much better detection limits.

An ion specific electrode is comparable to PP. It can measure free ion concentrations accurately only to a level of 10^{-7} M, 10-100 times higher than concentrations typically encountered in natural waters. Various ASV techniques are able to measure concentrations accurately down to 10^{-9} M, but much care is required because of many possible complications such as contamination, adsorption of organics on the mercury electrode, and dissociation of metal-ligand complexes during the actual analysis.

Metal-dissolved organic complexation has received considerable attention in the recent literature. Chau and Chan (1974) and Chau et al. (1974) defined the complexing capacity of a natural water as the amount of Cu that can be complexed per liter of 0.45 μ m filtered water at a fixed ionic strength and a buffered pH of 6. There are, however, other definitions proposed for complexing capacity (see Section 2.2).

To quantify complexing processes, measurements of stability constants for metal-organic complexes need to be made. However, usually a stability constant, which is a thermodynamic quantity based on activities, cannot be obtained due to considerable lack of information about the chemical properties of the complexing organic matter. These properties include the concentration of the organic ligand and the stoichiometry of complex formation; that is, the number of complexing sites available for metal complexation on these molecules is not known. Therefore a so-called conditional stability constant is obtained, which can be considered as an average stability constant for the different sites on the organic material. Conditional stability constants are labelled conditional because their value is valid only at fixed solution conditions such as pH, ionic strength and temperature (Ringbom 1963; Malcolm et al. 1968).

Several techniques for measuring complexing capacities (CC) and a large number of methods for determining conditional stability constants (CSC) are available. Due to inherent definitions and assumptions, results obtained with different CC and CSC methods cannot always be compared directly. An example is the concentration terms in which L_c , the total ligand concentration, is expressed.

It was suggested at the end of the previous Chapter (Section 1.3) that a well-established method for the determination of stability constants would be most suitable to study trace metal interactions with both particulate and dissolved material in natural aquatic systems. Since trace metal associations are easily influenced by alterations in the aquatic chemistry such as pH and concentrations, the method employed to investigate such associations should disturb the original water sample as little as possible. The next sections of this chapter discuss methods for determining complexing capacity and conditional stability constants. In particular, the δ - MnO_2 method (van den Berg 1979), which is the subject of this study, is discussed in some detail.

2.2 The Concept of Labile and Non-Labile Trace Metal-Organic Complexes and Methods to Measure Complexing Capacity

The complexing capacity of a natural water can be defined as the amount of trace metal (M) that is experimentally found to be complexed by ligands in solution. The potential capacity has been defined in various ways. The maximum amount of metal that could be bound if all acidic sites were bidentate and reactive is one way. The amount that can be calculated to be chelated on the basis of total

carboxylic or phenolic acidity, assuming that all reactive functional groups will form monodentate complexes (Gaskill 1978), is a second, but less frequently used way.

The best-known procedure for measuring CC's is that of Chau et al. (1974), who defined and used the concept of labile and strongly bound forms of metals in lakewaters (Chau and Chan 1974). Labile metals are determined as the ionic metal plus acetate-exchangeable metal. In some cases part of the strongly complexed metal is labile, if the ratio of complexing organics to total metal (L_t/M_t) $\gg 1$. Non-labile metal is the difference between total metal and labile metal. The analytical procedure is simple: Immediately after collecting a water sample it is filtered through a 0.45 μm membrane to remove all dispersed particles. 50 mL of sample with 0.5 mL of acetate buffer solution is analysed voltammetrically to give labile metal. Another 50 mL of sample is digested to give total metal concentration. The advantage of this method is that there is no necessity to concentrate the sample and therefore original existing equilibria in the sample are not altered. The high sensitivity of this procedure can be further increased by using longer deposition times on the Hg-electrode, although considering the L_t/M_t ratio in some samples, electrolysis times as short as possible are required. This method has been tested for four metals and the sensitivities obtained are: 0.2 $\mu\text{g/L}$ Zn, 0.4 $\mu\text{g/L}$ Cd, 0.7 $\mu\text{g/L}$ Pb and 0.5 $\mu\text{g/L}$ Cu.

A disadvantage of this method is that dissociation of complexes probably takes place during analysis, especially during the plating step. The nature of the complexes and the plating time strongly influence the extent to which such dissociations occur. This is

especially the case for waters where $L_t/M_t > 1$. Quantifying this so-called kinetic contribution is difficult since there is no theory on kinetic currents available for ASV, as there is for PP (Brinkman and Los 1964; van Leeuwen 1977, 1978; Stroes and Strijbis 1977). Labile metals determined by Chau's method therefore include the aquo-complexes and acetate-exchangeable metal and probably include part of the strongly bound metal.

Figura and McDuffie (1979) determined labile fractions of Cd, Cu, Pb and Zn in the presence of NTA, EDTA, glycine and humic acid, by using uptake on a Ca-Chelex resin. They found that the slow dissociation of soluble metal-ligand complexes can limit trace metal uptake by Chelex columns. Labile fractions determined by the Chelex method appear generally larger than the fractions obtained with the ASV method, indicating different timescales of measurement.

Chau et al (1974) also developed a voltammetric procedure, preceded by a titration, for measuring the concentration of ligands that are capable to bind Cu strongly. Copper was chosen because it associates strongly and non-specifically with the various ligands in natural waters. The amount of Cu complexed by a water sample is proposed as a measure of the copper complexing capacity of that water sample. The procedure again is simple. A sample of 0.45 μm filtered lake water is divided into several subsamples, each spiked with increasing amounts of Cu and allowed to equilibrate at 25°C for at least two hours. Cu is measured following the procedure described above. The complexing capacity (CC) is expressed in M of Cu equivalents, calculated from the intercept of the graph: ASV peak current (i) versus spiked Cu. By measuring the Cu binding capacity of various

known ligands, it was found by Chau et al. (1974) that this method would only work for Cu complexing agents with stability constants $>10^{13}$, which is approximately the strength of NTA. Experiments carried out at various pH's showed that the apparent CC of a sample is independent of the original pH only in the range 4-8.

Brezonik et al. (1976) provided evidence of the significant and sometimes severe changes that can be produced during ASV by sorption phenomena on the Hg-electrode surface at model sorbent concentrations representative of natural waters. They emphasized the need to discuss the possible implications of these effects with regard to the usefulness of ASV for analysis of CC in situ. Sorption seems to occur under natural and low pH conditions but some sorbents apparently inhibit electrochemical reactions more strongly at low than at neutral pH. In their opinion, the difference between the ASV signal for an untreated and acidified sample does not necessarily define the amount of metal present as non-labile complexes. Brezonik et al. (1976) questioned the assumptions on which the titration procedure for determining the Cu-CC are based, namely that the metal added during the titration of a water sample behaves exactly as all metals under natural conditions. They especially emphasized the possible long time required to reach true equilibrium status. Therefore they questioned the meaningfulness of CC concepts using Chau's principles.

Shuman and Woodward's (1973, 1977) ASV method to determine conditional stability constants (see Section 2.3.1) can also be used to measure the complexing capacity of the same water sample. Instead of extrapolating the graph of ASV response ($=fM^{2+}$) versus M_t (added) after the equivalence point to intercept the M_t axis, as Chau et al.

(1974) do, they use data points both before and after the equivalence point and obtain the equivalence point for CC by applying Gran (1952) principles.

Lazar et al. (1981) critically reviewed the ASV method. They suggested that the break in the Cu titration curve in seawater, as determined by ASV, could be due to the formation of a Zn-Cu inter-metallic compound (see also Chapter 6) formed in the Hg-electrode during the deposition stage of the ASV procedure.

Others, e.g. Ramamoorthy and Kushner (1975) and Guy and Chakrabarti (1976) have used an ion specific electrode (ISE) procedure to measure CC (Gaskill 1978). They plotted dialyzable metal versus total metal and called the breakpoint the CC. There is also the δ -MnO₂ method by van den Berg (1979) and van den Berg and Kramer (1979a,b) which is based on competition between unknown ligands and added δ -MnO₂ for trace metal (see Section 2.3.8).

Wilson and Kinney (1977) used a dialysis equilibration method to determine the CC's of aquatic humics and the commercial Aldrich humic acid. Truitt and Weber (1981 a,b) evaluated and used the dialysis titration technique as a method for determining the CC of soil-derived fulvic acid and some freshwater samples. They found that a statistical comparison of dialysis and Cu²⁺ - ISE results showed no difference in the ability of the two techniques to measure CC. Campbell et al. (1977) made use of the Cu(II) solubilization method published by Kunkel and Manahan (1973) to determine Cu-CC's of several rivers, but found that this method underestimated the true CC of natural waters. Blaser et al. (1980 a,b) proposed a spectrophotometric titration method to determine the maximum Fe or Cu binding ability of leaf litter extracts and the conditional stability

constants of the organo-metallic compounds. They checked this method against the dialysis method of Zunino and Martin (1977). The cobalt (III) complexation method developed by Hanck and Dillard (1977) eliminates many of the problems of metal complex lability by making use of inert metal complexes in determining the CC of natural waters.

A number of biological procedures to measure complexing capacities have also been proposed. Davey et al. (1973) used Cu titrations on concentrations of known chelators to illustrate that the growth of Thalassiosira pseudonana in response to Cu could be used to quantify the levels of the chelators to within 5%, at concentrations as low as 10^{-7} M EDTA. Gillespie and Vaccaro (1978) described a simple ^{14}C tracer bioassay technique which uses a copper sensitive bacterium to measure the Cu chelating capacity of seawater. Blaser et al. (1980 a,b) compared the CO_2 uptake response by algae in solutions with and without organic substances spiked with variable amounts of Cu. From this they were able to derive the maximum binding ability and the conditional stability constant for leaf litter extracts.

Batley and Florence (1976) proposed a classification of trace metal species in natural waters. It systematically determines soluble and insoluble binding agents separately and thus rather than complexing capacity (see definition at the beginning of Section 2.2) considers the overall binding capacity of natural waters. The scheme subdivides trace metal species in water samples in four classes of which three contain both organic and inorganic species such that a total of seven groups are identified. Separation methods include U.V. radiation and chelating resins. The scheme has been successfully applied to a range of seawater and freshwater samples. The advantages

of this scheme are that the techniques of U.V. radiation and chelating resin separation are less suspect with regard to contamination than filtrations.

2.3 Methods for the Determination of Conditioned Stability Constants of Trace Metal-Organic Complexes

Many procedures for the determination of conditional stability constants (CSC) for trace metal-organic (and/or - humic) complexes exist. These methods have been reviewed by Martell and Calvin (1952), Rossotti and Rossotti (1961), Beck (1970) and Gaskill (1978). This section examines the theory behind and the capabilities of eight procedures. Two methods are discussed in considerable detail, because they were evaluated during the course of this study. Shuman and Woodward's (1973,1977) ASV method (Section 2.3.1) was used in the preliminary phase of this study, to measure CSC's for Zn-organic complexes (see Section 2.4). The δ -MnO₂ method (Section 2.3.8), originally proposed by van den Berg (1979) is the subject of this work.

2.3.1 Anodic Stripping Voltammetry (ASV)

The speed and selectivity of ASV facilitate the study of the trace metal binding with ligands of natural or pollution origin (Allen et al. 1970) and is used extensively for determining CSC's. Most work has examined organic ligands. Shuman and Woodward (1973,1977) developed a method which uses a titration followed by ASV, to effectively estimate the conditional formation constant for the metal-ligand complex. The expressions involved are the following:

At equilibrium,



and the conditional stability constant is

$$K_{ML} = \frac{[ML^{n+}]}{[M^{n+}] [L]} \quad (2.2)$$

in which $[M^{n+}]$ = free metal ion concentration

$[L]$ = free ligand concentrations, i.e. ligand not
bound with metal

$[ML^{n+}]$ = metal ligand complex

k_f = rate constant (forward)

k_b = rate constant (back)

The electrode reaction is



in which $M(\text{Hg})$ = metal-Mercury amalgam.

The anodic stripping current is

$$i_a = \kappa [M^{n+}] \quad \text{or}$$

$$[M^{n+}] = \frac{i_a}{\kappa}$$

(2.4)

in which i_a = anodic stripping current (peak)

and κ = empirical constant, depending on characteristics of electrode and cell, stirring efficiency, time of plating, scanrate and diffusion characteristics of the metal ion.

Rearranging gives

$$[ML^{n+}] = M_t - \frac{i_a}{\kappa} \quad ; \quad (2.5)$$

M_t = total analytical metal concentration

$$\text{and } [L] = L_t - [ML^{n+}] = L_t - M_t + \frac{i_a}{\kappa} \quad ; \quad (2.6)$$

L_t = total analytical ligand concentration.

Therefore,

$$K'_{ML} = \frac{(M_t - \frac{i_a}{\kappa})}{(\frac{i_a}{\kappa})(L_t - M_t + \frac{i_a}{\kappa})} \quad (2.7)$$

In a titration, two regions of the titration plot (i_a vs added metal M_t) proved to be useful. At the beginning of the titration where

$L_t > M_t$,

$$[M^{n+}] = \frac{i_a}{\kappa} \ll M_t < L_t$$

Therefore,

$$K'_{ML} = \frac{M_t}{(\frac{i_a}{\kappa})(L_t - M_t)} \quad (2.8)$$

Plotting i_a vs $M_t/(L_t - M_t)$, in the case where L_t is known, will

give a slope of κ/K'_{ML} . At the end of the titration, far beyond the equivalence point which is the break in the titration curve, $M_t \gg L_t$.

$$\text{Therefore, } i_a = \kappa(M_t - L_t) \quad (2.9)$$

Again, by plotting i_a vs $(M_t - L_t)$ one obtains κ from the slope and therefore K'_{ML} can be calculated, assuming L_t is known. If L_t is unknown, a plot of i_a vs M_t yields a slope κ and an intercept $\kappa \cdot L_t$ from which L_t can be calculated (yielding the approximate complexing capacity). Then the data for the beginning of the titration, i_a vs $M_t/(L_t - M_t)$, can be plotted and K'_{ML} can be calculated from the slope κ/K'_{ML} .

Shuman and Woodward (1973, 1977) realised that their method of a titration followed by ASV uses, in fact, inaccurate measurements to estimate K'_{ML} for a metal-ligand complex. To investigate how accurate the results obtained by the above outlined approximations would be, they rearranged (2.7) to:

$$\text{or } \left(\frac{i_a}{\kappa}\right)^2 + \left(\frac{i_a}{\kappa}\right) \left\{ \frac{1}{K'_{ML} + L_t} - M_t \right\} - \frac{M_t}{K'_{ML}} = 0 \quad (2.10)$$

$$\frac{i_a}{i_{\max}} = \frac{1}{2} \left\{ [g-1 - (K'_{ML} \cdot L_t)^{-1}] + [(1 - g + (K'_{ML} \cdot L_t)^{-1})^2 + 4g(K'_{ML} \cdot L_t)^{-1}]^{1/2} \right\} \quad (2.11)$$

in which $i_{\max} = \kappa L_t$ and $g = M_t/L_t$.

This equation (2.11) holds for 1:1 complexes. It shows that the titration depends only on the product $K'_{ML} \cdot L_t$. It can be solved using a computer algorithm. To observe a break in the titration curve, $K'_{ML} \cdot L_t$ has to be > 1 . But for $K'_{ML} \cdot L_t$ as low as 10, estimates of K'_{ML} accurate to at least 20% can be made halfway up to the end point of the titration curve. An accuracy within 1% can be expected throughout 70% of the titration curve, when $K'_{ML} \cdot L_t > 10^3$.

The error caused by disregarding currents associated with dissociating complexes during the plating out step, increases with decreasing $K'_{ML} \cdot L_t$. Shuman and Woodward (1973) tried to quantify the effects of complex dissociation on stripping currents. They defined a general criterion for differentiating between strictly diffusion controlled and partly kinetic currents. The latter can be related to the rate constant of the dissociation reaction, by applying reaction layer theory.

Shuman and Woodward (1977) extended the original titration procedure for application to any stoichiometry. The principles are the same as for 1:1 complexes. K'_{ML} can again be calculated in two different ways: from approximation of titration data (end and start) by their plotting method (accuracy $\leq 20\%$) or by computerfitting of the data to the theoretical equation (2.11). In fact, the latter only serves to check how accurate the approximation method is.

To determine whether complex dissociation contributes to accumulation during pre-electrolysis, dissociation rate constants can more accurately be estimated using a rotating disk electrode (Shuman and Michael 1975, 1978; Shuman 1978). The rate constants obtained can be used to calculate the fraction of the total flux due to complex

dissociation. Shuman concludes that although corrections up to 20% can be made on K'_{ML} values, their application is not justified when the precision of the titration and the approximate manner with which the kinetic current was estimated are recognized.

Ernst et al. (1975) use DPP and DPASV to measure trace metal stability constants and apply the Lingane (1941) theory which calculates stability constants from the shift in peak potential:

$$E_{1/2} = E_{1/2}(\text{single ion}) - E_{1/2}(\text{complexed ion}) = (2.3RT/nF)$$

$$\log B_j [L]^j \quad (2.12)$$

in which

$$B_j = [M L_j^{n+}] / [M^{n+}] [L]^j.$$

Gaskill (1978) argues that some of the Lingane assumptions were not fulfilled, suggesting that Ernst et al.'s (1975) results are highly questionable.

ASV has also been used for trace metal - inorganic ligands stability constants measurements. Examples are Bradford (1973) (Zn-hydroxides) and Bilinski et al. (1976) (Hydroxo - and carbonato-complexes of Pb, Cu, Cd and Zn). ASV has also been applied in combination with gel filtration chromatography, to study the organic associations of Cu and Pb in seawater (e.g. Sugai and Healy 1978, see Section 3.6).

2.3.2 Ion Exchange Methods (IE)

The ion exchange method was originally proposed by Schubert (1948). Because the method is suitable for low metal concentrations, and metal-resin equilibria generally are rapid, it has found much application in the field of CSC's of trace metal - (natural) organic complexes.

Martell and Calvin (1952) proposed the following IE method.

From

$$K'_{ML} = \frac{(ML)_x}{(M)(L)^x} \quad (2.13)$$

one obtains $\log \left(\frac{\lambda_o}{\lambda} - 1 \right) = \log K'_{ML} + x \log (L)$, (2.14)
 in which $\lambda_o = (\text{metal on resin}) : (\text{metal in solution})$ ratio determined in an experiment without organics.

$\lambda = (\text{metal on resin}) : (\text{metal}_{\text{free}} + \text{metal}_{\text{complexed}})$ ratio determined in an experiment with organics present.

Other symbols are as defined for equations 2.1 and 2.2. A plot of $\log \left(\frac{\lambda_o}{\lambda} - 1 \right)$ versus $\log L$ will yield K'_{ML} and x .

are: Conditions for accurate determination of stability constants

- (i) L must not be resin exchangeable.
- (ii) Temperature, solution volume, ionic strength and the resin amount must all be held constant.
- (iii) A low metal- and a high resin-concentration will ensure a proper value for λ_o .
- (iv) $\text{Metal}_{\text{free}}$ must be in equilibrium with the resin, both in presence and absence of ligand.

- (v) L_t must be in great excess to ensure that $L = L_t$ and so that polynuclear complex formation is avoided.
- (vi) Molar ligand concentrations are required to calculate K'_{ML} . This can be a problem, since molar concentrations are not known when one attempts to measure unknown organic material.

Examples of workers who have applied the ion exchange method in one form or another are: Schnitzer and Skinner (1966,1967), Schnitzer and Hansen (1970), Schnitzer and Khan (1972), Stevenson and Ardakani (1972), Ardakani and Stevenson (1972), Zunino et al. (1972a,b, 1975), Allen et al. (1975) and Zunino and Martin (1977).

Galindo and Zunino (1978) discuss limits to the ion exchange method. The CSC's obtained are most reliable when working in L_t concentration ranges that bracket the value of $1/K'_{ML}$ for 1:1 ML complexes. For this range enough metal stays in solution to allow its accurate determination in successive experiments with increasing L_t concentrations. To measure reliable stepwise formation constants for ML_2 (i.e. 1:2) complexes, the intermediate species ML^+ should not be exchanged by the resin; otherwise Schuberts (1948) equations are no longer valid.

2.3.3 Ion Specific Electrode Method (ISE)

Buffle et al. (1977) showed that the use of an ISE makes it possible to measure the complexing ability of organic matter, without modifying the medium and without any pretreatment. Expressions used in this method are, for a Nernst response (at constant temperature and ionic strength):

$$E = E_0 + p \log (M^{++}) \quad (2.15)$$

in which E and E_0 have their usual meaning and $\alpha = (M_t)/(M^{++})$ or

$$\alpha = (M_t) \cdot 10^{(E_0 - E)/p} \quad (2.16)$$

For 1:1 complexes one can write:



and
$$B_1^* = \frac{(ML)(H^+)^x}{(M^{++})(H_x L)} \quad (2.18)$$

After defining $(L_t)/Mw = (H_x L)/v + (ML)/v$, (2.19)

in which (L_t) = concentration of ligand in g/L

Mw = g/mole metal equivalent

x = moles H^+ released per mole of sites (or ligand) complexed.

v = metal ions per complexing site (1 for 1:1 complex),

rewriting yields:

$$Y = \frac{(L_t)}{(M_t)} \cdot \alpha/\alpha-1 = \frac{Mw}{v} + \frac{Mw}{v} \frac{(H)^x}{B_1^*} \frac{\alpha}{(M_t)} \quad (2.20)$$

$((M_t) = (M^{++}) + (ML))$ as defined before, in moles/L.)

By plotting Y versus $\alpha/(M_t)$, the intercept with the Y-axis

yields the metal equivalent weight M_w of the organics, while the intercept divided by the slope yields K'_{ML} , the conditional stability constant ($K'_{ML} = B_1^*/(H^+)$).

Buffle et al. (1977) also derived a method for 1:2 (ML_2) complexes.

ISE's have a detection limit varying from 10^{-6} to 10^{-8} M, but below 10^{-7} M; most electrodes are not able to measure free ions very accurately and the slope of the calibration graph (electrode response vs. free metal concentration) changes rapidly to a smaller or even negative value. However, due to the developments in ISE technology over the last five years, which increased precision and sensitivity, ion specific electrodes have become quite popular.

Cheam (1973) and Manning and Ramamoorthy (1973) used a Cu^{2+} -ISE, to study the chelation of Cu with fulvic acid at low pH and to determine equilibrium constants for mixed ligand complexes of the type Cu^{2+} -fulvate-secondary ligand, as well as the stability constant for the 1:1 Cu^{2+} -fulvate complex. Ramamoorthy and Kushner (1975 a,b) used ISE to obtain both complexing capacity and stability constants for river water and soil fulvic acid. Nakagawa et al. (1975) described the use of the Cu(II) selective electrode to determine stability constants of Cu with acetate, ammonia, ethylenediamine, glycine, etc., but due to calibration problems in the lower limit calibration range, they were unsuccessful in obtaining Cu-NTA and Cu-EDTA stability constants with the ISE. Takamatsu and Yoshida (1978) used a combination of potentiometric titration (see Section 2.3.5) and ISE to determine apparent stability constants of Cu^{2+} , Pb^{2+} and Cd^{2+} complexes with humic acids. Saar and Weber (1980 a,b)

studied the complexation of lead (II) with fulvic acids derived from soil and river water, as measured by ISE and compared the results for lead with fulvic acid complexation of Cu and Cd. Their electrode response flattened out below about 10^{-5} M Pb^{2+} . They used a computer fitted polynomial for the calibration curve for Pb^{2+} . They described ways to avoid or correct difficulties with the lead (II) ISE, such as air oxidation of the surface and coatings by surface active substances such as fulvic acids on the electrode.

2.3.4 Method of Continuous Variation (CV)

Job's (1928) continuous variation technique has been used both to determine humic-trace metal ratio's (Schnitzer and Skinner 1963 and Schnitzer and Hansen 1970) as well as to estimate trace metal humic complex formation constants (Schnitzer and Hansen 1970). The principle of the method relies on the preparation of a series of solutions in which the sum of the total ligand and metal concentrations are kept constant, but in which their ratio $r = M_t/L_t$ is continuously varied. Expressions involved are:



$$M_t + L_t = C \text{ (constant)} \quad , \quad (2.22)$$

$$x = L_t / (M_t + L_t) \quad (2.23)$$

$$\text{and } r = M_t / L_t \quad (2.24)$$

At equilibrium, when $(1-x)$ units of M_t are mixed with x units of L_t , the following expressions hold:

$$[M] = C(1-x) - a[M_a L_b] \quad (2.25)$$

$$[L] = Cx - b[M_a L_b] \quad (2.26)$$

and

$$[M_a L_b] = K'_{M_a L_b} [M]^a [L]^b \quad (2.27)$$

At $x = x_{\max}$, $[M_a L_b]$ reaches a maximum; i.e. $d[M_a L_b]/dx = 0$ in the plot of $[M_a L_b]$ versus x . The expression $x_{\max} = b/(b+a)$, holds when equimolar units of M_t and L_t are mixed, (i.e. $r=1$) while in the case of non-equimolar units, x_{\max} depends on M_t , $K'_{M_a L_b}$ and r . Differentiating the expressions for $[M]$, $[L]$ and $[M_a L_b]$ with respect to x , setting $d[M_a L_b]/dx = 0$ and combining the 3 differential equations with the original expressions to eliminate $[M]$ and $[L]$, gives:

$$K'_{M_a L_b} \cdot M_t^{a+b-1} \cdot r^{b-1} \cdot a^{1-b} \cdot b^{1-a} [(b+ar)x_{\max} - b]^{a+b} = (r-1)^{a+b-1} [b - (b+a)x_{\max}] \quad (2.28)$$

Once b and a are known from an equimolar experiment, $K'_{M_a L_b}$ can be determined with non-equimolar solutions.

Instead of $[M_a L_b]$ versus x , usually Y versus x is plotted in which Y is the difference between the optical density (OD) of the solution containing the complex and the OD of the reactants M_t and L_t separately.

There are numerous conditions to be met before the method of continuous variation can give accurate ligand-metal ratio's and stability constants. The main ones are (Gaskill 1978):

(i) The ionic strength must be high, in order to ensure a constant b/a over the M_t range.

(ii) Y must be strictly linear with $[M_a L_b]$.

(iii) Only a single, mononuclear complex must be formed.

Often, many of the conditions are not met, especially when L is a humic substance, which makes the CV method not very practical for natural waters.

2.3.5 Potentiometric Titration Method (PT)

The potentiometric titration method is based on measuring the competition between protons and metal ions for complexing sites. The method has been used to measure stability constants for trace metal-humic acid complexes by (amongst others) Stevenson and Ardakani (1972), Stevenson (1976) and Stevenson (1977). Expressions involved are as follows (Stevenson 1977):

Defining

$$b_1 = \frac{(ML^+)(H^+)}{(HL)(M^{2+})} \quad \text{and} \quad b_2 = \frac{(ML_2)(H^+)}{(HL)(ML^+)} \quad (2.29/2.30)$$

gives $B_2 = b_1 b_2 = K_2 (K_1)^2$, in which $K_1 = \frac{(L^-)(H^+)}{(HL)}$, is the

dissociation constant of the ligand.

\bar{n} is Bjerrum's formation function, the average number of ligand molecules per metal ion or:

$$\bar{n} = \frac{(L_t) - (HL) - (L^-)}{M_t} = \frac{(ML^+) + 2(ML_2)}{(M^{2+}) + (ML^+) + (ML_2)} \quad (2.31)$$

which can be written in general form as

$$\bar{n} = \frac{\sum_{n=1}^N n(ML_n)}{(M^{2+}) + \sum_{n=1}^N (ML_n)} \quad (2.32)$$

This can be worked out to

$$\sum_{n=0}^{N=n} (\bar{n} - n) B_n (HL/H^+)^n = 0 \quad (2.33)$$

where n is the number of ligands per complex, with N the largest. B_n is the stability constant for the n th complex. For 1:2 complexes (i.e. one metal-two ligand) the following equation can be used to obtain the desired constants:

$$\frac{\bar{n}}{(\bar{n}-1)(HL/H^+)} = \frac{(2-\bar{n})(HL/H^+)}{(\bar{n}-1)} \cdot B_2^{-b_1} \quad (2.34)$$

Computer programs based on linear least squares analysis were developed for calculating (HL/H^+) and \bar{n} from the experimental data, and for estimating B_2 .

Stevenson (1977) also developed a revised approach to the PT

method. Swallow et al. (1978) used potentiometric Cu titrations to determine excretion of extracellular organic compounds by algae.

Takamatsu and Yoshida (1978) combined PT and ISE techniques to determine conditional stability constants for Cu^{2+} , Pb^{2+} and Cd^{2+} complexes with humic acids.

2.3.6 Gel Filtration Chromatography Method (GFC)

Mantoura and Riley (1975) used gel filtration chromatography for the estimation of stability constants of metal-ligand complexes. The method is in fact a form of zonal analysis. It consists of the following.

A TRIS-buffer solution with a known amount of complexing agent is injected into a Sephadex-G15 column. The latter is equilibrated with a flowing TRIS-buffer solution containing a known concentration of metal ion. The collected effluent fractions show first a peak, then a trough in total metal concentration with identical areas respectively below and above the curve of total metal vs. volume collected. The peak corresponds to the amount of complexed metal that is eluted from the column, the trough corresponds with the resultant metal deficiency in the column. Tris-(hydroxymethyl)-amino methane is used as a metal buffer. Besides buffering the pH, it provides a system capable of working at free metal concentrations down to 10^{-8} M for some metals.

After plotting the concentrations of trace metal in the various collected effluent fractions as a function of elution volume, the bound metal (M_b) and metal deficiency can be determined from the peak and trough areas of the plot. Providing the total ligand concentra-

tion (L_t) can be measured or is somehow known, $\bar{v} = M_b/L_t$ can be calculated. \bar{v} represents the number of moles of metal bound by the total concentration of ligand.

The estimation of the stability constant for the metal ligand complex requires three steps:

1. The concentration of buffer (TRIS) that is free to complex with the metal (=unprotonated TRIS) is calculated from

$$\text{pH} = \text{pK}_a + \log \frac{(\text{TRIS}_f)}{(\text{TRIS}_t) - (\text{TRIS}_f)} \quad (2.35)$$

2. The concentration of free metal ion (M_f) in the TRIS-buffer solution is calculated, using

$$(M_f) = \frac{(M_t)}{1 + \sum \beta_n (\text{TRIS}_f)^n}; \quad (\text{TRIS}_f) \gg (M_t) \quad (2.36)$$

Here $\beta_1, \beta_2, \dots, \beta_n$ are the successive stability constants of the TRIS-metal complex.

3. The association constant, K_o , is calculated from

$$K_o = (M_b) / (M_f)(L_t - M_b) \quad (2.37)$$

This formula should be used whenever only a single run is performed. However, it is preferable to do a whole series of runs, for which the following formula is valid:

$$\frac{\bar{v}}{M_f} = K_1 \cdot (n_1 - \bar{v}) \quad , \quad (2.38)$$

in which $\bar{v} = M_b/L_T$,

K_1 = stability constant of metal-ligand complex,

n_1 = number of metal binding sites per ligand molecule, and

i = type of complexing site where 1 equals the first site and 2 the second, weaker type of complexing site; 0 is the sum of 1 and 2.

By plotting \bar{v}/M_f versus \bar{v} , one obtains K_1 from the slope and n_1 from the intercept on the \bar{v} -axis. This is called a Scatchard plot analysis. K_1 (i.e. K_1 or K_2) is the overall or average stability constant for all sites of one type (i.e. 1 or 2). The overall K_0 is not the average of the individual constants for each type of complexing site as stated by Mantoura and Riley (1975) but is a weighted average given by $(n_1K_1 + n_2K_2)/(n_1 + n_2)$. This weighting reflects the varying contributions of stronger and weaker sites (Gaskill 1978).

Means et al. (1977) used GFC to evaluate trace metal-organic interactions in natural waters, while Sugai and Healy (1978) used a combination of ASV and GFC to examine Cu- and Pb- complexation with organics in seawater.

2.3.7 Dialysis Method (DI)

This method is based on the assumption that free metal ions can diffuse through dialysis bags, but that metal-organic complexes cannot. Bags containing organics are suspended in distilled water which contains metal. At equilibrium, no further diffusion occurs

because the free metal concentrations inside and outside the bag are the same. Measurements of the total metal concentrations on either side of the bag permits the calculation of the quantity of metal bound in metal-ligand complexes.

One significant problem results, because dialysis membranes usually carry a negative charge. This causes negative species in solution to experience a smaller effective dialysis membrane pore size, necessitating long equilibrium times (Guy and Chakrabarti 1977). The Donnan-membrane effect (caused by a lack of diffusible anions) can be overcome by adding enough inert electrolyte.

Wilson and Kinney (1977) used the dialysis equilibration principle to calculate Zn, Mn and Cu stability constants for humic material. They used modified equations from the biochemical literature to describe proton-metal-ion interactions on humic substances. They were able to experimentally determine intrinsic constants for the dissociation of the humics and formation of the metal complex. Intrinsic constants are equilibrium constants in the absence of electrostatic effects of other charged functional groups on the humic molecules. They are calculated from

$$K_{app} = K_{int} \exp(2 w z_1 z^*) \quad (2.39)$$

in which

K_{app} = apparent dissociation constant of a given group type,

K_{int} = dissociation constant of a group type on a polyion in a hypothetical chargeless state,

z_i = charge on the bound species (i.e. H^+ or M^{z+}),
 w = electrostatic interaction factor,
 and Z^* = average charge on the macroion at a given pH.

2.3.8 The δ -MnO₂ Method

Van den Berg (1979) and van den Berg and Kramer (1979a,b) developed an indirect measurement technique which involves a titration, a resin, and voltammetry to measure complexing capacities and conditional stability constants. The method was developed and tested for Cu. A certain amount of δ -MnO₂, calibrated for Cu uptake, is added to the sample, to act as a weak ion exchange resin. Titrating the sample, at constant pH and fixed ionic strengths with Cu causes the organic material present and the δ -MnO₂ to compete for the metal. The resin is removed from the sample (after 1 hr. equilibration time) by 0.45 μ m filtration and Cu in solution is measured by DPASV after acidifying the sample. The difference from ordinary IE procedures is that only a small amount of δ -MnO₂ is added to the sample, which presumably does not significantly alter the composition and/or existing equilibria in the natural water sample.

The important mass balance equations are (van den Berg 1979):

$$(Cu_{diss}) = (Cu^{2+}) + (CuOH^+) + (Cu-L) + (CuCO_3), \quad (2.40)$$

$$(Cu_t) = (Cu_{diss}) + (Cu_{ads}) \quad (2.41)$$

and $(L_t) = (L) + (Cu-L). \quad (2.42)$

In some systems, Cu_{diss} may include other inorganic complexes of Cu.

These are assumed negligible here. Carbonates can be removed by N_2 purging which simplifies the mass balance for Cu_{diss} even further. At equilibrium,



and

$$K'_L = \frac{(Cu-L)}{(Cu^{2+})(L)} \quad (2.44)$$

To describe Cu uptake on δ - MnO_2 , a Langmuir adsorption isotherm is used. This gave satisfactory results to van den Berg, although in fact the Langmuir theory cannot be applied in systems with increasing amounts of ions which affect the charge on the oxide. The Langmuir model is:

$$\Gamma_{ads} = \Gamma_{max} \frac{(Cu^{2+})}{1/B + (Cu^{2+})} \quad (2.45)$$

in which

Γ_{ads} = mole Cu adsorbed per mole MnO_2 ,

Γ_{max} = limiting or maximum value of Γ_{ads}

and B = binding constant representing the energy involved in adsorption.

The δ - MnO_2 surface can be calibrated for Cu uptake as follows: A solution containing δ - MnO_2 is titrated, at a certain pH and fixed ionic strength, with Cu. Depending on the pH of the δ - MnO_2 suspension, a known organic is added to keep enough Cu in solution (either

by preventing Cu-oxides and/or -hydroxides to precipitate or to keep an equal balance between Cu adsorbed and Cu dissolved). The amount of Cu adsorbed is determined from the mass balance (expression (2.41)). Cu_t is known, while Cu_{diss} can be measured in the sample, which is acidified after δ - MnO_2 is removed by 0.45 μ m filtration. The described procedure is called a calibration experiment hereafter. The Langmuir isotherm can be linearized and by plotting Cu^{2+} vs Cu^{2+}/Γ_{ads} , one can calculate B and Γ_{max} , the adsorption parameters, from the slope and the intercept of this plot. Once B and Γ_{max} are known, one can calculate Cu^{2+} concentrations from Γ_{ads} data measured during a titration with Cu of an unknown system (i.e. containing unknown complexing material) after addition of a known amount of calibrated δ - MnO_2 . The calculated Cu^{2+} concentration has to be corrected for Cu-hydroxides, depending on the pH at which the titration was performed. By purging the sample continuously with N_2 , the formation of $CuCO_3$ can be avoided, simplifying the calculations. Once the Cu^{2+} concentrations are known for each titration step, the total ligand concentration can be calculated as follows:

$$K'_L = \frac{(Cu-L)}{(Cu^{2+})(L)} \quad (2.44)$$

$$(L_t) = (L) + (Cu-L) \quad \text{or} \quad (L) = (L_t) - (Cu-L) \quad (2.42)$$

$$(Cu-L) = (Cu_{diss}) - (Cu^{2+}) - (Cu\text{-hydroxides}) \quad \text{from (2.40)}$$

Combination of these expressions gives:

$$K'_L = \frac{(Cu-L)}{(Cu^{2+})((L_t) - (Cu-L))} \quad (2.46)$$

Rearranging yields:

$$\frac{1}{K'_L} = \{(Cu^{2+}) (L_t) - (Cu^{2+}) (Cu-L)\} / (Cu-L) \quad (2.47)$$

or

$$\frac{(Cu^{2+})}{(Cu-L)} \cdot (L_t) - (Cu^{2+}) = \frac{1}{K'_L} \quad (2.48)$$

and eventually

$$\frac{(Cu^{2+})}{(Cu-L)} = \frac{1}{K'_L (L_t)} + \frac{(Cu^{2+})}{(L_t)} \quad (2.49)$$

A plot of $(Cu^{2+}) / (Cu-L)$ vs (Cu^{2+}) yields $1/(L_t)$ from the slope and $1/K'_L(L_t)$ from the intercept. Therefore K'_L , the conditional stability constant of the complex, and then L_t , the complexing capacity, can be calculated.

The main strong points of the δ - MnO_2 method are as follows (van den Berg 1979): The MnO_2 method has a sound theoretical basis and functions in an equilibrium situation with metal ions and ligands. No preconcentration of the ligands is necessary and the natural water sample is disturbed as little as possible. Even in such dilute systems as natural waters enough metal is kept in solution to be measured accurately, due to the weak adsorption character of MnO_2 . Also, this method can discriminate between two sites or two ligands, providing they are present in about equal concentrations and have sufficiently different stability constants to display their effect in the titration curve.

The following are possible drawbacks (van den Berg 1979): At pH's <6, the conditional stability constants of ligands in natural waters and the binding constant and adsorption capacity for δ -MnO₂ decrease greatly, causing determinations to become rather inaccurate due to increased solubility of Cu²⁺. In such cases, the Cu titration has to be performed at a suitable higher pH. Whenever the natural ligand concentration exceeds around 5 μ M, the sample should be diluted, because of foam formation and interferences during the ASV step (adsorption of organics on the Hg-electrode). The measurements become inaccurate when K'_L becomes much larger than B (e.g. if $\log K'_L > 10$ at pH 8, in van den Berg's case). It may also not be possible to discriminate between 2:1 (Cu₂L) and 1:2 (CuL₂) complexes with this method (van den Berg 1979).

2.4 Comparison Between the δ -MnO₂ Method and the Other Procedures with Respect to Results for CSC's

Van den Berg (1979) briefly compares the δ -MnO₂ method with most of the procedures described in Sections 2.3.1-2.3.7. From his conclusions, and from the descriptions of other CC- and CSC- methods in Section 2.3, it is clear that they all have limitations, on the basis of one or more of the following reasons:

- (i) A method is too insensitive, requiring one to work at unnaturally high (free) metal concentrations. The ion selective electrode is an example.
- (ii) A method is only applicable at relatively low pH values, e.g. the ion selective electrode. The large number of studies at low pH's

is illustrated in Figure 2.1; van den Berg's results and a few others are the exception. K'_{ML} results cannot be extrapolated to higher pH values due to electrostatic effects on the macromolecules.

- (iii) The ligand concentration needs to be high (10^{-4} - 10^{-3} M). This requires undesirable concentration procedures, such as in the ion exchange method.
- (iv) The ligand concentration needs to be known, either in moles/L, g/L or metal equivalent/L. This is required in ion exchange, ion specific electrode-, continuous variation-, gel filtration chromatography-, and Shuman's ASV- methods.
- (v) The procedure works only for strong complexes or in solutions having a high concentration of ligands; e.g. the ASV-methods.
- (vi) The method alters the natural system too much through additives and concentration procedures. The ion-exchange method and the Co(III) procedure for determining CC's are examples.
- (vii) The method is subject to interferences, for instance the ASV-, continuous variation- and dialysis-methods.
- (viii) The basic assumptions are not valid for natural systems, e.g. in the continuous variation method.

- (ix) A high ionic strength is required, e.g. in the dialysis method and the continuous variation method.
- (x) The method is very time consuming. An example is the dialysis method.

In Figure 2.1, the influence on the free Cu^{2+} concentration of a number of conditional stability constants (K'_{ML}) for Cu-natural organic complexes, reported in the literature, are compared. These constants are obtained with the methods described in Section 2.3 and are recalculated for Figure 2.1 in terms of α , which describes Cu^{2+} as a fraction of Cu_t (van den Berg 1979).

$$\alpha = \text{Cu}^{2+}/\text{Cu}_t \quad (2.50)$$

$$\text{or } \alpha = (K'_{ML} \cdot L_t + 1)^{-1} \quad (2.51)$$

The total ligand concentration (L_t) is set at 10^{-6} M, while the Cu_t concentration is 10^{-7} M in Figure 2.1, a situation fairly representative of natural waters. The $p\alpha$ and $p\text{Cu}^{2+}$ values, calculated with van den Berg's (1979) MnO_2 values for a number of K'_{ML} 's measured for fresh water bodies are represented by closed circles (see legend for Figure 2.1). The $p\alpha$ and $p\text{Cu}^{2+}$ values calculated with K'_{ML} values obtained by the other methods described in Section 2.3 are indicated by closed triangle symbols. The latter values are obtained from Gaskill (1978) who recalculated these K'_{ML} values to a common unit basis of metal equivalent per liter, from the different units of expressing the ligand concentration

used originally (e.g. moles/L, g/L, metal equivalent/L). The metal equivalent has the same units as van den Berg's K'_{ML} , since 1:1 complexation was assumed.

Except for the value reported by Mantoura and Riley (1975) at pH 8 for Cu, none of the values recalculated by Gaskill (1978) were obtained above pH 7; most of them are below pH 6. However, the K'_{ML} values obtained by van den Berg (1979) with the δ -MnO₂ method were all determined at $7.2 \leq \text{pH} \leq 8.4$.

Figure 2.1 illustrates that, in the chosen system, essentially all Cu^{2+} is uncomplexed below pH 5.0 and substantially uncomplexed in the pH range of 5-6, for all values of K'_{ML} obtained by the CSC-methods described in Sections 2.3.1-2.3.7. Van den Berg's results shows clearly that complexation becomes very significant at pH values greater than 6. There are few exceptions to this trend. This emphasizes the inadequacy of the other CSC-methods to predict effects at meaningful pH values. There is an obvious need for direct measurements of CSC's at pH values in the range 6-9 and this is made possible by the δ -MnO₂ method.

Figure 2.2 presents, in the same manner, the influence of some known organic ligands on the free Cu^{2+} concentration in the same system. The calculations for this Figure were performed with the computer program REDEQL2 (McDuff and Morel 1973). The stability constants used in the data bank of this program are obtained mainly from Sillen and Martell (1964), and were determined with a variety of methods, not further discussed here. Such known ligands can be used as a comparison for the behaviour of unknown ligands, shown in Figure 2.1. Ligands included in Figure 2.2 are oxalic acid, glutamic acid, alanine, glycine, aspartic acid, nocardamine, histidine and NTA. The acidity and stability con-

stants for Cu-NTA original included in REDEQL2 seemed far too high and the influence of these constants on the Cu^{2+} concentrations is indicated by a broken line. The constants were replaced by more appropriate ones (obtained from the literature, see also Chapter 8) and the influence of these is indicated by a solid line. Also included in Figure 2.2 are the influences on the Cu^{2+} concentration of conditional stability constants for the Cu-NTA complex obtained at several pH values by the $\delta\text{-MnO}_2$ method in this study. Closed circles indicate data reported by van den Berg (1979).

Figures 2.1 and 2.2 can be compared to liken the Cu-complexing behaviour of unknown organics to that of known ligands. It appears that the values determined by van den Berg (1979) for unknown ligands lie between the effects of aspartic acid and nocardamine or histidine on the Cu^{2+} concentration. The values given by Gaskill (1978) seem to follow the glycine line of influence on the Cu^{2+} concentrations, but this comparison cannot be extended much above pH 6 due to a lack of data at higher pH values.

Figure 2.1 Comparison of the effects of complexation between Cu and natural ligands on the Cu²⁺ concentration.

$$Cu_t = 10^{-7} \text{ M}; L_T = 10^{-6} \text{ M}; T = 20-25^\circ\text{C}$$

- van den Berg (1979), δ -MnO₂ method; I = 0.01

Organic	
1. Lake Ontario	8. Dickie 5
2. Bay of Quinte	9. Dickie 6
3. Lake Huron	10. Dickie 10
4. Whitewater	11. Lake Dickie
5. Gloucester Pool	12. Red Chalk 3
6. Onaping River	13. FA, soil
7. Windy	14. Red Chalk 4

- ▲ Gaskill (1978), all K' values recalculated to K' metal equivalent*

Organic	Method	I	Reference
1. peat HA	PT	0.01	Stevenson (1977)
2. leonardite HA	PT	0.01	" "
3. soil HA	PT	0.01	" "
4. lakewater FA	GFC	0.02	Mantoura + Riley (1975)
5. Aldrich HA	DI/GFC	0.1	Guy + Chakrabarti (1975)
6. soil FA	IE	0.1	Schnitzer + Hansen (1970)
7. soil FA	IE	0.1	Courpron (1967)
8. soil HA	IE	0.1	Courpron (1967)
9. SOM extract	IE	0.1	Geering + Hodgson (1969)
10. peat extract	IE	0.1	Allen et al. (1975)
11. poultry litter extract	IE	0.1	Tan et al. (1971)
12. pondwater	ISE	0.1	Buffle et al. (1977)
13. river water	ISE	0.1	" " " "
14. soil FA	ISE	0.1	Ramamoorthy + Manning (1973)
15. soil FA	ISE	0.1	Cheam + Gamble (1974)
16. Aldrich HA	DI	0.1	Wilson (1974)
17. K&K HA	ASV/POL.	0.1	Ernst et al. (1975)
18. pondwaters	ASV	0.1	Shuman + Woodward (1977)
19. soil FA	CV	0.1	Schnitzer + Hansen (1970)

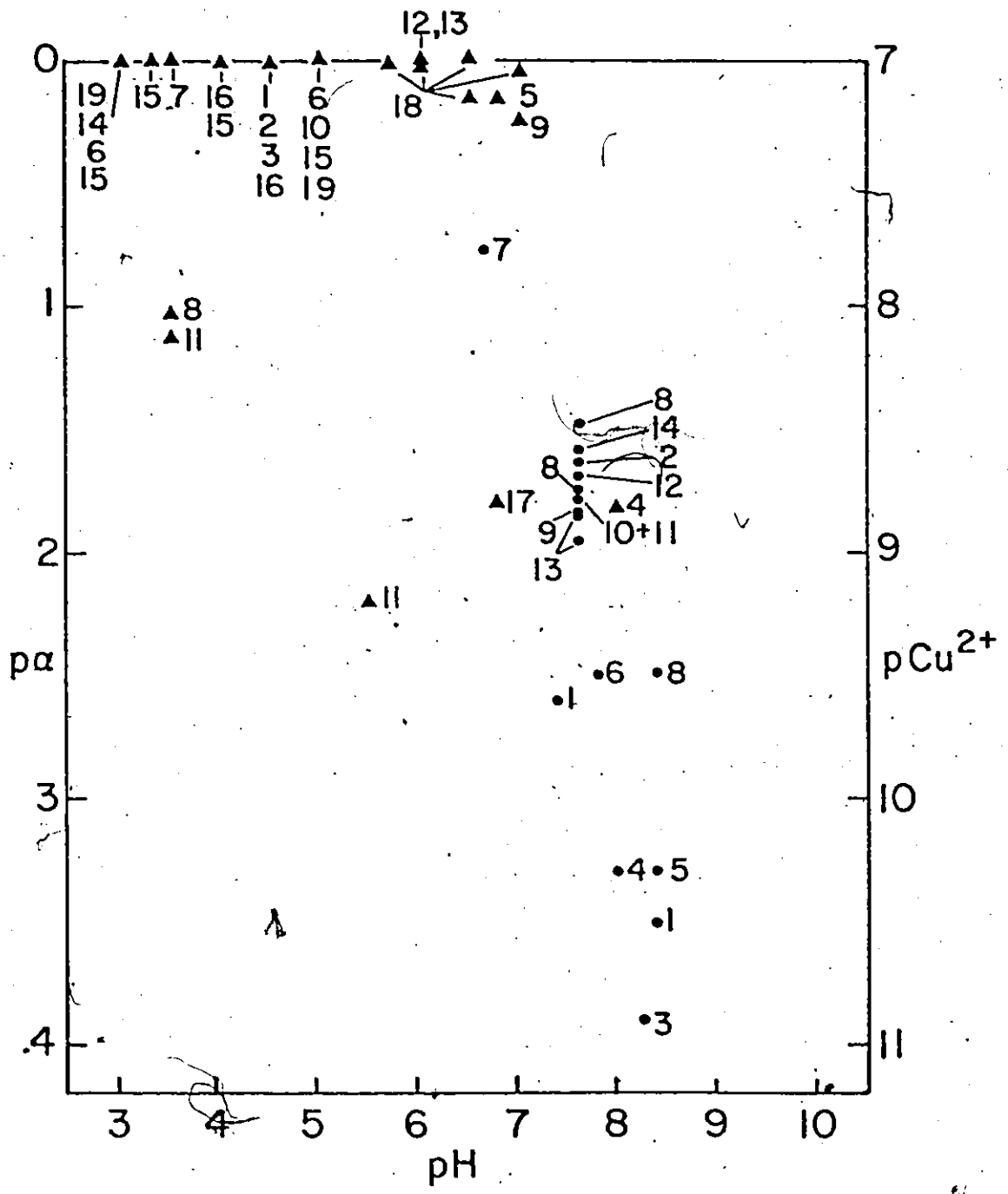


Figure 2.2 Influence of known organic ligands on the free Cu²⁺ concentration

$$Cu_t = 10^{-7} \text{ M}$$

$$L_t = 10^{-6} \text{ M}$$

$$I = 0.01$$

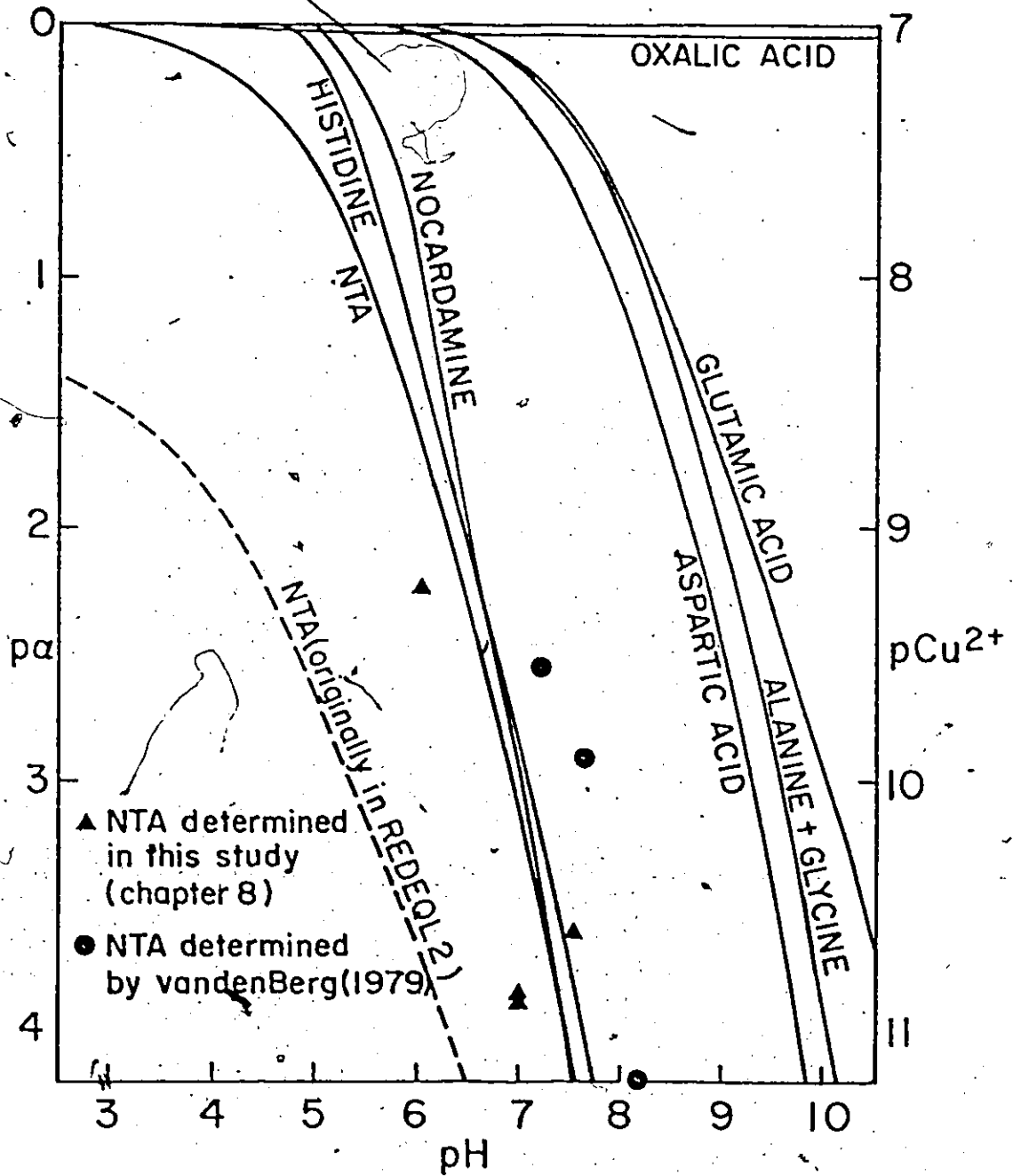
$$T = 20-25^\circ\text{C}$$

$$Cu_t = 1/\alpha \text{ Cu}^{2+}$$

$$\alpha = (K'_{ML} \cdot L_t + 1)^{-1}$$

Calculations performed with REDEQL2 (McDuff and Morel 1973) for all ligands. NTA-broken line indicates original stability constants for Cu-NTA included in REDEQL2, NTA-solid line indicates replaced stability constants for Cu-NTA, much lower than the original ones (see Chapter 8).

Also $K'_{\text{Cu-NTA}}$ values obtained with the $\delta\text{-MnO}_2$ method by van den Berg (●) (1979) and Stroes (▲) (this study, see Chapter 8) are included.



2.5 Evaluation of the δ -MnO₂ Method as Proposed by van den Berg (1979);
Further Formulation of Research Objectives

Several of the more feasible (i.e. simple) methods discussed in Section 2.3 were used during the orientation period of this study, prior to the developing of a research proposal. Shuman's method and Chau's procedure were used to determine complexing capacity values for several known organics, and natural water samples for Zn, while an attempt was made to calculate conditional stability constants with Shuman's method (Stroes 1979 and Stroes and Goudey 1979, unpublished results). The results were not encouraging, in part due to the ubiquity of Zn, causing contamination problems, but mainly because Shuman's method is limited to the middle range of ligands (i.e. not too weak or too strong complexing). The MnO₂ method seemed, therefore, more suitable compared to the others described in Section 2.3, for reasons discussed in Section 2.4.

In an attempt to reproduce the calibration curves for the adsorption parameters of Cu onto δ -MnO₂, prepared according to the prescriptions of van den Berg (1979), a number of difficulties were encountered. They are:

- (i) Γ_{\max} and $\log B$ values obtained by Stroes (1979, unpublished results) and by van den Berg (1979) did not compare. This is shown in Figures 2.3 and 2.4.
- (ii) Linearized Langmuir plots (Cu^{2+} versus $\text{Cu}^{2+}/\Gamma_{\text{ads}}$) displayed a clear and consistent deviation from linearity at the lower end of the line (see Figures in Chapter 7). It is hypothesized that this could have implications for the calculation of conditional stability constants.

(iii) The Transmission Electron Microscope (TEM) image of the δ -MnO₂ sample left over from van den Berg's experiments (see Figure 4.8, Chapter 4) differed markedly from the ones prepared and used in this study (see Figure 4.5, Chapter 4). Van den Berg's particles were fibrous while those freshly prepared for this study were spherical. No TEM images were made by van den Berg. It is possible that these fibres were formed by van den Berg's recipe, but it is more probable that they formed upon aging of the original spherical-shaped particles. If formed by van den Berg, the different particle shapes and surface areas have implications for the adsorption parameters Γ_{\max} and log B. If formed by aging processes, changes in the values of the parameters Γ_{\max} and log B with time can be expected.

A few other disconcerting matters arose from van den Berg's work. The conditional stability constant for the Cu-NTA complex could apparently not be determined accurately by the δ -MnO₂ method. However, as can be seen from Figures 2.1 and 2.2, NTA is only moderately stronger in complexing Cu than the natural organics measured by van den Berg. If, therefore, the measured K'_{ML} value for Cu-NTA was found to be too low, the K'_{ML} values for the natural organics could also have been on the low side. Adsorption of ligands, even known ligands, such as NTA and glycine, on the δ -MnO₂ surface was never checked. The recent literature has several examples describing extensive adsorption of organic material on surfaces such as hydrous oxides (see Chapter 1). Finally, conditional stability constants and total ligand concentrations for very weak 1:2 (and 2:1) complexes were only treated theoretically but not verified with actual measurements.

From the above considerations one specific goal devolves for this

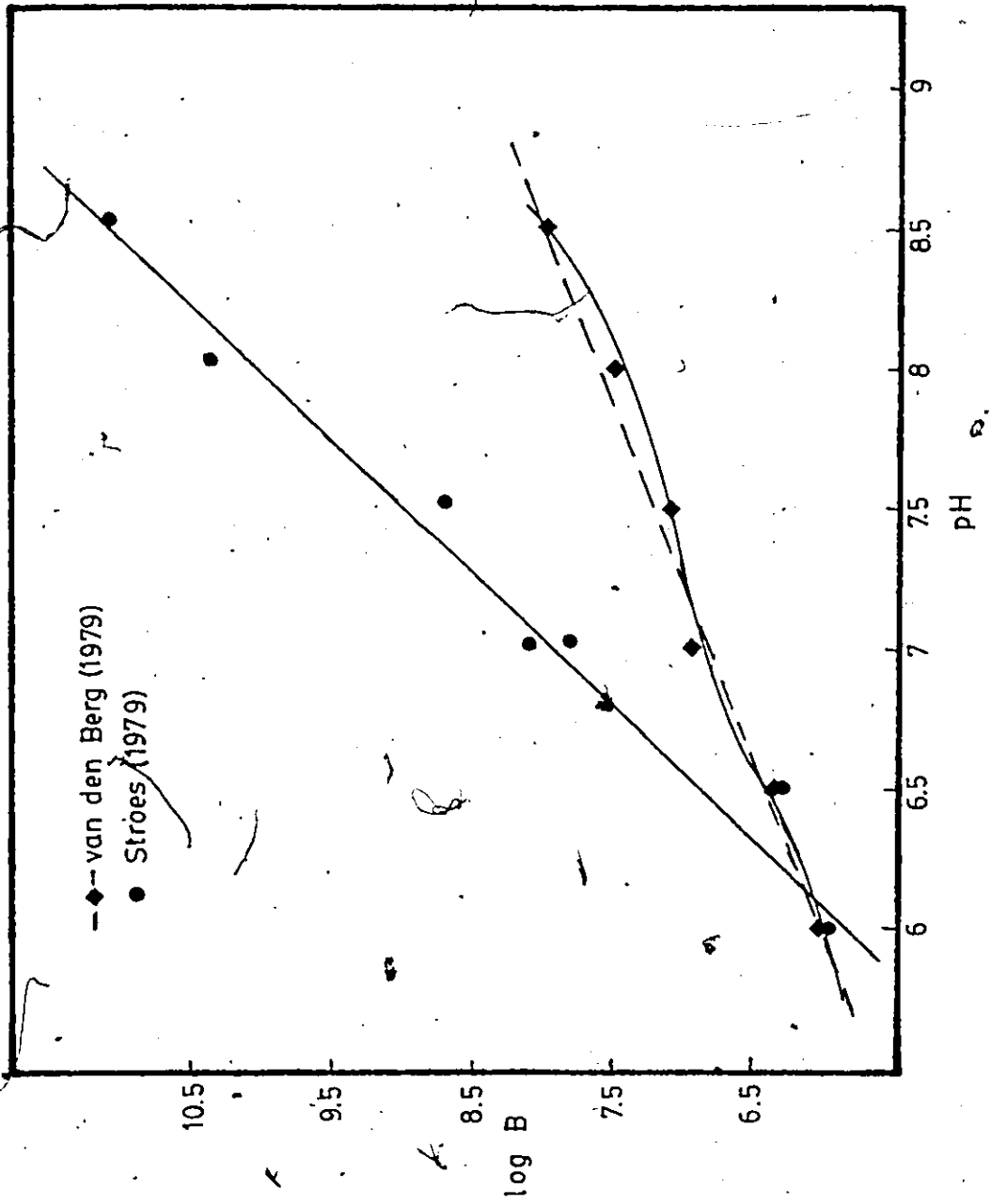


Figure 2.3 Comparison of the binding constant B for Cu adsorption on δ - MnO_2 , as obtained by van den Berg and in this work.

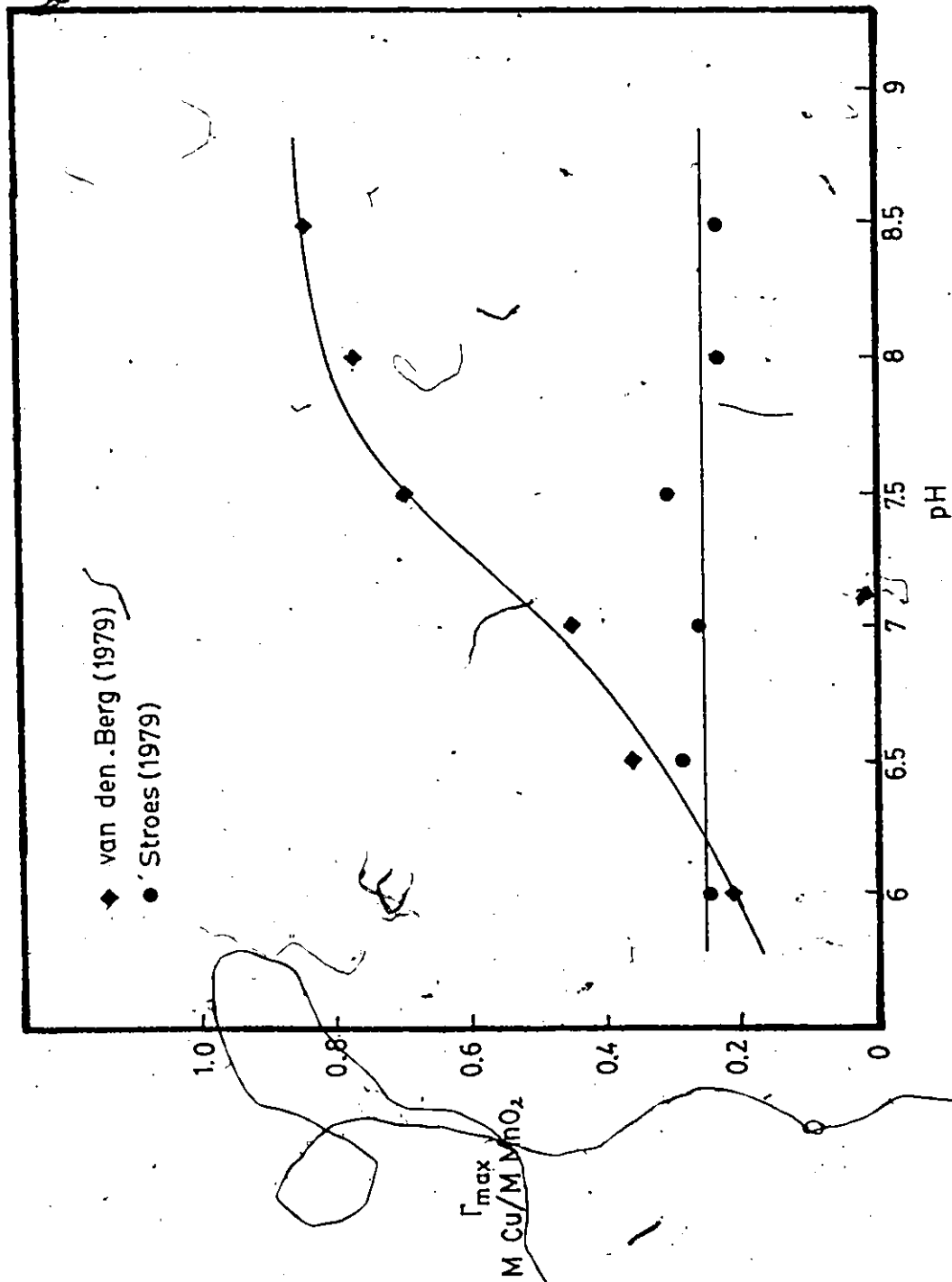


Figure 2.4 Comparison of the adsorption capacity Γ_{\max} for Cu adsorption on δ -MnO₂ as obtained by van den Berg and in this work.

work, namely to provide the δ -MnO₂ method with a solid, experimentally oriented basis, to match its principally sound theoretical basis. This requires that the following specific aspects be researched:

1. Natural and synthetic manganese IV oxides; structures of natural and synthetic δ -MnO₂'s; literature study of methods to synthesize δ -MnO₂ (Chapter 3).
2. Comparison of different recipes for δ -MnO₂ preparation; characterization of δ -MnO₂ samples; influence of aging (natural and simulated) on the surface structures as characterized by TEM (Chapter 4).
3. Literature review of existing adsorption models for hydrous oxides with emphasis on MnO₂; if necessary, development of a new but simple adsorption model for Cu uptake on δ -MnO₂, describing deviation from Langmuir linearity, constant adsorption capacity and pH dependence of B (Chapter 5).
4. Rigorous procedures on how to perform calibrations of the δ -MnO₂ surface for Cu adsorption; how to perform titrations to obtain conditional stability constants; investigation by ¹⁴C technique of adsorption of known organic ligands on the δ -MnO₂ surface with and without Cu present; checking of mass balances for Cu and known ligands (Chapter 6).
5. Adsorption behaviour of a number of different δ -MnO₂ surfaces with respect to:
 - reactivity towards Cu
 - reproducibility of the δ -MnO₂ surface characteristics
 - reproducibility of isotherms
 - influence of the presence of glycine on isotherms

- influence of natural and simulated aging processes on the adsorption performance of $\delta\text{-MnO}_2$
 - fitting of the adsorption results to a number of adsorption models, comparing them and choosing the most suitable model (Chapter 7).
6. Application of the most suitable adsorption model, to determine L_t and K'_{ML} values for a number of known ligands of varying adsorption strength (Chapter 8).

This study uses Cu as a model metal, and involves only known organics. Only after performing such a thorough study can assessments be made concerning (i) how well the $\delta\text{-MnO}_2$ method performs, with regard to reliability, ease and precision, in determining K'_{ML} values and L_t (i.e. complexing capacity) values, for trace metal-organic complexes, and (ii) how suitable it is as a routine and standard measurement technique for predicting the fate of trace metals in the aquatic environment.

In Chapter 1, it was emphasized that not only 0.45 μm filtered water samples should be assessed in trace metal speciation studies, but also unfiltered samples, since the particulate phase can possess important complexing capacities. That the $\delta\text{-MnO}_2$ method is very suitable for this, will be discussed in Chapter 10, where a recommended procedure for its use is outlined. $\delta\text{-MnO}_2$ could also represent a model particulate phase, capable of simulating the role of particles in the interactions of metals, ligands and surfaces in natural aquatic systems. The number of aqueous environments for which it could be a representative model awaits more research.

2.6. Summary

The various existing methods for determining complexing capacities and conditional stability constants for trace metal-organic complexes are discussed in this Chapter. The δ -MnO₂ method has a definite advantage over the existing methods, because of its capability to measure K'_{ML} values in untreated natural water samples, at pH's varying from 6 to 9; most other methods can only be applied at low pH's. However, a literature review and preliminary experimental analysis revealed that the δ -MnO₂ method has several problems, such as a deviation from the Langmuir adsorption model to describe Cu uptake on δ -MnO₂ at low Cu concentrations, the danger of organics adsorbing and hence modifying the δ -MnO₂ surface, and the uncertainty regarding the reproducibility of the δ -MnO₂ surface. These problems suggested several areas for research, whose scope and direction is outlined as the research performed and described in the next six Chapters.

CHAPTER 3

NATURAL AND SYNTHETIC MANGANESE (IV) OXIDES

3.1 Introduction

Hydrous manganese oxides have been an object of study in many areas of research. A considerable amount of knowledge about manganese oxides has been gathered because of the commercial use that manganese ores have found in the past in the manufacturing of dry cell batteries. The mineralogical characteristics of manganese ores are important in determining their electrochemical behaviour in such batteries. When the supply of natural, usable ore from Europe was not available during World War II, research on the synthetic production of a reactive MnO_2 increased considerably (McMurdie 1944; Otto et al. 1944; Storey et al. 1944; Copeland et al. 1947; Cole et al. 1947).

During the past few decades, the emphasis of study has shifted largely to the role manganese oxides play in controlling the concentrations and availability of (trace) metals in soil, freshwater and marine environments. Hydrous oxides of manganese have a high sorption capacity for trace metals and are ubiquitous. They can be found in clays, soils and sediments, particularly as manganese (and iron) oxide coatings on silicate minerals. These coatings increase the ratio of their chemical activity to concentration considerably (Jenne 1968). Concentrations of Co, Zn and other important trace metals in soils are quite high in the hydrous manganese oxides (Loganathan and Burau 1973). The existence,

in the marine environment, of manganese nodule formations, enormously enriched in trace metal concentrations relative to seawater, volcanic rocks and other sediments, has been known since the Challenger Expedition (1872-1876) (Davis 1973; Burns and Burns 1979). Recently, these nodules have also been recovered from the freshwater Great Lakes in the U.S.A. and Canada (Harriss and Troup 1969; Jeffries and Stumm 1976; Cahil 1981; Mudroch and Bistrichi 1981).

3.2 Formation and Deposition of Manganese Oxides

Two principal sources, weathering processes on the continents and submarine volcanism, cause manganese to enter the exogenic cycle in the form of the hydrated $\text{Mn}(\text{H}_2\text{O})_6^{2+}$ ion. The solubility of Mn^{2+} is controlled by rhodochrosite ($\text{MnCO}_3(\text{s})$) in the pH range of natural, carbonate-bearing waters. The solubility of higher-valent manganese oxides (MnO_x , $1 < x \leq 2$) is extremely low and analytically undetectable. Some Mn^{2+} is present in non-stoichiometric manganese oxides and can, via exchange processes, enter into solution (Stumm and Morgan 1970). Once dissolved, the fate of the Mn^{2+} ion is controlled by its rate of oxidation, which is proportional to pH, temperature, oxygen pressure and concentrations of solid and dissolved manganese (Burns and Burns 1979). Eventually, on the geological time scale, the dissolved and suspended phases of manganese all end up in depositional environments (oceans, great lakes), where a variety of processes results in different types of sediments.

Slow hydrogenous precipitation results mostly in vernadite ($\delta\text{-MnO}_2$) while coprecipitation with hydrated iron oxide phases creates deposits with Mn : Fe ratios of 0.5 - 2.0 (Burns and Burns 1979). The

small particle size of the suspended manganese phases, entering the oceans either via continental runoff or by in situ formation in estuarine areas (precipitation processes), results in the existence of large specific surfaces. These imply a significant adsorption capacity and, at the same time, very low settling velocities. Slow settling causes the particles to be transported by ocean currents to depositional environments far removed from the continents. Redox reactions involving organic matter can remobilize manganese in buried sediments, producing low valence-state forms of Mn and Fe; these ions are transported via pore water diffusion, as soluble Cl^- , HCO_3^- or organic complexes, to the oxic sediment-seawater interface, where oxidation reactions can take place.

All these oxidation, precipitation and deposition processes are slow compared to the formation of ferromanganese oxides in the vicinity of seafloor volcanism and hydrothermal activity (Burns and Burns 1979). Fe and Mn are leached from the volcanic rocks by seawater permeating in the seafloor, fractured as a result of volcanic heating. Some Mn and Fe may even come from juvenile mantle sources, transported upwards by the volcanic activity. The hydrothermal solution containing Mn and Fe in the form of chloride complexes, come eventually in contact with oxygenated seawater whereupon these complexes are hydrolysed and precipitate as amorphous or poorly crystalline oxides, due to oxidation reactions (Burns and Burns 1979). Extreme fractionation of Mn and Fe can occur in this type of deposit, since the oxidation kinetics of dissolved Mn^{2+} complexes are slower than those for soluble Fe^{2+} complexes. Deposition of todorokite and birnessite in hydrothermal deposits results from incomplete oxidation of Mn^{2+} .

3.2.1 Mn²⁺ Oxidation to MnO₂; Mechanisms and Pathways

According to the literature, there are several pathways along which MnO₂ can be formed under natural conditions:

1. chemical oxidation of Mn²⁺ or reduction of Mn⁷⁺
2. autoxidation of manganese
3. disproportionation of Mn₂O₃, Mn₃O₄ or MnOOH
4. biooxidation of Mn²⁺

Ad 1:

Manganese dioxide can be formed via reduction of Mn(VII) or oxidation of Mn(II). It appears however that, despite the various oxidation states possible for manganese, only the II and IV and maybe the III valence states are of any practical significance in nature (Jeffries and Stumm 1976). Normally, only Mn²⁺ can be found in anoxic waters, but both Mn²⁺ and Mn⁴⁺ oxides are encountered in oxygen-bearing waters.

The oxygenation kinetics for Mn²⁺ are autocatalytic and follow the rate law (Stumm and Morgan 1970):

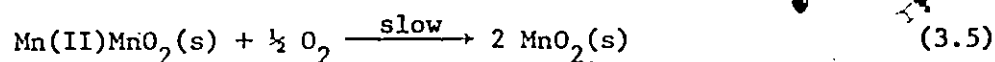
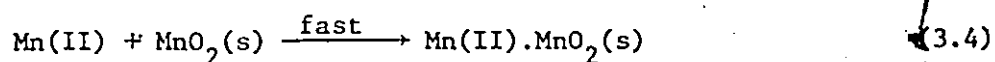
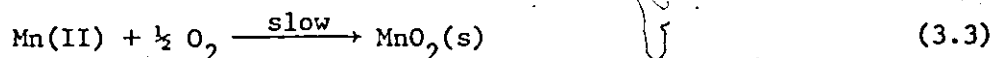
$$-\frac{d[\text{Mn}^{2+}]}{dt} = k_o [\text{Mn}^{2+}] + k[\text{Mn}^{2+}] [\text{MnO}_2] \quad (3.1)$$

in which the rate constant k is dependent on both pH (second order with respect to $[\text{OH}^-]$) and $p\text{O}_2$ (first order):

$$k = k' [\text{OH}^-]^2 p\text{O}_2 \quad (3.2)$$

Based upon their experimental findings regarding stoichiometry, oxidizing equivalents of the suspension in which oxidation takes place, and

average degrees of oxidation of the formed product(s), Stumm and Morgan (1970) visualize the autocatalytic reaction as follows:

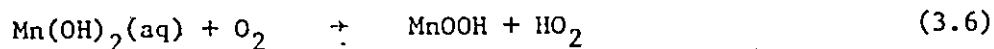


They also acknowledge that other mechanistic interpretations of these kinetics are possible. The products resulting from this process depend on reaction conditions such as pH and $p\text{O}_2$. Stumm and Morgan (1970) find that the products formed under high pH conditions resemble manganous manganite and $\delta\text{-MnO}_2$, the latter being one of the main hydrous manganese oxides which are stable at ordinary conditions of temperature, pressure and Eh. At pH 9.5, a product partly resembling hausmannite (Mn_3O_4) was identified by Stumm and Morgan (1970). According to Burns and Burns (1979) the above reaction series leads probably to vernadite ($\delta\text{-MnO}_2$).

From experiments with simulated lake water, Stumm and Giovanoli (1976) suggested that, particularly in continental waters, eventually a stable phase, manganite ($\gamma\text{-MnOOH}$) is formed with hausmannite (Mn_3O_4) as an oxidation intermediate; this occurs after Mn^{2+} is initially precipitated as either Mn(OH)_2 or MnCO_3 , depending on environmental circumstances.

Ad 2:

Kessick and Morgan (1975) studied the autoxidation of manganese (II) in aqueous solution at pH-values of ca.9. Their data indicate that the initial product of oxidation is a Mn(III) oxide; they reason that this is MnOOH rather than the more unstable γ -Mn₂O₃. They suggest that the rate determining step, for this reaction, which depends on pO₂ and [OH⁻]², involves a one-electron transfer:



From a thermodynamic point of view, the existence of Mn(OH)₂ (aq) in any appreciable concentration in free solution is unlikely. But Kessick and Morgan (1975) argue that a high concentration of Mn(OH)₂ could develop at the surface of the already precipitated product. This may occur because Mn²⁺ ions are strongly adsorbed on the surface of manganese dioxide at high pH and OH⁻ ions are potential determining ions for this type of surface. Under prolonged oxidizing conditions MnOOH can be further oxidized in aqueous solution.

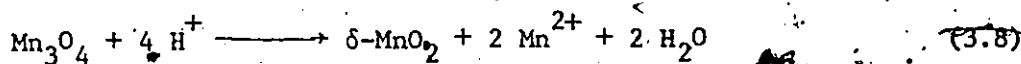
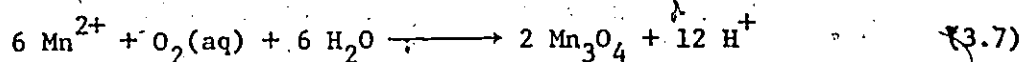
The properties of the end product of an oxidation process will depend on its rate of formation relative to its rate of coagulation and subsequent removal from the aqueous phase. An example is the formation of the δ -MnO₂ sheets which form part of the structure of ferromanganese nodules, found on the ocean floor. Under conditions of high pH (ca.8-9), the rate of initial oxidation can be presumed to be very rapid relative to the rate of coagulation and subsequent deposition; this allows extended contact with the aqueous phase and hence highly oxidized products

can and do in fact form. Even a slowly-forming oxide precipitate can be expected to be oxidized beyond $\text{MnO}_{1.5}$ as long as the rate of coagulation is much slower. Only when the latter approaches the initial oxidation rate, can products with the composition of $\text{MnO}_{1.5}$ be expected in aqueous precipitates. Any products with lower oxidation numbers that might be found in sediments must be the result of coprecipitation with Mn(II) -hydroxide or -carbonate.

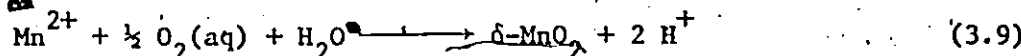
Ad 3:

Posselt et al. (1968a) briefly discuss the contention that manganese dioxide could form as a result of the disproportionation of Mn_2O_3 . This is a process in which polymerization of the tetrahydroxide Mn(OH)_4 would play an important intermediate role (Chevillot 1964). Two of the principal forms of soluble and colloidal manganese in oxygenated natural waters, which would influence disproportionation if present, may be Mn(OH)_4 and Mn(OH)_3 (Sillen 1961).

Hem (1978) proposes two other Mn^{2+} oxidation mechanisms, involving disproportionation of intermediary hausmannite or manganite. The intermediate reactions proposed for hausmannite are:



giving an overall reaction of:



The reaction involving manganite (γ -MnOOH) is:

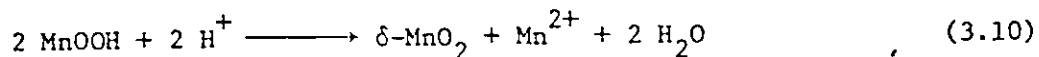


Figure 3.1 summarizes the relationships between various synthetic oxides of manganese (adapted from McKenzie 1971). It shows that the pathways from the lower to the higher oxides demand extreme conditions, which rarely occur in nature. Yet the lower oxides have not been found in soils. It is therefore probable that under natural conditions the oxidation of Mn^{2+} is favoured by bacterial action (McKenzie 1971).

Ad 4.

As mentioned above, oxidation of Mn^{2+} , caused by or catalyzed by bacterial action, is possible. A number of bacteria and fungi, which are responsible for the biological oxidation of Mn(II), have been identified (McKenzie 1977).

In fact, the influence of bacteria upon MnO_2 chemistry may be significantly underestimated by developments in the literature to date.

Burns and Burns (1979) discuss the survival of Mn^{2+} - containing todorokites in manganese nodules at the sediment - seawater - interface, in relation to the likelihood that micro-organisms catalyse the oxidation of Mn^{2+} , within the todorokite structure (see also Table 3.1). Replacement of Mn^{2+} by other divalent cations such as Ni, Cu, Zn, Mg, etc. which are not susceptible to oxidation, seems to stabilize and protect the todorokite lattice, by preventing the oxidation of Mn^{2+} to Mn^{4+} (see Section 3.3). They also describe a number of other known occasions in which the inorganic mechanism of manganese oxide deposition is modified

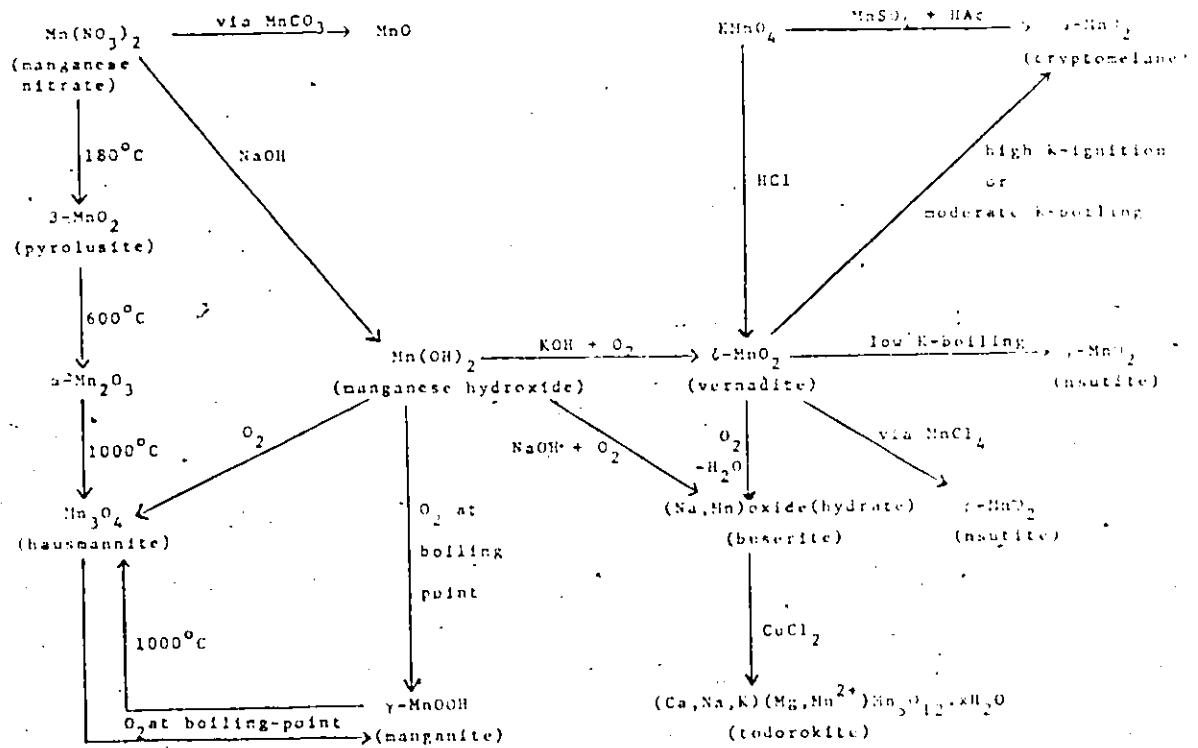


Figure 3.1 Relationships between the various synthetic oxides of manganese, obtained under laboratory conditions (adapted from McKenzie 1971). For reaction conditions, such as chemicals and reaction times involved, see McKenzie (1971).

or influenced by biological processes. On the other hand, reduction of manganese can occur under anaerobic circumstances in soils and sediments. There, bacterial oxidation of organic matter proceeds at such a rate that the dissolved O_2 supply is exhausted and the bacteria switch to using O_2 from the higher manganese oxides as a final electron acceptor (McKenzie 1977).

The above discussion indicates that there exists uncertainty about the exact pathway for oxidation of Mn^{2+} to MnO_2 under natural, or at least non-extreme laboratory conditions. Stumm and Morgan (1970) do not consider Mn^{3+} as an intermediate oxidation state. Both autoxidation and disproportionation theories are based on Mn^{3+} as an intermediate but disagree as to which Mn(III) oxide is involved. More data seem necessary before any firm conclusions regarding the exact pathway(s) can be drawn. Precipitation of MnO_2 is definitely dependent on pH and pO_2 conditions. Biological activity can also play an important role in the formation (or dissolution) of MnO_2 products. Figure 3.1 summarizes the different kinds of synthetic manganese oxides that can be obtained under laboratory conditions. Some of these reactions involve heat treatment, which could indicate that, under natural circumstances, they occur at a much lower rate, if at all.

3.3 Description of the Basic Structure of Some Ubiquitous Mn(IV) Oxides

More than twenty manganese (IV) oxide minerals have been found in continental manganese deposits, but only a few of these terrestrial minerals have been positively identified in the marine environment (Burns and Burns 1979). The mineralogy of these Mn(IV) oxides is com-

plicated by two significant phenomena. Firstly, there exists a large number of oxides and hydroxides in which substitution of Mn^{2+} and Mn^{3+} for Mn^{4+} occurs extensively. These replacements result in a change of the average Mn-O bond lengths, and consequently in the unit-cell parameters. Moreover, these Mn^{2+} (and even Mn^{3+}) ions can subsequently be replaced by other cations, such as Ni^{2+} , Cu^{2+} , Zn^{2+} , and Mg^{2+} . These cations give the oxide structures more stability (e.g. against oxidation or collapse), but at the same time it complicates the mineralogy of the oxides. The substitution of Mn^{2+} or Mn^{3+} for Mn^{4+} is necessarily accompanied by replacement of O^{2-} with OH^- to maintain electrical neutrality. Secondly, manganese ions in the oxide lattices may be oxidized or reduced without changing position in the structures. If the valence of a sufficient number of Mn ions changes, the oxide structure becomes mechanically unstable and rearranges into a new phase. It appears that a continuous series exists from MnO to MnO_2 within which there is a number of stable and meta-stable arrangements of atoms forming the well known minerals, many of which may cover a wide range of compositions (McKenzie 1977).

The fundamental structural unit in tetra-valent manganese oxides is the $[Mn^{IV}O_6]$ octahedron. Here six oxygens surround a central Mn^{4+} ion, in which the Mn^{4+} ions with their $[A]3d^3$ electronic configuration acquire exceptionally high Crystal Field Stabilization Energy (CFSE*) (Burns 1970). The basic $[MnO_6]$ octahedra in manganese oxide mineralogy are linked by corner- and edge-sharing to give a variety of chain,

* The total bonding energy between two elements is composed of three parts: the covalent energy, the ionic resonance energy and the CFSE; ability of one element to displace another from a crystal lattice will depend on the relative bonding energies of the two elements, and therefore also on their relative CFSE's (McKenzie 1972).

tunnel and layer structures (see Table 3.1). Edge sharing of $[\text{MnO}_6]$ octahedra and the close proximity of the Mn^{4+} ions to one another can also cause structural instability in, and cryptocrystallinity of, manganese oxide minerals. Added complexities besides these, are the existence of ordered and random vacancies in the $[\text{MnO}_6]$ octahedral arrangements, and the occurrence of domain structures and complex intergrowths of variable lattice periodicities (Burns and Burns 1979).

The most common method for identifying the often highly cryptocrystalline manganese oxide minerals has been by X-Ray Diffraction (XRD) analysis. However, due to the very small particle size of the material, coherent scattering of the X-rays is often reduced. This results in amorphous appearances (no diffraction pattern) or at best very broad, diffuse diffraction patterns. A further complication is, that certain d-spacings are common to several minerals, especially the values around 2.40-2.45 Å and 1.40-1.42 Å. These values represent the basic structural units of hexagonally, close-packed oxygens containing manganese ions in octahedral coordination. Due to these complications, identification using XRD techniques has not always produced unambiguous results (Burns and Burns 1979). Alternative and modern techniques such as Electron Diffraction (ED), Absorption Spectroscopy (AS) and Infrared Spectroscopy (IS) have provided more information about the complicated structures. Potter and Rossman (1979) argue that the latter is often a necessary alternative and at least a useful supplement to XRD analysis, because IS is sensitive to amorphous components, to those with short range order and to material with long range order.

Table 3.1 is compiled from data derived from Burns and Burns

(1979), McKenzie (1977), Giovanoli (1969), Potter and Rossman (1979) and Buseck and Turner (1981). Its objective is to provide a summary of the properties of the myriad number of MnO_2 structures found in the literature.

3.4 $\delta\text{-MnO}_2$ and Its Related Minerals

The structure of $\delta\text{-MnO}_2$ is discussed here in some detail, relative to other allied minerals. The manganese dioxide method, discussed in Chapter 2, uses $\delta\text{-MnO}_2$ as a resin, and the adsorption studies described in Chapters 6, 7 and 8 use this type of manganese dioxide extensively. A tabular summary is given at the end of this chapter, compiling the numerous preparation methods reported in the literature that presumably yield $\delta\text{-MnO}_2$.

Concluding from the literature examined in this research, the name $\delta\text{-MnO}_2$ was probably proposed first by McMurdie (1944). In his attempt to chemically produce an active battery grade manganese dioxide (by reducing KMnO_4 with heated, concentrated HCl), McMurdie (1944) encountered a variety that, to him, was not known to occur naturally, but seemed to be common among chemically produced manganese oxides. The X-ray patterns showed only two diffuse lines at 2.39 Å and 1.40 Å, suggesting that it was a very poorly crystallized form of cryptomelane ($\text{KMn}_8\text{O}_{16}$). Although McMurdie (1944) did not know $\delta\text{-MnO}_2$ to exist naturally, it appears to be one of the most common forms of mineralized manganese in soils, although other ions are always present in natural $\delta\text{-MnO}_2$ (Taylor et al. 1964).

Copeland et al. (1947) described a successful method for preparing a battery grade, highly oxidized 'active' manganese oxide by aerating freshly precipitated $\text{Mn}(\text{OH})_2$ in the presence of NaOH. This

Table 3.1 Crystallographic data for some Mn(IV) oxides

* McKenzie (1977)
 † Burns and Burns (1979)

Structure groups and families	Mineral, oxide or compound	Other names	Composition or approximate formula	Crystal class	cell parameters (Å)	Structure
Cyclic or tecto-(IV) oxides, framework or tunnel structures	Pyrolusite	β-MnO ₂ ; pollianite	true MnO ₂ stable modification Rutile-type	tetragonal	a=4.39; c=2.87	single chain structure, looking approximately down c
	Ramdehlite	-	true MnO ₂ metastable modification Diaspore-type	orthorhombic	a=4.53; b=9.27; c=2.87	double chains of edge-sharing (MnO ₆) octahedra parallel
Nephtite family	Ksurtite	γ-MnO ₂ α-MnO ₂	variable: (Mn ²⁺ , Mn ³⁺ , Mn ⁴⁺)(OH) ₂ partial substitution of Mn ²⁺ by Mn ³⁺ frequent	hexagonal	a=9.65; c=4.43	mixture of single and double chains, structural intergrowth of pyrolusite in ramdehlite Jilika, or vice-versa
	α-MnO ₂	-	MnO ₂	hexagonal	a=2.80; c=0.45	mixture of single and double chains, analogous to pyrolusite and nesutite, but with Mn ⁴⁺ ions randomly distributed over the octahedral interstices
Hollandite family	Nankinite	γ-MnOOH	MnOOH	monoclinic	a=8.88; b=5.25; c=5.71; β=90°	single chain structure, modeled on the structure of pyrolusite
	Hollandite	α-MnO ₂	Ba ₂ Mn ₈ C ₁₆ (Ba,K) ₁₋₂ Mn ₈ O ₁₆ ·xH ₂ O †	tetragonal or monoclinic	a=5.96; c=2.66 a=10.03; b=5.76; c=9.90; β=90° †	three-dimensional double-chain framework with large cavities, in which large cations and water can be accommodated

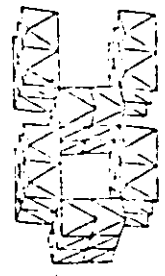
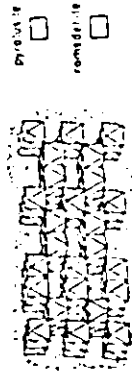
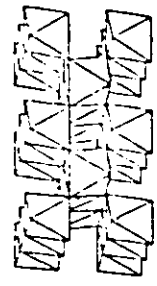


Table 3.1 cont.

Structure groups and families	Mineral, oxide or compound	Other names	Composition or approximate formula	Crystal class	cell parameters (Å)	structure
Cycle- or tecto-manganese (IV) oxides : ring-, framework- or tunnel structures	Cryptomelane	$\alpha\text{-MnO}_2$	$\text{K}_2\text{Mn}_8\text{O}_{16}$ or $\text{K}_{1-2}\text{Mn}_8\text{O}_{16}\cdot x\text{H}_2\text{O}$	tetragonal or monoclinic	$a=9.84; c=2.86$ $a=9.79; b=2.88$ $c=9.94; \beta=90.03^\circ$	as hollandite
	Coronadite	$\alpha\text{-MnO}_2$	$\text{Pb}_2\text{Mn}_8\text{O}_{16}$	tetragonal or monoclinic		as hollandite
	Romanechite	psilomelane	$(\text{Ba}, \text{K}, \text{Mn}^{2+}, \text{Co})_2\text{Mn}_5\text{O}_{10}\cdot x\text{H}_2\text{O}$	monoclinic or orthorhombic	$a=9.56; b=2.88; c=13.85; \beta=92.03^\circ$ $a=8.254; b=2.864; c=2.864$	treble chains, linked by double chains forming tube or tunnel structures in which large cations and water can be accommodated
Layer structures	Todorokite		variable: $(\text{Ca}, \text{Ba}, \text{K})(\text{Mg}, \text{Mn}^{2+})\text{Mn}_5\text{O}_{12}\cdot x\text{H}_2\text{O}$	monoclinic	$a=9.75; b=2.849; c=7.59; \beta=90^\circ$	tunnel structures, formed by $(\text{Mn}^{2+}, \text{Mn}^{3+})$ octahedra linked in double (12,n) chain and triple (13,n) formations, large cations and water can be accommodated in the tunnels
	Chalcophanite		$\text{Zn}_2\text{Mn}_6\text{O}_{14}\cdot 6\text{H}_2\text{O}$ (ideal formula)	triclinic	$a=7.55; b=7.54; c=8.22; \alpha=90^\circ; \beta=119.12^\circ; \gamma=120.0^\circ$	layers of edge-shared (MnO_6) octahedra, 7.26 Å apart and single sheets of water molecules, between which Zn^{2+} is located. (Stacking sequence along c-axis: -O-Mn-O-Zn- $\frac{1}{2}$ O-Zn-O-Mn-O-). Layer structure similar to chalcophanite
Phyllo-manganite (IV) oxides	synthetic $\text{Cd}_2\text{Mn}_3\text{O}_8$ and Mn_5O_8		$\text{Cd}_2\text{Mn}_3\text{O}_8$ $\text{Mn}_5^{2+}\text{Mn}_3^{4+}\text{O}_8$	monoclinic	$a=10.34; b=5.74; c=4.85; \beta=109.5^\circ$	
	Litjupharite		$(\text{Al}, \text{Li})\text{Mn}_2(\text{OH})_2$ $(\text{Mn}^{3+}, \text{Mn}^{2+})_2\text{O}_{12}$ $(\text{Al}, \text{Li})_2(\text{OH})_{12}$	monoclinic	$a=5.99; b=8.70; c=9.61; \alpha=100^\circ$	layers of edge-sharing (MnO_6) octahedra alternate with layers of $[(\text{Al}, \text{Li})(\text{OH})_6]$ octahedra, 9.5 Å apart, with no vacancies in either layer (stacking sequence along the c-axis: -O-Mn-O-OH-(Al, Li)-OH-O-Mn-O-).

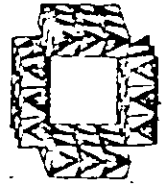


Table 3.1 cont.

Structure groups and families	Mineral, oxide or compound	Other names	Composition or approximate formula	Crystal class	cell parameters (Å)	structure	
Mnnesite family	Birnessite	δ-MnO ₂ , manganese-variety: (Na,Ca,K) manganite	disperse and disordered (Mg,Mn)Mn ₆ O ₁₄ ·5H ₂ O	hexagonal	a=2.85; c=7.08 - 7.31	contains layers of edge-shared (MnO ₆) octahedra separated by sheets of H ₂ O containing K ⁺ , Na ⁺ , Mn ²⁺ , Mn ³⁺ possibly other trace metals	
	Synthetic birnessite	"	Na ₄ Mn ₁₄ O ₂₇ ·9H ₂ O	orthorhombic	a=8.54; b=15.39; c=14.26		
	Synthetic birnessite	"	Mn ₇ O ₁₃ ·5H ₂ O	hexagonal	a=2.84; c=7.27	sodium-free form of the above	
	Buserite	10 X manganite oxide hydrate	variable, Na, Mn	hexagonal	a=8.41; c=10.01	oxidised layers of (MnO ₆) octahedra interspersed with layers of relatively unoxidised [Mn ^{II} (OH, H ₂ O)] ₂	
	Verdelite	β-MnO ₂	MnO ₂ ·nH ₂ O (R ₂ O, RO, R ₂ O ₃) R = Na, Ca, Co, Fe/Mn	hexagonal	a=2.86; c=4.70	two layer hexagonal packing of oxygen atoms and H ₂ O molecules in which the octahedra are statistically, but a little less than half, filled by Mn ²⁺ , the extent of which depends on content of H ₂ O, Na ⁺ , K ⁺ , Ca ²⁺ , Mg ²⁺ , Co ²⁺	
	Pyrochroite	Mn(OH) ₂	"	hexagonal	a=3.322; c=4.734	similar to brucite structure (Mg(OH) ₂ = hexagonal-rhombohedral layers of edge-shared (Mn(OH) ₆) octahedra in which each shares edges with 6 neighboring octahedra to form a two dimensional layer.	
	Other Mn Minerals	Rancieite	(Ca,Mn)Mn ₄ O ₉ ·9H ₂ O	"	hexagonal	a=2.84; c=7.07	
		Groutite	α-MnOOH	MnOOH	orthorhombic	a=4.36; b=10.70; c=2.85	
		Feltknechtite	β-MnOOH	MnOOH	hexagonal	a=3.32; c=4.71	
		Partridgeite	α-Mn ₂ O ₃	Mn ₂ O ₃			
Hausmannite		Mn ₃ O ₄	Mn ²⁺ Mn ₂ ³⁺ O ₄	tetragonal	a=5.76; c=9.41		

Structure not entirely disclosed, but mainly layers

yielded an oxide with oxidation states between 1.85 and 1.90. Buser et al. (1954) used different ratios of HCl, Mn^{2+} and $KMnO_4$ to precipitate manganese oxides, referring to their preparations as manganous-manganite or δ - MnO_2 , depending on whether the oxygen : manganese ratio was less or greater than 1.90. They noted that all filtrates of the precipitates were violet (from non-reacted permanganate) and that therefore the reaction could not be a complete one.

It appears that the structural ordering of MnO_2 diminishes with increasing oxidation number and that the two XRD basal reflections become weaker and finally disappear at a composition of about $MnO_{1.9}$.

The structure is described by Buser et al. (1954) as layers of Mn^{4+} and oxygen ions, mixed with layers of $Mn(OH)_2$. In the case where 4 Mn^{4+} ions are counteracted by 1 Mn^{2+} , $MnO_{1.8}$ results. With increasing oxidation, the number of $Mn(OH)_2$ layers decreases and the boundary of 1 Mn^{2+} ion and 8 Mn^{4+} ions has the composition $MnO_{1.89}$ while the orientation of the layers is such that XRD basal reflections disappear.

Jones and Milne (1956) describe the structure of MnO_2 as consisting of layers of 4 MnO_2 , interspersed with layers of $Mn(OH)_2 \cdot 2H_2O$. In the more highly oxidized samples, the interlayers of 4 MnO_2 and $Mn(OH)_2 \cdot 2H_2O$ no longer exist as regular structural units. Instead, there are only individual double layers which are randomly oriented. The result is that the basal reflections eventually disappear from the XRD patterns. They argue that 'manganous manganite' and δ - MnO_2 have been shown to have variously disordered forms of a distinct crystal phase and are not disordered forms of cryptomelane (α - MnO_2 or $K_2Mn_8O_{16}$) as was suggested by McMurdie (1944). However, synthetic manganous manganite and δ - MnO_2

are easily converted to cryptomelane or to $\gamma\text{-MnO}_2$, and therefore such oxides should occur only where temperatures have been low both during and since deposition.

Murray et al. (1968) describe the structure of manganese oxides as consisting of ordered layers of MnO_2 alternating with disordered layers containing metal ions coordinated with H_2O , OH^- and other anions. Results from his experiments indicate that the ordered layers which contain Mn^{4+} ions in sixfold coordination with O^{2-} are separated by a 10 Å disordered layer containing Mn^{2+} coordinated by O^{2-} , H_2O and OH^- .

Buser et al. (1954) attributed the difference in what they assume is manganous manganite and $\delta\text{-MnO}_2$ to differences in preparation methods (see Table 3.3). The abundant presence of Mn^{2+} induces precipitation of the former due to formation of $\text{Mn}(\text{OH})_2$ layers, while in the latter the slow formation of Mn^{2+} (by reduction of Mn^{7+} to Mn^{2+} , which is not added initially) partly prevents the formation of $\text{Mn}(\text{OH})_2$ layers which results in an oxide with higher oxidation state.

Bricker (1965) ~~however~~ suggested that the presence or absence of the basal reflections in the XRD patterns is a function of the particle size distribution rather than a result of different products. He recommended that the term manganous manganite be dropped in favour of $\delta\text{-MnO}_2$.

The nomenclature which has been developed to describe manganese dioxides is rather confusing. The name birnessite was proposed by Jones and Milne (1956) for the naturally occurring mineral, for which they propose a general formula of $(\text{Na}_{0.7}\text{Ca}_{0.3})\text{Mn}_7\text{O}_{14} \cdot 2.8 \text{H}_2\text{O}$. (This means presumably that sodium, calcium and water are located between pure MnO_2 layers). McKenzie (1977) asserts that birnessite refers to a group of

oxides of which some members have been known as δ -MnO₂, manganous manganite, 7 Å manganite, Mn(III) manganate (IV), manganous (II) manganate (IV) and NaMn (II, III) manganate (IV). Chuckrov et al. (1978a,b; in Burns and Burns 1979) claim that the name vernadite is preferred over δ -MnO₂ for poorly crystalline supergene hydrated manganese (IV) oxides that occur naturally. Their proposed formula for vernadite is MnO₂.m(R₂O, RO, R₂O₃).nH₂O, where R = Na, Ca, Co, Mn or Fe. If R = Fe, it is possible that Fe is part of the lattice, but more probable that it results as an ingrowth (a coprecipitation) of some ferric-hydroxide component. Burns and Burns (1979) provide some unity to the nomenclature by concluding that there are several types of birnessite; they propose a variable formula, (Na,Ca,K)(Mg,Mn)Mn₆O₁₄.5H₂O for the natural product.

Again, birnessites possess a double layer structure: the main layers consist of sheets of Mn^{IV}O₆ octahedra linked by sharing edges. The sheets are separated by a distance of about 7 Å, and are responsible for the basal reflections in the XRD pattern. The structure of the intermediate layers is not known in detail. They consist of Mn²⁺ and Mn³⁺ ions coordinated with OH⁻ ions and H₂O molecules, and may contain foreign ions such as Na, K, Ca and others. The oxides occur in disperse form and are non-stoichiometric (McKenzie 1977).

Several synthetic types are known, i.e. sodium-birnessite and sodium free-birnessite. They are synthesized as follows: First, sodium-buserite (which is the modern name for 10 Å manganite) is precipitated by oxidation of a fresh Mn(OH)₂ suspension in cold aqueous NaOH by molecular oxygen (the colder, the better; above 10°C, Mn₃O₄ (hausmannite) tends to form). According to Giovanoli et al. (1975), stable buserite

varieties can only form in the presence of suitable transition metal ions, which then are incorporated selectively into the lattice. Sodium-buserite, in which the ordered layers are separated by 10 Å disordered layers containing water, collapses to 7 Å sodium-birnessite ($\text{Na}_4\text{Mn}_{14}\text{O}_{27}\cdot 9\text{H}_2\text{O}$) when dried over P_4O_{10} in a vacuum (Burns and Burns 1979), due to water loss; no structural rearrangements are involved. Sodium-birnessite decomposes readily to manganite ($\gamma\text{-MnOOH}$) at room temperature (Jeffries and Stumm 1976). Alternatively it can form a related but sodium free compound of the analytical composition $\text{Mn}_7\text{O}_{13}\cdot 5\text{H}_2\text{O}$ when digested in HNO_3 (Burns and Burns 1979; Giovanoli 1970a,b). A second possible structure for sodium free birnessite is $\text{Mn}_7\text{O}_{12}\cdot 6\text{H}_2\text{O}$ (Giovanoli 1970 a,b). All authors agree that the influence of crystallite size, lattice disorder and partial substitutions of Mn^{4+} by Mn^{3+} makes it difficult to recognize particular members of the birnessite family, and that no member is a true modification of pure MnO_2 .

Historically, there have been some arguments as to whether or not $\delta\text{-MnO}_2$ and birnessite are members of the same group and whether or not $\delta\text{-MnO}_2$ is the proper name for naturally occurring forms. Accordingly, Giovanoli (1969) argues that $\delta\text{-MnO}_2$ and birnessite are two members of the same group, based on the fact that the two XRD lines of $\delta\text{-MnO}_2$ at 1.4 and 2.4 Å coincide with the two strongest lines for birnessite. Chukrov et al. (1978a,b) conclude on the basis of ED work, that birnessite and vernadite (or $\delta\text{-MnO}_2$) have different c-parameters and therefore should be regarded as different mineral species. This conclusion is supported by the IS work of Potter and Rossman (1979). Also, Electron Microscope (EM) pictures show (i) that leaflets of vernadite have smaller dimensions (tens of Ångströms) than flakes of birnessite, and (ii) that

vernadite leaflets are often curved, folded or rolled to resemble fibres (Burns and Burns 1979). Furthermore, Buser and Graf (1955) conclude that synthetic birnessite has a surface area of 30-40 m²/g compared to δ -MnO₂ with an average of ca. 300 m²/g.

Of concern to this research is the effect that aging has on the properties of birnessite and δ -MnO₂, and whether heat-treatment is a good simulation of aging.

Both birnessite and δ -MnO₂ can be easily transformed to cryptomelane by heat treatment. McMurdie (1944) discovered this process during a study on dry cell manganese batteries in which he tried to simulate the aging of poorly crystalline MnO₂ in the presence of NH₄⁺ ions (which form an integral part of such dry cells). Various artificial and natural MnO₂ samples were treated with saturated NH₄Cl solution at about 100°C on a steambath and also in an autoclave at 150°C. It was found that the morphological change in the oxides obtained after 3 to 4 hours in the autoclave was approximately equivalent to that obtained after 18 days on the steambath. McMurdie showed that there was no loss of available oxygen after heat treatment, but his EM pictures revealed that many of the artificial MnO₂ samples were converted to an acicular form. The fine needles were subsequently identified as cryptomelane by ED. Similar forms obtained in this work are shown in Figures 4.8 and 4.9 in Chapter 4. McMurdie (1944) only partially managed to determine the exact conditions required to promote this transformation. It seems that a low pH (≤ 3) and a certain amount of potassium (which is part of the cryptomelane structure) are necessary to induce conversion. Furthermore, during the conversion process by autoclaving, the pH of the

suspension shifted to more neutral values.

Buser et al. (1954) prepared a series of birnessite with very low K-contents (0.08-0.25%) which were converted to γ -MnO₂ or nsutite ((Mn²⁺, Mn³⁺, Mn⁴⁺)(O,OH)₂, Burns and Burns 1979) on boiling. Another series of birnessite with higher K concentrations (3.8-6.2% K), prepared by the same authors, were converted to cryptomelane (K₁₋₂Mn₈O₁₆·xH₂O, Burns and Burns 1979) on boiling. If however they removed most of the K by replacing it with Mn via leaching with a manganese salt, boiling resulted in transformation to γ -MnO₂, which is apparently more stable than cryptomelane (Buser et al. 1954).

Hence there appears to be a limiting lower concentration level for K, if cryptomelane is to form after boiling. McKenzie (1971) showed that there apparently is also an upper limit for the K content at which cryptomelane could be obtained by boiling. The upper limiting content is about 7% K, while the lower limit lies between 0.25-2.2% K (McKenzie 1971; Buser et al. 1954). The presence of some large cations is necessary to prevent the cryptomelane structure from collapsing (Byström and Byström 1950).

The general formula for cryptomelane is K_{2-y}Mn_{8-z}O₁₆ in which O may be replaced by OH and Mn by lower valence ions. y is always approximately equal to 1, so that the two K positions per unit cell are only half filled. The short K-K distance of 2.8 Å would make the structure unstable, due to repulsive forces between the cations, if all the K-sites were filled (Byström and Byström 1950). During the conversion of birnessite to cryptomelane there is a migration of some of the K from exchange sites of birnessite (i.e. adsorbed K) to the crystal lattice of cryptomelane, where it is no longer exchangeable (McKenzie 1971).

In summary, the requirements for transformation of birnessite (and/or $\delta\text{-MnO}_2$) to cryptomelane are: heat, low pH and a certain amount of potassium.

Another $\delta\text{-MnO}_2$ related structure which has received substantial attention is todorokite. Giovanoli et al. (1971) propose that todorokite is not a pure mineral species, but can be regarded as a partly decomposed busserite admixed with birnessite and manganite ($\gamma\text{-MnOOH}$). However, some mineralogists do not accept this view and they regard todorokite to be identical to 10 Å manganite (busserite) (Burns et al. 1975). Turner and Buseck (1979, 1981) describe tunnel structures for hollandites and todorokites, recently discovered using High Resolution Transmission Electron Microscopy (HRTEM) techniques. There appears to exist in these minerals a random fashion of intergrowths of differently sized tunnels (dimensions m by n), which results in the streaking of the diffraction patterns.

Turner and Buseck have devised a new nomenclature scheme to describe some minerals related to $\delta\text{-MnO}_2$. It is based on tunnel structures, and depends essentially on the dimensions of these tunnels, i.e. the number of octahedra surrounding them (see also the figures in Table 3.1). Table 3.2 shows this scheme. It appears that, if the number of intergrowths becomes very large, basically a layer structure results. Hence these tunnel structures provide the link with the layered structures of birnessite and busserite.

Table 3.2 Partial nomenclature scheme for manganese oxide structures

(from Turner and Buseck 1981)

Familyname	Common dimension (m)	variable dimension				sheeted end member (n \rightarrow ∞)
		n = 1	n = 2	n = 3	n = 4	
nsutite	1	T(1,1)	T(1,2)	T(1,3)	T(1,4)	
hollandite/ romanechite	2	T(2,1)	T(2,2)	T(2,3)	T(2,4)	birnessite
todorokites	3	T(3,1)	T(3,2)	T(3,3)	T(3,4)	buserite

3.5 Preparation of δ -MnO₂

The most common methods for δ -MnO₂ (or, manganous manganite or birnessite) preparation involve oxidation of manganous hydroxide and/or reduction of potassium permanganate, using a variety of oxidizing and reducing agents.

Table 3.3 is compiled from literature data in an attempt to summarize the methods for preparing δ -MnO₂. The table indicates the importance of factors such as pH, temperature, order and method of reagents addition, stirring, stoichiometry, type of oxidizing or reducing agent, washing and centrifuging, drying etc. There is obviously a considerable amount of variation in ways of preparation and reporting characteristics for δ -MnO₂. Some of this diversity could be due to the effect of crystal structure on the polarization of the surface. Healy and Fuerstenau (1965) consider the electrostatic field of oxide surfaces to control

both the adsorption and dissociation of water molecules at the solid-liquid interface. However, an equally important source of variation may be the sample preparation and subsequent treatment and aging, processes which have not been clearly documented in the literature. The history of the sample needs to be described thoroughly, because the dehydration of the surface as a result of drying, or aging while in solution can have a pronounced effect on the location of the $\text{pH}(\text{zpc})$ of the solid and hence influence adsorption characteristics. According to Murray (1974) aging is probably due to the condensation and dehydration of the oxide which may explain some of the variability that exists in the literature regarding the location of the $\text{pH}(\text{zpc})$ for $\delta\text{-MnO}_2$.

In order to investigate the influence of the precipitation process on resulting $\delta\text{-MnO}_2$ products, three batches of $\delta\text{-MnO}_2$ were prepared in this study according to the three basically different precipitation methods summarized in Table 3.3. These methods are:

- (i) oxidation of manganous-hydroxide or (-salt (ox),
- (ii) reduction of potassium permanganate using a variety of oxidizing and reducing agents (red),
- (iii) the so-called Guyard reaction, a redox process involving both Mn^{7+} from permanganate and Mn^{2+} from a manganous salt (redox).

Chapter 4 describes how these three batches of $\delta\text{-MnO}_2$ differ in specific characteristics and adsorption behaviour for Cu.

3.5.1 The Kinetics of the Reaction between Permanganate and Manganous Ions

A large number of the preparation methods summarized in Table 3.3

include the redox-reaction involving Mn^{7+} from permanganate and Mn^{2+} from manganous salt. This Guyard type of reaction is the principal method employed to precipitate δ - MnO_2 in this study, and the following section discusses some possible reaction pathways and mechanisms involved in this particular reaction.

Polissar (1935) discusses the influence of pH on the Guyard reaction. In acid solution, there appears to be an incubation period for the reaction between Mn^{2+} and MnO_4^- . The manganese dioxide formed in the course of the reaction acts as a catalyst (autocatalysis). Polissar (1935) tested the assumption of autocatalysis by addition of a manganese dioxide precipitate. He found that although the reaction was accelerated through this addition of manganese dioxide to the initial solution, the catalytic effectiveness depended on the pH at which this MnO_2 was formed. Precipitated in a neutral solution, MnO_2 seems far more effective than when prepared in acid solution. As a result of visual observations Polissar concludes that the 'neutral' solid is much more highly dispersed than the 'acid' solid, and that this difference in degree of dispersion can probably account for the higher catalytic effectiveness of the neutrally formed MnO_2 . It is however not clear whether this is a straight pH effect on particle formation (i.e., a low pH induces the formation of a smaller number of large particles). It is also possible that at low pH the overall ionic strength is higher; this would induce coagulation of the particulates and hence a reduction in total surface area available.

The autocatalytical effect and the variability of particle sizes can also be interpreted in terms of nucleation and crystal particle growth (W.J. Snodgrass, pers. comm. 1982): A certain period of time is required for nuclei to form (homogeneous or heterogeneous). Upon for-

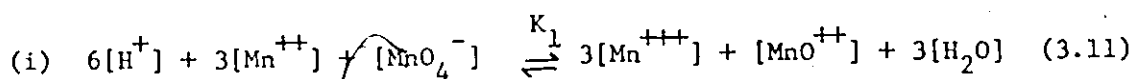
mation of nuclei, they aggregate together to form amorphous crystallites or crystals, while more nuclei are forming. Upon formation of these larger particles, crystal growth and secondary nucleation can occur, increasing the rate of removal of soluble Mn from solution (the effect observed by Polissar). If one were in favour of a straight pH effect upon particle size, one would have to argue as follows (W.J. Snodgrass, pers. comm. 1982):

At a low pH, the rate of loss of H^+ from hydration water molecules surrounding Mn^{4+} ($Mn^{4+} \cdot 4H_2O + Mn^{4+} \cdot OH^- \cdot 3H_2O + H^+ \rightarrow \text{----} \rightarrow Mn^{4+}(OH^-)_4$) is slower than at neutral pH because of the higher concentration of protons in solution. Loss of H^+ from hydration water is necessary to permit formation of nuclei, the basic building blocks of a crystallite. The slower rate of nucleation induces fewer particles to form, but allows those that do form to grow larger. On the other hand, at more neutral pH, nuclei form more rapidly, which then aggregate to form crystals. Nucleation and aggregation compete more effectively for solution forms of Mn^{4+} than does crystal growth, resulting in more particles of a smaller size.

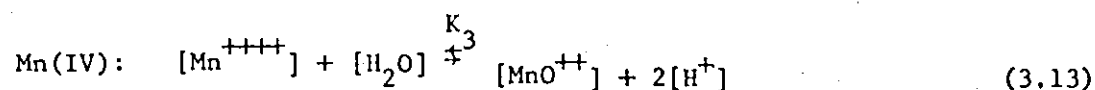
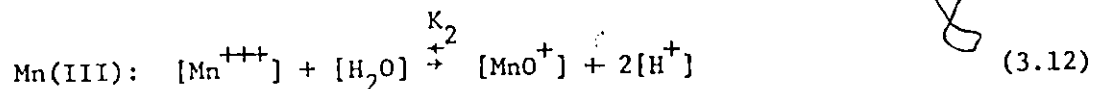
However, if one is in favour of a pH effect being secondary to the effect of ionic strength (Polissar's solutions of high pH have a high ionic strength) on particle size, then one can present a somewhat different argument:

Assuming the rate of nucleation and crystal growth are independent of pH will give a similar particle size distribution at both acidic and neutral pH values. However, a higher ionic strength associated with lower pH induces more aggregation of particles and hence fewer particles of larger size in the more acidic solution.

Adamson (1952) made a detailed study of the reactions that occur in an acid solution of manganous and permanganate ions to try and explain the autocatalytic- and pH- effects observed by Polissar (1935). From his observations, combined with Polissars research, Adamson hypothesized that a most reasonable assumption is that a rapid pre-equilibrium between Mn (II) and Mn (VII) in solution produces two intermediate valence states Mn (III) and Mn (IV). These intermediates subsequently undergo a slow electron exchange, which is disturbed by the appearance of MnO_2 . Adamson shed some light on the actual kinetics involved through the use of radioactive manganese and by measuring exchange rates (between radio-manganous and permanganate ions). He proposed that the most reasonable reaction mechanism which agreed with his observations are: (i) a rapid reversible equilibrium, involving Mn(III) and Mn(IV) (the intermediates), (ii) an electron exchange reaction and (iii) several competing reactions. They are the following:



This reaction is the sum of several steps involving Mn(III) and Mn(IV) from the hypothesized pre-equilibria which are supposed to be rapid:



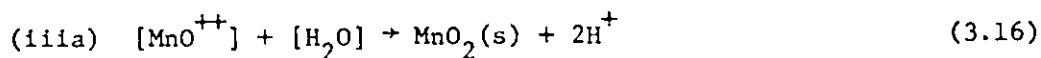
The values of K_2 and K_3 are such that in acid solution the principal forms of Mn(III) and Mn(IV) are $[\text{Mn}^{+++}]$ and $[\text{MnO}^{++}]$ as shown in the overall equilibrium reaction.



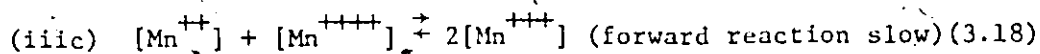
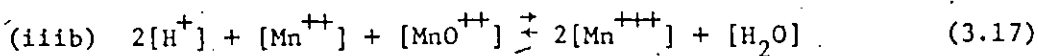
This is a non-instantaneous, measurably slow, electron exchange and the exchange reaction rate is:

$$R = k' [\text{MnO}^+] [\text{MnO}^{++}] \quad (3.15)$$

(iii) Competing reactions are:



This reaction is negligible in the absence of solid MnO_2 (see also Polissar 1935); but inhibits the electron exchange reaction (ii), once a trace of $\text{MnO}_2(\text{s})$ is formed. The effect of increasing the pH is the same.



Empirically, Adamson had found the following electron exchange rate by varying the concentrations of manganous, permanganate; and

hydrogen-ions, and using radiomanganous ions:

$$R = k [H^+]^a [Mn^{++}]^b [MnO_4^-]^c \quad (3.19)$$

in which $a = 1.3 \pm 0.3$; $b = 1.3 \pm 0.3$ and $c = 0.3 \pm 0.3$

By using the above proposed mechanisms, R can be expressed as:

$$R = k [H^+] [Mn^{++}]^{3/2} [MnO_4^-]^{1/2} \quad (3.20)$$

where $k = (k' \cdot 2 K_1 K_2^2 / 3)^{1/2} \quad (3.21)$

This expression for R agrees with the empirical equation within the limits of error. In the absence of solid, an equilibrium concentration is established of $[Mn^{++}]$, which drops considerably at the appearance of the solid. The concentration of each reactant in the exchange reaction is reduced and thus the exchange rate itself is reduced to a negligible value, and $MnO_2(s)$ is formed. In neutral or alkaline solution, electron exchange is negligible, since $MnO_2(s)$ is formed immediately.

From Adamsons work then, the rate of formation of MnO_2 is more rapid at more neutral pH than in acid solution. This agrees with Polissars findings of the higher catalytic effectiveness of neutrally formed MnO_2 . Explanations in terms of nucleation, aggregation and crystal growth were already given.

This research deals with the adsorption of Cu on δ - MnO_2 , formed via the Guyard reaction. The effect of pH on this reaction is clear: A more dispersive MnO_2 with a larger surface area is obtained, when the

reaction is allowed to proceed at neutral pH. A larger surface area implies a larger adsorption capacity. This should be kept in mind when interpreting the results of the adsorption studies of Cu on MnO₂. In Chapter 4 a precise description is given of the manner in which the Guyard reaction has been applied in this study.

3.6 Summary

Hydrous manganese oxides have been the object of study in many areas of research. Earlier publications deal with the electrochemical behaviour of MnO₂ in dry cell batteries. The natural formation and deposition of manganese oxides is a complicated process, controlled by factors such as pH, temperature, O₂ availability, carbonate- and manganese- concentrations. The oxidation of Mn²⁺ to MnO₂ occurs along several pathways, but there is uncertainty regarding the relative importance of the various possibilities.

The fundamental structural unit in tetravalent manganese oxides is the (Mn^{IV}O₆) octahedron. These units can be linked by corner- and edge- sharing to give a variety of chain, tunnel and layer structures, which complicates the identification of manganese minerals. Researchers do not always agree on the exact structure of δ-MnO₂ and whether the minerals known as δ-MnO₂, birnessite, manganous manganite and vernadite are identical. Currently, the general feeling seems to be, that δ-MnO₂ consists of layers of pure MnO₂, interspersed with layers containing Mn²⁺, Mn³⁺, H₂O, K⁺, Na⁺, Ca²⁺ and perhaps metal ions. Such a complicated varying structure does not help to resolve the arguments regarding the identity of the above mentioned minerals. Conversion of δ-MnO₂ to

cryptomelane is possible through heat treatment, which could indicate that such a process may occur at a much slower rate at low temperatures which would encompass a natural aging process. This is of importance to this study (see Chapter 4).

The precipitation of $\delta\text{-MnO}_2$ under laboratory circumstances is influenced by the pH. A product, obtained under neutral pH conditions is more dispersive and hence possesses a larger surface area. This has been explained with several arguments. It seems more likely that the explanation involving the formation of nuclei and subsequent aggregates is of more importance than ionic strength effects, although the latter cannot be excluded without more experimental details.

This Chapter aims to provide basic background information regarding the natural occurrence, mineralogy and structure of manganese oxides. In particular, $\delta\text{-MnO}_2$ is discussed, since it is the subject of this study. Knowledge of structure can be helpful in interpreting observed experimental results for the adsorption of Cu on artificially prepared $\delta\text{-MnO}_2$. Kinetic arguments can aid the understanding of the actual pathway(s) along which $\delta\text{-MnO}_2$ can be precipitated in the laboratory. This in turn can perhaps facilitate the interpretation of adsorption results.

Table 3.3 Formation and various characteristics of 'artificial' δ -MnO₂ (references are in chronological order).

Reference & principle of method	Description of method	Reaction formula as given in reference	Product	pH (apc)	Surface	X-ray pattern	Details
McHurdie 1944 REDUCTION	Reduction of KMnO ₄ with concentrated HCl whilst heating	not specified	δ -MnO ₂	n.m.	n.m.	two very diff- use lines at 2.39Å & 1.40Å	poorly crystallized form of cryptomelane (KMn ₈ O ₁₆)
Copeland, Griffith & Schertsinger 1947 OXIDATION	Aeration of freshly ppted Mn(OH) ₂ in NaOH solution	not specified	MnO _x 1.856xcl.9	n.m.	n.m.	pattern corres- ponds to the δ - MnO ₂ described by McHurdie 1944	product consists of extremely thin plate-like particles
Wadswley 1950 OXIDATION	Oxidation of manganese hydroxide in aqueous alkaline suspension	not specified	(Na,Mn)Mn ₃ O ₇ H ₂ O MnO ₂ 75.6% MnO 11.4%	n.m.	n.m.	strong line at 10.0 Å	electron micrograph shows very thin, over- lapping sheets, sharply different from δ -MnO ₂ or manganese-manganite barlike structures
Buser, Graf & Feitknecht 1954 REDUCTION	Fast oxidation of Mn ²⁺ salt with KMnO ₄	$3Mn^{2+} + 2MnO_4^- + 2H_2O \rightarrow 5MnO_2 + 4H^+$	mangan(II)- manganite: 4MnO ₂ ·Mn(OH) ₂ 2H ₂ O	n.m.	n.m.		
REDUCTION	Reduction of KMnO ₄ with heated (90°C) concentra- ted HCl	as above	theor. MnO 1.72	exper. MnO 1.74	n.m.	n.m.	All four products morphologically identical under the electron microscope
			MnO 1.86	MnO 1.82			
			MnO 2.1	MnO 1.88			
			MnO 2.4	MnO 1.94			
REDUCTION	Reduction of KMnO ₄ with heated (90°C) concentra- ted HCl	as above	theor. MnO 1.75	exper. MnO 1.706	n.m.	n.m.	EM. shows not a bar- like product, but aggregates of spherical particles
			MnO 2.00	MnO 1.79			
			MnO 2.25	MnO 1.89			
			MnO 2.50	MnO 1.945			

- continued -

Table 3.3 continued

Reference & principle of method	Description of method	Reaction formula as given in reference	Product	pH (zpc)	Surface	X-ray pattern	Details
Clemmer, Gattov & Heisick 1961 REDUCTION	A number of different procedures are described. In general, the reaction consists of a reduction of Mn^{2+} at neutral or alkaline pH at 20-100°C	not specified	δ - MnO_2	n.b.	around 30-50m ² /g, decreasing with temp. of formation	poorly crystallised products; patterns only show a few more or less diffuse lines	δ - MnO_2 becomes converted into α - Mn_2O_3 upon heating in air; δ - MnO_2 containing foreign ions becomes α - MnO_2 on annealing
Morgan & Stumm 1964	Generally either oxidation of Mn^{2+} or reduction of MnO_4^-	not specified	MnO_x 1.15x1.8 depending on pH, temp. etc.				
REDOX	Manganese perchlorate solutions of known strength are slowly added to a standardised $KMnO_4$ solution in a measured excess of NaOH and under thorough mixing conditions	$3Mn^{2+} + 2MnO_4^- + 2H_2O \rightarrow 5MnO_2 + 4H^+$	MnO_x 1.90x1.95 closely related to δ - MnO_2 or $Mn(III)$ manganite	2.8±0.3 by titration	not specified	low degree of crystallinity with only 4 or 5 lines	nonstoichiometry caused by uptake of Mn^{2+} by hydrous manganese dioxide that is formed in the reaction process
Cabano, Etienne & Laurent 1965 OXIDATION	Anodic oxidation at 90°C of Mn^{2+} salts in acid and at various current densities	not specified	γ - MnO_2 (manganite)	not reported	45-134m ² /g		
Healy, Herring & Fuerstenau 1966 REDUCTION	Reaction in excess $KMnO_4$ ensures oxidising conditions Reaction in deficient $KMnO_4$ produces reducing conditions	$2KMnO_4 + 8HCl + 2MnO_2 + 2KCl + 3Cl_2 + 4H_2O$ as above	MnO_x ; x<1.9 is called β - MnO_2 O : H = 1.7-1.9, is called $Mn(III)$ manganite, by elec. $3MnO_2 \cdot Mn(OH)_2$ or Mn_2O_3	1.5±0.5 by coagulation	BET; 2 300m ² /g BET; 70m ² /g	2 diffuse peaks at d-spacings of 1.45Å and 2.60Å diffuse peaks at d-spacings of 7.22, 3.66Å, 2.45 and 1.42Å	forms layered structure, the crystals being 2 to 3 atomic layers thick double layer structure; main layers contain Mn^{2+} in 6-fold coordination with O^{2-} , are separated by 10Å spacings which contains Mn^{2+} coordinated with O^{2-} , OH^- and H_2O

- continued -

Table 3.3 continued

Reference & Principle of Method	Description of method	Reaction formula as specified in reference	Product	pH (zpc).	Surface	X-ray pattern	Details
Posselt, Reifeger & Weber 1968 REDOX REDUCTION	Generally: oxidation-reduction reaction as combined in the Guyard reaction or by use of permanganate with a reducing agent	$3Mn^{2+} + 2MnO_4^- + 2H_2O \rightarrow 5MnO_2 + 4H^+$ $MnO_4^- + 2H_2O + \text{reducing agent} \rightarrow MnO_2 + 4OH^-$	$MnO (1+x)$ $0.14x \leq 0.95$ depending on conditions of formation	2.8-4.5 depending on actual measuring technique and/or slight differences in products	not reported	not reported	
REDOX	Specific: a specified amount of $MnSO_4$ is first introduced into 950ml of dist. water under rapid mixing conditions. After a pH adjustment, an amount of $KMnO_4$ is added	Guyard reaction (as above)	$\delta-MnO_2$	not reported	not reported	not reported	
Murray, Healy & Fuerstenaу 1968 REDUCTION	see Healy, Herring & Fuerstenaу 1966	$2KMnO_4 + 8HCl \rightarrow 2MnO_2 + 2KCl + 3Cl_2 + 4H_2O$	Mn(II) manganite	1.8±0.5	BET, 70m ² /g	see Healy, Herring and Fuerstenaу 1966	
Posselt, Anderson & Weber 1968a	An MnO_2 sol is prepared at constant pH and rapid mixing by simultaneous addition of $NaOH$ and $NaMnO_4$ to dist. water solutions of Mn^{2+} , Na^+ & ClO_4^-	Guyard reaction (as above)	$MnO (x+1)$ $0.14x \leq 0.95$ $\delta-MnO_2$ $\gamma-MnO_2$	range from 2.6-4.5	300m ² /g 150m ² /g	poor degree of cryst. note ordered	
McKenzie 1970	A mixture of 70g $MnSO_4 \cdot H_2O$ and 308g KOH in 2L water is oxidised by bubbling O_2 for 7 hours, which gives a strongly alkaline product (pH 9.9 after washing). Sample is washed until free from soluble salts and dried at 35°C	not specified	birnessite	1.84	78m ² /g (N_2 ads.)	not explicitly mentioned	corresponds to manganomanganite of Buser, Graf & Feitknecht 1954
	As above; after washing, the product is titrated to pH 7.4 with dilute nitric acid and washed again until free from soluble salts and dried at 35°C	not specified	birnessite	1.84	75m ² /g	not explicitly mentioned	

- continued -

Table 3.3 continued

Reference & Principle of Method	Description of Method	Reaction formula as specified in reference	Product	pH (zpc)	surface	X-ray pattern	Details
McKenzie 1970 (cont.) REDUCTION	196ml of conc. HCl is added slowly, under vigorous stirring to a boiling solution of 158g KMnO_4 in 2.5L water (compare McKenzie 1971). The mixture is boiled a further 10 min. before filtering. Same washing and drying procedure as mentioned above	not specified	birnessite	1.98	$32\text{m}^2/\text{g}$	not explicitly mentioned	corresponds to $\delta\text{-MnO}_2$ of Buser et al. 1954
McKenzie 1971 REDUCTION	Two moles of conc. HCl are added dropwise to a boiling solution of 1M KMnO_4 in 2.5L water, under vigorous stirring. After boiling for a further 10 min. the precipitate is filtered and washed	not specified	brown birnessite with 9.5% K	not reported	$32\text{m}^2/\text{g}$	not reported	large K excess prevents formation of $\gamma\text{-MnO}_2$
OXIDATION	A mixture of 0.4 moles MnSO_4 and 5.5 moles KOH in 2L water is cooled to 5°C and oxidised by bubbling O_2 for 5 hours	not specified	black birnessite with 9.0% K	not reported	$75\text{m}^2/\text{g}$	not reported	
Loganathan & Bura 1973; Loganathan Bura & Fuerstenau 1977 REDUCTION	$\delta\text{-MnO}_2$ is prepared in an excess of KMnO_4 to ensure oxidising conditions. The oxide is washed several times with demin. water, then a few times with 0.05N HClO_4 to remove as much K as possible. The oxide is next dried at 45°C , ground and pestled to 140 mesh & stored	$2\text{KMnO}_4 + 8\text{HCl} + 2\text{MnO}_2 + 2\text{KCl} + 3\text{C}_2\text{H}_5\text{OH} + 4\text{H}_2\text{O}$	$\delta\text{-MnO}_2$ or MnO , 1.92	1.40 by elec-phor; 1.60 m^2/g ; mob; 1.55 glycol; by subside retention; 2.45 & 1.41 μ (based on X-ray pattern)	BET: 2.45 & 1.41 μ (based on X-ray pattern)	low crystallinity; 3 or 4 diffraction lines at 7.3, 2.45 & 1.41 μ which does not permit definite identification as $\delta\text{-MnO}_2$	washing with acid does not change the structure of the oxide (based on X-ray pattern)
Gedde & Laitinen 1974 REDOX	Hydrous MnO_2 is prepared by slowly adding MnNO_3 solution to alkaline KMnO_4 solution (mole ratio 3:2:4). The pptc is filtered, washed with, and redispersed in dist. water. The pH is adjusted to 6 and the product is aged for 16 to 20 hours before use in experiments	$3\text{Mn}^{2+} + 2\text{MnO}_2 + 4\text{OH}^- + 2\text{H}_2\text{O} + 5\text{MnO}_2 + 4\text{H}_2\text{O}$ (Norgan and Stumm 1964)	MnOx 1.90-1.95	1.5-2.8 (assumed)	not reported	amorphous	no pronounced aging effect. in presence or absence of ads. Pb^{2+} ; only a slight decrease in recoverability upon aging

- continued -

Table 3.3 continued

Reference & Principle of Method	Description of method	Reaction formula as given in reference	Product	pH (zpc)	Surface	X-ray pattern	Details
Murray 1974 Murray 1975a Murray 1975b Murray 6 Dillard 1979	A known amount of KMnO_4 is added to a 4L erlenmeyer flask. An equivalent amount of NaOH is added to neutralize evolving acid to keep pH basic, which tends to create a situation kinetically favoring the oxidation of Mn(II) . Dist. water is added up to 3L and a stoichiometric amount of standardized MnCl_2 added dropwise whilst mixing. The pptc strength is down to 1x10 ⁻⁴	1974: $3\text{Mn}^{2+} + 2\text{MnO}_4^- + 4\text{H}^+$ $10\text{H}_2\text{O} + \text{MnO}_2 + 4\text{H}^+$ 1975a, b: $3\text{Mn}^{2+} + 2\text{MnO}_4^- + 2\text{H}_2\text{O} + 5\text{MnO}_2 + 4\text{H}^+$	MnO_2 1.92 or MnO_2	2.25 2.40 by electrophor.	BET (triplicate): 263.55 m ² /g by electrophor. 270 m ² /g	low degree of crystallinity with reflections at 7.4, 4.04, 2.43 and 1.63 Å	Particles have sizes from 0.2-1.0 μm and appear to be aggregates of much smaller, spherical-shaped particles
van den Berg 1975	To 1L twice dist. water of 0.01M KMnO_4 , stoichiometric amounts of Mn^{2+} & KNO_3 are added while the solution is kept around pH 7 by adding NaOH . After 1 hr. the colloid is centrifuged & redispersed in 0.01M KMnO_4 (3 times)	$3\text{Mn}^{2+} + 2\text{MnO}_4^- + 2\text{H}_2\text{O} + 5\text{MnO}_2 + 4\text{H}^+$	MnO_2 1.9%	2.5	not reported	not reported	
Gray, Malati & Raphael 1978	KMnO_4 is prepared batchwise by the slow addition, at 70°C of 0.1M KMnO_4 solution to a 2M H_2O_2 in 0.4M NaOH solution using a volume ratio of 3:20. The filtered product is twice resuspended in H_2O , refiltered and washed with H_2O until the pH of the effluent is 8.5. The product is dried at 45°C, ground, and stored in the dark at 22°C.	not specified	MnO_2 1.98	3.3 0.5	BET 4 m ² /g	d-spacing lines and relative intensities: 7.40 (72%) 3.86 (33%) 2.40 (32%) 1.41 (18%)	The low BET surface may be due to aging effects. However, Zn ²⁺ adsorption seems to indicate a surface area 50x BET
van den Berg 1979; van den Berg & Kramer; 1979a, b	MnO_2 is made by mixing stoichiometric amounts of KMnO_4 and KOH at neutral pH; a premixed solution of KMnO_4 and KOH is pipetted into a solution of MnCl_2 while vigorously stirring magnetically. The pptc is further purified by centrifugation and redispersion in dist. water	$\text{Mn}^{2+} + 2\text{MnO}_4^- + 2\text{H}_2\text{O} + 5\text{MnO}_2 + 4\text{H}^+$	MnO_2 x = 1.94 assumed from earlier expts. (van den Berg 1975)	n.m.	n.m.	amorphous up to two years	flocculate becomes finely dispersed upon stirring
McKenzie 1979	Birnessite is prepared by the action of HCl on hot KMnO_4 solution (see McKenzie 1971)	not specified	Birnessite with 9% K, reduced to 2% by wash- ing with 0.25M HClO_4	1.6	not reported	X-ray diffraction shows material similar to oxides used by Loganathan & Barau (1973) and Murray (1975a)	

CHAPTER 4

PREPARATION, CHARACTERIZATION AND AGING OF VARIOUS

 δ -MnO₂ SAMPLES4.1 Introduction

The structure and nomenclature for Mn(IV) oxides, especially δ -MnO₂ and related products discussed in Chapter 3, gives a picture of a field of research which is quite complex and often confusing. Much of the confusion is related to problems regarding proper characterization techniques. Table 3.3 indicates that, in general, hydrous manganese dioxides are characterized by a limited number of types of analyses; X-Ray Diffraction (XRD) patterns and the oxidation state of manganese are the main ones. But there appears to be considerable disagreement about the identity of certain Mn-oxides and the characteristics of specific oxides. Also, it seems that certain characterizing analyses do not always give unambiguous results regarding the identification of the material under study. For example, Jeffries and Stumm (1976), in their study of metal adsorption on a büserite (10A manganate) surface, realized that different Mn-oxides may exhibit substantially different surface and structural properties. The stress that they place upon the desirability to work with one, well-defined species of MnO₂ is well taken.

This study likewise emphasizes that a satisfactory characterization of the particular surface under study, is an absolute necessity for adsorption work. As mentioned in Chapter 2, difficulties

were encountered in reproducing the adsorption parameters for δ -MnO₂, as reported by van den Berg (1979) (see also Chapter 6). This was thought due to the form of Mn-oxide used, details of preparation, aging, or a combination of these factors. An extensive study was carried out to ascertain how far-reaching the effects of these factors are and how important they may be with respect to adsorption behaviour.

The following sections discuss general characteristics of δ -MnO₂ surfaces which are important for either identification of the product and/or for determining the reactivity of its surface with respect to adsorption. Then some characteristics for three principally differently prepared δ -MnO₂'s are presented along with a number of results for replicates of one of these preparations, for two commercially prepared MnO₂'s, and for variations of one particular preparation method. Any preparation method is hereafter called a recipe. The three different recipes involve respectively a redox-, reduction- and oxidation-reaction. The second section of this Chapter examines aging of the δ -MnO₂ surface, with emphasis on its morphology. This part of the study was initiated because a four year old δ -MnO₂ sample, a remnant of van den Berg's studies, showed totally different morphology from a freshly prepared δ -MnO₂ and in fact resembled cryptomelane, when examined under the Transmission Electron Microscope (TEM). Conclusions are then given concerning the major differences between the three different recipes and the effects of aging upon the morphology and adsorption behaviour of δ -MnO₂.

4.2 Characteristics of and Methods for Characterizing δ -MnO₂

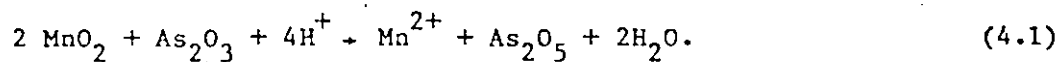
4.2.1 Oxidation State of Manganese in δ -MnO₂

The controversial relation between structure, oxygen:manganese ratio and nomenclature for hydrous Mn(IV) oxides is discussed in Chapter 3. The work of most research in this particular field is summarized in Table 3.3 and shows a range of oxidation numbers for MnO_x of roughly 1.70 $< x < 1.98$.

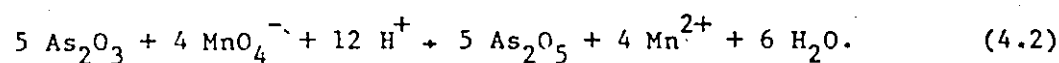
Determination of the oxidation number of a MnO_x product can be approached principally from two directions: one can determine the amount of oxygen present in the MnO_x chemically, and one can also attempt to determine the different oxidation states of Mn physically and/or chemically. Morgan and Stumm (1965) mentioned in their review of the pertinent literature that there appear to be relatively few possibilities for the determination of Mn(II) in the presence of other forms of manganese. They devised a chemical method, which used both filtration and colorimetric techniques, to quantitatively characterize the distribution of some of the different forms of manganese in a particular sample. However, this method is subject to a relatively large number of interferences and does not seem to have found wide application. Physical techniques to determine the oxidation state of Mn in a sample include Nuclear Magnetic Resonance - (NMR) and Electron Paramagnetic Resonance - (EPR) Spectroscopy.

Several methods are available to determine the amount of oxygen in MnO_x chemically. These methods can be distinguished on the basis of the type of sample (i.e. wet or dry) they require. An example of a 'wet' method is the latter part of the well-known Winkler method for dissolved

oxygen analysis, a procedure widely used in water quality research. In this study, a 'dry' method was chosen, which reduces Mn^{4+} to Mn^{2+} by adding excess As_2O_3 to a known amount of dried MnO_x , while afterwards the excess is back-titrated with permanganate to determine the amount of oxygen used. Reaction equations involved are (Belcher and Nutten 1967):



and



Permanganate, standardized with an arsenic solution, also serves an endpoint indicator. Calculation of the oxidation number for MnO_x can be done as follows (McKenzie 1970):

The amount of As_2O_3 used in (4.1) is calculated as MnO_2 on a weight basis. The difference between the initial weight of the MnO_x sample and the amount of MnO_2 determined, the residue, is assumed to be MnO . From the amounts of MnO_2 and MnO , the ratio Mn:O can be calculated. The assumption that $MnO_x - MnO_2 = MnO$ can only be backed up by a separate analysis of MnO_x for Mn, because in reactions (4.1) and (4.2) MnO_4^- is added which makes it impossible to do Mn determinations concurrently. The fraction MnO could possibly contain amounts of K and H_2O , which, if undiscovered, would influence the Mn:O ratio.

The results obtained with the above presented method, in this study, indicated that the amount of MnO calculated was likely over-estimated, and that results needed to be corrected for quantities of K and H_2O present in the residue. The samples were dried to constant weight at approximately $100^\circ C$ prior to the determination of the Mn:O

ratio. Some H_2O may stay attached to the MnO_2 surface at $100^\circ C$ or alternatively H_2O may be bound in the lattice, which would take higher temperatures to remove it. Potassium is one of the ingredients in the precipitation of MnO_2 (see Section 4.3). It can be either incorporated in the lattice in the imperfect layers (see Chapter 3, Section 3.4) or adsorbed on the MnO_2 surface, depending on the pH of the suspension. Drying does not remove K. McKenzie (1970) dried δ - MnO_2 samples at $105^\circ C$, after which the residual water content was determined by heating for two hours at $1000^\circ C$ in a silica tube furnace. Water which evaporated in the furnace was adsorbed on anhydrous magnesium perchlorate and weighed. McKenzie found 7.7-11.5% residual water in his birnessite (i.e. δ - MnO_2) samples. Such a percentage combined with large quantities of impurities (e.g. up to 10% of K) would imply a large correction for the values of x for δ - MnO_2 samples prepared in this study. It should be noted that McKenzie (1970) reports very specifically how residues were assessed. Other authors are not very explicit and usually restrict themselves to mentioning the principles of the method used to determine x (mostly a wet method) and the end results.

To assess K- and H_2O -contents, a number of K and Mn analyses using Atomic Adsorption Spectrometry (AA) are carried out to determine the ratio Mn:K in the MnO_x samples. Also, a limited number of Differential Thermal Analyses (DTA) combined with Thermo-Gravimetric Analyses (TGA) are performed to attempt to estimate the percentage water present, and to obtain an idea about the stability of the samples and the rate of water loss at elevated temperatures. A very limited number of Electron Spin Resonance (ESR) analyses are carried out to find indications of Mn^{2+} present in the MnO_x samples. Results for Mn:O ratios in the investigated

MnO_x samples, as well as results from AA, DTA, TGA and ESR analyses are discussed in Section 4.4.

4.2.2 Surface Area Analysis

Table 3.3 presents a range of values for the surface area of δ-MnO₂. The mean value seems to center around 300 m²/g. There are a number of options for measuring surface areas.

The classic BET-N₂ adsorption method (Brunauer, Emmett and Teller 1938) is based on the concept that for adsorption of gases in multi-molecular layers, there is a vapour pressure of a gas from which a uniform adsorbing surface, in equilibrium with the gas, will adsorb a monolayer. By adsorption of N₂ onto a surface at this particular pressure, a monolayer coverage of N₂ will result and from the total amount of gas adsorbed combined with the diameter of the N₂ molecule, the total surface area per unit weight of material can be calculated.

The equilibrium ethylene glycol retention method as described by Bower and Goertzen (1959) involves the equilibration of a sample with the glycol vapor pressure of a CaCl₂-glycol solvate. The surface area is calculated from the Dyal-Hendricks value for the amount of glycol required to form a monolayer on one m² of surface (Dyal and Hendricks 1950), the amount of glycol retained by the sample and the weight of the dried MnO₂ sample.

A method which measures surface area in suspension is negative adsorption of an ion of the same charge as the MnO₂ surface. Jeffries and Stumm (1976) used the negative adsorption of NO₃⁻ (Lyklema and van der Hul 1969; Huang and Stumm 1972) to determine the surface area of busserite.

The BET- and glycol retention- methods require drying of sufficient material prior to the adsorption process. In this study, only

very small amounts (0.4 to 0.8 gram total) of MnO_2 could readily be prepared per batch and this amount was not adequate for surface area analysis by the above methods. The possibility of precipitating more MnO_2 per batch by using for example 5 to 10 times the concentrations of chemicals was not thought desirable, since preparation of a certain kind of $\delta\text{-MnO}_2$ is apparently very sensitive to the concentration of the chemicals used (B. Dempsey, pers. comm. 1981).

In addition, a strong argument against using the surface area determination methods is that they require drying of the material which may alter the surface area and/or structure (e.g. busserite collapses to birnessite on water loss). A method for measurement in solution is most desirable

In this work approximate surface areas were obtained indirectly from the Cu-adsorption isotherms using the Langmuir theory. Moreover, the values for Γ_{max} (i.e. the maximum amount of Cu adsorbed per amount of MnO_2) were thought to be very suitable for comparing available surfaces of different batches of $\delta\text{-MnO}_2$. Such comparison is necessarily a relative one, but it suffices for characterization of $\delta\text{-MnO}_2$ surfaces which are supposedly identical or at least very similar.

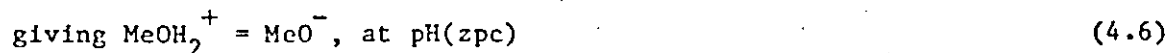
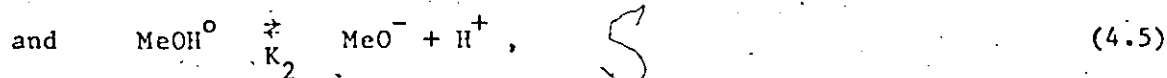
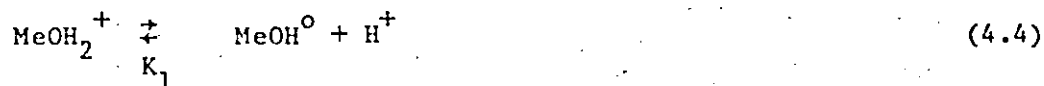
4.2.3 The pH of Zero Point of Charge

The $\text{pH}(\text{zpc})$, another characteristic of the $\delta\text{-MnO}_2$ surface, is the concentration of potential determining H^+ ions at which the surface has a net zero charge. The electrochemical double layer, counteracting surface charge at the interface can be pictured as follows:



This assumes that H^+ and OH^- are potential determining ions; for $\delta\text{-MnO}_2$ this is generally accepted as valid.

Murray (1974) proposed that the exact value of the $\text{pH}(\text{zpc})$ will depend on the relative acidity of the surface groups. The sequential reactions are:



and $[\text{H}^+_{\text{zpc}}] = [\text{K}_1\text{K}_2]^{1/2}$ (4.7a)

or $\text{pH}(\text{zpc}) = 1/2(\text{pK}_1 + \text{pK}_2)$ (4.7b)

K_1 and K_2 are the acidity constants of the surface sites. The location of the $\text{pH}(\text{zpc})$ will thus depend on such factors as the acidity of the metal (Me) ion (in this case manganese).

For metal oxides in aqueous solutions, there is a direct relation between the $\text{pH}(\text{zpc})$ (which is a characteristic property of the interface) and the electrostatic field strength of the solid (a characteristic property of the bulk lattice). This relation is of the form (Healy et al. 1966):

$$\text{pH}(\text{zpc}) = \frac{F \mu}{4.666 RT} + k, \quad (4.8)$$

where μ is the dipole moment of water, R the gas constant, T the absolute temperature and k a (positive) constant. F is the electrostatic field strength at the oxide surface. F is given by (Healy et al. 1966):

$$F = \frac{8\pi e}{r_c^2} \exp\left(-\pi \sqrt{2} \frac{r_a}{r_c}\right), \quad (4.9)$$

where e is the electronic charge and r_c the smallest cation-anion spacing in the crystal. r_a is the equilibrium distance between an adsorbed ion and a surface ion of the adsorbing surface directly below the adsorbed ion. Therefore,

$$\text{pH}(\text{zpc}) = A/r_c^2 + B, \quad (4.10)$$

in which A and B are positive constants for an oxide. This relation shows that the $\text{pH}(\text{zpc})$ increases with decreasing interionic distance r_c .

For more complex solids, such as some of the hydrous manganese oxides, in which the metal is likely to be in more than one valence state, the above is not applicable and:

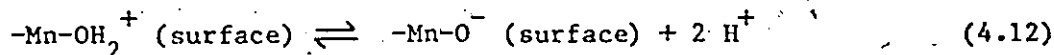
$$\text{pH}(\text{zpc}) = A'/(V)^{2/3} + B', \quad (4.11)$$

where V is the average volume of the unit cell. For $\delta\text{-MnO}_2$, $V = 42.9 \text{ \AA}^3$, which means a high degree of oxidation (Healy et al. 1966).

The above implies, that as the atomic packing in the lattice increases, the unit cell dimensions decrease and the electrostatic field above the lattice increases, which results in a higher pH(zpc).

By definition only that portion of the charge that is caused by the interaction of H^+ and OH^- ions with the surface, affects the surface charge (σ). But the pH(zpc) is lowered as a result of adsorption of other ions (Stumm et al. 1976). Hence pH(zpc) and pH(iep) (iep = isoelectric point; the pH where the effective surface charge is zero) are only identical in the absence of specific adsorption of other ions (i.e. metals).

According to Murray (1974), δ - MnO_2 has a pH(zpc) of around 2.25. Such a low value implies that, compared with most other metal oxides, MnO_2 is a relatively strong acid; which readily dissociates as:

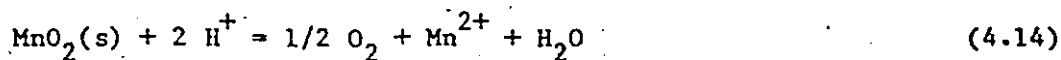


The equilibrium constant for the dissociation is:

$$K_{1,2} = \frac{[-Mn-O^- \text{ (surface)}]}{[-Mn-OH_2^+ \text{ (surface)}] \gamma^+} \cdot \left(\frac{\gamma^-}{\gamma^+}\right) \cdot \alpha [H^+]^2 \quad (4.13)$$

Its value is ca. $10^{-4.5}$ at pH(zpc) (Murray 1974).

It is generally accepted that H^+ and OH^- ions are potential determining for δ - MnO_2 but below pH 3.5, Mn^{2+} is released to the solution (Morgan and Stumm 1964) caused by the dissolution of MnO_2 , for which the following reaction is given by Morgan and Stumm (1965):



After $\text{H}^+/\text{Mn}^{2+}$ exchange, Mn^{2+} may be acting as a potential determining ion, and therefore the $\text{pH}(\text{zpc})$ is not entirely due to adsorbed H^+ ions at low pH.

Since the solubility of $\delta\text{-MnO}_2$ is very low (10^{-56}) at normal pH values, $\text{Mn}(\text{IV})$ solution species can be neglected.

In conclusion it can be said that, although some discrepancies do exist in the literature regarding the $\text{pH}(\text{zpc})$ for MnO_2 (see Table 3.3), the value can be assumed to lie between 1.4 and 4.5. This means that for pH values occurring in natural waters, the surface of colloidal hydrous manganese dioxides has a negative surface charge, which increases with pH.

In this study, the pH of zero point of charge was estimated for various MnO_2 's by determining the electrophoretic mobility of the particles at certain pH values in an electric field. The electrophoretic mobility (EM) is given by the relation (Riddick 1961):

$$\text{EM} = \frac{\epsilon \zeta E}{6\pi \eta} \cdot f \quad (4.15)$$

where EM/E = electrophoretic mobility per unit field strength ($\mu\text{cm}/\text{V}\cdot\text{sec}$)

E = electric field strength (V)

ϵ = dielectric constant of the medium (i.e. water)

η = dynamic viscosity of the medium Ns/m^2

f = factor depending on the shape and size of the particles as well as on the thickness of the electric double layer

ζ = zeta potential, located at a certain plane in the double layer (V)

By plotting the pH versus EM, one can approximate the value of the $pH(zpc)$, when no movement of the particles in the applied electric field is observed. Results are discussed in Section 4.4.

4.2.4 X-Ray Diffraction (XRD) Analysis

The basic structural hexagonal units of close-packed oxygen atoms, containing manganese in octahedral coordination can give rise to d-spacing values of around 2.40 - 2.45 Å and 1.40 - 1.42 Å for a number of MnO_x minerals, depending on the particle size of the oxides. Typically there are up to four d-spacing values reported for MnO_x with approximate values of 7.20 - 7.40 Å, 3.66 - 4.04 Å as well as the above given two d-spacing values. For very small particle sizes, coherent scattering of the X-rays is reduced, causing an amorphous appearance for minerals which in fact are crystalline (crypto-crystallinity). Table 3.3 summarizes a number of XRD analyses for $\delta-MnO_2$. In addition an example pattern (Buser et al. 1954) is given. It shows that with increasing value for x the basal reflections tend to gradually disappear. As a result of cryptocrystallinity, XRD analysis may not always be a suitable way to determine the identity of a particular manganese dioxide product under study. Electron Diffraction and Infrared Spectroscopy are alternatives.

In this research, XRD analysis was performed on most of the MnO_2 batches used. A range of $5^\circ < 2\theta < 60^\circ$ or $5^\circ < 2\theta < 85^\circ$ was scanned. (2θ is the irradiation angle) with $Cu/K2\alpha$ radiation. Results are given in Section 4.4.

4.2.5 Electron Microscopy

McMurdie (1944) was probably the first to use Electron Microscopy to study particle sizes and shapes of various natural and artificial MnO_2 's. The transformation of $\delta\text{-MnO}_2$ into cryptomelane upon aging and the importance of pH and K content in the samples has briefly been discussed in Chapter 3.

In this study TEM was used for two purposes. In the first place it was used to compare morphologies of differently prepared $\delta\text{-MnO}_2$ batches and to assess the accuracy of duplicated preparations of one particular $\delta\text{-MnO}_2$. Results are given in Section 4.4. In the second place TEM was used in a simulated aging study which had as objective to clarify the role of pH and K-content in the conversion of $\delta\text{-MnO}_2$ to cryptomelane. Results are presented in Section 4.6. A more detailed description of the findings of McMurdie (1944) and McKenzie (1971) is given here in addition to what was already mentioned in Chapter 3, to provide more comparison material for the results presented in Section 4.6.

McMurdie (1944) studied a number of synthetically prepared MnO_2 batches in relation to their shelf-life in dry-cell batteries. He found that samples which were identified by XRD and/or ED as $\delta\text{-MnO}_2$ could have vastly different morphologies as revealed by TEM analysis. However, treatment of these $\delta\text{-MnO}_2$'s in an autoclave at 150°C for three hours with NH_4Cl solution or on a steambath for 18 days resulted always in the formation of filamentous cryptomelane. A sample which upon XRD and ED analysis was identified as $\gamma\text{-MnO}_2$ (nsutite, which has a variable composition, see Table 3.1), also changed into cryptomelane. A sample containing two clearly distinguishable size fractions was identified via XRD and ED analysis as respectively pyrolusite and cryptomelane

(fine fraction). Heat treatment did not alter the appearance and identity of this sample.

McMurdie correlated these morphological characteristics to the reactivity of the forms of MnO_2 used for dry-cell battery production, but did not attempt to explain the mechanism for conversion into cryptomelane. He concluded that poorly crystallized materials such as γ or δ - MnO_2 were the most reactive initially, but would change to a less available form (cryptomelane) upon aging, negatively influencing the shelf-life of such batteries. More crystalline forms, such as cryptomelane and pyrolusite, are not as reactive initially as γ or δ - MnO_2 , but their capacity does not change much with aging, which implies that they have better shelf-life characteristics.

McKenzie (1971) investigated the conversion of birnessite ($=\delta$ - MnO_2) into cryptomelane. He used methods to prepare his samples comparable to some of the methods used in this study.

One sample (sample A) was prepared through adding concentrated HCl to a boiling solution of $KMnO_4$ which yielded a birnessite with 9.4% K.

Boiling for 24 hours did not change this sample, but when the K content was lowered to 5.1% by washing with dilute HCl, conversion to cryptomelane was easily obtained by boiling. Igniting the 9.4% K-birnessite at 400°C for 60 hours also converted the sample to cryptomelane. The morphology of this sample prior to conversion was vastly different from another sample (sample B) which was precipitated by bubbling O_2 through a suspension of manganese hydroxide in a solution of potassium hydroxide, yielding a product that was more difficult to convert to cryptomelane. Ignition resulted in a mixture of mainly cryptomelane and some birnessite, while boiling after acid washing, which lowered the K

content to 4%, yielded a mixture of mainly birnessite and some cryptomelane.

It is quite remarkable that McKenzie does not elaborate on the requirement, proposed by McMuride (1944), that the pH should be low in order to obtain a conversion to cryptomelane by heating. Acid washing was performed by McKenzie with the intention of decreasing the potassium content of the products to be converted. Since he does not report whether these conversions then also take place at low pH, it is not clear whether the pH or a particular K percentage, or both, control the conversion from birnessite (or $\delta\text{-MnO}_2$) to cryptomelane. How K could play a role in the conversion has been speculated upon by McKenzie, while the role of K in the stability of the cryptomelane structure has been explained by Byström and Byström (1950). This was discussed briefly in the previous Chapter in relation to the possible structure(s) of $\delta\text{-MnO}_2$.

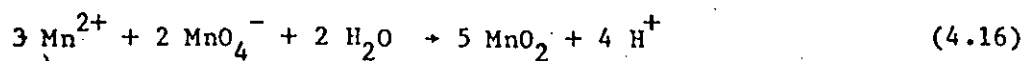
4.3 Preparation Methods Used in This Study

In order to investigate how important different preparation methods are for the ultimate properties of $\delta\text{-MnO}_2$ for use as a competing surface in trace metal speciation studies, several different batches were prepared and characterized for comparison. The preparation methods involved respectively a redox-reaction at neutral pH, a reduction at acid pH and an oxidation at alkaline pH. A number of other MnO_2 samples were included in this study. Two commercial MnO_2 samples were obtained from respectively Baker and Leco Chemical Companies. The Baker sample is true MnO_2 , or pyrolusite ($\beta\text{-MnO}_2$) according to Anderson et al. (1973). The Leco MnO_2 is especially

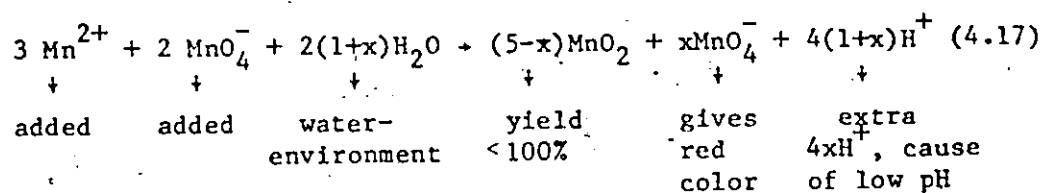
prepared for use in the Carbon/Sulphur Determinator by Leco Corporation, Michigan. The Leco MnO_2 is a highly efficient and speedy sulphur dioxide absorber from CO_2 gas, which evolves during organic carbon analysis. Two aged $\delta\text{-MnO}_2$ samples were included. A naturally aged $\delta\text{-MnO}_2$ was fortuitously available as a residue of van der Berg's (1979) work, while neutral MnO_2 , prepared for this research, was artificially aged by heat treatment in an autoclave (see Section 4.6).

All chemicals used in the fabrication of the $\delta\text{-MnO}_2$ batches were of reagent grade or better and all $\delta\text{-MnO}_2$ preparations aimed for a final concentration of 10^{-2} M MnO_2 , assuming a 100% yield. A detailed description of the above mentioned three recipes is given here.

The neutral recipe (adapted from van den Berg 1979) involves the following: 367 mg Mn metal (6.7×10^{-3} M) is dissolved in a minimum amount of conc. HNO_3 , diluted to a liter with deionized H_2O and neutralized with KOH. 632 mg KMnO_4 (0.4×10^{-2} M) and 450 mg KOH (0.8×10^{-2} M) are premixed in 100 mL deionized H_2O . To precipitate $\delta\text{-MnO}_2$, the 100 mL premixed solution is added rapidly, from a dripping buret, to 900 mL of the Mn^{2+} solution, under vigorously stirring on a magnetic stirrer, whilst keeping the pH constant manually by addition of small amounts of dilute HNO_3 or KOH. After adding the premix, the suspension is maintained at ca. pH 7.5 and stirred for an additional half hour. The $\delta\text{-MnO}_2$ suspension should actually not need pH correction, because stoichiometric amounts of base are used in the premix to counterbalance the evolving acid during the reaction. The equation for this redox reaction is



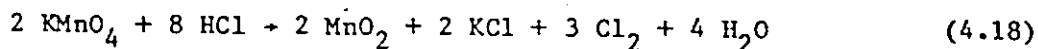
However, presumably due to an incomplete reaction, which manifests itself via an endproduct with pH 2-3, purple tinted from KMnO_4 residue, stoichiometric amounts of base added to the premix apparently cannot prevent a severe pH drop in the $\delta\text{-MnO}_2$ suspension, and pH correction during the precipitation reaction is necessary. This phenomenon was observed repeatedly in this research, while it was also noticed by van den Berg (pers. comm. 1981). A possible explanation can be obtained from the following reaction equation:



For $x = 1$, an eighty percent yield is obtained for MnO_2 and an extra $0.8 \times 10^{-2} \text{ M H}^+$ is formed which would result in a pH value of 2.1. Similarly, for $x = 1/2$ or $1/4$, respectively ninety and ninety-five percent yield is obtained for MnO_2 and the matching pH values are 2.4 and 2.7 respectively, when using the above equation. This coincides nicely with the observed pH when no correction is made. However, no yield measurements were done directly after the precipitation reaction to verify this explanation. It is also possible to imagine other explanations for evolving extra H^+ , but the evidence points in the direction of an incomplete reaction. The severe pH drop during the formation of $\delta\text{-MnO}_2$ should be avoided, because a neutrally formed MnO_2 is far more reactive according to Polissar (1935) (see Chapter 3). Therefore, pH correction is performed manually during the formation of the precipitate.

Once the precipitate is formed and stirred for an additional half hour at neutral pH, it is washed by centrifuging and resuspension in deionized H₂O. This cleaning procedure is followed by specific conductivity measurements in the resuspended δ-MnO₂ while the pH is maintained near neutral by adding dilute acid or base if necessary. The procedure is continued until the resuspended δ-MnO₂ displays a specific conductivity lower than that of a 10⁻⁴ M KCl solution, which generally requires three to four washings. During the purifying procedure, the very fine particle phase is lost (i.e. stays in the discarded supernatant) as a result of decreasing ionic strength which produces increasingly stable colloidal particles that cannot be centrifuged and are discarded with the supernatant. Reaction yield is measured after the washing procedure, by reducing a small amount of suspension with oxalic acid and measuring manganese by Atomic Absorption Spectrometry (A.A.). Overall yields are 70-85%, depending on the care taken during the cleaning process. Since the concentration of MnO₂ increased slightly with time, presumably through evaporation of water, A.A. measurements for Mn content were repeated every six to eight weeks. The δ-MnO₂ suspensions are stored in the dark at 4°C. The "neutral" procedure yielded δ-MnO₂'s III, VIb and XVc, all included in the comparison study.

The acid recipe (adapted from Healy et al. 1966) involves the following: approximately 1.8 g KMnO₄ (1.14 x 10⁻² M) and 3.4 mL conc. HCl (4 x 10⁻² M) (which means a slight stoichiometric excess of KMnO₄) are allowed to react in approximately 80 mL deionized H₂O. Attempts to perform the reaction at its dilute concentrations failed several times, presumably for kinetic reasons. The equation for this reaction is



The reaction, in concentrated form, is allowed to proceed for three hours and then diluted to one liter with deionized H_2O . The end-pH of the suspension is very low ($\text{pH} < 2.5$) and before starting the washing procedure, the suspension is titrated to pH 7 with KOH. Purification and storage are as described for the neutral recipe. The acid recipe yielded $\delta\text{-MnO}_2$ VIIIb for the comparison study.

The alkaline recipe (compare McKenzie 1971) involves the following: a mixture of 1.69 g $\text{MnSO}_4 \cdot \text{H}_2\text{O}$ (10^{-2} M) and 7.7 g KOH (0.138 M) in one liter deionized H_2O , is allowed to react in an ice-water bath for 4 1/2 hours while O_2 is bubbled through the suspension, causing an oxidation of Mn^{2+} to Mn^{4+} . The pH of the resulting $\delta\text{-MnO}_2$ suspension is > 13 and even after washing once, remains very high. After titrating the pH of the suspension down to neutral with HNO_3 , the purifying procedure is continued as described for the neutral recipe. This procedure yielded MnO_2 VIIb for the comparison study.

The commercial MnO_2 samples included in this comparison study are already described above. The naturally aged MnO_2 13 is a remnant of van den Berg's (1979) research, which was prepared according to his version of the neutral recipe. It was three to four years old at the time of this study. The artificially aged MnO_2 XXV-A is a sample prepared according to the neutral recipe as used in this study, with the exception that the washing procedure after precipitation was omitted, while the pH of the endsuspension was lowered to pH 2.2 with conc. HNO_3 . This sample was, to simulate the aging process, subjected to 120°C in an autoclave for three hours (at a pressure of ca. 1.4 kg/cm^2), after which

it was washed and stored as described above.

4.4 Results and Discussion of the Comparative Study

Oxidation states (x in MnO_x), percentages K and H_2O , XRD patterns and $pH(zpc)$ data are summarized in Table 4.1. Figures 4.1 and 4.2, respectively present the TGA data and the adsorption isotherms for Cu at pH 6. Figures 4.3 and 4.4 show the $pH(zpc)$ for several MnO_2 samples. Figures 4.5-4.11 show the TEM images of the δ - MnO_2 samples. Figures 4-12 and 4-13 illustrate the relationships between adsorption capacity and K and H_2O - content, respectively, of the δ - MnO_2 samples.

4.4.1 Oxidation States of the MnO_2 's

The values for x , shown in Table 4.1 are averages of at least two determinations. Typical standard deviations range from 0.01 to 0.06. The data for %K and H_2O are unique measurements on aliquots of MnO_2 samples that were filtered to dryness through a 0.45 μ Millipore membrane for the K determinations, or dried at ca. 100°C for the H_2O determinations. The values for x that are not corrected for K and H_2O content of the dried MnO_2 powders are too low compared to literature data. This suggested that either the arsenic method was at fault, or that the drying procedure of the MnO_2 samples prior to analysis created artifacts. The effectiveness of the arsenic method was established by analyzing the true MnO_2 sample (Baker). The value for x obtained for this sample was 1.99. A comparison was made between a drying procedure to constant weight in an oven at ca. 100°C and in a desiccator over $CaCl_2$ and H_2SO_4 . Results were virtually the same for both oven and desiccator dried samples, ruling out any disturbing effects that the high

Table 4.1 Characteristics for various differently prepared (δ -)MnO₂ surfaces

MnO ₂	precipitation method	x (not corr. for K & H ₂ O content) for K & H ₂ O assuming all Mn = MnO ₂ content)	K (% weight)	H ₂ O (% weight) from TGA at 100-350°C	x (corr. for K & H ₂ O content)	XRD for pattern	pH (zpc)
III	neutral	1.66	10.9	17.6	1.98	amorphous	1.7
VIb	neutral	1.72	10.1	10.8	1.96	amorphous	1.7
XVc	neutral	1.71	10.0	11.2	1.94	amorphous	n.m.
VIIb	alkaline	1.59	1.5	0	1.60	4.55 Å (MnSO ₄ ·H ₂ O)	1.5
VIIIb	acid	1.70	13.4	10.5	1.97	amorphous	n.m.
Baker	purchased	1.99	0 (according to specifications of manufacturer)	0	1.99	6.97 Å 4.13 Å 3.09 Å 2.39 Å 1.62 Å	n.m.
Leco	purchased	1.86	n.m.	0	n.m.	7.15 Å	n.m.
van den Berg 13	neutral*, naturally-aged	1.72	<4.9**	8.6	1.85	amorphous	n.m.
XXV-A	neutral, not washed, 3 hrs autoclaved	1.65	1.6	0	1.66	amorphous	n.m.

* = neutral method according to van den Berg (1979) ** = K measured in solid + liquid, n.m. = not measured

temperature in the oven may have had on the oxidation state of MnO_2 samples. Another possible cause for the too low values for x was K and/or H_2O content in the dried MnO_2 samples (see also Section 4.3.1). Measurements showed that the MnO_2 samples indeed contained certain amounts of K and H_2O .

As shown in Table 4.1, the values for x are, after correction for K and H_2O content, very similar to reported literature values, and agree closely for the neutral (III, VIb and Xvc) and acid (VIIb) samples. No correction for Mn^{2+} could be made, because ESR results failed to indicate any presence of Mn^{2+} in the dried $\delta\text{-MnO}_2$ samples. The corrections for K and H_2O content may not have been totally accurate for several reasons. The K content was determined along with Mn in a filtered volume sample of MnO_2 , while x was determined on a dry weight basis. Therefore, the K content (weight %) could only be calculated relative to Mn content, assuming that all Mn measured was in the MnO_2 form. This is only approximately true, a small amount of Mn is presumably present as Mn^{2+} , Mn^{3+} , $\text{Mn}(\text{OH})_2$ or MnO (see Chapter 3), although this could not be confirmed by ESR measurements. The calculated K content could, because of this, be slightly low. On the other hand, TGA was performed on the MnO_2 samples after they were dried at $\sim 100^\circ\text{C}$, some time (weeks) prior to TGA. Although the dry powders were stored in tightly capped glass vials, some moisture might have readsorbed prior to TGA, which then implies an overestimation of the percentage weightloss due to H_2O between approximately 100° and 350°C . This seems to have been the case for MnO_2 III (neutral) (H_2O content = 17.6%).

The alkaline MnO_2 VIIb has a much lower x value and since this sample scores significantly lower in K content and loses no weight (i.e.,

water) between 100 and 350°C, correction has virtually no influence on the value for x.

The naturally- and artificially- aged (neutral) MnO_2 (van den Berg 13; XXV-A) differ, both from each other and the fresh, neutral MnO_2 samples, with respect to x, K and H_2O content. The naturally aged sample contains only about half of the K compared to the fresh samples, while the H_2O content and the value for x are also lower. The heat treated sample has a low value for x, contains very little K, and has no easily removed H_2O . In this respect, it is very similar to the alkaline MnO_2 VIIb.

The Baker sample is pure MnO_2 (x = 1.99), contains no K according to manufacturers specifications and contains no water. The Leco sample has a value for x of 1.85, but no measurement for K content was performed.

4.4.1.1 TGA Results

The TGA results, shown in Figure 4.1, have already been discussed partly, in relation to the oxidation state.

TGA records the loss in weight with increasing temperature, due to dehydration or decomposition. Changes in weight are a result of the disruption and/or formation of various physical and chemical bonds at elevated temperatures, which leads to evolution of volatile products or formation of heavier reaction products. Any transition which a sample undergoes will result in liberation or absorption of energy by the sample (Willard et al. 1971). Differential Thermal Analysis (DTA) records the shift in energy by recording the temperature difference between the sample and a thermally inert reference material. The

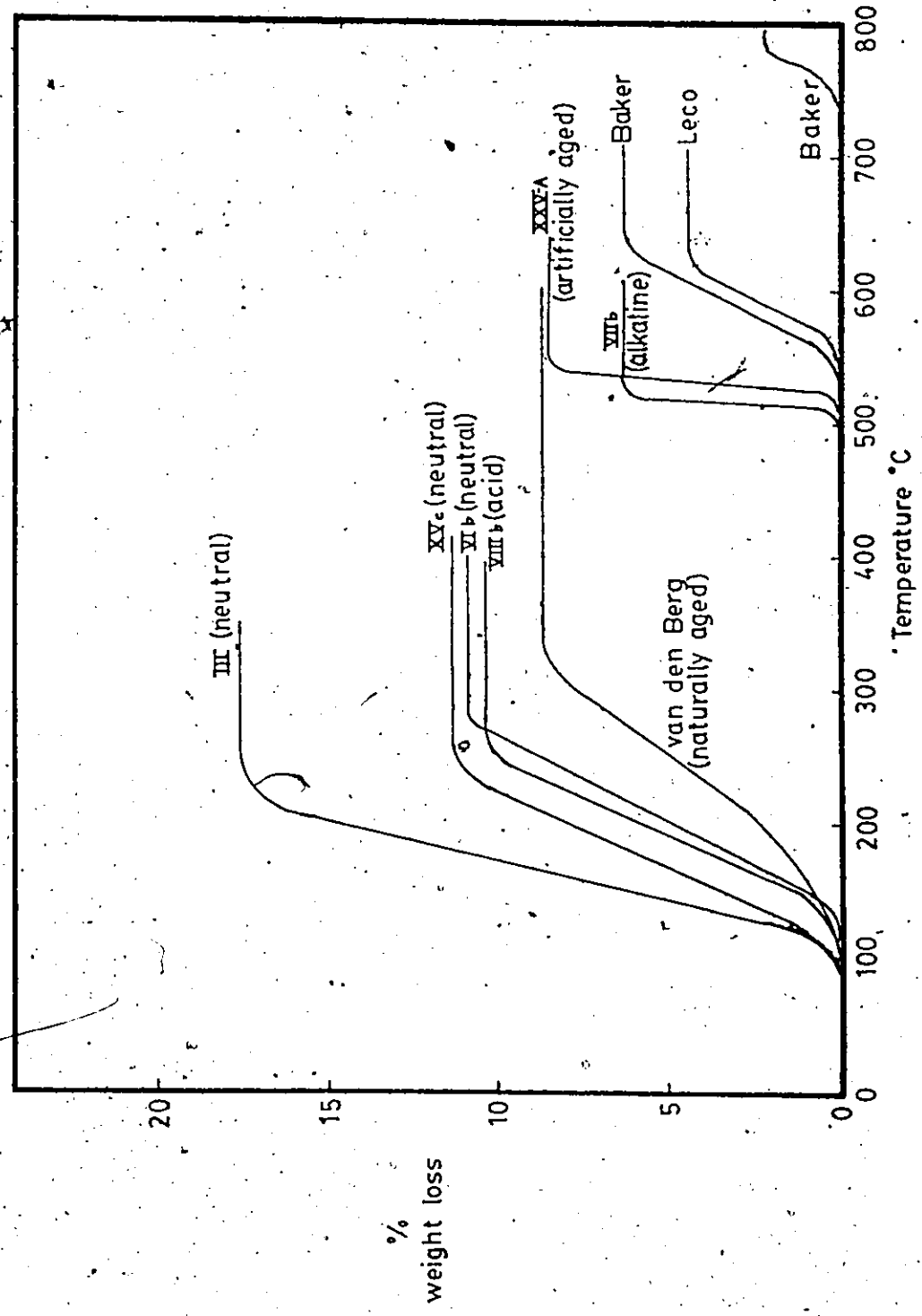
resulting differential temperature discloses at which temperature transitions occur and whether they are exo- or endo-thermic. Exothermic reactions involve (re)crystallization, oxidation or decomposition, while endothermic reactions include phase transitions and dehydration.

Thermal analyses are affected by experimental conditions, such as rate of heating, sample weight, etc. Apparently, the optimum conditions for DTA and TGA do not always coincide. It is also necessary to analyze the volatile reaction products to correctly assess the chemical or physical changes that take place.

For this study, the TGA and DTA results were obtained with a Nertzsch STA-409 Differential Thermal Analyzer. The rate of heating was 10°C/min. (starting just below 100°C) and was kept constant throughout all analyses. The samples were dried at ca. 100°C several weeks prior to DTA analysis and stored in glass vials. The sample weight varied for each analysis (due to lack of large amounts of dried δ -MnO₂), which could have caused some minor differences between the results for the samples. Unfortunately the DTA trace on the analyzer output was of very poor quality during analysis of the δ -MnO₂ samples. A badly drifting baseline prevented firm conclusions concerning the exo- or endo-thermic character of the losses for most analyses.

Figure 4.1 shows that weight loss in the region 100°C-350°C is very similar for the neutral and acid samples. Heating beyond 600°C did not result in any further weight loss. The naturally aged sample undergoes a more gradual weight loss but also obtains constant weight in the region 100°C - 350°C. Weight losses in this temperature range are most likely due to loss of structural water. Samples VIIb (alkaline) and XXV- A (artificially aged) undergo a sudden loss in weight around 500°C,

Figure 4.1 TGA analysis for various MnO₂'s. The right extent of each line indicates maximum temperature to which each sample was heated.



which could indicate decomposition. The highly crystalline Baker MnO_2 and the partly crystalline Leco sample finally undergo a more gradual weight loss between 550° and 650°C , possibly indicating decomposition or phase transition.

4.4.2 Surface Area Determinations

Surface area determinations were performed on a relative basis via adsorption capacity measurements. The adsorption behaviour for Cu at pH 6 is shown in Figure 4.2. The neutral and acid samples have a very similar adsorption capacity ($\mu\text{M Cu}/\mu\text{M MnO}_2$), while the naturally aged sample (MnO_2 13), MnO_2 VIIb, the artificially aged MnO_2 XXV-A and the Baker sample have increasingly lower adsorption capacities for Cu at pH 6. The same trend was observed at pH's 7 and 8 (see Chapter 7). For the Leco sample no adsorption data were obtained. Maximum adsorption capacities (Γ_{max}) are read from Figure 4.2, and can be used to calculate a relative surface area. For this, one has to assume that the Γ_{max} value represents a monolayer coverage of Cu. The radius of the adsorbing Cu ion can be assumed to be either $r_{\text{Cu}^{2+}}^{\text{ads}} = r_{\text{Cu}^{2+}} + r_{\text{H}_2\text{O}}$ or $r_{\text{Cu}^{2+}} + 2r_{\text{H}_2\text{O}}$. Table 4.2 gives results for both possibilities.

These results suggest that the assumption that the Cu^{2+} ion retains only its inner hydration sphere when adsorbing, leads to somewhat underestimated surface areas compared to the value of $300 \text{ m}^2/\text{g}$ generally quoted (see Table 3.3). On the other hand, the assumption that the Cu^{2+} ion retains both inner and outer hydration spheres when adsorbing leads to grossly overestimated surface areas. It is obvious that both the artificially aged MnO_2 XXV-A and the commercial Baker sample have surface areas far too low to qualify for $\delta\text{-MnO}_2$ characteristics. The surface

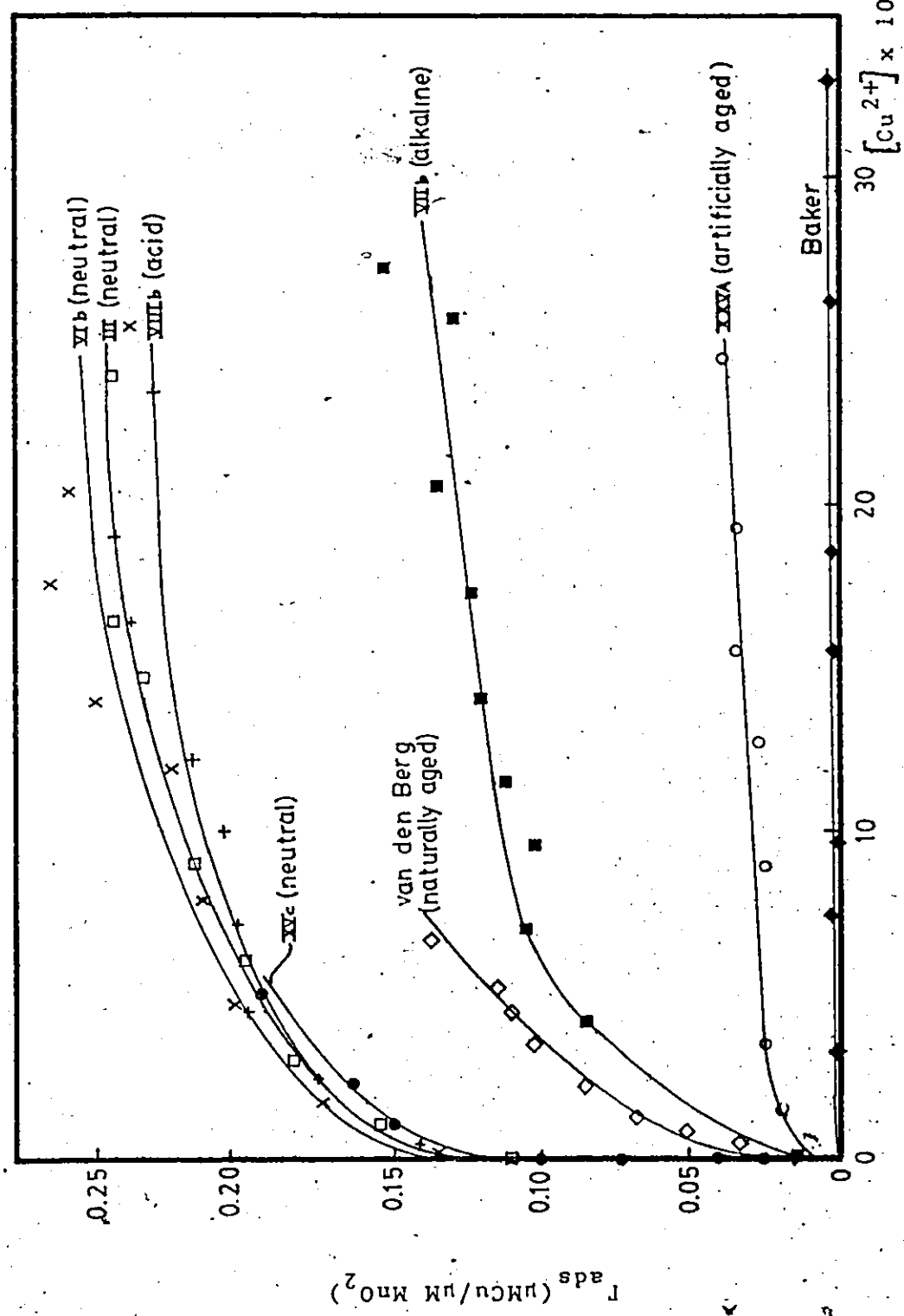


Figure 4.2 Adsorption isotherms for Cu on various MnO_2 's at pH 6.0, I = 0.01N KNO_3

\square III (neutral) \times VIIb (neutral) \square VIIIc (neutral) \times VIIIb (acid)
 \bullet van den Berg (naturally aged) \blacksquare VIIb (alkaline) \blacklozenge Baker
 \circ XXV-A (artificially aged, i.e. heat treated)

Table 4.2 Calculated surface areas for MnO₂'s

MnO ₂	r_{max} ($\mu\text{M Cu}/\mu\text{M MnO}_2$)	$r_{\text{Cu}^{2+ \text{ ads}}} = r_{\text{Cu}^{2+}} + r_{\text{H}_2\text{O}}$	surface area (m^2/g)	$r_{\text{Cu}^{2+ \text{ ads}}} = r_{\text{Cu}^{2+}} + 2r_{\text{H}_2\text{O}}$
III	0.240	235	640	
VIb	0.260	254	693	
XVc	0.192	188	512	
VIIb	0.148	145	395	
VIIIb	0.230	225	613	
van den Berg 13	0.150	146	400	
XXV-A	0.038	37	101	
Baker	0.002	2	5	

areas of the other MnO_2 samples all lie within a factor 2 of the generally reported value of $300 \text{ m}^2/\text{g}$ for $\delta\text{-MnO}_2$. More discussion regarding the relationship between surface area, adsorption capacity and percentages water and potassium is given in Section 4.4.6.

4.4.3 The pH of Zero Point of Charge

The pH of zero point of charge for various MnO_2 samples was determined by measuring the electrophoretic mobility of the particles at various pH values in an electric field, with a Zeta meter. The measurements were performed in a plexiglass cell. After filling this cell with a MnO_2 -suspension of known pH, an electric field is switched on and the rate and direction of movement of the MnO_2 particles observed through a microscope. After repeating this measurement a number of times at different pH values, the electrophoretic mobility (EM, in $\mu \text{ cm}/\text{V}\cdot\text{sec}$) can be plotted versus the pH and the $\text{pH}(\text{zpc})$ can be obtained by extrapolation to $\text{EM}=0$ (no movement). No buffer was used and no flow-through pump mechanism was available. Therefore, a sharp drop in the pH of the sample during the measurements due to electrolysis of water, could not be avoided.

Only a few reasonably accurate sets of data were obtained, and the resulting $\text{pH}(\text{zpc})$ values have been included in Table 4.1. Two sets of measurements (Figure 4.3) refer only to the pH before the electric field was applied. The third set of electrophoretic mobility data (Figure 4.4) is plotted versus the pH values observed before and after the electric field was applied.

Figure 4.3 shows good agreement between the MnO_2 's III and VIb, both prepared according to the "neutral" recipe. The $\text{pH}(\text{zpc})$ for both

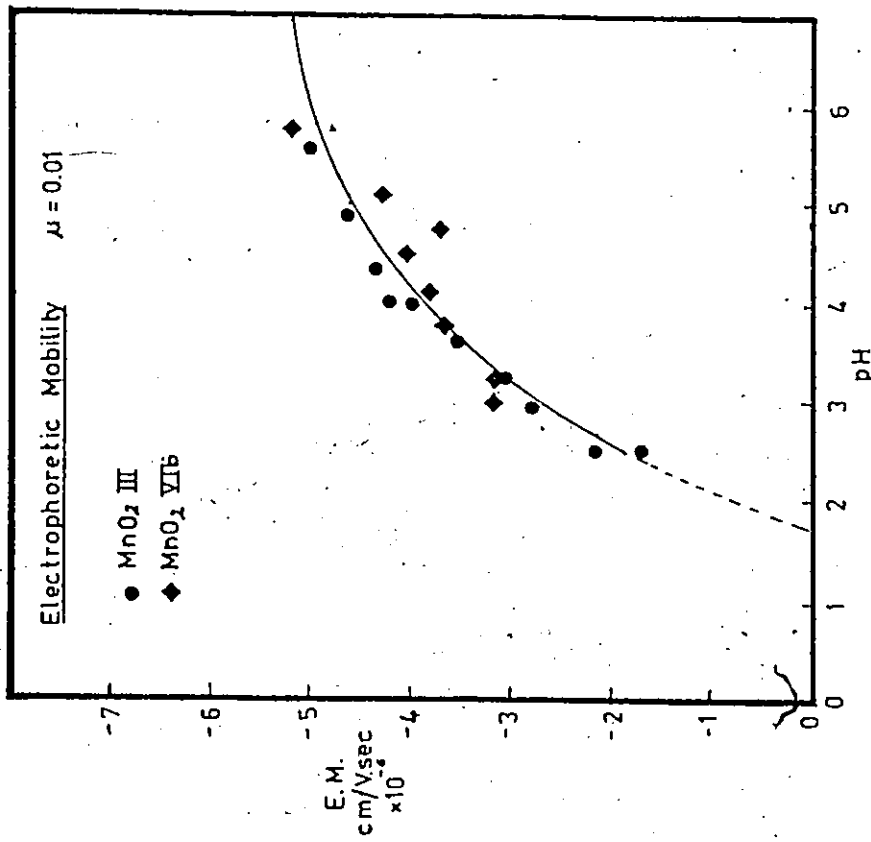


Figure 4.3 Electrophoretic mobility versus pH for MnO_2 's III and VIIb. pH measured before application of electric field only.

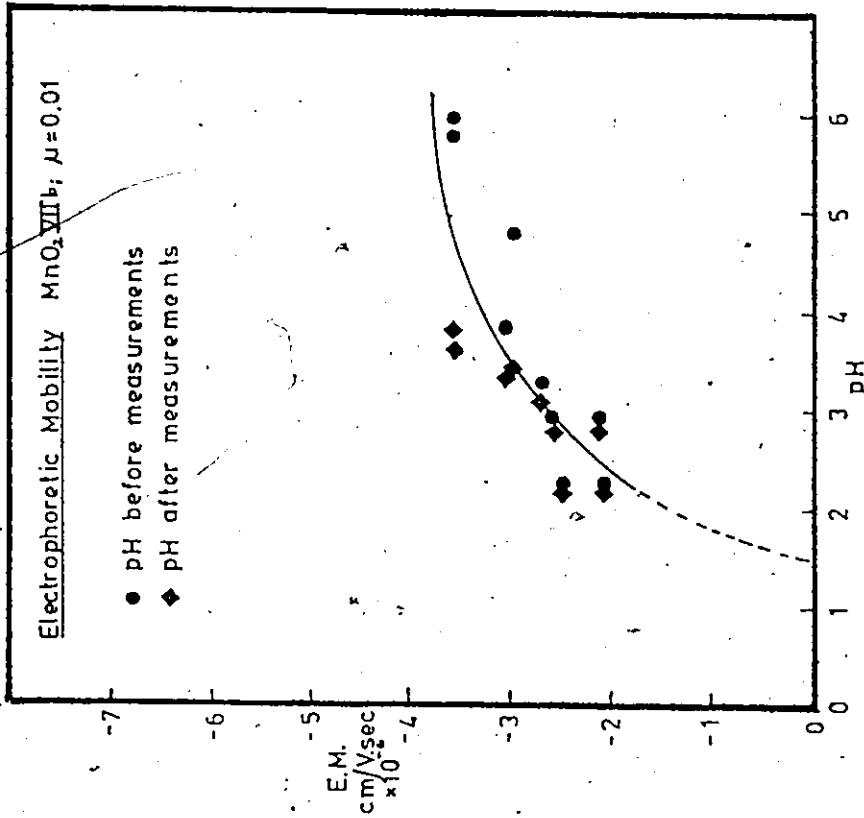


Figure 4.4 Electrophoretic mobility versus pH for MnO_2 VIIb. pH measured before and after application of electric field.

MnO₂ III and VIb as obtained by graphical extrapolation lies around pH 1.7 which compares favourably with literature data for δ-MnO₂, which vary from 1.5 to 2.8 (see Table 3.3). Figure 4.4 shows electrophoretic mobility data for MnO₂ VIIb, the "alkaline" sample plotted versus the pH values observed before and after the application of the electric field. The shift in pH is not always the same and depends obviously on the starting pH and electrophoresis time. The graphically obtained pH(zpc) for MnO₂ VIIb lies around pH 1.5. However, due to the obvious scatter of data points it would be better to conclude that the pH(zpc) lies between pH 1 and 2, which still compares fairly well with literature data. This implies that also the pH(zpc) obtained for MnO₂ III and VIb lies in the range 1-2, rather than "exactly" at pH 1.7. Another possible conclusion is that the pH(zpc) as obtained by the described method is not accurate enough to differentiate between MnO₂'s with slightly different values for pH(zpc). However, in comparison with the range of literature data for pH(zpc) given for δ-MnO₂ ($1.5 \leq \text{pH(zpc)} \leq 2.8$) it appears that MnO₂'s III, VIb and VIIb all qualify for the name δ-MnO₂. The other MnO₂'s included in this study were not analyzed for pH(zpc).

4.4.4 X-Ray Diffraction Results

X-Ray Diffraction results are largely non-informative. For all but three samples in this study, a completely amorphous XRD pattern was obtained. Of the prepared MnO₂'s included in Table 4.1, only MnO₂ VIIb (the alkaline sample) showed one peak in the XRD pattern, at a d-spacing of 4.55Å. This peak was identified as representative of MnSO₄·H₂O, one of the ingredients for the fabrication of this sample. This indicates that not all of the MnSO₄·H₂O used had been fully dissolved during the

precipitation of this sample with O_2 and that the washing procedure failed to remove the residue. XRD-analysis one year later on the same sample showed no peak at all, indicating that the $MnSO_4 \cdot H_2O$ residue had slowly dissolved with time. The other two samples showing distinct patterns were the commercial MnO_2 samples. The Baker MnO_2 showed the MnO_2 standard peaks at d-spacings of around 7.0, 4.2, 2.4 and 1.4 Å, while Leco MnO_2 showed one peak at a d spacing of 7.15 Å.

The Electron Microscopy study (described in Section 4.4.5) revealed that all samples included in this study had very small particle sizes. This probably caused cryptocrystallinity effects, which by some researchers is regarded as the reason for not obtaining characteristic XRD patterns. However, other researchers do not regard particle size as critical in obtaining an XRD pattern, but rather look at the layered structure of the more highly oxidized samples as the cause for amorphous XRD patterns. This was discussed previously in Chapter 3 (Section 3.4). In Section 4.4.6 the amorphous character of the samples in this study is discussed in relation to H_2O content. None of the samples qualifies for the name δ - MnO_2 based on the obtained XRD patterns, unless amorphous XRD patterns are accepted as characteristic for δ - MnO_2 .

4.4.5 Transmission Electron Microscopy Results

Figures 4.5-4.11 show the TEM morphology of the MnO_2 samples at various magnifications. The three neutral MnO_2 's III, VIb and XVC (Figure 4.5) all consist of uniform, very small round (or maybe hexagonal) particles (diameter $\approx 0.01 - 0.02 \mu m$), providing these samples with a large surface area. Such appearance does not resemble the TEM image given by McMurdie (1944) for δ - MnO_2 . A three hour autoclaving procedure, to simulate aging, had no effect on the morphology of these neutral

samples (see Section 4.6).

The acid sample MnO_2 VIIIb (Figure 4.6) consists of very thin, overlapping sheets, resembling flower petals, with an appearance of short fibres when "rolled up". The surface area of such thin sheets can be expected to be large. This acid MnO_2 VIIIb resembles McKenzies (1971) similarly prepared sample A, although McKenzie describes its appearance as fibrous. Autoclaving sample VIIIb does not change its morphology, unlike McKenzie's sample A, which apparently changed to filamentous cryptomelane upon boiling (see Section 4.2.5).

The alkaline MnO_2 VIIb (Figure 4.7) consists of relatively large, roundish particles (0.03 - 0.08 μm in diameter) vaguely resembling McKenzies (1971) sample B. It also contains very large crystals (0.25 - 0.35 μm in diam.) which are probably the undissolved $\text{MnSO}_4 \cdot \text{H}_2\text{O}$.

However, although in the XRD pattern the $\text{MnSO}_4 \cdot \text{H}_2\text{O}$ peak disappeared with time, the large crystals were still present in the TEM picture after a year. Autoclaving this sample turns it into a mixture of fibres and round particles, virtually identical to McKenzies heat-treated sample B, who identified the fibres and particles as respectively cryptomelane and birnessite.

The naturally aged MnO_2 13 sample (van den Berg) (Figure 4.8) consists of very thin, long fibres (diam. $\sim 0.01 \mu\text{m}$), a total change from the fresh neutral samples. Its appearance compares well with McMurdies (1944) heat-treated $\delta\text{-MnO}_2$. It should be mentioned here that the original TEM appearance of the naturally aged sample is not known and was not necessarily identical to one of the fresh neutral MnO_2 's (shown in Figure 4.5). XRD could not identify the naturally aged sample as cryptomelane, although both McMurdie (1944) and McKenzie (1971) recognized

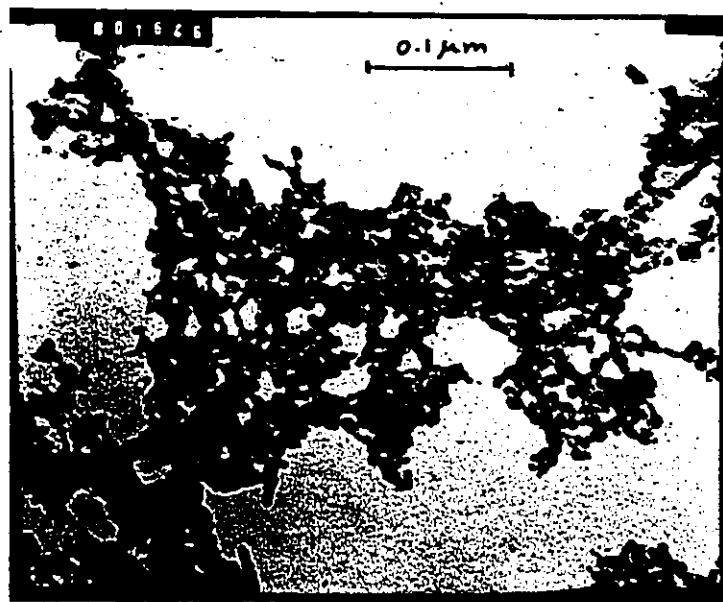


Figure 4.5 TEM appearance of δ -MnO₂'s : III, VIb and XVe (neutral).



Figure 4.6 TEM appearance of δ -MnO₂ VIIb (acid).

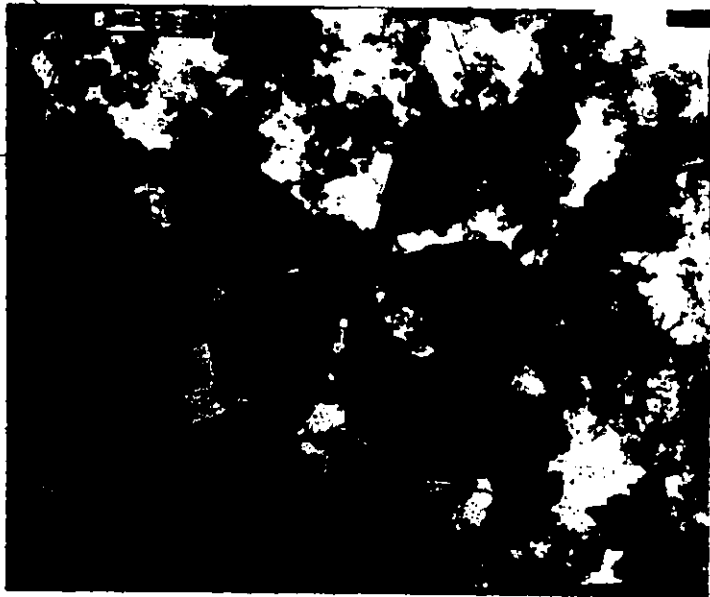


Figure 4.7 TEM appearance of $\delta\text{-MnO}_2$ VIIb (alkaline).

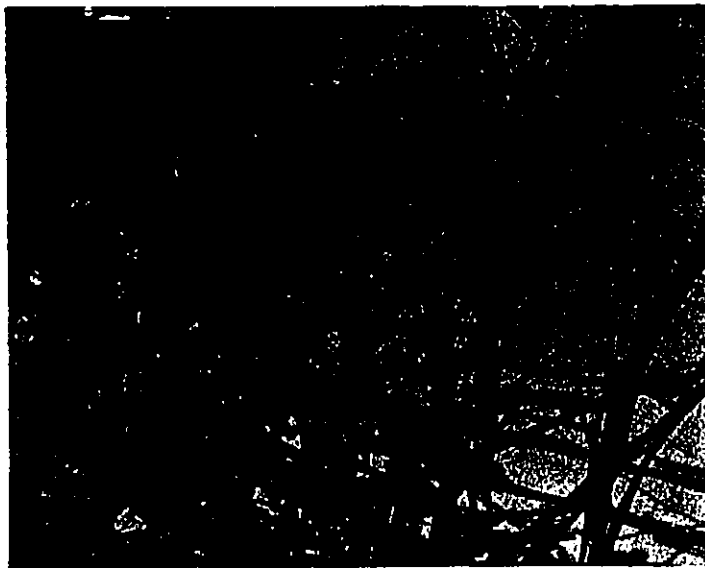


Figure 4.8 TEM appearance of MnO_2 13 (van den Berg, naturally aged).

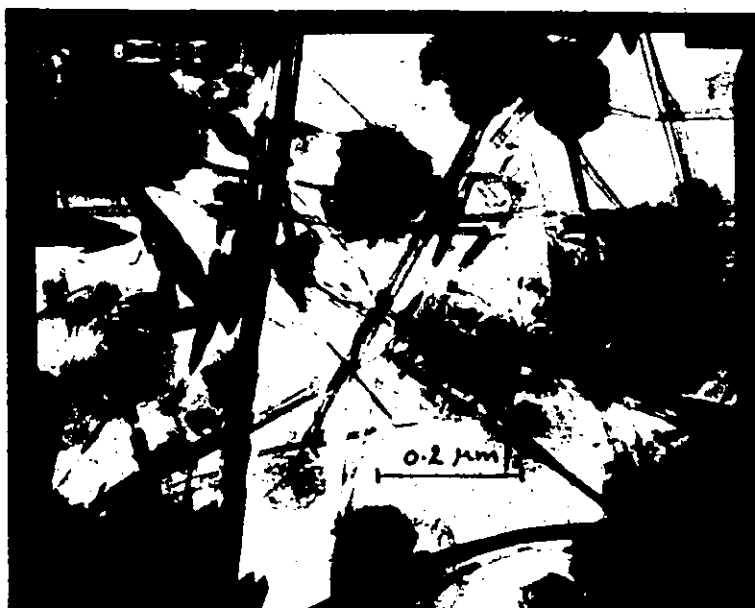


Figure 4.9 TEM appearance of MnO_2 XXV-A (artificially aged by heat treatment in autoclave).

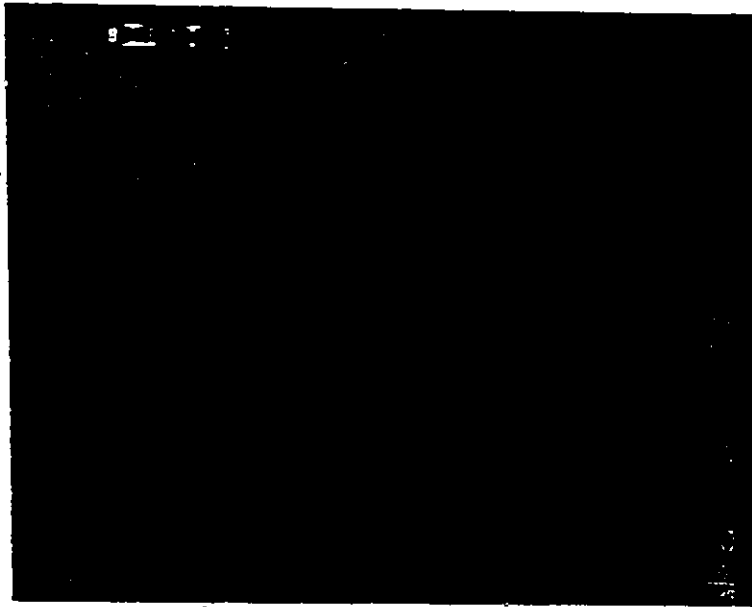


Figure 4.10 TEM appearance of Baker MnO₂ (commercial).

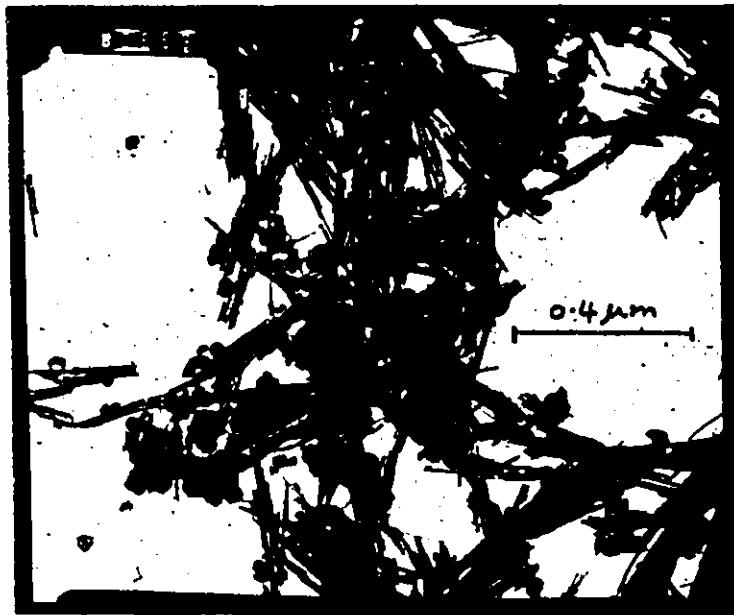


Figure 4.11 TEM appearance of Leco MnO₂ (commercial).

their heattreated samples as cryptomelane.

The heattreated (i.e. artificially aged) MnO_2 XXV-A (Figure 4.9) consists of a mixture of oblong shapes ($0.15 \mu m$ by $0.03 \mu m$), large hexagonal particles (diam. = $0.1 - 0.3 \mu m$) and long fibres (diam. = $0.015 - 0.05 \mu m$), unlike anything reported in the literature.

The Baker sample (Figure 4.10) consists of small shapes, resembling hexagonal particles in a wide variety of sizes ($0.01 - 0.05 \mu m$ in diam.), but clearly has a smaller surface area than the neutral samples.

The Leco sample (Figure 4.11) is a mixture of fibres (diam. = $0.03 - 0.04 \mu m$) and round or hexagonal particles (diam. = $0.01 - 0.02 \mu m$).

From comparison with the descriptions given by McMurdie (1944) and McKenzie (1971), no conclusions regarding the neutral samples qualifying for the name $\delta-MnO_2$, can be drawn, because neither of these authors used the neutral recipe to prepare $\delta-MnO_2$. The acid sample is $\delta-MnO_2$, while the alkaline sample is likely $\delta-MnO_2$. The naturally aged sample is cryptomelane according to its appearance. The other samples have either a mixed morphology and/or are not described by McMurdie or McKenzie.

4.4.6 Discussion of the Relationships Between Characteristics for $\delta-MnO_2$

4.4.6.1 Identification of $\delta-MnO_2$

In Table 4.3 the positive identification, as $\delta-MnO_2$, of the sample included in this study, is illustrated. Three positive characteristics out of five, and no negative ones, is proposed as a criterion for a positive identification. A negative characteristic, combined with three positive ones, is taken as doubtful, while anything less than three positive characteristics and more than one negative is taken as negative.

identification. Table 4.3 shows that the neutral MnO_2 's (III, VIb and XVC) and the acid MnO_2 (VIIb) are $\delta\text{-MnO}_2$, while the alkaline sample (VIIb) is perhaps $\delta\text{-MnO}_2$. The other samples are definitely not $\delta\text{-MnO}_2$. The following conclusions can be drawn regarding the three tested recipes for $\delta\text{-MnO}_2$. The Guyard reaction and reduction of Mn^{7+} yield $\delta\text{-MnO}_2$'s (III, VIb, XVC and VIIb) with conventional characteristics in agreement with literature data. TEM revealed striking differences in morphology for these otherwise so similar samples. Three repeats of the neutral recipe yielded samples that were virtually identical on all points of comparison. The alkaline MnO_2 VIIb, a product of the alkaline recipe, did not agree on all points with literature characteristics for $\delta\text{-MnO}_2$.

4.4.6.2 The Relationship Between Adsorption Capacity and Surface Area

Gray and Malati (1979a,b) found that the adsorption capacity of $\delta\text{-MnO}_2$ increased in the series: $\text{Ni}^{2+} < \text{Co}^{2+} < \text{Cd}^{2+} = \text{Zn}^{2+} < \text{Mn}^{2+}$. They tentatively used hydration enthalpies to estimate ionic radii and found that the above sequence coincides with a decrease in adsorption radius. Murray (1975a) and Murray (1975b) used the assumptions of $r_{\text{hydr.}} = r_{\text{cryst.}} + 2r_{\text{H}_2\text{O}}$ (inner and outer hydration sphere) respectively $r_{\text{hydr.}} = r_{\text{cryst.}} + r_{\text{H}_2\text{O}}$ (inner hydration sphere) to explain adsorption results on hydrous manganese dioxide. Gray and Malati (1979a,b) quoting Stern and Amis (1959), argued that Murray's assumptions produce values for $r_{\text{hydr.}}$ that disagree with some physical measurements. However, although their found adsorption order coincided with the calculated hydration radii, Gray and Malati (1979a,b) admitted that their calculation procedure involving hydration enthalpies might not be entirely correct.

Murray (1975b) investigated Co adsorption on hydrous manganese dioxide and found adsorption to plateau at a monolayer value greater than

Table 4.3 Identification of δ -MnO₂

+ = positive characteristic ? = doubtful characteristic
 - = negative characteristic x = not determined

MnO ₂	preparation method	characteristics				6-MnO ₂
		O ₂ number	surface area	pH (zpc)	XRD morphology	
III	neutral	+	+	+	?	yes
VIB	neutral	+	+	+	?	yes
XVC	neutral	+	+	x	?	yes
VIIB	alkaline	-	+	+	?	?
VIIIB	acid	+	+	x	?	yes
van den Berg 13	neutral, naturally aged	+	+	x	?	no
XXV-A	neutral, artificially aged	-	-	x	?	no
Baker	commercial	+	-	x	+	no
Leco	commercial	+	x	x	?	most likely no

what can be calculated assuming that Co ions retain their inner hydration sphere. This could indicate that, when specific adsorption occurs on hydrous manganese dioxide, the Co ions are not necessarily separated from the surface by a layer of water molecules, as found by James and Healy (1972) for Co on SiO_2 and TiO_2 . It could also mean that the assumption of $r_{\text{hydr.}} = r_{\text{cryst.}} + r_{\text{H}_2\text{O}}$ is incorrect, or alternatively that the surface area is under-estimated by whatever method was used to determine it, as was suggested by Davis (1978).

Anderson et al. (1973) concluded that the adsorption maxima for Ag adsorption on various types of poorly crystallized MnO_2 are not directly related to the amount of surface area available (in fact, there appears to be almost an inverse relation to surface area, but this is believed to be coincidental by these authors).

The surface areas calculated in this study (Section 4.4.2) indicate that, if the BET value of $300 \text{ m}^2/\text{g}$ quoted in the literature for $\delta\text{-MnO}_2$ can be trusted, Cu^{2+} ions retain at least their inner hydration sphere and maybe part of their outer hydration sphere. However, calculating surface areas from adsorption capacities necessarily assumes a positive relationship between surface area and capacity. According to Anderson et al. (1973), this is not necessarily the case. From Figures 4.5 to 4.11 an independent comparison of relative surface areas can be obtained: The order of decreasing surface areas is $\text{III} = \text{VIb} = \text{XV}_c \geq \text{VIIIb} > \text{van den Berg 13} \geq \text{VIIb} > \text{XXV-A} \geq \text{Baker} \geq \text{Leco}$.

From Figure 4.2, the order of decreasing adsorption capacity can be established as: $\text{III} = \text{VIb} = \text{XVc} = \text{VIIIb} > \text{van den Berg 13} > \text{VIIb} > \text{XXVA} \rightarrow \text{Baker}$.

These two orders follow each other closely which implies that

there is a positive correlation between surface area and adsorption capacity for Cu on δ -MnO₂.

4.4.6.3 The Correlation Between Adsorption Capacity and Percentages

K and H₂O in the Solid of MnO₂ Samples

Anderson et al. (1973) found that there is a positive relationship between the amount of foreign ions contained in the MnO₂ samples, and the amount of Ag⁺ they are able to adsorb. They proposed both surface exchange with Mn²⁺, K⁺ and Na⁺, as well as exchange with structural Mn²⁺, K⁺ and Na⁺ as mechanisms for the uptake of Ag by hydrous MnO₂. Loganathan and Bureau (1973) also proposed an adsorption model, wherein Mn is displaced from structural positions in MnO₂ by adsorbing ions (Co and Zn). The model is based on the fact that during adsorption of Na⁺, K⁺ or Ca²⁺ on δ -MnO₂ no detectable Mn was found in the solution phase, while during adsorption of Co²⁺ and Zn²⁺, Mn would appear in solution. Co released more Mn than Zn, which they explain with Crystal Field Stabilization Energy (CFSE).

In this study, the possibilities for exchange of Cu²⁺ with Mn²⁺ and/or K⁺ from the imperfect layers between the true MnO₂ layers or from surface sites, needs to be considered. However, Mn²⁺ could not be detected by A.A. in solution after adsorption of Cu²⁺ (see also Chapter 6). Release of K⁺ upon Cu²⁺ adsorption could not be measured due to the fact that the adsorption studies were carried out in 0.01 N KNO₃. Nevertheless, if adsorption would take place as exchange with both surface and structural K⁺, a positive correlation between adsorption capacity and %K should indicate this. Both K⁺ and Mn²⁺ apparently lodge in imperfect layers between true MnO₂ layers, containing water. Therefore, there may also be a positive correlation between %water and

adsorption capacity.

In Figure 4.12, Γ_{\max} is plotted versus percentage K (from Table 4.1), while in Figure 4.13, Γ_{\max} is plotted against the amount of weight (i.e. water) removed between 100° and 350°C. The linear least squares lines through these points have a correlation coefficient of respectively $R = 0.745$ and $R = 0.712$. One can speculate about the implications of these correlations for the adsorption mechanism. The question is, where in the $\delta\text{-MnO}_2$ structure are these H_2O molecules and K ions located? It was previously discussed how ordered layers of MnO_2 octahedra are interspersed with disordered layers, which presumably contain an array of foreign ions and water. Posselt et al. (1968a) and Gabano et al. (1965) visualize surface hydration in which the oxygen of the water molecules is chemically bound to structural manganese ions, leaving the hydrogen available for exchange with electrolyte ions (K^+ , Na^+ , etc.), Mn^{2+} or other adsorbing trace metals. Both Loganathan and Burau (1973, 1977) and Anderson et al. (1973) support the idea of two adsorption processes for trace metals. One is surface adsorption, i.e. exchange with H^+ , Mn^{2+} , Na^+ , K^+ , the other is exchange with structural Mn^{2+} and Mn^{3+} ions (Loganathan and Burau 1973, 1977) or structural Mn, K and Na (Anderson et al. 1973), presumably from the disordered layers. On the basis of CFSE and ionic radius (arguments used by Loganathan and Burau 1973, 1977, for Zn^{2+} adsorption of $\delta\text{-MnO}_2$ via exchange with structural manganese), Cu^{2+} could only replace Mn^{2+} (and not Mn^{3+}) in the disordered layers. However, no Mn^{2+} was found in the $\delta\text{-MnO}_2$ samples involved in this study by ESR, nor could A.A. detect any Mn in solution after Cu^{2+} adsorption onto the $\delta\text{-MnO}_2$'s (at pH's 6 - 8.5). It appears therefore that no Mn^{2+} is present in these $\delta\text{-MnO}_2$ samples, and that any residual Mn is of the

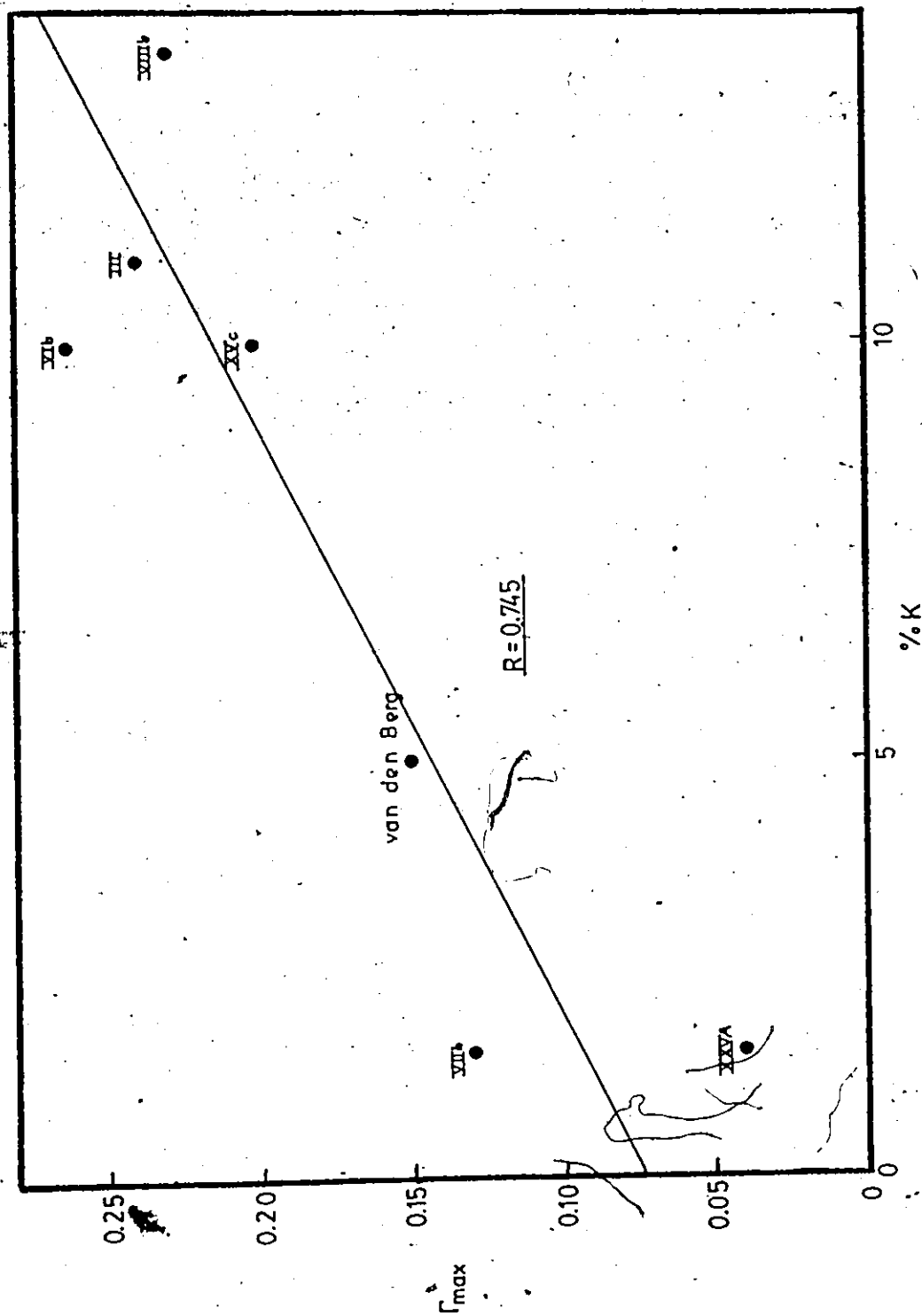


Figure 4.12 Relationship between maximum adsorption capacity and %K in solid for various MnO₂ samples.

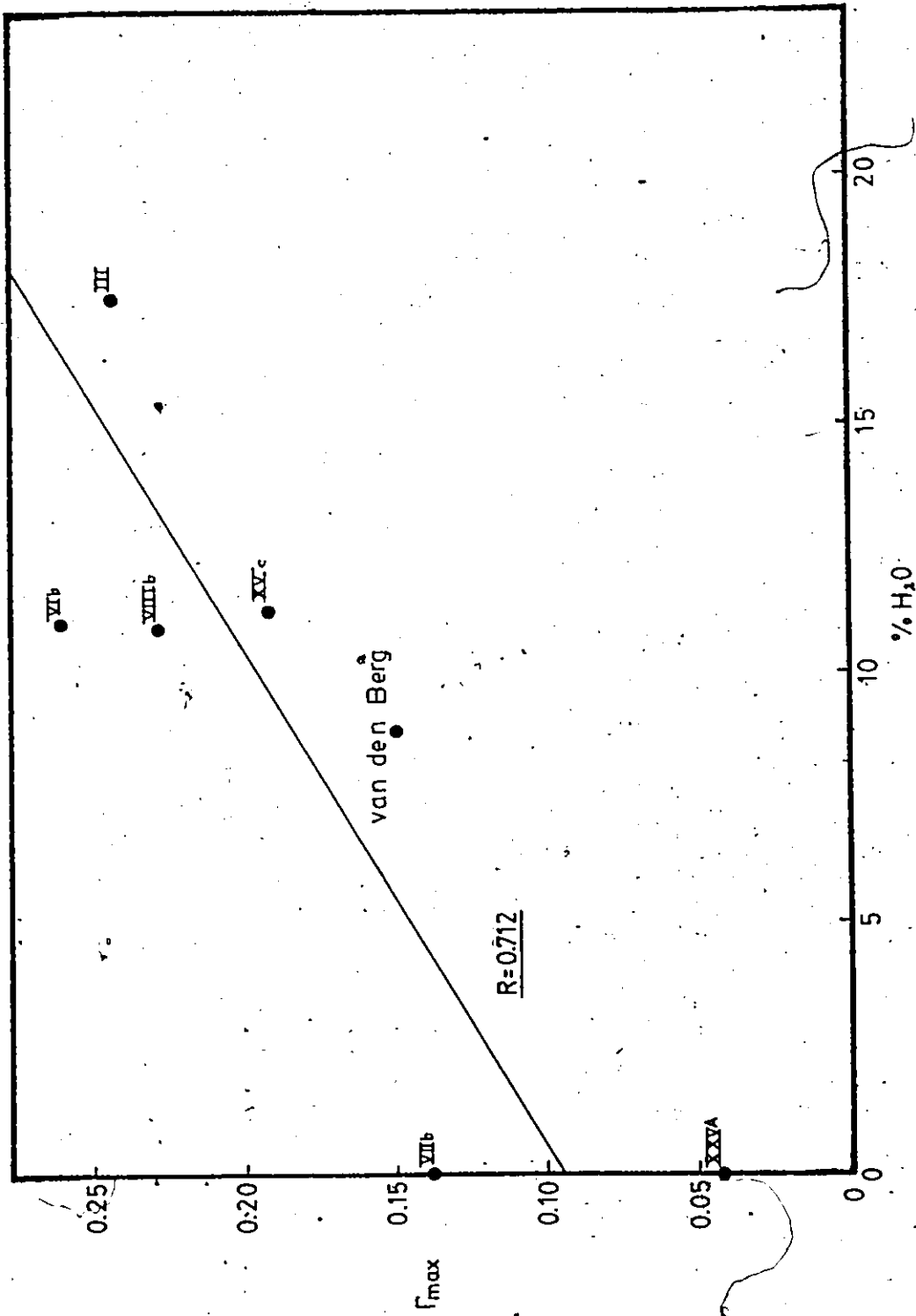


Figure 4.13 Relationship between maximum adsorption capacity and %H₂O in solid for various MnO₂ samples.

form Mn^{3+} rather than Mn^{2+} which explains why no Mn is found in solution after Cu^{2+} adsorption.

It is concluded here, that most likely, water is chemisorbed both at the oxide surface and in the imperfect layers between the MnO_2 octahedra, leaving the hydrogen free to exchange with potassium (from reaction ingredients), which in turn can exchange with Cu^{2+} ions during adsorption experiments. How available and accessible such imperfect layer sites are compared to surface sites remains as yet unanswered. Access to these sites may be diffusion controlled, but due to the very small particle size of δ - MnO_2 , it may also be that these imperfect layers are quite exposed and therefore accessible. The ratio of surface sites and interlayer sites can only be determined if these sites display different adsorption behaviour. Analysis of adsorption data for Cu on the δ - MnO_2 samples with a linearized Langmuir isotherm indicated indeed a non-constant binding constant for Cu on δ - MnO_2 . The implications of this, and the development of a new semi-empirical adsorption model for Cu onto δ - MnO_2 are discussed in Chapters 5 and 7.

4.4.6.4 The Relationship Between Particle Size, XRD Patterns, Oxidation State, and H_2O Content

In Chapter 3 (Section 3.4) it was discussed that δ - MnO_2 consists of ordered layers of true MnO_2 alternating with disordered layers containing metal ions coordinated with H_2O , OH^- and other anions (Murray et al. 1968). Jones and Milne (1956) described the structure of MnO_2 as consisting of layers of $4 MnO_2$, interspersed with layers of $Mn(OH)_2 \cdot 2 H_2O$. With increasing oxidation, the number of $Mn(OH)_2$ layers decreases and they no longer exist as regular structural units. Instead, there are only

individual double layers, randomly oriented, and this results in the disappearance of XRD patterns.

Bricker (1965) however suggested that the presence or absence of the basal reflections for MnO_2 in the XRD patterns is a function of particle size in the MnO_2 sample.

Figures 4.5 to 4.11 show that all MnO_2 samples in this study have very small particle sizes, including the commercial Baker MnO_2 (which is β - MnO_2 , or pyrolusite according to Anderson et al. (1973)). However, this sample which has a distinct XRD pattern does not contain any water and is pure MnO_2 . From this it can be concluded that the absence of imperfect layers containing water rather than the particle size of the sample plays a crucial role in the appearance of an XRD pattern for MnO_2 .

MnO_2 's VIIb, XXV-A and Leco also contain no water, but do contain some K in their lattice (see Table 4.1). These samples have oxygen numbers that are much lower than the ones for the δ - MnO_2 samples. This could imply that they only partly consist of MnO_2 layers, and are interspersed with, for instance, Mn_2O_3 layers in such a manner that again any XRD pattern for MnO_2 or Mn_2O_3 disappears.

4.4.6.5 The Influence of the pH of Formation on the δ - MnO_2 Surface Area

In Chapter 3 (Section 3.5.1) possible theories regarding the influence of the pH on the reactivity of the MnO_2 surface and the total surface area are discussed. Polissar (1935) observed that in an acid environment there appears to be an incubation period for the reaction between Mn^{2+} and MnO_4^- (the Guyard reaction). MnO_2 formed in the course of the reaction acts autocatalytically, but because it is formed at acid pH,

it appears less effective as a catalyst than an added neutrally formed MnO_2 . These effects were explained in terms of nucleation and particle growth.

The neutral $\delta\text{-MnO}_2$'s formed in this study have very small particle sizes, i.e. large surface areas, which agrees with the explanations given in Section 3.5.1. The alkaline sample has a smaller surface area, which can be explained by favouring an ionic strength effect over a pH effect. The acid MnO_2 does not display the expected smaller surface area. However, the first attempts to precipitate this particular sample at dilute concentrations of reagents, aiming at a yield of 10^{-2} M MnO_2 failed (see also Section 4.3). This can readily be explained by the effects observed by Polissar (1935); MnO_2 is formed under acid conditions, but autocatalytic effects are slow due to the fact that the MnO_2 is formed under acid conditions. The reaction under very concentrated reagent conditions is much faster. The obtained $\delta\text{-MnO}_2$ has a large surface area, which is not in agreement with the arguments of either pH - or ionic strength effects. The reasons for this must be sought in the fact that the reaction was allowed to proceed under such concentrated conditions, but how this can affect the particle size is not clear. Also neither the acid or the alkaline samples were precipitated via the Guyard reaction. Therefore, the details discussed in Chapter 3 (Section 3.5) regarding the reactions between manganous- and permanganate-ions (Adams 1952) may not apply here.

4.5 The Influence of Modifications of the Neutral Recipe on the Oxidation State and Morphology of $\delta\text{-MnO}_2$

It appears that oxidation state and morphology (and derived sur-

face areas) are very important characteristics for positive identification of $\delta\text{-MnO}_2$. In this Section, slight alterations to the neutral recipe are designed to investigate their effects upon the morphology and oxidation state of the produced $\delta\text{-MnO}_2$'s. Such alterations can possibly offer explanations for the completely different morphology displayed by various samples inherited from van den Berg's (1979) research. In Sections 4.3 and 4.4 it was assumed that a natural aging process caused the particular morphology, but no mention of such a natural process can be found in the literature. Although a natural aging process is still the most likely cause of the difference in appearance between the neutral samples and the van den Berg's MnO_2 's, modifications in the neutral recipe cannot be ruled out per se as a cause. Moreover, no TEM image of the fresh MnO_2 's prepared by van den Berg (1979) exist. Concurrently with the modifications in the neutral recipe, an investigation was carried out to determine the effects of pH and potassium content on the conversion of $\delta\text{-MnO}_2$ to cryptomelane as a result of an artificially induced aging process (i.e. under heat-treatment in an autoclave). This was done quite easily since part of the modifications in the recipe consisted of changes in pH and omitting of washing procedures, which influenced the K contents of the samples (see Section 4.6).

Table 4.4 compiles all the modifications that were investigated. The neutral recipe (adapted from van den Berg 1979) is split up in various steps as follows:

Step 1: 367 mg Mn metal (6.7×10^{-3} M) is dissolved in a minimum amount of conc. HNO_3 and diluted with deionized H_2O .

- Step 2: Neutralization of the Mn^{2+} solution with KOH, causing a brown precipitate or a dark yellow solution with no obvious precipitate.
- Step 3: 632 mg $KMnO_4$ (0.4×10^{-2} M) and 450 mg KOH (0.8×10^{-2} M) are premixed in 100 mL deionized H_2O .
- Step 4: 100 mL of the Mn^{7+} mixture is added rapidly to 900 mL of the Mn^{2+} solution from a dripping buret while correcting the pH, or instantly by a pipet, which causes a pH drop.
- Step 5: The pH is kept neutral manually in Step 4, by addition of small amounts of dilute HNO_3 or KOH, while vigorously stirring.
- Step 6: After adding the premixed Mn^{7+} solution to the Mn^{2+} solution, the suspension is kept at neutral pH and stirred for an additional half hour.
- Step 7: The precipitate is washed three to four times by centrifuging and resuspension in deionized water.
- Step 8: The pH is maintained near neutral during the washing procedure by adding dilute HNO_3 or KOH if necessary.
- Step 9: The δ - MnO_2 suspension is stored at neutral pH, or alternatively is stored at lower or higher pH after correction via acid or base addition.

MnO ₂	1	2	3	4	<u>steps</u>	5	6	7	8	9
III, V1b, Xvc	/	/	/	/	/	/	/	/	/	/
XIa	/	brown precipitate	/	pipet pH drops to 2.8	pH not corrected	pH 2.8	not washed	not performed	stored at pH 2.8	
XId	"	"	"	"	"	"	/	pH not corrected	stored at pH 7.0	
XIe	"	"	"	"	"	"	"	"	stored at pH 2.9	
XIIa	/	yellow solution	/	pipet pH drops to 2.9	/	/	not washed	not performed	stored at pH 6.8	
XIIC	"	"	"	"	"	"	/	/	7.4	
XIIIa	<	not neutralized	/	pipet pH drops to 2.5	pH not corrected	pH 2.5	not washed	not performed	2.5	
XIIIb	"	"	"	"	"	"	/	pH not corrected	7.0	
XIIIc	"	"	"	"	"	"	"	"	2.3	
XIVa	/	not neutralized	/	pipet pH drops to 2.5	/	/	/	/	7.7	
XIVb	"	"	"	"	"	"	"	"	2.8	
XVa	/	brown precipitate	/	/	/	/	not washed	not performed	6.9	
XVc	"	"	"	"	"	"	/	/	7.3	
XVd	"	"	"	"	"	"	"	"	2.8	
XVII	/	/	doubly concentrated premix	pipet pH inc. to 11.5	/	/	/	/	7.4	
XVIII	doubly concentrated Mn ²⁺ solution	/	/	/	/	/	/	/	7.0	

/ - according to standard procedure

Table 4.4 Modifications of the neutral recipe

The oxidation state for each of the "modified" neutral δ -MnO₂'s is given in Table 4.5. None of these results have been corrected for K or H₂O content. The numbers can therefore only be compared to the uncorrected data given for the neutral δ -MnO₂'s III, VIb and XVC in Table 4.1. It appears that the average oxidation number for the "modified" samples that were stored at low pH is 1.73 ± 0.03 , while the average value for the samples stored at high pH is 1.69 ± 0.020 . Although this is not a very significant difference, it indicates a trend. Samples that are stored at low pH tend to have less potassium adsorbed on their surface because of H⁺ exchange. Thus, their uncorrected oxygen numbers will be slightly larger than the uncorrected oxygen numbers for samples that are stored at higher pH's and therefore, have more potassium adsorbed on their surfaces. The pH at which the latter were stored tended to drop slightly, likely caused by K⁺/H⁺ exchange. In Table 4.6 (Section 4.6) percentages K are given for the samples included in Table 4.5.

The Transmission Electron Microscope images of the "modified" neutral δ -MnO₂ samples showed no differences from the morphology shown in Figure 4.5. One exception is sample XVIII, which was considerably more "thready" in appearance. All δ -MnO₂'s involved in this study were periodically (approximately once every three months over a period of three years) scrutinized under the TEM to discover any naturally occurring changes in morphology. No change occurred over this period of time (see also Section 4.6).

Without exception, all samples involved in this study were amorphous according to XRD analysis.

Consequently, it is concluded that apparently transient conditions during the preparation of neutral δ -MnO₂ are not the cause of the

Table 4.5 Oxidation state of the modified neutral δ - MnO_2 samples

MnO_2	pH stored	x in MnO_x (not corrected for K and residual H_2O)
XIa	2.8	1.73
XId	7.05	1.71
XIe	2.93	not determined.
XIIa	6.77	1.70
XIIc	7.37	1.70
XIIa	2.5	1.76
XIIb	7.01	1.69
XIIc	2.31	1.77
XIVa	7.73	not determined
XIVb	2.8	1.69
XVa	6.92	1.68
XVc	7.30	1.71
XVd	2.76	1.71
XVII	7.35	1.69
XVIII	6.95	1.65

difference in morphology between the δ -MnO₂ samples prepared for this study and the aged ones remaining from van den Berg's research.

4.6 Simulated Aging Study

McMurdie (1944) suggested that aging of manganese dioxides can be simulated by subjecting them to heat-treatment. The δ -MnO₂'s prepared for the comparison study described in Section 4.4 and the "modified" δ -MnO₂'s described in Section 4.5 were treated in an autoclave at approximately 120°C and 1.4 Kg/cm² pressure during three hours. Prior to this heat-treatment, the pH and K content of all the δ -MnO₂ suspensions involved were recorded, as well as the K content of each δ -MnO₂ solid. For the former, 1 mL of well-stirred δ -MnO₂ suspension was reduced with oxalic acid. For the latter, 1 mL of well-stirred δ -MnO₂ suspension was filtered to dryness through an 0.45 μ m millipore filter. The filter papers were thereafter reduced with oxalic acid. After reduction, K was measured by A.A. McMurdie (1944) believed that the pH was of vital importance in the conversion from δ -MnO₂ to cryptomelane, while McKenzie (1971) suggested that a certain percentage K was indispensable for the transformation to occur. The purpose of this aging study was to more accurately determine the precise role of a low pH and a particular K content in the solids, and to possibly even draw some conclusions regarding the conditions under which these conversions could take place without being induced by heat. The pH and K-percentage of the autoclaved samples were also measured. The results of this study are compiled in Table 4.6. Representative micrographs are presented in Figures 4.16 to 4.26.

Table 4.6 and Figures 4.16 to 4.26 show a number of interesting

developments. Firstly, autoclaving induces a raise in the pH of each suspension, except for MnO_2 VIIa, whose pH dropped. McMurdie (1944) also mentions a pH increase upon autoclaving. For the samples that were stored at neutral pH, an increase in pH upon heattreatment could perhaps be explained by the fact that carbonic acid (i.e. CO_2) escaped from the solutions. For the acid $\delta\text{-MnO}_2$ suspensions, such an explanation is not feasible.

Secondly it appears that, prior to heating, there is a relationship between pH and percentage K for the $\delta\text{-MnO}_2$ samples. This indicates a straight-forward H^+/K^+ exchange on the $\delta\text{-MnO}_2$ surface. A shift in pH upon autoclaving should necessarily also include a shift in K content for the $\delta\text{-MnO}_2$ samples. To establish whether this is the case, Figures 4.14 and 4.15 were assembled from the data in Table 4.6. The data for MnO_2 's VIIa, VIIb and XVIII are excluded from these Figures, since the former two are not really $\delta\text{-MnO}_2$'s (see Section 4.3) and the latter behaved totally differently from any of the other samples upon autoclaving. By performing linear least squares analysis, the relationships between pH and %K could be established. The correlation for each line is reasonable due to a considerable number of data points (18), although the scatter appears considerable. Correlation factor validation by performing an r -test indicates that the straight line relationships in Figures 4.14 and 4.15 are valid even at the 99.9% level. The equation for the lines are given in the Figures. By testing whether the slopes and intercepts of the lines are the same by performing a t -test at 95% confidence, it appears that the hypothesis that both slopes and intercepts are in fact the same, cannot be rejected. This means that based on the data presented in Table 4.6 and Figures 4.14 and 4.15, there is no statistical

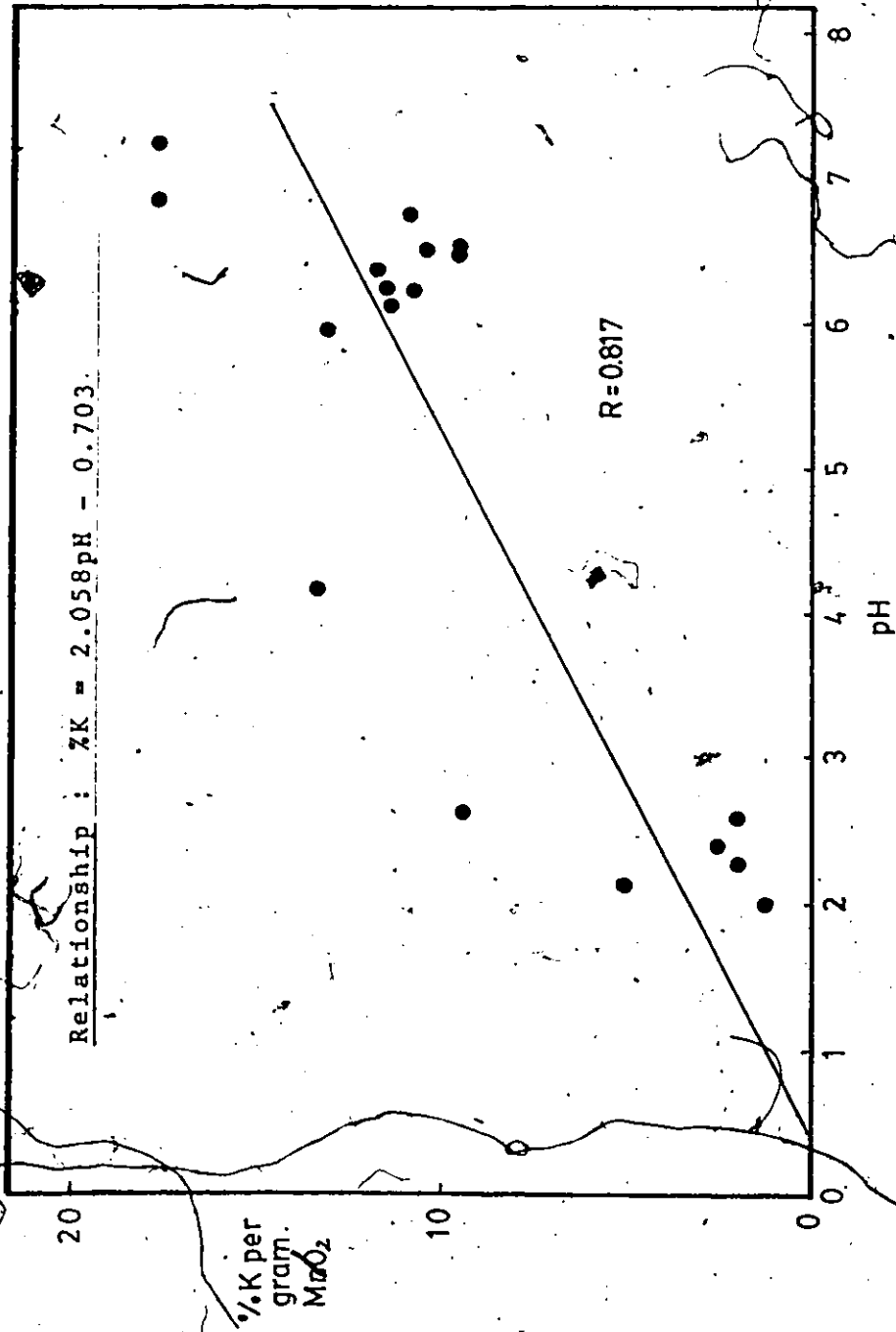


Figure 4.14 The relationship between pH and weight-percentage K in the δ -MnO₂ samples prior to heat-induced aging

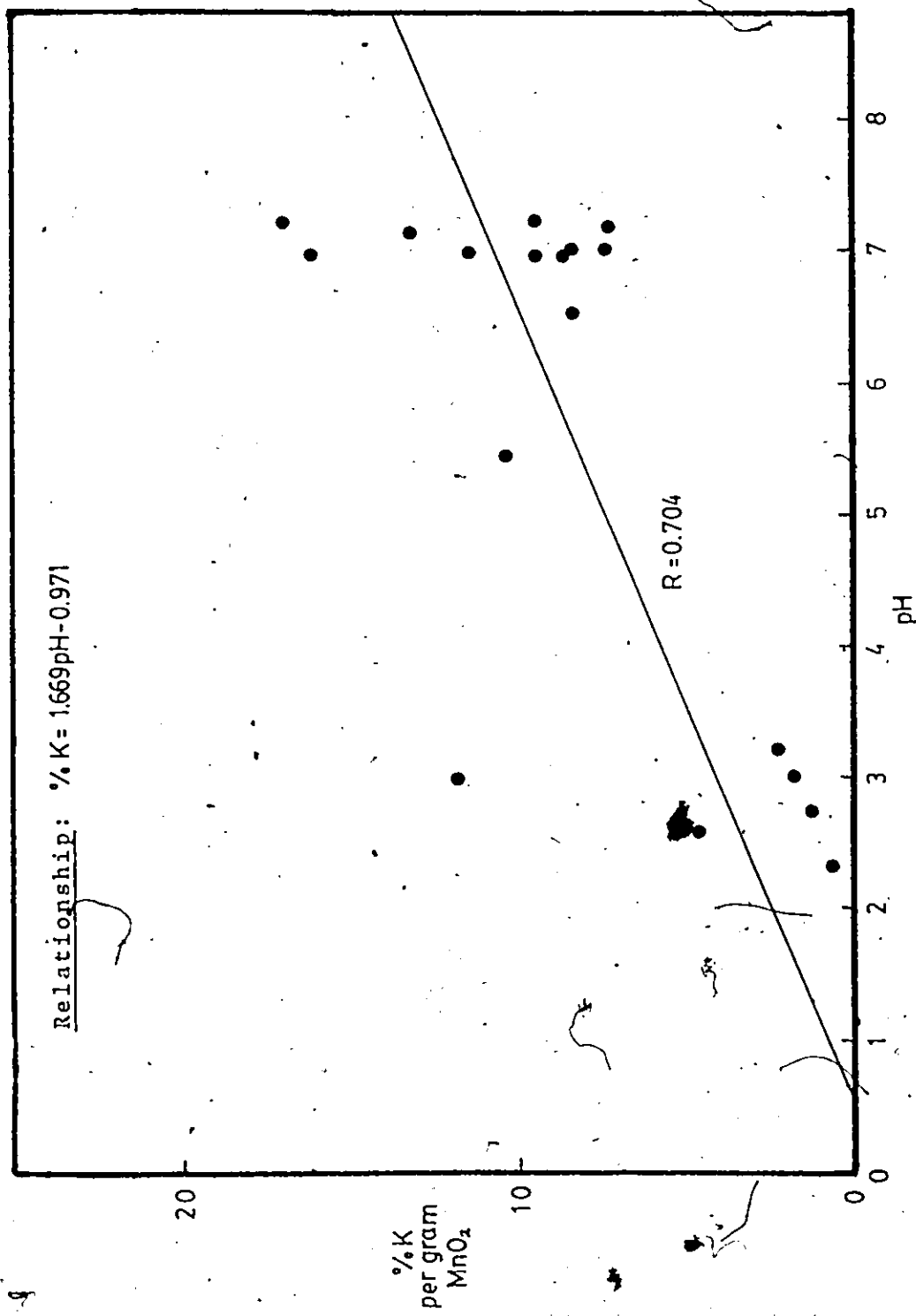


Figure 4.15 The relationship between pH and weight-percentage K in the δ -MnO₂ samples after heat-induced aging.

difference in the relationship between pH and %K before and after simulated aging. This implies that the shift in pH can explain the shift in percentage K in the δ -MnO₂ samples.

Thirdly, the morphologies of the δ -MnO₂'s before and after the simulated aging process were studied. All samples had the appearance of neutrally formed δ -MnO₂ as shown in Figure 4.5 prior to heat treatment. After three hours in an autoclave, some striking changes were apparent.

MnO₂ III had a neutral pH and a K content greater than 10% prior to heat treatment. Its appearance changed only slightly and became somewhat more "thready" upon autoclaving, as shown in Figure 4.16. The MnO₂'s VIa and b, with neutral pH and K content of more than 10%, underwent no visible changes in morphology. The "alkaline" MnO₂ VII forms an interesting case: sample VIIa, although stored in 0.01M KNO₃, has only a slightly higher K content than the MnO₂ VIIb batch (both have less than 3% K), while each MnO₂ VII sample possesses a pH of around 6 before the aging simulation process. The change in VIIa is complete: Figure 4.17 shows thick fibres which are neither similar to McMurdies (1944), nor to McKenzies (1971), fibrous material. This sample is the only one for which a pH drop was observed after autoclaving. MnO₂ VIIb however, showed only a partial conversion to fibrous material, which is illustrated in Figure 4.18. The change in MnO₂ VIIb closely resembles the transition observed by McKenzie (1971) for similar material. Both samples VIIa and VIIb were excluded from the data analysis presented in Figures 4.14 and 4.15 since they probably are not true δ -MnO₂'s.

Sample VIIIa, with a fairly low pH (4.13) but high K percentage (13.4%) did not change upon autoclave treatment. This again is in agreement with what McKenzie (1971) suggested for a similar sample, namely

that without lowering the K concentration in such a sample, no morphology change will take place. Sample XIa, one of the "modified" ones, possessed a very low pH and relatively high proportion K (9.5%), but upon autoclaving underwent a drastic change in appearance, as is shown in Figure 4.19. After heattreatment, this sample contained both fibres with a diameter of about 0.015 - 0.05 μm and large, hexagonal particles measuring 0.1 - 0.3 μm in diameter. Sample XIc of neutral pH and high K concentration, became very filamentous upon autoclaving (see Figure 4.20), resembling to some extent, the micrographs given by McMurdie (1944), although no acid-treatment was involved. MnO_2 XIe had both a low pH and very low K-content in its solid (2%) and changed to a sample with some thick fibres and again the very large hexagonal particles, but also particles of an oblong shape, measuring about 0.10 - 0.15 μm in length and 0.03 μm in width (Figure 4.21). These may be the hexagonal particles, in oblique or perpendicular view.

The MnO_2 's XIIa and c, both of neutral pH, with a high K percentage in their solids, did not change appearances. Figure 4.22 shows the change in XIIa, which had a very low pH, and low K content (5%). Again, a mixture of large hexagonal particles, filaments and oblong shapes was obtained. MnO_2 XIIb had a neutral pH and fairly high K-content, and did not change to filamentous or hexagonal morphology, but became more "thready" in appearance. MnO_2 XIIc, with a very low pH and K percentage, changed to a composition of hexagonal and oblong particles, but seemed to lack the fibres (Figure 4.23). MnO_2 XIVa did not change, but XIVb, low in both pH and K%, converted to very distinct hexagonal shapes with very little fibrous material (Figure 4.24).

The MnO_2 XV samples form a perfect summary of all of the above:

sample XVa, with neutral pH and high K content (17.8%) did not undergo a change in appearance, Sample XVc, having a neutral pH and lowered K content through washing (but still above 7%) changed reluctantly to a more filamentous morphology (Figure 4.25). MnO_2 Xvd, (Figure 4.24) possessing a low pH and hence a low K percentage in its solid, underwent the drastic change to hexagonal-, fibrous- and oblong- shapes of large proportions.

The non-stoichiometrically precipitated MnO_2 XVII, made with twice the amount $KMnO_4/KOH$ premix behaved according to what can be expected from a sample with neutral pH and high K%, i.e. no drastic changes were observed. Finally, MnO_2 XVIII (Figure 4.26) with its almost neutral pH and very low K concentration converted to a hitherto unencountered mixture of a few filaments and numerous triangular shapes measuring approximately 0.10 by 0.15 μm . This sample was not included in Figures 4.14 and 4.15 because of its different morphology.

Although the particles of the converted samples are larger than before autoclaving, XRD patterns were nevertheless still amorphous, preventing identification of the products. However, the threads, needles and filaments in most micrographs appear very similar to observations by McKenzie (1961) and McMurdie (1944), who both identified such shapes (with apparent varying thickness) as cryptomelane. It is therefore assumed that any filamentous material obtained in this study is cryptomelane. The oblong shapes have not been encountered before either in this study or in the literature, and form only a small fraction of the converted samples. They are likely perpendicular or oblique images of the hexagonal particles. The large hexagonal shapes resemble, to a certain extent, the particles of Baker MnO_2 (compare Figure 4.10), which was identified by Anderson et al. (1973) as pyrolusite. However,



Figure 4.16 TEM appearance of artificially aged MnO_2 III.

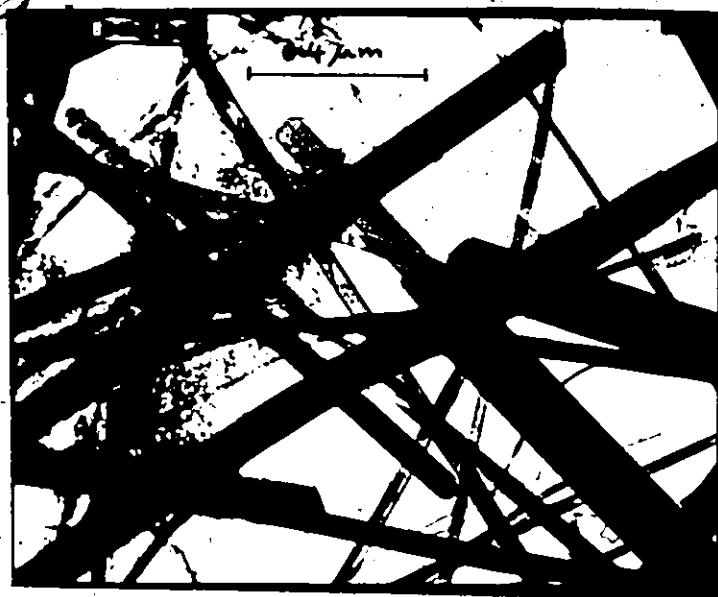


Figure 4.17 TEM appearance of artificially aged MnO_2 VIIa.

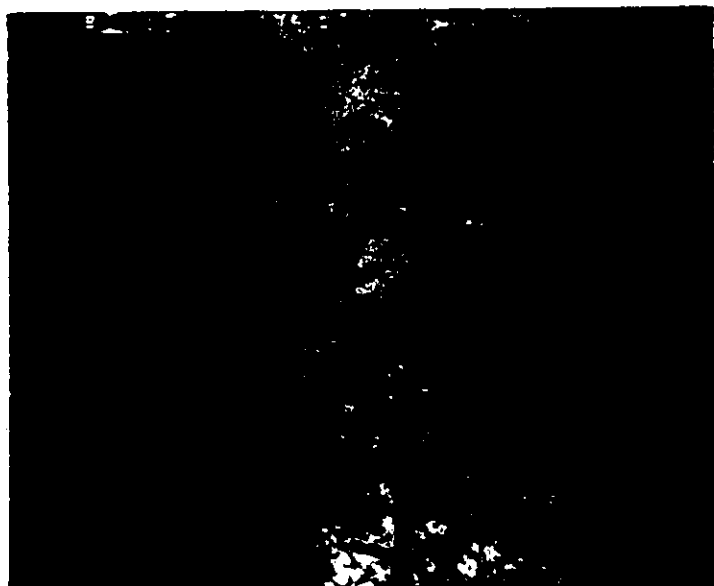


Figure 4.18 TEM appearance of artificially aged MnO₂ VIIb.



Figure 4.19 TEM appearance of artificially aged MnO₂ XIa.

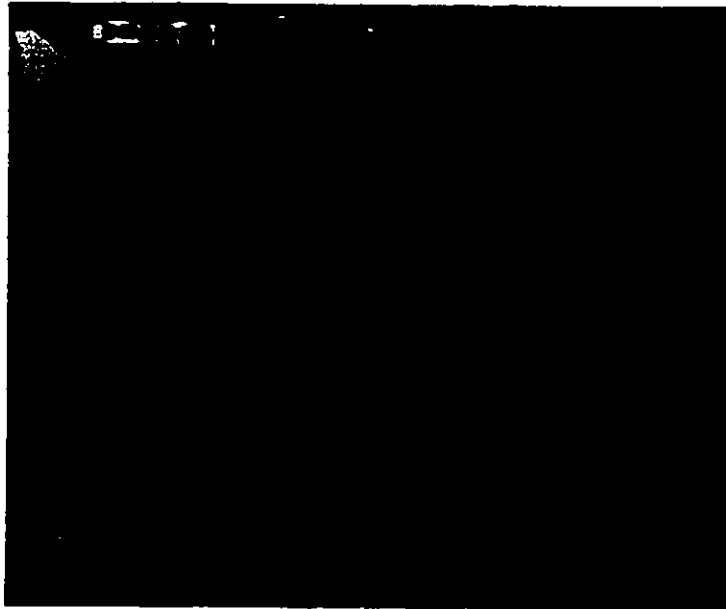


Figure 4.20 TEM appearance of artificially aged MnO₂ XId.

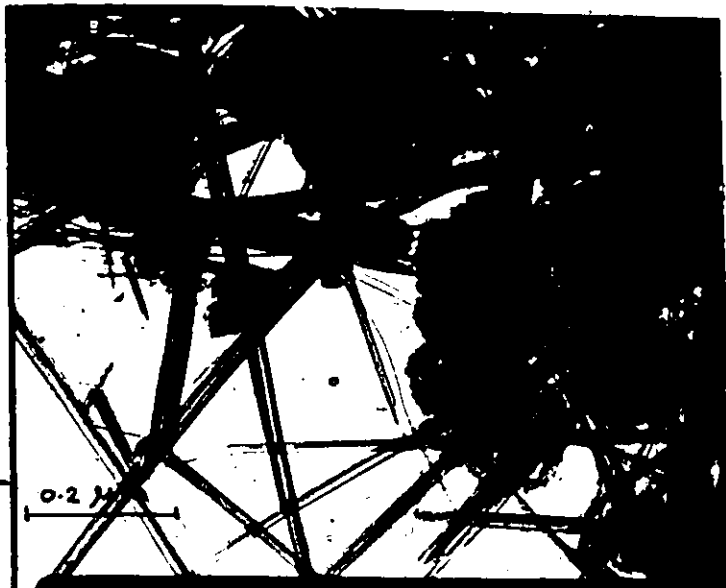


Figure 4.21 TEM appearance of artificially aged MnO₂ XIe.



Figure 4.22 TEM appearance of artificially aged MnO_2 XIIIa.

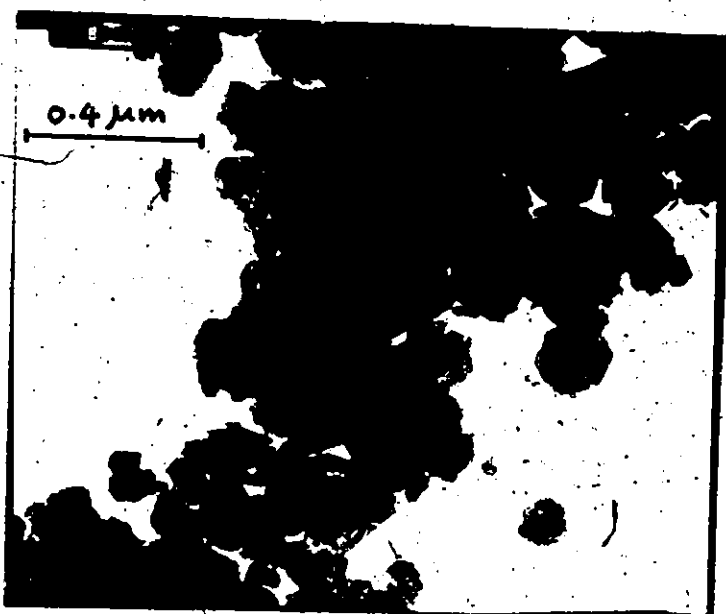


Figure 4.23 TEM appearance of artificially aged MnO_2 XIIIc.



Figure 4.24 TEM appearance of artificially aged MnO_2 XIVb.

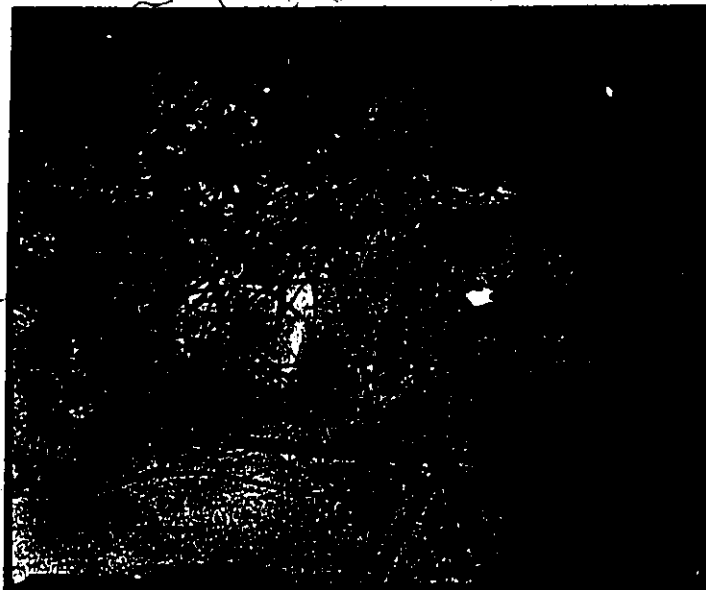


Figure 4.25 TEM appearance of artificially aged MnO_2 XVc.



Figure 4.26 TEM appearance of artificially aged MnO₂ XVIII.

Baker-MnO₂ is true MnO₂ (i.e. x=1.99) as shown in Section 4.3. Most converted samples with the three different shapes (filaments, hexagonals, oblongs) consist for the main part of the large hexagonal shapes. The oxygen number for such samples lies, according to the analysis of MnO₂ XXV-A in Section 4.3, around 1.66, after correcting for K- and H₂O content. Assuming that the filaments are cryptomelane (i.e. K₂Mn₈O₁₆) and the hexagonals are pyrolusite (β-MnO₂) would imply a higher oxygen number than 1.66 (after correcting for K and H₂O). It is therefore not likely that the hexagonal shapes are pyrolusite.

This study was initiated to establish the importance of pH and K content during the conversion of δ-MnO₂ into cryptomelane. McKenzie (1971), for his MnO₂'s, which were prepared with recipes resembling the "acid" and "alkaline" ones used in this study, stressed the point of a critical K concentration but did not mention the pH values at which he obtained the conversions to cryptomelane. In this study, a positive relationship between the pH and percentage K in the δ-MnO₂ samples was established. This relationship did not change significantly upon aging. This implies that upon a pH change the K content will change, regardless of a morphology change. This makes it virtually impossible to distinguish between pH- and K content- influences upon morphology changes. All that can be concluded from the above observations is more or less a confirmation of the results by McKenzie (1971), for MnO₂'s prepared according to an "acid" and "alkaline" recipe: Conversion does not seem to take place unless the K percentage is low (generally below 7%).

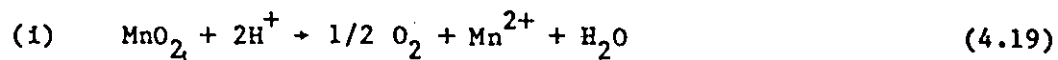
The slight changes to more filamentous appearances undergone by a number of "neutral" MnO₂'s with neutral pH values and K contents of 7-10% or more, resemble both McMurdies (1944) micrographs and van den Berg's

sample (Figure 4.8), although conversions are not nearly as extensive. This could indicate that morphology changes at neutral pH values and high K percentages do take place but at a very slow rate and/or to an incomplete degree. It is possible that even without heat-induction, these changes can in fact occur and that van den Berg's MnO_2 possesses a filamentous appearance as a result of a natural, time-dependent aging process which was favoured by optimum K conditions (K content of MnO_2 is <5%, see Table 4.1). However, the oldest samples made for this study are now well over 3 years old. The most recent TEM scrutiny did not disclose any positive changes towards this fibrous state, K percentages are, however, quite high (>10%) in most samples.

The above discussion indicates that cryptomelane can be formed from $\delta\text{-MnO}_2$ by heat-treatment under certain circumstances. The K-percentage appears crucial. In Chapter 3 it was discussed how the presence of some large cations such as K is necessary to prevent the cryptomelane structure from collapsing (Byström and Byström, 1950). McKenzie (1971) describes that during the conversion to cryptomelane there is a migration of some K from exchange sites to the crystal lattice, where it is no longer exchangeable. How too much K could prevent such a migration, or alternatively cause the cryptomelane to be unstable can be explained by observations by Byström and Byström (1950). They suggest that in the general formula for cryptomelane, $\text{K}_{2-y}\text{Mn}_{8-z}\text{O}_{16}$, y is always approximately equal to 1, so that the two K positions per unit cell are only half filled. The short K-K distance of 2.8 Å would make the structure unstable, due to repulsive forces between the cations, if all the K-sites were filled. If there were 2 K cations per unit cell ($\text{K}_2\text{Mn}_8\text{O}_{16}$), the K content would be >10%, which agrees well with the observation that at

such K percentages no conversion takes place. From observations with samples MnO₂ VIIa and VIIb it is obvious that conversions to cryptomelane are possible at approximately neutral pH providing the K content is low. The converted MnO₂ samples from van den Berg also had a neutral pH and a K-content <5% (see Table 4.1). This, combined with the above arguments regarding the role of K in cryptomelane stability, provides convincing evidence that for a conversion to cryptomelane the K percentage is crucial, and not a low pH.

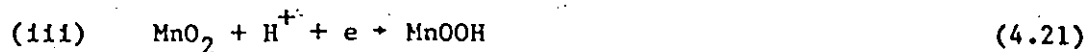
The role of a low pH is obscured by the fact that pH and K-percentage are related. A low pH necessarily means a low K-percentage. However, the samples converted at low pH show distinct differences from the autoclaved samples VIIa, VIIb and van den Berg's aged MnO₂ 13. It is proposed that in these conversions the pH and not the K content plays the most important role. The following reactions are thought of importance for the conversion at low pH to a mixture of unidentified manganese oxide surfaces:



(Morgan and Stumm 1965)



(Adamson 1952)



(Tari and Hiray 1982)



A combination of reactions i, ii and iii provides MnOOH (manganite) which via reaction iv goes to Mn_2O_3 (partidgeite, McKenzie 1977). Mn_2O_3 has an oxygen number of 1.5, reasonably close to 1.66 found for MnO_2 XXV-A. If one assumes that the samples are for a large part partidgeite (i.e. the hexagonal shapes) and for a small part cryptomelane, the oxidation number would lie around 1.7.

One final experiment was performed, to study the speed of the conversion of the low pH- low K- MnO_2 's to the fibrous and hexagonal shapes during the autoclave procedure. For this purpose, MnO_2 XXV was produced according to the normal "neutral" procedure with the exception that the $KMnO_4/KOH$ premix contained about 1 1/2 times the stoichiometric amount of KOH, so that neutralization of the precipitate was not necessary (the end-pH of the suspension was around 6). Half of this batch, MnO_2 XXV-N was washed five times, and stored at pH 7.7. The other half, MnO_2 XXV-A was brought to pH 2.2 and not washed prior to storage.

Shortly after their preparation, ten amounts of 25 mL of each of these two batches were transferred to Erlenmeyer flasks. These aliquots were covered with aluminium foil and autoclaved at 120°C and 1.4 Kg/cm². The progress of morphological changes was followed by removing a flask at a preset time from the autoclave (e.g. 0-15-30-45-60-90-120-150-180-240 minutes). Upon removal, they were cooled quickly in a cold-water bath, and their contents were studied under the TEM. The neutral sample XXV-N (K content 11.2%), the control, did not undergo any changes during the four hours in the autoclave, in agreement with the preceding study. The low pH-, unwashed sample (K-content in solid 8.0%) changed very rapidly and after half an hour the conversion was complete. This is shown in a sequence of micrographs in Figure 4.27a-c.

Figure 4.27 Morphological changes of δ - MnO_2 upon heat treatment as a function of time.

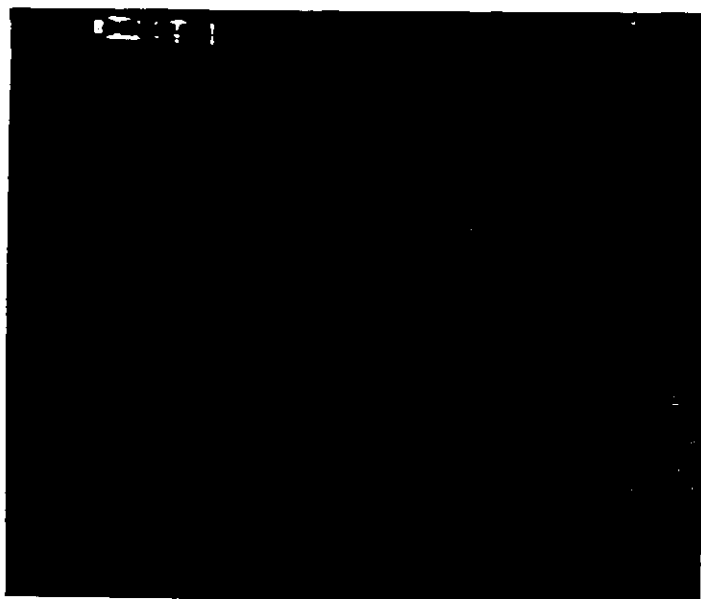


Figure 4.27-A TEM appearance of MnO_2 XXV-A, not autoclaved.

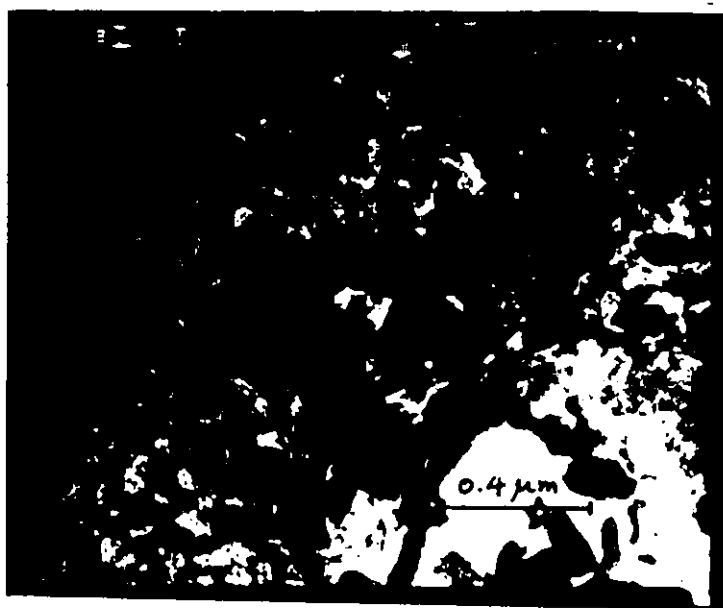


Figure 4.27-B TEM appearance of MnO_2 XXV-A autoclaved for 15 min at 120°C (250°F) and 1.4 kg/cm^2 (20 lbs/inch^2) pressure.



Figure 4.27-C TEM appearance of MnO_2 XXV-A autoclaved for 35 min at 120°C (250°F) and 1.4 kg/cm^2 (20 lbs/inch^2) pressure.

With regard to the time dependence of conversion to cryptomelane at low K content, it is worth mentioning that McMurdie (1944, see Chapter 3) obtained his conversion in two ways: one was rapid, through three hours in an autoclave at 150°C (although he does not mention whether this is the minimum amount of time required). The other process required 18 days on a steam bath at 100°C before conversion was achieved. This suggests the following type of relationship between time and temperature for these changes to occur:

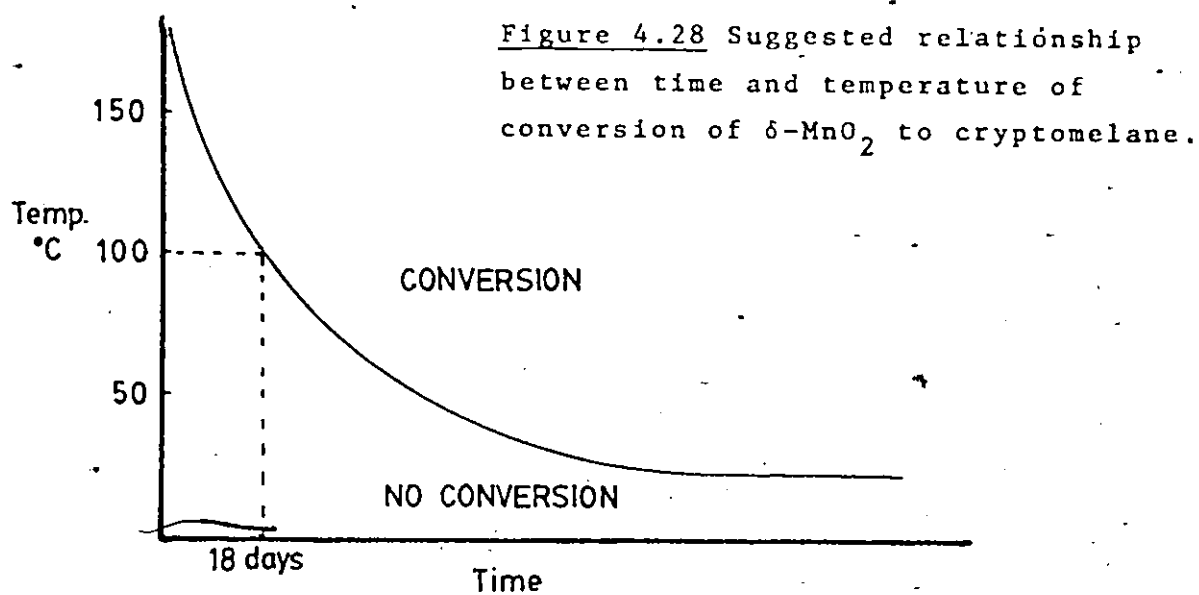


Figure 4.28 implies that the MnO_2 samples stored at 4°C will take a very long time to convert, and that only if certain circumstances regarding the K concentration are optimal. For instance, van den Berg's MnO_2 13 converted within three years at 4°C due to its low (<5%) K content. The samples prepared for this study did not convert in three years time at 4°C , due to their considerably higher (>10%) K content. The fact that during autoclaving of these samples some became more filamentous indicates perhaps that if the heat treatment had been continued longer, conversion would have been more drastic. It should be noted that in this study the temperature for three hours treatment did not exceed 120°C , while McMurdie reports conversions after three hours at 150°C . McKenzie (1971) reported a birnessite with 9.4% K, which did not convert into cryptomelane after boiling for 24 hours, but upon ignition at 400°C for 60 hours the sample did convert. These findings are all in agreement with the relationship suggested in Figure 4.28.

4.7 Summary and Conclusions

The literature reviewed in Chapter 3 provided some possible structures for $\delta\text{-MnO}_2$ and discussed the factors that play a role in the conversion of $\delta\text{-MnO}_2$ (or birnessite) to cryptomelane.

The characterization of various $\delta\text{-MnO}_2$'s, prepared according to different recipes, and the study on aging behaviour, carried out in this research and reported in this Chapter has narrowed the possible sources for the observed differences considerably. Taken together, this work allows a description of a general model structure for $\delta\text{-MnO}_2$. From positive relationships between the adsorption capacity and water- and potassium-content in the solid, and from amorphous XRD patterns, it is

concluded that δ -MnO₂ probably possesses a layer structure of perfect MnO₂ octahedra interspersed with layers containing a mixture of H₂O, OH⁻, K⁺ and H⁺ ions. Water is chemisorbed both at the oxide surface and in between the MnO₂ layers, leaving the hydrogen free to exchange with potassium (from reaction ingredients), which in turn can exchange with trace metals. The access to the interlayer sites may be diffusion controlled, but due to the small particle size of δ -MnO₂ it could also be that these sites are quite exposed and therefore just as accessible as the surface sites. The ratio of surface sites and interlayer sites can only be determined if these sites display different adsorption behaviour. The amorphous XRD pattern can be explained by the arrangement of a layer structure in a certain way. Particle size does not seem a feasible explanation for amorphous XRD patterns here.

A positive identification as δ -MnO₂ includes characteristics such as an oxygen number larger than 1.9 (after properly correcting for K and H₂O content), a large adsorption capacity (i.e. around 0.25 mol Cu²⁺/mol MnO₂), an amorphous XRD pattern, and a low pH(zpc) (i.e. between pH 1 and 2). The morphology of δ -MnO₂ seems variable. If prepared according to the neutral recipe, a distinct appearance of very small round particles should be apparent, while the acid recipe produces a δ -MnO₂ sample with a "flower-petal" appearance.

Of the three recipes investigated, the alkaline recipe did not produce δ -MnO₂. This particular sample has a lower oxidation number (1.6) than δ -MnO₂ and contained very little K and no H₂O.

Modifications of the neutral recipe did not have any noticeable effect on the morphology of the samples.

Heat-treatment to simulate the aging process produced several

2

trends: the potassium content should be lower than 7-10% to produce substantial conversion to cryptomelane at neutral pH values. At low pH values, the percentage K is also low, due to a positive relationship between these two factors. Conversion at low pH likely involves the formation of a manganese oxide with a lower oxidation number. Of the three distinctive shapes in such a converted sample, the most abundant hexagonals are possibly Mn_2O_3 while the filaments are likely to be cryptomelane. Conversions from acid-stored $\delta-MnO_2$ into the three shapes upon heat treatment is a very rapid process and is complete in approximately half an hour. A neutral-pH, high K-content (>10%) $\delta-MnO_2$ sample is protected from a rapid conversion to cryptomelane by the high K content which excludes cryptomelane stability. However, such samples generally become more filamentous in appearance during heat treatment, which indicates that there is a relationship between the time and temperature of the aging process. Such a relationship could readily explain the filamentous MnO_2 13 sample inherited from van den Berg's research.

CHAPTER 5

ADSORPTION MODELS

The problems encountered in this study by describing adsorption of Cu on δ -MnO₂ with the Langmuir isotherm instigated a thorough evaluation of existing adsorption theory with respect to adsorption behaviour of hydrous oxides in general. Adsorption models applied to hydrous manganese dioxide surfaces are especially emphasized in this evaluation. Based on findings (described in Chapter 7) such as deviation from Langmuir linearity, constant adsorption capacity and a linear pH dependence of adsorption strength in the pH range of 6 to 8.5, a semi-empirical adsorption model is derived, which accomodates these findings. This model is unique in that it combines both the simple Langmuir theory and the more complicated adsorption theory developed for hydrous oxides in general.

Adsorption models for hydrous oxides are discussed in Section 5.1, while in Section 5.2 adsorption models used to describe adsorption on MnO₂ are reviewed. Development of the new semi-empirical model to describe adsorption of Cu on δ -MnO₂ is presented in Section 5.3.

5.1 Adsorption Models for Hydrous Oxides

5.1.1 Introduction

The adsorption of metal ions such as Zn, Co and Cu onto hydrous

oxides such as Al_2O_3 and $\delta\text{-MnO}_2$ has often been described by a Langmuir isotherm (e.g. Morgan and Stumm 1964; Gabano et al. 1965; Posselt et al. 1968 a; Anderson et al. 1973; Gray and Malati 1979 a, b; Van den Berg 1979 etc). Although a few of its basic assumptions are occasionally violated (e.g. constant activity of the surface groups involved in the adsorption reactions), it has been found by many researchers that the Langmuir isotherm provides a good fit to many experimental data, and hence is a useful model for describing adsorption phenomena.

The Langmuir model can be derived as follows:

At kinetic equilibrium, the rate of adsorption equals the rate of desorption. Hence,

$$k_1 \text{Me}^{z+} S_0 = k_2 S_1 \quad (5.1)$$

where k_1 = adsorption rate constant
 k_2 = desorption rate constant
 Me^{z+} = equilibrium concentration of free trace metal ion
 S_0 = number of empty sites
 S_1 = number of filled sites
 z^+ = valency of trace metal ion

S_0 (in Langmuir terms) can be expressed as $\Gamma_{\text{max}} - \Gamma_{\text{ads}}$, where Γ_{max} is the maximum amount of moles of trace metal that can be adsorbed in monolayer configuration per unit surface area of hydrous oxide, and Γ_{ads} is the amount of moles of trace metal adsorbed per unit surface area of hydrous oxide at a certain metal concentration. Therefore $S_1 = \Gamma_{\text{ads}}$.

This yields:

$$k_1 \text{Me}^{z+} (\Gamma_{\text{max}} - \Gamma_{\text{ads}}) = k_2 \Gamma_{\text{ads}} \quad (5.2)$$

$$\text{or } \Gamma_{\text{ads}} = \frac{k_1/k_2 \text{Me}^{z+} \Gamma_{\text{max}}}{1 + \text{Me}^{z+} \cdot k_1/k_2} = \frac{\text{Me}^{z+} \Gamma_{\text{max}}}{k_2/k_1 + \text{Me}^{z+}} \quad (5.3)$$

k_2/k_1 is related to the energy of adsorption, and is often expressed as $1/B$ ($B = k_1/k_2$); the larger k_1 (the adsorption rate constant) the larger B and the smaller $1/B$.

There is a considerable amount of argument in the literature about the driving force behind adsorption of trace metal ions on charged hydrous oxide surfaces, e.g., what governs and determines the k_1/k_2 ratio. A very considerable amount of research regarding adsorption on hydrous oxides is described in recent literature and a substantial number of adsorption models has been put forward to describe the combination of processes that determine adsorption behavior of hydrous oxides (e.g., Westall and Hohl 1980). It is not always easy to compare these models and to discriminate between them on the basis of their structure, assumptions, and degree of complexity.

An attempt will be made here to first describe the general theory regarding charged particles and then to briefly discuss a number of adsorption models that have been formulated for these charged surfaces. Where possible, model assumptions regarding the adsorption sites and their locations (e.g., near or on the surface), are visualized.

5.1.2 Double Layer Theory

Hydrous oxides, like many other surfaces in natural waters, possess a charged surface. In general, the surface charge σ_0 of a

colloid or colloidal particle is a result of adsorption of potential determining ions (e.g., Ag^+ or I^- for AgI , H^+ or OH^- for hydrous oxides), imperfections in the lattice (e.g., clay minerals) or dissociation of surface groups (e.g., polyelectrolytes, hydrous oxides). Sometimes adsorption of nonpotential determining ions (such as trace metals on hydrous oxides) is also regarded as affecting the surface charge. At least two questions arise from this enumeration of charge determining conditions. They are: (i) Is the charge on a hydrous oxide determined by the uptake of H^+ and OH^- ions as potential determining ions (pdi) or should one regard this charge as a result of the dissociation of surface hydroxo groups? (ii) Does adsorption of trace metal ions affect the surface charge σ_0 itself or not? The latter is a matter of where one assumes the adsorption is located with respect to the surface itself, and how one imagines the structure of the electrical double layer surrounding hydrous oxides.

The electrical double layer theory was quantitatively formulated by two independent groups, Deryagin and Landau, and Verwey and Overbeek (Fleer and de Wit 1969). This DLVO theory is based on the following:

Assuming that a surface (e.g., hydrous oxide) has a charge, then this charge calls for a compensating charge by an excess of counter ions and a deficiency of co-ions in a diffuse double layer around the particle. The diffuse character is caused by the tendency to strive for maximum entropy. Figure 5.1 visualizes a negatively charged hydrous oxide and its surrounding diffuse double layer. The concentration of each of the ions at any location in the diffuse double layer is determined by a Boltzmann distribution:

$$\text{For a cation, } n_+(x) = n_o e^{-z_+ F\psi(x)/RT} \quad (5.4)$$

where n_o = the concentration of ions outside the influence sphere of the surface (bulk concentration)

$n(x)$ = the concentration of counter ions at distance x from the surface

z_+ = valency of the counter ions

$\psi(x)$ = Potential at x which is by definition the amount of work necessary to bring a positive unit of charge from infinity to x . The potential is negative if the surface charge is negative.

Figure 5.2 illustrates how the potential $\psi(x)$ in the double layer changes as a function of the distance to the surface. This relation is formulated as follows:

$$\psi(x) = \psi(o) + 2.3 RT/zF \log n_+(x)/n_-(x) \quad (5.5)$$

where $\psi(o)$ is the surface potential, given by:

$$\psi(o) = 2.3 RT/F \log \{H^+\}/\{H_o^+\} \quad (5.6)$$

$$\text{or } \psi(o) = 2.3 RT/F (pH_{zpc} - pH) \quad (5.7)$$

In this Nernst equation, R , T and F have their usual meaning. The relation between potential and space charge density in the double layer

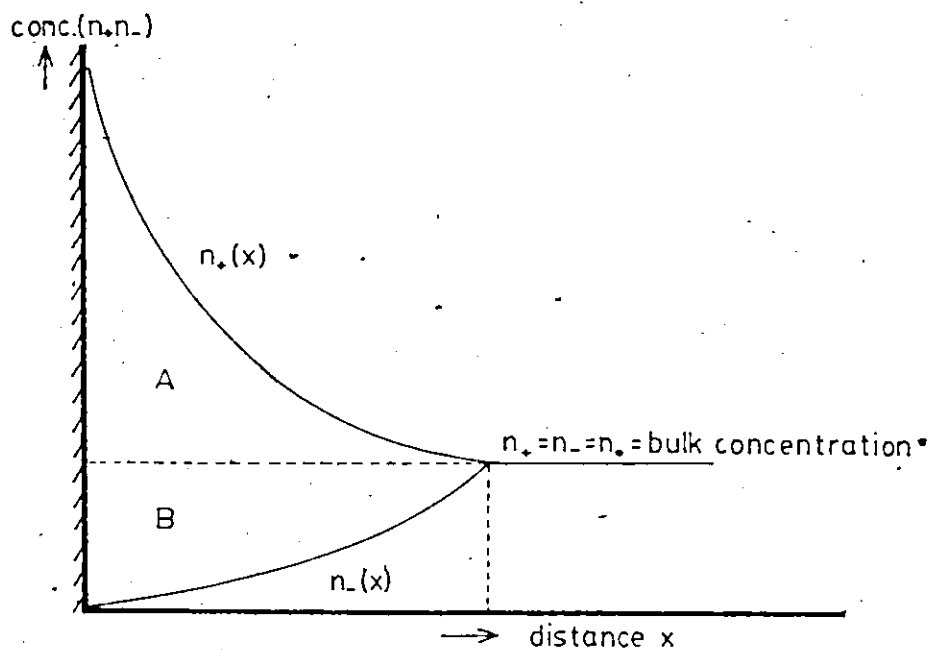


Figure 5.1 Charged surface and surrounding diffuse double layer (from Fler and de Wit 1969).
 area of A : excess of counter ions
 area of B : shortage of co-ions

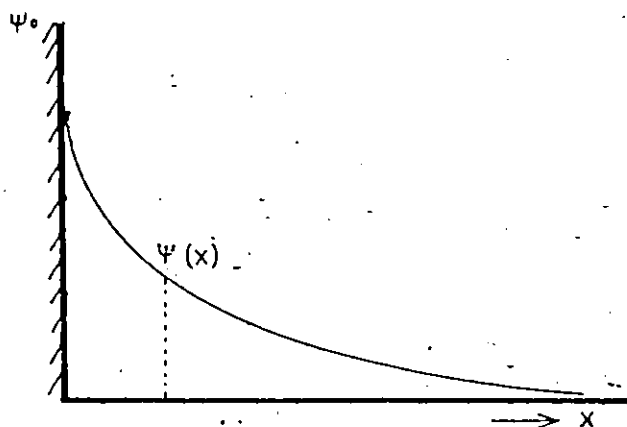


Figure 5.2 Change of potential (ψ_x) with distance (x) to the surface (from Fler and de Wit 1969).

is given by the Poisson equation:

$$d^2\psi/dx^2 = -4\pi\rho/\epsilon \quad (5.8)$$

where ρ = the charge density, i.e., $\rho = e(z_+n_+ + z_-n_-)$ (5.9)

or $\rho = zen_0(e^{-zF\psi(x)/RT} - e^{zF\psi(x)/RT})$ (5.10)

and ϵ = dielectric constant of the medium (e.g., water)

This can mathematically be reduced to:

$$\psi(x) = \psi(0) e^{-\kappa x}, \quad (5.11)$$

where $\kappa = \sqrt{8\pi n_0 z^2 e^2 / \epsilon kT} = \sqrt{10^{15} cz^2} \text{ cm}^{-1}$, (5.12)

in which c is the electrolyte concentration and z the valency of the electrolyte ions and $1/\kappa$ is by definition the thickness of the diffuse double layer. It is apparent that κ is determined by both the concentration and the valency, but more by the valency of the electrolyte ions. This in fact holds the key to colloid stability and Figure 5.3 serves to illustrate this.

The above presents the DLVO theory in its simplest form. The diffuse double layer (DDL) is often called Gouy-layer after one of two researchers, Gouy and Chapman, who quantitatively formulated the double layer theory independently. The DLVO theory only holds for a diffuse (as opposed to a compact) double layer. The only characteristic of the

ions involved, besides their concentration, is their valency. Accordingly, it offers no explanation for several observed effects: Adsorption progresses sometimes beyond what can be expected on the basis of electrostatic attraction, and the flocculation efficiency for various electrolyte ions with identical valencies and concentrations differs markedly.

The DLVO theory was corrected for ionic volume and specific adsorption effects by Stern (1924), who created a compact inner layer in the diffuse layer. The DLVO theory does not incorporate ionic volumes, but assumes so-called point charges. Due to this assumption, calculations with the Boltzmann equation showed that for a surface with a potential of -300 mV and a bulk concentration of electrolyte of 10^{-2} M, the concentration of ions adsorbed on the surface would be about 1600 M. It is apparent that a finite ionic volume sets an upper limit to the number of ions that can be adsorbed very near the surface. Furthermore, in the innermost part of the double layer, chemical forces between the surface and adsorbed ions other than the physical electrostatic force exist. These include van der Waals forces of attraction, H-bridge formation and real chemical bonding (in which ions lose their hydration spheres).

The compact inner part of the double layer, called the Stern layer, incorporates both ionic volume and specific adsorption. This is shown in Figure 5.4. As a result of finite ion volume in the Stern layer, there exists a charge free zone with a thickness of r_{ion} (or $r_{ion} + r_{water}$) in which the potential decreases linearly with distance from the surface as follows:

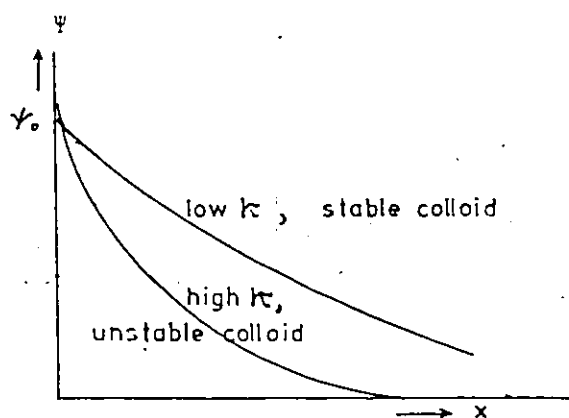


Figure 5.3 Qualitative relationship between colloid stability and thickness of the double layer (from Fler and de Wit 1969).

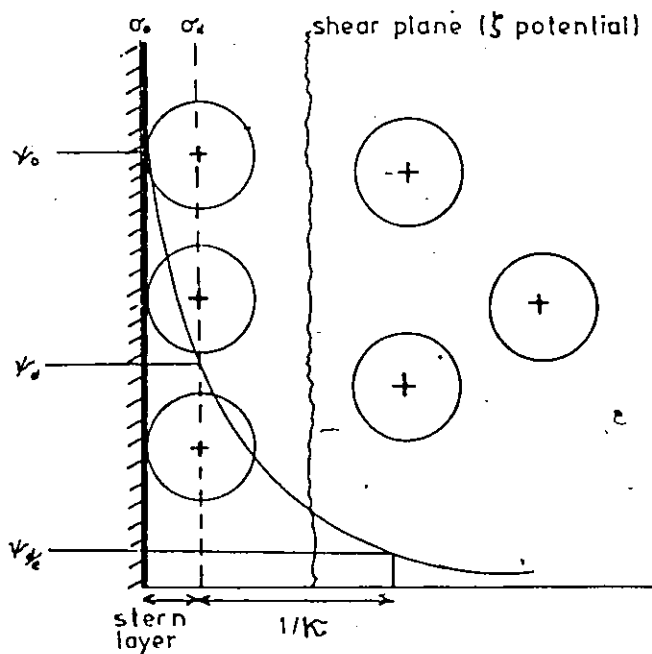


Figure 5.4 The Stern Layer (after Fler and de Wit 1969)

$$d/dx (d\psi/dx) = 0 \quad (5.13a)$$

and $d\psi/dx = c \quad (5.13b)$

A qualitative relation between charge and potential can be illustrated by the tangent to the potential curve in the diffuse double layer illustrated in Figure 5.5.

Grahame (1947) developed expression (5.14) to mathematically describe specific adsorption onto charged surfaces, which is located in the compact Stern plane:

$$\Gamma = 2 r C e^{-z F(\psi_d + \phi)/RT} \quad (5.14)$$

in which Γ = the adsorption density in the Stern layer

r = the radius of the adsorbed ion (may be hydrated)

C = equilibrium concentration in bulk solution

z = charge of the adsorbed ion

ψ_d = potential at the end of the Stern layer

ϕ = specific adsorption potential

In this classic theory, the surface potential is by definition determined by the amount of pdi or dissociated surface groups. The potential ψ_d at the end of the Stern layer is dependent on the amount of specific adsorption in the Stern layer. The relation between ψ_d and the charge in the diffuse double layer is given by the following Gouy-Chapman expression (Stumm et. al. 1970):

$$\psi_d = 0.05 \sinh^{-1} (\sigma_d / 11.74 C_o) \quad (5.15)$$

in which ψ_d = potential at end of Stern layer

σ_d = charge of the diffuse layer

C_o = electrolyte concentration in M

σ_d can be approximated by σ_o (the surface charge) in the case of no specific adsorption.

The Stern layer can in turn be divided into an inner and outer so-called Helmholtz plane, illustrated in Figure 5.6. The inner Helmholtz plane (IHP) is the plane where specific adsorption of ions other than indifferent electrolyte ions is located, while the outer Helmholtz plane (OHP) coincides with the plane of the compact layer adjacent to the specific adsorption layer in the Stern layer. The shear plane lies further into the diffuse double layer and only under very special circumstances such as low surface charge or low specific adsorption, can the potential at the shear plane be taken as very similar to the potential at the end of the Stern layer. The potential at the shear plane determines the stability of the system against coagulation, and cannot be measured directly, but can be assessed via flocculation studies. If a large amount of specific adsorption (i.e., super-equivalent adsorption) occurs, reversal of the sign of the diffuse double layer potential can result, which can be indicated by a reversed potential in the shear plane (i.e., ζ potential). Such a situation is illustrated in Figure 5.7.

5.1.3 Adsorption Models for Inorganic Cations

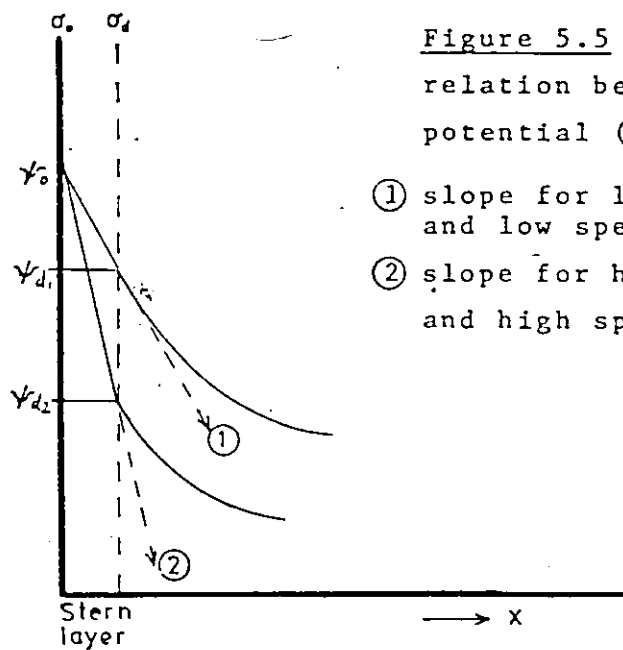


Figure 5.5 Qualitative relation between charge and potential (after Woods 1976).

- ① slope for low surface charge and low specific adsorption
- ② slope for high surface charge and high specific adsorption

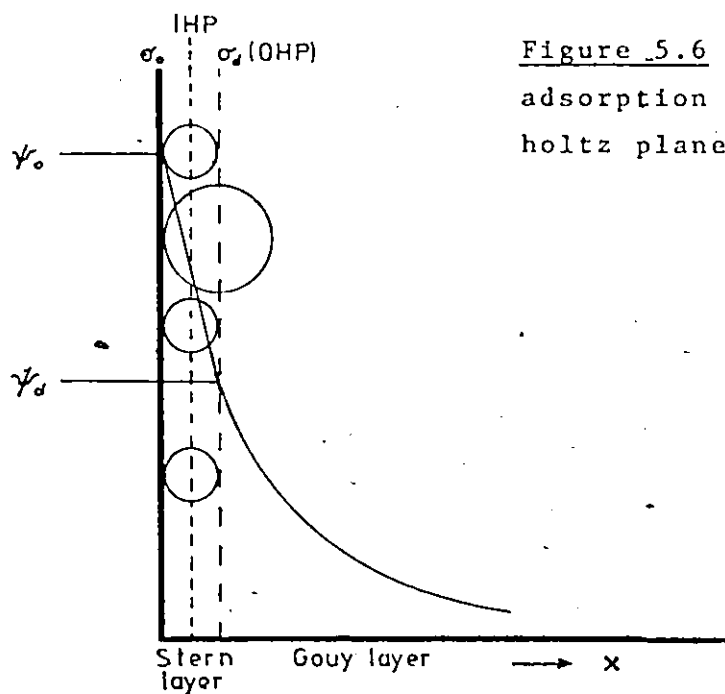


Figure 5.6 Finite specific adsorption in the inner Helmholtz plane (from Park 1975).

5.1.3.1 The Gouy-Chapman-Stern-Grahame-Model

This model, used for measurements concerning basic phenomena such as surface charge, colloid stability and electrokinetic potentials has in fact already been discussed qualitatively as a part of the double layer theory. It is probably better described as a theory than a model and consists of a number of expressions for adsorption density of adsorbed metal ions. These expressions are developed by respectively Gouy and Chapman (5.18), Stern (5.19) and Stern and Grahame (5.20) (see Section 5.13.3).

Adsorption of potential determining ions by hydrous oxides (H^+ and OH^-) is calculated from the difference between the consumption of acid or base by the particle suspension and that of a blank. From this, the surface charge can be calculated as follows:

$$\sigma_o = F(\Gamma_{H^+} - \Gamma_{OH^-}) = F(H^+ - OH^- + C_A - C_B)/A \quad (5.16)$$

in which σ_o = the surface charge (Coulombs/cm²)

F = Faraday constant

Γ_{H^+} and Γ_{OH^-} = analytical surface excesses for H^+ and OH^- ions (moles/cm²) respectively

C_A and C_B = acid respectively base consumption

A = surface area (cm²/g)

Adsorption of other ions is usually derived from the difference between the amount of ions added and their final solution concentration.

The pH of the zero point of charge for hydrous oxides can be found from the intersection point of σ_o - pH curves at different electro-

lyte concentrations, providing specific adsorption is absent.

The surface charge density and differential capacitance for many hydrous oxides appears to be much larger than the values measured for classic colloids such as Hg and AgI. Lyklema (1968) found that the actual values for σ_o for hydrous oxides tend to be higher, the more porous the surface is. Hence, he postulated the 'porous double layer' model, featuring a surface charge which is not confined to the surface proper but is distributed within some depth from the surface layer. The surface charge σ_o is partly compensated by counter ions which penetrate in the porous surface layer (σ_m) (Lyklema 1968), or in a 'gel layer' for non-porous surfaces (Perram 1973). Although the analytical surface charge depends on the concentration of p.d.i., the effective surface charge ($\sigma_o - \sigma_m$), as encountered in colloid stability studies and electrokinetic measurements, tends to become constant at some distance from the point of zero charge (Lyklema 1968).

Despite the high surface charge measured on oxides, the diffuse layer charge σ_d is relatively low. The maximum rate of change of the ζ -potential is seldom greater than 35 mV per pH unit or tenfold change in electrolyte concentration. This must mean that the capacitance C ($C = d\sigma_o/d\psi_o = \Delta\sigma_o/\Delta\psi_o$) (Davis et al. 1978a) for the inner layer is much larger than the capacitance for the diffuse layer and that the total double layer capacitance ($1/C_t = 1/C_{inner} + 1/C_{diffuse}$) is controlled primarily by the value of the diffuse layer capacitance. The inner layer capacitance is related by expression (5.17) to the distance between the surface and the plane of closest approach of counter ions (Davis 1978):

$$C_{\text{inner}} = \frac{\epsilon_{\beta} \epsilon_0}{\beta} = \frac{\epsilon_{\beta}}{1.131\beta} \quad \mu\text{F}/\text{cm}^2 \quad (\beta \text{ in nm}) \quad (5.17)$$

where ϵ_0 = permittivity of free space

ϵ_{β} = dielectric constant of the inner layer

β = distance between surface plane and plane of closest approach

The 'Gouy-Chapman-Stern-Grahame' theory has been used by various researchers. Levine and Smith (1971) derived a modified form of the Nernst equation with respect to H^+ and OH^- as potential determining ions on oxide surfaces and combined this with a model for the inner part of the double layer involving adsorption of both anions and cations of a supporting monovalent electrolyte. They also incorporated a discreteness-of-charge correction in their adsorption isotherms (discrete charges have electric fields different from smeared out charges (Woods 1976)). Breeuwsma and Lyklema (1973) studied adsorption of both cations and anions (alkali, alkali earth, chloride, nitrate, sulphate and phosphate) on Hematite ($\alpha\text{-Fe}_2\text{O}_3$) and found that most results could be explained satisfactorily in terms of the 'Gouy-Stern' theory.

5.1.3.2 The Adsorption-Hydrolysis Model

The above described adsorption theory fails to explain the sudden sharp increase in adsorption in a certain pH range. Hydrolysis of the adsorbing metal prior to adsorption is often invoked as an explanation, since this increase seems to coincide with the appearance of hydrolyzed metal species in solution (Matijević 1960, 1967). Matijević et al. (1960) have postulated that the adsorption of hydrolyzable metal ions is directly related to the presence of hydrolyzed species, and in fact a coagulation

technique is used to investigate the extent of metal ion hydrolysis. James and Healy (1972) have also emphasized that a hydrolyzed metal ion, because of its lower ionic charge and therefore reduced ion-solvent interaction, is the active species to be adsorbed preferably on oxide surfaces.

However, adsorption often occurs at a pH value considerably below the pH value where the first hydrolysis species appears. This is often used as a strong argument against the hydrolysis model. Stumm et al. (1976) compare the adsorption behaviour of aquo-metal ions with that of robust (kinetically inert) cation complexes such as $[\text{Co}(\text{NH}_3)_6]^{3+}$, $[\text{Co}(\text{NH}_3)_5\text{Cl}]^{2+}$ etc., which do not dissociate nor hydrolyze. They show that chemical interaction energies characterize the adsorption of aquo-metal ions primarily, while electrostatic interaction energies govern the adsorption of small, robust cation complexes (which therefore cannot cause charge reversal). Accordingly, the pH dependence of metal ion sorption onto a hydrous oxide surface can therefore be explained by the pH dependence of the activity of the surface ligand groups and the affinity of these ligand groups for the metal ion (Stumm et al. 1976). The hydrolysis of the latter prior to adsorption need not be invoked then.

5.1.3.3 The Ion-Solvent Interaction Model (James and Healy Model)

James and Healy (1972) attempted to fit experimentally obtained adsorption data for the adsorption of Co(II) on SiO_2 to the traditional adsorption isotherms based on the Gouy-Chapman-Stern-Grahame theory.

They used the following adsorption isotherms:

$$\Gamma_{Me}^{z+} = \{6.08 \times 10^{-11}/z\} \sqrt{C_{Me}^{z+}} \{\exp(z e \psi_0 / 2kT) - 1\} \quad (5.18)$$

(Gouy-Chapman)

$$\Gamma_{Me}^{z+} = 2 r C_{Me}^{z+} \exp\{-z e \psi_0 / kT\} \quad (5.19)$$

(Stern)

and
$$\Gamma_{Me}^{z+} = 2 r C_{Me}^{z+} \exp\{-z e (\psi_0 + \phi) / kT\} \quad (5.20)$$

(Stern-Grahame)

where Γ_{Me}^{z+} = adsorption density (mole/cm²) of adsorbed Me^{z+}

z = ionic charge

C_{Me}^{z+} = equilibrium concentration (mole/L)

ψ_0 = 59.2(pH_{zpc} - pH) (mV)

r = radius of ion

ϕ = specific adsorption (i.e., chemisorption) potential of an ion with charge z and radius r

None of these adsorption isotherms were found to fit the observed data if ψ_0 was used for the surface potential. Using $\psi_x < \psi_0$ or even ψ_d or the ζ -potential did not improve matters. However, they found that, if they used the parameters for the hydrolyzed metal species instead of the values for the free metal ions, they were able to fit the data to the Stern-Grahame model. Nevertheless, this did not explain why the unhydrolyzed species do not adsorb to a comparable extent in the Stern layer at the interface. In order to explain this, James and Healy (1972) designed a model which considers adsorption to be controlled by coulombic, solvation and specific chemical energy interactions as the ion approaches

the interface. The lowering of the ionic charge of metal ions through hydrolysis decreases the solvation energy which otherwise forms too large an energy barrier to allow the unhydrolyzed ion to approach the surface very closely.

A number of researchers had previously proposed electrostatic models for ϕ , all of which resulted in superequivalent adsorption with the term ϕ , a free energy, being negative, enhancing adsorption. James and Healy argued however that in order to explain the hypothesized adsorption of hydrolyzed cations in preference to free metal ions, an electrostatic term could not be used, since electrostatic adsorption will always be most favourable for the adsorption of free metal ions on negative surfaces. Yet, metal ions characteristically do not adsorb until a critical pH is reached. Therefore, they argued the need for a ϕ term that opposes adsorption rather than aids it. They found that this was possible by hypothesizing that ϕ accounts for changes in the secondary (i.e., outer) hydration sheath of the adsorbing ion, since a solvation energy term is the most likely to prevent adsorption. The inner hydration sheath remains undisturbed.

They separate the energy involved in cation adsorption into a simple coulombic term, $z e \psi_x$, and a secondary solvation energy term. Due to discreteness of charge, the coulombic term actually underestimates ψ_x . Therefore it is 'corrected', when necessary, with a 'chemical' free energy term, rather than by estimating the 'true' potential, using the model of Levine et al. (1967). Their overall model is given by the following equation:

$$\Delta G_{\text{ads } i}^{\circ} = \Delta G_{\text{coul } i}^{\circ} + \Delta G_{\text{solv } i}^{\circ} + \Delta G_{\text{chem } i}^{\circ} \quad (5.21)$$

$\Delta G_{\text{ads } i}^{\circ}$ is to be calculated for every ion (i) considered capable of adsorbing. It is tacitly assumed that $\Delta G_{\text{ads } i}^{\circ}$ is independent of the fractional coverage of the surface. This assumption is appropriate if the adsorbed ions or molecules are considered to be hydrated, which implies that they cover a relatively large area per adsorption site, compared with the area that would be covered by the bare or free ion itself.

The free energy term $\Delta G_{\text{ads } i}^{\circ}$ can then be used in the Grahame expression to calculate the adsorption density as follows:

$$\Gamma_i = 2r_{\text{hydr}} C_i \exp(-\Delta G_{\text{ads } i}^{\circ}/RT), \quad (5.22)$$

providing that the density is less than monolayer coverage. If both C_i and $\Delta G_{\text{ads } i}^{\circ}$ are large, then the complete (or extended) Stern expression must be used (see also Section 5.1.3.5.4).

To obtain the total adsorption density, the adsorption density for each ion or species has to be calculated from:

$$\Gamma_{\text{Me } i} = \Gamma_{\text{Me } i}^{z+} + \Gamma_{\text{Me(OH)}_n}^{z-n} \quad (5.23)$$

This can be done by deriving a Langmuir expression analogous to (5.3):

$$\theta = \frac{\sum_i K_i \text{Me}_i}{1 + \sum_i K_i \text{Me}_i}, \quad (5.24)$$

in which θ is the fraction of surface sites covered by Me_i . The uncovered fraction $(1-\theta)$ equals $\Gamma_{\max} - \Gamma_{\text{ads}}$ in the earlier derived Langmuir isotherm (5.2):

To calculate the fractional coverage of one particular species, one can use the expressions (Stumm and Morgan 1970):

$$\theta_i = \frac{K_i Me_i}{1 + \sum_i K_i Me_i} \quad (5.25)$$

$$\Delta G_{\text{ads } i}^{\circ} = -R T \ln K_i \quad (5.26)$$

and $K_i = \exp (-\Delta G_{\text{ads } i}^{\circ} / RT)$. (5.27)

The expressions for the three free energy terms are given by James and Healy (1970) as follows:

$$\Delta G_{\text{coul } i}^{\circ} = z_i F \Delta \psi_x \text{ (joule/mole)} \quad (5.28)$$

where $\Delta \psi_x = \frac{2 R T}{z F} \ln \frac{(e^{zF\psi_0/2RT} + 1) + (e^{zF\psi_0/2RT} - 1)e^{-\kappa x}}{(e^{zF\psi_0/2RT} + 1) - (e^{zF\psi_0/2RT} - 1)e^{-\kappa x}}$ (5.29)

(for derivation, see Stumm and Morgan 1970, p. 460)

Here $\psi_0 = 2.3 RT / zF (\text{pH}_{\text{zpc}} - \text{pH})$

$\kappa = 0.328 \times 10^{10} (I)^{1/2}$ = thickness of the double layer (m^{-1})

$x = r_{\text{ion}} + 2r_{\text{water}}$ (m)

z_i = valency of adsorbing ion

z = valency of background electrolyte

For $\Delta G^\circ_{\text{solv } i}$ two different expressions can be used, depending on the assumptions one makes regarding the manner in which the sorbing ion approaches the surface. For the case where the primary hydration sheath of the ion and the water adsorbed on the solid do not overlap, James and Healy derive that:

$$\Delta G^\circ_{\text{solv } i} = \frac{z_i^2 e^2 N}{32\pi r_e \epsilon_0} \left(\frac{1}{\epsilon_{\text{int}}} - \frac{1}{\epsilon_{\text{bulk}}} \right) + \frac{z_i^2 e^2 N}{32\pi (r_e + 2r_w) \epsilon_0} \left(\frac{1}{\epsilon_{\text{solid}}} - \frac{1}{\epsilon_{\text{int}}} \right)$$

(joule/mole). (5.30)

where z = charge on the ion

N = Avogadro's number

e = electronic charge

ϵ_0 = permittivity of free space

ϵ_{int} = dielectric constant of material in the interface

ϵ_{bulk} = dielectric constant of material in the bulk solution

ϵ_{solid} = dielectric constant of material in the adsorbing surface

r_e , r_w , and r_{ion} = radii of adsorbed species, see Figure 5.8

The second, more likely situation is where the primary hydration sheath of the ion includes the adsorbed water on the solid surface, i.e., the primary hydration sheath and adsorbed water overlap. The following expression is obtained for such a situation:

$$\Delta G^\circ_{\text{solv } i} = \frac{z_i^2 e^2 N}{16\pi \epsilon_0} \left(\frac{1}{r_{\text{ion}} + 2r_w} - \frac{r_{\text{ion}}}{2(r_{\text{ion}} + 2r_w)^2} \right) \left(\frac{1}{\epsilon_{\text{int}}} - \frac{1}{\epsilon_{\text{bulk}}} \right) + \frac{z_i^2 e^2 N}{32\pi \epsilon_0} \left(\frac{1}{r_e + 2r_w} \right) \left(\frac{1}{\epsilon_{\text{solid}}} - \frac{1}{\epsilon_{\text{int}}} \right)$$

(joule/mole) (5.31)

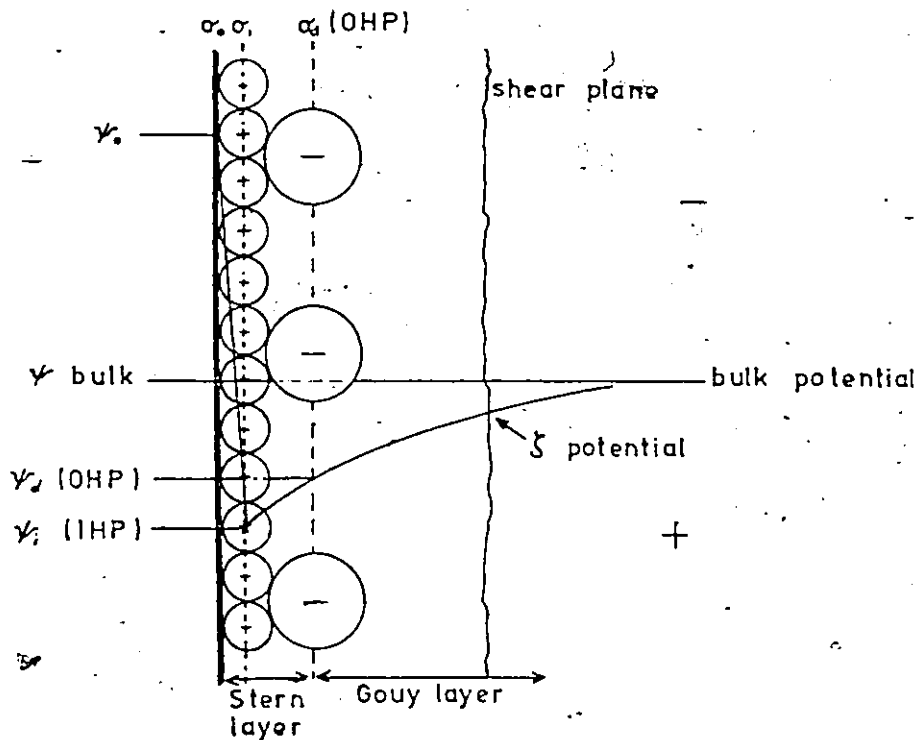


Figure 5.7 Super equivalent adsorption resulting in sign reversal for the ζ potential (after Park 1975).

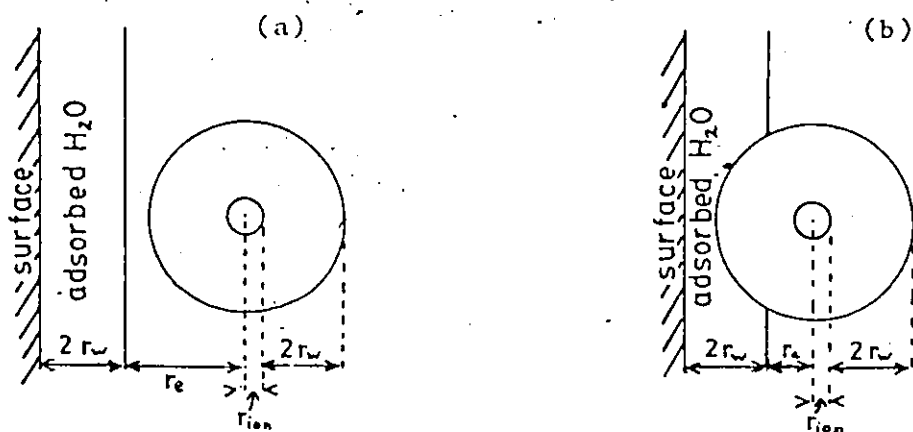


Figure 5.8 Possible locations for an adsorbed ion (from James and Healy 1972)

- Primary hydration sheath of ion and adsorbed water on the surface do not overlap.
- Primary hydration sheath of ion includes adsorbed water on the surface or, in other words, the primary hydration sheath and adsorbed water overlap.

$$\text{where } \epsilon_{\text{int}} = \left(\frac{\epsilon_{\text{bulk}} - 6}{1 + (1.2 \times 10^{-17})(d\psi/dx)x^2} \right) + 6 \quad (5.32)$$

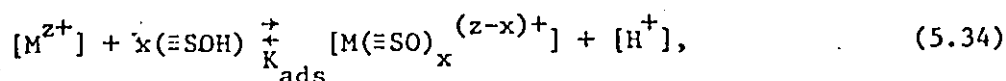
$$\text{and } \frac{d\psi}{dx} = -2\kappa \frac{RT}{zF} \sinh(zF \Delta\psi x / 2RT) \text{ V/m} \quad (5.33)$$

ϵ_{int} is the dielectric of the interface, the property which makes the major contribution to the secondary solvation energy term as the ion approaches the surface. The two situations regarding the possible locations of an adsorbed ion can be pictured as shown in Figure 5.8. For insulating oxides, which have a low ϵ_{solid} , $\Delta G_{\text{solv } i}^{\circ}$ is of considerable magnitude.

$\Delta G_{\text{chem } i}^{\circ}$ is chosen differently for each metal but is the same for each species of one metal. Some typical $\Delta G_{\text{chem } i}^{\circ}$ values can be calculated from the thermodynamic functions given by Dugger et al. (1964).

5.1.3.4 The Ion Exchange Model

The pH dependence of adsorption for a metal ion on a hydrous oxide can be characterized in terms of a mass law relationship, if adsorption of the metal ion is assumed to follow a course similar to complexation with a weak acid and if the activity of the solid phase (c.q. of the surface groups involved in adsorption) remains unchanged by the adsorption process. The surface reaction can be treated according to mass law theory, as first applied for adsorption by Kurbatov et al. (1951a,b):



$$K_{\text{ads}} = \frac{[\text{M}(\equiv\text{SO})_x^{(z-x)+}] [\text{H}^+]^x}{[\text{M}^{z+}] (\equiv\text{SOH})^x} \quad (5.35)$$

$$\text{and } \log \frac{[\text{M}(\equiv\text{SO})_x^{(z-x)+}]}{[\text{M}^{z+}]} = \log \frac{[\text{M}^{z+}]_{\text{sorbed}}}{[\text{M}^{z+}]_{\text{solution}}} = A + x \text{ pH} \quad (5.36)$$

where $A = \log K_{\text{ads}} + x \log (\equiv\text{SOH})$

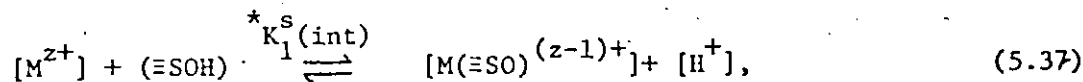
Morgan and Stumm (1964) and Posselt et al. (1968) however pointed out that the basic condition of constant sorbent activity during adsorption is not satisfied. Although both found a straight line relationship when plotting $\log [\text{M}^{z+}]_{\text{adsorbed}} / [\text{M}^{z+}]_{\text{solution}}$ versus pH, they conclude that the derived value for x has no chemical meaning.

Dugger et al. (1964) used this model in their adsorption study of twenty metal ions on silica. Free energies of the bonds between the surface and metal ions were determined at such pH values that cation hydrolysis was largely avoided. Dugger et al. (1964) stressed this point, because they had found that $\log K_{\text{ads}}$ varied linearly with $\log K_1^*$, the first hydrolysis constant for the adsorbing metal in question. This led to the observation that increased adsorption and the appearance of hydrolysis processes in solution were positively correlated. However, Davis (1978) claims that there is no need to avoid certain pH values to exclude hydrolyzed species. Providing such species are positively charged, they can still take part in ion exchange reactions and do not need to be excluded from the model.

The ion exchange model has at least two disadvantages. Firstly, one has to assume that the surface charge is constant. Secondly, the model is not very general, since it is not applicable to surfaces which do not have H^+ and OH^- as potential determining ions.

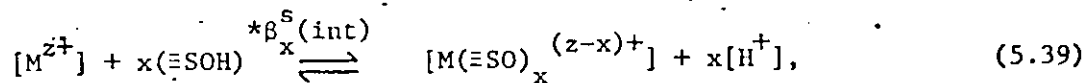
5.1.3.5 The Surface Complex Formation- or Site Binding- Model

Schindler et al. (1976) proposed a model, similar to that of Huang and Stumm (1973), which corrects for the fact that the activity of the surface groups cannot be regarded as constant upon adsorption. The model is as follows:



$$\text{or } K_1^S(\text{int}) = \frac{(e^{(z-1)F\psi/RT}) [H^+] \{ [M(\equiv\text{SO})^{(z-1)+}] \}}{[M^{z+}] \{ (\equiv\text{SOH}) \}} \quad (5.38)$$

In more general terms it follows that:



$$\text{or } \beta_x^S(\text{int}) = \frac{(e^{(z-x)F\psi/RT}) [H^+]^x \{ [M(\equiv\text{SO})_x^{(z-x)+}] \}}{[M^{z+}] \{ (\equiv\text{SOH})^x \}} \quad (5.40)$$

in which [] are concentrations of species in solution (M) and

{ } are concentrations of surface species (mole/kg surface)

This kind of equilibrium constant is called an intrinsic microscopic formation constant and is valid for solutions of constant ionic strength. ψ stands for the potential difference between the sites of $[M(\equiv\text{SO})_x^{(z-x)+}]$ and the bulk of the solution.

The possibility of mixed complex formation at the surface (e.g., $[M(\text{OH})_m(\equiv\text{SO})_x^{(z-x-m)+}]$) is not included in this site-binding model.

However, Davis (1978) argues that there is no reason to exclude mixed complexes from adsorption models and the model of James and Healy (1972) in fact incorporates such mixed complexes.

In the course of his investigations, Schindler et al. (1976) found that, surprisingly, ψ could be approximated by a constant or even zero value, without leading to serious difficulties.

Combining expression (5.40) and $\psi = RT \ln(10)/F (\log[H^+] - \log[H^+]_{zpc})$, the following relation between β_x^s and pH can be predicted:

$$\log \beta_x^s = \log \beta_x^s(\text{int})^s + (z-x)(\log[H^+]_{zpc} - \log[H^+]) \quad (5.41)$$

However, it appears that the dependence of k_1^s (or β_x^s) on the surface charge and $\log[H^+]$ is much smaller than the above relation predicts. Davis (1978) argues that such an inadequacy of the physical (electrostatic) correction term is a major disadvantage of the surface complexation model, and proposes an improvement (see Section 5.1.3.5.4; Triple Layer Model).

Schindler et al. (1976) find, like Dugger et al. (1964), a linear relationship between $\log K_1^s$ and $\log K_1$ (first hydrolysis constant), indicating that the ligand properties of the OH-groups on the surface are not basically changed by the proximity of the surface (silica in this case). Again, such a straight line relationship provides an explanation for the often observed coincidence of hydrolysis and adsorption.

According to Davis (1978), the reactions assumed for the development of the surface charge in the site-binding model are too simple.

They force the assumption of a very high capacitance for the inner region of the double layer, to obtain agreement with the, for most oxides observed, high surface charge and low diffuse layer charge (Yates et al. 1974).

The main advantage of the surface complexation or site-binding model is that it is simple compared with for instance the James and Healy model, which in addition to its complexity assumes no interaction between surface sites. The site-binding model has been used with considerable success by various researchers to describe adsorption behaviour of dilute metal ions at constant ionic strength, in systems where the chemical interaction with the surface was dominant (e.g., Schindler et al. 1976; Hohl and Stumm 1976).

According to Westall and Hohl (1980) there are many models which could be categorized as 'surface complexation' models. These models all describe hydrolysis and adsorption at metal oxide surfaces, and may be expressed with similar mass law and material balance equations. They all possess a fixed number of adsorption sites. The main difference between these models is how the electrical double layer is conceptualized in each model, or in other words, where in each model adsorption is located. Westall and Hohl (1980) compare five such surface complexation models, for well-defined, crystalline surfaces and provide a very clear description of the various double layer models involved. This comparison is now reviewed in some detail.

5.1.3.5.1 Constant Capacitance Model

This model was used by Stumm et al. (1976) and Hohl and Stumm

(1976). It conceptualizes the electrical double layer as shown in Figure 5.9-a. The surface charge σ_o is determined by H^+ and OH^- ions and there exists a linear relationship between the surface charge and potential $\sigma = a\psi_o$, where a is a constant which varies for each adsorption isotherm. This means that the capacitance is constant, i.e., $C = \Delta\sigma_o / \Delta\psi_o$, but not fixed. All specifically adsorbed ions contribute to the surface charge and experience ψ_o , while non-specifically adsorbed counter ions are excluded from the surface layer (Westall and Hohl 1980).

5.1.3.5.2 The Diffuse Layer Model

This model was used by Stumm et al. (1970) and Huang and Stumm (1973) and conceptualizes the double layer as shown in Figure 5.9-b. The charge-potential relationship in this model is identical to the one used in the Gouy-Chapman (G-C) model, but contains a fixed number of surface sites implied in a surface complexation model, which the G-C model does not have. Stumm et al. (1970) argue that in a simple model one can compute ψ_o from the surface charge by setting $\psi_o = \psi_d$, where ψ_d is the potential at the plane of closest approach, i.e., the Stern layer. They also assume that ideally, σ_d may be considered nearly equal to σ_o and analogous to expression (5.15), one can use the following equations for the relation between ψ_o and σ_o :

$$\psi_o = 0.05 \sinh^{-1} (\sigma_o / 11.74 C_o) \quad (5.42)$$

or
$$\sigma_o = (8 \epsilon \epsilon_o R T I)^{1/2} \sinh (F\psi_o / 2 R T) \quad (5.43)$$

which, for low ψ_0 ($\psi_0 < 25\text{mV}$) can be approximated by:

$$\sigma_0 = (8 \epsilon \epsilon_0 R T I)^{1/2} F \psi_0 / 2 R T \quad (5.44)$$

in which ϵ = dielectric of the medium (i.e., surface)

ϵ_0 = dielectric of free space

This is in fact also a constant capacitance model, but the capacitance in this case is fixed. As in the constant capacitance model, all specifically adsorbed ions are assumed to contribute to the charge σ_0 and experience the potential ψ_0 (Westall and Hohl 1980).

5.1.3.5.3 Stern Models

Bowden, Posner and Quirk (1977) present a completely general theory which can be used to describe both anion and cation adsorption on amphoteric oxide surfaces. The interface model is very similar to the basic Stern model developed for an AgI surface in which the potential determining ions Ag^+ and I^- are part of the surface, or in other words fit into the AgI lattice. In Bowden et al.'s model the H^+ and OH^- ions are assigned to the immediate surface where they contribute to the surface charge σ_0 and experience the potential ψ_0 (Westall and Hohl 1980). This is visualized in Figure 5.9-c. Other specifically adsorbed ions are assigned to the Inner Helmholtz Plane (IHP), contributing to the charge σ_1 and experiencing the potential ψ_1 . All non-specifically adsorbed ions are assigned to the diffuse layer. C_1 is the capacitance in the region between the surface and the IHP, while the potential at the OHP equals the potential at the IHP. This implies that the region

between IHP and OHP has a very large capacitance, which can be made clear as follows:

$$C_1 = \frac{\sigma_o}{\psi_o - \psi_1} \text{ and } C_2 = \frac{\sigma_o}{\psi_1 - \psi_d} \text{ in which } C_2 \rightarrow \infty \text{ as } \psi_1 = \psi_d.$$

Stern (1924) proposed a model for the Hg surface in which the pdi are not part of the Hg structure (as in AgI), but are located at the IHP, where also the electrostatically attracted electrolyte ions are located. This means that the actual surface layer has zero charge. Figure 5.9-d shows such a situation for oxide surfaces in which H^+ and OH^- are pdi. In addition, there is a diffuse layer, either separated from the IHP by a Helmholtz capacitance (the so-called Extended Stern Model) or not. Figure 5.9-d also visualizes the extended model.

This Stern model is different from the others in that it assigns both chemically and electrostatically bound ions to the same plane, which results in a lower surface charge than calculated by the other models. For the same reason, the potential predicted by the Stern model is lower than predicted by any of the other models discussed.

5.1.3.5.4 The Triple Layer Model

This model was proposed by Yates et al. (1974) and extensively used by Davis (1978), Davis et al. (1978) and Davis and Leckie (1978a,b; 1979; 1980). It is visualized in Figure 5.9-e. The surface charge σ_o is calculated from mass balance and electroneutrality considerations. For a hydrous oxide in a NaCl background electrolyte, the equations are:

$$\sigma_o = 10^6 F/A ([SOH_2^+] + [SOH_2^+Cl^-] - [SO^-] - [SO^-Na^+]) \mu C/cm^2, \quad (5.45)$$

while σ_1 is given by

$$\sigma_1 = 10^6 F/A ([SO^-Na^+] - [SOH_2^+Cl^-]) \mu C/cm^2, \quad (5.46)$$

$$\text{and } \sigma_o + \sigma_1 + \sigma_d = 0, \quad (5.47),$$

$$\text{where } \sigma_d = -11.74 \sqrt{C} \sinh (ze\psi_d/2kT) \mu C/cm^2. \quad (5.48)$$

C = bulk concentration of electrolyte (M)

This model accommodates in the innermost layer only H^+ and OH^- ions which contribute to σ_o and experience the potential ψ_o (Westall and Hohl 1980). A region of constant capacitance C_1 ($\psi_o - \psi_1 = \sigma_o/C_1$) separates the surface from the IHP, where the electrolyte ions are assigned to by this model. These electrolyte ions form 'ion pairs' (Yates et al. 1974) with oppositely charged surface groups. Davis (1978) argues that it is better to speak of 'surface complexes' but stresses the point that this does not imply a particular bonding structure. The 'surface complex' forming ions contribute to σ_1 and experience ψ_1 . The IHP and OHP are separated by a region of constant capacitance C_2 ($\psi_1 - \psi_d = -\sigma_d/C_2$), while the potential at the OHP is ψ_d and the charge σ_d (diffuse layer charge).

According to Davis (1978), the formation of these 'surface complexes' readjusts the acid-base equilibrium on the surface and therefore affects the surface charge σ_o . The surface charge can thus be considered as determined by the net number of protons released or

consumed by all surface reactions and not just by the formation of ionized surface species such as $[\text{SO}^-]$ and $[\text{SOH}_2^+]$.

The surface species are distributed among the total number of sites available, N_s ($\mu\text{C}/\text{cm}^2$), as follows:

$$N_s = 10^6 F/A \{ [\text{SOH}_2^+] + [\text{SOH}_2^+ \text{Cl}^-] + [\text{SOH}] + [\text{SO}^-] + [\text{SO}^- \text{Na}^+] \} \quad (5.50)$$

$$[\text{SOH}_2^+] = [\text{SOH}] [\text{H}^+] [\exp(-e\psi_o/kT)] / K_{a1}^{\text{int}} \quad (5.51)$$

$$[\text{SO}^-] = [\text{SOH}] / [\text{H}^+] [\exp(e\psi_o/kT)] K_{a2}^{\text{int}} \quad (5.52)$$

$$[\text{SO}^- \text{Na}^+] = [\text{SOH}] [\text{Na}^+] / [\text{H}^+] \exp[(e\psi_o - e\psi_1)/kT] * K_{\text{Na}^+}^{\text{int}} \quad (5.53)$$

$$[\text{SOH}_2^+ \text{Cl}^-] = [\text{SOH}] [\text{H}^+] [\text{Cl}^-] \exp[(e\psi_1 - e\psi_o/kT)] / * K_{\text{Cl}^-}^{\text{int}} \quad (5.54)$$

This set of equations can be solved numerically with known values for the interfacial properties N_s , K_{a1}^{int} , K_{a2}^{int} , $*K_{\text{Na}^+}^{\text{int}}$, $*K_{\text{Cl}^-}^{\text{int}}$, C_1 and C_2 . The intrinsic stability constants for a hypothetical isolated site can be determined from the apparent (conditional) stability constants, which can be calculated from the bulk solution concentrations. This involves applying mass law equations to potentiometric titration data, plotting these apparent stability constants against the calculated surface charge and extrapolating the apparent stability constants to zero charge conditions.

Davis (1978) gives a method to determine the intrinsic constants which is different from the way in which Stumm and coworkers and

Schindler determined these, since the latter do not include surface-complex induced charge.

In the triple layer theory, it is assumed that the surface possesses a chemisorbed water layer which may adsorb or release protons to form the ionized surface sites, which cause σ_0 . The theory also assumes that electrolyte ions cannot quite reach this σ_0 plane, but approach the surface closely to form the σ_1 plane. Because of the intervening chemisorbed water layer, an approaching electrolyte ion may obtain a chemisorbed water molecule as part of its hydration layer (compare the James and Healy model), which constitutes a chemical bonding. Such a sharing of water molecules allows a very close approach to the σ_0 plane. This is consistent with the experimental observations and model calculations of a high inner capacitance, given by:

$$C_1 = \epsilon \epsilon_1 / \beta \quad \mu\text{F}/\text{cm}^2 \quad (5.55)$$

$$C_1 = \epsilon_1 / 1.131\beta \quad \mu\text{F}/\text{cm}^2 \quad (5.56)$$

in which β is the distance between σ_0 and σ_1 (in nm), while ϵ_1 is the relative dielectric strength in the inner region. From the above expression, it can be easily seen that the closer the electrolyte ions can approach the σ_0 plane, the higher the capacitance for the inner region.

The mean location of all specifically adsorbed ions is also assumed to be in the σ_1 plane. For Me^{2+} adsorption in NaNO_3 electrolyte the triple layer theory gives:

$$\sigma_0 = [\text{SOH}_2^+] + [\text{SOH}_2^+ \text{-NO}_3^-] - [\text{SO}^-] - [\text{SO}^- \text{-Na}^+] - [\text{SO}^- \text{-Me}^{2+}], \quad (5.57)$$

$$\sigma_1 = [\text{SO}^- \text{-Na}^+] + 2[\text{SO}^- \text{-Me}^{2+}] - [\text{SOH}_2^+ \text{-NO}_3^-], \quad (5.58)$$

$$[\text{SO}^- \text{-Me}^{2+}] = [\text{SOH}][\text{Me}^{2+}]/[\text{H}^+] \exp[(e\psi_0 - 2e\psi_1)/kT] * K_{\text{Me}^{2+}}^{\text{int}} \quad (5.59)$$

The triple layer site-binding model as described above has been favoured by the results of Smit et al. (1978a,b). By using radiotracer techniques they found that sodium ions penetrate a solid phase (vitreous silica) less than 0.3 nm and that the formation of a gel layer is unlikely. This favours the triple layer site-binding model over the other site-binding models for the explanation of the fact that satisfactory agreement between calculated and observed zeta potentials can only be obtained by assuming that the surface potential ψ_0 is less than what can be calculated by using the Nernst equation:

$$\psi_0 = 2.303 RT/F(\text{pH}_{\text{zpc}} - \text{pH}). \quad (5.7)$$

5.1.3.5.5 Comparison of Surface Complexation- or Site-Binding- Models

Westall and Hohl (1980) compared the predictive powers for each of these five site-binding models at different ionic strength situations. The fit of experimental acid-base titration data (for $\gamma\text{-Al}_2\text{O}_3$ in 0.1 M NaClO_4) to each of these five models appears to be equally excellent. The simple (i.e. conditional) models determine their fitting parameters for each ionic strength, but in the more complicated models, the parameters are applicable over a much wider range of experimental conditions. Westall and Hohl argue that the parameters for each of

these models (e.g. equilibrium constants and capacitances) should not be directly compared since they are not based on the same assumptions regarding location of adsorption. Only the fit obtained by each model, can be compared.

The models in Sections 5.1.3.5.1 and 5.1.3.5.4 were compared for predicting the experimental observations for an acid-base titration for TiO_2 (rutile) in respectively 0.1, 0.01, and 0.001 M KNO_3 . Again, for both models, very good agreement was obtained between predicted and observed data. Such agreement is especially remarkable for model 5.1.3.5.1, the constant capacitance model. In terms of the Stern model, the constant capacitance model can be regarded as the 'high ionic strength' limiting case of the basic Stern model, because at high ionic strength, the diffuse double layer capacitance is much greater than the compact layer capacitance. This leaves the total capacitance approximately equal to the compact layer capacitance. Along the same line, the diffuse layer model, model 5.1.3.5.2 can be regarded as the 'lower ionic strength' limiting case of the basic Stern model.

Westall and Hohl (1980) concluded that in the situation where a prediction of 'mass balance' is required, all models are equally accurate, but that none of these models is able to uniquely describe and separate the adsorption energies (chemical and electrostatic) involved at the oxide-water interface, and hence allow accurate statements concerning the mechanism of adsorption. Furthermore, the values for the 'intrinsic' (non-conditional) chemical surface complexation energies are really only valid for the model with which they were derived. They argue as follows: The 'intrinsic' constants are found via extrapolating to zero charge

conditions, a procedure which is influenced by the assumptions made for the properties of the interface (e.g., where the adsorption is located, values of capacitances, number of interface layers), which vary from model to model. Since no unique physical and electrostatic model exists at present, reported 'intrinsic' constants should always be accompanied by a description of the assumptions for the interface model for which they were found. Comparison of chemical constants is only valid if they are derived for the same electrostatic and physical model.

5.1.4 Models for Adsorption of Anions and Metal-Ligand Complexes

Adsorption of inorganic anions on hydrous oxide surfaces in aqueous systems has been described with the ion-exchange (c.q. ligand-exchange) model (see Section 5.1.3.4) for the adsorption of nitrate, sulphate and phosphate on goethite and α -chromia by Yates and Healy (1975), and for phosphate on hematite by Bréeuwsma and Lyklema (1973) and Bowden et al. (1977). The adsorption of arsenate onto aluminum oxide has been modeled by Malotki and Anderson (1976) and Anderson et al. (1976).

Much data and knowledge regarding the adsorption of organic materials on surfaces has been collected in the field of soil science. A few representative studies are those of Healy (1971), Schnitzer and Khan (1972), Orlov et al. (1973) and Rubio and Matijevic (1979).

Healy (1971) discusses the principles of selective adsorption of organics such as small organic molecules (e.g., amino acids), surfactants, polymers and organic sols onto inorganic surfaces which have the

properties of a simple inorganic oxide. The total free energy of adsorption can be expressed as:

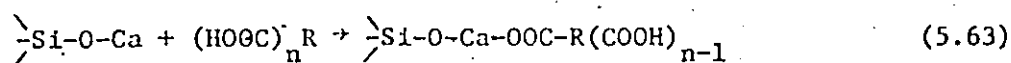
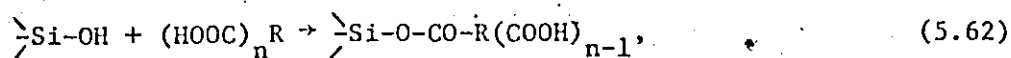
$$\Delta G_{\text{ads } i} = \sum_{\text{all } i} \Delta G_i \quad (5.60)$$

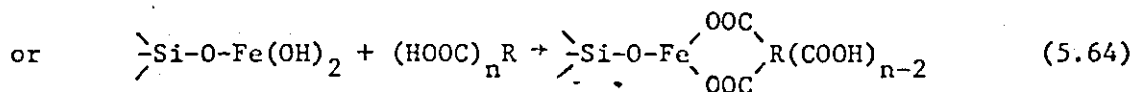
$$\text{or } \Delta G_{\text{ads}} = \Delta G_{\text{coul}} + \Delta G_{\text{solv}} + \Delta G_{\text{hydr.bond}} + \Delta G_{\text{vdwaals}} + \Delta G_{\text{chem}} \quad (5.61)$$

The way in which each of these energies contributes to the overall energy of binding varies with molecular structure of the organic and the surface structure and controls selective uptake.

Schnitzer and Khan (1972) discuss some reactions of metal-hydroxides and -oxides with humic and fulvic acids. They mention that freshly precipitated Fe^{3+} and Al^{3+} hydroxides adsorb humics and fulvics (with the Al^{3+} hydroxides being more active in this respect than the Fe^{3+} hydroxides), while under certain circumstances solubilization of some Fe^{3+} and Al^{3+} can occur.

In a review, the interaction of humic substances with minerals and the nature of their bond is discussed by Orlov et al. (1973). Interactions between humics and minerals is shown to be possible because of the bonding of the hydroxyl groups on humic acids with the OH groups of minerals or via the formation of mineral bridges. Khan (1969), quoted by Orlov et al. (1973) suggested the following possibilities:





These reaction schemes do not show any participation of the very active nitrogen-containing groups on humic acids, but it is expected that such groups can play an important role in the adsorption of organics on mineral surfaces (Orlov et al. 1973).

Rubio and Matijevic (1979) studied the interaction of EDTA with β -FeOOH particles over a wide pH-, temperature- and concentration- range with respect to the adsorption of the chelating agent and the simultaneous dissolution of the solid. They concluded that the chemical binding energy (ΔG_{chem}) between EDTA and the cation of β -FeOOH particles represents the major contribution to the overall free energy of adsorption (ΔG_{ads}) in the pH range where uptake of EDTA by the surface was observed. Adsorption of EDTA seemed to inhibit dissolution of the β -FeOOH particle, but when, above a certain pH value, the adsorption of EDTA decreased, the leaching of ferric species increased considerably. A minimum surface coverage seemed to be needed in order to inhibit the dissolution of iron.

However, possible adsorption of organic material onto hydrous oxides in aquatic systems in the presence of trace metals and adsorption of metal-organic complexes is often avoided in adsorption studies, by the use of relatively uncomplicated laboratory systems. Although it has been known for some time now that natural particles in seawater are likely to be coated with adsorbed organic material (Neihof 1972); only very recently has such a phenomenon been considered for freshwater model systems. Bourg and Schindler (1978), Bourg et al., (1979) and Bourg (1979) describe the adsorption of complexed trace metals using the surface

complexation model (see Section 5.1.3.5) of Schindler et al. (1976) and Hohl and Stumm (1976). Adsorption of Cu(II) at the silica-water interface in the presence of 2,2'-bipyridine or ethylenediamine is best explained in terms of formation of ternary surface complexes which are more stable than the ones formed between the surface and free Cu(II) ions. Such a model was applied to a natural water situation with chosen, 'suitable' surface equilibrium constants. Although they realize that the predictions for Cu-speciation with such a model is affected by the choice of the equilibrium constants, they conclude that the general trends are nevertheless valid and that the presence of ternary surface complexes cannot be ignored or neglected.

Davis (1978) and Davis and Leckie (1978a) determine the role of complexing ligands and pH in affecting trace metal adsorption at the sediment/water interface in a number of experimental model systems. Their results suggest that the distribution of trace metals in natural water systems is likely controlled by binding on surfaces of colloidal particles coated with organic (humic) material, rather than on surfaces of simple hydrous oxides.

Davis (1978) and Davis and Leckie (1978b, 1980) applied the triple layer site-binding model to describe adsorption of dilute inorganic and organic anions and even metal-ligand complexes on hydrous oxides. Ligands studied included (amongst others) sulfate, chloride, thiosulfate, glutamic acid and histidine, while amorphous iron oxide served as model-surface. For inorganic anions it was found that often two surface reactions need to be invoked (involving the free anion and the protonated species) if satisfactory agreement between observed and

predicted adsorption isotherms, for uncomplexed anions such as arsenate and sulfate is to be obtained. The modeling of the adsorption of glutamic acid and salicylic acid appeared less successful with this triple layer model, possibly due to the fact that not all the surface sites present (defined as the number of sites that exchange protons rapidly with tritium) are available for such larger organic ligands. Assuming that each organic anion occupies several surface sites improves the model fit somewhat. Such an approach fails, however, for the modeling of more complex systems containing, for instance, Cu and salicylic acid. It is possible that one needs to discriminate between exterior and interior surface sites, with different affinities for organics and metals. Davis (1978) finds that, although the modeling of metal-organic ligand adsorption on hydrous oxide surfaces with the triple layer model was unsuccessful, the effect of inorganic ligands such as thiosulfate and chloride on Ag(I) adsorption could be reasonably described with the same model.

Kummert and Stumm (1980) and Stumm, Kummert and Sigg (1980) propose a constant capacitance model for the specific adsorption of organic and inorganic weak acids and anions on hydrous oxide surfaces. They use a ligand exchange model based on the surface complexation idea. However, they assign the specifically adsorbed species to the same surface layer as where the H^+ and OH^- ions are located, and include in the surface charge (fixed by pdi ions) the charge caused by the adsorbed ligands. This is shown in the following charge balances (after Stumm, Kummert and Sigg 1980):

no specific adsorption:

$$\sigma_o = [\text{SO}^-] - [\text{SOH}_2^+] = (C_B - C_A + [\text{H}^+] - [\text{OH}^-]) / A \quad (5.65)$$

specific adsorption of Me^{2+} :

$$\begin{aligned} \sigma_o = [\text{SO}^-]^* - [\text{SOH}_2^+]^* - [\text{SOMe}^+] &= (C_B^* - C_A^* + [\text{H}^+] - [\text{OH}^-] \\ &+ 2[\text{Me}^{2+}] - 2[\text{Me}^{2+}]_T) / A \end{aligned} \quad (5.66)$$

specific adsorption of L^{2-} (unprotonated):

$$\begin{aligned} \sigma_o = [\text{SO}^-]^* - [\text{SOH}_2^+]^* + [\text{SL}^-] &= (C_B^* - C_A^* + [\text{H}^+] - [\text{OH}^-] \\ &- 2[\text{L}^{2-}] + 2[\text{L}^{2-}]_T) / A \end{aligned} \quad (5.67)$$

specific adsorption of HL^- :

$$\begin{aligned} \sigma_o = [\text{SO}^-]^* - [\text{SOH}_2^+]^* - [\text{S}_2\text{L}^+] &= (C_B^* - C_A^* + [\text{H}^+] - [\text{OH}^-] \\ &- [\text{L}^-]) / A \end{aligned} \quad (5.68)$$

specific adsorption of H_2L :

$$\begin{aligned} \sigma_o = [\text{SO}^-]^* - [\text{SOH}_2^+]^* + [\text{S}^-] &= (C_B^* - C_A^* + [\text{H}^+] - [\text{OH}^-] \\ &- [\text{HL}^-] - 2[\text{L}^{2-}]) / A \end{aligned} \quad (5.69)$$

Here C_A and C_B are the concentrations of strong acid and base used in the alkalimetric and acidimetric titrations to determine the surface charges; A is the amount of surface used (kg/L) and $*$ means the concentrations in the presence of specifically adsorbing ions.

They find that specific adsorption depends on the acid-base behaviour of the surface, the properties of the specifically adsorbing ions and on the affinity of the surface metal ion for the ligand. The equilibrium constants for the surface reactions are found to be directly correlated to the equilibrium constants for the same reactions in solution (e.g. the equilibrium constant for surface complexation of an organic acid with for instance $\gamma\text{-Al}_2\text{O}_3$ is related to the equilibrium constant for the solute reaction between the ligand and Al^{3+}). Solute complexation reactions involve innersphere complexes; the fact that such a good relationship is found between surface and solution complexation constants can be regarded as an indication that surface complexation reactions also involve innersphere complexes (e.g. adsorbent and adsorbate share water molecules at the interface). They conclude that the simple model used in their study is in good agreement with their experimentally observed data and they quote the findings of Westall and Hohl (1980) regarding the use of the simplest possible models for mass balance description.

5.2 Adsorption Models for Trace Metal Adsorption on MnO_2

The adsorption models discussed in the first part of this Chapter have largely been derived for hydrous oxides other than manganese dioxide. The main reason for this may be because there are many types

of manganese dioxide for which identification, especially for the more amorphous varieties, can be difficult (see Chapter 3). Yet a large amount of research on the adsorption behaviour of MnO_2 has been reported in the literature and the following section gives a brief review of some of this work.

Murray et al. (1968) discuss the adsorption of metal ions onto hydrous manganese dioxide in terms of the double layer theory, namely as potential determining adsorption (H^+ and OH^-), as surface inactive or diffuse double layer adsorption (e.g. Na^+ , K^+) and as surface active or specific adsorption (e.g. Co^{2+} , Ni^{2+} and Cu^{2+}). Their experimental results show that only at low concentrations of Na^+ and K^+ is adsorption onto MnO_2 (manganous manganite) strongly pH dependent and located only in the double layer. At high concentrations (i.e. $> 0.1 M$), the adsorption becomes pH independent which is tentatively explained as incorporation of the Na^+ and K^+ ions into the MnO_2 lattice, due to the structure of ordered Mn^{4+} and disordered Mn^{2+} layers in the oxide.

Murray et al.'s results, however, can be explained in a different way, by applying the triple layer model of Davis (1978). Davis shows that surface acidity constants are dependent on ionic strength and explains this by the formation of 'surface complexes', which influence the dissociation of the surface hydroxo groups (formation of 'ion pairs' or 'surface complexes' in the Inner Helmholtz Plane). At very low electrolyte concentrations, the surface dissociation plays an important role in determining the surface charge and the $[SO^-]$ and $[SOH_2^+]$ surface groups cannot be ignored. However, at high electrolyte concentrations, the release or uptake of surface protons is entirely controlled by the

formation of 'surface complexes', and hence the surface charge becomes pH independent. $[\text{SO}^-]$ and $[\text{SOH}_2^+]$ groups can be disregarded and the surface charge is determined by the amount of 'ion pairs' formed (e.g. $[\text{SO}^- \text{Na}^+]$). Unfortunately at very high ionic strength, this model does not hold, possibly due to various factors such as non-ideal behaviour of ionic solutions at high ionic strength and the physical limit to the number of counter ions at the surface in 'ion pairs' (Davis 1978).

Adsorption of such ions as Co^{2+} , Ni^{2+} and Cu^{2+} on MnO_2 , is assumed by Murray et al. (1968) to be dependent on a relatively large specific adsorption potential, since it was observed that these ions adsorb in considerable amounts near the pH_{zpc} , where electrostatic (Coulombic) and solvation energy terms are negligible or absent. They use Grahame's expression (5.14) to calculate specific adsorption energies. They also observe that the adsorption behaviour of Co^{2+} (compared to Ni^{2+} and Cu^{2+}) deviates from the theory and they suggest the oxidation of Co^{2+} to Co^{3+} on the surface on MnO_2 as a possible explanation for this (see also p. 233).

Many researchers describe adsorption of trace metal ions on manganese dioxide with a Langmuir isotherm (which is basically a special case of the mass law equation). They justify such a model with a statement that, although it is realised that the basic model assumptions are not always fulfilled, the fit of the observed isotherms to the Langmuir equation is excellent (e.g. Morgan and Stumm 1964, Gabano et al. 1965, Posselt et al. 1968a, Anderson et al. 1973, Gray and Malati 1979a,b, van den Berg 1979 etc.).

Other workers picture an ion exchange process as the mechanism for trace metal adsorption on hydrous manganese dioxide:

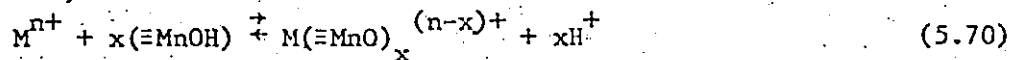


Figure 5.10 sketches two possible cases for an ion exchange process;

either one or two moles of H^+ are exchanged for one mole of divalent metal.

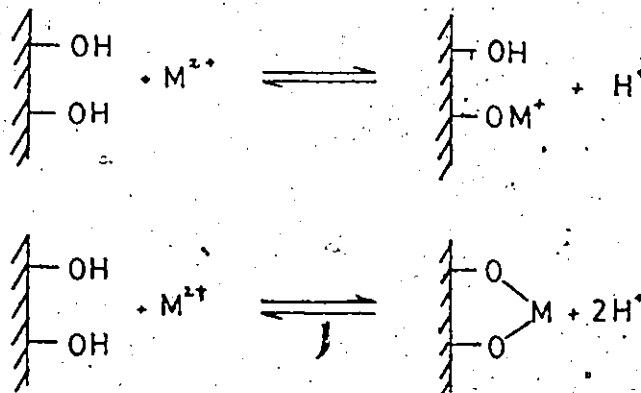
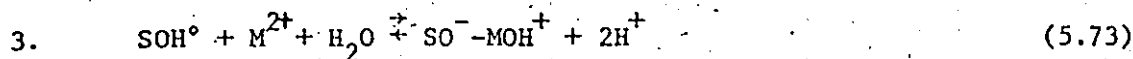
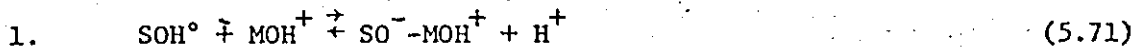


Figure 5.10
Ion exchange mechanisms
for trace metal ad-
sorption on hydrous
manganese dioxide

McKenzie (1979) considers three possible surface exchange reactions of which two differ from the above. They are:



McKenzie argues that at lower pH values models 1 and 2 are dominant, but that at higher pH's model 3 becomes more important. However, one could also argue that model 3 should be more likely at lower pH and especially that model 1 should take over at higher pH, since it involves the direct adsorption of MOH^+ , which under lower pH conditions can only occur under very special circumstances (see also p. 225). Another point is that of

the above three models, only model 2, the adsorption of free metal ion, can cause charge reversal of the diffuse double layer. The other two can only change the charge to zero, but not beyond.

The selectivity of transition metal ions for hydrous manganese dioxide as found by Murray (1975a) (from calculated specific adsorption potentials: $\text{Co} > \text{Mn} > \text{Zn} > \text{Ni} > \text{Ba} > \text{Sr} > \text{Ca} > \text{Mg}$) does not follow the Irving Williams order ($\text{Zn} < \text{Cu} > \text{Ni} > \text{Co} > \text{Fe} > \text{Mn}$; Stumm and Morgan 1970) nor the order found by Huang and Stumm (1973) for specific adsorption of cations on hydrous $\gamma\text{-Al}_2\text{O}_3$ ($\text{Mg} > \text{Ca} > \text{Sr} > \text{Ba}$). The Irving Williams order is a reasonably well-established rule for the sequence of complex stability and has been explained using crystal field theory. Considering this, Murray (1975a) suggests that the factors controlling the selectivity involve more than the crystal field stabilisation energies as proposed by Loganathan and Burau (1973).

Murray (1975a) argues in favour of the model proposed by James and Healy (1972) (discussed in Section 5.1.3.3). The James and Healy model can be summarized as follows: The adsorption of hydrolyzable metal ions at the solid-solution interface occurs as a result of changes in the Coulombic, solvation and specific chemical energy interactions. They consider (i) metal oxides with a low dielectric constant (ϵ) for which ion-solvent interactions present a barrier to close approach of highly charged ions to the solid-solution interface, and (ii) metal oxides with a high dielectric constant, for which the change in solvation energy for an ion following adsorption is small compared with adsorption onto low ϵ metal oxides. For high ϵ metal oxides, Coulombic and specific terms dominate the free energy of adsorption and therefore significant

amounts of specific adsorption can occur. Hydrrous manganese dioxide is such a high ϵ oxide.

However, it appears that James and Healy (1972), Loganathan and Bureau (1973) as well as Murray (1975a) all accept the need to invoke the concept of surface precipitation by metal hydroxy species to explain the very high adsorption densities and charge reversals found at high pH's.

Microelectrophoretic mobilities of hydrrous MnO_2 in the presence of adsorbed metals such as Zn or Co, show that in a very narrow pH range (pH 5-7), the ζ -potential changes from negative to positive, a charge reversal caused by a suddenly steeply increasing adsorption in this narrow pH range. A large number of investigators describe this sudden increase in adsorption to hydrolysis of the adsorbing metal. Loganathan et al. (1977) carried out investigations over a wide pH range for the adsorption of Co and Zn on hydrrous MnO_2 . They consider hydrolysis as a possible cause of the sudden increase in adsorption, but argue that the presence of $CoOH^+$ and $ZnOH^+$ species could cause this sudden increase only if their affinities for the surface are much higher than those of the free ions, because the concentration of the free ions is 100 to 500 times larger than the concentration of the hydrolyzed species in the region of abrupt adsorption increase. This observation does not contradict the model of James and Healy (1972) who point out the considerable reduction in the solvation term for hydrolyzed species. Such a reduction could give the hydrolyzed species a large adsorption edge over the unhydrolyzed ions.

Stumm et al. (1976), however, argue that it is the oxide surface itself that causes the rapid increase in adsorption. Loganathan et al.

(1977) in their study with Zn, point out that the abrupt increase in adsorption can also be explained by assuming the δ -MnO₂-water interface region as a hypothetical volume element where Zn(OH)₂ is less soluble than in pure solution. In this case, interface 'precipitation' could occur, causing adsorption to increase, depending on metal concentration as well as the pH. This model is consistent with the large surface densities found by Loganathan et al. (1977), which can only partly be accounted for by the observed exchange with bound H⁺ and structural Mn²⁺, and exceed normal monolayer quantities by a large amount. It is possible that a surface hydroxide may be nucleating or precipitating even though conditions are not achieved for formation of Co(OH)₂ and Zn(OH)₂ in the bulk solution (Loganathan et al. 1977). Healy et al. (1968) also suggest that at the oxide-solution interface the OH concentration might be higher than in the bulk solution and that therefore nucleation of a hydroxy precipitate might occur at pH values lower than would be expected for solutions. Loganathan et al. (1977) suggest that the fact that the mobility curve (electrophoretic mobility) of Zn(OH)₂ coincides with that of δ -MnO₂, onto which Zn is adsorbed at high pH and high Zn-concentrations in their studies, indicates that δ -MnO₂ under these circumstances behaves like a Zn(OH)₂ surface.

The same authors suggest that there are three regions of adsorption to be distinguished. For Zn- and Co- adsorption onto MnO₂ they are:

- (1) pH < 5: sorption due to exchange with bound H and interchange with structural manganese as well as adsorption in the diffuse double layer. The latter is due to an increase with pH of the pH dependent surface charge, which in its turn increases the

inner layer counter ion population (M^{2+} , MOH^+) to a point where the shear plane potential (Zeta-potential) changes from negative to positive and thus attracts anions including OH^- while repelling cations. The change in shear plane potential occurs roughly at the boundary of region 1 and 2.

- (2) pH 5-6: In this region some sorption of hydroxy species and/or the formation of polynuclear hydroxy species occurs within the shear plane. Alternatively, one could consider this as the region where progressive nucleation of a hydroxy precipitate in the interfacial zone might occur.
- (3) pH > 6: This region exhibits a slowly decreasing shear plane potential. At high sorption densities the δ - MnO_2 surface again goes through a zpc, approximating the zpc of $M(OH)_2$ (e.g. in the case where M is Zn), because, with progressive nucleation of hydroxides, the force field of the original δ - MnO_2 surface is completely shielded from the new hydroxide-surface.

This three-region model is not applicable to the adsorption of Ca onto δ - MnO_2 , because Ca does not adsorb in the inner layer.

According to Hofmeister (Posselt et al. 1968a), the affinity for exchange adsorption of various ions onto hydrous oxides is generally (with few exceptions): $Li^+ < Na^+ < K^+ < Rb^+ < Cs^+ < Mg^{2+} < Ca^{2+} < Sr^{2+} < Ba^{2+} < Al^{3+}$ etc. To explain this specific order, it is argued that affinity is a function of the ionic radius. Within a given group of elements, the larger the crystalline ionic radius, the larger is the exchange affinity. This phenomenon is related to the solvation of the ions. The smaller the crystalline ionic radius, the greater is the actual ionic radius of the

hydrated ion. The strongly hydrated ions are less likely to undergo exchange sorption because of their increased size, which necessarily introduces steric hindrance.

Gray and Malati (1979b) determined the apparent heat of adsorption for various trace metals on δ -MnO₂ at pH values of 6 to 7, and at various temperatures, fitting their observations to a Langmuir isotherm. They found that the adsorption capacity of δ -MnO₂ increased in the series: Ni²⁺ < Co²⁺ < Cd²⁺ = Zn²⁺ < Mn²⁺. To compare this order with the hydrated radii of the adsorbing ions, they tentatively used hydration enthalpies to estimate these values and calculated the following numbers: Ni²⁺ = 3.04 Å; Co²⁺ = 3.00 Å; Cd²⁺ = 3.02 Å; Zn²⁺ = 3.02 Å and Mn²⁺ = 2.95 Å, which follow the expected trend of a decrease in the hydrated radius with an increase in the crystalline ionic radius. Apparently, the assumption of $r_{\text{hydr}} = r_{\text{cryst}} + 2r_{\text{H}_2\text{O}}$, as used by Murray (1975a) produces values that disagree with some physical measurements (Gray and Malati, quoting Stern and Amis 1959). However, although their adsorption order coincides with the calculated hydration radii, Gray and Malati admit that the calculation procedure involving hydration enthalpies might not be entirely correct.

Hydrous oxides are considered to have a strongly structured, probably hydrogen bonded and chemisorbed water layer immediately adjacent to their surfaces. The metal ion binding at the hydrous oxide surface is not necessarily accompanied by the dehydration of the metal ion or by a full displacement of a H₂O molecule at the oxide surface; the change in hydration can occur by a rearrangement of H₂O molecules during the adsorption process. Stumm et al. (1976) suggest that a part of the

hydration sheet of the cation may be substituted by the surface environment (chemisorbed water) of the oxide lattice while James and Healy (1972) assume either no loss of, or an overlap of the primary hydration sheath with surface-adsorbed water.

Murray's (1975b) work suggested that the adsorption of Co onto hydrous manganese dioxide induced loss of H_2O from the hydrated ion - that adsorption appears to plateau at a monolayer value that is greater than what would be calculated assuming that the cobalt ions retain their inner hydration sphere. This means that, when specific adsorption occurs on hydrous manganese dioxide, the cobalt ions are not necessarily separated from the surface by a layer of water molecules, as found by James and Healy for cobalt on SiO_2 and TiO_2 . The use of $r_{hydr} = r_{cryst} + r_{H_2O}$ may be incorrect, or alternatively the surface area may be underestimated by whatever method was used to determine it, as is suggested by Davis (1978).

Several researchers have proposed exchange of adsorbing ions with structural ions in $\delta-MnO_2$. Anderson et al. (1973) find that the adsorption maxima for silver adsorption on various types of poorly crystallized MnO_2 are not directly related to the amount of surface area available. In fact, there appears almost an inverse relation to surface area, although this is believed to be coincidental by these authors. From their studies they conclude that there is a positive relationship between the amount of foreign ions contained in the MnO_2 samples and the amount of silver they are able to adsorb. As a mechanism for the uptake of silver by hydrous MnO_2 , they propose that both surface exchange with Mn^{2+} , K^+ , Na^+ and H^+ , as well as exchange with structural Mn^{2+} , K^+ and

Na⁺ occurs.

Loganathan and Burau (1973) propose an adsorption model, whereby Mn is displaced from structural positions in MnO₂ by adsorbing metal ions (Co and Zn). The model is based on their findings that adsorption of Na⁺, K⁺, or Ca²⁺ onto δ-MnO₂ caused no detectable Mn to be found in the solution phase, while during Co²⁺ and Zn²⁺ adsorption, Mn would appear in solution. Little is known about the valency state of lower-valency Mn in manganese dioxides. The Mn³⁺ state is known to be stable in the octahedral sites of the oxides hausmannite and bixbyte (McKenzie 1970). Similarly, Mn³⁺ may exist in the disordered layers between the main ordered layers in δ-MnO₂ (see Chapter 3). The fact that Co adsorption releases more Mn than Zn adsorption could possibly be explained on the basis of crystal field theory with a model wherein Zn replaces only Mn²⁺ from the disordered layers, whereas Co replaces both Mn²⁺ and Mn³⁺, thereby gaining in crystal field stabilization energy.

Adsorption onto hydrous MnO₂ has been found to depart from Langmuir linearity at low metal concentrations by Gabano et al. (1965) and Loganathan and Burau (1973). These researchers find that the adsorption of Zn onto γ-MnO₂ and Co and Zn onto δ-MnO₂, respectively, fit a Langmuir equation only above a certain equilibrium concentration of metal in solution (e.g. > 1 x 10⁻⁴ M for Co and Zn at pH4). Gabano et al. (1965) explain this deviation from a single site Langmuir expression at low Zn concentrations by variations in adsorption energy at low coverages, but not in terms of discrete adsorption sites on MnO₂. Loganathan and Burau (1973) propose that this deviation from Langmuir linearity at low concentrations and the simultaneous release of Mn, is

due to Co and Zn interchange with the Mn in the disordered layers of $\delta\text{-MnO}_2$. This theory infers that there are additional adsorption sites with different sorption affinities for metal ions in the structure of $\delta\text{-MnO}_2$ from those on the surface. Besides exchange with H^+ (Ca^{2+} adsorption) and double layer adsorption (Na^+ and K^+), they propose two more sites: exchange with Mn^{3+} (Co^{2+}) and with Mn^{2+} (Co^{2+} , Zn^{2+}). The order of decrease in sorption energies at these sites is: structural Mn^{3+} > structural Mn^{2+} > bound H^+ . The deviation of Langmuir linearity at low concentrations, as found by Loganathan and Bureau (1973) and Gabano et al. (1965), is shown in Figures 5.11 and 5.12.

Loganathan and Bureau (1973) propose that, instead of a single Langmuir equation, it would be better to use a double one in these cases. They show that at high concentrations and high surface coverage, the slope of an ordinary single-site linear Langmuir plot gives a valid estimate for the total maximum adsorption capacity of the two sites together. Because of the differences found for Ca, Co and Zn adsorption they attempt to estimate the surface capacity for exchange with surface bound H^+ by the adsorption of Ca^{2+} . Then they use simple arithmetic to estimate the capacities of structural Mn^{2+} and Mn^{3+} exchange by subtracting the adsorption maximum for Ca from the adsorption maximum for Zn and subtracting the adsorption maximum for Zn from the adsorption maximum for Co respectively. By comparing these calculations with manganese released into solution, these authors conclude that the model is in fair agreement with the experimental data. However, there is a discrepancy of a factor 1.5-2 between measured and calculated Mn^{2+} and Mn^{3+} release upon exchange with Zn and Co. This may be significant.

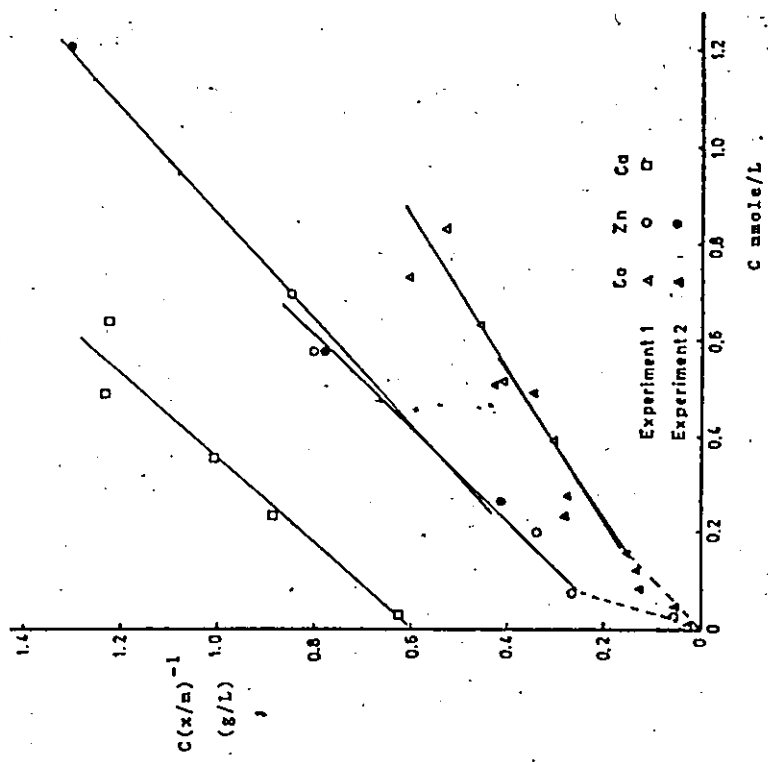


Figure 5.11 Langmuir plot of data for sorption of Co, Zn and Cs by 0.015g δ -MnO₂ at pH 4, (from Loganathan and Bura 1973).

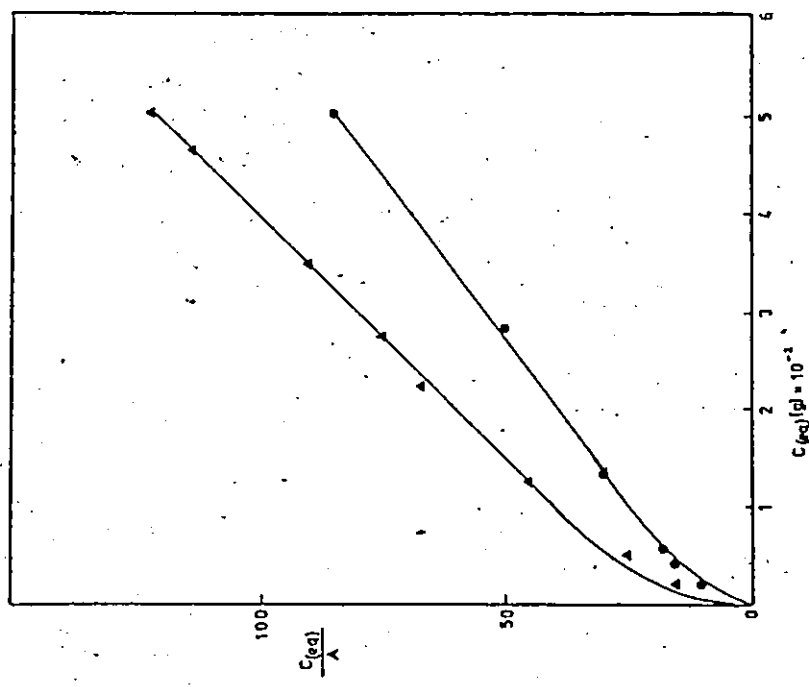


Figure 5.12 Langmuir adsorption isotherms for Zn adsorption at pH 7 for two γ -MnO₂'s with different specific surfaces, (from Gabeno, Etienne and Laurent 1965). \circ = γ -MnO₂, 70m²/g; Δ = γ -MnO₂, 102m²/g.

The replacement of structural manganese by an 'adsorbing' ion, to explain a second site for adsorption, is a plausible mechanism. To investigate the viability of such a site for Cu on the basis of Crystal Field Stabilization Energy (CFSE), Table 5.1 was constructed from various literature sources. Based on CFSE, it is apparent that Cu^{2+} could displace Mn^{2+} from the disordered layers and so give the MnO_2 lattice a more stable configuration. On the basis of ionic radii, this is less likely, but perhaps still possible, since the gain in CFSE is reasonably high. CFSE values for Zn are not particularly favourable for Mn^{2+} displacement by Zn^{2+} nor is the ionic radius value. However, Mn^{2+} displacement by Zn^{2+} is mentioned by Loganathan and Bureau (1973) and a second adsorption site for Zn^{2+} on $\gamma\text{-MnO}_2$ is found by Gabano et al. (1965). Cu^{2+} cannot replace either Mn^{3+} (in the disordered layers) or Mn^{4+} (in edge shared octahedrals) on the basis of CFSE values.

The suggestion that Co^{3+} ions penetrate into the solid phase of MnO_2 to replace either Mn^{3+} or Mn^{2+} is not completely satisfactory to Murray (1975a), because of the large discrepancy in ionic radii between Co^{3+} , Mn^{2+} and Mn^{3+} (see Table 5.1). To explain laboratory adsorption results for Co adsorption, several authors have proposed the oxidation of Co^{2+} to Co^{3+} at the MnO_2 surface (Murray et al. 1968; McKenzie 1970; Burns 1976 and Burns and Burns 1977). Murray and Dillard (1979) strengthen this theory by presenting direct chemical confirmation of the presence of Co^{3+} adsorbed from Co^{2+} solution onto MnO_2 . Their proposal that the Co^{3+} ion is subsequently stabilized by filling vacancies in the edge shared $[\text{MnO}_6]$ octahedra follows the suggestions of Burns (1976) and Burns and Burns (1977) who propose that Co^{3+} could substitute for

Table 5.1: CFSE's of selected ions in an octahedral field

<u>ion</u>	<u># of 3d electrons</u>	<u>electronic configuration</u>	<u>CFSE (kcal/mol)</u>		<u>ionic radius</u>	
Mn ⁴⁺	3	t _{2g} ³	94.0*	79**	A 0.54 ^{+c}	
Mn ³⁺	4	t _{2g} ³ e _g ¹	36.0*	35.9**	0.65 ^{+c}	
Mn ²⁺	5	t _{2g} ³ e _g ²	0*	0**	0.82 ^{+c}	
Co ³⁺ low spin	6	t _{2g} ⁶	127.5*	45**	0.525 ^c	0.53 ⁺
Co ²⁺ high spin	7	t _{2g} ⁵ e _g ²	21.3*	17.1**	0.74 ⁺	
Ni ²⁺	8	t _{2g} ⁶ e _g ²	29.6*	29.3**	0.69 ^c	
Cu ²⁺	9	t _{2g} ⁶ e _g ³	21.6*	22.2**	0.72 [#]	
Zn ²⁺	10	t _{2g} ⁶ e _g ⁴	0*	-	0.74 [#]	

* Data from Loganathan and Bureau (1973): all values except that of Mn⁴⁺ were obtained from Burns (1970), the value of Mn⁴⁺ was calculated from parameters given by Figgis (1966).

** Data from McKenzie (1970): with the exception of the value for Mn⁴⁺ these values were taken from McClure (1957), the CFSE of Mn⁴⁺ in an oxide structure is not known and the value shown in the above Table is an approximate value calculated from parameters given by Figgis (1966, p. 244).

+ Data from Burns (1976)

c Data from Murray (1957b)

Data from van den Berg (1975)

Mn⁴⁺ ions, due to the close agreement between the ionic radii of Co³⁺ and Mn⁴⁺. This proposed mechanism involves initial adsorption of Co²⁺, subsequent oxidation to Co³⁺ by Mn⁴⁺, and replacement of the displaced manganese by low-spin Co³⁺ in the [MnO₆] octahedra or in vacancies.

Murray and Dillard (1979) were able to demonstrate the presence of Co³⁺ on the surface of MnO₂ by using X-Ray Photoelectron Spectroscopy (XPS). This technique enables the measurement of the binding energy of specific core atomic electrons. This binding energy is dependent on the oxidation state and the coordination number of the adsorbed metal ion. Brulé et al. (1980) also advocate this technique for the direct analysis of manganese dioxide surfaces to monitor the adsorption of metal ions.

Dempsey and Singer (1980) investigated the competitive influence of Ca on the adsorption of Zn by the δ-MnO₂ surface. They attempted to fit their Zn-adsorption data to the James and Healy model but found this not possible due to the fact that they encountered an adsorption capacity which increased with pH (the James and Healy model assumes a constant maximum adsorption capacity, as does the Langmuir model). Also, assuming that Zn adsorbs without losing its primary hydration sheath ($r_{\text{ads}} = r_{\text{ion}} + 2r_{\text{H}_2\text{O}}$, as used by James and Healy), coverages exceeding a monolayer were found. Their attempt to use a so-called competitive Langmuir approach for the Ca-Zn-MnO₂ system involved the description of the adsorption isotherms for Ca and Zn adsorption as follows:

$$q_e = \frac{Q_{\text{Zn}} B_{\text{Zn}} (\text{Zn})}{1 + B_{\text{Zn}} (\text{Zn})} + \frac{Q_{\text{Ca}} B_{\text{Zn}} (\text{Zn})}{1 + B_{\text{Zn}} (\text{Zn}) + B_{\text{Ca}} (\text{Ca})} \quad (5.74)$$

Here q_e is equal to the amount of Zn adsorbed per amount of MnO_2 present. The model assumes that Ca can only compete at (Q_{Ca}/Q_{Zn}) of the surface sites available for Zn, while $[(Q_{Zn} - Q_{Ca})/Q_{Zn}]$ sites are restricted to Zn adsorption. Their results showed that the adsorption of trace quantities of Zn was only slightly affected by the presence of abundant amounts of Ca. The competition appeared to decrease with increasing pH and became insignificant at pH 7. In all cases they found that the competitive behaviour of Ca was less than predicted by the competitive Langmuir equation but no explanation for this was given.

There are a number of contentions that surface repeatedly in adsorption studies involving hydrous manganese dioxide. One of these is the maximum adsorption capacity. Some researchers find an increase in Γ_{max} with pH (amongst them: Morgan and Stumm 1964, for Mn^{2+} on $\delta-MnO_2$; Gabano et al. 1965, for Zn^{2+} on $\gamma-MnO_2$; van den Berg 1979, for Cu^{2+} on $\delta-MnO_2$ and Dempsey and Singer 1980, for Zn^{2+} on $\delta-MnO_2$). Some investigators explained this by an increase or decrease in the uptake of potential determining ions (OH^- and H^+) with higher pH, creating more adsorption sites. However, models such as the James and Healy model, the Langmuir model and the mass law equation all assume a constant maximum capacity independent of pH. In order to use such models, researchers are forced to apply them at constant pH values only. However, the condition of constant maximum adsorption capacity seems very reasonable if one conceptualizes the adsorption of trace metals on hydrous oxides as being a surface complexation- or exchange- process with surface H^+ . The reason why such a constant capacity is not found could possibly be the presence of mechanisms other than thermodynamically reversible.

adsorption. For example, surface precipitation as a function of pH may occur. Also, the formation of insoluble metal-hydroxides or -oxides should not be ruled out in the higher concentration regions. The fact that there exists a lot of disagreement in the literature about the formation constants of species such as $Zn(OH)_2$ (Zirino and Yamamoto 1972; Bradford, 1973) and $Cu(OH)_2$ (Vuceta and Morgan 1977) provides evidence for such a possibility. Precipitation of metals would be experienced as adsorption since it takes the metals out of solution.

Factors such as the relative kinetics of adsorption on a surface and the formation of hydrous oxides may play a keyrole in higher concentration regions. Adsorption takes metal out of solution, and the total metal concentration can be higher in the presence of an adsorbing surface than in the absence of such a solid without the danger of precipitation. However, one could argue that non-immediate mixing and a temporary non-uniform pH in solution directly after a metal addition may produce localized effects of precipitation which may or may not be totally reversible.

Another point of discussion is the time reported as required to reach (apparent) equilibrium in some of the above mentioned studies on MnO_2 adsorption behaviour. Table 5.2 gives a summary of this.

Very little is known about the adsorptive behaviour of organic materials on δ - MnO_2 . Adsorption studies on δ - MnO_2 involving organic acids and amino acids and their effect on trace metal adsorption have not been reported. From the studies of adsorption of organics on other hydrous oxides, however, it seems very likely that MnO_2 will adsorb organic substances.

Table 5.2 Adsorption of trace metals on δ -MnO₂; time required to reach equilibrium

Reference	MnO ₂	metal adsorbed	pH	ionic strength	temperature	time	details
Morgan and Stumm 1964	δ -MnO ₂	Mn	various	0.01	25°C	1 hour	50% exchange in 5 minutes
Gabeno, Etienne & Laurent 1965	γ -MnO ₂	Zn	7.0	2.0	25°C	15 hours	
Murray, Healy & Fuerstenaue 1968	manganese manganite	Ni, Cu, Co, K, Na	various	0.0005	25±0.05°C	several hours	
Posselt, Anderson & Weber 1968	δ -MnO ₂	Ag, Hn, Ba, Ca, Mg, Sr, Na	5.0	0.01	not reported	0.5 hour	0.5 hour reaction time 5-10 min. to reach equilibrium
Loganathan & Burau 1973	δ -MnO ₂	Na, Co, Zn	4.0	0.001	24±0.5°C	1 hour 1-2 days	
Gedde & Latinen 1974	δ -MnO ₂	Pb, Cd, Zn, Th	various	not reported	not reported	3 hours	
Murray 1975a	δ -MnO ₂	Co, Ni, Mn, Zn, Ca, Hg, Sr, Ba	various	0.1	not reported	1 hour	time necessary to reach equilibrium is a function of the amount of pH change
Loganathan, Burau & Fuerstenaue 1977	δ -MnO ₂	Zn, Co, Ca	3.5 - 10.0	0.001	24±0.5°C	2 days	
van den Borg 1979	δ -MnO ₂	Cu	6.0 - 9.0	0.01	25°C	1 hour	
McKenzie 1979	birnessite	Pb, Cu, Mn, Zn	4.0	0.02 - 0.25	not reported	1 hour	
Dempsey & Singer 1980	δ -MnO ₂	Zn, Ca	6.0 - 8.5	0.01	22 - 25°C	0.5 hour	40 minutes reaction time 30 minutes to reach equilibrium

In a study on the adsorption of neutral, cationic and anionic tensioactive organic materials (such as nonylphenoxynonylethoxyethanol, p-dodecylbenzyltrimethylammoniumchloride and dodecylbenzenesulfonate respectively) on hydrous MnO_2 , Posselt et al. (1968a) found not much adsorption other than for the cationic organic solute. They concluded that ionic forces of attraction are the principal forces involved in the sorption of such organic species on hydrous MnO_2 .

Rosell and Babcock (1968) (quoted by Schnitzer and Khan 1972) found that a mixture of humic and fulvic acid extracted from a loam soil and a peat had a much stronger effect than 10^{-3} M EDDHA or EDTA, at pH 9, on the leaching of manganese from manganese oxides and hydroxides. This could be explained by a number of phenomena such as redox reactions between the Mn-oxides and humic substances, chelation of $\text{Mn}(\text{OH})_2$ and the higher, hydrated Mn-oxides by the humics and autoxidation of the humic mixture, resulting in an increase in functional metal-complexing groups. Apparently, humic materials are responsible for maintaining a high concentration of complexed manganese in solution in soils of high pH where Mn would normally precipitate as the hydroxide.

Guy et al. (1975) and Guy and Chakrabarti (1976) investigated metal speciation for a model system, containing potassium bentonite, hydrous MnO_2 , both solid and soluble humic acid, tannic acid and bicarbonate. They considered the following metal control mechanisms: metal-clay colloid ion exchange reactions; metal adsorption on hydrous oxides; metal adsorption on humic acid-clay colloids; metal-inorganic anion complexes, and metal-organic ligand complexes. No consideration was given to the possibility of adsorption of the organic ligands on the

hydrrous oxide. It was found however, that MnO_2 could be solubilized via reduction to Mn^{2+} by polyhydric phenols such as pyrogallol, gallic and tannic acid, because these substances are able to lower the p_e of the solution (e.g. $p_e = 20.42 + \frac{1}{2} \log [H^+]^4/[Mn^{2+}]$, Stumm and Morgan 1970).

A considerable amount has been written about the measured and/or calculated ratio's of H^+ released per amount of metal adsorbed on hydrrous MnO_2 . There are various ways to determine this release:

- 1) The pH dependence for adsorption of a metal ion on a hydrrous oxide can be characterized in terms of mass-law relationships, if adsorption of the metal ion M^{n+} is assumed to follow a course similar to complexation with a weak acid and if the activity of the solid phase is assumed to be unchanged by the sorption reaction. The process can then be treated according to mass law theory, as first applied for adsorption by Kurbatov et al. (1951) (see Section 5.1.3.4). Morgan and Stumm (1964) and Posselt et al. (1968a) however point out that the basic condition of constant sorbent activity during adsorption is not satisfied in the case of δ - MnO_2 . Although both groups found a straight line relationship when plotting $\log \{ [M^{n+}]_{\text{sorbed}} / [M^{n+}]_{\text{solution}} \}$ versus pH, they conclude that the value obtained for x , has no chemical meaning.
- 2) An automatic titrator can be used to keep the pH constant during the adsorption process. From the amount of base added, the amount of H^+ released can be calculated.
- 3) The change in pH of the oxide suspension can be measured before and after metal adsorption.

Reported values for the ratio's vary. Rather than discuss them here, a summary is given in Table 5.3.

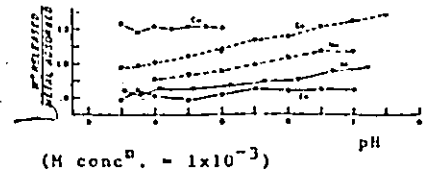
Reference	MnO ₂	metal adsorbed	pH	ionic strength	temperature	Y	details
Morgan & Stumm 1964	δ-MnO ₂	Mn	4.5 5.0 5.4 6.4 7.0 7.5 8.2	0.01	25°C	1.0 1.0 1.0 1.1 1.1 1.3 1.7	
Lögnathan & Burau 1973, 1977	δ-MnO ₂	Zn Co	4.0 4.0	0.001 0.001	24±0.5°C 24±0.5°C	2.10±0.26 2.10±0.05	acid-washed δ-MnO ₂ Y = (H ⁺ released - Na adsorbed - K adsorbed) / (M adsorbed - Mn released)
Gadde & Laitinen 1974	δ-MnO ₂	Pb Cd Zn Th	6.0 6.0 6.0 6.0	not reported	not reported	1.4 1.3 1.1 0.38	
van den Berg 1975	δ-MnO ₂	Pb Mn	6.5-3.7	0.01	25°C	0.86 0.47	
Murray 1975a	δ-MnO ₂	Co Co Co Mn Mn Ni Zn	various	0.1	not reported	1.02 1.09 0.99 0.87 0.94 1.18 0.74	M conc ⁿ = 1x10 ⁻³ = 7.5x10 ⁻⁴ = 5.0x10 ⁻⁴ = 1.0x10 ⁻³ = 5.0x10 ⁻⁴ = 1.0x10 ⁻³ = 1.0x10 ⁻³
Murray 1975a	δ-MnO ₂	Cu, Co Mn, Ni Zn	3.5-7.5	0.1	not reported	 (M conc ⁿ = 1x10 ⁻³)	
McKenzie 1979	Birnes-site	Pb Cu Mn Zn Pb	4.0 4.0 4.0 4.0 4.0	0.0028 0.0054 0.0065 0.012 0.018 0.028 0.059 0.26 0.02 0.25 0.02 0.25 0.02 0.25 0.02 0.25	not reported	2.05 1.73 1.58 1.27 1.16 1.10 1.07 0.99 1.13 1.07 1.23 1.14 1.08 1.00 1.06 1.00	shows effect of ionic strength on the ratio H ⁺ released/metal adsorbed

Table 5.3 Adsorption of trace metals on δ-MnO₂; H⁺ released per M²⁺ adsorbed (= Y).

One particular case should perhaps be emphasized since it solves some of the discrepancies in the literature. Loganathan and Burau (1973) propose that all cations which take place in the exchange process during adsorption should be taken into account to calculate Y, the ratio of H^+ released to M^{2+} adsorbed. For a M^{2+} solution, containing Na^+ , K^+ and $\delta-MnO_2$,

$$Y = \frac{H^+ \text{ released}}{M^{2+} \text{ sorbed}} = \frac{H^+ \text{ released} - Na^+ \text{ sorbed} - K^+ \text{ sorbed}}{M^{2+} \text{ sorbed} - Mn \text{ released}} =$$

$$\frac{\text{bound } H^+ \text{ released}}{M^{2+} \text{ interchanged with bound } H^+} \quad (5.75)$$

Na^+ is part of the electrolyte used to impose a certain ionic strength, while K^+ leaked from the pH electrode. They obtain a value for Y of 2 for Co and Zn at low pH (see Table 5.3). But their work is criticized by McKenzie (1979) who points out that the ratio H^+ released/ M^{2+} adsorbed is strongly influenced by the ionic strength, since at low ionic strength an acid washed MnO_2 has mainly H^+ ions in its double layer. In the case of adsorption of a divalent metal ion, one H^+ is released from the surface, but also the negative charge decreased by one, causing another H^+ to be released from the double layer. This effect is reduced as the ionic strength is increased and the diffuse layer becomes increasingly saturated with K^+ or whatever is used as electrolyte. In such cases, only one H^+ is released (from the surface) per M^{2+} adsorbed and one K^+ from the double layer. At high ionic strength and neutral pH values, all H^+ on the surface is replaced by K^+ , and adsorption of M^{2+} will not

result in any H^+ release.

In general, it can be concluded that, although adsorption on MnO_2 has been extensively studied, the models most widely used to predict and describe the processes involved have been the relatively simpler ones that were derived for hydrous oxides in general. Most researchers investigate adsorption of trace metals on hydrous MnO_2 (and hydrous oxides in general) by keeping both adsorbent and adsorbate constant whilst varying adsorption by changing the pH over a range of values. In the cases where the trace metal concentration in solution was varied (i.e. effectively a titration of the MnO_2 surface with metal), models such as the Langmuir expression and mass law approach seem most popular. This emphasizes the often empirical character of most studies. Explicit statements and theories of the exact location of adsorption in the electrical double layer is rarely found for work on the MnO_2 surface. Furthermore, while the limitations of the Langmuir model with respect to non-constant surface activity of the participating surface groups are mentioned by most researchers, no attempt is usually made to make corrections for this, although this would be possible by using one of the more advanced models discussed in Section 5.1. In the next Section, possible locations for adsorbed metal ions on the δ - MnO_2 surface are discussed. An adsorption model for Cu on the δ - MnO_2 surface is derived that corrects for non-constant surface activity of the participating surface groups. This model is very simple in that it is of a Langmuir form, but at the same time it complies with the assumptions of the more advanced adsorption models.

5.3 Development of a Model for Cu Adsorption on δ -MnO₂

5.3.1 Qualitative Discussion of the Influence of Hypothesized Surface- and Double Layer- Configurations on the Surface Charge of δ -MnO₂

In this study, Cu²⁺ uptake by δ -MnO₂ was determined by measuring the amount of copper remaining in solution. Initially, the Langmuir isotherm model (equation 5.3) was used to fit the data. Adsorption experiments were generally performed at low free Cu²⁺ concentrations for various reasons, e.g. to avoid precipitation of Cu(OH)₂. However, at such low copper concentrations, the linearized form of a Langmuir expression could not describe the observed data satisfactorily - a clear deviation from linearity was observed at low surface coverage (see Section 7.3.2 of Chapter 7). This indicates that the binding energy was larger at low coverage of the surface than at the higher values.

The literature (Section 5.2) suggests several explanations for such a deviation from linearity. They include:

- (i) Simultaneous occurrence of mono - and bidentate adsorption.
- (ii) The existence of a second adsorption site with different affinity for Cu²⁺.
- (iii) Possible simultaneous adsorption of both Cu²⁺ and CuOH⁺.

Another possible explanation is suggested by this research. The δ -MnO₂ surface has a large capacity for trace metal uptake (see the isotherms in Figure 4.2). If one pictures the adsorption process as a complexation with surface hydroxyl groups, then it follows that the density of these surface groups is high, with the consequence that mutual influences cannot be disregarded. With increasing pH, the surface

will become more negative and it will be more difficult for the surface to part with additional H^+ ions, which has consequences for the acidity constant(s) of the surface and hence the surface charge σ_0 , as determined by the potential determining ions. Using Davis' (1978) concept, the surface and its electrical double layer possess three charge planes. The first plane, at the plane of the surface groups on the $\delta\text{-MnO}_2$ surface, has a surface charge σ_0 , which, because of the low pH_{zpc} of $\delta\text{-MnO}_2$, is strongly negative at the pH values used in this study (pH 6 - 8.5). The second plane, the plane of closest approach for non-potential determining ions, possesses the charge σ_1 , caused by either 'ion pair' formation between electrolyte ions and surface groups or by specific adsorption of trace metal ions. The amount of 'ion-pairs' or specific adsorption found in this plane depends on the surface charge and also on a chemical factor, for specifically adsorbed trace metals. But the surface charge σ_0 is itself influenced by the presence, in the σ_1 plane, of non-potential determining ions. How extensive this influence is, depends on factors such as the density of the surface groups (which determines the spacing between the adsorbed ions) and on how close the σ_1 plane is located to the σ_0 plane. The third plane, the σ_d plane, finally, possesses the charge of the diffuse double layer.

The $\delta\text{-MnO}_2$ surface, in the absence of specific adsorption, but featuring 'ion-pair' formation in the presence of background electrolyte (Davis 1978) can be conceptualized to be in various states, depending on the pH and ionic strength. The following series of Figures schematically examines some possible combinations of surface-, 'ion-pair', and diffuse double layer-configurations:

Case I/ the $\delta\text{-MnO}_2$ surface at a pH below pH_{zpc}

Figure 5.13.a shows the surface of $\delta\text{-MnO}_2$ in the absence of background electrolyte. The surface is strongly positively charged and because of the proximity of the positive groups causing mutual repulsion, there will be a tendency to lower this surface charge. In other words, it is easier in this case for the surface to part with an additional H^+ than in a situation where the surface groups are spaced so far apart that they do not exert any influence on each other. This lowering tendency is indicated by two down-pointing small arrows to the left of σ_0 , two, because there are two positive groups indicated; if it were one, the influence would be smaller and indicated by one arrow. In the absence of background electrolyte, there is no 'ion-pair' formation in the σ_1 plane. The counter-ions in the diffuse double layer are indicated by OH^- ions, although this is hypothetical, because at such low pH electro-neutrality would require that other negative ions outnumber the OH^- ions.

Figure 5.13.b shows the surface in the presence of low concentration background electrolyte (KNO_3). Both the absence and presence of limited 'ion-pair' formation is indicated. The tendency to lower surface charge due to mutual repulsion of the positive surface groups is again represented by down-pointing arrows on the left side of σ_0 . The influence of the NO_3^- ion, adsorbed in the σ_1 plane, tends to keep the positive charge unchanged, which is indicated by an upward pointing small arrow to the right side of σ_0 . In this latter case, the charge of the σ_d plane is reduced due to 'ion-pair' formation in the σ_1 plane.

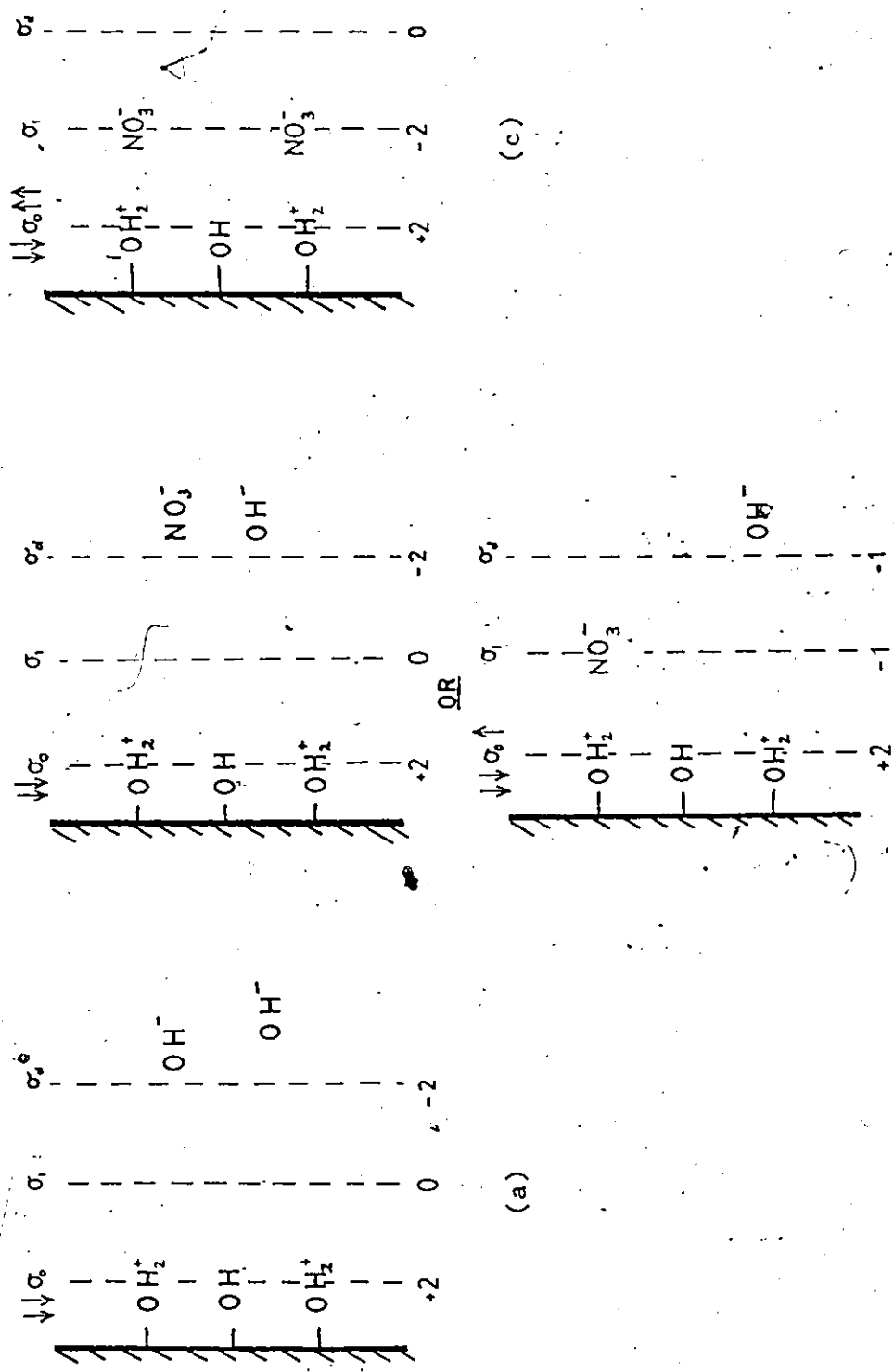


Figure 5.13 The $\delta\text{-MnO}_2$ surface at a pH below pH_{zpc}

- a) no background electrolyte
- b) low background electrolyte
- c) high background electrolyte

Figure 5.13.c shows the surface in the presence of high ionic strength. There is sufficient 'surface complexation' with the electrolyte ions, to reduce the σ_d charge to zero. If one assumes that the mutual influence of all surface groups and all 'ion-pairs' is of equal but opposite strength, then the surface in Figure 5.13.c should behave similar to a situation in which surface groups were spaced widely apart and 'surface complexation' had no effect on them. However, it does not seem likely that both effects cancel each other, because surface groups and 'ion-pairs' lie in different planes.

Case II: the δ -MnO₂ surface at the pH_{zpc}

Figure 5.14 shows the surface of δ -MnO₂ and the electrical double layer at the pH_{zpc}. Figure 5.14.a presents the situation where no background electrolyte is present (hypothetical) while Figure 5.14.b. illustrates the situation at low background electrolyte concentration without and with the possibility of limited 'ion-pair' formation in the σ_1 plane. Figure 5.14.c shows the situation at high electrolyte concentration. Arrows on the left respectively right of the σ_0 plane indicate the influence of the surface groups and 'ion-pairs' on the surface charge σ_0 qualitatively.

Case III: the δ -MnO₂ surface at a pH above pH_{zpc}

The situation at and near the δ -MnO₂ surface for a pH above pH_{zpc} is illustrated in Figure 5.15. The case of no background electro-

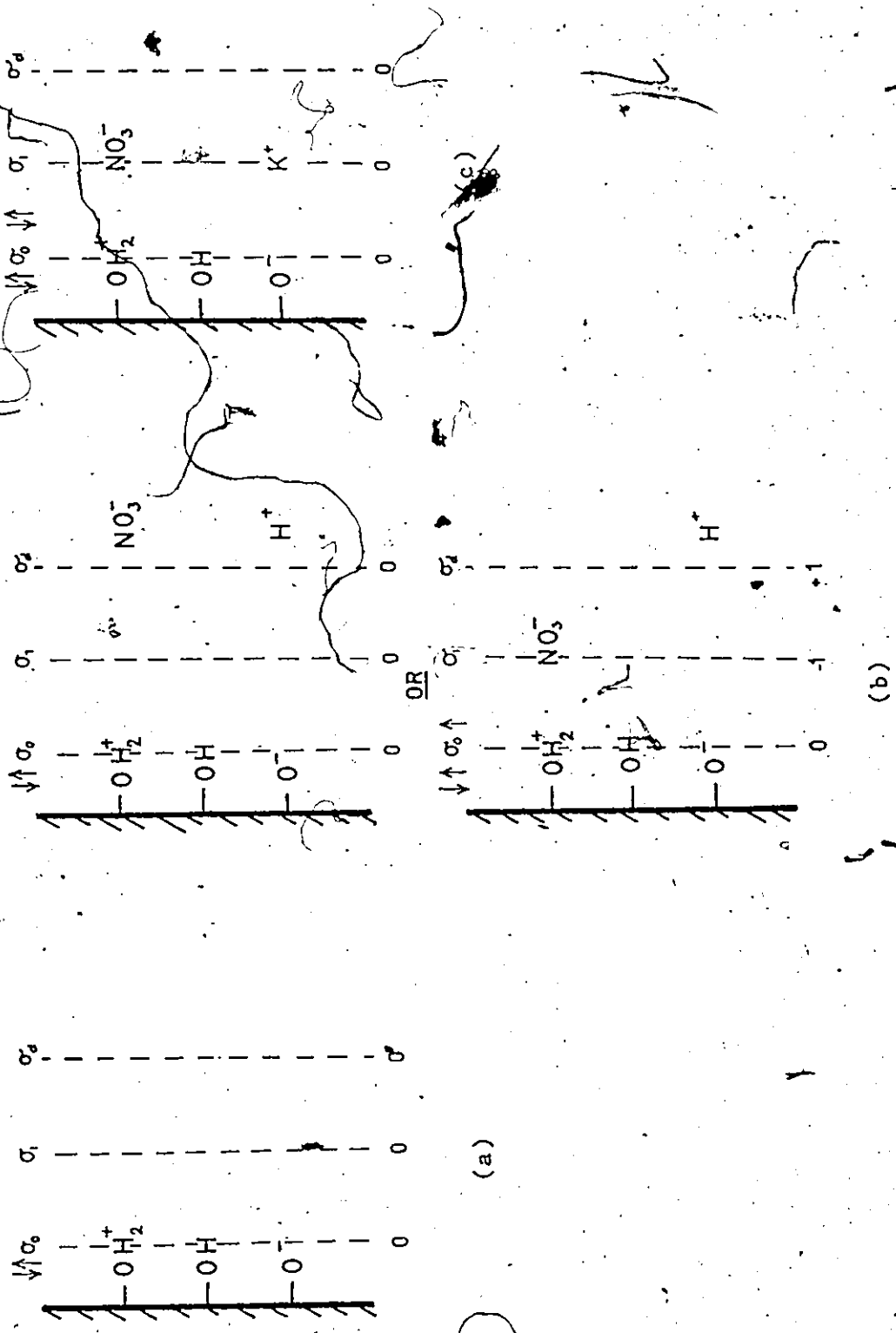


Figure 5.14 The $\delta\text{-MnO}_2$ surface at pH_{zpc}

a) no background electrolyte b) low background electrolyte
 c) high background electrolyte

lyte present is shown in Figure 5.15.a. A low background situation is presented in Figure 5.15.b. In Figure 5.15.c 'ion-pair' formation is shown for the high background electrolyte case. The arrows indicate the qualitative effect of the surface groups and 'ion-pairs' on σ_o .

Case IV: the δ -MnO₂ surface at high pH.

Figure 5.16.a shows the situation at the surface and in the diffuse double layer for the δ -MnO₂ surface at high pH. In Figure 5.16.b several possibilities are sketched for low background electrolyte concentrations, while Figure 5.16.c does the same for high electrolyte situations.

It should be emphasized that Cases I-IV and Figures 5.13-5.16 merely serve as an illustration of possible surface and electrical double layer configurations. No quantitative values should be attached either to the number of surface groups or 'ion-pairs' indicated, since only a tiny part of the surface is sketched. Again, the arrows indicating the influence of these surface groups and 'ion-pairs' on the surface charge σ_o , have only a qualitative meaning.

5.3.2 Discussion of the Influence of Cu²⁺ Adsorption on the Surface

Charge σ_o of δ -MnO₂

In this study, adsorption of Cu²⁺ onto δ -MnO₂ was studied at pH values varying from 6 to 8.5 and at a constant ionic strength (0.01 M KNO₃). The pH_{zpc} for δ -MnO₂ is around pH 1.5 - 2.0 (see Chapter 4). This implies that the δ -MnO₂ surface is strongly negatively charged at the pH values at which the experiments were performed. This, combined with an

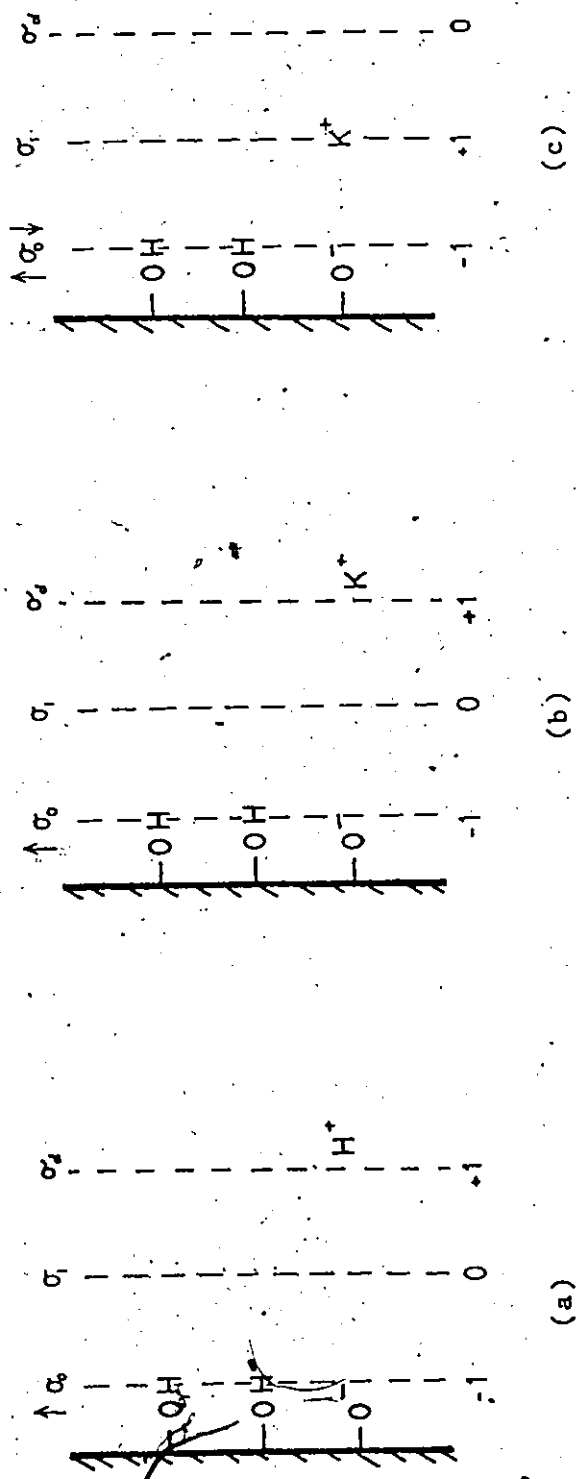


Figure 5.15 The $\delta\text{-MnO}_2$ surface at a pH above pH_{zpc}

- a) no background electrolyte
- b) low background electrolyte
- c) high background electrolyte

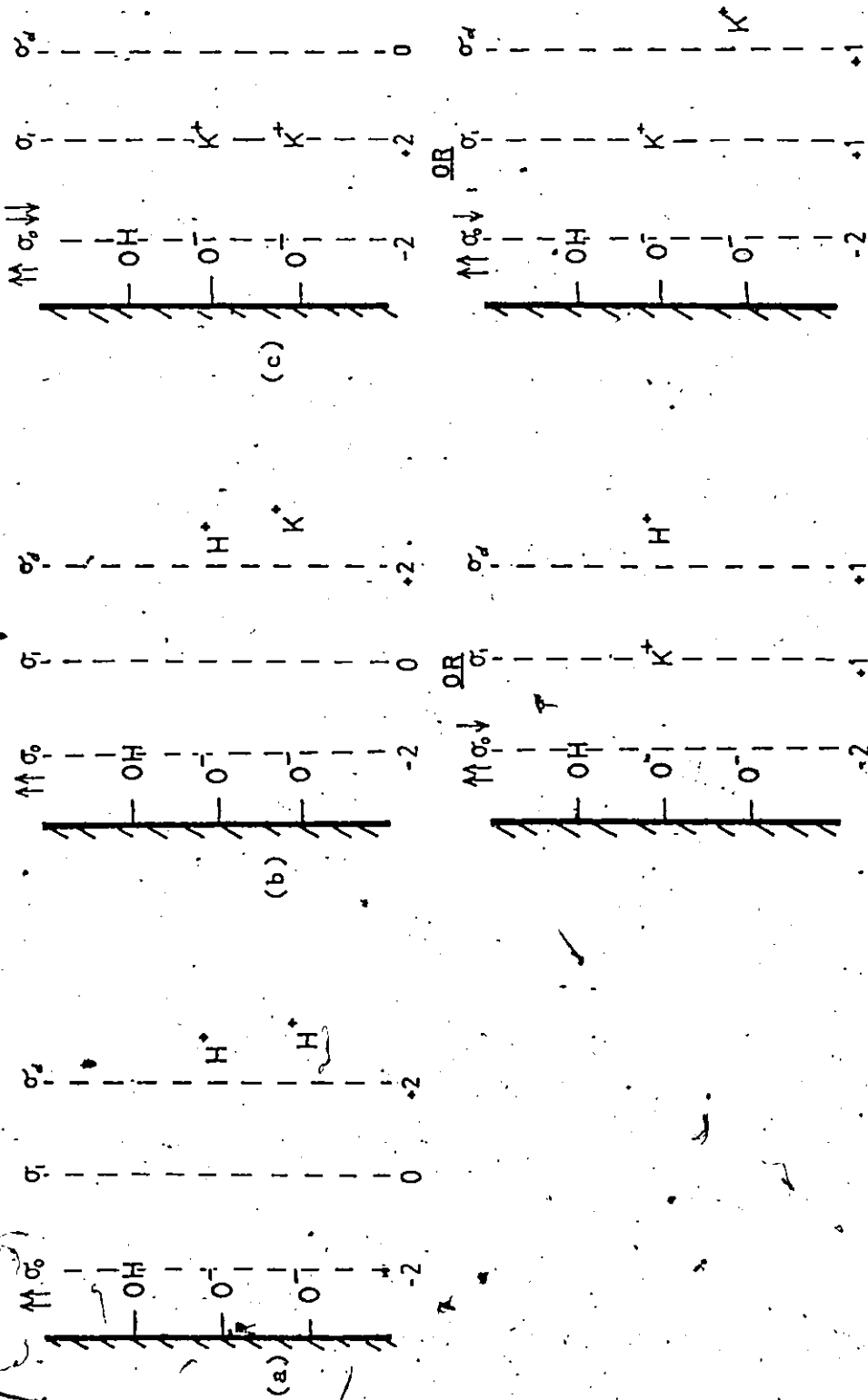


Figure 5.16 The $\delta\text{-MnO}_2$ surface at high pH

- a) no background electrolyte
- b) low background electrolyte
- c) high background electrolyte

ionic strength of 0.01 M KNO_3 , implies that the structure of the $\delta\text{-MnO}_2$ surface and surrounding electrical double layer is most suitably compared to the situation sketched in Figure 5.16.c.

It is assumed in the following discussion on adsorption of Cu^{2+} that the influence of the surface groups on the surface charge, due to mutual repulsion, is counteracted by 'ion-pair' formation to a certain extent. The overall effect of surface group repulsion and 'ion-pair' formation on the surface charge σ_0 is regarded as a constant effect (i.e., as a straight line relationship). This is underscored by Figure 5.17 which shows that the influence of the pH, at constant ionic strength, on the surface charge σ_0 is represented by a more or less straight line at pH values a few units away from the pH_{zpc} . The higher the ionic strength, the closer to the pH_{zpc} the relationship between pH and σ_0 becomes constant (i.e., a straight line). Assuming a pH_{zpc} of 1.5 - 2, for the $\delta\text{-MnO}_2$ surface, and given the fact that the experiments in this study were performed at $6 < \text{pH} < 8.5$, it seems reasonable that the assumption of a constant overall effect of surface group repulsion and 'ion-pair' formation is valid.

The situation sketched in Figure 5.16.c is considered as representative of the state of the $\delta\text{-MnO}_2$ surface prior to adsorption of Cu^{2+} . This situation is expanded schematically in Figure 5.18, where it is illustrated how the surface and electrical double layer configuration changes upon progressing adsorption of Cu^{2+} . Cu^{2+} ions are assumed to exert a larger influence on the individual surface groups than electrolyte ions adsorbed in the σ_1 plane, for reasons such as valency and proximity to the surface groups. This is indicated qualitatively by

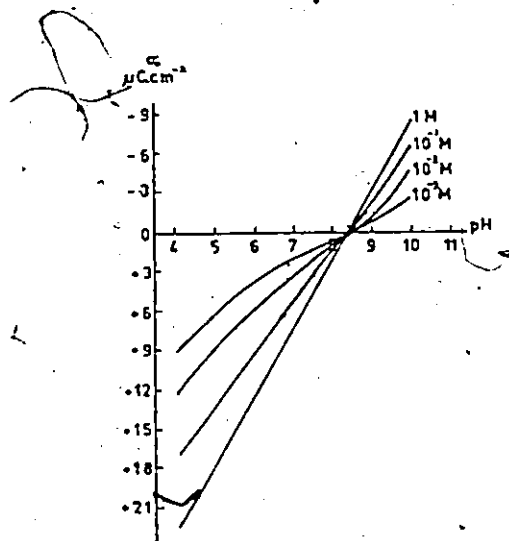


Figure 5.17 (from Breeuwens and Lyklema 1971). Surface charge of synthetic hematite ($\alpha\text{-Fe}_2\text{O}_3$) as a function of pH in the presence of four different concentrations of KCl. (Note: Similar trends are shown in several figures of Davis 1978).

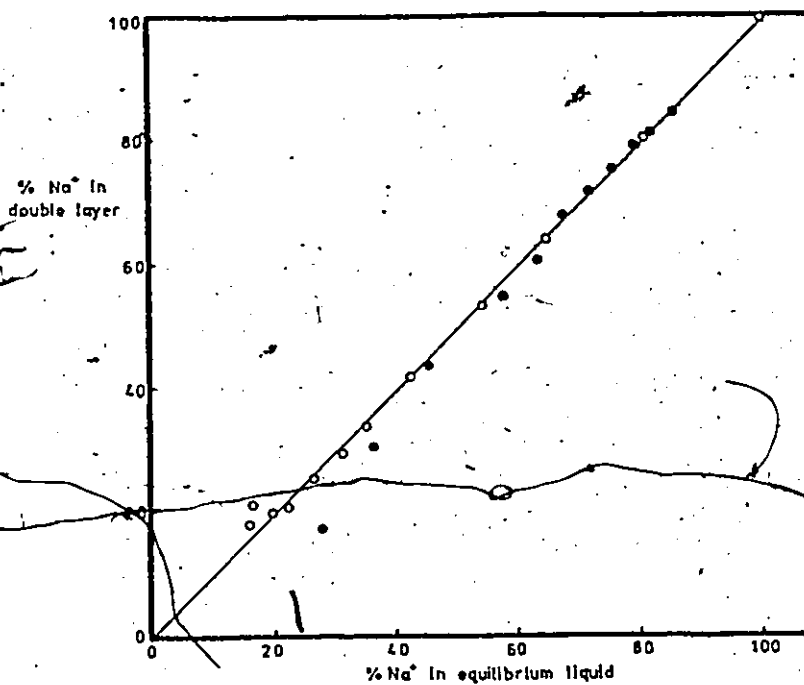


Figure 5.19 Exchange of Na^+ for H^+ in the double layer of Ag-I sol. (from Kruyt 1952).

larger arrows to the right of σ_0 as compared to the basic situation. For example, one could imagine that a stronger binding Cu^{2+} ion can get closer to the surface than an 'ion-pair'-forming electrolyte ion. This depends on the extent of loss of the hydration sphere, and the ionic radius (i.e., the charge density) of the adsorbing ion. It can also be seen from Figure 5.18 that with increasing adsorption the charge in the σ_1 plane (IHP) becomes very high. This will consequently start to form a barrier to further approach of positively charged Cu^{2+} ions to this plane. Therefore, although the surface charge σ_0 tends toward a more negative (and stronger binding) value, the presence of increasing amounts of Cu^{2+} in the σ_1 plane exceeds this effect in the opposite direction. The net effect will be a negative influence on progressing adsorption (note that the influence exerted by the Cu^{2+} ions on each other in the σ_1 plane is neglected here).

The conceptual model for Cu^{2+} adsorption on $\delta\text{-MnO}_2$ arising from the sequence of sketches in Figure 5.18 can be compared to literature data for Y, the ratio of H^+ released per metal ion adsorbed (Table 5.3 in Section 5.2). Y varies from less than one to more than two in this Table. The sequence in Figure 5.18 suggests that it is mainly K^+ that is released in these cases: Either two K^+ ions are released per Cu^{2+} ion adsorbed, or zero to one. The latter release is accompanied by the attraction into the diffuse double layer of charge-balancing NO_3^- ions. The situations sketched are highly simplified. If one imagines a large number of surface groups, it is easy to see that instead of the attraction of NO_3^- ions into the diffuse layer, extra K^+ could be expelled from the diffuse layer, to effectuate the same charge balance. Since in the

Figure 5.18 surface and double layer configurations of the $\delta\text{-MnO}_2$ surface for progressing Cu^{2+} adsorption.

Figure 5.18a

basic situation
no Cu adsorption

Figure 5.18b

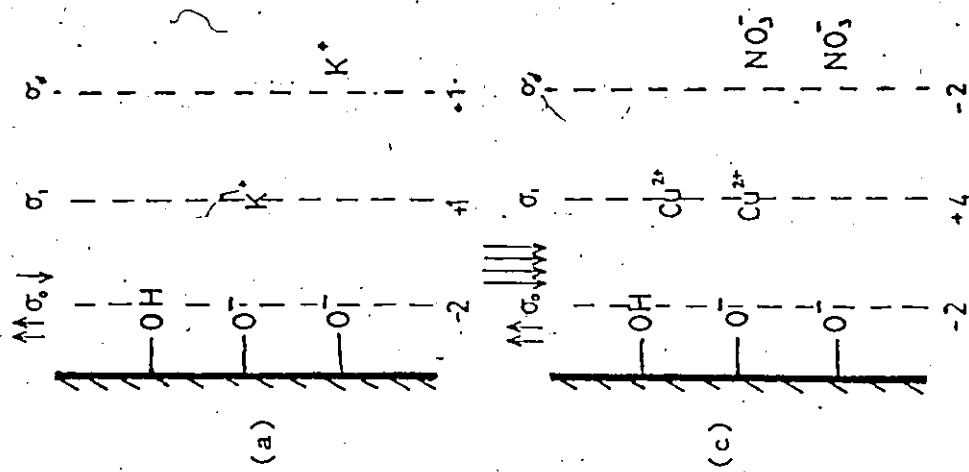
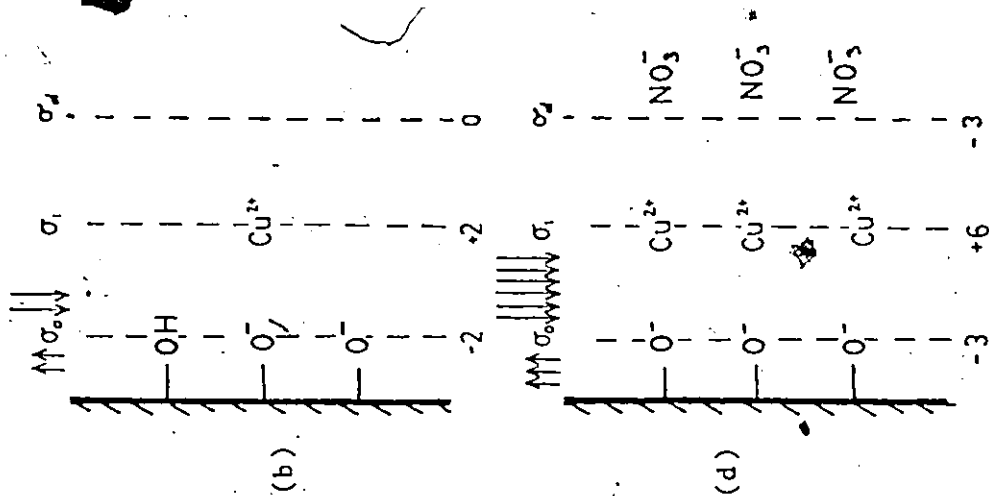
Adsorption of Cu^{2+} ions causes release of twice as much K^+ ions, both from the σ_1 plane and from the diffuse double layer; σ_d is reduced and eventually goes to zero.

Figure 5.18c

adsorption of more Cu^{2+} ions causes a charge reversal of σ_d ; negative counter ions abound in the diffuse double layer.

Figure 5.18d

adsorption of large amounts of Cu^{2+} facilitates the release of more H^+ from the surface, which creates more surface sites; adsorption continues until all potential sites are filled, but adsorption becomes increasingly more difficult with the filling of most sites, due to the formation of a charge barrier in the σ_1 plane (see text).



Handwritten scribbles and a large number '15' on the right side of the page.

studies described in Chapters 6 and 7, no measurements of uptake or release of background electrolyte were performed in concurrence with the Cu adsorption experiments, no conclusions regarding the exact charge balancing process can be drawn. Also, the way in which the surface is represented in the sketches of Figure 5.18 may not be correct. In this Figure, release of K^+ outnumbers release of H^+ by far, unless a much less negative surface is assumed and exchange with OH-groups on the surface rather than with O^- groups occurs. But this goes against literature data which show a highly negative MnO_2 surface in the pH range where the experiments were performed. It is also plausible that besides K^+ , there is H^+ in the diffuse double layer. But since the K^+ concentration is many orders of magnitude higher than the H^+ concentration in the here performed experiments, this is not likely. Figure 5.19 illustrates this.

Another possibility is to assume that Cu^{2+} adsorbs in a different fashion. Figure 5.20 shows various possibilities for Cu^{2+} adsorption, based on suggestions by McKenzie (1980) (see Section 5.2). Figure 5.20a illustrates the basic situation. In Figure 5.20b and 5.20c Cu^{2+} is adsorbed in a bidentate fashion releasing respectively $2K^+$ - or one K^+ - and one H^+ - ion per Cu^{2+} ion adsorbed. In Figure 5.20d and 5.20e, hydrolysis of the Cu^{2+} ion prior to adsorption is illustrated, releasing one K^+ - and one H^+ - or $2H^+$ - ions per Cu^{2+} ion adsorbed. There are more possibilities to imagine than are illustrated in Figure 5.20. However, none of the mechanisms in Figure 5.20 results in a charge reversal for σ_d , which is often observed in the literature (i.e., reversal of sign for the zeta-potential); the illustrated mechanisms can only cause the

σ_d charge to be reduced to zero.

In conclusion it can be said that it is not exactly clear which adsorption process would be most favourable. It has been observed that H^+ is released upon adsorption; hence processes featuring release of K^+ ions only, seem unlikely. But the fact that not always exactly 2 H^+ ions are found to be released upon adsorption of 1 Cu^{2+} , combined with the often found charge reversal of the diffuse double layer, indicates that most likely a mixture of the processes illustrated in Figures 5.19 and 5.20 occurs. It has been argued above, that it is reasonable to assume that the pH effect on the surface charge is either cancelled or is linear at a relatively high constant ionic strength at pH values several units away from the pH_{zpc} , due to the effect of 'ion-pair' formation. It has also been argued above that, although increasing adsorption of Cu^{2+} in the σ_1 plane has a tendency to reduce the surface charge σ_o (and hence favour more adsorption), this tendency is by far exceeded by the high charge in the σ_1 plane. This high charge, caused by increasing Cu^{2+} adsorption, induces a substantial Coulombic barrier to further adsorption in this plane. This energy barrier increases with progressing adsorption.

5.3.3 Model Development

In this section, a simple model is developed, which includes the above discussed effects. The general adsorption equation for Cu^{2+} on $\alpha\text{-MnO}_2$ is:

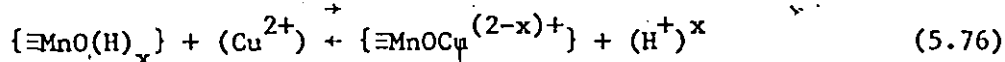


Figure 5.20 Alternative possibilities for the adsorption of Cu^{2+} ions on the $\delta\text{-MnO}_2$ surface

Figure 5.20a

basic situation
no Cu^{2+} adsorbed

Figure 5.20b

bidentate adsorption of Cu^{2+}
releasing one K^+ ion from the
'ion-pair' plane and one from
the diffuse double layer

Figure 5.20c

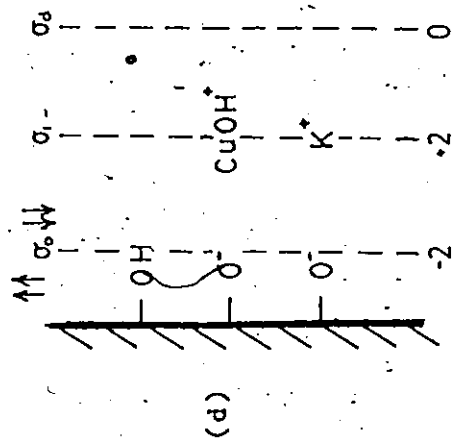
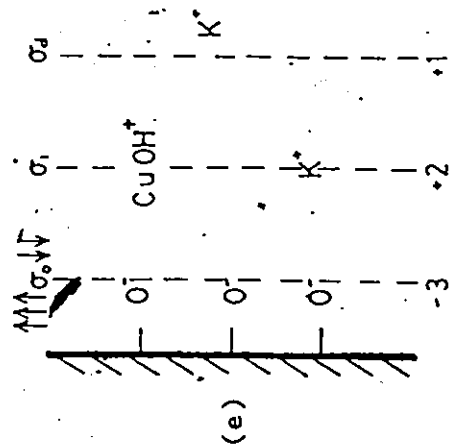
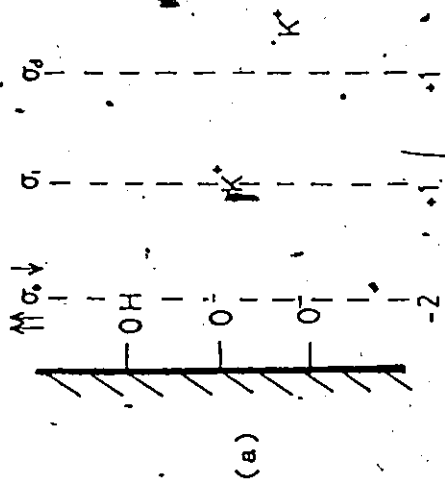
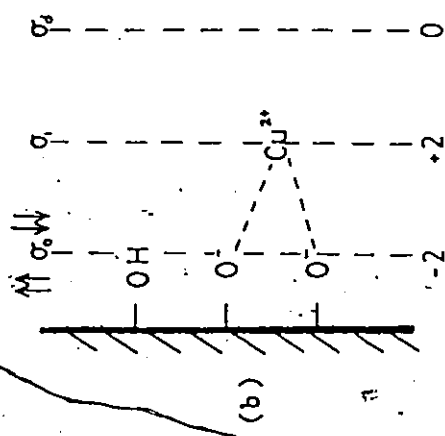
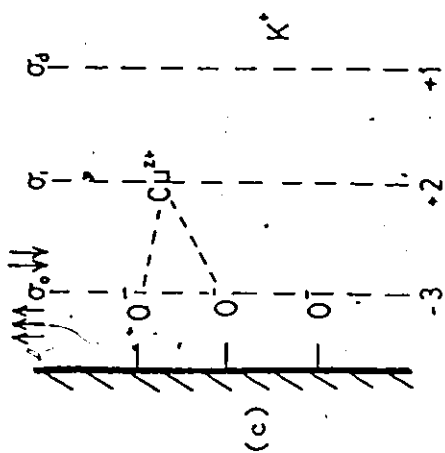
bidentate adsorption of
 Cu^{2+} releasing one H^+
from the surface and one
 K^+ from either the σ_1
plane or the diffuse
double layer

Figure 5.20d

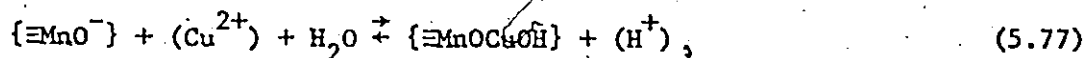
adsorption of hydrolysed Cu^{2+} ,
releasing one H^+ from the hydration
reaction and one K^+ from either
the σ_1 plane or the diffuse double
layer

Figure 5.20e

adsorption of hydrolysed
 Cu^{2+} , releasing one H^+
from the hydration
reaction and one H^+ from
the surface



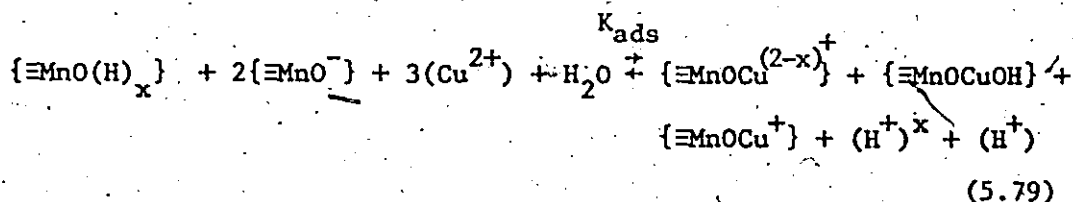
Alternatively, adsorption can be pictured as (McKenzie 1980):



or simply:



Adding all three processes together yields:



Assuming that:

$$\{\equiv\text{MnO}(\text{H})_x\} + 2\{\equiv\text{MnO}^-\} = \text{the free sites} = \Gamma_{\text{max}} - \Gamma_{\text{ads}}, \quad (5.80)$$

and:

$$\{\equiv\text{MnOCu}^{(2-x)+}\} + \{\equiv\text{MnOCuOH}\} + \{\equiv\text{MnOCu}^+\} = \text{the occupied sites} = \Gamma_{\text{ads}} \quad (5.81)$$

and: $3(\text{Cu}^{2+})$ = the solution concentration of Cu^{2+} in equilibrium with the occupied sites,

and that:

$$(\text{H}^+)^x + (\text{H}^+) = (\text{H}^+)^n \quad (5.82)$$

the following can be written:

$$K_{\text{ads}} = \frac{\Gamma_{\text{ads}} (H^+)^n}{(\Gamma_{\text{max}} - \Gamma_{\text{ads}}) (Cu^{2+})} \quad (5.83)$$

or:

$$\Gamma_{\text{ads}} = \frac{\Gamma_{\text{max}} (Cu^{2+})}{(H^+)^n / K_{\text{ads}} + (Cu^{2+})} \quad (5.84)$$

However, the effect of adsorption on the surface charge is ignored in this derivation. Schindler (1976) derived an equation which corrects for the fact that the activity of the surface groups is not constant due to the changing charge effect (see Section 5.1.3.5 of this Chapter). Applying such a correction to the above equation yields:

$$K'_{\text{ads}} / e^{(2-n)\psi/kT} = \frac{\Gamma_{\text{ads}} (H^+)^n}{(\Gamma_{\text{max}} - \Gamma_{\text{ads}}) (Cu^{2+})} \quad (5.85)$$

or:

$$\Gamma_{\text{ads}} = \frac{\Gamma_{\text{max}} (Cu^{2+})}{\frac{(H^+)^n}{K'_{\text{ads}}} e^{(2-n)\psi/kT} + (Cu^{2+})} \quad (5.86)$$

in which K'_{ads} is not an actual equilibrium constant, but a 'surface equilibrium' constant related to the maximum number of available surface sites (which here is assumed to be constant and independent of pH). Also, it is assumed that n is a constant and independent of pH (in other words, that the different reactions probably taking part in the adsorption process have a constant ratio).

According to Schindler (1976), ψ is the difference between the surface potential and the bulk solution potential. For the case presented

here, either the surface potential ψ_0 or the potential at the plane of closest approach (ψ_1) can represent the surface potential in the Schindler correction.

Davis (1978) shows that $\psi_0 - \psi_1 = \sigma_1 / C_1$, assuming a constant capacitance between the two planes. It has been shown in the previous discussion that C_1 is dependent on both 'ion-pair' formation and specific adsorption of Cu^{2+} of which the latter only is variable (constant ionic strength). Therefore it is proposed that the potential difference between the surface and the bulk depends almost entirely on σ_1 , i. e. on the amount of Cu^{2+} adsorbed (Γ_{ads}) in this plane. With this in mind, the following equation for the description of Cu^{2+} adsorption on the $\delta\text{-MnO}_2$ surface is proposed:

$$\Gamma_{\text{ads}} = \frac{\Gamma_{\text{max}} (\text{Cu}^{2+})}{\frac{(\text{H}^+)^n}{B} e^{-(1-\Gamma_{\text{ads}}/\Gamma_{\text{max}})} + (\text{Cu}^{2+})} \quad (5.87)$$

in which the expression $\frac{(\text{H}^+)^n}{B} e^{-(1-\Gamma_{\text{ads}}/\Gamma_{\text{max}})}$ represents the overall bindings energy involved. $B \neq K'_{\text{ads}}$, and both the effect of pH and σ_1 are included, as well as several adsorption mechanisms.

As concluded before, the effect of the pH on the surface charge at constant ionic strength is assumed to be linear at pH values a few units away from pH_{zpc} (concealed in B). 'Ion-pair' formation is not excluded, but is assumed to have a linear effect on σ_0 , and is combined with the pH effect in B. The above equation shows that, if adsorption of Cu^{2+} is minimal, the overall bindings energy term has its smallest value (strongest adsorption), while at almost complete coverage of the surface, the overall bindings energy term has

its largest value and in fact becomes almost constant. These trends are in agreement with deviations from linearity at lower surface coverages observed in the literature and in this study, when using a simple linearized Langmuir adsorption isotherm, to model trace metal adsorption on $\delta\text{-MnO}_2$.

The adsorption data obtained in this study have all been fitted to the above presented 'Implicit' Langmuir equation. Independent of the above derived model, adsorption data have been fitted (in Chapter 7) to a Single Langmuir isotherm (equation 5.3) and a Double Langmuir isotherm. Both these isotherms can only be used at a constant pH. The Double Langmuir model, given in equation (5.88) represents the possibility that besides 1:1 surface complexation, exchange with a second site can occur:

$$\Gamma_{\text{ads}} = \frac{\Gamma_{\text{max}_1} (\text{Cu}^{2+})}{\frac{1}{B_1} + (\text{Cu}^{2+})} + \frac{\Gamma_{\text{max}_2} (\text{Cu}^{2+})}{\frac{1}{B_2} + (\text{Cu}^{2+})} \quad (5.88)$$

It is possible to combine the Double Langmuir model with the Implicit Langmuir, to correct for the fact that progressing adsorption causes a Coulombic barrier to further adsorption. There are two possibilities. In equation (5.89) mono - and bidentate adsorption with fixed stoichiometry is modeled, while equation (5.90) estimates the stoichiometry for the two sites (i.e. does not assume that one site is for mono-, the other is for bidentate binding). The equations are:

$$\Gamma_{\text{ads}} = \frac{\Gamma_{\text{max}_1}(\text{Cu}^{2+})}{\frac{(\text{H}^+)}{B_1 e^{(1 - \frac{\Gamma_{\text{ads}}}{\Gamma_{\text{max}_1}})}} + (\text{Cu}^{2+})} + \frac{\Gamma_{\text{max}_2}(\text{Cu}^{2+})}{\frac{(\text{H}^+)^2}{B_2 e^{(1 - \frac{\Gamma_{\text{ads}}}{\Gamma_{\text{max}_2}})}} + (\text{Cu}^{2+})}, \quad (5.89)$$

$$\text{and } \Gamma_{\text{ads}} = \frac{\Gamma_{\text{max}_1}(\text{Cu}^{2+})}{\frac{(\text{H}^+)^{n_1}}{B_1 e^{(1 - \frac{\Gamma_{\text{ads}}}{\Gamma_{\text{max}_1}})}} + (\text{Cu}^{2+})} + \frac{\Gamma_{\text{max}_2}(\text{Cu}^{2+})}{\frac{(\text{H}^+)^{n_2}}{B_2 e^{(1 - \frac{\Gamma_{\text{ads}}}{\Gamma_{\text{max}_2}})}} + (\text{Cu}^{2+})}. \quad (5.90)$$

These last two models are not used in Chapter 7 to fit the obtained adsorption data to; mono - and bidentate - binding are implied in the derivation for the Implicit Langmuir model, with the restraint that the ratio of both reactions is a constant independent of pH and Cu^{2+} concentration. It is also possible that Cu^{2+} can exchange with lattice Mn^{2+} . Such an exchange probably does not contribute to a charge barrier in the σ_1 plane, and an Implicit Langmuir function is probably not the correct way to model such a process. The possibility of direct adsorption of CuOH^+ has not explicitly been explored in the above models, although the formation of CuOH^+ during the adsorption process is considered in the derivation of the Implicit Langmuir expression.

Surface precipitation has also not been considered in the above discussion. In this work, the experiments performed were all carried out at such concentrations of free Cu^{2+} that $\text{Cu}(\text{OH})_2(\text{s})$ and/or CuO precipitations were avoided (see Chapter 6). This does not necessarily exclude surface-precipitation. However, the fact that constant maximum

adsorption capacities were found for different pH values indicates that surface precipitation likely did not occur. Moreover, by assuming that the maximum adsorption capacity represents monolayer coverage, a surface area could be calculated for $\delta\text{-MnO}_2$ in close agreement with the prevailing literature value of approximately $300\text{ m}^2/\text{g}$ (see Chapter 4).

The energy barrier caused by mutual repulsion between Cu^{2+} ions for extensive adsorption in the σ_1 plane of Cu^{2+} ions can be compared to the so-called Frumkin Fowler expression for gas-adsorption. This expression has been derived with statistical thermodynamics for gas adsorption on a surface where the gas molecules interact laterally with an energy of magnitude w between two molecules, resulting in a larger barrier to further adsorption than if they did not interact: The Frumkin Fowler expression is (Lyklema 1976):

$$\frac{\Gamma_{\text{ads}}/\Gamma_{\text{max}}}{1 - \Gamma_{\text{ads}}/\Gamma_{\text{max}}} e^{(z w \Gamma_{\text{ads}}/\Gamma_{\text{max}})/kT} = k_1 P \quad (5.91)$$

in which:

Γ_{ads} = amount of adsorbed gas

Γ_{max} = maximum amount of available sites

k_1 = constant (relating adsorption to gas pressure)

P = equilibrium gas pressure

z = coordination number (e.g. how many molecules interact with each other)

w = interaction energy between two molecules

As long as the term w is constant and z is low, this expression can

be worked out to a form, very similar to the implicit Langmuir equation as follows:

$$\Gamma_{\text{ads}} = \frac{\Gamma_{\text{max}} P}{1/k_1 e^{(zw\Gamma_{\text{ads}}/\Gamma_{\text{max}})/kT} + P} \quad (5.92)$$

But w itself is a function of the amount of adsorption and the coordination number. The average interaction energy \bar{w} , is given by

$$\bar{w} = w z \Gamma_{\text{ads}} / 2 \Gamma_{\text{max}} \quad (5.93)$$

For the Implicit Langmuir isotherm it was assumed that the adsorbed Cu^{2+} ions in the σ_1 plane interact mainly with the surface groups, and influence σ_0 while it is tacitly assumed that they do not interact laterally in the σ_1 plane, or if they do, the interaction causes a linear effect upon σ_0 throughout the adsorption isotherm. This might not be correct. Lateral interaction can also be compared to movement of adsorbed molecules or ions over the surface, rather than being located in one place. It seems not unrealistic to imagine that, with each additional Cu^{2+} ion adsorbed in the σ_1 plane, not only an extra 2 positive charge units are added to this plane, which increases the barrier to further adsorption, but also the interaction between adsorbed Cu^{2+} ions increases, and instead of the term $e^{(1-\Gamma_{\text{ads}}/\Gamma_{\text{max}})}$ a term of the form $e^{(1-(\Gamma_{\text{ads}}/\Gamma_{\text{max}})^2)}$ would be more appropriate, as follows from equations (5.92) and (5.93). However, in this study, reasonably good results were obtained with the above described Implicit Langmuir expression (5.87), which does not include extensive lateral interaction between adsorbed

Cu²⁺ ions.

5.4 Summary and Conclusions

Adsorption of Cu onto δ -MnO₂ forms a central part of this work. As mentioned previously, adsorption results that were fitted to a linearized form of the Langmuir equation, apparently deviated from linearity, especially at low coverages of the δ -MnO₂ surface. In order to find an explanation for this, the literature was reviewed in the first part of this Chapter with respect to adsorption models generally developed for hydrous oxides. Such a review provides the theoretical background which is needed to apply one or more of these models to the specific case of Cu - δ -MnO₂ interactions. A review of the literature with respect to applications of adsorption models for δ -MnO₂ revealed that only simple models, such as the Langmuir equation, have been applied.

The Implicit Langmuir model developed in this work to describe Cu²⁺ adsorption onto δ -MnO₂ at a constant ionic strength (0.01 N KNO₃) and in the pH range 6 - 8.5, attempts to create a link between the first (general adsorption theory) and second (adsorption on δ -MnO₂) part of this chapter. The model has been developed with complicating factors such as non-constant activity of involved surface groups and various adsorption mechanisms in mind. The Implicit Langmuir model accounts for the influence of these factors on the overall bindings constant by taking into account the relative surface coverage at each adsorption point, and by estimating the pH dependency of the bindings constant. At the same time it was attempted to keep the model as similar to a Simple Langmuir equation as possible.

The Implicit Langmuir model that emerged from this attempt requires only adsorption measurements (and a non-linear least squares computer program). No additional acidity constants for the surface groups nor a calculation of surface charge are necessary. The main advantage of the Implicit Langmuir model over a Single Langmuir equation is that it is able to describe adsorption of trace metals on δ -MnO₂ more accurately at low solution concentrations and low coverages of the δ -MnO₂ surface. At this point it seems appropriate to recall the reasons for which Cu adsorption onto δ -MnO₂ are studied in this work. The δ -MnO₂ method, described in Chapter 2, was developed to determine conditional stability constants for Cu-organic complexes in natural waters. It is important that adsorption of Cu (and other metals) on δ -MnO₂ is known precisely since from this, free Cu²⁺ concentrations in solution are calculated. And these, in turn are involved in the calculation of conditional stability constants. The latter are usually derived at both the low ligand- and low metal- concentrations, characteristically found in natural waters. Since a low ligand concentration necessitates the use of only a small quantity of δ -MnO₂ as a competing surface for the metal which is also present in low (i.e. trace) concentration, it is obvious that especially the area of low surface coverage of the δ -MnO₂ surface needs to be modeled properly. The Implicit Langmuir model is capable of doing this. At the same time the model is simple enough to be used with only the need for measurements of amount of metal uptake by δ -MnO₂ in the presence of unknown ligand, the Cu concentration remaining in solution and the pH.

CHAPTER 6

EXPERIMENTAL PROCEDURES AND THEIR EVALUATION (MASS BALANCES
AND LIGAND ADSORPTION)6.1 Introduction

In this Chapter, the experimental procedures and important technical details, pertaining to the procedures, are discussed. A description of the equipment, chemicals and calibration procedures can be found in Appendix I. As outlined at the end of Chapter 2, one of the purposes of this research has been to investigate the adsorption behaviour of δ -MnO₂ in relation to its proposed use as a resin in metal speciation studies. Copper was chosen as a model trace metal in the experiments which involved a number of differently prepared δ -MnO₂ batches, described in Chapter 4. Although one is referred to Appendix I for most technical details, a description of the actual adsorption procedure is given in Section 6.2. Chemicals and stock solutions necessary for the adsorption experiments are also described in Appendix I. Upper (and lower) limits of amounts of Cu that can be added safely (i.e. without risk of precipitation) during the adsorption procedure are discussed in Section 6.3. Ionic strength fluctuations caused by acid- and base-additions to keep the pH constant during the adsorption process, Mn release during the adsorption of Cu on δ -MnO₂ and DPASV problems

during Cu-analysis are also discussed in Section 6.3. There are many factors that can cause a deficiency in the Cu mass balance during the adsorption procedure. Section 6.4 deals extensively with problems regarding the mass balance. Difficulties can arise when MnO_2 particles adsorb on glassware. These are considered in Section 6.5. Complications caused by adsorption of glycine on δ - MnO_2 and/or glassware are discussed in Section 6.6, while the same is done for other ligands (NTA, aspartic acid) in Section 6.7. Finally, an example-calculation to work out the results from a calibration- and a titration-experiment is given in Section 6.8.

6.2 Adsorption Procedures

All adsorption isotherms were obtained at a constant pH value, while the amount of Cu was varied. Each adsorption experiment was performed as follows: In an acid-cleaned, preweighed, 500 mL Erlenmeyer flask, containing a tefloncoated stirringbar, 5 mL of a 10^{-2} M stock solution of δ - MnO_2 and 2.5 mL of a 2 M electrolytically cleaned KNO_3 solution are added to about 200 mL of distilled, deionized, organic free water and then diluted to 500 mL (by weight). The flask is placed in a thermostated waterbath of $25^\circ C \pm 1^\circ$ and the solution is stirred magnetically. After immersing the pH-electrode and a degassing tube for prepurified N_2 gas, the MnO_2 suspension is purged for one hour at pH=5, to remove CO_2 , before the experiment actually starts. Complete degassing is indicated by a constant pH. After degassing, a small quantity of 10^{-2} M Cu^{2+} solution is added and the pH is adjusted to the particular value, at which the Cu titration is to be performed, by dropwise addition of dilute base. If for the first point of the adsorption isotherm a "blank" is required, no Cu^{2+} is added at this point, and only the pH is adjusted. After the

first Cu addition, an equilibration period of one hour is allowed. During this time, the solution is continuously stirred and degassed, while the pH is kept constant manually by adding minute quantities of dilute acid or base. After the equilibration period, a sample is taken as follows: the flask is quickly removed from the waterbath, dried and weighed. Approximately 20 mL of sample are filtered through an acid cleaned 0.45 μm millipore filter by pouring the solution directly from the flask. This 20 mL fraction is used to rinse the filter membrane and filtrate flask, and discarded. The procedure is repeated and a second 20 mL fraction of filtrate is transferred to a nalgene sample bottle (30 mL capacity), acidified with approximately 200 μL nitric acid (1% dilution factor) and stored. The flask with MnO_2 is again weighed and placed back in the waterbath. More Cu^{2+} is added and the pH is adjusted to the required value.

The sampling procedure, as described above, requires about 5 minutes, while it takes approximately 10 minutes for the pH to become stable again after a Cu addition (the Cu stock solution has a very low pH). Forty-five minutes are allowed to reach equilibrium after each subsequent Cu addition, once the pH is stable. During these equilibration periods, pH corrections are occasionally necessary; the pH is kept constant within ± 0.03 pH units maximum deviation. Eight to ten samples are taken per isotherm. This requires up to twelve hours, but with some careful preparations prior to the experiment, as many as 4 adsorption isotherms can be obtained simultaneously. Once a complete set of samples is collected, they are stored at 4°C until analysis for Cu by Differential Pulse Anodic Stripping Voltammetry (DPASV). By subtracting the amount of Cu in solution from the total amount of Cu added, the

adsorbed fraction can be calculated. The free Cu^{2+} concentration can be calculated from the dissolved amounts by using equilibrium chemistry concepts. Frequently the aid of the computer program REDEQL2 (McDuff and Morel 1974) is invoked to facilitate the calculations. The data are then fitted to a Langmuir adsorption isotherm of the form:

$$\Gamma_{\text{ads}} = \Gamma_{\text{max}} \frac{(\text{Cu}^{2+})}{1/B + (\text{Cu}^{2+})} \quad (6.1)$$

For explanation of the parameters, see Chapter 5; equation (5.3). This expression can be linearized, and a plot of $(\text{Cu}^{2+})/\Gamma_{\text{ads}}$ versus Γ_{ads} should yield a straight line. In this study, a clear deviation from the expected linearity has been observed. Possible causes are discussed in Chapter 5, while Chapter 7 shows the results for a number of isotherms at various pH's.

In future, the above described adsorption experiment will be called a calibration experiment, since the $\delta\text{-MnO}_2$ surface is calibrated for Cu uptake, and its adsorption parameters Γ_{max} and B can be used in a titration experiment.

A titration experiment determines, via titration with Cu, the amount of an unknown ligand present in solution as well as the conditional stability constant for the Cu-ligand complex. Such a titration experiment is performed in virtually the same manner as a calibration experiment. Instead of organic free water, water containing organic matter is used (either a natural water sample or a known laboratory solution). From the amount of Cu adsorbed on the added $\delta\text{-MnO}_2$ (Γ_{ads}), the free Cu^{2+} concentration can be calculated by using the adsorption parameters Γ_{max}

and B determined in the calibration experiment. A Cu mass balance will yield the Cu-ligand (Cu-L) concentration (after correction for CuOH^+ and $\text{Cu}(\text{OH})_2$) and a plot of (Cu^{2+}) vs. $(\text{Cu}^{2+})/(\text{Cu-L})$ should yield a straight line from which the total ligand concentration and the conditional stability constant can be derived via linear least squares analysis. In Section 6.8, a complete example of a calibration- and titration experiment is given.

6.3 Difficulties Associated with Experimental Procedures

The above describes the basic procedure for obtaining adsorption isotherms. However, a number of points deserve special attention. They include (i) the determination of the maximum and minimum amounts of Cu that should and can be added safely during a calibration (or titration) procedure, (ii) ionic strength fluctuations caused by acid- and/or base additions to keep the pH constant during the adsorption experiment, (iii) Mn release during adsorption of Cu on $\delta\text{-MnO}_2$ and (iv) DPASV problems (i.e. peak depression) during Cu analysis afterwards.

6.3.1 Upper (and Lower) Limits of Cu Addition

To obtain meaningful results from adsorption experiments, it is necessary, for arithmetical reasons, that the amount of Cu adsorbing on $\delta\text{-MnO}_2$ is roughly in balance with the amount of Cu that remains in solution. Since at the start of a calibration of a new MnO_2 batch its adsorption strength is unknown, it generally takes some trial and error to arrive at the optimal Cu concentration range.

At low pH values (e.g. 6.0, 6.5), no addition of a known (organic) ligand is necessary to ensure a reasonable amount of Cu in solution with-

out danger of precipitating it in the form of CuO or Cu(OH)_2 . However, without ligand competition, the proportion of Cu that adsorbs will be fairly large compared to the amount that remains dissolved. Therefore, although the amount of Cu added should not be too large because of precipitation problems, it should not be too small at the beginning of an isotherm either, since otherwise very little Cu remains in solution and contamination can become a problem during storage and analysis for total dissolved Cu (e.g. filtration, glassware, etc.). If contamination at low concentrations occurs, the first point(s) of a linearized Langmuir plot ($\text{Cu}^{2+}/\Gamma_{\text{ads}}$ vs. Cu^{2+}) are too high and these data can not be used for linear least squares analysis to determine Γ_{max} and $\log B$. Figure 6.1 (data points 1 and 2) illustrates this case.

On the other hand, additions of Cu should not be too large since otherwise Cu may precipitate to be subsequently filtered off with the MnO_2 and adsorbed Cu. The adsorbed quantity will therefore appear larger than in fact is the case; this results in the upper part of the linearized Langmuir plot being curved. Figure 6.1 illustrates this: data points 8, 9 and 10 cannot be used for linear least squares analysis to determine the adsorption parameters Γ_{max} and B . This problem can be solved to some extent by adding a known amount of ligand which prevents precipitation of Cu. Addition of glycine has often been applied during the calibration experiments performed for this study.

Van den Berg (1979) reports for $\delta\text{-MnO}_2$ calibration: "500 mL of 100 μM manganese dioxide is titrated with copper at a fixed pH and a constant temperature (25°C) and ionic strength (0.01 M KNO_3). Copper additions range from 10-100 μM . Subsamples are filtered, acidified and analyzed by DPASV, which gives very accurate results and linear

response in the range of importance, 0.01-10 μ M of copper. At pH's greater than 7, copper becomes increasingly insoluble. A 35 μ M solution of glycine has been used to increase the dissolved copper concentrations at these pH's".

Initially, calibrations were performed according to these instructions. However, this resulted in the loss of at least 3 to 5 points per 10-point experiment, due to the above mentioned upper and lower effects (Figure 6.1, data points 1, 2, 8, 9 and 10). It seems necessary to perform a number of theoretical calculations prior to calibration, to determine the practical minimum and maximum Cu addition limits, in order to prevent the loss of data points. The computer program REDEQL2 (McDuff and Morel 1974) can be used to calculate Cu(OH)₂ precipitation conditions. Unfortunately the databank of this program does not contain data for CuO precipitation. The following illustrates how upper (and lower) limits of "safe" Cu addition can be calculated.

The solution equilibrium of Cu (in solutions void of carbonates and other ligands) may be controlled by reactions involving CuO(s):



$$\frac{(\text{Cu}^{2+})}{(\text{H}^+)^2} = *K_{\text{so}} = 7.65 \quad , \text{Stumm and Morgan 1970, p.167-168}.$$

and perhaps Cu(OH)₂(s):



One of the reasons that it is difficult to predict free Cu²⁺ concentrations in solution, is that generally there exists considerable disagree-

ment in the literature about the formation constants of trace metal hydroxides such as $Zn(OH)_2$ and $Cu(OH)_2$ (Vuceta and Morgan 1977; Zirino and Yamamoto 1972; Bradford 1973; Baes and Mesmer 1976, in McBride 1982).

The linearized Langmuir solution can be rewritten as:

$$\frac{1}{\mu M Cu_{ads} / \mu M \delta-MnO_2} = \frac{1}{B} \cdot \frac{1}{\Gamma_{max}} \cdot \frac{1}{[Cu^{2+}]} + \frac{1}{\Gamma_{max}} \quad (6.4)$$

or

$$\frac{\mu M \delta-MnO_2}{Cu_t - Cu_{diss}} = \frac{1}{B} \cdot \frac{1}{\Gamma_{max}} \cdot \frac{1}{[Cu^{2+}]} + \frac{1}{\Gamma_{max}} \quad (6.5)$$

in which: Cu_t = total added Cu

$$Cu_{diss} = [Cu^{2+}] + [CuL^+] + [CuL_2] + [CuOH^+] + [Cu(OH)_2]$$

where $[CuL^+]$ and $[CuL_2]$ are Cu-glycine complexes.

Equilibrium constants required to solve the above equation for Cu_{diss} are given in Appendix II.

Consider only the limits imposed by the solubility of CuO : From the solubility constant for CuO , the maximum amount of free Cu^{2+} that can exist in solution without causing a precipitate can be calculated.

Glycine is added to keep more Cu in the dissolved fraction. Table 6.1 shows the upper boundaries for Cu^{2+} in solution at various pH values as well as the upper limit of dissolved Cu in the presence of 50 μM glycine. The calculations can be done either by using the computer

program REDEQL2 or alternatively by hand, by expressing $[\text{CuL}^+]$, $[\text{CuL}_2]$, $[\text{CuOH}^+]$ and $[\text{Cu}(\text{OH})_2]$ in $[\text{Cu}^{2+}]$ and $[\text{L}^-]$ and substituting the maximum allowable free $[\text{Cu}^{2+}]$ concentration and solving for $[\text{L}^-]$.

Table 6.1 Upper limits for Cu^{2+} and Cu_{diss} to avoid CuO precipitation

pH	max. free Cu^{2+} allowable from $*K_{\text{so}}$	μM	Cu_{diss} allowable in presence of 50 μM glycine, calculated with REDEQL2
6.0	44.7	μM	$\gg 40 \mu\text{M}$
6.5	4.47		~ 26
7.0	0.447		~ 12
7.5	0.0447		~ 10
8.0	0.00447		~ 8
8.5	0.000447		~ 7

Assuming a certain MnO_2 concentration and using reasonable values for Γ_{max} and B (e.g. previously reported values), one can estimate the maximum amount of Cu_t that can be added safely. Once initial values for the adsorption parameters of the unknown $\delta\text{-MnO}_2$ are obtained, these calculations can be refined. If one wants to be absolutely sure that no CuO can precipitate during the calibration of a MnO_2 with unknown but suspected low adsorption capacity and/or strength, one should treat the solution as if no $\delta\text{-MnO}_2$ were present and adhere to the maximum allowed Cu_{diss} concentrations shown in Table 6.1:

Calibrations at pH 7.0 and 7.5 were made for a very "fresh" δ -MnO₂ and deliberately taken too far as compared with the predictions of Table 6.1 using K_{SO}^* . Figures 6.2a and b display linearized Langmuir plots for these experiments. For pH 7.0, precipitation starts slightly before the predicted maximum free Cu²⁺ concentration is reached, while for pH 7.5 precipitation starts around the expected value. It should be noted here that such calculations can only be of an approximate character because there are errors associated with (i) the equilibrium constants which influence the calculated values for free Cu²⁺ concentrations, and with (ii) the values used for Γ_{max} and B which influence the maximum Cu_t concentrations allowable.

In addition to the precipitation of CuO, the possible precipitation of Cu(OH)₂ must be taken into account. Consider the values of Cu²⁺, if only Cu(OH)₂ precipitates: To avoid problem concentration ranges, maximum values of Cu_{diss}⁻ (and corresponding Cu_t⁻) concentrations, which avoid Cu(OH)₂(s) precipitation, are calculated and presented in Table 6.2. Addition of a strongly adsorbing MnO₂ allows Cu_t to be larger than calculated for the absence of any adsorbing surface.

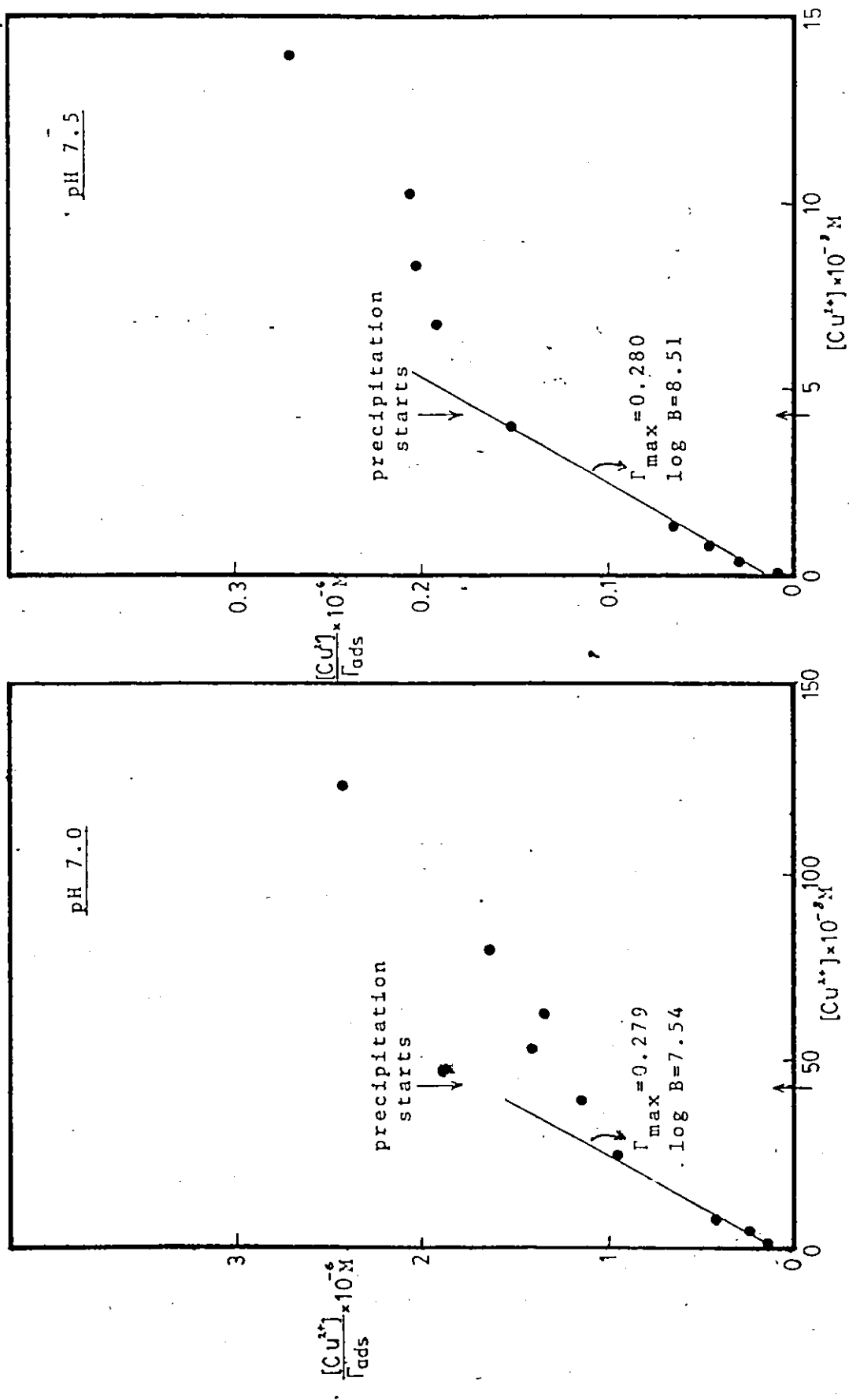


Figure 6.2 Calibration of δ -MnO₂ at pH's 7.0 and 7.5, illustrating CuO precipitation.

Table 6.2 Upper limits for Cu^{2+} and Cu_{diss} concentrations to avoid $\text{Cu}(\text{OH})_2(\text{s})$ formation calculated with REDEOL2

pH	max. free Cu^{2+} allowable in presence of 50 μM glycine	corresponding max. Cu_{diss} permitted
6.0	269 μM	$\gg 40$ μM
6.5	26.9	$\gg 40$
7.0	2.69	~ 34
7.5	0.269	~ 23
8.0	0.0269	~ 20
8.5	0.00269	~ 18

By comparing Tables 6.1 and 6.2, one observes that precipitation of CuO occurs well before the limits of $\text{Cu}(\text{OH})_2$ precipitation over the pH range of 6-8.5. Hence, to obtain meaningful adsorption isotherms, the free Cu^{2+} concentration should stay below the values given in Table 6.1.

6.3.2 Ionic Strength Fluctuations

The ionic strength increases throughout an adsorption experiment, due to the addition of small amounts (μL 's) of Cu^{2+} in the form of highly acidic, concentrated $\text{Cu}(\text{NO}_3)_2$ and the subsequent adjustment of the pH of the MnO_2 suspension with small quantities of dilute KOH. A drastic change in ionic strength certainly has effects on adsorption characteristics (see also Chapter 5, Table 5.3).

Changes in specific conductance were used to estimate shifts in ionic strength during the course of adsorption experiments. The conductivity of a number of typical experimental MnO_2 suspensions ($\sim 80 \mu\text{M } \delta\text{-MnO}_2$, 0.01 M KNO_3) was measured after the adsorption experiments were completed. The ionic strength of these suspensions was estimated using the linear relationship between ionic strength and specific conductance obtained with standard KNO_3 solutions. It appeared that the ionic strength during a typical adsorption experiment changes from 0.010 to 0.012 over the entire experiment. Such a small change in ionic strength is not expected to have an important effect on activities and hence adsorption isotherms.

6.3.3 Mn Release During Cu Adsorption

It is possible that the replacement of Mn^{2+} (or possibly Mn^{3+}) from the imperfect MnO_2 lattice by adsorbing Cu might create a second adsorption site. In fact, this is reported by Loganathan and Bureau (1973; see Chapter 5). This possibility was investigated for an adsorption experiment in which Cu was adsorbed onto the δMnO_2 surface, in a solution devoid of substances such as organics. The subsamples resulting from this experiment were not acidified (as is the usual practice) in order to be able to perform DPASV on these samples at a plating-out potential (-1.7 V) low enough to determine potentially present Mn^{2+} . (Mn^{2+} plates out at -1.45 V ; in acidified samples one cannot apply such a low potential, due to H_2 development which coats the Hg electrode). No Mn was detected in these samples.

However, a small amount of Zn ($\sim 0.3 \mu\text{M}$) was present in each subsample. It was proposed that perhaps Zn was present on the $\delta\text{-MnO}_2$

surface, and exchanged for Cu, hence creating an adsorption site with different affinity for Cu. However, one can argue against this possibility since the amount of Zn detected is very small compared to the total concentration levels of Cu adsorption. Moreover, the amount of Zn detected in each subsample stays virtually constant throughout the experiment ($\approx 0.3 \mu\text{M}$). If Zn was exchanging for Cu, then one should find an increasing amount of Zn in subsequent subsamples, proportional to the amount of Cu adsorbed. This does not seem to be the case, and it is quite likely that the Zn contamination occurs elsewhere in the experimental process.

For instance, during the scrubbing of the subsamples to remove oxygen before DPASV measurements, N_2 gas is bubbled through a vanadium oxygen scrubber solution, which contains a Zn-Hg amalgam, before it enters the sample solution. This could be a source of Zn contamination, and is possibly proportional to the time during which N_2 is bubbled through the solution. However, the same level of Zn was found for a sample which was scrubbed for 5, 10 and 15 minutes consecutively. It is therefore not certain where this relatively small Zn contamination comes from. It cannot result from acidification, since no HNO_3 was added to the subsamples. It is not expected that this small amount of Zn has a significant influence on the adsorption of Cu onto the MnO_2 surface. Since no Mn^{2+} was found in any of the subsamples of a calibration of the $\delta\text{-MnO}_2$ surface for Cu adsorption, it is not likely that exchange of Cu for Mn causes a second adsorption site.

6.3.3.1 Intermetallic Interferences

With respect to the reliability of the DPASV analysis

for dissolved Cu, some attention should be given here to the phenomenon of intermetallic interferences in Anodic Stripping Voltammetry (ASV). Gerlach and Kowalski (1982) report a number of findings with regard to the Cu-Zn-Hg system. It appears that the interaction of Zn with Cu in Hg has been investigated repeatedly, mainly because of the increased use of ASV for trace metal analysis of environmental samples in which frequently Zn and Cu are the most abundant trace metals present. The Zn peak is depressed in the presence of Cu as a result of an intermetallic Zn-Cu compound formed in the mercury drop, but apparently the effect of Zn on the Cu peak is very small. This might be due to another peak from the oxidation of the intermetallic compound at a potential very close to the potential at which Cu is oxidized (Shuman and Woodward 1976). Gerlach and Kowalski (1982) report a depression of 9% for 0.083 μM Cu in the presence of 0.2 μM Zn, but in the same solution the depression of the Zn peak is 22%.

However, for intermetallic compounds to form, the plating potential during ASV has to be such that both Zn and Cu are reduced to end up in the Hg drop. This is the case during simultaneous analysis of several trace metals in a sample. In this study, the reduction of Cu was always performed at a potential of -200 mV, well above the potential at which Zn is reduced (\sim -900 mV). Even in the case of a small amount of Zn contamination (as mentioned above) in some subsamples, intermetallic Zn-Cu compounds could not have formed to give false (i.e. too low) Cu determinations. This point is emphasized since the deviation from Langmuir linearity as found for the Cu adsorption isotherms in this study could be artificial if too low Cu concentrations were measured at low surface coverage of $\delta\text{-MnO}_2$, due to this analytical problem.

6.3.4 Depression of Cu Peaks During DPASV Analysis

Problems were encountered during DPASV analysis to determine Cu_{dissolved} concentrations. It was found that standard additions of Cu in an acidified, filtered sample solution (no organics) yielded lower concentrations of Cu compared to standard additions in acidified organic free water of the same ionic strength. Initially it was thought that possibly manganese would pass through the 0.45 μm filterpaper and cause peak depression (intermetallic interference) during the analysis. Manganese was measured by Atomic Absorption Spectrometry (A.A.) in the subsamples of calibrations of MnO_2 at pH 6.0 and 6.5. These samples are most likely to contain manganese, because the pH might drop temporarily (few minutes) directly after the addition of acid Cu solution during a calibration experiment. Also, Loganathan and Burau (1973, 1977; see Chapter 5) have reported that Mn exchanges for Cu. A.A. analysis showed a concentration of less than 0.08 ppm (1.46 μM) Mn, which is close to the detection limit of A.A analysis for Mn, in all subsamples. To investigate whether such a small amount of Mn could cause peak depression, Cu was measured in absence and presence of Mn in organic free water in 3 experiments. They are:

Experiment 1: organic free water, unfiltered, acidified, ionic strength 0.01;

Experiment 2: organic free water, filtered through an uncleaned 0.45 μm filterpaper (first 20 mL's filtrate discarded), acidified, ionic strength 0.01;

Experiment 3: organic free water, filtered through an acid cleaned (HNO_3) 0.45 μm filterpaper (first 20 mL's filtrate discarded), acidified, ionic strength 0.01 .

The results (corrected for blank etc.) are presented in Table 6.3.

Table 6.3 Peak depression of Cu during DPASV

		(peak) current μA		
Concentration		Experiment 1	Experiment 2	Experiment 3
2 μM	Cu^{2+}	11.38	9.34	11.19
id. + 1.46 μM	Mn^{2+}	11.45	9.25	11.44

From Table 6.3 it can be concluded that it is improper cleaning of the 0.45 μm filterpapers rather than the presence of Mn which is causing the peak depression. Possibly some polymer from the filterpapers enters the sample solution, which then depresses the Cu peak by adsorbing on the mercury electrode. Initially, the filter papers were not cleaned with acid because any residual trace of acid might strip some of the adsorbed Cu from the MnO_2 during the filtration-procedure. The filterpapers were rinsed with sample instead, but this does not appear adequate. Therefore, filterpapers were acid-treated and rinsed with large amounts of deionized water prior to use.

It was also noted that the presence of glycine caused a slight peak depression (4.5 - 8%). Glycine does not complex with Cu at low pH (acidified sample solution pH=1) and therefore it is more likely that glycine adsorbs on the mercury electrode. This could be investigated,

and the effect avoided, by irradiating the samples with U.V. light prior to ASV. Irrespectively, calibration of polarographic response to Cu^{2+} should always be performed in the sample solution itself by standard additions. In this study it was assumed that the effect of glycine on DPASV analysis was constant throughout one set of samples from the same adsorption experiment. Polarograph calibrations were done by standard additions in two sample solutions per set of samples.

6.4 Mass Balance for Cu

The calibration procedure described in Section 6.2 does not include a check on the mass balance for Cu throughout the experiment. A considerable number of the adsorption isotherms obtained in this study never underwent a control with respect to the Cu mass balance. Initially, it was assumed that, if glass adsorption or contamination occurred at all, during the 10 -- 12 hrs. experiments in the Erlenmeyer flasks, it would be a negligible factor, due to the relatively high (i.e. certainly no trace-) total metal- concentrations at which the experiments were performed.

However, since the obtained isotherms did not follow the Langmuir theory at low surface coverage (deviation from linearity), it seemed necessary to rule out any possible artifacts with respect to this deviation. Therefore, a mass balance check for Cu was instituted, to ascertain whether glass adsorption or contamination would occur during the actual experiments, or during post-experimental procedures such as filtration, storage and analysis.

Contamination and glass adsorption of trace metals is a well-known problem. Laxen and Harrison (1981) and Smith (1978) investigated

respectively cleaning methods for polythene containers prior to their use for determination of trace metals in freshwater samples, and sources of Cu and Cd contamination in small biological samples. Laxen and Harrison (1981) recommend that sample containers be routinely cleaned with 10% HNO_3 during a 48 hr. soak both for preliminary cleaning of new bottles and for routine cleaning, to prevent sample contamination. Smith (1978) describes some filter-washing techniques investigated by Wallace et al. (1977) for Whatman and Nucleopore filterpapers and recommends that filters be soaked for 24 hr. in 1 M HNO_3 and rinsed with distilled water.

Subramanian et al. (1978) and Masseur and Maessen (1981) investigated the losses for a number of trace metals from respectively natural riverwaters, distilled water and artificial seawater by sorption on various container surfaces. Subramanian et al. (1978) find that for storage of synthetic- and river-water samples in Pyrex and Nalgene containers, a loss of Cu occurs above pH 4.0. Most of the loss, (e.g. 35% at pH 6.0 and 50% at pH 8.0) occurs in one day and no further loss is observed up to 30 days. Total Cu concentrations used in Subramanians study are based on riverwater analysis and fall in the range of 0-50 ng/mL ($\approx 0-0.8 \mu\text{M}$). Subramanian et al. (1978) conclude that the best way to preserve natural water samples is acidification of the samples with HNO_3 to a pH ≤ 1.5 , and storage in Pyrex glass or Nalgene linear polyethylene containers, of which the latter are less expensive, lighter, more durable and easier to handle.

In their detailed study on sorption losses of trace metals, Masseur and Maessen (1981) find that the various factors can be categorized as follows:

- (1) chemical form and concentration of the trace metals involved (e.g. free or complexed ion)

- (ii) solution characteristics such as pH, complexing agents, suspended matter, dissolved gases, micro-organisms, etc.
- (iii) container properties: chemical composition, surface roughness, surface cleanliness, specific surface (i.e. available surface per amount of liquid), and history of containers such as age, cleaning method, previous samples, exposure to heat, etc.
- (iv) external factors such as temperature, contact time, light- and agitation-exposure.

They give particular attention to the specific surface, i.e. the ratio of the inner container surface in contact with solution, to the volume of the solution, and find that the larger this ratio, the more sorption occurs. No results for Cu are reported by these authors; but they have included Cu in a large summary table containing literature references on sorption losses of 41 elements from aqueous solutions under different experimental conditions. Their general recommendations are reduction of contact time and specific surface, and acidification with a strong acid ($\text{pH} < 2.0$). If the latter is not possible for reasons such as speciation studies, the use of radiotracers, added directly after sampling in known concentrations, will provide a check on sorption losses during storage. They also mention that sample containers may exhibit erratic sorption characteristics after several days storage. The same holds for repeatedly used sample vessels.

Sorption and/or contamination of Cu could potentially occur in many places during the adsorption-, sampling-, and storage-procedures, for the experiments described here and in Chapter 7. Contamination problems are largely ruled out because of the use of Analar Grade

chemicals, generally high total Cu levels (1-30 μM , depending on the experiment) and rigorous cleaning methods (e.g. 48 hours soaking in 10% HNO_3 of all glassware, polyethylene sample bottles (Nalgene, 30 mL) and Millipore filterpapers involved - for details see Appendix I). The only remaining potential contamination spot exists at the lower concentrations of an adsorption isotherm, in cases where adsorption is strong enough so that very little free Cu^{2+} stays in solution. However, this is usually rather obvious (see Figure 6.1), and such contaminated data points are excluded from further calculations. Sorption problems are avoided in the sample storage step by acidifying each subsample after filtration with 1% Aristar HNO_3 (pH 1.2 - 1.0).

As described in Section 6.2, the actual adsorption experiments are performed in Pyrex Erlenmeyer flasks, at pH values varying from 6.0 to 8.5. At this stage in the experimental procedure, there is potential for Cu sorption losses. Thus, an addition was made to the experimental procedure, discussed in Section 6.2, to assess sorption effects. Through this addition, not only Cu sorption phenomena, but also MnO_2 - and glycine- sorption losses (see Sections 6.8 and 6.9) can be evaluated. The addition consists of the following:

The filterpapers through which the sample solution is filtered at intervals of 1 hr. and on which MnO_2 plus adsorbed Cu is deposited, are filtered to dryness and stored in plastic petri dishes at 4°C .

Prior to analysis, the filterpapers are reduced in 25 mL oxalic acid (0.5 M); this dissolves the MnO_2 and adsorbed Cu. After dilution to 50 mL with deionized H_2O , the solutions are analyzed for Cu and Mn by A.A. Standards and blanks for Cu and Mn are prepared in the same oxalic acid medium to avoid matrix effects.

The difference between total Cu added and the sum of Cu on the filterpapers and Cu in the filtrates is large, suggesting that quite an amount of Cu has disappeared. Table 6.4 gives a typical example of the extent of this lack of mass balance. According to the filtrate analyses (by DPASV), more Cu is adsorbed on the MnO_2 surface than is recovered from the MnO_2 when analyzing the filterpapers. However, the amount of Cu missing appears to vary widely from experiment to experiment, and on some occasions the Cu mass balance does add up to the total amount of added Cu.

There are several possible answers to the problem of the missing

Cu:

- (1) In a pH range of 6.0 - 8.5, Cu can adsorb on the walls of the Erlenmeyer flask during the actual adsorption experiment. However, occasional DPASV analysis of overall, non-filtered but acidified samples taken at the end of the experiments recovered almost all of the total Cu added. If there exists any glass adsorption at all, it is certainly not in the quantities necessary to account for the missing Cu in Table 6.4. But it should be mentioned here that DPASV analysis of a non-filtered, acidified sample containing MnO_2 particles appeared difficult and did not always yield unambiguous results (e.g. repeat analysis of the same acidified overall end-sample gave varying results). Therefore some additional evidence is needed to test whether Cu does (not) disappear in the experimental phase of the adsorption experiments.
- (2) Cu can adsorb during the filtration step. The filter support is made from sintered glass (glass frit), which therefore must have a

Table 6.4 Adsorbed, dissolved and total Cu concentrations of a typical calibration experiment displaying mass balance irregularities

Experiment * 010381 : MnO₂ XVe - pH 6.0 - 50μM glycine added.

Cu _t added	Cu _{diss} (DPSAV)	Cu _{ads} (A.A.)	equil.time	Cu _{missing}	% of Cu _t missing
μM	μM	μM	hrs.	μM	
1.9995	0.1190	1.413	1	0.467	23.4
4.1827	0.1307	3.597	2	0.455	10.9
6.5505	0.1506	5.495	3	0.905	13.8
9.1470	0.3215	7.657	4	1.169	12.8
12.0485	0.5910	9.569	5	1.889	15.7
15.3098	1.738	11.244	6	2.328	15.2
19.0114	3.702	12.270	7	3.039	16.0
23.3093	6.189	13.307	8	3.813	16.4
28.5318	10.310	14.483	9	3.739	13.3

* Note : a complete overview of all experiments performed is given in Appendix III. The identification number of each experiment is the date on which it was performed, supplemented by the specific MnO₂ batch used, the pH at which the experiment was performed and whether or not glycine was added to keep sufficient Cu soluble.

very large surface area. Although the supports were acid soaked and well rinsed with deionized water and sample solution prior to use and in between filtration steps, possible sorption of Cu in the filterhead cannot be ruled out per se, without further investigation.

- (3) Cu may disappear in the polyethylene sample bottles prior to d.p.a.s.v. analysis. However, this is adequately prevented by acidifying the sample solutions to pH \approx 1.
- (4) Cu may disappear in the sample flasks in which the filter papers are reduced prior to A.A. analysis (i.e. 100 mL Pyrex glass Erlenmeyer flasks). On several occasions, an overall, non-filtered sample, taken at the end of an adsorption experiment, was reduced with oxalic acid and measured for total Cu by A.A. analysis. The amount of Cu recovered appeared considerably lower (12-17%) than the total added concentration, indicating that perhaps the oxalic acid reduction procedure causes the Cu deficit.

To find an answer to the disappearance of Cu, an experiment was set up similar to the general description in Section 6.2. MnO_2 was omitted, and instead of 10 Cu additions at one pH, 2 Cu additions were made at two different pH values. Any unaccounted for Cu must then be due to sorption onto glassware or filtration equipment. The results of this experiment showed the following:

- (i) Cu does not sorb over the timespan of two hours on the walls of the Erlenmeyer flask in which the experiments are performed.
- (ii) The Cu contents, as measured by A.A., of HNO_3 acidified filtered and unfiltered subsamples were identical. This means that no sorption occurs during the filtration step.
- (iii) The Cu contents of filtered and unfiltered subsamples diluted once with 0.5 M oxalic acid solution, as measured by A.A., were

virtually identical; this is additional evidence that the filtration step does not cause the discrepancy. However, the Cu content of these oxalic acid-diluted subsamples was not always consistent with the subsamples that were acidified with HNO_3 , although the slight differences cannot offer an explanation for the amounts of Cu missing in Table 6.4.

A definite answer to the "missing Cu mystery" has not been found.

Adsorption on vessel walls can be ruled out as an explanation.

DPASV measurements on acidified subsamples, stored in conscientiously cleaned Nalgene bottles, are also not suspect. And although it was not proven in the above described experiment, the step in which the filterpapers are reduced with oxalic acid, seems most suspect. Several possibilities can be argued:

- (i) It might be possible that oxalic acid does not completely reduce the MnO_2 particles and hence not all Cu is freed, although visible observations contradict this: all MnO_2 particles disappear in a few minutes after immersing the filterpapers in the oxalic acid solution.
- (ii) The freed Cu could adsorb on the glassware with or without help from the oxalic acid molecules. However, Cu standards were always made up at the same time, in the same oxalic acid solution; this renders this possibility highly unlikely.
- (iii) The filterpapers in the oxalic acid solutions may adsorb Cu (or Cu-oxalic acid complex); this would result in a lower Cu concentration measured by A.A. Cu standards did usually not include the presence of a filterpaper.

- (iv) Cu measurements by A.A. may somehow be negatively influenced by the presence of Mn from the dissolved MnO_2 particles. Cu standards did not always contain Mn in the amounts present in the sample solutions.

In summary, it can be concluded that:

- (i) Cu disappears, because the mass balance for the total amount of Cu added does not close.
- (ii) Sorption during the experiments in the Erlenmeyer flasks, during the filtration procedure or during storage and subsequent DPASV measurements are absent or negligible and cannot account for the large deficit of approximately 10% in the Cu mass balance.
- (iii) Most likely, a cause must be sought in the step where MnO_2 on the filterpapers is reduced with oxalic acid. However, exploring most possibilities in this direction have not resulted in a satisfactory answer to the Cu deficit.

The example data shown in Table 6.4 can be used to show the effect that the missing Cu has on the values calculated in this research for the adsorption parameters Γ_{max} and $\log B$. Assuming that at least the amount of dissolved Cu as measured by DPASV is correct, the free Cu^{2+} concentration can be calculated (using REDEQL2). The amount of Cu adsorbed can be obtained in two ways; by using $\text{Cu}_{\text{adsorbed}} = \text{Cu}_{\text{total added}} - \text{Cu}_{\text{dissolved}}$ and by using $\text{Cu}_{\text{adsorbed}}$ as obtained from the analysis of the filterpapers. By plotting Cu^{2+} vs. $\text{Cu}^{2+}/\Gamma_{\text{ads}}$ one obtains for the former the adsorption parameters $\Gamma_{\text{max}} = 0.258$ and $\log B = 6.876$, for the latter

$\Gamma_{\max} = 0.215$ and $\log B = 6.857$. While Γ_{\max} differs significantly (20%) in this case, B differs only slightly (4.5%). If one rejects the DPASV data totally and assumes that the $\text{Cu}_{\text{adsorbed}}$ data obtained by analyzing the filterpapers is correct, different values for $\text{Cu}_{\text{dissolved}}$ and hence Cu^{2+} will result, which will influence both the values for Γ_{\max} and $\log B$. The results reported in Chapter 7 all assume the DPASV results to be correct and the adsorbed amounts of Cu are calculated by subtracting the dissolved amount from the total amount of Cu added.

6.5 Mass Balance for MnO_2

The calibration procedure described in Section 6.2 does not include a mass balance check for MnO_2 throughout the experiment. It is important however, that this is assessed, because the amount of surface area present is a factor in the overall adsorption of Cu on MnO_2 . The literature indicates that MnO_2 can adsorb on container walls. Subramanian et al. (1978) quote Jenne (1968) regarding the fact that hydrous manganese oxides coat silicate surfaces. They conclude that their measured losses of Mn from natural- and synthetic-water samples may therefore be due to adsorption of the hydrous oxide on the container surface, especially the glass surface.

In this study, adsorption of MnO_2 particles onto glassware was clearly visible in several cases. In particular the MnO_2 batches with low adsorption capacities for Cu (see Figure 4.6) such as MnO_2 XXV-A and MnO_2 Baker adsorbed strongly on glass and plastic surfaces. As a standard procedure the amount of MnO_2 added per experiment was calculated by taking a well-stirred sample from the stock solution, reducing it with oxalic acid and measuring the Mn (in μM) concentration by A.A.

analysis. The introduction of the analysis of the filterpapers to check the mass balance for Cu, allowed that the Mn concentration during each point of the adsorption experiments could be measured.

Mn concentrations for a typical nine-point adsorption experiment are shown in Table 6.5.

The last tabulated sample is an unfiltered overall sample taken at the end of the experiment. The results do not show a clear trend and it can therefore not be concluded with certainty whether MnO_2 adsorbs on the glass container walls. The total amount of MnO_2 present per titration for use in calculating Γ_{ads} values, is taken equal to the average of the ten numbers, as shown in Table 6.5, because of this uncertainty. If MnO_2 does adsorb on the glass walls of the experiment vessels, the question arises whether it is still capable of adsorbing Cu^{2+} as if it were free in solution. Glass adsorption of Cu-containing MnO_2 could be the major cause of the Cu mass balance deficit if one argues as follows: From Table 6.5 it is seen that the maximum amount of MnO_2 disappearing during an adsorption experiment is $(73-65) = 8 \mu\text{M}$. Assuming a maximum adsorption capacity of $0.25 \mu\text{M Cu}/\mu\text{M MnO}_2$ (a realistic value, see Chapter 7), this could account for $2 \mu\text{M Cu}$ missing at the end of an experiment. However, this is all very speculative and needs further investigation.

6.6 Mass Balance for Glycine

Glycine is used in most of the adsorption experiments, to keep sufficient Cu in solution to be measured accurately by DPASV and to prevent Cu from precipitating, either as CuO or Cu(OH)_2 (see Section 6.3). Whether glycine influences the adsorption behaviour of the MnO_2 surface as a result of adsorption of glycine on MnO_2 is a question of concern.

Table 6.5 Typical Mn concentration Variations during an adsorption experiment

Experiment 010381 MnO_2XVc - pH 7.0 - 50 μM glycine added

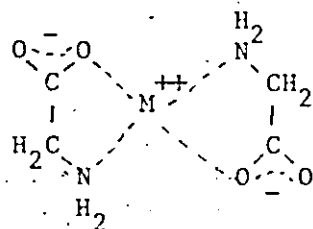
Cu_t added	Mn_t measured	
μM	μM	
0.9986	72.97	
2.0728	70.86	
3.2301	73.36	Mn_t (average) =
4.5053	68.75	$69.45 \pm 2.77 \mu\text{M}$
5.9059	71.17	
7.4625	67.84	
9.2134	66.56	
11.2398	64.94	
13.5973	66.30	
13.5973	70.60	

The effects of glycine adsorption can potentially display themselves in several ways:

- (1) Adsorption of glycine could either increase, decrease or have no effect on the number of Cu-adsorption sites on the MnO_2 surface and on the strength of the binding between Cu and MnO_2 .
- (2) Adsorption of glycine would remove ligand from solution. The remaining glycine would be less effective for the purpose of keeping Cu in solution and/or preventing Cu precipitation.
- (3) Adsorption of glycine could occur in the form of adsorption of Cu-glycine complexes. This would affect the adsorption capacity of MnO_2 for Cu and reduce the amount of glycine present in solution.
- (4) Adsorption of glycine could occur via a complexation reaction between already adsorbed Cu and glycine. This should not affect the adsorption capacity or strength considerably, but does remove ligand from solution.

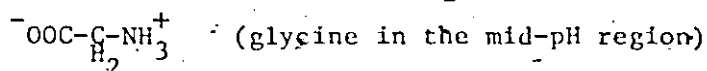
There appears to be little literature on the adsorption behaviour of glycine (and other amino acids) in general and onto MnO_2 in particular. Groenewegen and Sachtler (1972) investigated the chemisorption of glycine from vapor onto silica-supported nickel. The infrared spectrum which shows the glycine to be present on the surface in the anionic form indicates that glycine interacts with the nickel metal through the carboxyl group as well as through the NH_2 group. Although it is not known whether 1:2 or 2:1 complexes are formed on this surface, it is known that in complexes of several bivalent metal ions with glycine in solution, the oxygen atoms have different positions with respect to the metal ions.

This is illustrated by:



It is possible that glycine exists in a similar structure on the silica-supported nickel surface.

Davis (1979) and Davis and Leckie (1979) investigated the adsorption behaviour of glycine on amorphous iron oxide ($\text{pH}_{\text{zpc}} = 8$). In the mid-pH region glycine exists primarily as the zwitterion with a localized charge on the COO^- and NH_2^+ groups:



Davis (1979) finds that amorphous iron oxide has little affinity for the zwitterion, either coulombically or chemically. Less than 3% adsorption of glycine is observed in the pH region 4-10 for very low concentrations (10^{-6}M glycine). Higher concentrations are expected to yield even less adsorption.

Van den Berg (1979) argues against the adsorption of glycine, because in his titration with glycine (at constant Cu_t and MnO_2 concentrations), the conditional stability constant for the Cu-glycine complex could be produced quite accurately at pH 6.0. A similar experiment was performed during this study and is discussed in Section 7.7. of Chapter 7. However, it is argued here that, although the conditional stability constant for the Cu-glycine complex obtained is very satisfactory, this does not necessarily preclude adsorption of part of the glycine. Van den Berg (1979) also reasons that, if during the titration of an (un)known

ligand, the ligand adsorbs, the plot of Cu^{2+} vs. $\text{Cu}^{2+}/\text{Cu-L}$ will be curved. However, in this study a number of experiments have been performed in which known ligands are treated as unknown material. The plots of Cu^{2+} vs. $\text{Cu}^{2+}/\text{Cu-L}$ of a number of weaker ligands deviate vastly from straight lines, while others exhibit curvature. Yet this could have been caused by a number of different factors, such as 1:2 or 2:1 complexes and not just by adsorption of ligand on MnO_2 . Therefore the suggestion that obtaining a curved line means ligand adsorption must be rejected, as well as the opposite assumption that obtaining a straight line means no adsorption.

It is also found in this study (see Chapter 7, Section 7.7) that calibration of the MnO_2 surface with and without glycine present at pH 6 or 7 usually yields stronger adsorption for solutions with glycine present. From such results it is tempting to conclude that the presence of glycine modifies the surface to such an extent that increased adsorption is the result. But it has also been observed that replicate isotherms for the same MnO_2 batch obtained in the presence or absence of glycine under identical experimental conditions are not consistent in the Γ_{max} and $\log B$ values they yield. It is therefore concluded that the above discussed experiments have not provided enough unambiguous evidence to draw conclusions regarding adsorption of glycine (and other ligands used).

Hence, to investigate the possibility of glycine adsorption onto MnO_2 in the experimental systems of this study, it was decided to use ^{14}C -labelled glycine (Amersham), with a maximum activity of 1 $\mu\text{Ci/L}$. This also permits one to make a glycine mass balance at the same time. The following experimental modification to the normal calibration

procedure described in Section 6.2 was designed: Instead of reducing the MnO_2 containing filterpapers collected after each filtration step in 25 mL 0.5M oxalic acid, the filterpapers are immersed, in 25 mL Erlenmeyer flasks in 5 mL of a saturated oxalic acid solution. One mL of the reduced MnO_2 mixture is counted to detect any ^{14}C -labelled glycine present on the filterpapers, while the other 4 mL's are diluted and analyzed for Cu and Mn by A.A., to obtain their respective mass balances. One mL of filtrate is also counted. Blank samples and standards for counting are taken before and directly after addition of ^{14}C -labelled glycine to the experiment vessel. An overall (i.e. bulk), non-filtered sample is taken at the end of each adsorption experiment, to detect the removal of glycine during the actual experiment by such mechanisms as glass adsorption.

^{14}C -counting results for Cu- MnO_2 adsorption experiments involving 50 μM glycine at pH values of 6 and 7 are shown in Tables 6.6a to 6.6f. Cu^{2+} is calculated from the amount of Cu_t added, while Cu adsorbed is derived from the difference between Cu_t added and the amount of Cu measured in the filtrate by DPASV. Glycine is calculated from the ^{14}C -counting results of the filtrates. Glycine adsorbed is derived from the ^{14}C -counting results of the filterpaper solutions while glycine missing is calculated by subtracting $\text{glycine}_{\text{filtrate}} + \text{glycine}_{\text{adsorbed}}$ from 50 μM , the amount of glycine initially added.

From Table 6.6 it is clear that the fraction of glycine missing seems to occur in a rather erratic fashion for the MnO_2 batches Xvc and 13 (van den Berg). MnO_2 Xvc seems to adsorb very considerably at pH 6.0 on 240781, but hardly anything is adsorbed a month earlier at the same pH, on 210681, or at pH 7.0 on 280681. For van den Berg's MnO_2 , the

Table 6.6 Counting results for ¹⁴C-labelled glycine adsorption experiments
 The precision shown in the glycine data is imposed by counting statistics.

Table 6.6a: Experiment 240781 - MnO₂XVc - pH6.0 -
 50µM ¹⁴C-labelled glycine added

Cu ₂ added (µM)	Cu _{ads} (DPASV) (µM)	Gly. filtrate (µM)	Gly. ads. (µM)	Gly. missing (µM)	counting stats.
0.0	-	31.02±7%	11.31±5%	7.67	
2.1966	2.1843	30.01 "	10.28 "	9.71	
4.6029	4.5842	28.76 "	10.21 "	11.03	
7.2874	7.1726	30.41 "	8.99 "	10.60	
10.2266	9.7877	31.38 "	9.08 "	9.54	
13.6313	11.9948	33.11 "	8.74 "	8.15	
15.6371	13.1649	32.82 "	8.43 "	8.75	
18.2263	14.3923	30.09 "	8.03 "	11.88	
21.5992	15.6085	29.09 "	8.96 "	11.95	
21.5992	overall bulk sample (non-filtered)	47.09 "	-	2.91	

Table 6.6b: Experiment 210681 - MnO₂XVc - pH7.0 -
 50µM ¹⁴C-labelled glycine added

Cu ₂ added (µM)	Cu _{ads} (DPASV) (µM)	Gly. filtrate (µM)	Gly. ads. (µM)	Gly. missing (µM)	counting stats.
0.0	-	50.33±1.5%	0.099±10%	-0.429	
2.1719	2.1591	50.07 "	0.160±7%	-0.230	
4.5401	4.5204	50.67 "	0.298 "	-0.968	
7.1422	7.0734	47.96 "	0.443 "	1.597	
10.0151	9.7238	48.91 "	0.638 ±5%	0.452	

Table 6.6 continued : Counting results for ¹⁴C-labelled glycine adsorption experiments

Table 6.6c: Experiment 280681 - MnO₂XVc - pH 7.0 - 50 μM ¹⁴C-labelled glycine added

Cu ₂ added (μM)	Cu _{ads.} (DPASV) (μM)	gly. filtrate (μM)	gly. ads. (μM)	gly. missing (μM)	counting stats.
0.0	-	sample lost	1.303±3%	-	-
2.1732	2.1707	46.83±1.5%	1.313 "	1.857	-
4.5445	4.5312	46.48 "	1.905 "	1.615	-
7.1708	7.1302	45.91 "	2.349 "	1.741	-
10.1444	9.9379	45.10 "	2.582 "	2.318	-
11.8017	11.3096	45.52 "	2.719 "	1.761	-
13.7015	12.7914	45.45 "	2.773 "	1.777	-
18.1183	14.9810	45.61 "	2.727 "	1.663	-
20.7734	16.5072	44.37 "	2.723 "	2.837	-

Table 6.6d: Experiment 210781 - MnO₂ J3 (van den Berg) - pH 6.0 - 50 μM ¹⁴C-labelled glycine added

Cu ₂ added (μM)	Cu _{ads.} (DPASV) (μM)	gly. filtrate (μM)	gly. ads. (μM)	gly. missing (μM)	counting stats.
0.0	-	37.09±5%	6.06±3%	6.85	-
2.1896	1.9859	37.19 "	5.71±5%	7.10	-
4.5995	3.9631	36.97 "	6.04±3%	6.99	-
7.2633	5.4209	sample lost	6.58±5%	-	-
10.2194	7.2432	sample lost	6.04±5%	-	-
13.5630	8.9983	37.04±5%	5.83 "	7.13	-
17.4195	10.4662	37.73 "	5.81 "	6.46	-
21.9590	11.7579	sample lost	5.46 "	-	-
27.3926	15.0804	35.79±5%	5.38 "	8.83	-
27.3926 overall	sample	48.44 "	-	1.56	-

Table 6.6 continued: Counting results for ¹⁴C-labelled glycine adsorption experiments

Table 6.6e Experiment 210781 - MnO₂ 13 (van den Berg) - pH 7.0 - 50µM ¹⁴C-labelled glycine added

Cu ₂ added (µM)	Cu ads. (DPASV) (µM)	gly. filtrate (µM)	gly. ads. (µM)	gly. missing (pH)	counting stats.
0.0	-	37.61±5%	5.64±3%	6.75	
2.1945	1.9863	37.50 "	6.69 "	5.81	
3.4109	3.1268	37.60 "	5.21±5%	7.19	
4.7585	4.2053	37.50 "	5.74±3%	6.76	
6.2938	5.3327	36.44 "	6.16±5%	7.40	
9.7364	7.5074	37.54 "	5.34 "	7.12	
11.7452	8.8994	36.90 "	sample lost	-	
14.1630	10.4491	37.66 "	5.07 "	7.27	
17.1615	12.0900	35.67 "	4.95 "	9.38	
17.1615	overall sample	48.72±3%	-	1.28	

Table 6.6f Experiment 210781 - MnO₂ 13 (van den Berg) - pH 8.0 - 50µM ¹⁴C-labelled glycine added

Cu ₂ added (µM)	Cu ads. (DPASV) (µM)	gly. filtrate (µM)	gly. ads. (µM)	gly. missing (pH)	counting stats.
0.0	-	37.22±5%	4.99±5%	7.79	
2.1811	1.9217	36.46 "	4.41 "	9.13	
3.3908	3.0321	36.30 "	4.41 "	9.29	
4.7405	4.0871	37.09 "	4.52 "	8.39	
6.2555	5.1975	35.28 "	4.72 "	10.00	
9.6888	7.3010	36.10 "	4.76 "	9.14	
11.6931	8.6943	37.09 "	sample lost	-	
14.1571	10.0366	37.27 "	4.81±5%	7.92	
17.1711	11.8649	37.43 "	4.26 "	8.31	
17.1711	overall sample	49.70	-	0.30	

amount of glycine adsorbed at pH 6.0 and 7.0 on 210781 is considerable, while a simultaneous experiment at pH 8.0 shows a somewhat lower adsorption of glycine. However, it is quite clear that, with the exceptions of the experiments involving $\text{MnO}_2 \cdot \text{XVc}$ at pH 6.0 on 210681 and at pH 7.0, on 280681, the mass balance for glycine shows a substantial deficit. Similar to the mass balance for Cu, a considerable amount of glycine is missing (up to 20%) after all fractions are added up. But bulk samples taken at the end of the various experiments indicate that there apparently is very little glass adsorption during the actual experiment (1-5%). The disappearance of so much glycine must therefore take place during either the filtration step, or the filterpaper reduction phase and successive counting procedure.

To investigate this, an experiment was carried out in concurrence with the experiment that attempted to find a solution to the Cu budget deficit (see Section 6.4). The following procedure was used:

In the same fashion as in an ordinary adsorption experiment, the solution was prepared in the Erlenmeyer flask, but MnO_2 is not added. Prior to adding any Cu, and immediately after ^{14}C glycine is added, a 1 mL sample is taken for counting (sample #1). After degassing for 1 hr. at pH \approx 5.0 and with still no Cu present, another sample is taken to determine the amount of glycine that disappears during this hour (sample #2). At time 1 hr. 10 μM Cu is added and the pH increased from ca. 5.0 to 6.0, whereafter an equilibrium time of 1 hr. is allowed, during which the pH is kept at exactly 6.0 by manual additions of dilute acid or base, as necessary. After this period, two 1 mL samples are taken. Of these samples, one is counted directly (sample #3), while the other is diluted with 4 mL saturated oxalic acid solution, to determine the possible

effect of oxalic acid on the ^{14}C detection. One mL of this oxalic acid mixture is counted (sample #4).

Approximately 70 mL are filtered through an acid cleaned 0.45 μm Millipore filter. The first 20 mL are discarded (as in an ordinary adsorption experiment). Of the next 50 mL of filtrate, 1 mL is counted directly (sample #5) and 1 mL is diluted with 4 mL saturated oxalic acid, of which mixture again 1 mL is counted (sample #6). One mL of the filtrate is mixed with 4 mL saturated oxalic acid to which the used filterpaper is added, and again 1 mL of this is counted (sample #7). The rest of the filtrate is used for the Cu mass balance study.

Next, the Cu concentration is doubled to approximately 20 μM and the pH increased from 6.0 to 7.0. One mL of the experimental solution is counted directly after this second addition to serve as a second standard (sample #8), while after another hr. of equilibration time at constant pH, two 1 mL samples are taken of which one is counted directly (sample #9) while the other is diluted with the saturated oxalic acid (sample #10). Another 70 mL are filtered and again the first 20 mL filtrate are discarded. One mL filtrate is counted directly (sample #11) and one mL is diluted with oxalic acid solution prior to counting (sample #12). Finally, one mL of filtrate is diluted with 4 mL oxalic acid to which the used filterpaper is added, of which mixture 1 mL is taken for counting (sample #13).

The results of this study are shown in Table 6.7, and the following calculations can be made:

From the difference between sample #7 and sample #6 the amount of counts on the filterpaper at pH 6.0 can be calculated to be 428.5 counts. One mL of 50 μM . ^{14}C solution has 338.3 counts (sample #1), representing

Table 6.7 Adsorption of ¹⁴C-labelled glycine on glassware and filter papers

Sample #	Description of sample	counts per minute	counting statistics	µM glycine
1	initial solution containing 50 µM ¹⁴ C-glycine	338.3	± 3%	50.00 ± 1.50
2	initial solution, 1 hr. degassed at pH~5	337.1	± 3%	49.82 ± 1.49
3	10 µM Cu ²⁺ added, equilibrated for 1 hr @ pH6.0	336.2	± 3%	49.69 ± 1.49
4	same as #3, dil: 5x with sat. oxalic acid soln.	65.9	± 7% (5x)	48.70 ± 3.41
5	filtrate of #3 (first 20 ml discarded)	226.9	± 3%	33.54 ± 1.01
6	same as #5, dil. 5x with sat. oxalic acid soln.	52.9	± 7% (5x)	39.09 ± 2.74
7	same as #6, used filterpaper of #5 added	138.6	± 5% (5x)	102.42 ± 5.12
8	Cu conc ⁿ . inc. to ~20 µM, pH inc. to 7.0	330.5	± 3%	48.85 ± 1.47
9	same as #8, equilibrated for 1 hr at pH 7.0	314.2	± 3%	46.44 ± 1.39
10	same as #9, dil. 5x with sat. oxalic acid soln.	66.7	± 7% (5x)	49.29 ± 3.45
11	filtrate of #9, first 20 ml discarded	230.0	± 3%	33.99 ± 1.02
12	same as #11, dil. 5x with sat. oxalic acid soln.	53.2	± 7% (5x)	39.31 ± 2.75
13	same as #12, used filterpaper of #11 added	121.5	± 5% (5x)	89.79 ± 4.49

0.05 μM of ^{14}C . This means that on the filterpaper 0.063 μM ^{14}C is present. For pH 7.0, the same calculation can be made (using samples #13 and #12) and in this case, 0.052 μM ^{14}C is present on the filterpaper. Glycine seems to disappear as a result of the filtration process, as can be seen from comparing samples #3 and #5 and samples #9 and #11. At pH 6.0, 0.0162 μM $^{14}\text{C}/\text{mL}$ disappears or 1.134 μM ^{14}C per 70 mL. Only a fraction of this amount, 0.063 μM (=5.6%) is found back on the filterpaper, the rest must have adsorbed on the filtration equipment glassware, in particular on the filterhead. For pH 7.0, 0.0124 μM $^{14}\text{C}/\text{mL}$ disappears, or 0.871 μM ^{14}C per 70 mL, of which 0.052 μM (or 6.0%) is found back on the filterpaper.

What does this loss mean with respect to the experimental data in Table 6.6 a-f? An example calculation using the adsorption data of Table 6.6d is shown in Table 6.8. This particular adsorption experiment was performed with MnO_2 13 (van den Berg) at pH 6, in the presence of 50 μM ^{14}C -labelled glycine, on 210781.

The largest uncertainty in the calculations shown in Table 6.8 lies in the calculation of the ^{14}C adsorption on the filterpaper itself. Filterpaper adsorption includes glycine in the amount of water retained in and on the filterpaper because even when filtering dry, there will always be some residual water left in and on the filterpaper, and this water contains ^{14}C . It is also possible that, when MnO_2 particles are built up as a filtercake on the filterpaper, they could trap some additional water, increasing the amount of ^{14}C on the filterpaper not really associated with MnO_2 . This is an unknown factor and needs further investigation. For the sample calculations shown in Table 6.8, an average percentage (5.8%) of the total amount of ^{14}C glycine that

Table 6.8 Example calculation showing the influence of ¹⁴C-labelled glycine adsorption on filtration equipment on the data for adsorption of ¹⁴C-labelled glycine on MnO₂ (data from Table 6.6d, MnO₂ 13, van den Berg, pH 6.0, 50μM ¹⁴C-labelled glycine present).

At time 0 hour, 50 μM ¹⁴C-glycine has 437.6 ± 3% counts/mL; this means that 0.05 μM ¹⁴C-glycine has 437.6±3% counts. It is assumed that an average of 6.0 + 5.6 = 5.8% of the total amount of ¹⁴C which disappears is due to filterpaper (fp) adsorption.

C _t added (μM)	equil. time (hr.)	counts/mL filtrate	ml's filtered	counts on filterpaper	times 5 dilution	μMoles ¹⁴ C on fp	counts disappeared per mL	μMoles ¹⁴ C per amount filtered	5.8% ¹⁴ C (μMoles) on fp	μMoles ¹⁴ C ads. on MnO ₂ equipment	μMoles ¹⁴ C ads. on MnO ₂ (μM)	μM/Urea
0.0	2	332.5±5%	42.82	427.9±3%	2139.5	0.244	105.1	0.514	0.0298	0.270	0.214	5.00
2.1896	3	333.3	40.73	386.1±5%	1930.5	0.221	104.3	0.485	0.0281	0.264	0.193	4.74
4.5936	4	331.5	41.37	432.3±3%	2161.5	0.247	106.1	0.501	0.0291	0.254	0.218	5.27
7.2633	5	lost	36.11	393.8±5%	1969.0	0.225	-	-	-	-	-	-
10.2194	6	lost	38.26	383.8	1919.0	0.219	-	-	-	-	-	-
13.5630	7	332.1	39.69	384.3	1921.5	0.220	105.5	0.478	0.0277	0.258	0.192	4.84
17.4195	8	337.7	38.76	374.5	1872.5	0.216	99.9	0.442	0.0256	0.228	0.188	4.86
21.9590	9	lost	36.25	332.4	1662.0	0.190	-	-	-	-	-	-
27.3926	10	321.9	43.76	390.4	1952.0	0.223	115.7	0.579	0.0336	0.356	0.189	4.33
27.3926	10	overall sample; amount of ¹⁴ C Glycine disappeared during the actual experiment is 1.45 μM										

disappears from the initial solution is assumed to be due to adsorption on the filterpaper. But because this 5.8 percentage is determined in the absence of MnO_2 , it is very well possible that, in the presence of MnO_2 , adsorption by the filterpaper is higher, due to trapped liquid. Therefore, the sample calculation gives only an approximate estimate of the amounts of ^{14}C -glycine adsorbed on MnO_2 , filterpaper and glassware.

It is not clear, why the amount of unaccounted for ^{14}C -glycine varies for identical experimental conditions (e.g. Table 6.6 a, b, c). In this context a number of potential "trouble-spots" can either be dismissed, or are emphasized, by the following:

- (i) Experiments have always been performed in the manner described in Section 6.2, additions such as filterpaper-analysis for Cu and ^{14}C and filtrate analysis for ^{14}C do not alter the basic procedure.
- (ii) Treatment of all glassware, filterpapers and sample bottles has always been as described in Appendix I.
- (iii) The glass-frit filterhead used in the various experiments has not always been the same piece of glass, although throughout one experiment usually the same filterhead is used. Adsorption capacities could have varied from filterhead to filterhead, causing large differences in ^{14}C disappearance.
- (iv) Acid washing, subsequent rinsing and drying (in a 60-80° oven) of the filterpapers could have caused some differences in the adsorption capacities for water of the individual filterpapers.

This, however, does not seem likely.

From Table 6.6.a-f it can be seen that, excluding the experiments in Tables 6.6.b and 6.6.c, the amount of ^{14}C associated with the MnO_2 on the filterpaper and/or adsorbed on the filterpaper, is remarkably

constant. Glycine seems to adsorb directly at the beginning of the adsorption experiments to a certain extent, without the intervention or help of Cu. Subsequent additions of Cu do not appear to significantly alter the amount of glycine adsorbed.

According to Davis (1979), glycine in the pH range of 4-10 is mainly present in the zwitterion form, while MnO_2 at these pH values is strongly negatively charged. If glycine does adsorb, it most likely involves the NH_3^+ group attaching to the negative MnO_2 surface. Whether it uses adsorption sites which otherwise would be used by Cu, is not certain, but this is very likely. However, since the carboxyl group likely protrudes into the solution, Cu can still complex with the adsorbed glycine, and in fact this protruding group may add to the ease with which Cu can adsorb, causing both stronger and more adsorption at a certain Cu_t concentration than without glycine adsorbing on the MnO_2 surface. However, these are mostly speculations and need further investigation.

The amount of ^{14}C found on the filterpapers is remarkably constant. Also, the experiments in Tables 6.6.b and 6.6.c show virtually no ^{14}C on the filterpapers. These two facts combined seem to indicate that all ^{14}C present on the filterpapers must be associated with the filterpapers themselves and not with the MnO_2 deposited on the filterpapers. There is no reasonable explanation for the fact that two identical experiments for MnO_2 XvC at pH 6 give such different results with respect to ^{14}C adsorption, other than an artifact caused by filterpaper adsorption and/or trapped water on the filterpapers. Moreover, a comparison between the experiments tabulated in Table 6.6 and the MnO_2 -free experiment shown in Table 6.7 indicates that the amount of ^{14}C recovered in the filtrate is very similar for the experiments where a considerable amount of ^{14}C is

apparently missing.

The sample calculation in Table 6.8 shows that after correcting for 5.8% adsorption associated with the filterpaper itself, there is still 8.7 - 10.5% adsorption of ^{14}C on the filterpapers, associated with deposited MnO_2 . However, the 5.8% is a minimum value, obtained in the absence of MnO_2 and may in fact be much larger in the presence of MnO_2 for reasons already stated. There are reasons to assume that most probably glycine does not adsorb onto MnO_2 in any substantial amounts (i.e. >5-10%), and that any indication otherwise is a result of artifacts such as glassware - and filterpaper adsorption and water trapped in and on the filterpapers. More experiments are needed, however, to prove this incontrovertibly. A procedure avoiding a filtration step, or a differently designed filterhead (no glass frit), would be desirable. Centrifugation of the the MnO_2 particles may be possible, although there too, many problems may arise with glassware adsorption. More discussion on glycine adsorption will follow in Chapter 7, where isotherms obtained both in the presence and absence of glycine are presented.

6.7 Adsorption of Other Ligands

6.7.1 Aspartic Acid

One experiment was performed with ^{14}C labelled aspartic acid in an identical way to the ^{14}C glycine experiments. Results are shown in Table 6.9.

The figures in Table 6.9 show that a little aspartic acid adsorbs onto the MnO_2 surface (0.3 to 1.4%). The small amounts found on the filterpapers could be due largely to water on the filterpapers or trapped

Table 6.9 Adsorption of aspartic acid on MnO₂

Experiment 210681, MnO₂XVc²⁻ pH 6.0 - 48μM ¹⁴C-
labelled aspartic acid added

Cu _t added (μM)	Cu _{ads.} (DPASV) (μM)	aspartic acid (filtrate) (μM)	aspartic acid (adsorbed) (μM)	aspartic acid (missing) (μM)
		counting stats.	counting stats.	
0.0	-	47.94±2%	0.087±10%	-0.027
2.1730	2.1486	45.88 "	0.154 "	1.966
4.5503	4.4993	47.06 "	0.255± 7%	0.685
7.1815	7.0000	47.19 "	0.333 "	0.477
10.1054	9.4050	49.23 "	0.579± 5%	-1.809
11.7620	10.4107	40.46 "	0.574 "	6.966
13.6773	11.0057	45.81 "	0.536 "	2.726
15.9484	11.9101	48.37 "	0.690 "	-1.060
18.7884	12.5570	49.07 "	0.637 "	-1.707

between the MnO_2 particles. These results strongly resemble the trends for MnO_2 XvC with glycine at pH 6.0 (experiment in Table 6.6.b) and to a lesser extent the results at pH 7.0 (experiment in Table 6.6.c). Aspartic acid is very similar in structure to glutamic acid. Davis (1979) finds considerable adsorption of glutamic acid on amorphous iron oxide below the pH_{zpc} , where the surface is positive, but virtually no adsorption above the pH_{zpc} . Apparently, a positive surface is needed, which means that most likely the adsorption reaction involves the terminal carboxyl group, and not the amino group, since Davis (1979) found that results obtained with glycine showed that there exists little interaction between the iron oxide and zwitterion. The $\delta\text{-MnO}_2$ surface has a pH_{zpc} around 1-2 and its surface is strongly negatively charged in the pH range 6-8.5. In the case of aspartic acid, there is a gradual increase in adsorption with increasing Cu concentration, which could mean that Cu adsorbed on MnO_2 provides a surface more positive and therefore more suitable to aspartic acid adsorption. However, the adsorbed amounts of aspartic acid are very small, compared to the amounts of Cu adsorbed.

6.7.2 Adsorption of NTA

Two experiments have been performed to establish the adsorption behaviour of NTA in the absence and presence of Cu, at pH's 6.0 and 7.0. Table 6.10 represents the results for these experiments. It can be seen from this Table that very little ^{14}C NTA is present on the filterpapers (0.2 - 0.4%). Whether the ^{14}C NTA found on the filterpapers is actually adsorbed on the MnO_2 or just associated with the filterpaper, is not known. However, the amounts present on the filterpapers are so small that they can be neglected. The missing amounts of NTA (8-20%), can be attributed to adsorption in the actual experimental phase on the walls of the Erlenmeyer flask, because the quantity missing is equal to the amount of NTA missing in the unfiltered acidified endsample (after 10 hours experimental equilibrium time). NTA is therefore easier to interpret than glycine.

6.8. Example Calculations for a Calibration - and a Titration -

Experiment

A calibration of the $\delta\text{-MnO}_2$ surface for Cu uptake precedes a titration experiment. In a titration, the conditional stability constant for a Cu-unknown organic complex and the concentration of the organic is determined with the help of $\delta\text{-MnO}_2$. In a calibration experiment, the adsorption parameters Γ_{max} and B are determined (see equation 6.1) for the $\delta\text{-MnO}_2$ surface. The procedure is described in Section 6.2. Table 6.11 contains the necessary data and calculations. By plotting Cu^{2+} vs. $\text{Cu}^{2+}/\Gamma_{\text{ads}}$, as is shown in Figure 6.3, one obtains Γ_{max} from the slope and log B from the intercept and the slope. There is a clear deviation from linearity, but for the time being this is ignored and a straight line is drawn through all points, since the calculations merely serve as an example.

Table 6.10 Adsorption behaviour of NTA on MnO₂ at pH 6.0 and 7.0

Experiment 240781 - MnO ₂ at pH 6.0 - 8.096 μ M ¹⁴ C-labelled NTA added											
Cu _t added (μ M)	Cu _{ads.} (DPASV) (μ M)	NTA filtrate (pH)	NTA _{ads.} (pH)	NTA missing (pH)	counting stats.	Cu _t added (μ M)	Cu _{ads.} (DPASV) (μ M)	NTA filtrate (pH)	NTA _{ads.} (pH)	NTA missing (pH)	counting stats.
0.0	-	7.385±3Z	0.017±15Z	0.69Z		0.0	-	7.937±1.5Z	0.914±7Z	0.145	
2.1966	2.1843	6.884 "	0.020 "	1.192 "		4.3229	0.6099	7.797 "	0.017 "	0.282	
4.6029	4.5842	6.603 "	0.023 "	1.470 "		6.6756	1.5814	7.789 "	0.018 "	0.288 p	
7.2474	7.1726	6.431 "	0.029 "	1.636 "		11.8861	5.1744	7.748 "	0.032 "	0.316	
10.2266	9.7877	6.283 "	0.031 "	1.732 "		14.7767	7.8231	7.654 "	0.042±5Z	0.400	
13.613	11.9948	6.453 "	0.033 "	1.610 "		18.0201	11.0843	7.693 "	0.049 "	0.354	
15.6371	13.1649	6.568 "	0.032 "	1.496 "		19.8620	12.4371	7.571 "	0.051 "	0.474	
18.2263	14.3923	6.287 "	0.036 "	1.773 "		24.0882	16.0902	7.662 "	0.045 "	0.389	
21.5992	15.6085	6.315 "	0.036 "	1.745 "		26.5473	18.6703	7.609 "	0.045 "	0.462	
21.5992	bulk unfiltered and sample: NTA present = 6.359 μ M, missing NTA = 1.737 μ M										

Table 6:11 Example calculation for a calibration experiment

Experiment 280681 - MnO₂XVc - pH 7.0 - no glycine or other organic material present

Cu_t added (μM)	$Cu_{diss.}$ (DPASV) (μM)	$Cu_{ads.}$ (μM)	$\Gamma_{ads.}$	Cu^{2+} (REDEQL2) (μM)	$Cu^{2+}/\Gamma_{ads.}$ (μM)
3.0942	0.00256	3.09164	0.0421	0.09929×10^{-2}	2.358×10^{-2}
4.2838	0.00697	4.27683	0.0582	0.27034	4.645
5.6052	0.01180	5.59340	0.0762	0.45804	6.011
7.0876	0.02658	7.06102	0.0962	1.03252	10.733
8.7969	0.04122	8.75568	0.1193	1.59915	13.404
10.7781	0.05345	10.72465	0.1462	2.07435	14.188
13.1335	0.16490	12.96861	0.1767	6.39478	36.190
16.0688	0.24360	15.81520	0.2155	9.83519	45.638

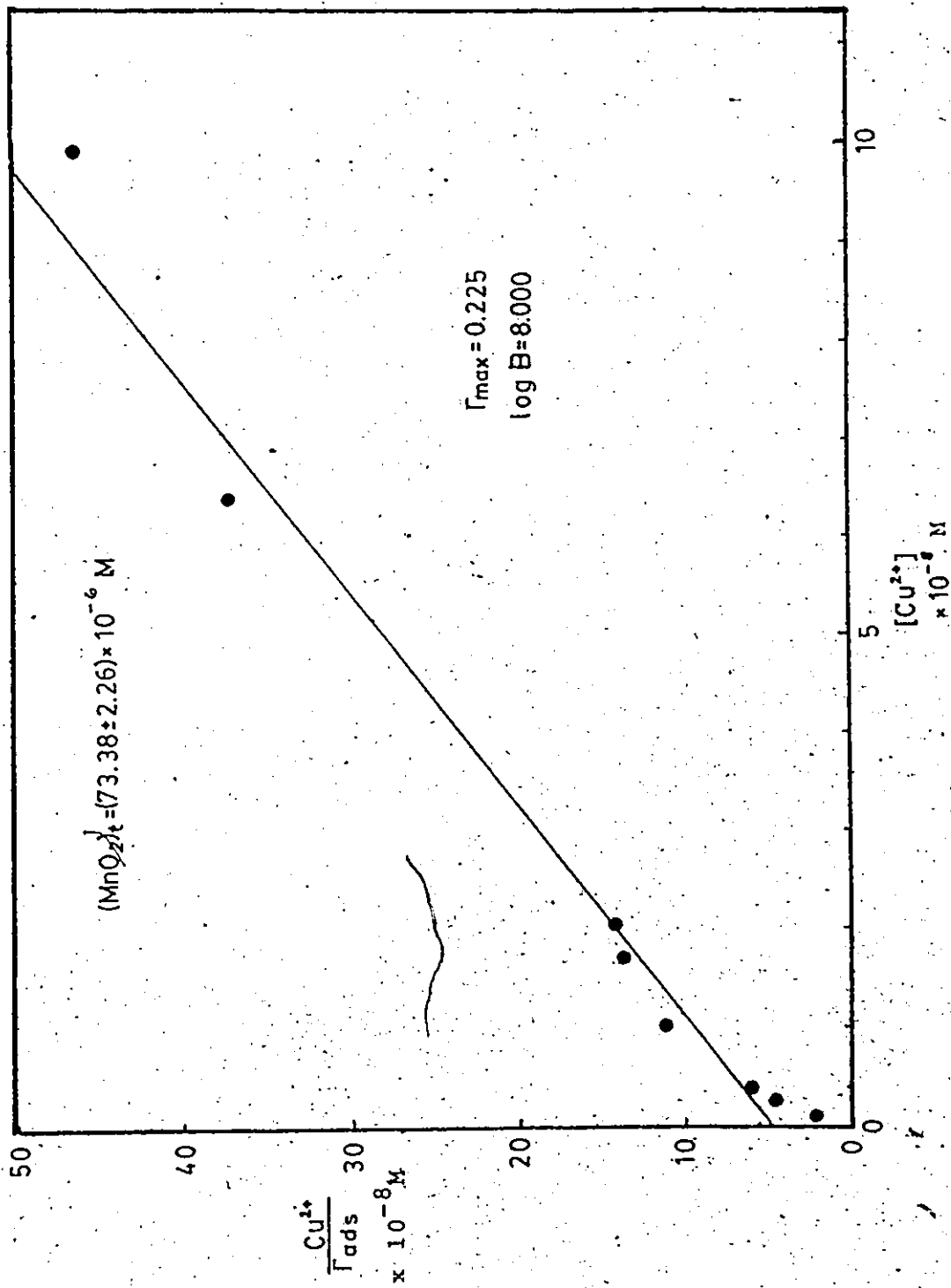


Figure 6.3 Example calibration of MnO_2 XVC for Cu adsorption at pH 7.0, no organics present.

As an example for a titration experiment, NTA is treated as if it were an unknown ligand and titrated in the presence of MnO_2 Xvc. Table 6.12 contains the necessary data and calculations. The Cu^{2+} concentrations in this table are calculated from the amount of adsorbed Cu and by using the values for the adsorption parameters Γ_{max} and $\log B$ for MnO_2 Xvc, obtained in the preceding calibration experiment (see Table 6.11 and Figure 6.3). The formula used is derived from expression (6.1) which can be written as:

$$\text{Cu}^{2+} = \frac{\Gamma_{\text{ads}} \times 10^{-\log B}}{\Gamma_{\text{max}} - \Gamma_{\text{ads}}} \quad (6.6)$$

The stability constants used to calculate CuOH^+ and Cu(OH)_2 concentrations can be found in Appendix II. The last two adsorption points in Table 6.12 can not be calculated due to the fact that the amount of free Cu^{2+} is too large (*) - only an amount of $44 \times 10^{-2} \mu\text{M}$ Cu^{2+} is allowed at pH 7.0, due to the possibility of Cu precipitation (see Section 6.3). The titration at these two points has been taken too far; hence all ligand is taken up and any additional Cu added will exist as free Cu, and might precipitate as CuO . This would cause Γ_{ads} for the last titration point to be too high (maximum for $\Gamma_{\text{ads}} = \Gamma_{\text{max}}$ as obtained in the previous example). By plotting Cu^{2+} vs. $\text{Cu}^{2+}/\text{Cu-L}$, as is shown in Figure 6.4, L_t , the total ligand concentration is found from the slope, while the conditional stability constant for the Cu-NTA complex is found from the slope and the intercept. The calculated values are:

$$L_t = 7.35 \mu\text{M} \quad (\text{compare the added amount of } 8.096 \mu\text{M NTA}).$$

and $\log K' = 9.27$ (compare the value in Sillen and Martell (1964) of approximately 9.7).

Table 6.12 Example calculation for a titration experiment
Experiment 280681 - MnO₂XVc - pH 7.0 - 8.096 μM NTA added

Cu _t (μM)	Cu _{diss} (μM)	Cu _{ads} (μM)	Γ _{ads}	Cu ²⁺ (x10 ⁻²) (μM)	CuOH ⁺ (x10 ⁻²) (μM)	Cu(OH) ₂ (x10 ⁻²) (μM)	Cu-L (μM)	Cu ²⁺ /Cu-L x 10 ⁻⁴
4.3229	3.7137	0.6092	0.00836	0.03887	0.00389	0.04164	3.7129	1.0469
6.6756	5.0942	1.5814	0.02169	0.10745	0.01075	0.11513	5.0919	2.1102
11.8861	6.7117	5.1744	0.07098	0.46424	0.04642	0.49743	6.7016	6.9273
14.7767	6.954	7.8231	0.1073	0.91853	0.09185	0.98420	6.9341	13.2467
18.0201	6.936	11.0843	0.1521	2.10328	0.21033	2.25367	6.8903	30.5251
19.8620	7.425	12.4371	0.1706	3.16285	0.31629	3.3890	7.3563	42.9950
24.0882	7.998	16.0902	0.2207	52.8996	-	-	-	-
26.5473	7.877	18.6703	0.2561	-	-	-	-	-

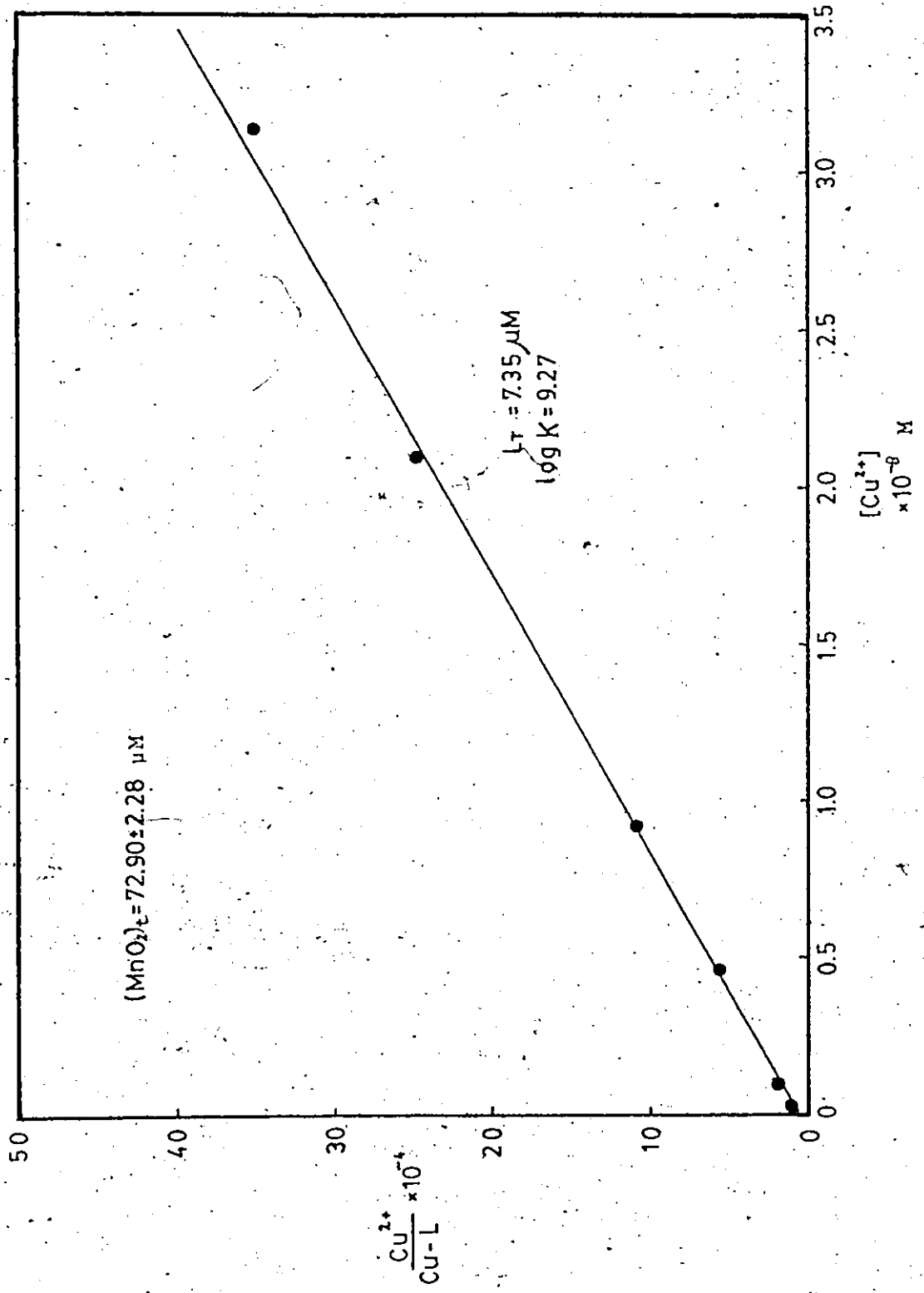


Figure 6.4 Example titration of 8.096 μM NTA at pH 7.0 in the presence of $\text{MnO}_2 \text{ Xvc}$.

Both L_t and $\log K'$ are somewhat smaller than expected. For L_t this can be explained by the fact that NTA adsorbs on the walls of the experiment vessel. The actual NTA concentration at the end of the titration is $7.60 \mu\text{M}$, found by ^{14}C analysis. The fact that NTA forms bidentate complexes with Cu also contributes to the ligand concentration calculated being lower than the concentration added. The overall binding constant between Cu and NTA is also affected by bidentate complex formation and appears weaker in this case. NTA will be discussed in more detail in Chapter 8.

6.9 Summary

This Chapter describes the experimental procedures used in this study and probable sources of discrepancies, in considerable detail to provide enough information for a thorough understanding of the adsorption experiments performed. Advisable Cu-concentration ranges are determined, to avoid precipitation of Cu at the upper end of adsorption isotherms and to secure sufficient Cu for accurate analysis at the lower end of isotherms.

The basic procedures for both a calibration and a titration experiment are described in Section 6.2. These procedures can be extended to perform mass balances for Cu, MnO_2 and glycine by simply reserving the filterpapers from each filtration step, reducing them in oxalic acid and analyzing for Cu and Mn by A.A. and for glycine by ^{14}C counting. A sample calculation for both a calibration and a titration is given.

The effects of contamination by organics, Mn and/or Zn in the

subsamples, on the measurement of Cu by DPASV are discussed, as well as possible fluctuations in ionic strength during experiments.

The deficit in the Cu mass balance, although not totally resolved, is probably due to the oxalic acid reducing step. ^{14}C experiments suggest that the hypothesized adsorption of glycine onto the $\delta\text{-MnO}_2$ surface is in fact not due to adsorption, but largely a result of artifacts such as glassware and filterpaper adsorption. The adsorption of glycine onto $\delta\text{-MnO}_2$ seems negligible and does not greatly affect the adsorption characteristics of the $\delta\text{-MnO}_2$ surface for Cu. Ligands such as NTA and aspartic acid do not adsorb to any considerable extent on the surface of $\delta\text{-MnO}_2$. The experimental errors and artifacts considered in this Chapter make it possible to compare the results presented in the next Chapter on a more direct basis, even though all discrepancies are not fully resolved.

CHAPTER 7

ADSORPTION BEHAVIOUR OF DIFFERENT δ -MnO₂ SURFACES FOR Cu
IN THE pH RANGE 6 TO 8.57.1 Introduction,

Proper modeling of adsorption of Cu onto the δ -MnO₂ surface is crucial to the successful use of δ -MnO₂ as a competing surface in trace metal speciation studies. In Chapter 4, a number of different MnO₂ surfaces was investigated and compared with regard to various physical and chemical characteristics. Adsorption behaviour for Cu at pH 6 was briefly compared and positively correlated with H₂O and K content respectively.

In this Chapter, an extensive comparison is made between adsorption behaviour for the various δ -MnO₂ surfaces included in this study. The pH and the range of Cu-concentrations are master variables in the obtaining of adsorption isotherms. These isotherms can be expressed in terms of r_{ads} , the amount of Cu adsorbed per amount of surface, and the free Cu²⁺ concentration remaining in solution. The relationship between r_{ads} and the free Cu²⁺ concentration can be expressed in terms of various adsorption models, discussed in Chapter 5 (Section 5.1.3).

General adsorption behaviour, for the various δ -MnO₂'s; expressed in terms of r_{ads} and [Cu²⁺], is visually compared and discussed in Section 7.2. Five types of comparisons are made:

- (1) Three δ -MnO₂'s, precipitated according to an acid, neutral and alkaline recipe are compared with regard to the reactivity of their surfaces towards Cu (Section 7.2.1).
- (2) The reproducibility of the 'neutral' surface is tested by adsorbing Cu onto three identically precipitated 'neutral' batches of δ -MnO₂ (Section 7.2.2).
- (3) Duplicate isotherms are obtained for the three 'neutral' δ -MnO₂ surfaces to explore reproducibility of isotherms (Section 7.2.3).
- (4) The influence of the presence of glycine on the shape of the isotherms is examined (Section 7.2.4).
- (5) The influence of both natural and heat-induced aging-processes, on the adsorption behaviour of the 'neutral' δ -MnO₂ surface, is investigated (Section 7.2.5).

In Section 7.3, the isotherms obtained are computer fitted to respectively the Single-, the Double- and the Implicit- Langmuir models. The fits to these models can be compared statistically on the basis of Residual Sum of Squares after Regression (RSS) data. Comparison of model parameters, obtained with various sets of adsorption data, for a particular model, can be made statistically through the use of a t-test for pooled standard deviations.

7.2 Adsorption Isotherms Obtained for a Number of Different δ -MnO₂ Surfaces

Adsorption isotherms visualize the relationship between the amount of adsorption on the surface and the amount of adsorbate remaining in solution. In this work, the former is expressed as r_{ads} , the amount of Cu (in μM) adsorbed per amount of surface (δ -MnO₂, in μM). The latter is presented by the amount of free (i.e. uncomplexed) Cu^{2+} in solution.

The data for all adsorption isotherms obtained for Chapter 7 can be found in Appendix III, expressed in terms of r_{ads} and $p[\text{Cu}^{2+}]$. Each isotherm is identified by the date on which it was obtained, by the δ -MnO₂ surface used, the pH of the solution and whether or not glycine was present to facilitate the keeping in solution of enough Cu. An example of an experimental code is as follows:

Experiment: 130979, MnO₂ III, pH6, no glycine

This denotes an adsorption experiment of Cu on δ -MnO₂ III (a 'neutral' surface) at pH 6 in the absence of glycine, on September 13, 1979. The date is given so that the age of the surface can be estimated (see Chapter 4, Table 4.1, for the dates on which the various surfaces were fabricated). In Appendix III, all data are grouped by particular surface. For instance, all data regarding δ -MnO₂ surface III are given consecutively, even though they are not all discussed together in Sections 7.2 and 7.3.

7.2.1 Comparison of the Adsorption Behaviour of a 'Neutral', 'Acid' and 'Alkaline' δ -MnO₂ Surface

Table 7.1 summarizes the pertinent data for the experiments that

were performed to compare adsorption of Cu onto a 'neutral', 'acid' and 'alkaline' δ -MnO₂ surface. The recipes, according to which these δ -MnO₂'s were precipitated were discussed in detail in Chapter 4.

Figures 7.1 to 7.4 show the adsorption isotherms at three pH values for the 'neutral', 'alkaline' and 'acid' δ -MnO₂ surfaces. In most cases, glycine was added to maintain sufficient soluble Cu. Figures 7.1, 7.3 and 7.4 show that the 'neutral' δ -MnO₂ (VIb) and the 'acid' δ -MnO₂ (VIIIb) have a very similar adsorption capacity over the pH range 6-8, with the 'neutral' surface having a slightly higher capacity. This similarity in adsorption behaviour is remarkable because Figures 4.5 and 4.6 show that these surfaces differ vastly in appearance. The 'alkaline' MnO₂ (VIIb) possesses a considerably lower adsorption capacity.

Figure 7.2 illustrates the influence of glycine on the adsorption isotherms. Table 7.1 shows that the experiments at pH 6 with and without glycine present were performed over virtually identical total Cu concentration ranges. However, the presence of glycine reduces both the amount of Cu available for adsorption and the free Cu²⁺ concentration in solution, shifting the isotherms to the left, and producing more data points in the lower parts of the isotherms. The importance of this shift is discussed in Section 7.3.2, where results are fitted to a linearized Single Langmuir model.

Figure 7.2 also shows a very steep isotherm for the 'acid' MnO₂ (VIIIb). The reason for this is unclear and an experimental artifact (possibly precipitation) is suspected because in the other three cases (Figures 7.1, 7.3 and 7.4) such behaviour is not observed.

Differences in adsorption capacity for the three surfaces should be due to either differences in affinity for Cu and/or differences in the

total surface area per amount of δ -MnO₂ material. However, for one particular δ -MnO₂, adsorption capacity differences may also occur; it is possible that the same amount of MnO₂ (in μ M Mn) may not always have the same surface area, due to undetected variations in particle size and porosity. In addition, MnO₂ was added volumetrically to the solution in which the adsorption experiment was to be performed. Analysis for Mn indicated that such a procedure did not always deliver exactly the same amount of MnO₂, although in all cases the same pipet was used, and the stock-solution of MnO₂ was vigorously stirred for 1/2 hr. prior to taking a volumetric aliquot.

The results shown in Figures 7.1 to 7.4 lead to the conclusion that from visual comparison, the adsorption capacity for the 'neutral' MnO₂ (VIb) and the 'acid' MnO₂ (VIIIb) appears similar. The capacity of the 'alkaline' MnO₂ surface is considerably lower.

7.2.2 Comparison of the Adsorption Behaviour of Three Identically Precipitated 'Neutral' δ -MnO₂ Batches

Figures 7.5 to 7.8 show adsorption isotherms obtained for three different batches of 'neutrally' precipitated δ -MnO₂ (MnO₂'s III, VIb and XVC), all 5 to 6 months old at the time of the adsorption experiments. Table 7.2 provides the pertinent data for the experiments visualized in these Figures.

From Figures 7.5 to 7.8 it is apparent that, with the exception of the data for pH 8, the adsorption capacity of the 'neutral' δ -MnO₂ batches varies. Figure 7.5 shows that at pH 6, in the absence of glycine, MnO₂'s VIb and XVC behave similarly, although the isotherm for MnO₂ XVC was not taken to its maximum capacity. This renders the

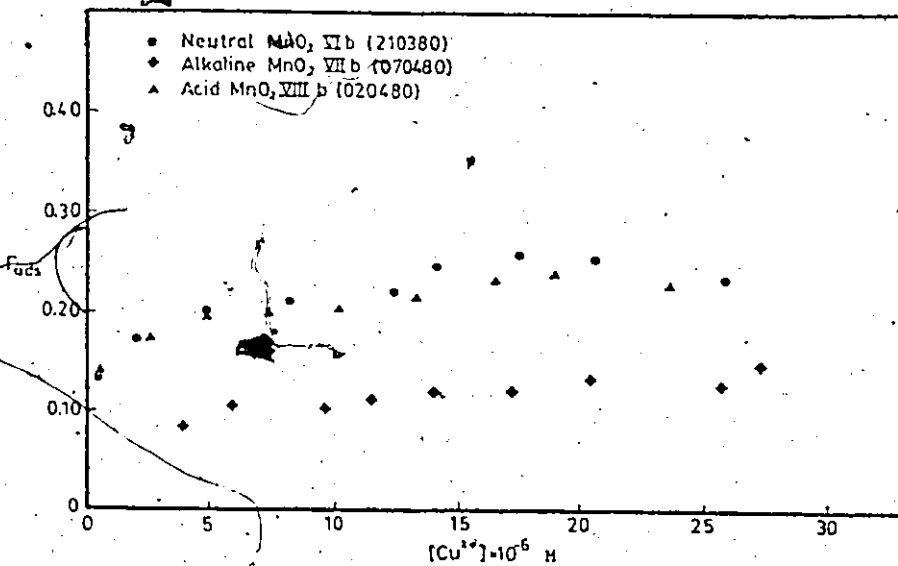


Figure 7.1 Adsorption isotherms for three differently prepared δ - MnO_2 batches, at pH 6.0, no glycine present.

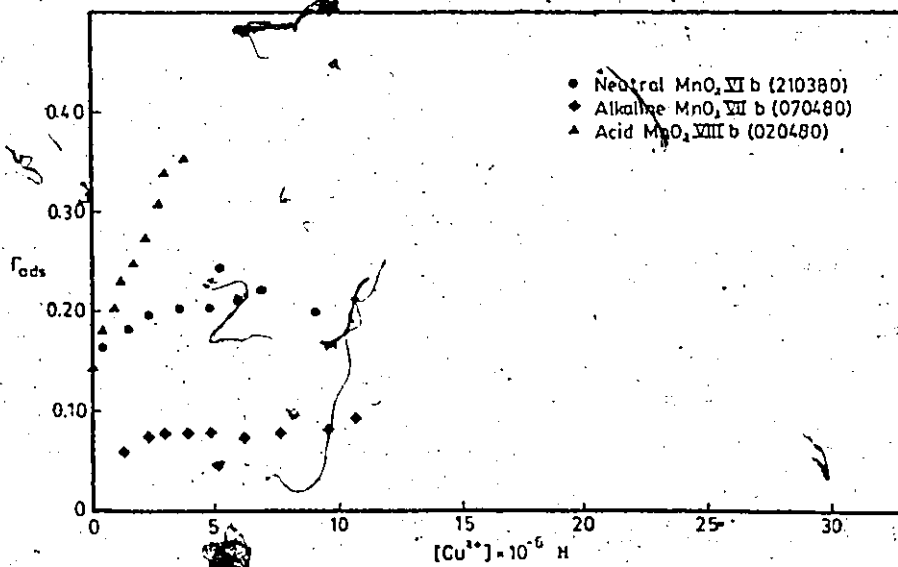


Figure 7.2 Adsorption isotherms for three differently prepared δ - MnO_2 batches, at pH 6.0, 50 μM glycine present.

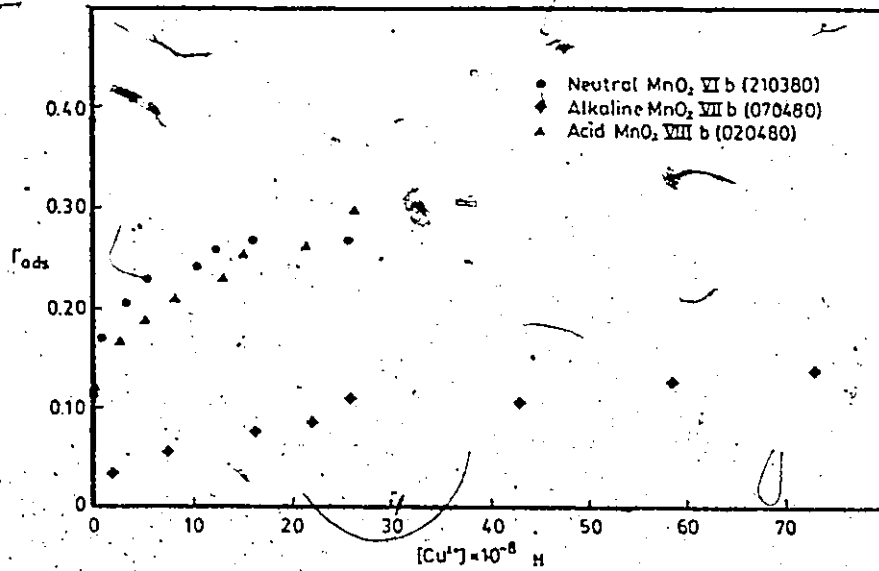


Figure 7.3 Adsorption isotherms for three differently prepared δ -MnO₂ batches, at pH 7.0, 50 μ M glycine present.

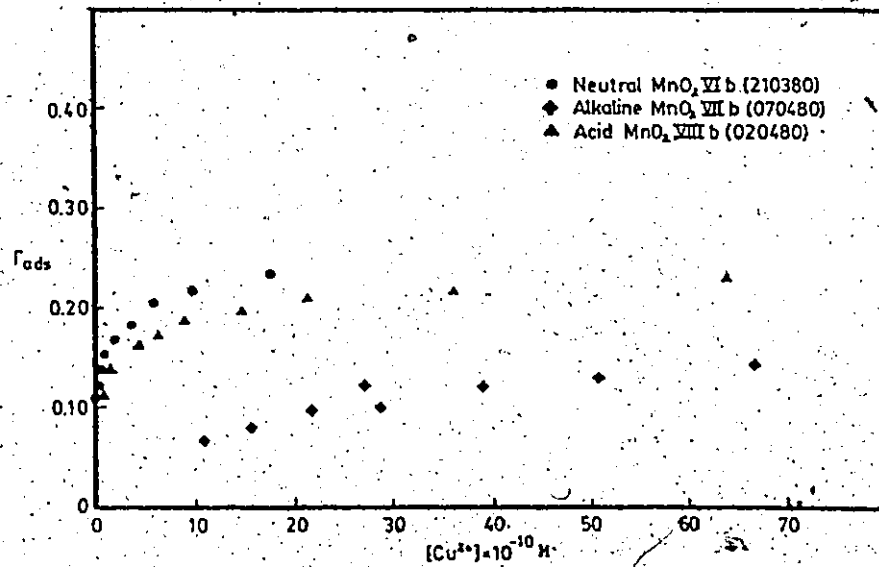


Figure 7.4 Adsorption isotherms for three differently prepared δ -MnO₂ batches, at pH 8.0, 50 μ M glycine present.

Table 7.1 Experimental conditions for comparison study involving a neutral δ - MnO_2 (VIIb), an alkaline δ - MnO_2 (VIIIb) and an acid δ - MnO_2 (VIIIb)

Cu ₂ range ^a (μM)	Glycine conc. (μM)	Fig.	pH	MnO ₂ ^b	exp. date	Cu ₂ range ^a (μM)	Glycine conc. (μM)	pH	MnO ₂ ^b	Fig.	exp. date
10.0-42.9	-	7.1	6.0	VIIb (neutral)	210380	10.0-44.7	-	6.0	III	7.5	130979
10.0-3-41.5	50.0	7.2	6.0	VIIb	210380	10.0-41.8	-	6.0	VIIb	7.5	210680
4.0-30.1	50.0	7.3	7.0	VIIb	210380	2.2-16.4	-	6.0	XVc	7.5	120681
8.0-22.0	50.0	7.4	8.0	VIIb	210380	14.3-41.5	50.0	6.0	VIIb	7.6	210380
						2.0-28.5	50.0	6.0	XVc	7.6	010381
10.0-38.1	-	7.1	6.0	VIIIb (alkaline)	070480	4.0-29.4	50.0	7.0	III	7.7	170979
10.0-37.4	50.0	7.2	6.0	VIIIb	070480	4.0-30.1	50.0	7.0	VIIb	7.7	210380
4.0-29.7	50.0	7.3	7.0	VIIIb	070480	8.0-22.3	50.0	8.0	III	7.8	270979
8.0-21.5	50.0	7.4	8.0	VIIIb	070480	8.0-22.0	50.0	8.0	VIIb	7.8	210380
						1.0-13.0	50.0	6.0	XVc	7.8	010381

^a MnO₂ III made on 030379

VIIb 220180

XVc 220181

10.0-39.2 - 7.1 6.0 VIIIb (acid) 020480

10.0-37.8 50.0 7.2 6.0 VIIIb 020480

4.0-31.1 50.0 7.3 7.0 VIIIb 020480

8.0-26.6 50.0 7.4 8.0 VIIIb 020480

^b MnO₂ VIIb made on 220180

VIIIb 230180

VIIIb 230180

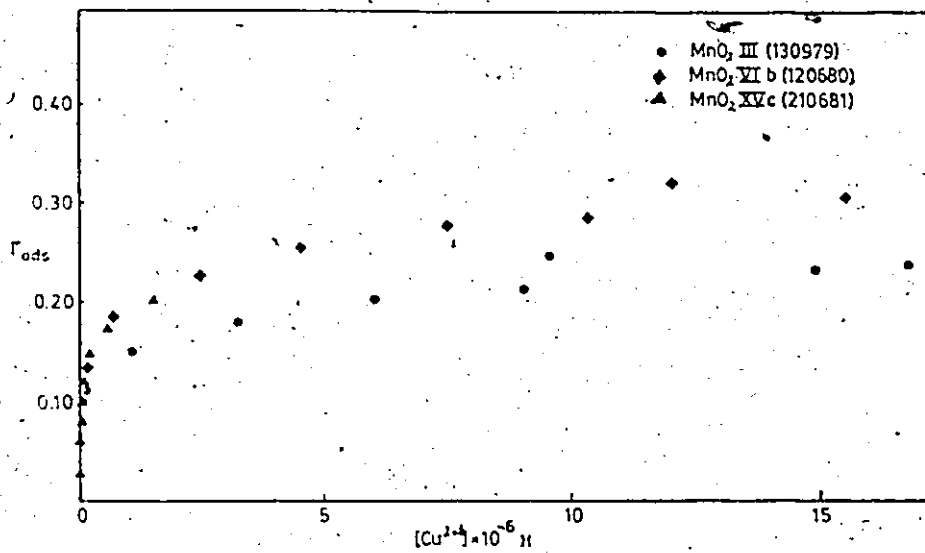


Figure 7.5 Adsorption isotherms for three identically prepared 'neutral' δ -MnO₂ batches, at pH 6.0, no glycine present.

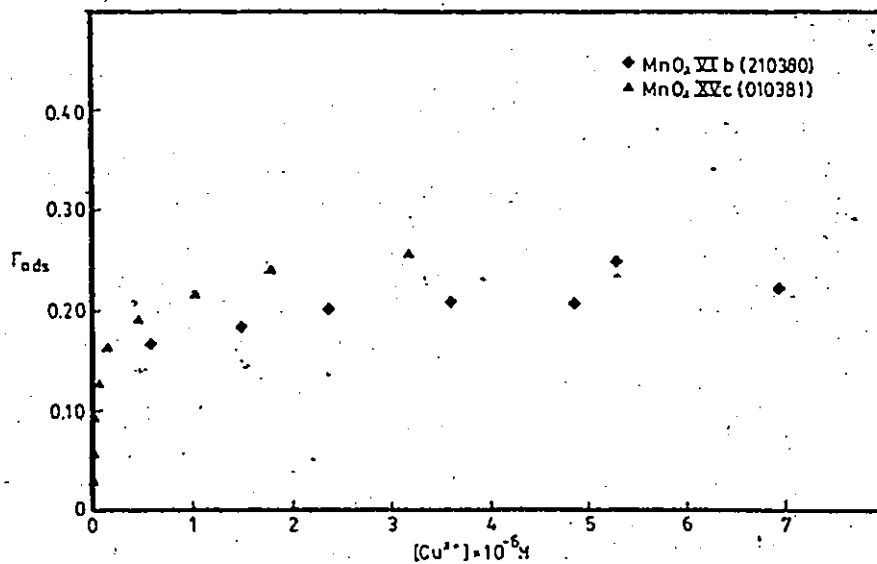


Figure 7.6 Adsorption isotherms for two identically prepared 'neutral' δ -MnO₂ batches, at pH 6.0, 50 μ M glycine present.

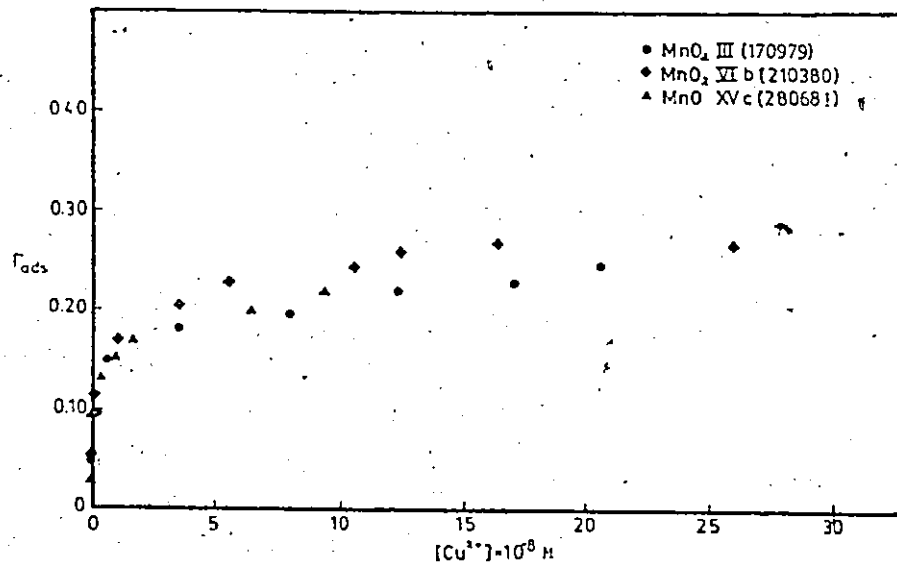


Figure 7.7 Adsorption isotherm for three identically prepared 'neutral' δ -MnO₂ batches, at pH 7.0, 50 μ M glycine present.

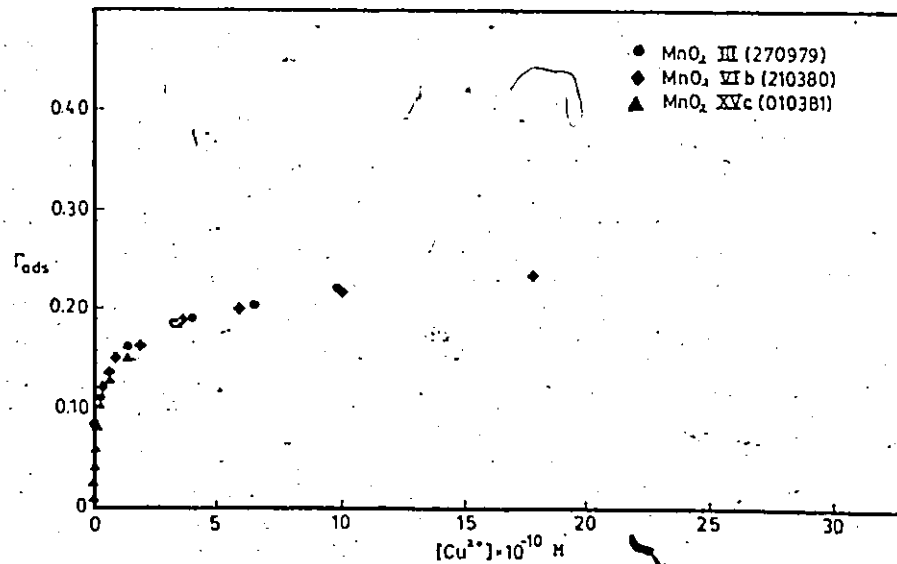


Figure 7.8 Adsorption isotherm comparison for three identically prepared 'neutral' δ -MnO₂ batches, at pH 8.0, 50 μ M glycine present.

comparison somewhat dubious. Nevertheless, it appears that under these experimental conditions, the adsorption capacity of MnO_2 III is significantly less than for the other two 'neutral' surfaces. Figure 7.6 indicates that adsorption isotherms for MnO_2 's VIb and Xvc differ at pH 6, in the presence of glycine. No data for MnO_2 III were obtained for this particular condition. These results contradict the similar behaviour of MnO_2 VIb and Xvc shown in Figure 7.5. At pH 7.0, in the presence of glycine (Figure 7.7) the three MnO_2 's also differ in adsorption capacity, but the variations are smaller than for pH 6 (Figures 7.5 and 7.6). Finally, at pH 8, in the presence of glycine (Figure 7.8) all three 'neutral' $\delta\text{-MnO}_2$ surfaces appear to have virtually identical adsorption capacities.

These results lead to the conclusion that, from visual comparison of adsorption isotherms, reproducibility of a 'neutral' $\delta\text{-MnO}_2$ surface with constant adsorption characteristics for Cu, is poor for adsorption at pH 6.0, but improves for adsorption at higher pH's (7.0 and 8.0).

7.2.3 Reproducibility of Adsorption Isotherms for 'Neutrally' Prepared $\delta\text{-MnO}_2$'s at pH Values in the Range 6 to 8

The 'neutral' $\delta\text{-MnO}_2$ surface was studied more extensively than the 'acid' or 'alkaline' ones. One of the objectives of the adsorption studies was to investigate the reproducibility of isotherms. A considerable number of isotherms for the various 'neutral' surfaces ($\delta\text{-MnO}_2$'s III, VIb and Xvc, see Section 7.2.2) were duplicated for this purpose. Table 7.3 contains the relevant data regarding the experimental conditions under which these duplicates were obtained. All results are plotted in Figures 7.9 - 7.18 for direct visual comparison. Only a

Table 7.3 Experimental conditions for the experiments investigating reproducibility of isotherms for a 'neutral' δ -MnO₂ surfaces

Cu _t range (μ M)	Glycine Conc. (μ M)	pH	MnO ₂ *	Fig.	Exp.Date
4.0-33.6	50.0	7.0	III	7.9 ⁺	170979
17.9-29.1	50.0	7.0	III	7.9	240979
4.0-28.8	50.0	7.5	III	7.10	170979
15.9-31.2	50.0	7.5	III	7.10	240979
16.0-30.5	50.0	7.5	III	7.10	081079
1.0-22.4	50.0	7.5	III	7.10	160381
5.0-18.9	50.0	8.5	III	7.11 ⁺	270979
2.0-18.8	50.0	8.5	III	7.11	160381
10.0-42.9	-	6.0	Vib	7.12	210380
9.9-41.8	-	6.0	Vib	7.12	150580
10.0-40.8	-	6.0	Vib	7.12	290580
10.0-41.8	-	6.0	Vib	7.12	120680
10.0-41.5	50.0	6.0	Vib	7.13 ⁺	210380
40.0	0-167	6.0	Vib	7.13	150580
10.0-40.0	50.0	6.0	Vib	7.13	290580
10.0-40.9	50.0	6.0	Vib	7.13	290580
10.0-40.2	50.0	6.0	Vib	7.13	120680
1.0-21.5	-	6.0	XVc	7.14 ⁺	210481
2.2-16.4	-	6.0	XVc	7.14	210681
3.1-17.2	-	7.0	XVc	7.15 ⁺	210481
3.1-16.1	-	7.0	XVc	7.15	280681
6.6-28.5	50.0	6.0	XVc	7.16 ⁺	010381
2.2-10.0	50.0	6.0	XVc	7.16	210681
2.2-21.6	50.0	6.0	XVc	7.16	240781
4.5-13.6	50.0	7.0	XVc	7.17 ⁺	010381
2.2-20.8	50.0	7.0	XVc	7.17	280681
2.1-13.9	50.0	8.0	XVc	7.18	010381
4.0-25.8	**80.0(asp)	8.0	XVc	7.18	080481
4.0-25.5	80.0(ala)	8.0	XVc	7.18	080481
6.2-26.7	80.0(glu)	8.0	XVc	7.18	080481

*MnO₂ III made on 050379

Vib 220180

XVc 220181

+ Figures can be found in Appendix IV

**asp = aspartic acid

ala = alanine

glu = glutamic acid

number of these Figures is contained in the main text of this Section. For the remaining Figures one is referred to Appendix IV.

Figures 7.10, 7.12 and 7.18 illustrate the general trend occurring from all of Figures 7.9 - 7.18; reproducibility of adsorption isotherms for 'neutral' δ -MnO₂ surfaces is low at pH 6, both in the presence and absence of glycine, and for all three 'neutral' surfaces. The reproducibility improves at pH 7, although less data are available at this pH for comparison. At a pH of 7.5-8.5, reproducibility appears good to excellent. It should be emphasized that the above noted trend is based on visual comparison only and not on a numerical data comparison. For the latter, the data have to be fitted to a particular model first, before statistical comparison of adsorption-parameters can be performed. This will be done in Section 7.3. At this point, it is concluded that reproducibility of isotherms for a 'neutral' δ -MnO₂ surface is generally poor.

7.2.4 Adsorption Isotherms for Various 'Neutral' δ -MnO₂ Batches in the Presence and Absence of Glycine

To obtain adsorption isotherms at pH values of 7 and higher, it is necessary to add a certain amount of glycine to the solution. Glycine serves to keep enough Cu in solution for accurate measurement, and at the same time prevents the formation of Cu-hydroxide and/or Cu-oxide precipitates (see also Chapter 6, Section 6.3.1). To investigate whether the addition of glycine influences the shape of the isotherms, a comparison needs to be made between isotherms obtained under similar experimental conditions, in the presence and absence of glycine. Such a comparison is most readily made at pH 6, because at this pH, precipitation of Cu is not

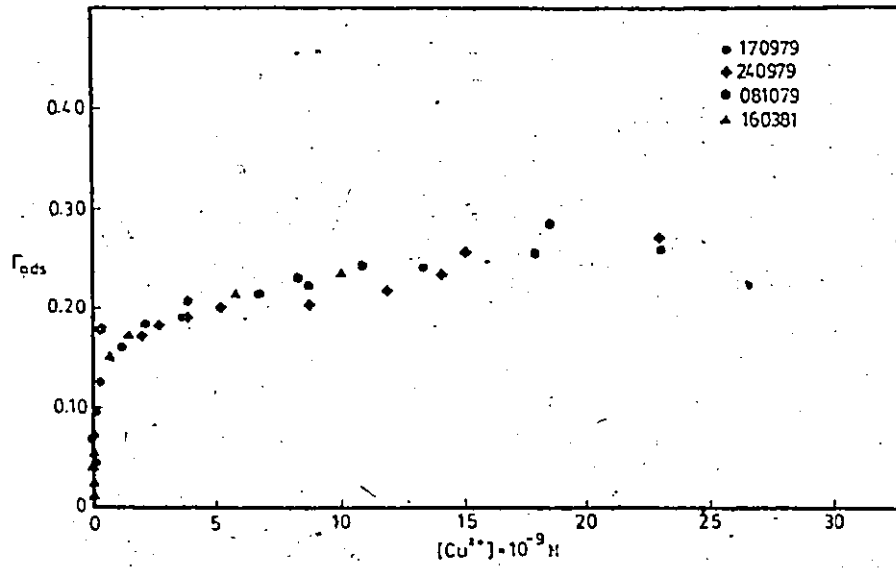


Figure 7.10 Duplicate isotherms at pH 7.5, in the presence of 50mM glycine, for MnO_2 III.

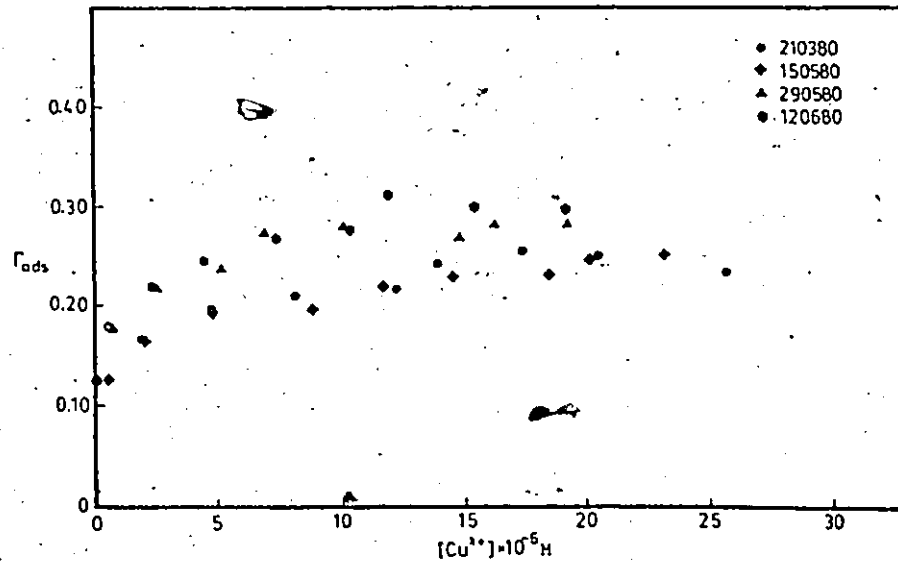


Figure 7.12 Duplicate isotherms at pH 6.0 in the absence of glycine for MnO_2 Vib.

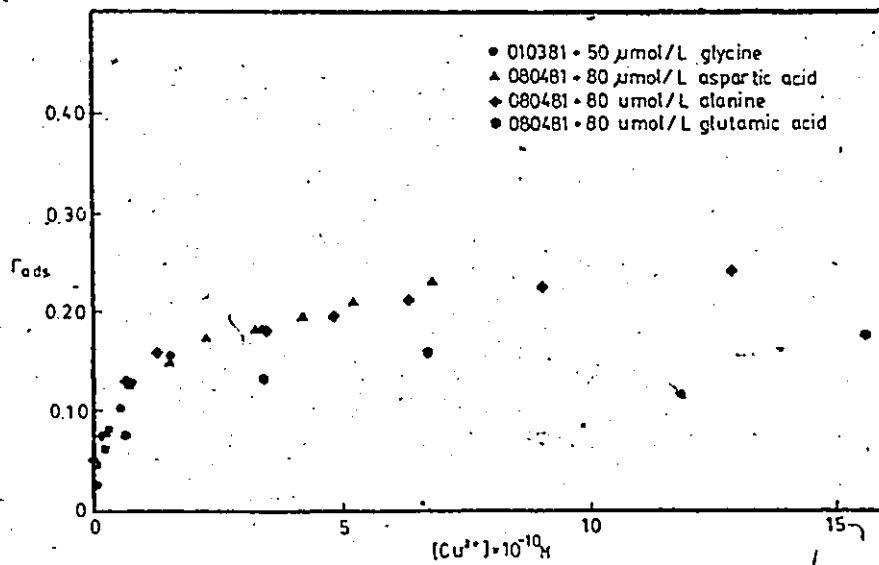


Figure 7.18 Duplicate isotherms at pH 8.0 in the presence of four different amino acids for $\text{MnO}_2\text{-XVc}$.

a problem. With some care, a comparison can also be performed at pH 7, but not at pH 8.

The three 'neutral' δ -MnO₂ surfaces III, VIb and XVC were used to investigate the influence of glycine on adsorption isotherms. Table 7.4 contains the pertaining data regarding experimental conditions.

For δ -MnO₂ III, one comparison was made at pH 6.5. The results are shown in Figure 7-19. The isotherms appear different in shape, but from Table 7.4 it can be seen that the C_u-range (total Cu added) is not similar for each of the isotherms. This could have caused at least part of the observed difference.

For δ -MnO₂ VIb, three comparisons were made at pH 6. The results are plotted in Figures 7.20, 7.21 (both in Appendix IV) and 7.22 (in Text). The visual differences in the isotherms do not seem to be smaller or larger than the differences in the duplicate isotherms, discussed in Section 7.2.3. Statistical testing of the data (in Section 7.3) will provide more information on the real differences between the isotherms.

For δ -MnO₂ XVC two comparisons were made at pH 6 and at pH 7. The results are illustrated in Figures 7.23 and 7.24 for pH 6 and Figures 7.25 and 7.26 for pH 7. Figures 7.23 and 7.25 are contained in the Text, while Figures 7.24 and 7.26 can be found in Appendix IV. The differences between the isotherms in these Figures appears large, with the exception of Figure 7.23. However, again, the visual differences do not appear much larger than some of the differences observed for duplicate isotherms in Section 7.2.3.

Differences occur when comparing isotherms obtained in the presence and absence of glycine for the 'neutral' δ -MnO₂ surfaces III,

Table 7.4 Comparison of adsorption isotherms obtained for 'neutral' δ -MnO₂ surfaces in the presence and absence of glycine

Cu _t range (μ M)	Glycine Conc. (μ M)	pH	MnO ₂ *	Fig.	Exp. Date
2.0-25.6	50.0	6.5	III	7.19	160381
17.9-29.0	-	6.5	III	7.19	130979
10.0-41.8	-	6.0	Vib	7.20 ⁺	120680
10.0-40.2	50.0	6.0	Vib	7.20	120680
10.0-40.8	-	6.0	Vib	7.21 ⁺	290580
10.0-40.0	50.0	6.0	Vib	7.21	290580
10.0-42.9	-	6.0	Vib	7.22	210380
14.3-41.5	50.0	6.0	Vib	7.22	210380
2.2-18.8	48 asp**	6.0	XVc	7.23	210681
2.2-16.4	-	6.0	XVc	7.23	210681
2.2-10.0	50.0	6.0	XVc	7.23	210681
2.2-18.8	48 asp**	6.0	XVc	7.23	210681
2.2-16.4	-	6.0	XVc	7.23	210681
2.1-21.5	-	6.0	XVc	7.24 ⁺	210481
2.0-28.5	50.0	6.0	XVc	7.24	010381
3.1-16.1	-	7.0	XVc	7.25	280681
2.2-20.8	50.0	7.0	XVc	7.25	280681
3.1-17.2	-	7.0	XVc	7.26 ⁺	210481
4.5-13.6	50.0	7.0	XVc	7.26	010381

* MnO₂ III made on 050379
 Vib. 220180
 XVc 220181

⁺ These Figures can be found in
 Appendix IV

**asp = aspartic acid

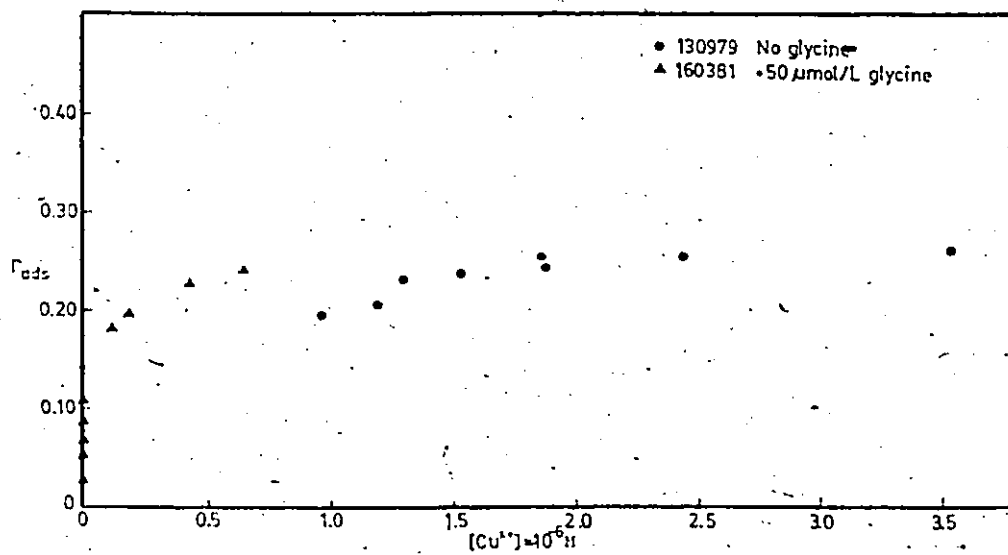


Figure 7.19 Isotherms in the presence, and absence, of glycine, for MnO_2 III at pH 6.5.

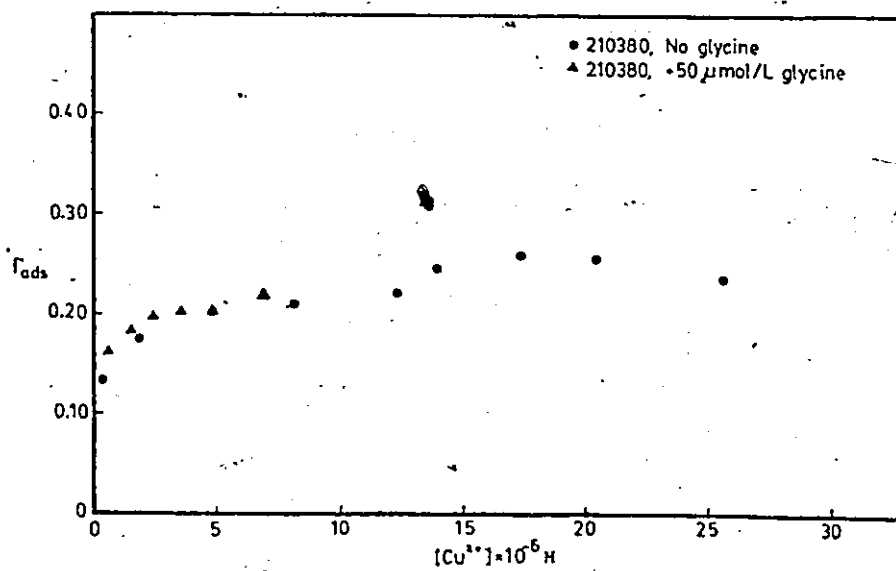


Figure 7.22 Isotherms in the presence, and absence, of glycine at pH 6.0, for MnO_2 V1b (220180).

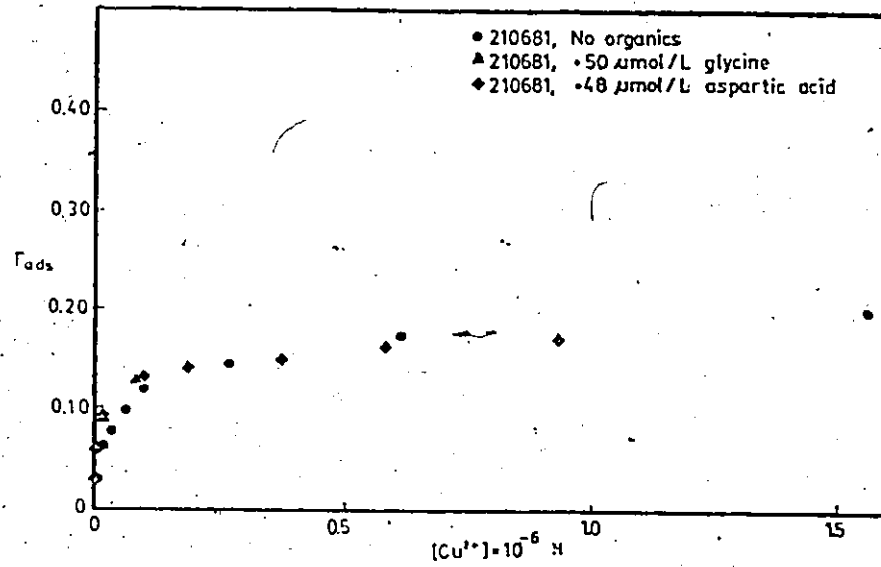


Figure 7.23 Isotherms in the presence, and absence, of organics (amino acids) at pH 6.0, for MnO_2 XVe (220181).

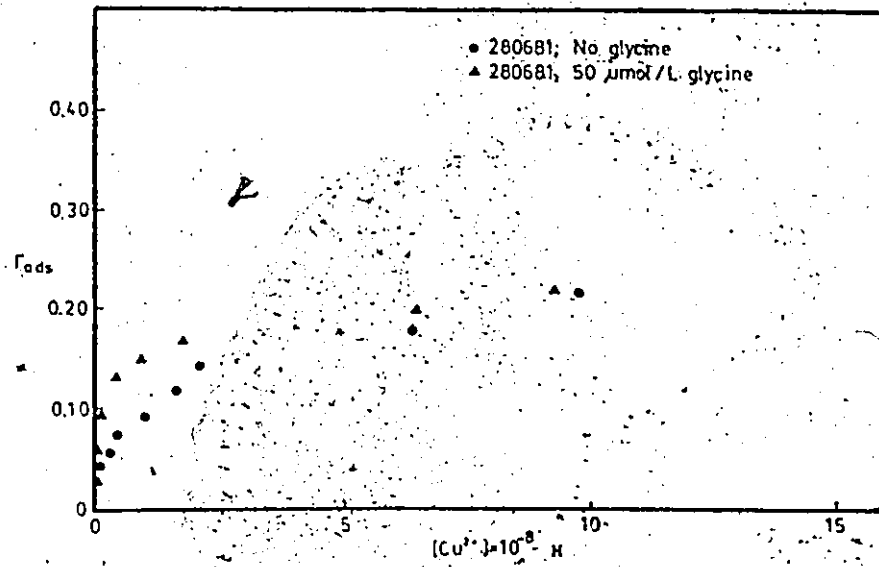


Figure 7.25 Isotherms in the presence, and absence, of glycine at pH 7.0 for MnO_2 XVe (280681).

V1b and Xvc. These differences are either due to the influence of glycine on the adsorption characteristics of the surface or to experimental fluctuations, as illustrated in Section 7.2.3.

In Chapter 6, adsorption of glycine on the δ -MnO₂ surface was investigated. The results indicated that glycine does not adsorb in any substantial amount on δ -MnO₂. The direct influence of glycine on the adsorption characteristics of the δ -MnO₂ surface can therefore be excluded. The presence of glycine in solution, however, does shift an adsorption isotherm to the left compared with an isotherm obtained in the absence of glycine. Both the terms Γ_{ads} and Cu^{2+} are negatively influenced by the presence of glycine. Nevertheless, this should not influence the shape of the isotherms, unless they are not 'uniform' throughout the whole adsorption region and for instance adsorption is stronger at low coverage of the surface. This will be discussed in more depth in Section 7.3.

7.2.5 Comparison of Adsorption Isotherms for a Naturally and an Artificially Aged δ -MnO₂ Surface

The results of natural aging, as well as that of simulated, heat-induced aging of δ -MnO₂, which can take the form of recrystallization from round particles to fibrous cryptomelane, is discussed in Chapter 4. Figure 4.8 shows a TEM image of a naturally aged, 'neutral' δ -MnO₂ (MnO₂ 13), a remnant of van den Berg's (1979) work. Figure 4.9 shows the TEM appearance of an artificially treated 'neutral' δ -MnO₂ surface (MnO₂ XXV-A).

Adsorption isotherms were obtained for each of these two MnO₂ surfaces. Table 7.5 provides information regarding the experimental

Table 7.5 Experimental conditions for comparison study involving
a naturally aged and an artificially aged 'neutral' δ - MnO_2

Cu _t range (μM)	Glycine conc. (μM)	pH	MnO ₂ *	Fig.	Exp. Date
2.0-29.4	-	6.0	XXV-A	7.27	280581
2.0-22.9	-	6.0	13	7.27	240781
2.0-34.2	50.0	6.0	XXV-A	7.28 ⁺	280581
2.2-27.4	50.0	6.0	13	7.28	190781
2.0-20.5	50.0	7.0	XXV-A	7.29 ⁺	280581
2.2-17.2	50.0	7.0	13	7.29	190781
2.0-18.6	50.0	8.0	XXV-A	7.30 ⁺	280581
2.2-17.2	50.0	8.0	13	7.30	190781
2.0-22.9	-	6.0	13	7.31	240781
2.2-27.4	50.0	6.0	13	7.31	190781

* MnO₂ 13 presumably prepared in either 1977 or 1978

+ MnO₂ XXV-A made on 250851, 4 hr. autoclaved

Figures in Appendix IV

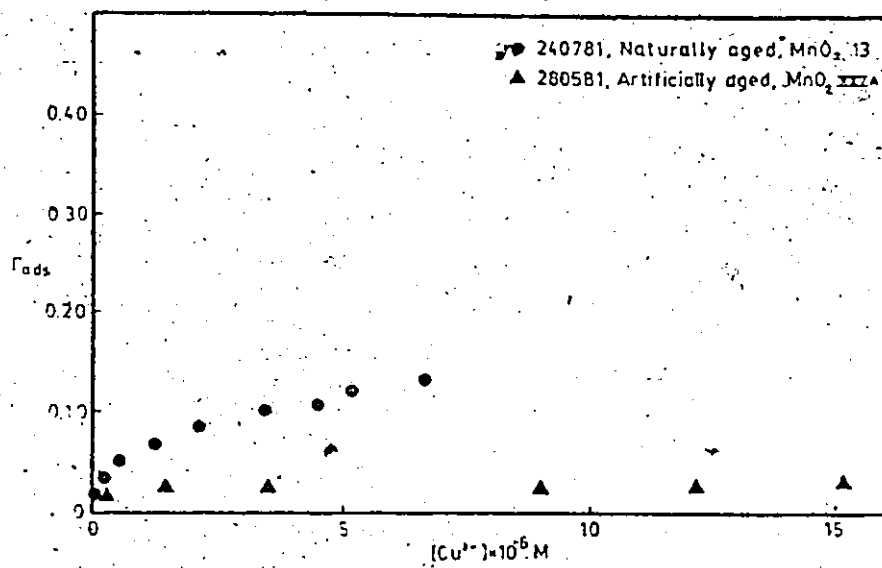


Figure 7.27 Comparison of isotherms for a naturally and artificially aged neutral MnO₂ at pH 6.0, in the absence of glycine.

conditions for which isotherms were obtained. Figures 7.27 to 7.30 visually compare the differences in the adsorption isotherms for the aged surfaces. Figure 7.27 is contained in the text, to illustrate the extent of the difference. Figures 7.28-7.30 can be found in Appendix IV. These Figures show essentially the same differences as illustrated by Figure 7.27, at different pH values. Figure 7.31 (in Appendix IV) compares the isotherms for MnO_2 13 obtained at pH 6 in the absence and presence of glycine.

The naturally aged MnO_2 13 possesses approximately half of the adsorption capacity of 'neutral' non-aged δ - MnO_2 surfaces. This reduction in adsorption capacity is most likely caused by a reduction in total surface area per amount of MnO_2 , as a result of the recrystallization to fibrous cryptomelane. Difference is observed for isotherms obtained at pH 6 in the presence and absence of glycine (Figure 7.31, Appendix IV). This difference must be due to experimental fluctuations, since in Chapter 6 it was shown that glycine does not adsorb in important quantity on the MnO_2 13 surface.

The artificially aged MnO_2 XXV-A has an extremely low adsorption capacity, most likely due to a considerable reduction in surface area as a result of the heat-induced aging process.

7.3 The Fit of the Adsorption Results to Three Adsorption Models; Statistical Comparison of Adsorption Parameters and Model Fit

7.3.1 Introduction

In Section 7.2, adsorption results were presented and visually compared, for a number of different δ - MnO_2 surfaces. Here, the results

are fitted to three adsorption models which were discussed and/or derived previously in Section 5.3 of Chapter 5. The adsorption models have the following forms:

1. Single Langmuir:

$$\Gamma_{\text{ads}} = \Gamma_{\text{max}} \frac{\text{Cu}^{2+}}{1/B + \text{Cu}^{2+}} \quad (7.1)$$

2. Double Langmuir:

$$\Gamma_{\text{ads}} = \Gamma_{m1} \frac{\text{Cu}^{2+}}{1/B_1 + \text{Cu}^{2+}} + \Gamma_{m2} \frac{\text{Cu}^{2+}}{1/B_2 + \text{Cu}^{2+}} \quad (7.2)$$

3. Implicit, Single Langmuir:

$$\Gamma_{\text{ads}} = \Gamma_{\text{max}} \frac{\text{Cu}^{2+}}{(\text{H}^+)^n / (B \cdot e^{(1-\Gamma_{\text{ads}}/\Gamma_{\text{max}})}) + \text{Cu}^{2+}} \quad (7.3)$$

The adsorption parameters which are determined by these models are Γ_{max} , the maximum amount of Cu adsorbed per amount of surface and B, the bindings constant related to the bindings energy involved. For Model 2, the Double Langmuir, Γ_{max} and B are split up in respectively Γ_{m1} , and Γ_{m2} and B_1 and B_2 . For Model 3, the bindings energy is made up from B, $(\text{H}^+)^n$ and $e^{(1-\Gamma_{\text{ads}}/\Gamma_{\text{max}})}$, where n is the third parameter estimated. Note that B is not the same for each of these models.

7.3.2 The Single Langmuir Model

One of the reasons that this extensive study on the adsorption

behaviour of δ -MnO₂ surfaces was undertaken, was the fact that the Single Langmuir adsorption parameters Γ_{\max} and B obtained for a 'neutral' δ -MnO₂ surface did not agree with the values obtained by van den Berg (1979) for a 'neutral' δ -MnO₂. This is illustrated in Figures 4.3 and 4.4 (Chapter 4). Another observation, equally important in inducing this study, was the fact that the linearized form of the Single Langmuir model did not appear linear at low coverage of the surface. The data in Figures 7.1 to 7.31 have all been fitted to linearized Langmuir isotherms, and almost without exception, deviation from linearity is observed at the lower end of the isotherms. Figures 7.32 to 7.34 illustrate this. Figure 7.32 is the linearized presentation of Figure 7.1, Figure 7.33 corresponds to Figure 7.10 and Figure 7.34 shows the linearized data of Figure 7.22.

The importance of this non-linear behaviour is obvious, if one tries to estimate the adsorption parameters for the Single Langmuir model by linearizing the data, followed by linear least squares analysis. Such a process was proposed for the δ -MnO₂ method, published by van den Berg (1979), who recommends the particular method of linearizing the Langmuir equation used in Figures 7.32 - 7.34, namely plotting Cu^{2+} versus $\text{Cu}^{2+}/\Gamma_{\text{ads}}$. Another way would be to plot $1/\text{Cu}^{2+}$ versus $1/\Gamma_{\text{ads}}$. However, van den Berg argues that by using the latter, in which the reciprocal of the Cu^{2+} concentration is the independent variable, a number of data points representing low Cu^{2+} concentrations will be at high $1/\text{Cu}^{2+}$ values and these points will have a strong influence on the slope of the line even though these data may contain relatively large errors due to for instance contamination problems. Also, by plotting $1/\text{Cu}^{2+}$ versus $1/\Gamma_{\text{ads}}$, the more accurate data obtained for higher Cu^{2+} concentrations tend to group together, reducing their influence on the

slope in favour of the more inaccurate data. In short, either way of plotting weights the data and hence influences the adsorption parameters obtained via linear regression analysis.

The deviation from linearity at low coverages of the surface implies that there, the adsorption strength is larger than at higher coverage of the surface. If two isotherms are obtained for the same surface at identical pH, but over a different C_u range, then one isotherm will contain more data points in the lower coverage range than the other, and hence the values for B obtained via linear regression will differ. If one would analyze only equivalent points, (i.e. the same number of points in a shared Cu^{2+} concentration range), the same value for B should be found. Table 7.6 shows the validity of the above discussion for duplicate isotherms in the presence of glycine obtained for MnO_2 , III. It should be noted that for comparison of isotherms obtained in the presence and absence of glycine, the above argument is even stronger; glycine pulls more data points toward the lower end of the isotherms, causing even larger differences in the results obtained from linear regression.

The above arguments imply that for accurate estimation of Single Langmuir model adsorption parameters, a non-linear regression method should be used, so that there is no weighting of the data points. However, this will not solve all the problems. The Langmuir model is set up such that from the lower part of the isotherm, B is estimated, while the upper part estimates Γ_{max} . A proper estimate of both B and Γ_{max} can only be obtained from data which cover the whole of the isotherm. From Figures 7.1 to 7.31 it is obvious that this was not always the case for the experiments performed in this study.

Table 7.6 CO_2 concentration ranges and linearized Single Langmuir adsorption parameters for duplicate isotherms obtained for the 'neutral' $\delta\text{-MnO}_2$ surface at pH values 7.0 - 8.5

Cu ²⁺ range (μM)	glycine conc. (μM)	pH	MnO ₂	Fig.	exp. date	regression analysis for all data		regression analysis for data adjusted to same number of data points in shared Cu ²⁺ range			
						Γ_{max}	$-\log B$	Cu ²⁺ range (μM)	# of points	Γ_{max}	$-\log B$
4.0 - 33.6	50.0	7.0	III	7.9	170979	0.241	8.13	3-22x10 ⁻²	5	0.262	7.67
17.9 - 29.1	50.0	7.0	III	7.9	240979	0.256	7.80	3-22 "	5	0.258	7.76
4.0 - 28.8	50.0	7.5	III	7.10/7.33	170979	0.261	9.20	0.5-13x10 ⁻³	4	0.256	9.03
15.9 - 31.2	50.0	7.5	III	"	240979	0.284	8.67	0.5-13 "	4	0.248	8.94
16.0 - 30.5	50.0	7.5	III	"	081079	0.284	8.90	0.5-13 "	4	0.265	8.97
1.0 - 22.4	50.0	7.5	III	"	160381	0.238	9.60	0.5-13 "	4	0.248	8.94
5.0 - 18.9	50.0	8.5	III	7.11	170979	0.226	11.02	1-6x10 ⁻⁵	3	0.230	11.01
2.0 - 18.8	50.0	8.5	III	7.11	160381	0.209	11.42	1-6 "	3	0.210	11.17

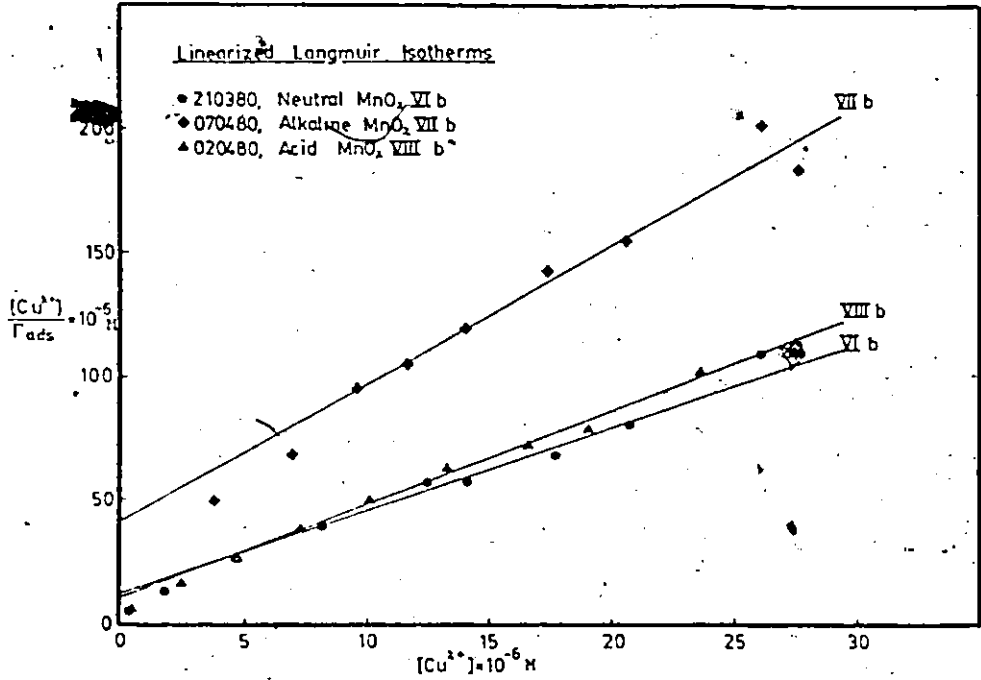


Figure 7.32 Linearized Single Langmuir adsorption isotherms for three differently prepared MnO₂ batches, at pH 6.0, no glycine present.

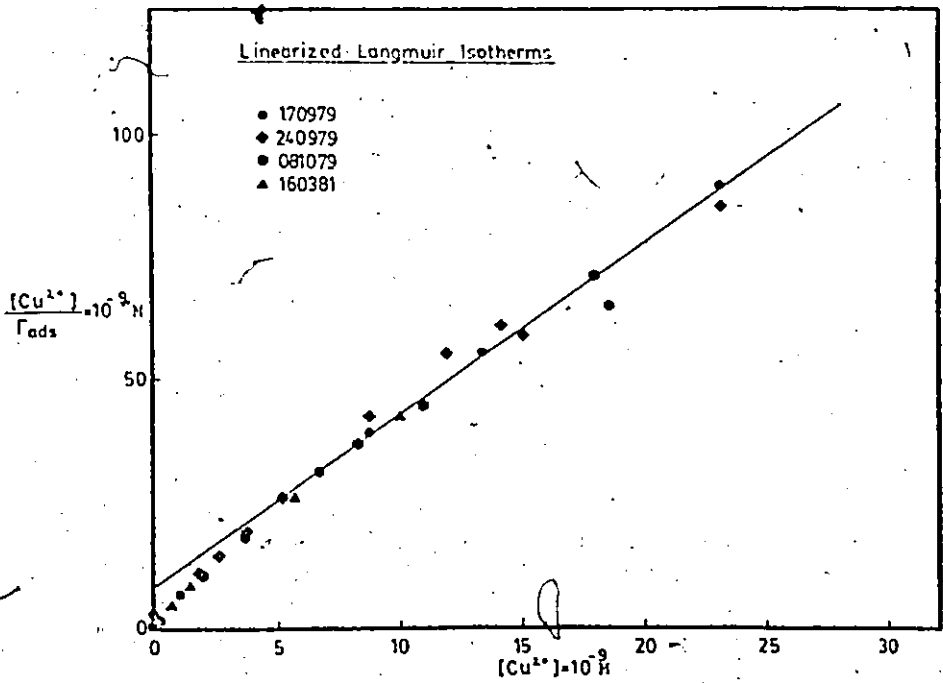


Figure 7.33 Linearized Single Langmuir isotherms for MnO₂ III, at pH 7.5, in the presence of glycine.

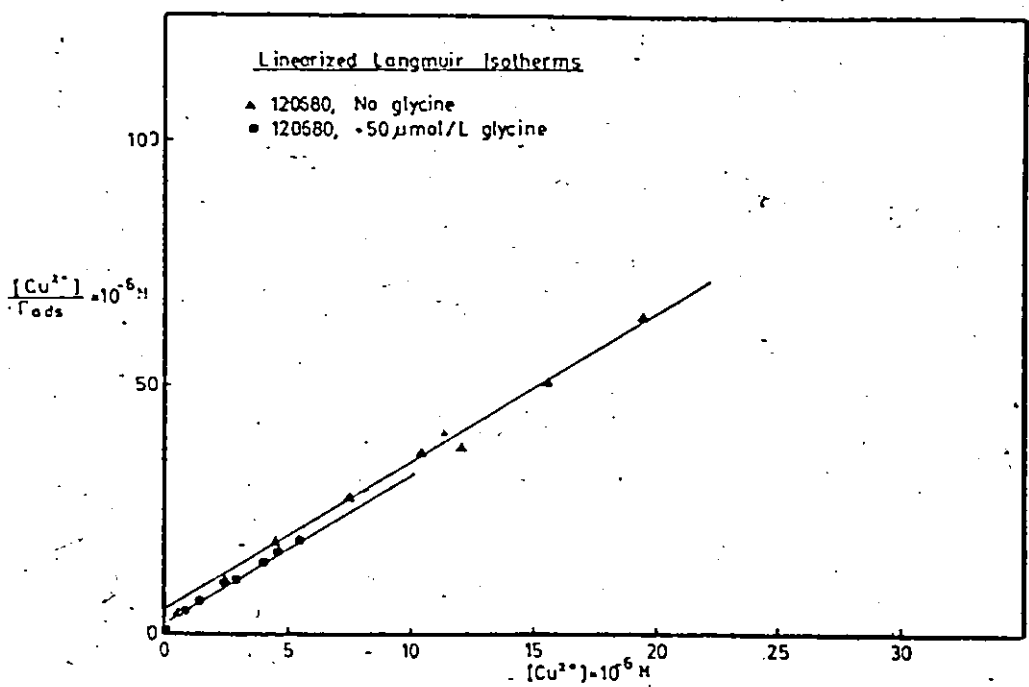


Figure 7.14 Linearized Single Langmuir isotherms for MnO₂ Vib. at pH 6.0, in the presence and absence of glycine.

It should be kept in mind that for the time being, the deviation from linearity is merely an observation, revealed by the linearized Single Langmuir equation. The model does not predict this, and a proper fit to either the linearized model or the non-linear model will not be possible. Nevertheless, the non-linear model is suitable for testing whether the adsorption isotherms obtained and compared in Section 7.2 are identical or not.

In Table 7.7, a comparison is made between estimates for the adsorption parameters B and Γ_{\max} obtained by both linear regression and non-linear regression analysis of the adsorption data presented in Figures 7.1 to 7.31 (Sections 7.2.1 to 7.2.5). For the linear regression analysis, a simple pocket calculator was used, which yielded values for B and Γ_{\max} , but no standard deviations. For the non-linear regression analysis, a computer program called UWHAUS (after Meeter 1965) was used, which yields estimates for B and Γ_{\max} , their 95% confidence limits, from which standard deviations can be calculated, correlation coefficients and Residual Sum of Squares (RSS) data. These data can all be found in Appendix III, along with the Γ_{ads} and $p[\text{Cu}^{2+}]$ data that were used to plot Figures 7.1 to 7.31. A computer printout of UWHAUS is contained in Appendix V.

While Table 7.7 lists the values for the parameters Γ_{\max} and B (arranged by Figure), Table 7.8 contains statistical calculations which make the comparison of these parameters possible on the basis of a t -test. The values for t (i.e. $t_{\Gamma_{\max}}$ and t_B) are obtained from pooled standard deviations and are calculated as follows:

To test the hypothesis $p_1 = p_2$, one has to calculate

Table 7.7 Comparison of linear and non-linear regression values of the adsorption parameters Γ_{\max} and B

Figure	MnO ₂	pH	glycine	exp. date	linear regression		non-linear regression ⁺ 1 standard deviation, (1σ)	
					log B	Γ_{\max}	log B	Γ_{\max}
7.1	VIb	6.0	-	210380	6.02	0.255	6.32 ± 0.14	0.2411 ± 0.0093
	VIIb	6.0	-	070480	5.33	0.161	5.40 ± 0.10	0.1548 ± 0.0084
	VIIIb	6.0	-	020480	5.94	0.243	6.42 ± 0.14	0.2227 ± 0.0074
7.2	VIb	6.0	+	210380	7.09	0.210	6.65 ± 0.19	0.2185 ± 0.0096 [†]
	VIIb	6.0	+	070480	5.92	0.089	6.38 ± 0.20	0.0820 ± 0.0039
	VIIIb	6.0	+	020480	6.14	0.397	6.22 ± 0.17	0.3732 ± 0.0379 [†]
7.3	VIb	7.0	+	210380	8.20	0.271	8.81 ± 0.16	0.2444 ± 0.0108
	VIIb	7.0	+	070480	7.14	0.153	6.85 ± 0.13	0.1515 ± 0.0140
	VIIIb	7.0	+	020480	7.70	0.293	8.27 ± 0.22	0.2469 ± 0.0164
7.4	VIb	8.0	+	210380	10.19	0.239	10.50 ± 0.002	0.2157 ± 0.0065
	VIIb	8.0	+	070480	8.66	0.189	8.67 ± 0.07	0.1882 ± 0.0126
	VIIIb	8.0	+	020480	9.17	0.234	10.06 ± 0.005	0.2139 ± 0.0054
7.5	III	6.0	-	130979	6.06	0.249	6.40 ± 0.15	0.2334 ± 0.0096
	VIb	6.0	-	120680	6.15	0.315	6.53 ± 0.15	0.2919 ± 0.0125
	XVc	6.0	-	210681	7.20	0.206	7.32 ± 0.07	0.1911 ± 0.0086
7.6	VIb	6.0	+	210380	7.09	0.210	6.65 ± 0.19	0.2185 ± 0.0096 [†]
	XVc	6.0	+	010381	6.88	0.258	6.97 ± 0.08	0.2469 ± 0.0116
	III	7.0	+	170979	8.13	0.241	8.45 ± 0.11	0.2281 ± 0.0085
7.7	VIb	7.0	+	210380	8.20	0.271	8.81 ± 0.16	0.2444 ± 0.0108
	XVc	7.0	+	280681	8.64	0.218	9.09 ± 0.08	0.1902 ± 0.0109
	III	8.0	+	270979	10.37	0.226	10.56 ± 0.001	0.2106 ± 0.0043
7.8	VIb	8.0	+	210380	10.19	0.239	10.50 ± 0.002	0.2157 ± 0.0065
	XVc	8.0	+	010381	10.38	0.205	10.34 ± 0.001	0.2060 ± 0.0044
	III	7.0	+	170979	8.13	0.241	8.45 ± 0.11	0.2281 ± 0.0085
7.9	III	7.0	+	240979	7.80	0.256	7.86 ± 0.05	0.2512 ± 0.0043 [†]
	III	7.5	+	170979	9.20	0.261	9.56 ± 0.04	0.2349 ± 0.0141
	III	7.5	+	240979	8.67	0.284	9.83 ± 0.02	0.2492 ± 0.0126
	III	7.5	+	081079	8.90	0.284	8.87 ± 0.10	0.2660 ± 0.0102 [†]
7.10	III	7.5	+	160381	9.60	0.238	9.89 ± 0.01	0.2132 ± 0.0100
	III	8.5	+	270979	11.02	0.226	-	-
	III	8.5	+	160381	11.42	0.209	-	-
	VIb	6.0	-	210380	6.02	0.255	6.32 ± 0.14	0.2411 ± 0.0093
7.11	VIb	6.0	-	150580	5.80	0.262	6.13 ± 0.11	0.2418 ± 0.0085 [†]
	VIb	6.0	-	290580	6.20	0.293	6.36 ± 0.08	0.2842 ± 0.0075
	VIb	6.0	-	120680	6.15	0.315	6.53 ± 0.15	0.2919 ± 0.0125
	VIb	6.0	+	210380	7.09	0.210	6.65 ± 0.19	0.2185 ± 0.0096 [†]
7.12	VIb	6.0	+	150580	5.99	0.280	5.97 ± 0.06	0.2817 ± 0.0071 [†]
	VIb	6.0	+	290580	6.41	0.263	6.91 ± 0.15	0.2364 ± 0.0094
	VIb	6.0	+	290580	6.83	0.218	7.19 ± 0.26	0.2193 ± 0.0129
	VIb	6.0	+	120680	6.52	0.299	7.30 ± 0.22	0.2600 ± 0.0133
	XVc	6.0	-	210481	6.88	0.193	7.45 ± 0.18	0.1502 ± 0.0103
7.13	XVc	6.0	-	210681	7.20	0.206	7.32 ± 0.07	0.1991 ± 0.0086
	XVc	7.0	-	210481	7.60	0.251	7.74 ± 0.10	0.2475 ± 0.0206
7.14	XVc	7.0	-	280681	8.00	0.225	7.98 ± 0.12	0.2188 ± 0.0169

continued.

Table 7.7 cont.

Figure	MnO ₂	pH	glycine	exp. date	linear regression		non-linear regression [†]	
					log B	Γ_{max}	1. standard deviation (1 σ) log B	Γ_{max}
7.16	XVc	6.0	+	010381	6.88	0.258	6.97 ± 0.08	0.2469 ± 0.0116 [†]
	XVc	6.0	+	210681	7.96	0.150	8.01 ± 0.12	0.1475 ± 0.0129 [†]
	XVc	6.0	+	240781	7.23	0.155	7.74 ± 0.15	0.1371 ± 0.0077
7.17	XVc	7.0	+	010381	8.69	0.221	8.46 ± 0.15	0.2572 ± 0.0436 [†]
	XVc	7.0	+	280681	8.64	0.218	9.09 ± 0.08	0.1902 ± 0.0109
7.18	XVc	8.0	gly	010381	10.38	0.205	10.34 ± 0.001	0.2060 ± 0.0044
	XVc	8.0	asp	080481	10.19	0.238	-	-
	XVc	8.0	ala	080481	10.26	0.245	10.52 ± -	0.2176 ± -
	XVc	8.0	glu	080481	9.44	0.237	9.71 ± 0.01	0.2161 ± 0.0073
7.19	III	6.5	+	160381	7.87	0.239	6.43 ± 0.14	0.2136 ± 0.0097
	III	6.5	-	130979	6.50	0.284	6.50 ± 0.11	0.2737 ± 0.0098 [†]
7.20	VIIb	6.0	-	120680	6.15	0.315	6.53 ± 0.15	0.2917 ± 0.0125
	VIIb	6.0	+	120680	6.50	0.299	7.30 ± 0.22	0.2600 ± 0.0131
7.21	VIIb	6.0	-	290580	6.20	0.293	6.16 ± 0.08	0.2642 ± 0.0075
	VIIb	6.0	+	290580	6.41	0.261	6.41 ± 0.15	0.2363 ± 0.0094
7.22	VIIb	6.0	-	210380	6.02	0.255	6.32 ± 0.14	0.2411 ± 0.0093
	VIIb	6.0	-	210380	7.09	0.210	6.65 ± 0.19	0.2185 ± 0.0096 [†]
7.23	XVc	6.0	asp	210681	7.55	0.173	7.32 ± 0.08	0.1607 ± 0.0051
	XVc	6.0	-	210681	7.20	0.206	7.32 ± 0.07	0.1911 ± 0.0065 [†]
	XVc	6.0	gly	210681	7.26	0.150	8.01 ± 0.12	0.1475 ± 0.0129 [†]
7.24	XVc	6.0	-	210481	6.88	0.193	7.45 ± 0.18	0.1525 ± 0.0103
	XVc	6.0	+	010381	6.80	0.261	6.97 ± 0.08	0.2469 ± 0.0116 [†]
7.25	XVc	7.0	-	280681	8.00	0.225	7.98 ± 0.11	0.2182 ± 0.0169 [†]
	XVc	7.0	+	280681	8.64	0.218	9.09 ± 0.08	0.1902 ± 0.0109
7.26	XVc	7.0	-	210481	7.68	0.251	7.74 ± 0.10	0.2475 ± 0.0206 [†]
	XVc	7.0	+	010381	8.69	0.221	8.46 ± 0.15	0.2572 ± 0.0436
7.27	XXV-A	6.0	-	280581	5.64	0.038	5.20 ± 0.23	0.0320 ± 0.0024
	13	6.0	-	240781	5.93	0.148	5.82 ± 0.10	0.1542 ± 0.0115 [†]
7.28	XXV-A	6.0	+	280581	5.64	0.039	5.57 ± 0.20	0.0400 ± 0.0064 [†]
	13	6.0	+	190781	6.09	0.159	5.56 ± 0.14	0.1708 ± 0.0209 [†]
7.29	XXV-A	7.0	+	280581	7.43	0.032	8.17 ± 0.18	0.0238 ± 0.0029
	13	7.0	+	190781	7.58	0.144	7.54 ± 0.10	0.1443 ± 0.0122 [†]
7.30	XXV-A	8.0	+	280581	9.01	0.029	9.03 ± 0.004	0.0289 ± 0.0006
	13	8.0	+	190781	9.23	0.147	9.24 ± 0.02	0.1457 ± 0.0050
7.31	13	6.0	-	240781	5.93	0.148	5.82 ± 0.10	0.1542 ± 0.0115 [†]
	13	6.0	+	190781	6.09	0.159	5.96 ± 0.14	0.1708 ± 0.0209 [†]

- indicates parameters could not be calculated with UWIABS, no convergence within 50 iterations

† indicates a data set having a significant correlation between Γ_{max} and B at the 5% level (two-tailed t-test)

$$S_p = \sqrt{\frac{\text{d.o.f.}_1 \times (\text{std}_1)^2 + \text{d.o.f.}_2 \times (\text{std}_2)^2}{\text{d.o.f.}_1 + \text{d.o.f.}_2}} \quad (7.4)$$

$$\text{and } t_{\text{calc.}} = \frac{|p_1 - p_2|}{S_p \sqrt{\frac{1}{\text{obs}_1} + \frac{1}{\text{obs}_2}}} \quad (7.5)$$

in which p = parameter value (i.e. Γ_{max} or B)

d.o.f. = degrees of freedom

std = standard deviation^o

obs = number of observations

$t_{\text{calc.}}$ has to be compared with a t -value obtained from a t -distribution Table (Draper and Smith 1966) at the appropriate confidence level and combined degrees of freedom. If $t_{\text{calc.}} > t_{\text{Table}}$, then the hypothesis $p_1 = p_2$ is rejected. If $t_{\text{calc.}} < t_{\text{Table}}$, the hypothesis $p_1 = p_2$ is not rejected.

When comparing the linear- and non-linear regression values for Γ_{max} and B in Table 7.7, it can be concluded that the non-linear regression procedure increases the value for $\log B$ while reducing the value for Γ_{max} . This is due to the fact that the linear procedure puts more emphasis on the plateau part of the isotherm, from which Γ_{max} is derived. Therefore, using a non-linear regression procedure to estimate values for Γ_{max} and B is a step in the right direction.

However, when comparing the non-linear regression values for Γ_{max} and B for duplicate experiments and identically made surfaces in Table 7.7, large differences are apparent. These differences are partly due to

experimental fluctuations, but also partly due to the character of the model: If an experiment obtains more data at the lower (i.e. steeper) end of the isotherm, then a reasonable estimate is obtained for B, while the estimate for Γ_{\max} is not very accurate. If more data are obtained for the flat upper part of the isotherm, the estimate for Γ_{\max} will be accurate, while B is estimated too low. To amend this, a large number of data points is necessary over the entire range of the isotherm. It is more difficult to correct for the experimental fluctuations, because there seems to be no particular reason why they occur. One can only speculate that total surface area present is not always accurately determined and that local, irreversible precipitation processes may contribute to inaccurate and irreproducible results.

Although the use of a non-linear regression procedure to estimate proper values for Γ_{\max} and B is an improvement over the use of the linearized model, the problem of a non-constant value of B is not solved by using the Single Langmuir model.

The statistical tests performed in Table 7.8 (on the adsorption parameters obtained by non-linear regression) to compare the isotherms in Figures 7.1 to 7.31 show that for most Figures, the isotherms are statistically different. For Figures 7.1 to 7.4, only the isotherms for MnO_2 's VIb ('neutral') and VIIIb ('acid') are compared, because it was obvious from visual comparison that MnO_2 VIIb ('alkaline') differed considerably in adsorption behaviour from MnO_2 's VIb and XVC. MnO_2 's VIb and XVC appear to have similarities, but in none of the cases are the isotherms statistically indistinguishable.

Every comparison made for the 'neutral' surfaces III, VIb and XVC (Figures 7.5 to 7.8) resulted in statistically different isotherms,

except for one case at pH 8 (Figure 7.8) where the values of Γ_{\max} were statistically indistinguishable for two isotherms.

Duplicate isotherms for MnO_2 III ('neutral') at pH 7 and 7.5 (Figures 7.9 to 7.11) are statistically different, while the comparison made for pH 8.5 could not be tested statistically due to the fact that no values for B and Γ_{\max} could be obtained with the non-linear regression procedure.

Duplicate isotherms for MnO_2 VIb ('neutral') at pH 6 without glycine present (Figure 7.12) showed that several isotherms were statistically different, several were indistinguishable for either B or Γ_{\max} and in one case two isotherms were statistically indistinguishable for both B and Γ_{\max} . Duplicate isotherms for MnO_2 VIb ('neutral') at pH 6 in the presence of glycine (Figure 7.13) were statistically different, with the exception of two cases in which isotherms were indistinguishable for either B or Γ_{\max} , but never for both.

The duplicate isotherms for MnO_2 Xvc ('neutral') at pH 6 (no glycine, Figure 7.14) have statistically indistinguishable values for B, but differ for Γ_{\max} values. The duplicate isotherms at pH 6 (with glycine, Figure 7.16), and pH 7 (without glycine, Figure 7.15 and with glycine, Figure 7.17) are all statistically different, while the isotherms obtained at pH 8 could not be compared mutually due to lack of values for Γ_{\max} and B from non-linear regression.

The isotherms obtained in the presence and absence of glycine under identical pH-conditions for the 'neutral' MnO_2 's III, VIb and Xvc (Figures 7.19 to 7.25) are all statistically different.

No statistical tests were performed for the comparison of the isotherms for the naturally and artificially aged MnO_2 surfaces 13 and

Table 7.8 Comparison of non-linear regression values of the adsorption parameters Γ_{max} and B on the basis of a pooled t-test

Figure	MnO ₂	pH	glycine	exp. date	d.o.f.	$t_{\Gamma_{max}}$	t_B	$t_{d.o.f.,95\%}$	conclusion
7.1	Vib	6.0	-	210380	14	4.660	1.450	2.145	$\Gamma_1 = \Gamma_2$ rejected $B_1 = B_2$ not rejected
	VIIIb	6.0	-	020480					
7.2	Vib	6.0	+	210380	13	11.145	4.930	2.160	statistically different †
	VIIIb	6.0	+	020480					
7.3	Vib	7.0	+	210380	14	0.383	5.371	2.145	$\Gamma_1 = \Gamma_2$ not rejected $B_1 = B_2$ rejected
	VIIIb	7.0	+	020480					
7.4	Vib	8.0	+	210380	14	0.641	293	2.145	$\Gamma_1 = \Gamma_2$ not rejected $B_1 = B_2$ rejected
	VIIIb	8.0	+	020480					
7.5	III	6.0	-	130979	15	11.576	1.779	2.131	$\Gamma_1 = \Gamma_2$ rejected $B_1 = B_2$ not rejected
	Vib	6.0	-	120680					
	Vib	6.0	-	120680	13	19.162	13.899	2.160	statistically different
	XVc	6.0	-	210681					
	III	6.0	-	130979	14	9.762	15.196	2.145	statistically different
	XVc	6.0	-	210681					
7.6	Vib	6.0	+	210380	13	5.461	-5.431	2.160	statistically different †
	XVc	6.0	+	010381					
7.7	III	7.0	+	170979	14	3.576	4.375	2.145	statistically different
	Vib	7.0	+	210380					
	Vib	7.0	+	210380	13	10.309	5.190	2.160	statistically different
	XVc	7.0	+	280681					
	III	7.0	+	170979	13	8.076	11.889	2.160	statistically different
	XVc	7.0	+	280681					
7.8	III	8.0	+	270979	15	2.041	75.96	2.131	$\Gamma_1 = \Gamma_2$ not rejected $B_1 = B_2$ rejected
	Vib	8.0	+	210380					
	Vib	8.0	+	210380	14	3.721	174.58	2.145	statistically different
	XVc	8.0	+	010381					
	III	8.0	+	270979	15	2.316	361.30	2.131	statistically different
	XVc	8.0	+	010381					
7.9	III	7.0	+	170979 240979	13	6.95	8.26	2.160	statistically different †
7.10	III	7.5	+	170979 240979	14	2.273	19.891	2.145	statistically different
	III	7.5	+	170979 081079	15	5.571	26.257	2.131	statistically different †
	III	7.5	+	170979 160381	13	3.622	32.34	2.160	statistically different
	III	7.5	+	240979 081079	15	3.212	47.53	2.131	statistically different †
	III	7.5	+	240979 160381	13	6.469	7.284	2.160	statistically different
	III	7.5	+	081079 160381	14	11.028	83.170	2.145	statistically different
7.11	III	8.5	+	270979 160381	cannot be compared statistically, no values for B and Γ_{max}				
7.12	Vib	6.0	-	210380 150580	14	0.167	1.569	2.145	$\Gamma_1 = \Gamma_2$ not rejected † $B_1 = B_2$ not rejected
	Vib	6.0	-	210380 290580	14	10.858	0.169	2.145	$\Gamma_1 = \Gamma_2$ rejected $B_1 = B_2$ not rejected

continued.

Table 7.8 cont.

figure	MnO ₂	pH	glycine	exp. date	d.o.f.	t_{\max}	t_B	$t_{d.o.f., 95\%}$	conclusion	
7.12 (cont)	Vib	6.0	-	210380 120680	14	9.826	2.776	2.145	statistically different	
	Vib	6.0	-	150580 290580	14	1.278	7.375	2.145	$\Gamma_1 = \Gamma_2$ not rejected \dagger^x $B_1 = B_2$ rejected	
	Vib	6.0	-	150580 120680	14	9.970	4.914	2.145	statistically different	
	Vib	6.0	-	290580 120680	14	1.589	2.619	2.145	$\Gamma_1 = \Gamma_2$ not rejected $B_1 = B_2$ rejected	
7.13	Vib	6.0	+	210381 290580A	13	3.890	3.102	2.160	statistically different \dagger	
	Vib	6.0	+	210381 290580	13	0.144	3.312	2.160	$\Gamma_1 = \Gamma_2$ not rejected \dagger $B_1 = B_2$ rejected	
	Vib	6.0	+	210381 150580	13	15.670	5.427	2.160	statistically different \dagger	
	Vib	6.0	+	210381 120680	13	4.144	4.280	2.160	statistically different \dagger	
	Vib	6.0	+	290580A 290580	14	3.222	2.340	2.145	statistically different	
	Vib	6.0	+	290580A 150580	14	11.566	8.937	2.145	statistically different \dagger	
	Vib	6.0	+	290580A 120680	14	4.347	3.454	2.145	statistically different	
	Vib	6.0	+	150580 290580	14	11.264	4.195	2.145	statistically different \dagger	
	Vib	6.0	+	150580 120680	14	4.324	5.985	2.145	statistically different \dagger	
	Vib	6.0	+	120680 290580	14	6.602	0.987	2.145	$\Gamma_1 = \Gamma_2$ rejected $B_1 = B_2$ not rejected	
	7.14	XVc	6.0	-	210481 210681	11	7.215	1.410	2.201	$\Gamma_1 = \Gamma_2$ rejected $B_1 = B_2$ not rejected
	7.15	XVc	7.0	-	210481 280681	11	2.978	4.064	2.201	statistically different
7.16	XVc	6.0	+	010381 210681	9	13.913	11.893	2.262	statistically different \dagger	
7.17	XVc	7.0	+	010381 280681	13	4.203	11.298	2.160	statistically different \dagger	
7.18	XVc	8.0	gly gly asp ala	010381 080481 080481 080481	cannot be compared statistically, no values for B and t_{\max} from EWHAUS \dagger					
7.19	III	6.5	- +	140979 160381	14	13.076	13.825	2.145	statistically different \dagger	
7.20	Vib	6.0	+	120680 120680	14	5.253	4.949	2.145	statistically different	
7.21	Vib	6.0	+	290580 290580	14	11.925	6.346	2.145	statistically different	
7.22	Vib	6.0	+	210380 210380	13	4.953	3.406	2.160	statistically different \dagger	
7.23	XVc	6.0	+	210681 210681	8	7.263	9.458	2.306	statistically different \dagger	
	XVc	6.0	- asp	210681 210681	12	8.580	10.051	2.179	statistically different \dagger	
	XVc	6.0	gly asp	210681 210681	8	2.807	3.326	2.306	statistically different \dagger	
7.24	XVc	6.0	+	010381 210481	12	17.353	4.847	2.179	statistically different \dagger	
7.25	XVc	7.0	+	280681 280681	12	4.031	14.003	2.179	statistically different \dagger	
7.31	XVc	6.0	+	190781 240781	13	2.071	2.270	2.160	$\Gamma_1 = \Gamma_2$ not rejected \dagger^x $B_1 = B_2$ rejected	

\dagger involves data sets where one or the other or both have a significant correlation between t_{\max} and B

\times examination of the RSS surface of the joint probability distribution of the two parameters might provide a less ambiguous conclusion

XXV-A (Figures 7.26 to 7.30). Visual comparison indicated that these isotherms were vastly different. The comparison for MnO_2 13 in Figure 7.31 finally indicated that the isotherms obtained at pH 6 in the presence and absence of glycine are statistically different for B, but not for Γ_{max} .

It can be concluded from the above discussion and Tables that:

- The Single Langmuir model does not correct for deviations from linearity at low coverages of the surface. These deviations imply that the bindings strength is not constant throughout the isotherm.
- The use of a linearized Single Langmuir isotherm tends to overestimate the value for Γ_{max} and underestimate the value for B.
- It is inherent to the Langmuir model that datapoints at the lower end of the isotherm are responsible for the estimation of B, while data points at the upper end estimate Γ_{max} . A proper distribution of data points throughout the isotherm is necessary.
- The use of a non-linear Single Langmuir isotherm to estimate B and Γ_{max} is an improvement over the use of a linearized Single Langmuir model, since the former does not favour datapoints in a particular area of the isotherm. However, no correction is made for the fact that B is not constant throughout the isotherm.
- A large number of data points covering the whole area of the isotherm for each pH is necessary to obtain reasonable estimates for B and Γ_{max} , and to avoid strong effects from experimental fluctuations.
- Correlation coefficients between the Single Langmuir model parameters Γ_{max} and B were unacceptably high in a number of cases (see Appendix III).

7.3.3 The Double Langmuir Model

Loganathan and Burau (1973), for Co and Zn, and Gabano et al (1968), for Zn, have previously reported a deviation from Langmuir linearity at low coverages of the MnO_2 surface. Gabano et al (1968) make no attempt to explain this, but Loganathan and Burau (1973) ascribe this deviation to a second adsorption site on the MnO_2 surface, where Co and Zn exchange for Mn^{3+} and/or Mn^{2+} , from the $\delta\text{-MnO}_2$ lattice (see Chapter 5, Section 5.2). Although no evidence of exchanged Mn was found in solution in this study (see Chapter 6, Section 6.3.3), one could still argue in favour of the presence of a second adsorption site on the surface of MnO_2 , with different affinity for Cu.

If a much stronger binding site dominates the adsorption initially, while the other, weaker site becomes more important towards saturation of the stronger site, then this could explain both the curvature at the beginning and the straight(er) upper parts of the linearized Langmuir plots. Initially, B will change as a function of Γ_{ads} , until the stronger site is completely filled, after which B becomes constant.

The adsorption data from the previous section have therefore been fitted to such a Double Langmuir expression, using a non-linear regression fitting procedure (after Meeter 1965). The parameter values, 95% confidence limits and correlation coefficients can be found in Appendix III. Table 7.9 contains the parameter values for Γ_{max_1} , Γ_{max_2} , $\log B_1$, and $\log B_2$ and their standard deviations. No graphical presentation is given for this model.

Because only 8 to 10 datapoints are available per adsorption isotherm and the Double Langmuir model requires the estimation of 4

parameters, only 4 to 6 degrees of freedom remain after fitting. This is the reason that the 95% confidence limits for the estimated parameters are often rather large (see Appendix III). Estimates for parameters could not be obtained in all cases with the non-linear regression procedure, due to very slow convergence and/or exceeding of the computer output file (i.e. 50 iterations). Slow convergence was in most cases caused by the fact that the datapoints essentially fitted different functions than a Double Langmuir model, for instance a Single Langmuir equation (expression (7.1)) or functions of the forms:

$$\Gamma_{\text{ads}} = C + \Gamma_{m2} \frac{\text{Cu}^{2+}}{1/B + \text{Cu}^{2+}} \quad (7.6)$$

or

$$\Gamma_{\text{ads}} = \Gamma_{m1} \frac{\text{Cu}^{2+}}{1/B + \text{Cu}^{2+}} + C \cdot \text{Cu}^{2+} \quad (7.7)$$

It is expected that, if the adsorption data could be described accurately by the Double Langmuir model, a particular pattern for the parameters would emerge; i.e. more or less constant values for Γ_{m1} and Γ_{m2} with B-values affected in a similar way by pH variations. However, this appeared only so in a very small amount of cases. Using a t-test on pooled standard deviations, it can be shown that Double Langmuir isotherms that are not statistically different, can only be found in Figures 7.5, 7.9, 7.12 and 7.18. In all other cases, either the obtained parameter values are statistically different or there is no model fit, or the estimated parameters describe models that are essentially different from a Double Langmuir model. The following conclusions can therefore be drawn regarding this model:

Table 7.9 Comparison of the double Langmuir regression parameters

Fig.	MnO ₂	pH	gly.	exp.date	$r_{m_2} \pm 1\sigma$	$r_{m_2} \pm 1\sigma$	$\log B_1 \pm 1\sigma$	$\log B_2 \pm 1\sigma$	function
7.1	VIIb	6.0	-	210380	0.1463±0.0643	0.1373±0.0420	7.15±1.14	5.14±0.65	double Langmuir
	VIIb	6.0	-	070480	-	-	-	-	no fit
	VIIIB	6.0	-	020480	-	-	-	-	no fit
7.2	VII	6.0	+	210380	-	-	-	-	no fit
	VIIb	6.0	+	070480	0.0455± X	0.0365± X	6.38± X	6.38± X	double L., large errors
	VIIIB	6.0	+	020480	0.1460±0.0335	0.9542±1.1284	7.66±0.79	4.88±0.72	equation (7.7)
7.3	VIIb	7.0	+	210380	0.1652±0.0221	0.1355±0.0195	9.20±0.14	7.17±0.31	double Langmuir
	VIIb	7.0	+	070480	0.0476±0.0679	0.1528±0.0610	7.79±1.31	6.25±0.95	double Langmuir
	VIIIB	7.0	+	020480	0.1629±0.0163	0.6311±0.9395	8.77±0.10	5.99±0.85	double Langmuir
7.4	VIIb	8.0	+	210380	0.1510±0.0071	0.1240±0.0077	10.99±0.08	9.10±0.13	double Langmuir
	VIIb	8.0	+	070480	0.1878±0.1381	0.9183E-08± X	8.67±0.41	4.34± X	equation (7.7), large errors
	VIIIB	8.0	+	020480	0.1504±0.0106	0.0985±0.0076	10.55±0.11	8.84±0.14	double Langmuir
7.5	III	6.0	-	130979	0.1262±0.0465	0.1453±0.0347	7.38±0.94	5.31±0.43	double Langmuir
	VIIb	6.0	-	120680	0.1741±0.0232	0.1765±0.0176	7.30±0.24	5.26±0.22	double Langmuir
	XVc	6.0	-	210681	0.1252±0.0175	0.1072±0.0142	7.70±0.11	6.21±0.29	double Langmuir
7.6	VII	6.0	+	210380	-	-	-	-	no fit
	XVc	6.0	+	010381	-	-	-	-	no fit
7.7	III	7.0	+	170979	0.1698±0.0248	0.1169±0.0334	8.86±0.18	6.79±0.49	double Langmuir
	XVc	7.0	+	280681	0.1204±0.0141	0.1178±0.0122	9.66±0.14	7.64±0.24	double Langmuir
	VIIb	7.0	+	210381	0.1652±0.0221	0.1355±0.0195	9.20±0.14	7.17±0.31	double Langmuir
7.8	III	8.0	+	270979	0.1683±0.0062	0.1677±0.0614	10.81±0.04	8.76±0.30	double Langmuir
	VIIb	8.0	+	210380	0.1510±0.0071	0.1240±0.0077	10.99±0.08	9.10±0.13	double Langmuir
	XVc	8.0	+	010381	-	-	-	-	no fit
7.9	III	7.0	+	170979	0.1698±0.0248	0.1169±0.0334	8.86±0.18	6.79±0.49	double Langmuir
	III	7.0	+	240979	0.1636±0.1676	0.1177±0.1236	8.73±3.98	6.98±1.19	double L., large errors
7.10	III	7.5	+	170979	0.0868±0.0534	0.1777±0.0474	10.74±1.29	8.73±0.46	double Langmuir
	III	7.5	+	240979	0.1774±0.0162	0.2109±0.0583	2.70± X	7.61±0.33	equation (7.7)
	III	7.5	+	081079	-	-	-	-	no fit
	III	7.5	+	160381	0.1554±0.0198	0.1302±0.0388	10.16±0.09	8.23±0.52	double Langmuir
7.11	III	8.5	+	270979	-	-	-	-	no fit
	III	8.5	+	160381	-	-	-	-	no fit
7.12	VIIb	6.0	-	210380	0.1463±0.0643	0.1373±0.0420	7.15±1.14	5.14±0.65	double Langmuir
	VIIb	6.0	-	150580	-	-	-	-	no fit
	VIIb	6.0	-	290580	0.1523±0.0898	0.1535±0.0796	7.04±0.77	5.60±0.46	double Langmuir
	VIIb	6.0	-	120680	0.1741±0.0232	0.1765±0.0176	7.30±0.24	5.26±0.22	double Langmuir
7.13	VIIb	6.0	+	210380	-	-	-	-	no fit
	VIIb	6.0	+	150580	0.1441± X	0.1377± X	5.97± X	5.97± X	single L., large errors
	VIIb	6.0	+	290580	-	-	-	-	no fit
	VIIb	6.0	+	290580	-	-	-	-	no fit
	VIIb	6.0	+	120680	0.1680±0.0097	0.2143±0.0281	8.04±0.14	5.42±0.17	double Langmuir
7.14	XVc	6.0	-	210481	0.1065±0.0095	0.1191±0.0323	7.79±0.09	5.44±0.32	double Langmuir
	XVc	6.0	-	210681	0.1252±0.0175	0.1072±0.0142	7.70±0.11	6.21±0.29	double Langmuir
7.15	XVc	7.0	-	210481	0.1157± X	0.1317± X	7.74± X	7.74± X	single L., large errors
	XVc	7.0	-	280681	0.0479±0.0326	0.2041±0.0238	9.42±1.16	7.56±0.27	double Langmuir

continued...

Table 7.2 cont

Fig.	NaCl ₂	pH	gly.	exp. date	$\Gamma_{n_2} \pm 1\sigma$	$\Gamma_{n_2} \pm 1\sigma$	$\log B_1 \pm 1\sigma$	$\log B_2 \pm 1\sigma$	function
7.16	XVc	6.0	+	010381	-	-	-	-	no fit
	XVc	6.0	+	210681	0.1475? ?	0.3867E-09? ?	8.01? ?	4.59? ?	equation (7.7)
	XVc	6.0	+	240781	0.0954±0.0095	0.1115±0.0378	8.13±0.11	5.85±0.37	double Langmuir
7.17	XVc	7.0	+	010381	0.1799± X	0.0772± X	8.46± X	8.46± X	single L., large errors
	XVc	7.0	+	280681	0.1204±0.0141	0.1178±0.0122	9.66±0.14	7.64±0.24	double Langmuir
7.18	XVc	8.0	gly	010391	-	-	-	-	no fit
	XVc	8.0	asp	080481	0.1326±0.0135	0.3245±0.1942	10.88±0.09	8.81±0.43	double Langmuir
	XVc	8.0	ala	050481	0.1447±0.0111	0.2262±0.0881	11.09±0.10	8.79±0.34	double Langmuir
	XVc	8.0	glu	080481	0.1582±0.0114	0.5545±1.3603	10.14±0.10	7.49±1.29	double Langmuir
7.19	III	6.5	+	160381	0.1610±0.0234	0.1836±0.1579	8.66±0.13	6.09±0.82	double Langmuir
	III	6.5	-	150579	0.1403± X	0.1334± X	6.51± X	6.51± X	single L., large errors
7.20	VIIb	6.0	-	120680	0.1741±0.0232	0.1765±0.0176	7.30±0.24	5.26±0.22	double Langmuir
	VIIc	6.0	+	120680	0.1680±0.0097	0.2143±0.0281	8.04±0.14	5.42±0.17	double Langmuir
7.21	VIIb	6.0	-	290581	0.1523±0.0898	0.1535±0.0796	7.04±0.77	5.60±0.46	double Langmuir
	VIIb	6.0	+	290580	-	-	-	-	no fit
7.22	VIIc	6.0	-	210390	0.1463±0.0643	0.1373±0.0420	7.15±1.14	5.14±0.65	double Langmuir
	VIIc	6.0	+	210380	-	-	-	-	no fit
7.23	XVc	6.0	asp	210681	0.1339±0.0102	0.0790±0.0464	8.01±0.08	6.02±0.62	double Langmuir
	XVc	6.0	-	210681	0.1252±0.0175	0.1072±0.0142	7.70±0.11	6.21±0.29	double Langmuir
	XVc	6.0	gly	210681	0.1475? ?	0.3867E-09? ?	8.01? ?	4.59? ?	equation (7.7) unknown errors
7.24	XVc	6.0	-	210481	0.1065±0.0095	0.1191±0.0323	7.79±0.09	5.44±0.32	double Langmuir
	XVc	6.0	+	010381	-	-	-	-	no fit
7.25	XVc	7.0	-	280681	0.0479±0.0326	0.2041±0.0238	9.42±1.16	7.56±0.27	double Langmuir
	XVc	7.0	+	280681	0.1204±0.0141	0.1178±0.0122	9.66±0.14	7.64±0.24	double Langmuir
7.26	XVc	7.0	-	210481	0.1157± X	0.1317± X	7.74± X	7.74± X	single L., large errors
	XVc	7.0	+	010381	0.1799± X	0.0772± X	8.46± X	8.46± X	single L., large errors
7.27	XXV-A	6.0	-	280581	-	-	-	-	no fit
	13	6.0	-	240781	0.1503± X	0.1421± X	18.02± X	7.21± X	equation (7.6) large errors
7.28	XXV-A	6.0	+	280581	-	-	-	-	no fit
	13	6.0	+	190781	-	-	-	-	no fit
7.29	XXV-A	7.0	+	280581	-	-	-	-	no fit
	13	7.0	+	190781	0.0501±0.0248	0.2574±0.2184	8.25±0.34	6.57±0.68	double Langmuir
7.30	XXV-A	8.0	+	280581	0.1472±1.1189	0.1685E-08± X	8.93±3.81	4.42± X	equation (7.7), large errors
	13	8.0	+	190781	0.0693±0.0239	1.287±12.626	9.73±0.21	7.32±4.65	double Langmuir, large errors
7.31	13	6.0	-	240781	0.1503± X	0.1421± X	18.02± X	7.21± X	equation (7.6), large errors
	13	6.0	+	190781	-	-	-	-	no fit

- could not be determined

X large number

? no standard deviations given

- no particular pattern exists in the values for Γ_{m_1} , Γ_{m_2} , B_1 and B_2 for duplicate experiments and/or identical surfaces.
- a considerable number of data sets could not be fitted to the Double Langmuir model. Either no fit at all was obtained, or an essentially different function emerged from the fitting procedure.
- The number of degrees of freedom is rather small, due to a maximum of 10 datapoints while 4 parameters need to be estimated per isotherm. The datasets that can be fitted to a Double Langmuir model, can therefore be fitted rather well (i.e. Residual Sum of Squares is small) but the 95% confidence limits for the parameters are generally large, see Appendix III).
- Correlation coefficients between the parameters (see Appendix III) were unacceptably high for almost all cases.

7.3.4 The Implicit Langmuir Model

The adsorption data presented in Figures 7.1 to 7.31 have also been fitted to the Implicit Langmuir model. This model was derived in Chapter 5 (Section 5.3.3). It contains a correction for the fact that the bindings energy is not constant but changes with increasing adsorption density on the surface. It also incorporates the pH in the overall bindings energy which means that for this model, all data obtained per surface, can be used to estimate its three parameters. This improves the statistics considerably, and makes the model very general.

A non-linear regression procedure (computer program UWHAUS, after Meeter 1965) was used to fit the data to the model. In Chapter 5 (Section 5.3.3), the model was derived in the following form:

$$\Gamma_{\text{ads}} = \Gamma_{\text{max}} \frac{\text{Cu}^{2+}}{\frac{(\text{H}^+)^n}{B e^{(1-\Gamma_{\text{ads}}/\Gamma_{\text{max}})}} + \text{Cu}^{2+}} \quad (7.3)$$

in which term $(\text{H}^+)^n / B e^{(1-\Gamma_{\text{ads}}/\Gamma_{\text{max}})}$ predicts the overall bindings energy. To facilitate computer fitting and to avoid negative values for the parameter B in the above expression, the term for the bindings energy can be written as:

$$\text{bindings energy} = (\text{H}^+)^n / 10^b \cdot e^{(1-\Gamma_{\text{ads}}/\Gamma_{\text{max}})} \quad (7.8)$$

and the parameters to be estimated for the Implicit Langmuir model are Γ_{max} , n and b.

Table 7.10 contains the values for the adsorption parameters for MnO_2 surfaces III, VIb, XVc (all 'neutral' surfaces), VIIb ('acid'), VIIIb ('alkaline'), 13 (naturally aged) and XXV-A (artificially aged). For MnO_2 III, 1979 and 1981 data are fitted separately. The data obtained for MnO_2 III in 1981 can therefore also be used for model verification, which is shown in Figures 7.35 to 7.37. Figures 7.38 to 7.40 illustrate how the Implicit Langmuir model predicts the deviation from linearity, when linearizing the model.

Figures 7.35, 7.36 and 7.37 indicate an excellent coincidence of model predictions and observations that were not used to establish the model, with one exception. At pH 6.0, at the lower end of the isotherm, estimates are below the observed values. This generally good agreement between model predictions and observations underscribes the validity of the Implicit Langmuir model and at the same time the stability of the

MnO₂ III surface; the Implicit Langmuir parameters were calculated from experiments performed in 1979, while the verification experiments were performed in 1981, 1 1/2 - 2 years later, on the same surface. It is felt that such a verification gives the model good credibility.

Figures 7.38 shows how the Implicit Langmuir model predicts the deviation from linearity at the lower end of the isotherm for MnO₂ VIIb at pH 6. The model predictions agree very well with actual observations for MnO₂ VIIb at pH 6, presented in Figure 7.32. Figure 7.39 shows linearized predictions for MnO₂ III at pH 7.5 and compares reasonably well with actual data for MnO₂ III at pH 7.5 presented in Figure 7.33. The predictions for MnO₂ VIb at pH 6, shown in Figure 7.40, also agree well with the actual data obtained for MnO₂ VIb at pH 6, as illustrated in Figure 7.34.

The parameter values in Table 7.10 can be compared statistically with the use of a t-test. For MnO₂'s VIIb, VIIIb, 13 and XXV-A, the differences are obvious. Of the four, 'neutral' surfaces, the parameters for MnO₂ Xvc are clearly different, but for MnO₂'s III and VIb, the parameter values seem very similar and the standard deviations of the parameters for MnO₂'s III and VIb overlap. However, a t-test showed that they are statistically different. This may be due to the large number of degrees of freedom and the chemical meaning of such a t-test is doubtful in this case.

For the Implicit Langmuir model, the following conclusions can be drawn:

- The model predicts deviation from linearity at the lower end of the isotherm.
- The deviation from linearity predicted by the model agrees

Table 7.10 Model parameters for the Implicit Langmuir model

MnO ₂	# of data used	$\Gamma_{\max} \pm 1\sigma$	$n \pm 1\sigma$	$b \pm 1\sigma$
III (neutral) (1979 data)	95	0.2425±0.0054	1.852±0.054	-4.782±0.432
III (neutral) (1981 data)	25	0.2271±0.0276	1.754±0.156	-3.963±1.329
Vib (neutral)	97	0.2543±0.0057	1.874±0.064	-4.828±0.423
XVc (neutral)	112	0.1988±0.0076	1.655±0.063	-3.119±0.453
VIIb (alkaline)	34	0.1613±0.0126	1.770±0.046	-5.563±0.343
VIIIb (acid)	36	0.2502±0.0123	1.439±0.128	-1.969±0.984
13 (naturally aged)	33	0.1709±0.0123	1.604±0.032	-4.018±0.268
XXV-A (artificially aged)	30	0.0365±0.0032	1.519±0.070	-3.559±0.546

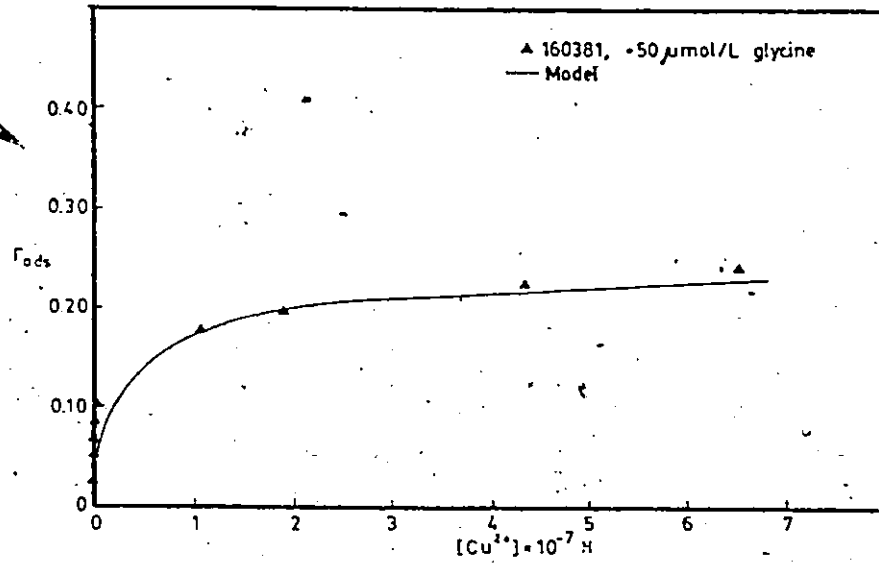


Figure 7.35 Verification of the Implicit Langmuir model for MnO_2 III, at pH 6.5, with new data (1981) for MnO_2 III.

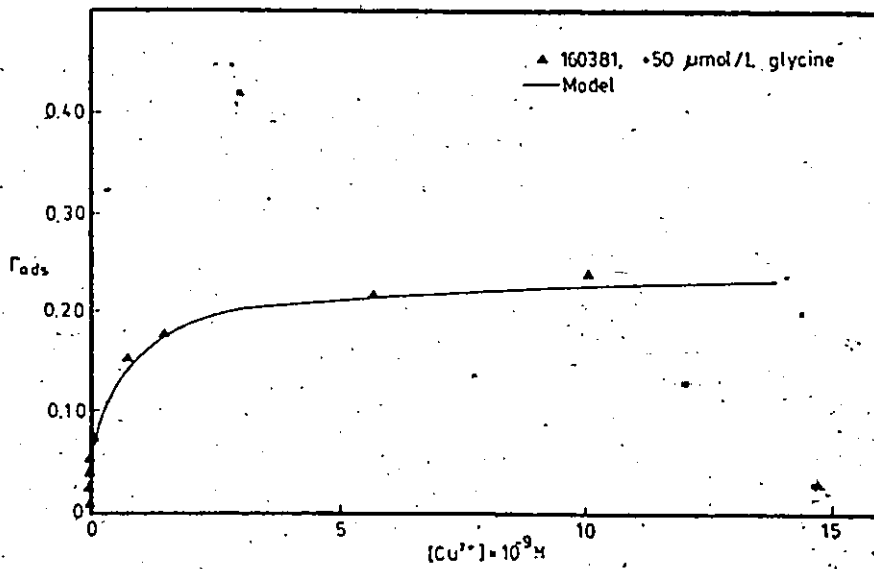


Figure 7.36 Verification of the Implicit Langmuir model for MnO_2 III with new (1981) data for MnO_2 III, at pH 7.5.

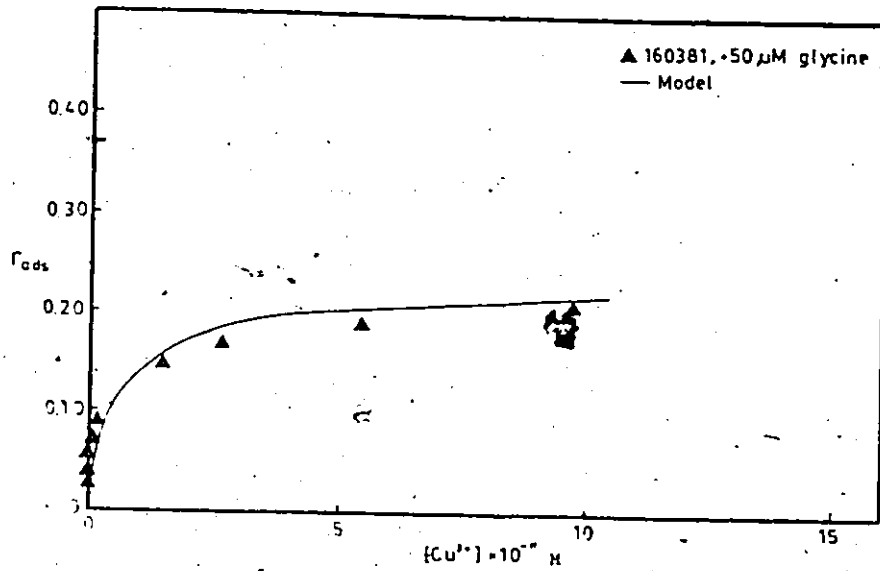


Figure 7.37 Verification of the Implicit Langmuir model for MnO_2 III with new (1981) data for MnO_2 III, at pH 8.5.

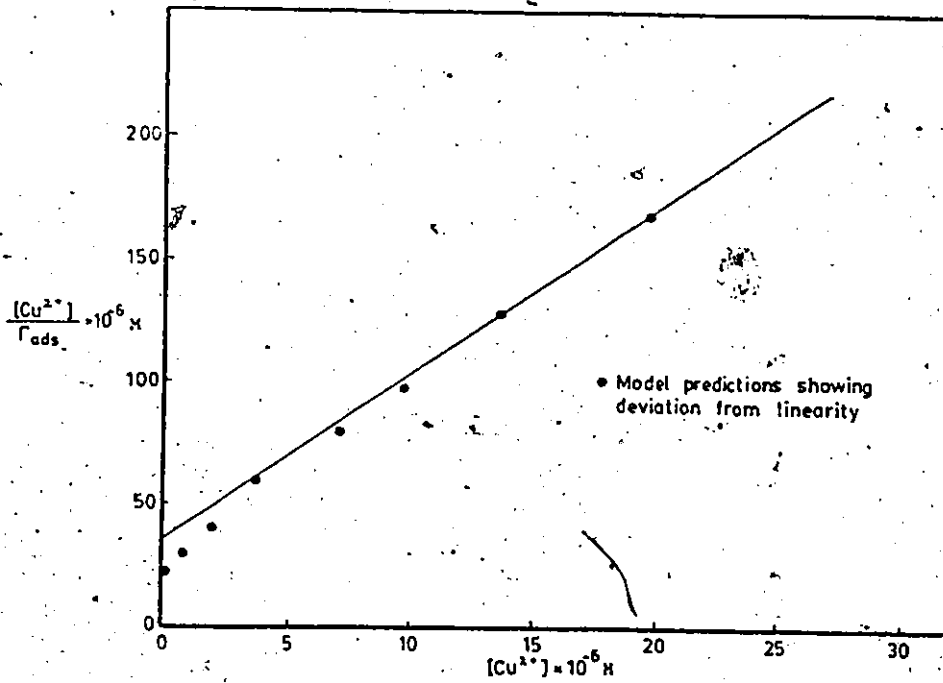


Figure 7.38 Linearized Implicit Langmuir model for MnO_2 VIIb ('alkaline'), at pH 6.0 (compare MnO_2 VIIb data in Figure 7.32).

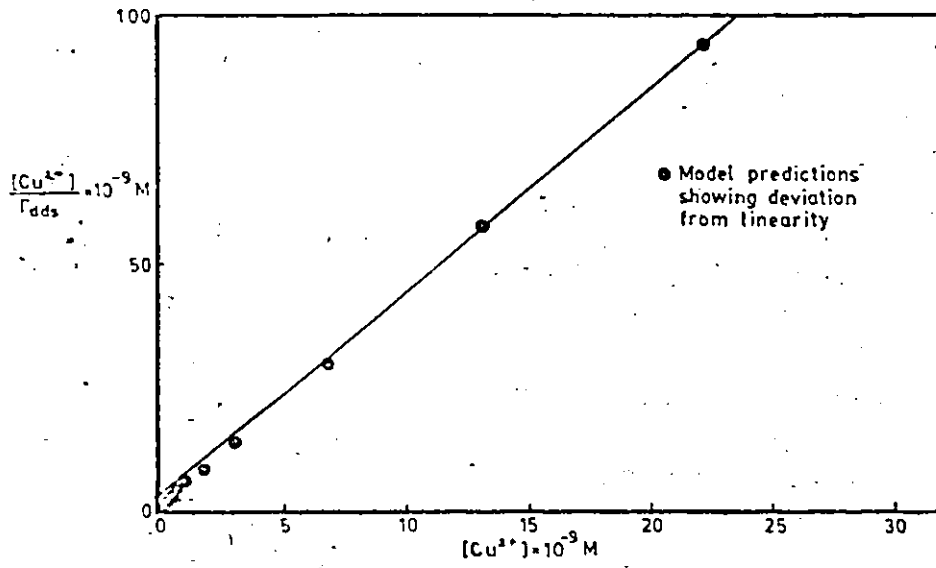


Figure 7.39 Linearized Implicit Langmuir model for MnO_2 III ('neutral') at pH 7.5

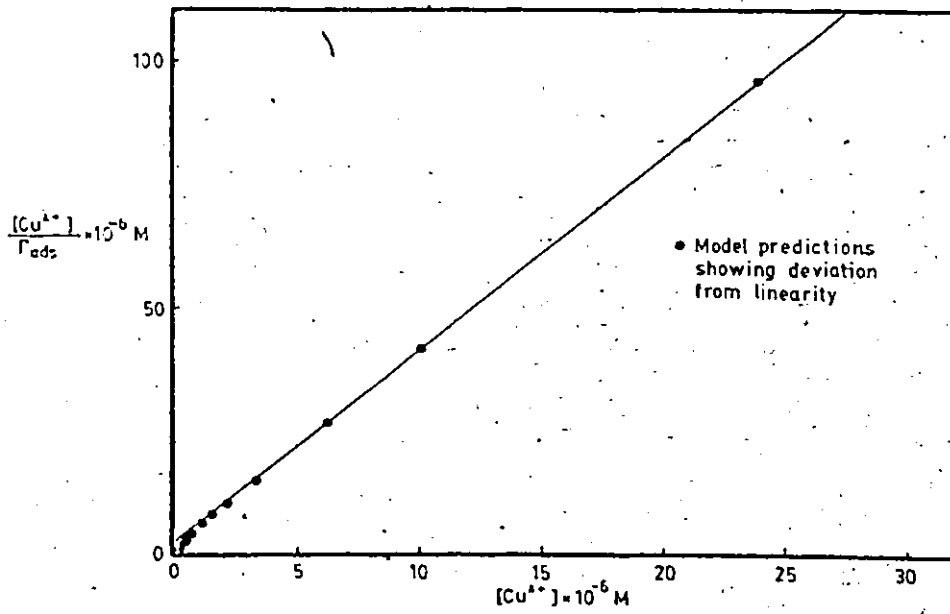


Figure 7.40 Linearized Implicit Langmuir model for MnO_2 VIb ('neutral') at pH 6

generally well with observations.

- Model verification with data that were not used to establish the model parameters is good.
- The model incorporates the pH in the term representing the bindings energy, which makes the model very general.
- Model parameters for three of four 'neutral' MnO_2 surfaces are very similar and their standard deviations overlap. However, a t-test indicated that these model parameters are statistically different, but the chemical meaning of this is doubtful.

7.3.5 Comparison of Model Fit for the Single-, Double- and Implicit Langmuir Models

In Sections 7.3.2 to 7.3.4 the Single-, the Double- and the Implicit Langmuir models were discussed with respect to the adsorption data. The fit of these models to the data can be likened to each other by comparing the Residual Sums of Squares after Regression. Table 7.11 gives the values for the summation of Residual Sum of Squares (ERSS) for the four 'neutral' MnO_2 's III (1979), III (1981), VIb and Xvc, the 'alkaline' MnO_2 VIIb, the 'acid' MnO_2 VIIIb, the naturally aged MnO_2 13 and the artificially aged MnO_2 XXV-A. For the Single- and Double-Langmuir models, several data sets did not result in a model fit, and hence ERSS does not include a value for RSS for these data sets. In Table 7.11 it is indicated how many data sets could not contribute to ERSS. The individual values of RSS for each data set can be found in Appendix III.

From Table 7.11 the following general trends can be derived: ERSS for model 1 (Single Langmuir) and model 3 (Implicit Langmuir) are generally in the same order of magnitude and do not differ more than a

factor 2 or 3. Σ RSS for model 1 is always lower than for model 3, which is not surprising, since model 1 is much less general than model 3, and the fit can therefore be much closer. The picture for model 2 is less clear: for MnO_2 's III (1981), VIb, Xvc and VIIIb the values for Σ RSS are 1 to 2 orders of magnitude smaller than for models 1 and 3. However, for MnO_2 's III (1979) and VIIb they are of the same order of magnitude, while for MnO_2 's 13 and XXV-A they are 2 orders of magnitude larger. Also, Σ RSS values for model 2 are incomplete by as much as 4 data sets. Moreover, model 2 is even more specific (i.e. less general) than model 1, and a good fit (with large confidence limits but small RSS) is relatively easy to obtain.

The comparison in Table 7.11 is made in an attempt to facilitate the ultimate choice of a model as the best one to describe adsorption of Cu onto δ - MnO_2 . However, in that respect, Table 7.11 is not very helpful, because it merely compared values for Σ RSS without regard for other model characteristics such as prediction of non-linearity, generality, etc. Therefore, Table 7.12 is composed to compare the features of each model on a more realistic basis. This comparison clearly shows the superiority of the Implicit Langmuir model, with its main merits of generality and proper prediction of non-linearity.

7.3:6 Bindings Energy Variations and Kurbatov Plots for the Implicit Langmuir Model

The Implicit Langmuir model appears to be the best model to describe the adsorption of Cu onto δ - MnO_2 from the comparison made in Table 7.12. In this Section, the dependence of the bindings energy on the surface coverage and the solution pH, is illustrated. The meaning of the

Table 7.11 Comparison of model fit by means of Residual Sums of Squares (RSS) after regression

MnO ₂ III (neutral)	model 1* ERSS = 0.305 E-01	excludes 1 set
	model 2 ERSS = 0.640 E-01	excludes 3 sets
	model 3 RSS = 0.524 E-01	includes all sets
MnO ₂ III (new) (neutral)	model 1 ERSS = 0.047 E-01	excludes 1 set
	model 2 ERSS = 0.005 E-01	excludes 1 set
	model 3 RSS = 0.370 E-01	includes all sets
MnO ₂ VIb (neutral)	model 1 ERSS = 0.380 E-01	includes all sets
	model 2 ERSS = 0.031 E-01	excludes 4 sets
	model 3 RSS = 0.868 E-01	includes all sets
MnO ₂ XVe (neutral)	model 1 ERSS = 0.213 E-01	excludes 1 set
	model 2 ERSS = 0.059 E-01	excludes 2 sets
	model 3 RSS = 1.290 E-01	includes all sets
MnO ₂ VIIb (alkaline)	model 1 ERSS = 0.166 E-02	includes all sets
	model 2 ERSS = 0.101 E-02	excludes 1 set
	model 3 RSS = 0.638 E-02	includes all sets
MnO ₂ VIIIb (acid)	model 1 ERSS = 0.197 E-01	includes all sets
	model 2 ERSS = 0.011 E-01	excludes 1 set
	model 3 RSS = 0.553 E-01	includes all sets
MnO ₂ 13 (van den Berg) (naturally aged)	model 1 ERSS = 0.194 E-02	includes all sets
	model 2 ERSS = 35.83 E-02	excludes 1 set
	model 3 RSS = 0.300 E-02	includes all sets
MnO ₂ XXV-A (artificially aged)	model 1 ERSS = 0.449 E-03	includes all sets
	model 2 ERSS = 22.02 E-03	excludes 3 sets
	model 3 RSS = 0.459 E-03	includes all sets

* model 1 = Single Langmuir
 model 2 = Double Langmuir
 model 3 = Implicit Langmuir

Table 7.12 Comparison of model features for the Single-, Double and Implicit-Langmuir models

model features	Single Langmuir	Double Langmuir	Implicit Langmuir
generality ¹	-	--	++
ease of model fitting ²	+	--	++
parameter comparison ³	±-	-	±
prediction of non-linearity ⁴	-	+	+
model fit by ERSS ⁵	+	±	-

1 Does the model allow use of all data in one model fit, ie. is the pH incorporated in the model?

2 Can a fit be obtained for each data set with non-linear regression analysis?

3 Are parameter values statistically indistinguishable (t-test)?

4 Does the model predict deviation from linearity at the lower end of a linearized isotherm?

5 Does the model fit result in a small value for the overall sum of RSS after regression?

parameter n is discussed in relation to so-called Kurbatov plots.

Table 7.13 presents Implicit Langmuir values for the bindings energy for most of the MnO_2 surfaces discussed in this Chapter. The values are given as negative logarithms (pB), calculated with the appropriate Implicit Langmuir expression, at pH 6.0 to 8.0, for respectively no adsorption and maximum adsorption. The results in Table 7.13 show that the 'neutral' MnO_2 's III and VIb are very similar in pB values, while the 'neutral' MnO_2 Xvc agrees better with these two as the pH increases. MnO_2 's VIIb ('alkaline'), VIIIb ('acid') and 13 (naturally aged) fall below the neutrally prepared surfaces in values for pB , while MnO_2 VIIIb approaches the 'neutral' MnO_2 's closest.

A few words should be said about the meaning of the Implicit Langmuir parameter n . In Chapter 5, possibilities for measuring the ratio of H^+ released per amount of metal adsorbed (Y) on hydrous MnO_2 are discussed, while Table 5.3 summarizes literature values for Y . Kurbatov plots of $\log(M^{n+})_{\text{adsorbed}} / (M^{n+})_{\text{solution}}$ versus pH, which should yield a straight line with a slope indicating the ratio Y , are criticized (Morgan and Stumm 1964, Posselt et al. 1968a) because sorbent activity is not constant during progressing adsorption. However, the Implicit Langmuir model does correct for this via the $\exp(1 - \Gamma_{\text{ads}} / \Gamma_{\text{max}})$ factor and n can therefore be considered as the number of moles of H^+ released per mole of Cu^{2+} specifically adsorbed.

Table 7.13 Comparison of bindings constants (log B) for the Implicit Langmuir models, for the various MnO_2 's involved in this study, at pH values of 6, 7 and 8

no adsorption	δ - MnO_2 surfaces					
	III	Vib	XVc	VIIb	VIIb'	13
$\Gamma_{ads} = 0$						
pH = 6.0	6.73	6.84	7.26	5.49	7.11	6.09
pH = 7.0	8.60	8.72	8.90	7.26	8.54	7.75'
pH = 8.0	10.46	10.60	10.55	9.03	9.97	9.41
maximum adsorption						
$\Gamma_{ads} = \Gamma_{max}$						
pH = 6.0	6.30	6.41	6.83	5.06	6.68	5.65
pH = 7.0	8.16	8.29	8.47	6.83	8.10	7.32
pH = 8.0	10.03	10.16	10.11	8.59	9.53	8.98

Table 7.14 Possible adsorption reactions for Cu on MnO₂

1. Monodentate $\text{MnOH}^{\circ} + \text{Cu}^{2+} \rightarrow \text{MnO}^{-}\text{-Cu}^{2+} + \text{H}^{+}$
2. Bidentate $2\text{MnOH}^{\circ} + \text{Cu}^{2+} \rightarrow \begin{array}{c} \text{MnO}^{-} \\ \diagdown \\ \text{Cu}^{2+} \\ \diagup \\ \text{MnO}^{-} \end{array} + 2\text{H}^{+}$
3. Hydrolysis prior to adsorption $\text{MnOH}^{\circ} + \text{CuOH}^{+} \rightarrow \text{MnO}^{-}\text{-CuOH}^{+} + \text{H}^{+}$
4. Surface hydrolysis $\text{MnOH}^{\circ} + \text{Cu}^{2+} + \text{H}_2\text{O} \rightarrow \text{MnO}^{-}\text{-CuOH}^{+} + 2\text{H}^{+}$

As already discussed in Chapter 5, there are several ways in which Cu can adsorb on MnO_2 . Table 7.14 illustrates this.

The second and fourth reaction can produce 2H^+ per Cu^{2+} , while only reaction 1 can bring about charge reversal of the diffuse double layer. Reaction 3 has not directly been considered in the derivation of the Implicit Langmuir model (see Chapter 5, Section 5.3.3). Some researchers (e.g. James and Healy 1972) argue in favour of reaction 3, others, for instance Stumm et al. (1976), do not find it necessary to invoke hydrolysis prior to adsorption and choose reaction 4; while Loganathan and Bureau (1977) regard both reactions as possible explanations for their observed results. If CuOH^+ would adsorb, one could argue that one then has to set up the Langmuir isotherm dependent on CuOH^+ (e.g. plot CuOH^+ versus $\text{CuOH}^+/\Gamma_{\text{ads}}$) instead of Cu^{2+} , but the CuOH^+ concentration is dependent on both the Cu^{2+} concentration and the pH and these factors are both already included in the Implicit Langmuir isotherm. This can be easily seen as follows:

$$\text{Assume: } \Gamma_{\text{ads}} = \frac{\Gamma_{\text{max}} \cdot \text{CuOH}^+}{\frac{(\text{H}^+)^n}{\text{B.e.} (1 - \Gamma_{\text{ads}}/\Gamma_{\text{max}})} + \text{CuOH}^+} \quad (7.9)$$

$$\frac{(\text{Cu}^{2+})(\text{OH}^-)}{(\text{CuOH}^+)} = 10^{-6} \quad \text{and} \quad (\text{CuOH}^+) = (\text{Cu}^{2+})/(\text{H}^+) \cdot 10^{-8}$$

(see Appendix II for stability constants)

$$\text{then: } \Gamma_{\text{ads}} = \frac{\Gamma_{\text{max}} \cdot (\text{Cu}^{2+})/(\text{H}^+) \cdot 10^{-8}}{\frac{(\text{H}^+)^n}{\text{B.e.} (1 - \Gamma_{\text{ads}}/\Gamma_{\text{max}})} + (\text{Cu}^{2+})/(\text{H}^+) \cdot 10^{-8}}$$

$$\begin{aligned}
 &= \frac{\Gamma_{\max} \cdot \text{Cu}^{2+}}{B \cdot 10^{-8} \cdot e^{(1-\Gamma_{\text{ads}}/\Gamma_{\max})} \cdot (\text{H}^+)^n \cdot \text{H}^+} + \text{Cu}^{2+} \\
 &= \frac{\Gamma_{\max} \cdot \text{Cu}^{2+}}{B' \cdot e^{(1-\Gamma_{\text{ads}}/\Gamma_{\max})} \cdot (\text{H}^+)^{n'}} + \text{Cu}^{2+} \tag{7.10}
 \end{aligned}$$

which shows that the Implicit Langmuir model does accommodate possible adsorption of CuOH^+ as well as the other three reactions as seen from the derivation of the Implicit Langmuir model in Chapter 5, Section 5.3.3.

Table 7.10 illustrates that the n values found for the $\delta\text{-MnO}_2$ surfaces involved in this study lie between 1.5 and 2. Combined with the fact that some researchers report a charge reversal of the diffuse double layer upon adsorption, it must be concluded that most likely a combination of the above four reactions occurs during adsorption. Note that the Implicit Langmuir model assumes that the percentage of each participating reaction is constant throughout the pH region investigated (pH 6-8.5). This does not seem to cause grave problems considering the reasonable fit of the data to the model and the fact that the values for log B calculated with the Single Langmuir model seem to increase linearly with pH in most cases as can be seen from log B values in Table 7.7.

Kurbatov plots for the Implicit Langmuir model will produce a straight line with slope n and a varying intercept depending on the value of Γ_{ads} :

$$\log (\Gamma_{\text{ads}} / \text{Cu}^{2+}) = n \text{ pH} + \log B + \log \frac{(\Gamma_{\max} - \Gamma_{\text{ads}})}{e^{(\Gamma_{\text{ads}}/\Gamma_{\max} - 1)}} \tag{7.11}$$

(Compare expression (7.11) to a single Langmuir Kurbatov plot which has the form:

$$\log (\Gamma_{\text{ads}} / \text{Cu}^{2+}) = n \text{ pH} + \log B + \log (\Gamma_{\text{max}} - \Gamma_{\text{ads}}) \quad (7.12)$$

Figures 7.41 - 7.46 show Kurbatov plots of the Implicit model for MnO_2 's III, VIb and XVC ('neutral'), VIIb ('alkaline'), VIIIb ('acid') and 13 (naturally aged). The solid lines represent the model predictions at several values of Γ_{ads} , while the symbols depict actual data points at Γ_{ads} values close to those used in the model calculations. However, this necessarily leads to a spread in the Γ_{ads} values used, which is indicated in the caption of the Figures.

The fit for MnO_2 III (Figure 7.41) is good at higher coverage of the surface, but there appears to be a deviation from the model at lower pH values when surface coverage is scanty.

MnO_2 VIb (Figure 7.42) shows reasonable agreement between model and observations, perhaps with the exception of the lower $\Gamma_{\text{ads}} = 0.11$ value.

Figure 7.43 illustrates very good agreement between model and data for MnO_2 XVC, at low surface coverages, with a slight deviation at pH 6.0. At adsorption levels close to maximum capacity however, model predictions stay far below the actual observations, although the slope of the line seems quite correct. Reasons for this must be sought in the fact that most data obtained for MnO_2 were in the lower surface coverage range.

Model calculations and actual data points agree reasonably well for both MnO_2 's VIIb and VIIIb (Figures 7.44 and 7.45). For MnO_2 13

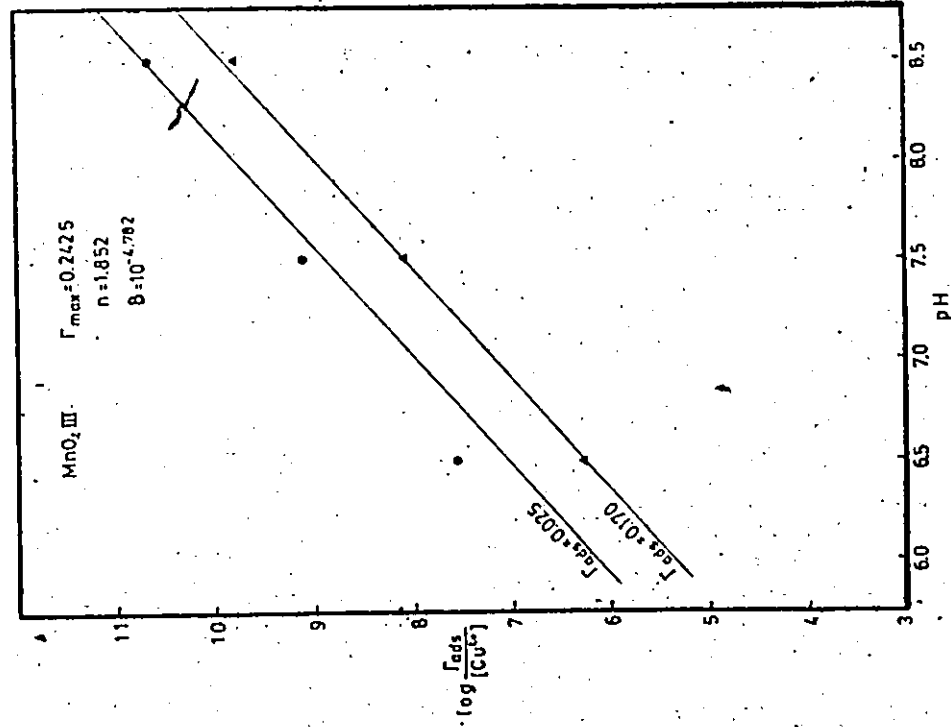


Figure 7.41 Kurbatov plot of the Implicit Langmuir model for MnO₂ III.

- exp. 160381 0.0247 $\Gamma_{ads} < 0.0257$ (+glycine)
- ▲ exp. 160381 0.165 $\Gamma_{ads} < 0.178$ (+glycine)
- model predictions at various values of Γ_{ads}

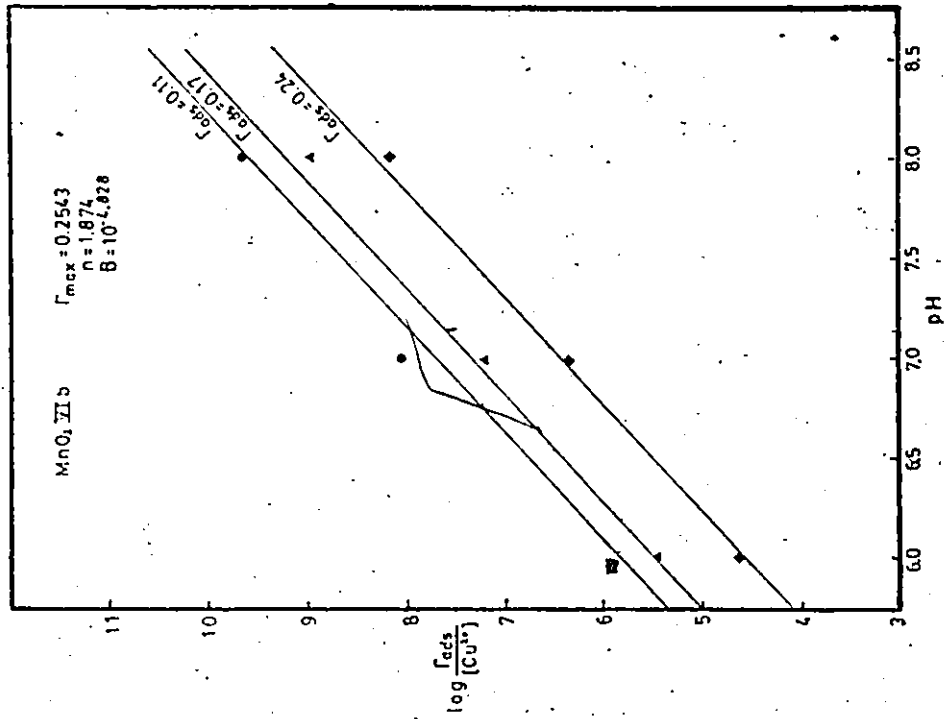


Figure 7.42 Kurbatov plot of the Implicit Langmuir model for MnO₂ VIIb.

- exp. 210380 (+glycine) 0.1094 $\Gamma_{ads} < 0.114$
- ▲ exp. 210380 (+glycine) 0.1634 $\Gamma_{ads} < 0.171$
- ◆ exp. 210380 (+glycine) 0.2365 $\Gamma_{ads} < 0.242$
- model predictions at various values for Γ_{ads}

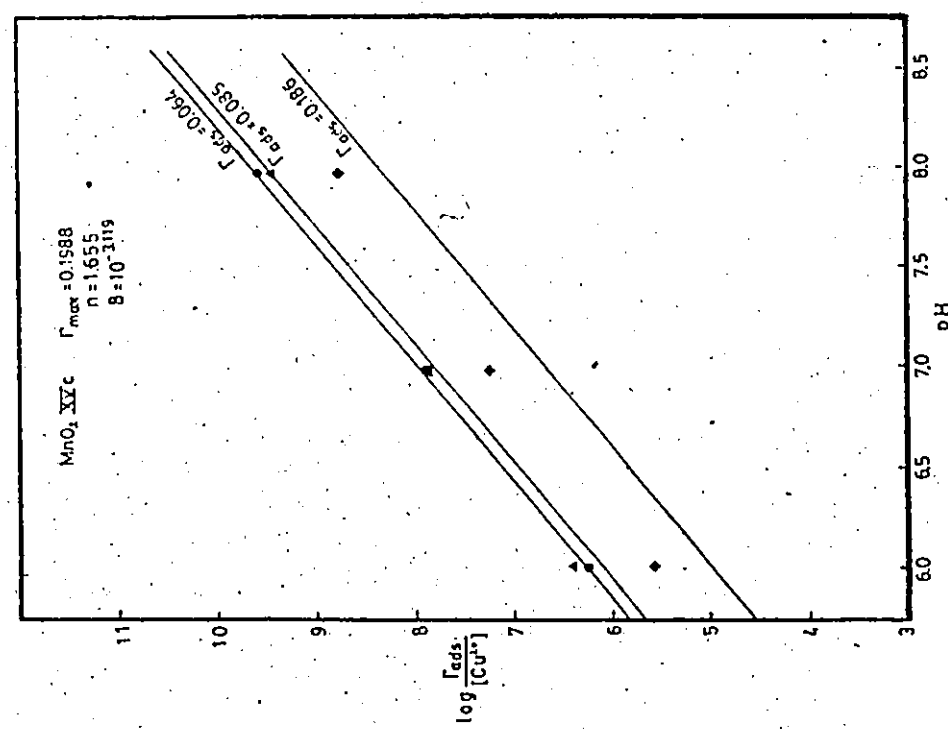
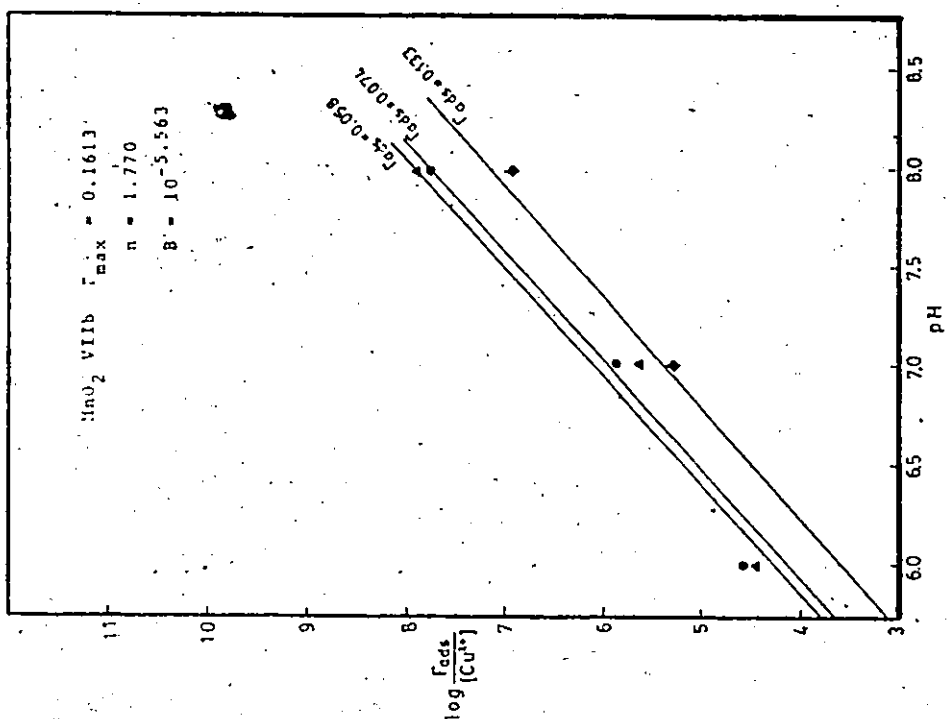


Figure 7.43 Kurbatov plot of the Implicit Langmuir model for MnO₂ XVe. Figure 7.44 Kurbatov plot of the Implicit Langmuir model for MnO₂ VIIb.

- exp. 0.10381 (+glycine) 0.056Γ_{ads} < 0.064
- ▲ exp. 0.10381 (+glycine) 0.084Γ_{ads} < 0.088
- ◆ exp. 0.10381 (+glycine) 0.185Γ_{ads} < 0.187
- model predictions for various values of Γ_{ads}

- exp. 0.070480 (+glycine) 0.056Γ_{ads} < 0.063
- ▲ exp. " " 0.072Γ_{ads} < 0.078
- ◆ exp. " " 0.130Γ_{ads} < 0.136
- model predictions for various values of Γ_{ads}

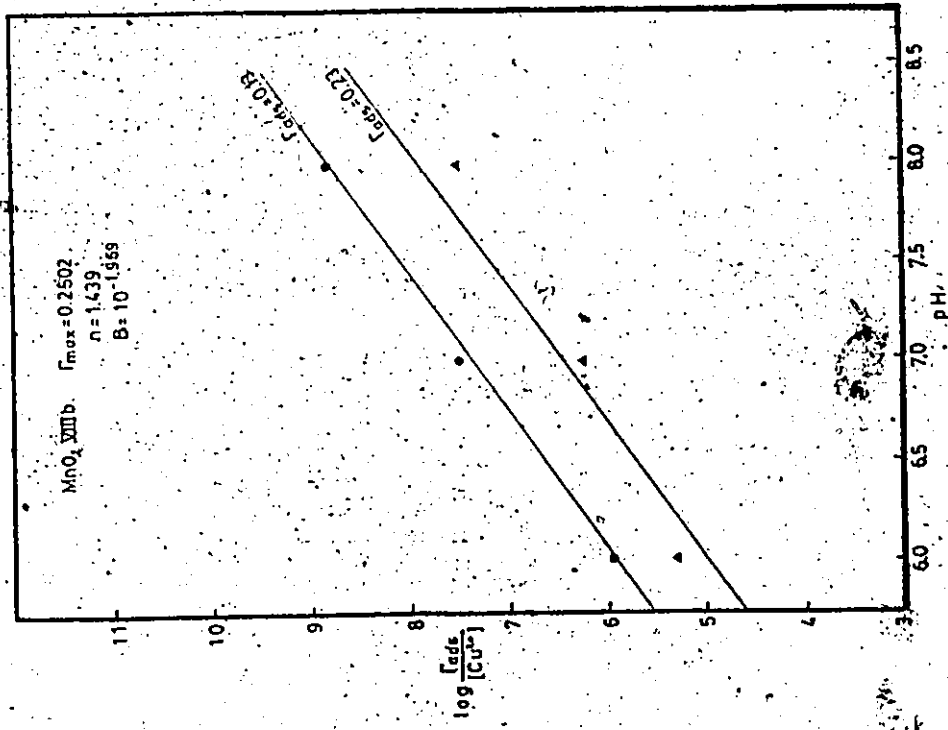


Figure 7.65 Kurbatov plot of the implicit Langmuir model for MnO₂ VIIIb.

- exp. 0.20480 (+glycine) 0.119 Γ_{ads} $\Gamma_{ads} < 0.140$
- ▲ exp. 0.20480 (+glycine) 0.230 Γ_{ads} $\Gamma_{ads} < 0.231$
- model predictions for various values of Γ_{ads}

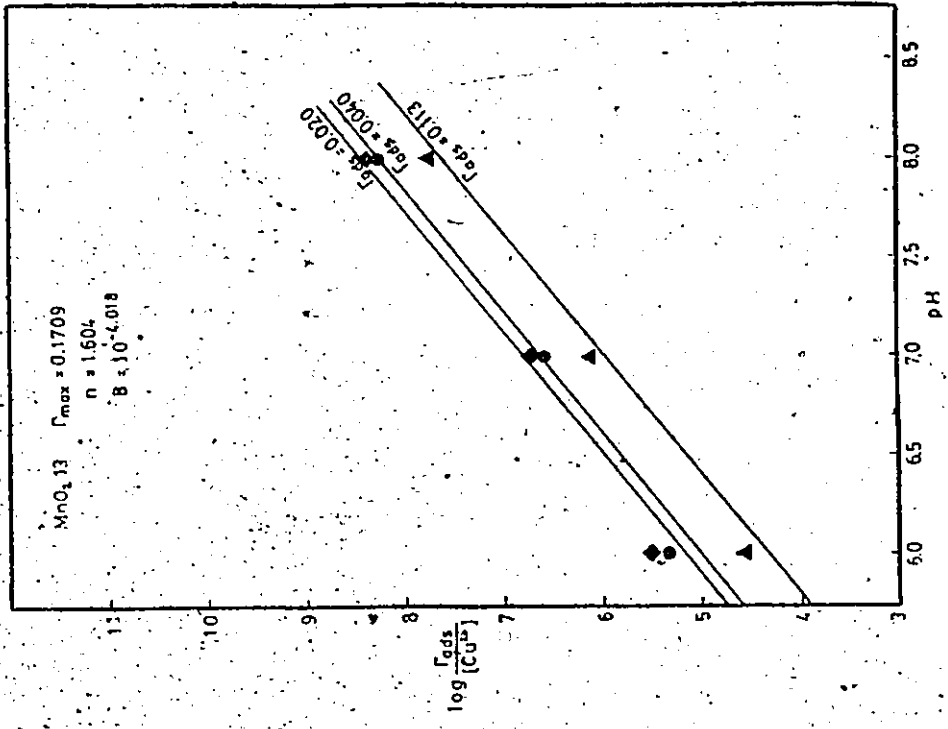


Figure 7.66 Kurbatov plot of the implicit Langmuir model for MnO₂ IJ.

- exp. 190781 (+glycine) 0.039 Γ_{ads} $\Gamma_{ads} < 0.044$
- ▲ exp. 190781 (+glycine) 0.107 Γ_{ads} $\Gamma_{ads} < 0.117$
- ◆ exp. 190781 (+glycine) 0.020 Γ_{ads} $\Gamma_{ads} < 0.021$
- model calculations for various values of Γ_{ads}

(Figure 7.46) the fit is good at low coverages except at pH 6.0, while at higher coverage the model predictions stay below the data points.

It can be concluded that ~~Kurbatov~~ plots show very good agreement between the data points and the Implicit Langmuir expression in the medium coverage ranges at all pH values $6.0 < \text{pH} < 8.0$, while on occasion at adsorption close to maximum capacity the model calculations fall below the data points, with preservation of the predicted slope. In several cases it seems that at low coverage and low pH (6 - 7), data points are higher than model predictions, indicating that the Implicit Langmuir model might still overestimate free Cu^{2+} concentrations to some extent at minimal adsorption and low pH.

7.4. Summary and Conclusions

This Chapter examines the adsorption behaviour of a number of different $\delta\text{-MnO}_2$ surfaces, and attempts to find a most suitable adsorption model.

In Section 7.2, adsorption behaviour for the various $\delta\text{-MnO}_2$'s is compared visually on several bases:

- Three $\delta\text{-MnO}_2$'s, precipitated according to a 'neutral', an 'alkaline' and an 'acid' recipe are compared. The 'neutral' and 'acid' surfaces appear to behave very similarly which is surprising, because their morphology is vastly different. The 'alkaline' surface has considerably less adsorption capacity.
- The reproducibility of the 'neutral' recipe is tested by adsorbing Cu onto three identically prepared 'neutral' $\delta\text{-MnO}_2$ surfaces. From visual comparison it is clear that reproducibility of the

'neutral' surface, in general, is poor.

- Duplicate isotherms were obtained for the three 'neutral' surfaces. Reproducibility of isotherms appears poor.
- Isotherms obtained at identical pH values in the presence and absence of glycine, for the 'neutral' surfaces did not compare very well. However, the fluctuations observed were similar to those observed for duplicate isotherms and it is unlikely that glycine changes the adsorption-behaviour of the surfaces. However, glycine does cause a decrease in both Γ_{ads} and free Cu^{2+} concentration, which has consequences for the estimation of model parameters. This is due to the observed non-linearity at the lower end of the linearized adsorption isotherm.
- The natural aging process appears to reduce adsorption capacity for the 'neutral' δ - MnO_2 surface by a factor of 1.5. The heat-induced aging process reduces the adsorption capacity very drastically. Both effects can be attributed to a reduction of available surface area, apparent from Transmission Electron Microscopy morphology data in Chapter 4.

In sections 7.3.1 to 7.3.3, the adsorption data were fitted to three related, but different adsorption models of the Langmuir form.

- The Single Langmuir model estimates the parameters Γ_{max} , the maximum amount of Cu that can be adsorbed per amount of MnO_2 and B, which is a constant related to the bindings energy involved. The visual comparisons made in Section 7.2 are substantiated by performing a t-test on the model.

parameters obtained by analysis. According to the Single Langmuir model parameters, duplication of results is extremely poor. An observation was made that although the Single Langmuir model should be linearizable, the experimental data shows a clear deviation from linearity at low coverage of the surface. This has important consequences for the Single Langmuir model parameters, which are usually estimated by linear regression, favouring the data at high surface coverage. A non-linear regression procedure improves this. However, it is inherent to the Langmuir model in general, that data at low surface coverage estimate the bindings energy, while data at high surface coverage estimate the maximum adsorption capacity. Hence it is necessary to obtain a large number of data points over the whole range of the isotherm in order to obtain reasonable estimates for the model parameters. The Single Langmuir model is only applicable for data obtained at the same pH and does not predict the observed deviation from linearity.

The Double Langmuir model assumes that there are two adsorption sites on the $\delta\text{-MnO}_2$ surface with different affinity for Cu. Γ_{max} is divided into Γ_{m_1} and Γ_{m_2} , while the bindings energy is also split into two components. This model does predict deviation from linearity, if the two components which make up the total bindings energy are noticeably different. However, this model is even more specific and less flexible than the Single Langmuir model. Non-linear regression data did not show a particular pattern for the model parameters. Model fit was hard to obtain in a considerable number of cases, due to the fact that the data basically fitted to

different functions. T-tests performed on model parameters indicated that reproducibility is extremely poor for this model.

The Implicit Langmuir model predicts that the binding energy of Cu on MnO_2 reduces in value with progressing coverage of the surface. The model also incorporates the pH in the overall value for the binding energy. This model is very flexible because it can accommodate adsorption data obtained for different pH values to estimate model parameters. Comparison of values for model parameters for the 'neutral' surfaces indicates very good agreement. However, a t-test indicated that these very similar model parameters are statistically different. Because of the correlation between parameters, a joint confidence analysis is needed to confirm the validity of these findings.

In Section 7.3.4, the three Langmuir shaped models are compared on five points. The Implicit Langmuir model is clearly the most suitable of the three, to describe adsorption of Cu onto $\delta\text{-MnO}_2$. The main advantages of this model are that:

- it is a very simple model, easy to understand and use,
- it incorporates the pH into the binding energy, which makes the model very general,
- it corrects for changes in surface charge, by taking the surface coverage into account for the estimation of the binding energy,
- it predicts the amount of H^+ that is released per amount of Cu^{2+} adsorbed, and in many cases gives good agreement with Kurbatov plots,

-it has a constant value for Γ_{\max} , which was found experimentally and,

-it predicts a higher binding energy at low coverage of the surface (which was observed experimentally) and a more or less constant binding energy at higher Γ_{ads} (also observed).

In the following Chapter, this model is tested regarding its accuracy for the determination of a conditional stability constant for NTA.

CHAPTER 8

USE OF THE IMPLICIT LANGMUIR MODEL IN THE CALCULATION OF
CONDITIONAL STABILITY CONSTANTS8.1 Introduction

Conditional stability constants and total ligand concentrations for a number of Cu-organic complexes, are calculated in this Chapter, from experimental data using the Implicit Langmuir model. The 'neutral' $\delta\text{-MnO}_2$'s are used in the experiments. The performance of the Implicit Langmuir model, in some cases is compared to results achieved by using a simple linearized Single Langmuir function. NTA and amino acids such as glycine, aspartic acid, alanine and glutamic acid are treated as models for unknown ligands. The calculated conditional stability constants and total ligand concentrations are compared to literature values and total concentrations of ligand added, so that the validity of the $\delta\text{-MnO}_2$ - method and, moreover, the suitability of the Implicit Langmuir model can be assessed.

8.2 Results for NTA

Possible errors, due to the use of a linearized Single Langmuir model, in the estimation of free Cu^{2+} , ligand concentrations and conditional stability constants have been discussed previously (Chapter 2; Section 2.5). The extent of such errors can be assessed by treating known organic material as models for unknown ligands and NTA is very suitable as such.

In the following Sections, a number of comparisons is made:

- (i) Stability and acidity constants for NTA and the Cu-NTA complex are evaluated from literature data.
- (ii) Adsorption parameters derived from both the linearized Single Langmuir model and the Implicit Langmuir model are used to calculate conditional stability constants for the Cu-NTA complex, from titration experiments.
- (iii) Titration results for a number of NTA concentrations at various pH values are evaluated.
- (iv) The influence of correcting for $\text{Cu}(\text{OH})^+$ and $\text{Cu}(\text{OH})_2$ formation on the calculation of conditional stability constants for the Cu-NTA complex from titration data, are investigated.

8.2.1 Evaluation of Values for NTA Acidity and Stability Constants

The acidity constants for NTA are generally well established in the publications of Sillen and Martell (1964, 1971) while the stability constants for Cu-NTA complex formation vary considerably. The computer program REDEQL2 (McDuff and Morel 1973) applies substantially higher equilibrium constants, but these are values extrapolated to zero ionic strength, while the program performs conversions in its calculations depending on the imposed ionic strength conditions. Table 8.1. gives a summary of constants listed by Sillen and Martel (1964, 1971) and REDEQL2.

The REDEQL2 constants appear high compared with the values from Sillen and Martel (1971), especially for the Cu-complexing constants. For the calculations presented in this Chapter, Sillen and Martell (1971)

Table 8.1 Equilibrium constants for NTA (literature data)

source	T °C	I	(H) ₁ (L) ₁ log K _{a1}	(H) ₂ (L) ₁ log K _{a2}	(H) ₃ (L) ₁ log K _{a3}	(Cu) ₁ (L) ₁ log K ₁	(Cu) ₁ (L) ₂ log K ₂
Sillen & Martell '64	20	0.1	9.73	2.5	1.9	12.7-13.1	-
Sillen & Martell '64	20	+ 0	10.33	2.94	1.65	-	-
Sillen & Martell '64	20	+ 0	10.7	3.07	3.03	-	-
Sillen & Martell '71	20	0.1	9.73	2.5	1.9	11.5-13.05	3.3
Sillen & Martell '71	20	+ 0	-	-	-	-	-
REDEQL2	25	+ 0	10.5	3.2	2.2	14.5	2.6

Table 8.2 Calculated equilibrium constants for NTA and Cu-NTA at I = 0.01 N KNO₃

Equilibrium	log K (I=0.1 KNO ₃)	log K (calc. at I=0)	log K (calc. at I=0.01)
(HL ²⁻)/(H ⁺)(L ³⁻)	9.73	10.37	10.11
(H ₂ L ⁻)/(H ⁺)(HL ²⁻)	2.5	2.91	2.74
(H ₃ L)/(H ⁺)(H ₂ L ⁻)	1.9	2.09	2.01
(CuL ⁻)/(Cu ²⁺)(L ⁻)	11.5	12.78	12.26
	12.7	13.98	13.46
	13.10	14.38	13.86

- values are used for the acidity constants and the first stability constant. The second complex is ignored for reasons discussed later in this Section. The chosen acidity and stability constants can be converted from 0.1 to 0.01 ionic strength via the Extended Debye-Hückel approximation (Stumm and Morgan 1970 p. 82-84). After first recalculating the given stability- and acidity- constants to zero ionic strength, one can then calculate their respective values at an ionic strength of 0.01 N. The results are listed in Table 8.2.

The conditional stability constant at any given pH can now be calculated. For example, the test case discussed in Section 8.2.2 is for a pH of 7.5. The conditional stability constant at pH 7.5 and $I = 0.01 \text{ KNO}_3$, for the Cu-NTA complex, is calculated with the following expressions:

$$[\text{HL}^{2-}] = 10^{10.11} \cdot 10^{-7.5} [\text{L}^{3-}] = 10^{2.61} [\text{L}^{3-}] \quad (8.1)$$

$$[\text{H}_2\text{L}^-] = 10^{2.74} \cdot 10^{-7.5} \cdot 10^{2.61} [\text{L}^{3-}] = 10^{-2.15} [\text{L}^{3-}] \quad (8.2)$$

$$[\text{H}_3\text{L}] = 10^{2.01} \cdot 10^{-7.5} \cdot 10^{-2.15} [\text{L}^{3-}] = 10^{-7.64} [\text{L}^{3-}] \quad (8.3)$$

$$[\text{CuL}^-] = 10^{12.26} [\text{Cu}^{2+}] [\text{L}^{3-}] \quad (8.4)$$

$$K'_L = \frac{[\text{CuL}^-]}{[\text{Cu}^{2+}][\text{free NTA}]} = \frac{10^{12.26} [\text{Cu}^{2+}] [\text{L}^{3-}]}{10^{2.61} [\text{Cu}^{2+}] [\text{L}^{3-}]} = 10^{9.65}$$

$$(\text{at pH } 7.5, I = 0.01) \quad (8.5)$$

Note that if one does not ignore the second complex, K'_L will depend on the concentration of L^{3-} which changes, at constant NTA concentration and pH, with the amount of complexed Cu:

$$K'_L = \frac{[CuL^-] + [CuL_2^{4-}]}{[Cu^{2+}] [free\ NTA]} = \frac{10^{12.26} \{1 + 10^{3.3} [L^{3-}]\}}{10^{2.61}} \quad (8.6)$$

Only if $[L^{3-}]$ becomes larger than about $1\ \mu M$ will this second complex have any influence on K'_L . This is not probable for the experiments performed in this study (e.g. $NTA_c = 2-8\ \mu M$, $pH = 6-8$; therefore one can ignore this complex).

By adjusting the range of Cu-NTA stability constants from Sillen and Martell (1971) (see Table 8.2) to an ionic strength of 0.01, it appears that $9.65 \leq \log K'_L \leq 11.25$ at $pH\ 7.5$.

8.2.2 Testcase: Titration of $2\ \mu M$ NTA at $pH\ 7.5$, Using MnO_2 , III as Resin

A testcase is now discussed in considerable detail to show the influence of the linearized Single Langmuir model and the Implicit Langmuir expression on the value for K'_L . At the same time, the importance of a proper correction for Cu-hydroxide formation is established. The experimental data, in the form of Tables and Figures, are given, along with the end results, to aid this discussion.

The 'neutral' δ - MnO_2 , III was used as the adsorbing surface for a titration of $2\ \mu M$ NTA with Cu (exp. 081079) at $pH\ 7.5$. The calibration of this surface, using $87.6\ \mu M$ MnO_2 and $50\ \mu M$ glycine (exp. 240979, see Figure 7.10), was performed on the same day as the actual

titrations, at the same pH of 7.5. The free Cu^{2+} concentrations for this calibration experiment were calculated with REDEQL2 (McDuff and Morel 1973). (Note that in the calculation of free Cu^{2+} for the calibration of the $\delta\text{-MnO}_2$ surface, with REDEQL2, corrections are made for hydroxide formation using $K_1 = 10^{5.99}$ and $K_2 = 10^{14.03}$). Linear least squares analysis of the linearized Single Langmuir plot of Cu^{2+} vs. $\text{Cu}^{2+}/\Gamma_{\text{ads}}$ yielded values for Γ_{max} of 0.284 and for log B of 8.673.

The adsorption parameters Γ_{max} and B, derived above, are now used to calculate the free Cu^{2+} concentration in the titration of 2 μM NTA with Cu, using the Γ_{ads} data from the titration. The Cu-NTA concentration is calculated from $(\text{Cu}_{\text{dissolved}} - \text{Cu}^{2+} - \text{Cu}(\text{OH})^+)$. The $\text{Cu}(\text{OH})^+$ concentration is calculated from the equilibrium $\text{Cu}(\text{OH})^+ / (\text{Cu}^{2+})(\text{OH}^-) = 10^{6.00}$. No corrections are made for $\text{Cu}(\text{OH})_2^{\circ}$ formation. The results of these calculations are given in Table 8.3 and in Figure 8.1.

Figure 8.1 shows that the first 6 points of the titration results form a straight line. From these 6 data points, a total ligand concentration of 2.06 μM is calculated and a conditional stability constant for the Cu-NTA complex of $10^{8.99}$. By comparison, van de Berg (1979) finds the following conditional stability constants for Cu-NTA, using the MnO_2 method:

$$\text{pH } 7.2 \quad \log K'_L = 8.55 \pm 0.18$$

$$\text{pH } 7.6 \quad \log K'_L = 8.9 \pm 0.4$$

$$\text{pH } 8.2 \quad \log K'_L = 10.2 \pm 0.4$$

However, the data of Sillen and Martell (1971) (see Section 8.2.1) suggest a range of values for K'_L of 9.65 to 11.25 at pH 7.5. Apparently,

the total ligand concentration (L_T) obtained from the titration experiment is correct, but $\log K'_L$ is much too low (by a log factor of 0.66-2.26).

There are several possible causes for this difference.

- (i) The MnO_2 method gives rise to incorrect results
- (ii) Adsorption of ligand (in this case NTA) changes the adsorption characteristics of MnO_2 and decreases the amount of ligand in solution
- (iii) Corrections for hydroxide formation are not correct
- (iv) The literature range of values for K'_L given by Sillen and Martell (1971) is incorrect and/or the adjustments to an ionic strength of 0.01 are in error

Ad (i)

The linearized Single Langmuir plot obtained for the calibration of the MnO_2 III surface for Cu uptake at pH 7.5 shows a deviation from linearity at low coverage of the surface. Because of the weighting given by linear least squares analysis to high surface coverage data, the values for Γ_{max} and B, estimated by linear regression using all 10 calibration points, will overestimate the free Cu^{2+} concentrations in the lower Γ_{ads} range. It is in this range that the first 6 titration data points for the NTA titration are located. Because NTA is a strong ligand, essentially all dissolved Cu is in the Cu-NTA complex, providing that total dissolved Cu is not larger than the total dissolved NTA concentration. Hence, it does not matter whether either 10^{-8} or 10^{-10} moles of free Cu^{2+} is subtracted from the total amount of dissolved Cu, the value for the Cu-NTA concentration is still estimated exactly in a

Figure 8.1 Titration of 2 μM NTA at pH 7.5

(exp. 081079)

Titration of 2 μM NTA at pH 7.5, using Single Langmuir parameters for $\delta\text{-MnO}_2$ III ($\Gamma_{\text{max}} = 0.284$; $\log B = 8.673$) and correcting for Cu(OH)^+ formation only ($\log K = 6.00$)

The inset is an enlargement of the lower part of the graph.

Input: $L_t = 2 \mu\text{M}$ (added)

$$9.65 \leq \log K'_L \leq 11.25 \text{ (Sillen and Martell, 1971)}$$

Results: $L_t = 2.06 \mu\text{M}$

$$\log K'_L = 8.99$$

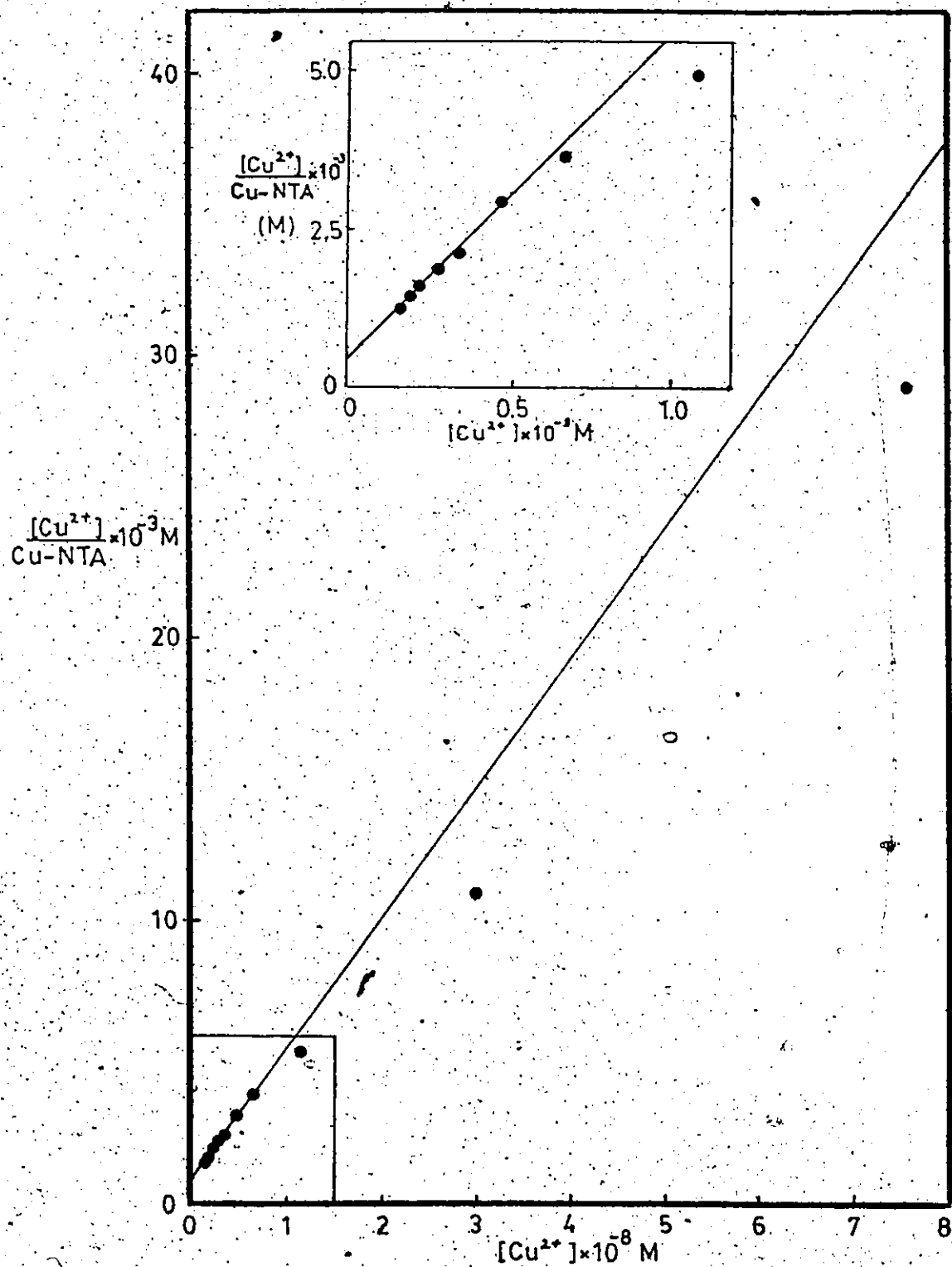


Figure 8.1 Titration of 2 μM NTA at pH 7.5

Cu _{total} (M)	Cu _{dissolved} (M)	Cu _{adsorbed} (M)	Γ_{ads}	Cu ²⁺ (M)	Cu(OH) ⁺ (M)	Cu-NTA (M)	Cu ²⁺ /Cu-NTA
11.866x10 ⁻⁶	1.297x10 ⁻⁶	10.569x10 ⁻⁶	0.121	0.159x10 ⁻⁸	0.050x10 ⁻⁸	1.295x10 ⁻⁶	1.228x10 ⁻³
12.954	1.319	11.635	0.133	0.188	0.060	1.317	1.428
14.157	1.431	12.726	0.145	0.223	0.071	1.428	1.562
15.506	1.504	14.002	0.160	0.276	0.087	1.500	1.840
16.997	1.646	15.351	0.175	0.344	0.109	1.642	2.096
18.681	1.618	17.063	0.195	0.470	0.149	1.612	2.916
20.639	1.831	18.808	0.215	0.668	0.211	1.822	3.666
22.940	2.192	20.748	0.237	1.083	0.343	2.572	4.973
25.755	2.609	23.146	0.264	2.852	0.902	2.572	11.091

Table 8.3 Calculation of Cu species in the 2 μ M NTA titration experiment using Single Langmuir parameters.

The ligand concentration is treated as unknown; the adsorption parameters Γ_{max} and B from the MnO₂ III calibration experiment and the Γ_{ads} data from the titration experiment are used for the calculation of Cu²⁺ concentrations; Cu-NTA concentrations are calculated from the Cu-mass balance. Cu-NTA values are corrected for Cu(OH)⁺ formation, by using $K_{Cu(OH)^+} = 10^{6.00}$.

relative sense. By plotting Cu^{2+} vs. $\text{Cu}^{2+}/\text{Cu-NTA}$, one obtains a straight line whose slope is relatively insensitive to Cu^{2+} concentration and yields the correct total NTA concentration. This occurs even if the free Cu^{2+} concentration is overestimated by several orders of magnitude. The value of the intercept is much more influenced by errors in the Cu^{2+} concentration. Because the conditional stability constant is determined by the value of the intercept, its calculated value can be in error by up to several orders of magnitude.

An error can also occur at the other end of the graph. Once the ligand, in this case NTA, is almost saturated with Cu, the Cu^{2+} concentration increases rapidly. But at this point one may be underestimating the Cu^{2+} concentration by using the linear regression calibration values for Γ_{max} and B. This would imply that Cu-NTA is overestimated and that the plot of Cu^{2+} versus $\text{Cu}^{2+}/\text{Cu-NTA}$ will display a break which could be mistaken for an indication of a second site on the ligand or a second ligand.

Therefore, on the one hand, over- and under-estimating of Cu^{2+} does not necessarily mean an effect on Cu-NTA, and therefore not on the slope, from which L_t is obtained. But on the other hand the value obtained for $\log K_L^i$ is strongly affected. Thus this example of NTA demonstrates the probable size of error associated with calculating $\log K_L^i$ with adsorption parameters obtained with the linearized Single Langmuir isotherm. But in dealing with an unknown natural organic ligand, one might well accept the value for $\log K_L^i$ as being correct.

Ad (ii):

Adsorption of NTA on the δ - MnO_2 surface was ruled out in Chapter 6 (Section 6.7.2) and cannot have caused the discrepancy between literature values and experimental results for K'_L .

Ad (iii):

Another reason for possible errors in $\log K'_L$ values is that the Cu species, calculated for the NTA titration in Table 8.3, are not corrected for $\text{Cu}(\text{OH})_2^\circ$ formation. Calibration results to calculate the adsorption parameters for the δ - MnO_2 surface were corrected for $\text{Cu}(\text{OH})_2^\circ$ formation, because Cu^{2+} concentrations were calculated with REDEQL2.

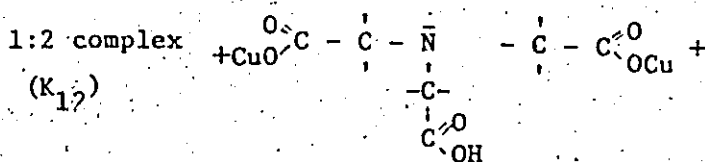
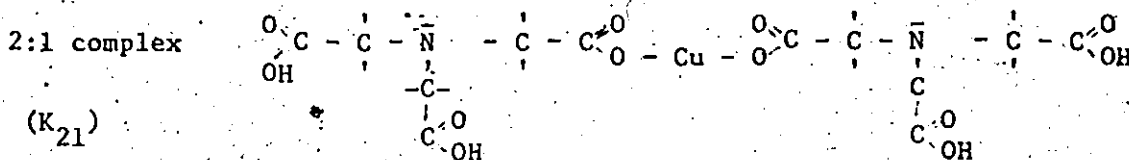
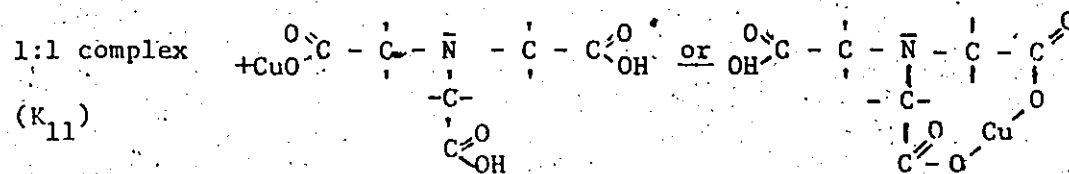
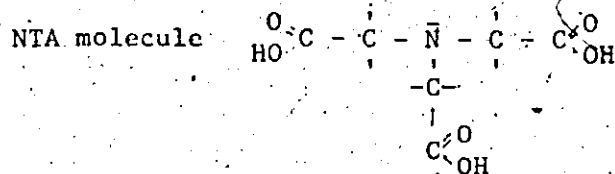
The titration data for NTA (Figure 8.1) show a clear break in the graph near the equivalence point of NTA (i.e. 2 μM). This can mean several things: either there exists a second site on the ligand (Cu_2L) or the data beyond the equivalence point are not corrected properly for hydroxide formation. Around the equivalence point, the free Cu^{2+} concentration suddenly increases drastically. This will be counteracted by $\text{Cu}(\text{OH})^+$ and possibly $\text{Cu}(\text{OH})_2^-$ formation, depending on the magnitude of this increase. Corrections with the proper constants are absolutely necessary in the region near and beyond the equivalence point of the titration.

The break in the titration graph can also mean that the increase in free Cu^{2+} beyond the equivalence point was so large that $\text{Cu}(\text{OH})_{2(s)}$ and/or CuO was precipitated and subsequently filtered off together with the MnO_2 , or maybe even precipitated on the surface of MnO_2 . This was also discussed in Chapter 6, Section 6.3.1. This results in Γ_{ads} being too large and Cu^{2+} being too small, and hence causes the break in the titration results.

As discussed before, REDEQL2 and Sillen and Martell (1971) both include a CuL_2 complex for NTA, but its K is such that L^{3-} has to become rather large (i.e. extremely low Cu^{2+} and very high pH) to have any influence whatsoever on the conditional stability constant for Cu-NTA. Neither Sillen and Martell (1964, 1971) nor REDEQL2 include complexes of the form:

$$K_{ln} = \frac{[\text{M}_n \text{L}]}{[\text{M}] [\text{M}_{n-1} \text{L}]} \quad (8.7)$$

which indicates that complexes of more than one Cu-ion with one NTA molecule are not considered. However, the structure of NTA suggests that several combinations of Cu with NTA are possible:



It is possible that in solution a mixture of these complexes occurs, depending on the experimental conditions. In Section 8.2.1, the 2:1 combination has been ruled out as unimportant for this particular study. If a 1:2 complex forms, the effect of it would be most obvious near the saturation of the ligand on a 1:1 basis. The presence of such a second site on the NTA molecule cannot be discriminated from a case in which two ligands are present in the same concentration but with different stability constants (van den Berg 1979), and the presence of a second ligand or site will indeed cause curvature followed by a second straight line in the plot of Cu^{2+} versus $\text{Cu}^{2+}/\text{Cu-NTA}$.

Ad(iv):

The correctness of published stability constants is difficult to evaluate. The fact that Sillen and Martell (1971) give a range of values for K'_L is an indication of the uncertainty that exists regarding the strength of the Cu-NTA complex. Adjustment of the K'_L values to 0.01 ionic strength was done (in Section 8.2.1) by means of a standard method, which is necessarily an approximation. It should therefore be emphasized that literature values, adjusted for ionic strength, may be subject to a certain degree of error. Whether this can account for the large discrepancy found between the literature and experimental value for K'_L is doubtful and in fact does not seem likely.

Three aspects are now investigated: i) proper correction for $\text{Cu}(\text{OH})^+$ and $\text{Cu}(\text{OH})_2^0$ formation; ii) recalculation of the above reported titration results using the Implicit Langmuir model and iii) the pos-

sibility of a second site on the NTA molecule for Cu. The third issue is examined in a separate Section (8.2.3).

The influence of correcting for Cu-hydroxide formation can be examined by using different stability constants for the $\text{Cu}(\text{OH})^+$ and $\text{Cu}(\text{OH})_2^0$ complexes. Two sets of calculations were performed. They are:

1 - Correction for $\text{Cu}(\text{OH})^+$ only, using a K of $10^{6.3}$, which was measured by van den Berg (1979). The results are given in Table 8.4. Linear least squares analysis for these results do not differ much from the first set of calculations with $K_{\text{Cu}(\text{OH})^+} = 10^{6.00}$. Note that in the results in Table 8.4, the last 3 points have a Cu-NTA concentration larger than 2 μM which is not possible for 1:1 or 2:1 complexes.

2 - Correction for both $\text{Cu}(\text{OH})^+$ and $\text{Cu}(\text{OH})_2^0$ using respectively $K_{\text{Cu}(\text{OH})^+} = 10^{6.3}$ and $K_{\text{Cu}(\text{OH})_2^0} = 10^{14.03}$. The results are given in Table 8.5.

Note that two of the last three data points have a calculated Cu-NTA concentration $> 2 \mu\text{M}$. Again, this is not possible for a 1:1 complex.

The reason for it must be sought in an underestimation of the Cu^{2+} concentration at these points which leads to an error in the mass balance for Cu and hence Cu-NTA. The use of a linearized Single Langmuir expression to calculate Γ_{max} and log B may be blamed for the underestimation of the Cu^{2+} concentration at the last three titration points. The reasons for this were previously discussed in Chapter 2 (Section 2.5) and Chapter 7 (Section 7.3.2).

The data presented in Tables 8.4 and 8.5 were used to calculate the NTA concentration and the conditional stability constant for the Cu-NTA complex. The results are listed in Table 8.8.

Table 8.4 Recalculation of Cu species in the 2uM NTA titration
(adjustment of Cu(OH)^+ correction)

$\text{Cu}_{\text{dissolved}}$ (M)	Cu^{2+} (M)	$\text{Cu(OH)}^+ (K=10^{6.3})$ (M)	Cu-NTA (M)	$\text{Cu}^{2+}/\text{NTA}$
1.297×10^{-6}	0.159×10^{-8}	0.100×10^{-8}	1.294×10^{-6}	1.228×10^{-3}
1.319	0.188	0.119	1.316	1.429
1.431	0.223	0.141	1.427	1.562
1.504	0.276	0.174	1.500	1.841
1.646	0.344	0.217	1.640	2.098
1.618	0.470	0.297	1.610	2.919
1.831	0.668	0.421	1.820	3.670
2.192	1.083	0.683	2.174	4.981
2.609	2.852	1.799	2.562	11.130
2.761	7.640	4.821	2.636	28.979

The results are calculated using single Langmuir parameters $\Gamma_{\text{max}} = 0.284$ and $\log B = 8.673$, and correction for Cu(OH)^+ formation is made by using $K_{\text{Cu(OH)}^+} = 10^{6.3}$.

Table 8.5 Recalculation of Cu-species in the 2uM NTA titration (Cu(OH)_2 correction)

$\text{Cu}_{\text{dissolved}}$ (M)	Cu^{2+} (M)	$\text{Cu(OH)}^+ (K=10^{6.3})$ (M)	$\text{Cu(OH)}_2 (K=10^{14.03})$ (M)	Cu-NTA (M)	$\text{Cu}^{2+}/\text{NTA}$
1.297×10^{-6}	0.159×10^{-8}	0.100×10^{-8}	1.704×10^{-8}	1.277×10^{-6}	1.245×10^{-3}
1.319	0.188	0.119	2.014	1.296	1.451
1.431	0.223	0.141	2.389	1.403	1.589
1.504	0.276	0.174	2.957	1.470	1.878
1.646	0.344	0.217	5.686	1.604	2.145
1.618	0.470	0.297	5.036	1.560	3.013
1.831	0.668	0.421	7.158	1.749	3.820
2.192	1.083	0.683	11.604	2.058	5.262
2.609	2.852	1.799	30.559	2.257	12.637
2.761	7.640	4.821	81.863	1.817	42.030

The results are calculated using single Langmuir parameters $\Gamma_{\text{max}} = 0.284$ and $\log B = 8.673$. Correction for Cu(OH)^+ formation is made by using $K_{\text{Cu(OH)}^+} = 10^{6.3}$, and for Cu(OH)_2 by using $K_{\text{Cu(OH)}_2} = 10^{14.03}$.

The NTA titration results are also analyzed by using the Implicit Langmuir model parameters derived for MnO_2 III. These parameters are (see also Chapter 7, Table 7.10) $\Gamma_{\text{max}} = 0.2425$, $n = 1.852$ and $b = -4.782$. The Cu-speciation for the NTA titration experiment is calculated considering two cases, designed, as above, to estimate the influence of hydroxide formation correction. Case 1, presented in Table 8.6 calculates Cu-speciation, while only the formation of $\text{Cu}(\text{OH})^+$ is considered. Case 2, presented in Table 8.7, considers the formation of both $\text{Cu}(\text{OH})^+$ and $\text{Cu}(\text{OH})_2^0$.

The use of the Implicit Langmuir adsorption parameters Γ_{max} , n and x , derived for $\delta\text{-MnO}_2$ III causes a problem. The value for Γ_{max} is 0.2425, which is smaller than the last two values obtained for Γ_{ads} in the NTA titration experiment (see Table 8.3). These last two titration points can therefore not be used in the calculation of the NTA concentration and the conditional stability constant for the Cu-NTA complex. Measuring Γ_{ads} values $> \Gamma_{\text{max}}$ can have several causes: (i) In Chapter 7 poor reproduction of isotherms was discussed. The Implicit Langmuir model derives an average value for Γ_{max} . (ii) Near the equivalence point for NTA, Cu^{2+} concentration increases drastically, which could cause precipitation of $\text{Cu}(\text{OH})_2(\text{s})$ and/or CuO . This would manifest itself as adsorption of Cu, causing larger than realistic values for Γ_{ads} . (iii) The surface area of $\delta\text{-MnO}_2$ per mole Mn is probably not constant, causing errors in the calculated Γ_{ads} values (Γ_{ads} is defined as the amount of Cu in moles adsorbed per amount of MnO_2 in moles). (iv) The amount of $\delta\text{-MnO}_2$ present during the titration may have been underestimated. $\delta\text{-MnO}_2$ was dispensed volumetrically to the solution and

Table 8.6 Recalculation of Cu-species in the 2uM NTA titration (using Implicit Langmuir parameters)

Cu _{dissolved} (M)	Cu ²⁺ (M)	Cu(OH) ⁺ (K=10 ^{6.3}) (M)	Cu-NTA (M)	Cu ²⁺ /Cu-NTA
1.297x10 ⁻⁶	4.796x10 ⁻¹⁰	3.076x10 ⁻¹⁰	1.296x10 ⁻⁶	3.700x10 ⁻⁴
1.319	6.142	3.875	1.318	4.660
1.431	7.895	4.982	1.430	5.522
1.504	10.939	6.902	1.502	7.282
1.646	15.529	9.798	1.643	9.449
1.618	26.600	16.783	1.614	16.484
1.831	54.507	34.392	1.822	29.914
2.192	303.000	191.180	2.143	141.418
2.609	-	-	-	-
2.761	-	-	-	-

The results are calculated using the implicit Langmuir parameters for δ-MnO₂ III, $i_{max} = 0.2425$, $n = 1.852$ and $b = -4.782$. Correction for Cu(OH)⁺ formation is made by using $K_{Cu(OH)^+} = 10^{6.3}$.

Table 8.7 Recalculation of Cu-species in the 2uM NTA titration (using Implicit Langmuir parameters and Cu(OH)₂ correction)

Cu _{dissolved} (M)	Cu ²⁺ (M)	Cu(OH) ⁺ + Cu(OH) ₂ (M)	Cu-NTA (M)	Cu ²⁺ /Cu-NTA
1.297x10 ⁻⁶	4.796x10 ⁻¹⁰	5.441x10 ⁻⁹	1.291x10 ⁻⁶	3.714x10 ⁻⁴
1.319	6.142	6.969	1.311	4.683
1.431	7.895	8.847	1.421	5.555
1.504	10.939	12.412	1.490	7.339
1.646	15.529	17.620	1.627	9.546
1.618	26.600	30.181	1.585	16.781
1.831	54.507	61.845	1.764	30.905
2.192	303.00	343.790	1.818	166.670
2.609	-	-	-	-
2.761	-	-	-	-

The results are calculated using the implicit Langmuir parameters for δ-MnO₂ III, $i_{max} = 0.2425$, $n = 1.852$ and $b = -4.782$. Correction for Cu(OH)⁺ and Cu(OH)₂ formation is performed by using $K_{Cu(OH)^+} = 10^{6.3}$ and $K_{Cu(OH)_2} = 10^{14.03}$.

a certain amount of MnO_2 per volume was assumed. Due to the particulate nature of MnO_2 this may not always have been accurate and caused errors in the calculated Γ_{ads} values.

The results of all these calculations have been plotted (not shown) and analyzed by linear regression. The values for L_t (the calculated NTA concentration) and K'_L (the calculated conditional stability constant for the Cu-NTA complex) are summarized in Table 8.8. Analysis was done for all data points (10), the first 8 points and the first 6 points. Reasons for this were that most calculations showed a break in the plot around point 7 and that only the first 8 points could be included in the analyses that used the Implicit Langmuir adsorption parameters for $\delta\text{-MnO}_2$ III.

It is concluded from Table 8.8 that the use of the Implicit Langmuir adsorption parameters certainly gives better results for K'_L than the use of the adsorption parameters derived from the linearized Single Langmuir model. Results for the total NTA concentrations are generally 7 - 15% too low. However, glass adsorption of NTA on the vessel walls during the titration experiment results in the disappearance of 8 - 20% of the NTA (Chapter 6, Section 6.7.2), which can easily account for the difference. It is also concluded that correction for $\text{Cu}(\text{OH})_2^{\circ}$ formation has a noticeable influence on the calculations for both L_t and K'_L . Therefore, both $\text{Cu}(\text{OH})^+$ and $\text{Cu}(\text{OH})_2^{\circ}$ should be corrected for routinely.

8.2.3 The Possibility of 1:2 Complex Formation

Van den Berg (1979) describes how one can calculate the concen-

Table 8.8 Summary of titration results for NTA (2 mM) at pH 7.5

Model used	correction for.		all 10 points L _T log K'	first 8 points L _T log K'		first 6 points L _T log K'		break at point 7 ?	
	Cu(OH) ⁺	Cu(OH) ₂							
single Langmuir logK=6.0			n.c.	n.c.	n.c.	2.06	8.99	yes	
single Langmuir logK=6.30			2.72	8.62	2.42	8.77	1.903	9.13	yes
single Langmuir logK=6.30			1.864	10.031	2.72	8.82	1.82	9.17	yes
implicit single Langmuir logK=6.30			-	-	2.18	9.24	1.732	9.793	yes
implicit single Langmuir logK=6.30			-	-	1.83	9.603	1.694	9.836	no

- n.c. = not calculated

- = not possible to calculate

The literature value is $9.65 \leq K' \leq 11.25$

tration and conditional stability constant of either a second ligand or a second site on the first ligand, if one finds a curvature followed by a second straight line in the plot of Cu^{2+} vs. $\text{Cu}^{2+}/\text{Cu-L}$. An iterative procedure is used. For NTA, a second site on the NTA molecule (Cu_2L) should be considered if a break in the titration curve is found. Cu_2L is determined as:

$$[\text{Cu}_2\text{L}] = [\text{Cu}_t] - [\text{Cu}^{2+}] - [\text{Cu}(\text{OH})^+] - [\text{Cu}(\text{OH})_2^c] - [\text{CuL}] \quad (8.8)$$

Cu_t and Cu^{2+} and hence $\text{Cu}(\text{OH})^+$ and $\text{Cu}(\text{OH})_2^c$ are all known. CuL can be calculated with L_t and K'_L obtained from the first straight line:

$$[\text{CuL}] = K'_L [\text{Cu}^{2+}] [L_t - [\text{CuL}]] \quad (8.9)$$

or

$$[\text{CuL}] = \frac{K'_L [\text{Cu}^{2+}] L_t}{1 + K'_L [\text{Cu}^{2+}]} \quad (8.10)$$

One can then plot Cu^{2+} vs. $\text{Cu}^{2+}/\text{Cu}_2\text{L}$ and obtain L_S and K'_S for the second site on the NTA molecule, where L_S is the concentration of the second site and K'_S the conditional stability constant. These values can then be used to correct L_t and K'_L , by recalculating CuL from:

$$[\text{CuL}] = [\text{Cu}_t] - [\text{Cu}^{2+}] - [\text{Cu}(\text{OH})^+] - [\text{Cu}(\text{OH})_2^c] - [\text{Cu}_2\text{L}] \quad (8.11)$$

in which

$$[\text{Cu}_2\text{L}] = \frac{K'_S [\text{Cu}^{2+}] L_S}{1 + K'_S [\text{Cu}^{2+}]} \quad (8.12)$$

Replotting Cu^{2+} versus $\text{Cu}^{2+}/\text{CuL}$ gives a better estimate for L_t and K'_L which in turn can be used to recalculate L_S and K'_S . Van den Berg (1979) suggests that two or three iterations should give values for L_t , L_S , K'_L and K'_S with an error much smaller than the error which probably is introduced by the measurement itself.

A titration of 4 μM NTA at pH 8.0 was performed in this study, and deliberately taken far beyond the first equivalence point, to investigate whether there is a second site for Cu on NTA. MnO_2 Xvc was used as resin and 40 μM glycine was added to prevent precipitation reactions beyond the first equivalence point, in case of lack of such a second site. The results are shown in Figure 8.2. The data set for this experiment is given in Table 8.9.

The first 4 data points represent Cu-NTA, the 1:1 complex. From the slope and intercept of the plot Cu^{2+} vs. $\text{Cu}^{2+}/\text{CuL}$ it can be calculated that $L_t = 4.02 \mu\text{M}$ and $\log K'_L = 11.58$, while the last three points, uncorrected for L_t and K'_L , yield an L_S of 9.56 μM and $\log K'_S$ of 9.88. According to van den Berg, these last three points only give a true indication of $(L_t + L_S)$ but what K'_S stands for in this case is not certain. However, with the values of L_t and K'_L , values for Cu_2L can be calculated for the last three points and hence better estimates for L_S and K'_S can be obtained from the plot Cu^{2+} vs. $\text{Cu}^{2+}/\text{Cu}_2\text{L}$ which in turn can be used to calculate corrected values for L_t and K'_L . This process has been repeated several times and the results are shown in Table 8.10.

Two iterations show that L_t for the 1:1 complex has a value of 3.64 μM , which is 9% lower than the input of 4 μM NTA. Since 8--20% of the NTA added can disappear during a titration, (presumably through

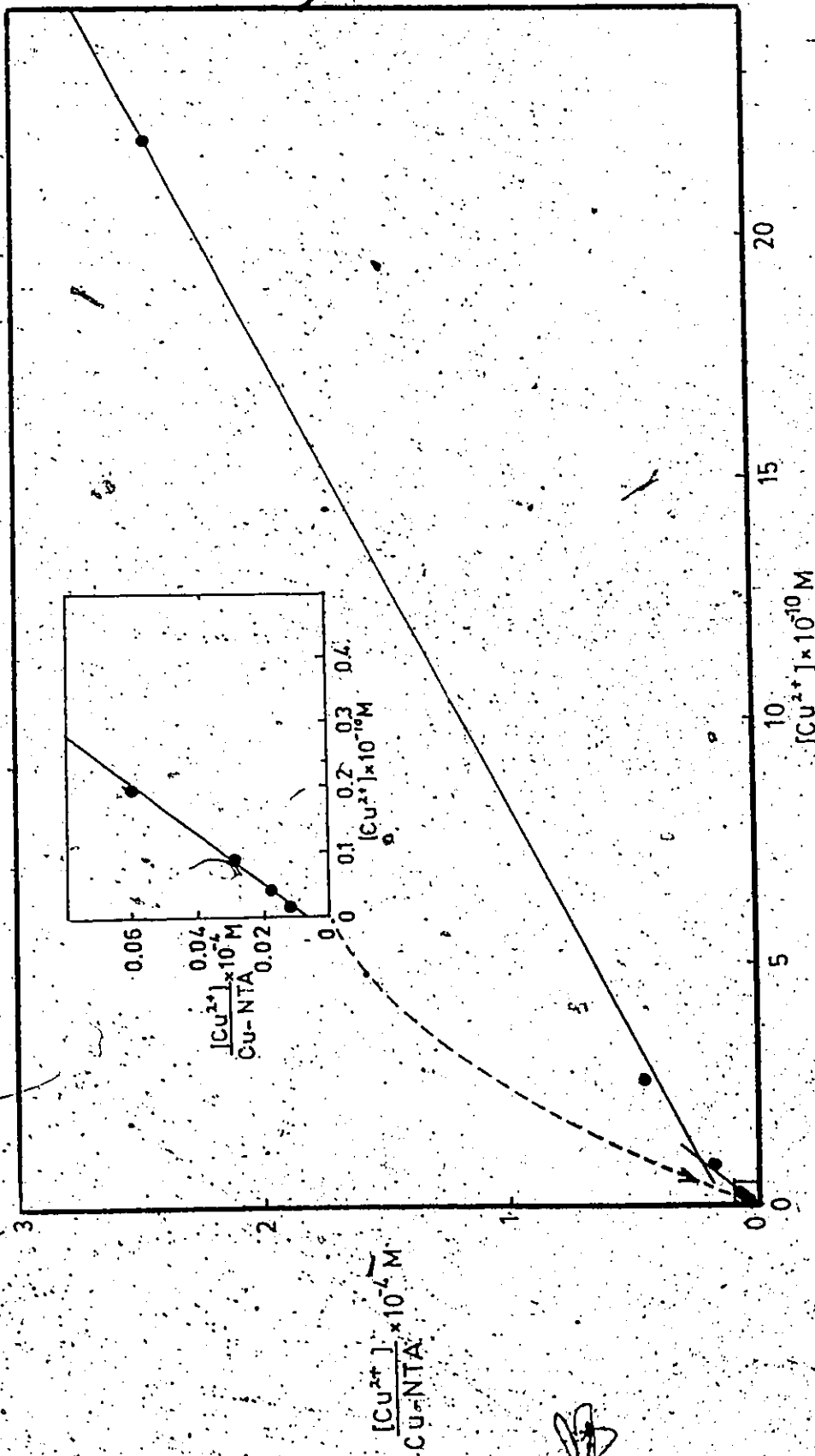


Figure 8.2 Titration of 4µM NTA (and 40µM Glycine) at pH 8.0, using MnO₂ Xvc with. Implicit Langmuir adsorption parameters, ($\Gamma_{max} = 0.1988$; $n = 1.655$; $b = 3.119$)

Table 8.9 Titration of 4 μ M NTA at pH 8.0

Cu ²⁺ (M)	Γ_{ads}	Cu ²⁺ (M)	Cu(OH) ⁺ (M)	Cu(OH) ₂ (M)	Cu _{diss} (M)	CuL (M)	$\frac{Cu^{2+}}{CuL}$
1.999x10 ⁻⁶	0.0088	0.0138x10 ⁻¹⁰	0.0138x10 ⁻¹⁰	1.479x10 ⁻¹⁰	1.274x10 ⁻⁶	1.274x10 ⁻⁶	0.010
4.171	0.0220	0.0395	0.0395	4.233	2.366	2.366	0.016
6.570	0.0420	0.0883	0.0883	9.462	3.267	3.266	0.027
9.262	0.0670	0.2029	0.2029	21.741	3.517	3.515	0.057
15.318	0.1246	0.9010	0.9010	96.544	5.089	5.079	0.177
18.784	0.1603	2.7028	2.7028	289.610	5.621	5.591	0.483
24.991	0.1915	21.9235	21.9235	2349.15	9.270	9.031	2.427

MnO₂ XVe, implicit Langmuir parameters $\Gamma_{max} = 0.1988$; $n = 1.655$; $B = -3.119$; 40 μ M glycine present.

Table 8.10. Values for L_t , L_s , K'_L and K'_S calculated by iterative method

number of iterations	L_t (μM)	$\log K'_L$	L_s (μM)	$\log K'_S$
0	4.02	11.58	9.56 ($L_t + L_s$)	9.88 (=?)
0	4.02	11.58	6.31	9.23
1	3.72	11.64	6.04	9.37
2	3.64	11.66	6.08	9.39

glass adsorption during the experiment, see Chapter 6) the value of 3.64 μM NTA can be accepted as correct. The value for $\log K'_L$ is found to be 11.66, on the high side but in the range of literature values corrected for ionic strength ($10.15 \leq \log K'_L$ at $\text{pH } 8 \leq 11.75$). Note that the presence of a second site for Cu on the NTA molecule has only a small influence on $\log K'_L$ for the first site. This is caused by the fact that $K'_{11} \gg K'_{12}$.

For the 1:2 complex (Cu_2L), the data are necessarily less accurate, due to the fact that they are based on few data points and possibly because 40 μM glycine is present. The value calculated for $(L_t + L_s)$ from the plot Cu^{2+} vs. $\text{Cu}^{2+}/\text{Cu-L}$ is 9.56 μM , which is too high and should be approximately 7.5 - 8 μM , i. e. twice the amount of NTA added. The calculated value for L_s after two iterations from the plot Cu^{2+} vs. $\text{Cu}^{2+}/\text{Cu}_2\text{L}$ is 6.08 μM , which is also too high and should be approximately

equal to L_t . The fact that both $(L_t + L_s)$ and L_s are too high could be due to either a third site on the NTA molecule or to a second ligand, in this case the 40 μM glycine added. There are too few data points to conclude with any certainty which of the two possibilities is most likely.

In conclusion it can be said that, although this is not a very accurate example, it provides an interesting illustration of the potential of the MnO_2 method, and shows the existence of a second and possibly third site on the NTA molecule for Cu.

8.2.4 Other Results for NTA at pH 6 and 7

Three other titrations were carried out, involving 4 to 8 μM NTA, at pH 6 and 7, to establish the conditional stability constants for the Cu-NTA complex in the pH range 6 - 8. MnO_2XVc (Implicit Langmuir parameters $\Gamma_{\text{max}} = 0.1988$; $n = 1.655$ and $b = -3.119$) was used as adsorbing surface. Figures 8.3 and 8.4 show titration results at pH 7, while Figure 8.5 presents titration results at pH 6.

Figure 8.3 illustrates a titration of 8 μM NTA (which was labelled with ^{14}C), at pH 7. This experiment was followed by ^{14}C determinations to assess adsorption of NTA on glassware or loss of NTA by other factors during the titration (see also Chapter 6, Section 6.7.2). The ^{14}C content appeared to decrease gradually during the experiment, indicating glass adsorption. An average value for the ^{14}C -NTA concentration is therefore used as the true concentration, i.e. 7.68 μM NTA. From the plot of Cu^{2+} versus $\text{Cu}^{2+}/\text{Cu-NTA}$, a concentration of 7.36 μM NTA is found, a deviation of -4.2%. $\log K'_L$ lies anywhere between 9.15 and

10.75 according to literature data (Sillen and Martell 1971). Van den Berg (1979) calculates a literature value for $\log K'_L$ of 9.7 at pH 7. The value for $\log K'_L$ determined from Figure 8.3 is 9.82. This agrees very well with the literature value quoted by van den Berg (1979) and lies well within the 9.15 - 10.75 range calculated from data by Sillen and Martell (1971). The value obtained for $\log K'_L$ is not corrected here for the fact that NTA possesses a second site for Cu. However, in Section 8.2.3 it was shown that the influence of a second site on K'_L for the first site is very small.

The data presented in Figure 8.3 were also analyzed in Chapter 6, using Single Langmuir adsorption parameters for the calibration of the MnO_2 surface. This yielded a value of 7.35 μM for L_c , identical to the above, while a value of 9.2 was obtained for $\log K'_L$, considerably lower than the above determined value.

Figure 8.4 displays the results of a titration of 4 μM NTA at pH 7.0. This experiment was not checked by using ^{14}C labelled NTA and hence an average concentration for NTA available for complexation with Cu was not determined experimentally. The typical range of 8 - 20% NTA disappearing due to glass adsorption during a titration experiment, established in Chapter 6 (Section 6.7.2), means that the available NTA concentration for this experiment must have been in the range of 3.68 - 3.20 μM . Assuming an average value of approximately 3.40 μM NTA, the experimentally determined concentration of 3.02 μM NTA is approximately 11% too low. The value for $\log K'_L$ of 9.86 is almost identical to the value obtained from the experiment shown in Figure 8.3.

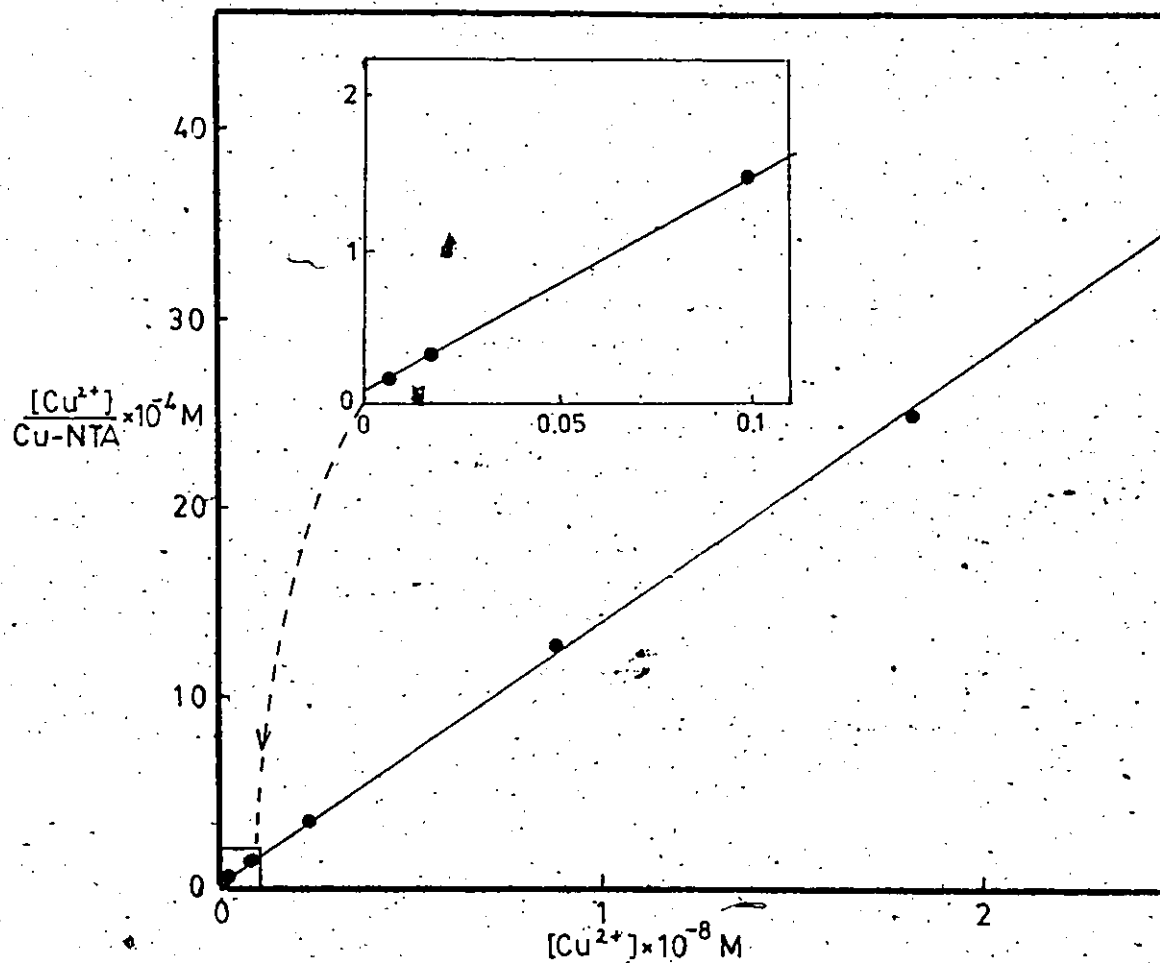
Figure 8.5 presents titration results for 8 μM NTA at pH 6.0.

According to ^{14}C analysis the true concentration range for NTA in this experiment has been 7.39 - 6.28 μM with an average of 6.56 μM . The plot of Cu^{2+} versus $\text{Cu}^{2+}/\text{Cu-NTA}$ shows a break after the first 6 data points. Because there are only two data points available after this break, no precise direction for a second straight line could be determined and hence no calculations could be performed for the second part of the plot. The L_t concentration determined from the first 6 data points is 5.73 μM , 12.6% too low, while the value for $\log K_L'$ is 8.23, on the low side, but within the literature range of $8.15 \leq \log K_L' \leq 9.75$, at pH 6.0.

The experiments shown in Figures 8.3, 8.4 and 8.5 yielded L_t concentrations that are low by 4 - 13%, even after allowing for NTA disappearance due to glass adsorption (8 - 20%). There are several possible explanations.

- (i) The formation of a Cu(NTA)_2 complex is possible; this would result in L_t appearing lower than in fact is the case. Previously (Section 8.2.1), the possibility of such a complex was ruled out on grounds of the concentration of L^{3-} . However, it should be re-considered with regard to the results for L_t .
- (ii) NTA is biodegradable, which could change its concentration during a titration.

Van den Berg (1979) analyzed the possible formation of a CuL_2 complex in considerable detail. He gives an example calculation at typical natural water pH values (pH 7-8) for $L_t = 0.2\text{-}100 \mu\text{M}$, $\log K_{11}$ (1:1 complex) = 8 and $\log K_{21}$ (2:1 complex) = 5, while the Cu^{2+} concentration varies from 10^{-9} to 10^{-5} M. At a total ligand concentration of 0.2 μM , the concentrations of CuL and free L never become high enough to

Figure 8.3 Titration of 8 μM NTA at pH 7.0 (exp. 280681)

Titration of 8 μM NTA at pH 7, using the Implicit Langmuir model for MnO_2 Xvc.

Input : $7.77 \leq L_t (\mu\text{M}) \leq 7.54$ (determined from ^{14}C data)
 $9.15 \leq \log K'_L \leq 10.75$ (from literature data)

Results: $L_t = 7.36 \mu\text{M}$

$\log K'_L = 9.82$

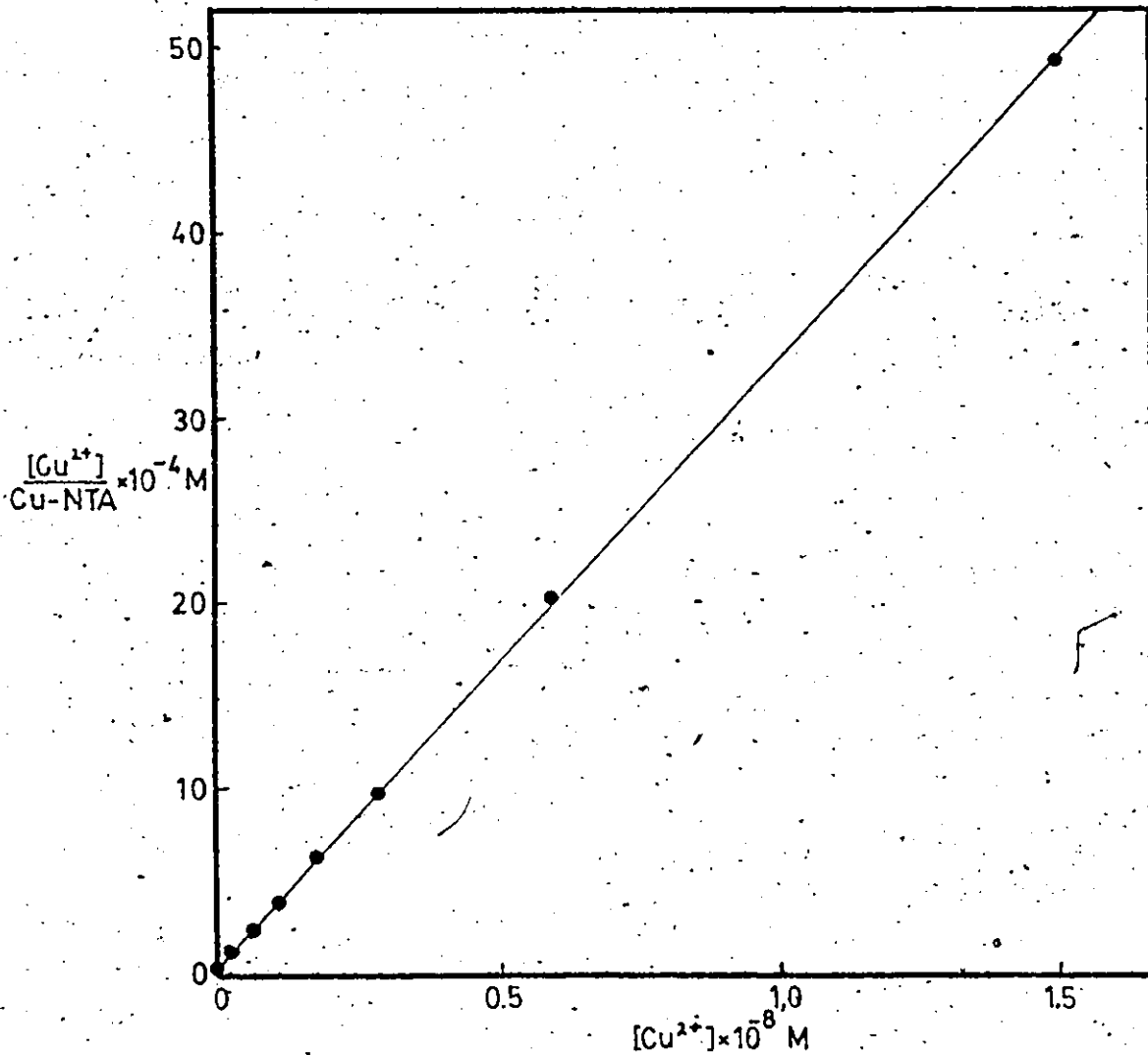


Figure 8.4. Titration of 4 μM NTA at pH 7.0 (exp. 010381)

Titration of 4 μM NTA at pH 7, using the Implicit
Langmuir model for MnO_2 XVe.

Input : $3.68 \leq L_t (\mu\text{M}) \leq 3.20$ (estimated from ^{14}C data)
 $9.15 \leq \log K'_L \leq 10.75$ (from literature data)

Results: $L_t = 3.02 \mu\text{M}$

$\log K'_L = 9.86$

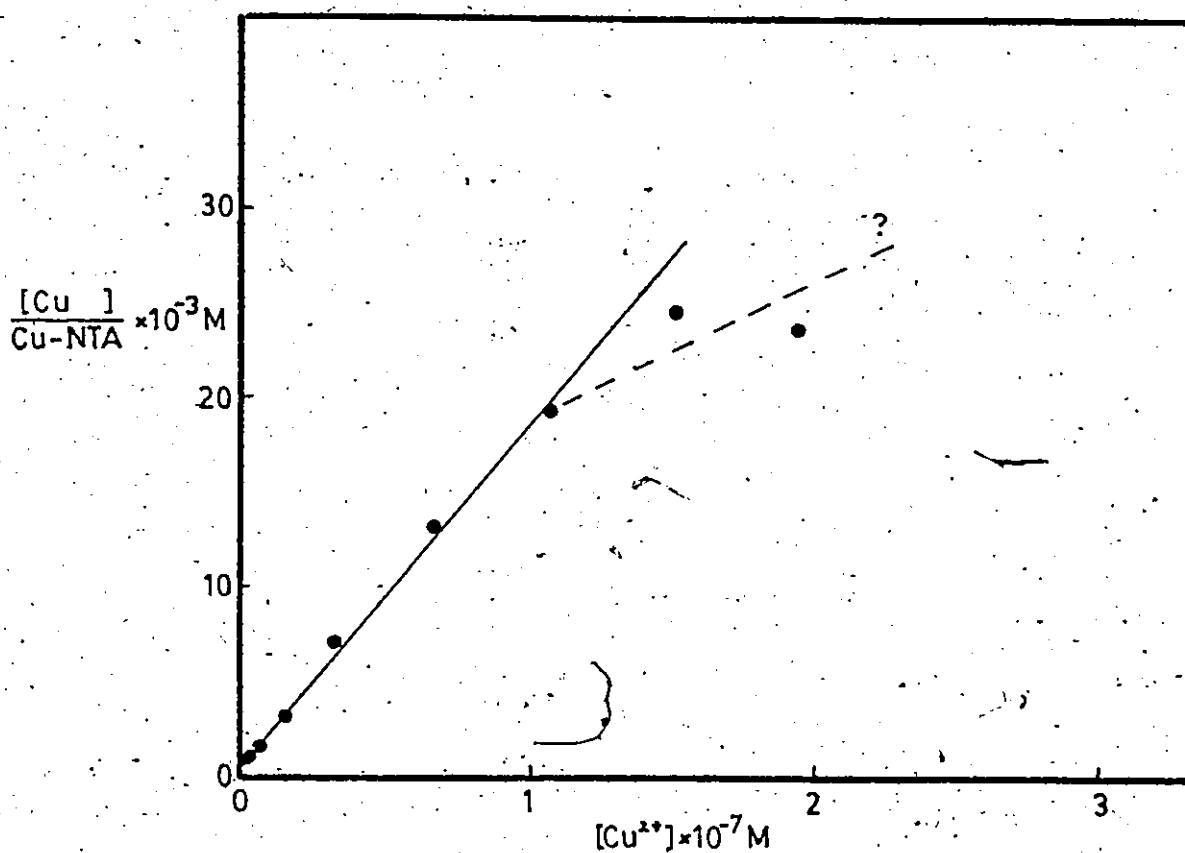


Figure 8.5 Titration of 8 μ M NTA at pH 6.0 (exp. 240781)

Titration of 8 μ M NTA at pH 6, using the Implicit
Langmuir model for MnO₂ Xvc

Input : 7.39 \leq L_t (μ M) \leq 6.28 (estimated from ¹⁴C data)
8.15 \leq logK'_L \leq 9.75 (calculated from literature
data)

Results: L_t = 5.73 μ M

logK'_L = 8.23

induce the formation of CuL_2 , the 2:1 complex. But when L_t is 100 μM , CuL_2 is the most important species from $\text{Cu}^{2+} = 10^{-9}$ M to $\text{Cu}^{2+} = 10^{-7.5}$

It is still an important species at higher Cu^{2+} concentrations. The concentration of CuL_2 increases with increasing L_t concentration and this effect would extend to higher Cu^{2+} concentrations. If K_2 were higher than the value used in the example calculation, the above would occur at lower ligand and metal concentrations. However, for the NTA titrations described in Figures 8.1 to 8.5 ($12.26 \leq \log K_{11} \leq 13.86$, $\log K_{21} = 3.3$ and $2 \mu\text{M} \leq \text{NTA}_t \leq 8 \mu\text{M}$), $\text{Cu}(\text{NTA})_2$ will not form in measureable amounts. Hence, this complex does not provide an explanation for the low values for L_t calculated from the titration data.

Another explanation could be sought in the fact that NTA is biodegradable. During the titration experiments, which lasted 10 to 12 hrs., no particular precautions were taken to suppress biological activity. Biodegradation of NTA to CO_2 and H_2O does not necessarily remove ^{14}C from solution, but makes it incapable of Cu complexation. Chau and Shiomi (1972) show that the Cu-NTA complex is very resistant biologically, and that an unadapted bacteria population takes 4 - 11 days to initiate uncomplexed NTA decay. For the titrations discussed above, organic free water was used and spiked with NTA from a bulk solution which had no visible growth of bacteria in it. During the experiments, increasingly more NTA is complexed with Cu, leaving only the uncomplexed NTA fraction available for biodegradation. Decay of NTA due to unadapted bacteria in the titration experiments is improbable. The possibility of adapted bacteria being present in the NTA bulk solution is equally improbable because there was no visible growth over several months.

It is concluded that experimental error is the only plausible explanation for the too low L_c concentrations determined, although the type of error is unclear.

8.3 Determination of the Conditional Stability Constant for Glycine

Table 8.11 summarizes acidity and stability constants for glycine and Cu-glycine complexes, taken from Sillen and Martell (1971) ($I = 0.1 \text{ KNO}_3$), recalculated for respectively 0 and 0.01 ionic strength via a method by Stumm and Morgan (1970), and taken from REDEQL2 (for $I = 0$ and 0.01). The conditional stability constant for the overall Cu-glycine complex at pH 6.0 can be expressed as:

$$K'_{\text{Cu-gly}} = \frac{[\text{Cu-L}^+] + [\text{Cu-L}_2]}{[\text{Cu}^{2+}]\{[\text{L}^-] + [\text{HL}] + [\text{H}_2\text{L}^+]\}} = \frac{10^{8.70}[\text{Cu}^{2+}][\text{L}^-] + 10^{16.04}[\text{Cu}^{2+}][\text{L}^-]^2}{[\text{Cu}^{2+}]\{[\text{L}^-] + 10^{3.8}[\text{L}^-] + [\text{L}^-]\}} = \frac{10^{8.70} + 10^{16.04}[\text{L}^-]}{10^{3.8}} \quad (8.13)$$

If one ignores the second complex, $\log K'_{\text{Cu-gly}}$ is independent of $[\text{L}^-]$ and has a value of 4.90 at pH 6.0, and $I = 0.01 \text{ KNO}_3$, while REDEQL2 would give 4.78 for identical circumstances. When taking Cu-L_2 formation into account, K'_L changes slightly with the L_c concentration, due to the influence of the $[\text{L}^-]$ term.

An experiment was performed, to determine the conditional stability constant for the Cu-glycine complex at pH 6.0. A mixture of 40 μM Cu and 72.6 μM MnO_2 VIb ('neutral') was titrated with glycine in ten steps (0 - 167 μM glycine, exp. 150580). The Implicit Langmuir model for MnO_2 VIb was used to calculate the results (adsorption parameters: $\Gamma_{\text{max}} = 0.2543$;

Table 8.11 Equilibrium constants for glycine and Cu-glycine

equilibrium reaction	log K (Sillen & Martell 1971)			log K (REDEQL2 1973)	
	I = 0.1	I = 0.0	I = 0.01	I = 0.0	I = 0.01
$\frac{[\text{Cu-L}^+]}{[\text{Cu}^{2+}][\text{L}^-]}$	8.60	8.99	8.70	8.7	8.41
$\frac{[\text{CuL}_2]}{[\text{Cu-L}^+][\text{L}^-]}$	7.20	7.43	7.34	7.3	7.01
$\frac{[\text{H}_2\text{L}^+]}{[\text{HL}][\text{L}^+]}$	2.51	2.47	2.48	2.3	2.32
$\frac{[\text{HL}]}{[\text{H}^+][\text{L}^-]}$	9.70	9.89	9.80	9.9	9.63

$n = 1.874$; $b = -4.828$). Several data points at the beginning of the titration could not be used owing to Γ_{ads} values being in excess of the Γ_{max} limit of 0.2543 set by the Implicit Langmuir model for MnO_2 Vib. The results are given in Table 8.12.

A calibration of the MnO_2 Vib surface (with no glycine present) was performed at the same time as the titration with glycine was carried out. The results for this calibration yielded Single Langmuir adsorption parameters $\Gamma_{max} = 0.262$ and $\log B = 5.80$ (exp. 150580, see Appendix III). These parameters were also used to calculate K'_L from the titration data, and the results are shown in Table 8.13.

A third analysis was carried out on these data, using Cu^{2+} concentrations directly measured during the titration, with a Cu-specific electrode. This electrode had a poor resolution below Cu^{2+} concentrations of 10^{-7} M (see Appendix VI), but nevertheless gives an independent comparison. The results are shown in Table 8.14.

Finally, one can use the measured $Cu_{dissolved}$ data and the input concentrations for total glycine in REDEQL2 to compare the computer calculations with the calculations presented in Tables 8.12-8.14, since REDEQL2 uses slightly different stability constants. The results are shown in Table 8.15.

Average values for $\log K'_{Cu-glycine}$ are summarized in Table 8.16, to compare the calculations presented in Tables 8.12 to 8.15.

Table 8.16 shows that results (i), (iii) and (iv) are close to the literature values for $\log K'_L$. It appears that, although the value derived from analysis with the Implicit model is on the high side, it is still much better than the value obtained with a Single Langmuir model.

Table 12 Titration of 40 μ M Cu and 72.6 μ M MnO₂ Vib with glycine (0 - 167 μ M) at pH 6.0. Calculation of K'_{Cu-gly} using Implicit Langmuir parameters (Γ_{max} = 0.2543, n = 1.874, b = -4.828).

Cu _T (μ M)	L _T (μ M)	Γ_{ads}	Cu _{diss} (μ M)	Cu ²⁺ (μ M)	CuL + CuL ₂ (corrected for hydroxides) (μ M)	free L _T (μ M)	log K' _L
40	0	0.270	20.377	-	-	-	-
40	10.921	0.258	21.239	-	-	-	-
40	23.031	0.250	21.823	23.919	-	-	-
40	50.494	0.257	21.372	-	-	-	-
40	81.893	0.233	23.030	3.971	18.979	62.914	4.88
40	100.254	0.214	24.463	1.777	24.463	75.790	5.26
40	122.735	0.214	24.463	1.777	24.463	98.272	5.14
40	149.679	0.189	26.294	0.875	25.401	124.278	5.37
40	167.051	0.188	26.320	0.858	25.445	141.606	5.32

Table 8.13 Calculation of K'_L Cu-gly using Single Langmuir parameters ($\Gamma_{max} = 0.262$ and $\log B = 5.80$)

Cu _{diss} (μM)	Cu ²⁺ (μM)	Cu-L + Cu-L ₂ (corrected for hydroxides) (μM)	free L (μM)	log K'_L
20.377	-	-	-	-
21.239	101.99	-	-	-
21.823	32.94	-	-	-
21.372	81.276	-	-	-
23.030	12.705	10.325	71.568	4.055
24.463	7.050	17.413	82.841	4.474
24.463	7.050	17.413	105.322	4.370
26.294	4.094	22.200	127.479	4.629
26.320	4.017	22.303	144.748	4.584

Table 8.14. Calculation of K'_L Cu-gly using Cu²⁺ data measured by Cu electrode

Cu _{diss} (μM)	Cu ²⁺ (μM)	Cu-L + Cu-L ₂ (corrected for hydroxides) (μM)	free L (μM)	log K'_L
20.337	4.5	-	-	-
21.239	4.5	16.739	-	-
21.823	4.5	17.323	5.708	5.82
21.372	3.5	17.872	32.622	5.19
23.030	3.2	19.830	62.063	5.00
24.463	3.2	21.263	78.991	4.92
24.463	2.6	21.863	100.872	4.92
26.294	2.6	23.694	125.985	4.86
26.320	2.2	24.120	142.931	4.88

Table 8.15 Calculation of K' Cu-gly using experimental data for Cu_{diss} and total glycine concentrations and the computer program REDEQL2.

Cu_{diss} (μM)	Glycine _t (μM)	Cu^{2+} (μM)	$Cu-L + Cu-L_2$ (corrected for hydroxides) (μM)	L_{free} (μM)	K' Cu-gly
20.377	0	20.377	-	-	-
21.239	10.921	15.551	5.248	5.625	4.778
21.823	23.031	11.878	9.550	13.186	4.785
21.372	50.494	6.511	14.791	34.682	4.814
23.030	81.893	4.282	18.197	61.674	4.838
24.463	100.254	3.784	20.417	75.876	4.852
24.463	122.735	2.970	21.380	97.747	4.867
26.294	149.679	2.530	23.442	120.255	4.886
26.320	167.051	2.192	23.988	138.071	4.899

Table 8.16: Average values for K' Cu-gly calculated from the same data set with different methods

Calculation method	presented in Table:	average $\log K'$ Cu-gly
(i) Implicit Langmuir model	8.12	5.19 ± 0.20
(ii) Single Langmuir model	8.13	4.42 ± 0.23
(iii) Cu-specific electrode	8.14	5.08 ± 0.34
(iv) REDEQL2	8.15	4.84 ± 0.04

Literature value for K'_L (ignoring CuL_2) calculated with constants from Table 8.11		4.90
Literature value for K'_L (ignoring CuL_2) calculated with REDEQL2 constants from Table 8.11		4.78

Table 8.16 shows that the latter (result ii) is considerably too low when compared to literature values.

The literature values for $\log K'_L$ given in Table 8.16 ignore formation of a CuL_2 complex. This causes the calculated values to be on the low side. A slight increase of $\log K'_L$ with increasing L_t concentration is expected and the extent of such an increase is shown in Table 8.15 where experimental results were analyzed with REDEQL2. Both data sets shown in Tables 8.12 and 8.13 exhibit the expected increase of $\log K'_L$ with increase in ligand concentration, although the range seems quite erratic. The Cu-specific electrode data yield a slightly decreasing range of values for $\log K'_L$ with increasing L_t , which is presumably due to inaccuracies of the Cu^{2+} electrode.

In conclusion, it can be said that the previous calculations show that the conditional stability constant for the Cu-glycine complex at pH 6.0 can be determined accurately by using the Implicit Langmuir model. The results obtained with a Cu-specific electrode also yield an accurate value for $\log K'_{\text{Cu-glycine}}$. The results obtained with a Single Langmuir model are clearly too low when compared to literature values.

8.4 The Effect of the Cu/MnO_2 Ratio on the Adsorption of Cu onto

$\delta\text{-MnO}_2$ VIb at pH 6.0

The usual amount of MnO_2 added per titration or calibration lies between 70 and 90 μM while Cu additions at pH 6 normally range anywhere from 1 to 43 μM (at higher pH values, less Cu is added). This means that the Cu_t/MnO_2 ratio varies from approximately 0.01 to 0.50. To assess the influence of this ratio on the adsorption process, an experi-

ment was designed in which a mixture of 40 μM Cu_t and 100 μM glycine was titrated with MnO_2 VIb ('neutral') at pH 6.0 (exp. 290580, see Appendix III). The results of this titration are shown in Table 8.17. Cu^{2+} concentrations were calculated from the amount of Cu measured in solution (i.e. Cu_{diss}), with REDEQL2.

Figure 8.6 shows the isotherm obtained for this experiment (i.e. Γ_{ads} vs. Cu^{2+}) while in Figure 8.7 the results are plotted according to the linearized Single Langmuir expression (i.e. $\text{Cu}^{2+}/\Gamma_{\text{ads}}$ vs. Cu^{2+}).

It appears that if the Cu_t/MnO_2 ratio exceeds 0.50, initially a slow adsorption increase is observed, which increases very rapidly at a ratio of approximately 1.15, at which point the free Cu^{2+} concentration becomes almost a constant. This could indicate that precipitation of Cu on the MnO_2 surface takes place, increasing the adsorption capacity far beyond the limit set by surface complexation. The actual mechanism of such a surface precipitation process is not clear. From Figure 8.7 it can be seen that with the Cu_t/MnO_2 ratio decreasing to 'normal' values near or below 0.5, the adsorption pattern resembles the observed behaviour for MnO_2 VIb (see Figures 7.12 to 7.14). Analysis of the last three points according to a linearized single Langmuir isotherm gives $\Gamma_{\text{max}} = 0.323$ and $\log B = 6.19$. This value of Γ_{max} is somewhat higher than the values measured for MnO_2 VIb via ordinary adsorption isotherms at pH 6 (see Table 7.7). This could perhaps be explained as follows: At the beginning of this particular experiment the Cu_t/MnO_2 ratio is extremely large, possibly causing surface precipitation. Upon lowering the ratio by adding more MnO_2 , the surface precipitate redissolves, but the kinetics may be relatively slow compared to the surface precipitation reactions, or alternatively the surface precipitation process is partially irreversible.

Table 8.17 Results for titration of 40 μ M Cu_t and 100 μ M glycine with MnO₂ VIB at pH 6.0

MnO ₂ VIB (μ M)	Cu _t /MnO ₂ VIB	Cu _{diss} (μ M)	Γ_{ads}	Cu ²⁺ (REDEQL2) (μ M)
7.454	5.37	28.098	1.587	4.5396
24.501	1.63	27.962	0.491	4.5121
34.591	1.15	27.609	0.358	4.4306
46.202	0.93	24.470	0.337	3.7946
59.537	0.67	23.152	0.283	3.5375
75.192	0.53	19.484	0.273	2.8552
94.309	0.42	17.133	0.242	2.4439
118.091	0.34	11.997	0.237	1.6142

Table 8.18 Equilibrium constants for aspartic acid, alanine and glutamic acid, from REDEQL2

aminoacid	complexes	log K (I=0.0)	log K (I=0.01)
aspartic acid	(H)1 (L)1	9.7	9.63
	(H)2 (L)2	13.6	13.46
	(H)3 (L)1	14.9	14.96
	(Cu)1 (L)1	8.9	8.71
	(Cu)1 (L)2	16.0	15.72
alanine	(H)1 (L)1	9.9	9.83
	(H)2 (L)1	12.3	12.25
	(Cu)1 (L)1	8.7	8.51
	(Cu)1 (H)2	15.9	15.62
glutamic acid	(H)1 (L)1	10.0	9.84
	(H)2 (L)1	14.3	14.07
	(H)3 (L)1	16.7	16.49
	(Cu)1 (L)1	8.9	8.53
	(Cu)1 (L)2	15.5	15.13

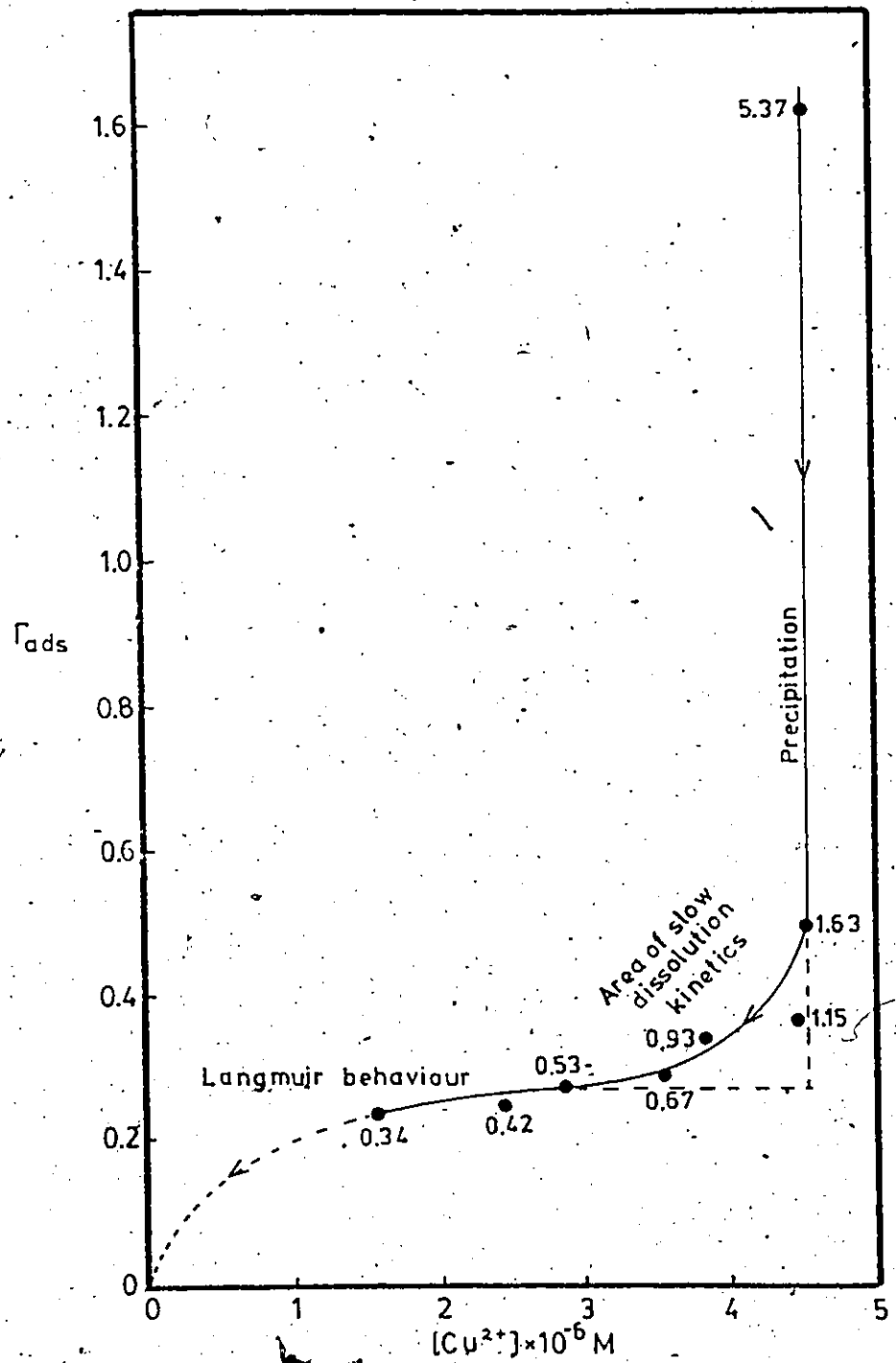


Figure 8.6 Adsorption isotherm for the titration of 40 μ M Cu and 100 μ M glycine with MnO₂ VIB (7.5 - 120 μ M) at pH 6.0. \rightarrow indicates direction of titration expt.

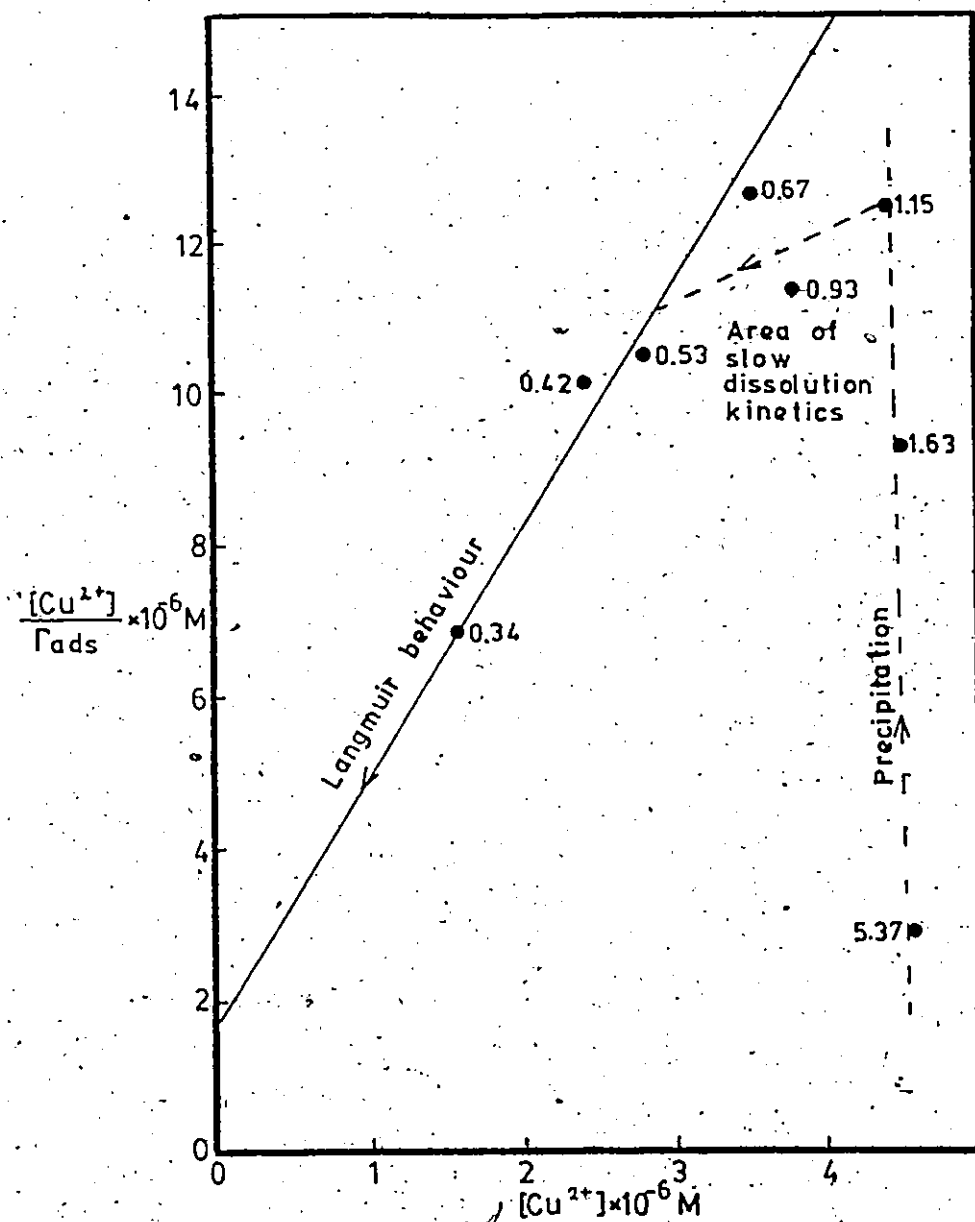


Figure 8.7 Linearized Single Langmuir isotherm for the titration of 40 μ M Cu and 100 μ M glycine with MnO₂ VIB (7.5 - 120 μ M) at pH 6.0.
 → indicates direction of titration expt.

(In Figures 8.6 and 8.7 the proposed areas of precipitation, slow dissolution kinetics and Langmuir behaviour are indicated). However, more experiments are needed to prove this.

One significant conclusion from this titration with MnO_2 is, that the Cu_t/MnO_2 ratio is important in determining the amount of adsorption beyond the obvious surface complexation plateau, which represents a monolayer according to the Langmuir theory. Also, this effect might partially explain why van den Berg (1979) (and others) find such high values for Γ_{max} (and/or a Γ_{max} increase with pH); their critical Cu_t/MnO_2 ratio could well have exceeded 0.5. For instance, van den Berg (1979) reports calibrations of the $\delta\text{-MnO}_2$ surface for Cu uptake at a concentration of $100 \mu\text{M MnO}_2$ and a Cu_t concentration range of $10 - 100 \mu\text{M}$ which results in a Cu_t/MnO_2 ratio range of $0.1 - 1.0$.

8.5 Titration of Other Amino Acids

Experiments were carried out to determine the Cu- conditional stability constants for several amino acids, at pH 8.0 using MnO_2 Xvc. The amino acids that were treated as 'unknown' organics are aspartic acid, alanine and glutamic acid. These ligands complex Cu rather weakly and therefore high concentrations of ligand were used in the titration experiments, so that complexation could be observed.

These same experiments were previously discussed in Chapter 7 (Figure 7.18), where they were used to help establish the Implicit Langmuir adsorption parameters for the 'neutral' $\delta\text{-MnO}_2$ Xvc surface ($\Gamma_{\text{max}} = 0.1988$; $n = 1.655$; $b = -3.119$).

To treat these experiments here as titrations of 'unknown' ligands, the above Implicit adsorption parameters cannot be used to

analyze the data, because these parameters were obtained partially with the data of these particular titrations. Therefore, calibration data for MnO_2 XVe at pH 6, 7 and 8 (performed on 010381, in the presence of 50 μM glycine) were fitted to the Implicit Langmuir model. This provided estimates for adsorption parameters that are independent from the amino acid experiments to be analyzed. The adsorption parameters obtained are: $\Gamma_{\text{max}} = 0.2668$; $n = 1.597$ and $b = -2.982$. Except for the value of Γ_{max} , these values resemble the originally obtained values for MnO_2 XVe quite closely (i.e. $\Gamma_{\text{max}} = 0.1988$; $n = 1.655$ and $b = -3.119$).

The titration results for aspartic acid, alanine and glutamic acid were analyzed, using these independent Implicit adsorption-parameters. Cu^{2+} and Cu-L concentrations were calculated from the Γ_{ads} data and the measured amount of Cu in solution. Also, the dissolved Cu data were used to calculate Cu^{2+} and Cu-L (= $\text{CuL} + \text{CuL}_2$) concentrations with REDEQL2, for comparison with the Implicit Langmuir data. This was done because it was anticipated that problems might arise due to factors such as the weakness of the ligands, the formation of CuL_2 complexes in solution and perhaps adsorption of ligands (especially glutamic acid) on the MnO_2 surface. The results of these calculations and comparisons are shown graphically in Figures 8.8, 8.9 and 8.10. A summary of the complexes and their stability constants used in REDEQL2 is given in Table 8.18. With these values, the conditional stability constants at pH 8 and $I = 0.01$ can be expressed as:

$$\text{for aspartic acid} \quad K'_L = \frac{10^{8.71} + 10^{15.72} [\text{L}^-]}{10^{1.63} + 10^{-2.26} [\text{L}^-]} \quad (8.14)$$

$$\text{for alanine } K'_L = \frac{10^{8.51} + 10^{15.62} [L^-]}{10^{1.83}} \quad (8.15)$$

$$\text{for glutamic acid } K'_L = \frac{10^{8.53} + 10^{15.13} [L^-]}{10^{1.84}} \quad (8.16)$$

Recalling the arguments made by van den Berg (1979) which were discussed in Section 8.2.3, the situation is now such that the ligand concentration is high (80 μM), K_{21} (for CuL_2) has a value very similar to K_{11} , and the Cu^{2+} concentration is well below $10^{-7.5}$, which means that CuL_2 (the 2:1 complex) is the most important species throughout the whole titration. This necessarily implies that the correct L_t concentration cannot be derived from the slope of the plot of Cu^{2+} versus $\text{Cu}^{2+}/\text{CuL}$.

Figures 8.8 and 8.9 show good agreement between Implicit Langmuir and REDEQL2-calculated data points, if one disregards one or two high data points on the left side of the plot. Agreement for Figure 8.10 is poor. However, all three Figures show an upward trend for data points on the left side of the plot. This means that there the Cu^{2+} concentration is estimated too high and/or the Cu-ligand concentration too low. The REDEQL2 data were calculated with measured Cu dissolved data and give no problems other than expected (2:1 complex formation, see above). Hence, if the $\text{Cu}_{\text{dissolved}}$ data are correct, the $\text{Cu}_{\text{adsorbed}}$ and Γ_{ads} data, from which the Cu^{2+} concentrations are calculated, must be correct. The only feasible cause for the particular curvature found in the data points in all three Figures is that Γ_{ads} is not in equilibrium with the free Cu^{2+} concentration. This is possible if the Cu-L complex (or Cu-L_2) adsorbs on the surface. In such a case, Cu^{2+} is overestimated and Cu-L (i.e.

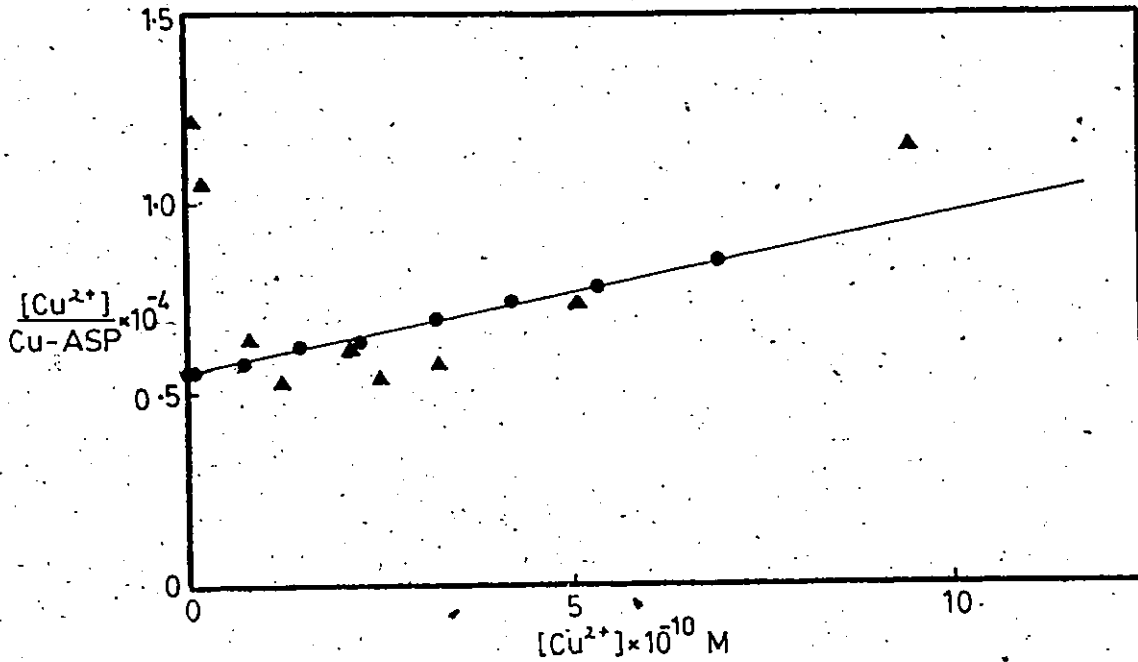


Figure 8.8 Titration of 80 μ M aspartic acid in the presence of MnO₂ XVe at pH 8 (exp. 080481)

$\log K'_{Cu-asp} = 8.05$ from equilibrium constants in Table 8.18
 aspartic acid = 80 μ M (added)

▲ data points calculated with Implicit model. They yield
 (excluding the first two points on left):- $\log K'_L = 9.18$
 $L_t = 14.80\mu\text{M}$

● same data, calculated for aspartic acid with REDEQL 2.
 They yield: $\log K'_L = -8.89$

$L_t = 23.57 \mu\text{M}$

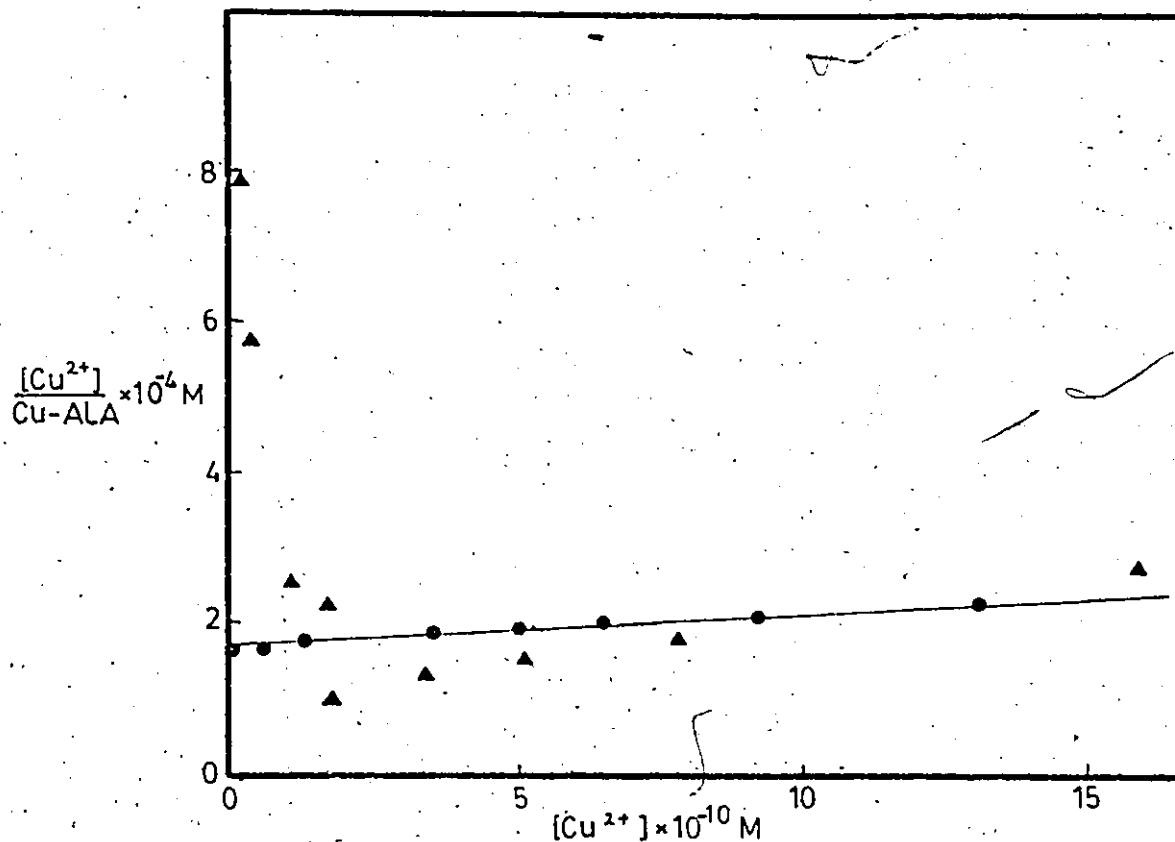


Figure 8.9 Titration of 80 μ M alanine in the presence of MnO_2 Xvc at pH 8.0

$\log K'_{\text{Cu-ala}} = 7.82$ from equilibrium constants in Table 8.18
alanine = 80 μ M

▲ data points calculated with Implicit model.
They yield (after excluding the first two points on the left) : $\log K'_L = 8.56$

$$L_t = 18.09 \mu\text{M}$$

● same data, calculated for alanine with REDEQL 2. They yield : $\log K'_L = 8.39$

$$L_t = 24.22 \mu\text{M}$$

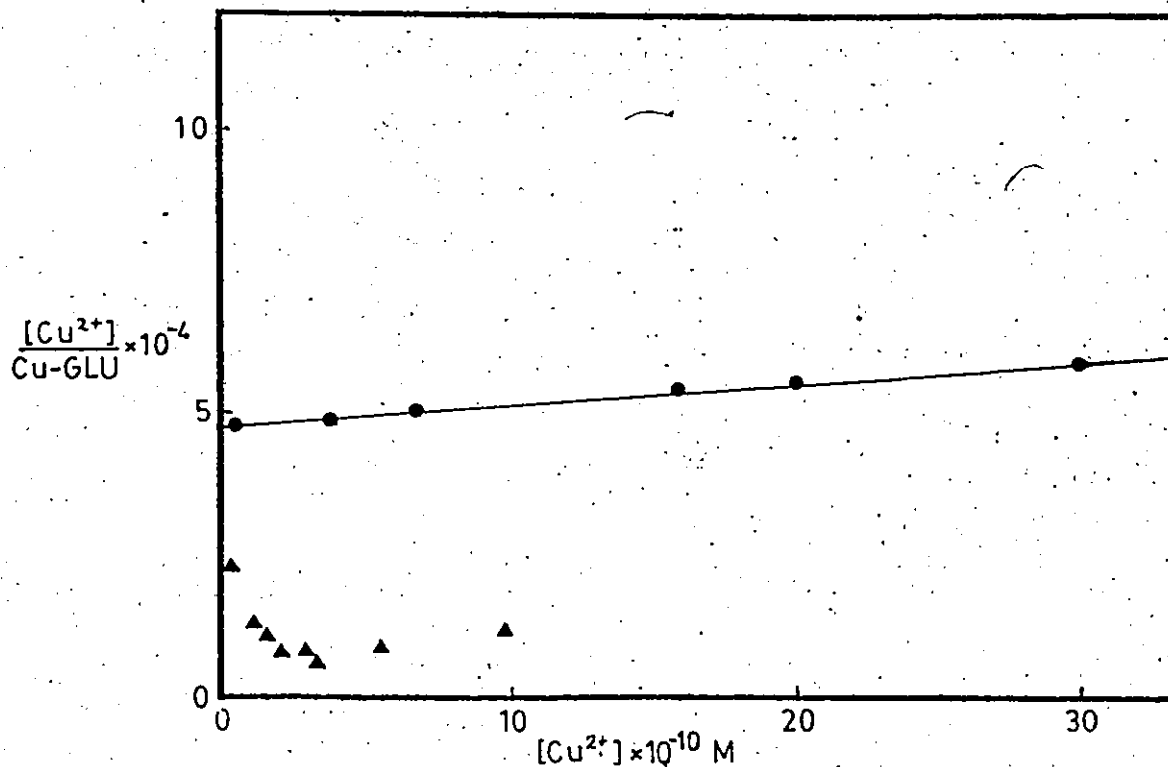


Figure 8.10 Titration of 80 μ M glutamic acid in the presence of MnO₂ KVC at pH 8.0

$\log K'_{\text{Cu-glu}} = 7.39$ from equilibrium constants in Table 8.18
glutamic acid = 80 μ M (added)

▲ data points calculated with Implicit model.
They yield (after excluding the first point on the left) : $\log K'_L = 8.08$

$$L_t = 95.08 \mu\text{M}$$

● same data, calculated for glutamic acid with REDEQL 2. They yield : $\log K'_L = 7.87$

$$L_t = 28.14 \mu\text{M}$$

$(Cu-L + Cu-L_2)$ is underestimated. The fact that later in the titration experiments, behaviour of the data points seems normal, could indicate that the initially adsorbed $Cu-L$ complex desorbs when more Cu^{2+} becomes available for direct adsorption (Cu_t increases during the titration). Adsorption of Cu^{2+} must then be favourable over $Cu-L$ or $Cu-L_2$ adsorption. However, these are speculations and need more investigation. Values for $\log K'_L$ and L_t were calculated for each amino acid, from both the experimental and REDEQL2 data, plotted in Figures 8.8, 8.9 and 8.10. The experimental data all showed a $Cu_{dissolved}$ (and hence $Cu-L$) concentration range from 0.1 - 8 μM , indicating that minimally 72 μM of ligand was uncomplexed. Taking the acidity constants into account, a value for the $[L^-]$ concentration of approximately 1 μM is calculated. This value can be used to calculate the approximate true value for K'_L , using the above expressions (8.14-8.16). K'_L and L_t values for each amino acid, calculated from experimental data, REDEQL2 data and the equilibrium expressions are summarized in Table 8.19. Table 8.19 also contains values for $\log L_t \cdot K'_L$ since this product is important in determining the concentration of free Cu^{2+} in solution:

$$Cu^{2+} = \alpha Cu_t, \quad (8.17)$$

$$\text{where } \alpha = \frac{1}{[K'_L \cdot L_t] + 1} \quad (\text{van den Berg 1979}) \quad (8.18)$$

It can be concluded from Table 8.19 that although $\log K'_L$ and L_t values differ for all 3 methods of calculating them, the product of

$K'_L \cdot L_t$ agrees very closely for alanine and reasonably closely for aspartic acid. For glutamic acid however, the difference between the experimental and the calculated $K'_L \cdot L_t$ products is almost an order of magnitude. It is not clear why this is the case. Alanine is very similar to glycine in structure, and likely does not adsorb on the δ - MnO_2 surface. Glutamic and aspartic acid are also very similar in structure. Aspartic acid was found not to adsorb in any significant amounts on MnO_2 at pH 6.0 in this study. However, Davis (1979) reports that glutamic acid adsorbs on amorphous iron oxide, most likely involving the terminal carboxyl group in the surface bond formation. Hence, adsorption of glutamic acid (with or without Cu mediation) could be an explanation for the observed discrepancy between experimental and theoretical results for glutamic acid. This should be further investigated with ^{14}C labelled glutamic acid. In addition ^{14}C studies should be performed to assess alanine and aspartic acid adsorption onto δ - MnO_2 at pH 8, since this seems to be the only feasible explanation for the observed trends in Figures 8.8 to 8.10.

In conclusion, it can be said that, although for weak ligands that are capable of forming 2:1 (CuL_2) complexes, for which K_{11} and K_{21} are very similar, the produced values for L_t and K'_L with the MnO_2 method are not correct individually, their product, determining the amount of free Cu^{2+} in solution, resembles the theoretical value very closely.

8.6 Summary and Conclusions

The Single- and Implicit Langmuir model are compared for their ability to determine conditional stability constants and total ligand

concentrations for NTA and glycine at pH values varying from 6 to 8. The Single Langmuir model produces K'_L values that are considerably lower than literature values. The Implicit Langmuir model yields K'_L values that agree well with the range of values obtained from the literature. This provides good validation for the Implicit Langmuir adsorption model and its underlying assumptions. Figure 8.11 summarizes the results obtained for NTA in this study, with the Implicit Langmuir model, and compares these results to literature values and values obtained by van den Berg (1979) with the Single Langmuir model.

The Implicit Langmuir model is capable of assessing the formation of 1:2 (Cu_2L) complexes. For NTA, a second adsorption site for Cu was found. The conditional stability constant for this site (K'_{12}) is more than two orders of magnitude lower than the conditional stability constant of the first site (K'_{11}). Values for K'_{12} are not given in the literature.

L_t values determined with the Implicit model tend to be low for NTA (5-12%), for which there is no ready explanation.

It was shown that correction for both $\text{Cu}(\text{OH})^+$ and $\text{Cu}(\text{OH})_2^0$ formation has a large influence on the titration results, and should be routine procedure.

The Implicit Langmuir model has been proven very useful in the estimation of K'_L and L_t for high concentrations of relatively weak, 1:1 (CuL) and 2:1 (CuL_2) complex forming ligands. Although the obtained individual values for K'_L and L_t are incorrect, their product, which governs Cu^{2+} concentration in solution, agrees with literature values for the product $L_t \cdot K'_L$.

A titration with MnO_2 finally showed that the Cu_t/MnO_2 ratio is

most important in obtaining reliable values for Γ_{\max} , the maximum adsorption capacity, representing a monolayer in the Langmuir theory. All experiments in this study are for ratios ≤ 0.5 . It was shown that an increase in this ratio greatly affects the results, probably by enhancing surface precipitation processes, causing adsorption capacities, far exceeding the limits of a surface complexation model.

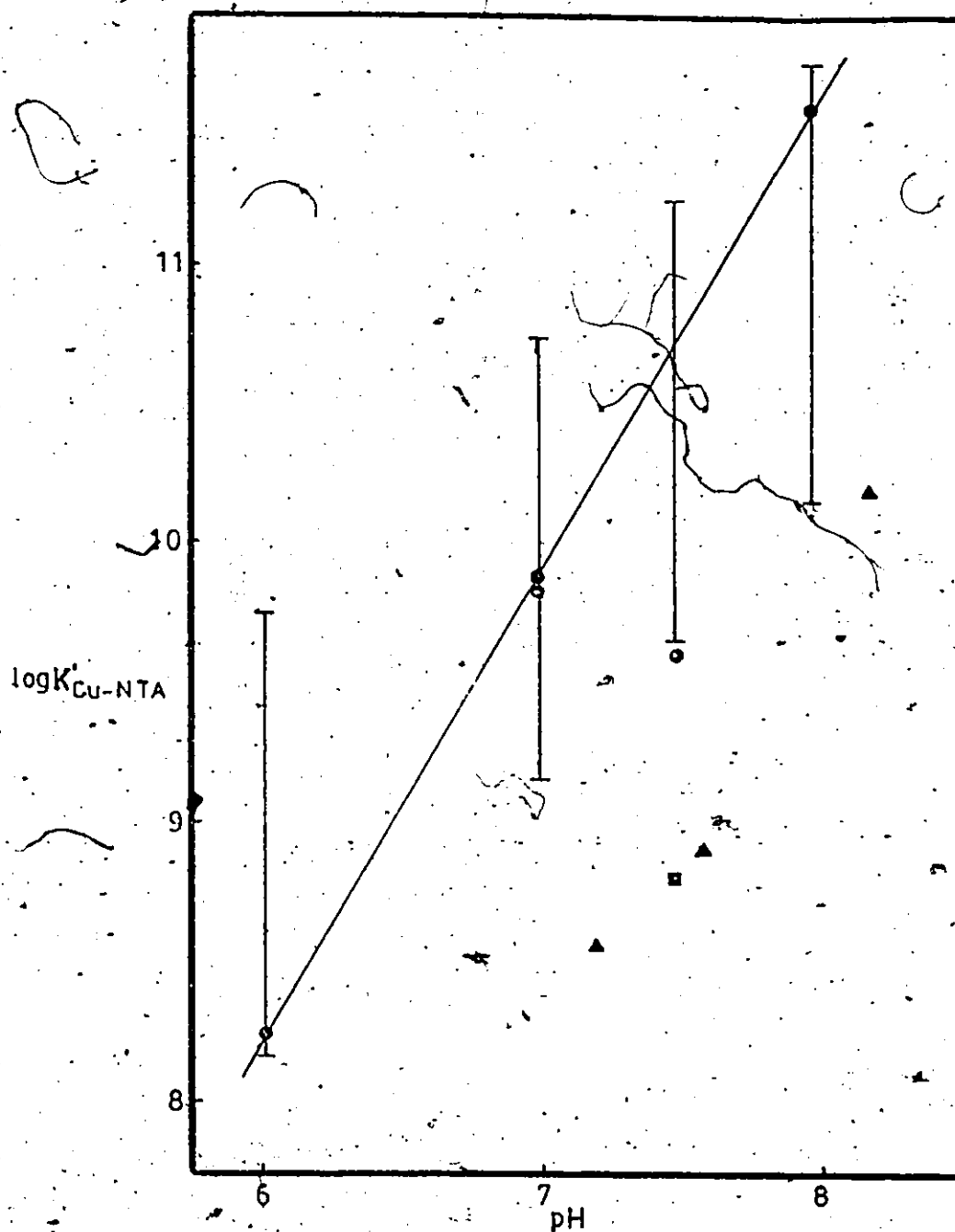


Figure 8.11 Summary of conditional stability constants for the Cu-NTA complex

- data from this study, obtained with the Implicit Langmuir function
- | literature data (Sillen and Martell 1964, 1971)
- ▲ van den Berg's (1979) data, obtained with the Single Langmuir function
- data obtained in this study with the Single Langmuir function

CHAPTER 9

APPLICATIONS OF δ -MnO₂ RESEARCH IN ENVIRONMENTAL ENGINEERING9.1 Introduction

Adsorption behaviour of δ -MnO₂ has been investigated with emphasis on the use of this surface as a resin in trace metal speciation studies. Chapter 1 pointed out why knowledge of the relations between trace metals and inorganics, organics and particulates is crucial for the prediction of the fate of these metals in natural waters. Once the type and strength of the most dominating relationships are known, one can apply an engineering approach to the overall modeling of the (equilibrium) state of affairs of trace metals in the water bodies under study.

The MnO₂ method provides a very straightforward and simple way for obtaining necessary conditional stability constants for equilibrium calculations. However, this research established that the MnO₂ method is more complicated than was originally proposed because

- (i) Adsorption of Cu on δ -MnO₂ did not display Langmuir behaviour at low surface coverage.
- (ii) Surface-preparation and -aging aspects with their inherent effects on surface properties, including adsorption behaviour, were not sufficiently known.
- (iii) Certain (unknown) organic material may adsorb on the δ -MnO₂ surface, with or without trace metals as a link. This would likely change ordinary adsorption behaviour.

All three aspects have been assessed in this study, and the new,

semi-empirical adsorption model derived in Chapter 5 and used in Chapters 7 and 8, is one of the results. The Implicit Langmuir expression has a sound basis, in that the parameters are derived for a set of adsorption data in a certain pH range, and verified for an independent set of data obtained for the same surface over an identical pH range. The model is simple, easy to use and understand, because it is based on the mass law expression, written in Langmuir terms, but takes the surface charge changes as a result of adsorption into account. The model does not rely on specified surface charge and -potential values, but is at the same time not in contradiction with the principles of the triple layer model which describes the adsorption area surrounding a charged particle. Thus, a simple, adequate model, describing adsorption of trace metals onto $\delta\text{-MnO}_2$ in the pH range 6 to 8.5, has evolved.

The Implicit Langmuir model developed here can be applied in various environmental engineering situations. This is discussed in section 9.2. The information obtained from the surface-aging and characterization study, and the results obtained for the model ligand NTA, are also very useful in the assessment of a number of environmental engineering problems. This is exemplified in Sections 9.3 to 9.5.

9.2 Speciation Studies : General

The $\delta\text{-MnO}_2$ method, improved with the implicit Langmuir adsorption model for Cu adsorption on $\delta\text{-MnO}_2$, is able to provide both the ligand concentration (assuming a 1:1 complex with Cu, or in other words the complexing capacity) and the conditional stability constant for any

non-sorbing Cu-ligand complex. Other metals can be used; the δ -MnO₂ surface must then be calibrated for these metals (van den Berg 1979). One objective for water quality management is to estimate the metal toxicity; present evidence shows that the free metal ion is the toxic species. For any freshwater body, the concentration and conditional stability constant of the dominating ligand can be measured and then used to calculate trace metal (e.g. Cu) speciation. For this purpose, one can begin very simply, by only considering the dominant inorganic ligands. This would be appropriate for an oligotrophic lake. Ligands such as carbonate and hydroxyl ions can be measured and stability constants for trace metals are generally well-established in the literature. (If not, the δ -MnO₂ method can also be used to determine conditional stability constants for inorganic ligands). The system can be made progressively more complicated by considering organic ligands in the case of more eutrophic and/or polluted water bodies. Van den Berg (1979) found one dominating ligand or site for all but one of the natural water samples investigated in his study. One can use the δ -MnO₂ method to determine the conditional stability constant and concentration of this particular ligand or site, and calculate the combined effects of inorganic ligands and the organic site, on Cu speciation at the particular pH for which the conditional stability constant was determined.

Speciation calculations are greatly facilitated by use of such existing equilibrium computer programs as REDEQL2 (McDuff and Morel 1973), MINEQL (Westall et al. 1976), etc. Once a conditional stability constant is determined, one can look in the data bank of such programs for a model ligand which has a stability constant very similar to the

one of the natural organic ligand, at the particular pH for which it was obtained, and include this model substance (in the concentration measured) in the equilibrium calculations one wants to perform. Replacing the stability constant(s) of a known ligand in the data bank of the computer program with the natural organic constant(s) is difficult, since one does not know the effect of pH on the constant(s). Other mechanisms which can be modeled simultaneously include precipitation of solids, adsorption and redox reactions.

Equilibrium models have been applied widely for calculation of metal speciation in the presence of various ligands and surfaces. The majority of calculations have involved surfaces such as silica. Morel et al. (1975) examined the possible solids which could form to explain observed metal concentrations in the Los Angeles County wastewater treatment plant effluent; silica was used as an adsorbing surface. For Cu there are few studies reported in which the calculation of Cu speciation is given in the presence of both organic ligands and an adsorbing surface. No such studies are discussed by Nriagu (1979) for natural systems, in his review on Cu in the environment.

Guy et al. (1975) studied metal distributions in a model system containing MnO_2 , bentonite and colloidal humic acids as adsorbing surfaces, and humic and tannic acid as organic ligands. Cu was included in this study.

The calculations of Hoffman and Eisenreich (1981) are an excellent example of equilibrium calculations for freshwater systems. They use the above approach to explain the unusually high Mn and Fe concentrations observed in the hypolimnion in Lake Mendota, Wisconsin, during summer stratification. Due to the higher surface water temperature in summer,

the hypolimnion becomes isolated from the epilimnion, causing O_2 depletion in the former; there is no mixing with oxygenated surface water, and no photosynthesis, because the hypolimnion is usually located below the photic zone. The increase in CO_2 from respiration causes the pH to drop while O_2 depletion forces bacterial utilization of sulphates as O_2 source, resulting in release of H_2S . The combined effect is a lowered pH and a low pE which causes dissolution of precipitates such as hydrous oxides and/or release of adsorbed or complexed metal ions. By analyzing field data, Hoffman and Eisenreich (1981) were able to estimate the likelihood of certain mechanisms (i.e. dissolution, desorption, etc.). By incorporating model-surfaces (e.g. $\delta-MnO_2$, $\alpha-SiO_2$) and -ligands besides actually measured ones in their calculations with REDEQL2, they were able to predict, reasonably well, the observed elevated concentrations of Mn and Fe. In their case, the James and Healy (1972) model was used for adsorption on hydrous oxide surfaces. However, in this model it is tacitly assumed that the free energy of adsorption (ΔG_{ads}^0) is independent of the fractional coverage of the surface. In Chapter 7 it was shown that, adsorption strength decreases with increasing coverage of the surface in the case of Cu adsorption on $\delta-MnO_2$, a surface included in Hoffman and Eisenreich's study. Westall and Hohl (1980) found no difference in mathematical correctness for adsorption models such as the constant capacitance model, diffuse layer model, the basic or extended Stern model or the triple layer model (see Chapter 5). The Implicit Langmuir model developed here incorporates the dependence of fractional surface coverage and is mathematically very simple, yet is based on the constant capacitance model. Therefore, incorporating the Implicit Langmuir function for the modeling of trace metal adsorption on hydrous oxides in general in computer programs such

as REDEQL2, seems very promising for speciation calculations for natural water systems. However, this cannot be done as yet, since the Implicit model has been developed and verified for adsorption of Cu on δ -MnO₂ only for a limited pH range, and needs application to other hydrous oxides and trace metals.

Adsorption of Cu on δ -MnO₂ is applicable in the modeling of natural water situations for more than just equilibrium calculations. Its most apparent use, (described above), is as a powerful tool for determining conditional stability constants and complexing capacities, and also as a promising general model for describing adsorption of trace metals on hydrous oxides.

Once the chemical model procedure has been set up, stability constants have been chosen or obtained, and controlling mechanisms and model substances have been determined, one can combine the equilibrium calculations in an engineering system, controlled by engineering parameters, which can be fixed or variable (i.e. inflow, outflow, etc.). The engineering systems can also be described relatively simply, e.g. ... a completely mixed system (lakes, bays), or in a more complicated fashion such as a dispersed plug flow system (streams or rivers) (Thomann 1972).

9.3 Speciation Studies with Emphasis on NTA and δ -MnO₂

This work has dealt in detail with the adsorption of Cu on δ -MnO₂. Inherently, the speciation of Cu in laboratory systems where an organic ligand (e.g. NTA, glycine) and an inorganic surface (δ -MnO₂) compete with each other for Cu²⁺, formed a central part of this study.

A natural water system may be viewed as a similar system, albeit far more complex because of the existence of other ions, ligands and surfaces besides Cu, NTA or glycine and δ -MnO₂. To environmental engineers

it is important to know what kind of ligands and adsorbing surfaces do occur in certain aquatic systems, and whether their concentrations are such that they can significantly complex metals.

Organic ligands in natural waters are found in the dissolved organic carbon (DOC) fraction. Typical concentrations are of the order of 0.3×10^{-3} M (as carbon). DOC is composed of a variety of organic ligands, from simple amino acids to very complex humic substances. Amino acids are relatively weak with respect to complexing Cu, while humics have the ability to bind Cu strongly. From Figures 2.1 and 2.2, it can be concluded that both glycine and NTA possess complexation strengths in the range of those of unknown natural organics. In the following paragraphs the influence of the presence of NTA in natural water systems will be exemplified.

NTA has been introduced into detergents as a substitute builder for polyphosphate since ca. 1970. As a result of this replacement, NTA has found its way into the environment and typical concentrations in various aquatic systems have been calculated on the assumption that wastewater has a concentration of 10 mg NTA/L. The results are summarized in Table 9.1 (Snodgrass 1983, U.S. Dept. of Interior 1968). In this Table, the effects of the Ontario watershed on Lake Erie are separated from those of the U.S. side because NTA was not widely used as a substitute builder during the 1970's in the U.S. Also, the figures given in Table 9.1 for the 'no treatment' case are improbable, because NTA is biodegradable (see Section 9.3.1). Evidence suggests that wastewater treatment is able remove 90% of the NTA. The calculations for the Grand River illustrate the effects of wastewater treatment plant discharges as well as flood flow and low flow conditions on the NTA concentration in riverwater.

Table 9-1 Calculated concentrations of NTA for various aquatic environments⁺

Environment	NTA		Dominant Complex [*]
	ug/L	M	
<u>Lake Erie</u> ^{** §}			
Ontario Watershed	16	8.5×10^{-8}	Cu-NTA
Ontario Watershed with 90% removal	1.6	8.5×10^{-9}	Cu-NTA
U.S. + Ontario watershed	140	7.5×10^{-7}	Cu-NTA
U.S. Watershed with 50% removal + Ontario Watershed with 90% removal	72	3.8×10^{-7}	Cu-NTA
<u>Grand River, Ontario (350,000 people)</u>			
283 m ³ /s (10,000 cfs), no treatment	65	3.5×10^{-7}	Cu-NTA
283 m ³ /s (10,000 cfs), 90% removal	6.5	3.5×10^{-8}	Cu-NTA
14 m ³ /s (500 cfs), no treatment	1300	6.9×10^{-6}	Cu, Pb, Zn, Fe with NTA
14 m ³ /s (500 cfs), 90% removal	130	6.9×10^{-7}	Cu-NTA
<u>Hamilton Harbour, no treatment</u>			
	500	2.7×10^{-7}	Cu, Pb, Zn, Fe with NTA
<u>Hamilton Harbour, 90% removal</u>			
	50	2.7×10^{-7}	Cu-NTA
<u>Wastewater Treatment Plant</u>			
Influent	10,000	5.3×10^{-5}	Ca-NTA
Effluent	1,000	5.3×10^{-5}	Cu, Pb, Zn, Fe with NTA

+ Calculations assume no removal (i.e. degradation) in the aquatic system. However, according to Swisher et al. (1973), it is probable that NTA decays very much slower at low concentrations (ca. 10^{-6} M and lower) than at higher concentrations.

* From calculations of Lerman and Childs (1973). For waters typical of Lake Erie, they use:

Ca(II) 1×10^{-3} M	Sr(II) 2×10^{-8} M	Co(II) 3×10^{-8} M	CO ₃ ²⁻ 1×10^{-3} M
Na(I) 5×10^{-4} M	Fe(III) 1.5×10^{-6} M	Cd(II) 2×10^{-8} M	Cl ⁻ 7.5×10^{-4} M
Mg(II) 2.5×10^{-4} M	Pb(II) 3×10^{-7} M	Ni(II) 1×10^{-9} M	SO ₄ ²⁻ 3×10^{-4} M
Cu(II) 2×10^{-6} M	Ba(II) 1.5×10^{-7} M	Fe(II) 1×10^{-12} M	PO ₄ ³⁻ 1×10^{-6} M
Mn(II) 2×10^{-6} M	Ni(II) 1×10^{-7} M		

** Calculations based upon 1.9 million people in the Ontario watershed and 15 million people in the U.S. Lake Erie watershed using a discharge to Lake Erie of 450L (100 gallons) per capita per day and an NTA concentration of 10 mg/L in the influent to Lake Erie.

† Calculations for Hamilton Harbour assume that the exchange flow with Lake Ontario is three times the hydraulic inflow.

§ Ref: U.S. Dept. of Interior, Lake Erie Report (1968).

The last column of Table 9.1 presents estimates of the dominant trace metal - NTA complex for a water modeled after Lake Erie (with respect to trace metal concentrations, see Legend of Table 9.1). The calculations are made by Lerman and Childs (1973). Generally, for NTA concentrations of 10^{-6} M (~ 200 $\mu\text{g/L}$) and lower, the existence of a Cu-NTA complex is predicted, which ties up approximately 80% of the NTA. In the range of 5×10^{-6} M NTA, Cu-NTA is still the dominant complex, but Pb, Fe and Zn complexes also become important. For NTA concentrations greater than 10^{-5} M, Ca-NTA ties up 80-90% of the NTA. Hence, it may be concluded that for this particular water, the Cu-NTA complex will be one of significant concern. In Section 9.3.1, it will be further discussed why the existence of the trace metal - NTA complex is important with regard to trace metal toxicity and mobilization.

The presence of MnO_2 is perhaps harder to assess compared to organic molecules. The formation and occurrence of MnO_2 was discussed in Chapter 3. The more significant form in which MnO_2 occurs in nature with regard to trace metal speciation, is likely as coatings on various surfaces (i.e. as amorphous or cryptocrystalline precipitates). Jenne (1968) and others persuasively argue that surface coatings of hydrous oxides of Mn and Fe on clays and sands etc., form a dominant surface onto which adsorption of metal ions can occur in certain aquatic systems such as rivers. They argue that without the surface area expansion due to such coatings, the quantity of Fe and Mn minerals would be insufficient to explain observed metal correlations with Fe and Mn. The degree to which $\delta\text{-MnO}_2$ adsorption characteristics, determined in this work, are an adequate description of the behaviour of such natural hydrous Mn oxide coatings awaits further study. However, theoretically the following can be calculated :

Table 3.3 indicates that for 'artificial' $\delta\text{-MnO}_2$'s, on average, 1g of $\delta\text{-MnO}_2$ has a surface area of approximately 300 m^2 . A figure of approximately $240 \text{ m}^2/\text{g MnO}_2$ was found in this study from the maximum amount of Cu that could be adsorbed per amount of $\delta\text{-MnO}_2$. For this, monolayer coverage of the $\delta\text{-MnO}_2$ surface was assumed, as well as a radius for adsorbed Cu of $r_{\text{Cu}^{2+}}^{\text{ads}} = r_{\text{Cu}^{2+}} + r_{\text{H}_2\text{O}}$ (see Table 4.2).

From the TEM image in Chapter 4, of $\delta\text{-MnO}_2$ (Figure 4.5), it can be calculated that typical $\delta\text{-MnO}_2$ particles (in a laboratory system) have a diameter of approximately 200 \AA (10^{-8} m). This, combined with the surface area, allows one to calculate the surface area and volume per particle and the amount of particles per gram $\delta\text{-MnO}_2$ which then yields a density for $\delta\text{-MnO}_2$ particles of 1.25 g/cm^3 .

For riverwater with a suspended solids content of 25 mg/L , the following calculation can be made. It is assumed that the suspended solids consist of spherical clay particles, with a diameter of $2 \times 10^{-6} \text{ m}$ and a density of 2 g/cm^3 and are coated with a thickness of 100 \AA (10^{-8} m) MnO_2 . From the volumes of the clay- MnO_2 particle and the clay particle, and the densities of clay and $\delta\text{-MnO}_2$, it can be calculated that a suspended solids content of 25 mg/L consists of 2.93×10^9 clay- MnO_2 particles/L. This number, combined with the volume of MnO_2 per particle, the MnO_2 density and molecular weight, yields a content of $5.33 \times 10^{-6} \text{ \mu M}$ ($4.64 \times 10^{-4} \text{ g}$) MnO_2 per liter. The surface area of the clay- MnO_2 particle combined with the number of particles yields a surface area of $3.75 \times 10^{-2} \text{ m}^2/\text{L}$. This implies that the MnO_2 surface coating has a surface area of $80 \text{ m}^2/\text{g MnO}_2$, while the clay- MnO_2 particle has a surface area of $1.5 \text{ m}^2/\text{g}$ suspended solids. Had the amount of MnO_2 per clay- MnO_2 particle not existed as a coating but as a spherical particle, then

a total surface area for the mass of MnO_2/L ($4.64 \times 10^{-4} \text{ g}$) of $56 \times 10^{-4} \text{ m}^2/\text{L}$ can be calculated, which yields a surface area of $12 \text{ m}^2/\text{g MnO}_2$.

The above clearly emphasizes the importance of surface coatings. The adsorption capacity of $\delta\text{-MnO}_2$ for Cu is typically $0.25 \text{ M Cu}/\text{M MnO}_2$ (see Chapter 7) which means that the suspended solids in the river system can bind approximately $1.3 \text{ }\mu\text{M Cu}$. Typical natural water systems contain amounts of Cu varying from 10^{-7} to 10^{-6} M (Lerman and Childs (1973) use a concentration of $2 \times 10^{-6} \text{ M Cu}$ for Lake Erie water). This implies that the surface coatings of MnO_2 on the above model river system can reduce the amount of free Cu in solution considerably.

9.3.1 NTA, A Case Study

Conditional stability constants for the Cu-NTA complex were determined in this study at pH 6, 7 and 8 with the $\delta\text{-MnO}_2$ method, using the Implicit Langmuir function. As discussed in Chapter 8, the values obtained fall in the range of literature data reported for the Cu-NTA complex. From Figures 2.1 and 2.2 in Chapter 2, it can be seen that NTA is a strong Cu complexing ligand and is therefore suitable as a model substance in equilibrium calculations involving Cu. For Zn complexation, NTA is also very comparable in complexation strength with a number of natural organics (Stroes 1979). NTA can become a very important factor in trace metal speciation for natural water situations, as was shown in Section 9.2. It is therefore obviously important to determine its stability constant(s) as accurately as possible in order to assess its effect on metal speciation. This work has shown that the improved $\delta\text{-MnO}_2$ method no longer underestimates the complexing strength of NTA. The following case study illustrates the possible (complicated) effects of NTA, entering the aquatic environment via wastewater discharges

or effluents of wastewater treatment plants.

About fifteen years ago, proposals to limit phosphate contents of detergents challenged the detergent industry to investigate possible substitutes for phosphate. NTA seemed one of the most promising but it was soon realised that NTA could cause several problems in case its concentration should increase in natural waters.

The nitrilotriacetate molecule contains three carboxyl groups and one amino nitrogen. It is an effective complexing agent and forms stable complexes with many di- and polyvalent metals. It is therefore possible that certain metals which are tied up in sparingly soluble salts in sediments will dissolve as a result of formation of metal-NTA complexes. Whether this will actually occur depends on the thermodynamic stability and solubility constants, and the total activities of the species involved. However, it can also be argued that an increase in NTA concentration can cause a decrease of free metal-ion concentration in waters containing a certain amount of dissolved trace metals.

It has been shown that NTA and most trace metal - NTA complexes are biologically degradable. However, degradation times (to concentrations below detection limit) vary considerably and are dependent on the state of adaption of the bacteria population and on the metal that is associated with the NTA. Recent evidence shows that NTA decays much more rapidly at high concentrations than at low concentrations (Swisher et al. 1973). Chau and Shiomi (1972) give a number of degradation times, obtained for non-adapted bacteria populations.

Table 9.2 Degradation times* for metal-NTA complexes

M-NTA complex	Degradation time (days)	M-NTA complex	Degradation time (days)
Al	6	Fe	17
Cr	6	Pb	25
Mn	10	Ni	108 (not degr.)
Zn	16	Hg	108 (")
Mg	13	Cu	149 (")
Ca	13	Cd	60

* degradation times to NTA concentrations below detection limits

The above numbers should be interpreted with caution in natural situations since they are obtained under laboratory conditions. Ni, Hg, Cu and Cd-NTA complexes seem very stable but this might be due to the relatively high total metal concentrations used in this study (20 x natural levels). Release of free metal ions as a result of degradation of the NTA-complex might have killed the bacteria population. Under natural circumstances degradation might be more likely.

Chau and Shiomi (1972) also discuss a number of experiments performed under natural circumstances in Lake Ontario. In summary the conclusions derived from the results of this study are: NTA indeed mobilizes trace metals from bottom sediments. Release starts soon (hours) after NTA is added to the water system and increases during a number of days. Decay of NTA starts 4-11 days after NTA spiking, reflecting the dependence on the adaption state of the bacteria present.

A number of days after NTA has disappeared from solution, the metal levels in solution fall to their original pre-NTA levels, which is explained by re-formation of the original insoluble metal complexes. Nitrate is an end product of NTA degradation and it is found that nitrate levels in solution rise during and after the disappearance of NTA. Phosphate levels seem to drop during NTA decay as a result of increased microbiological activity caused by the NTA spiking.

These observations make it possible to construct the following argument regarding increase and decrease of metal toxicity in the case of point source discharges of NTA:

If the receiving aquatic system contains high concentrations of free metal ions (due to a poor ligand composition), discharge of NTA will at least temporarily decrease the toxicity by complexing the free metal ions. Both the bacteria present and the metal involved determine if and at what rate this metal-NTA complex is decomposed. If degradation occurs, the metal returns eventually to its free ionic state and toxicity is restored unless in the meantime the concentration of other ligands has changed (increased). If the complex cannot be decomposed, then it keeps the metal in solution in the non- (or at least less) toxic complexed form and a more or less permanent lower toxicity is obtained. In the case of a highly toxic metal, an attempt by the bacteria to utilize the metal-NTA complex can result in release of so much free toxic metal ion that the bacterial population is killed and degradation stops.

If the aquatic system to which NTA is discharged contains a low concentration of metal in solution but has a relatively high metal concentration tied up in its sediments, NTA can cause solubilization of metals from these sediments. Successive degradation (for which the same arguments hold as in the above case) of the metal-NTA complexes increases the free metal ion concentration in the water phase and toxicity increases. Whether or not these free metal ions will go back to their original insoluble forms or will become complexed by other ligands depends entirely on the composition of the water, and on biological decomposition of NTA.

The above arguments hold specifically for point source discharges. In the case where NTA is continuously discharged into the natural aquatic environment, a permanent level of NTA may be expected and either originally free or solubilized metals will continually be bound and re-bound, thus keeping the concentrations of free metal ions low. This permanent NTA level may therefore play an important role as a carrier in transporting metals from one place to another. NTA is not usually regarded as directly toxic for higher organisms but some controversial data on teratogenic effects of NTA in the presence of Cd(II) and methyl mercury chlorides have been observed with mice and rats (Raspor et al. 1977). Also, metal-NTA complexes can be ingested by water organisms (e.g. in particular form) and therefore trace metals could become more concentrated in the foodchain as a result of increasing levels of NTA in natural water systems.

The effects of NTA on speciation and toxicity can be directly compared with the effects that unknown organics are expected to exert

on speciation. The δ -MnO₂ method can provide the necessary information to quantify these effects. Figures 2.1 and 2.2 and Table 9.1 provide a comparison of the effects that both model ligands and natural organic materials have on the speciation of Cu in a simple model system, and a natural water situation.

9.4 Radioactive (Fuel) Waste Disposal

The information gathered in this research on both the appearance and adsorption behaviour of δ -MnO₂ is not only useful for natural water speciation studies, but has also a potential application in the field of radioactive waste management and disposal.

Koons et al. (1980) have shown that during the weathering of diabase (a rock of basaltic composition), elements such as Co, Cr, Mn, Sc, Th, U, Zn and the heavy rare earth elements are associated with Fe oxides. The same holds for the elements As, Co, Cr, Sc, Th, U and Zn during the weathering of granite. Concentrations of Mn were too low so that the effects of Mn-oxides could not be separated from those of Fe-oxides. However, from the literature, summarized by Chao and Theobald (1976) and Means et al. (1978a); it appears that Mn-oxides are better trace metal scavengers than Fe-oxides. McLaren and Crawford (1973) concluded that the adsorption of Cu onto common soil constituents follows the order: Mn oxides > organic matter > Fe oxides > clay minerals. Balistreri and Murray (1981, 1982) studied the surface chemistry of both goethite and δ -MnO₂ in major ion seawater with the purpose to eventually shed some light on the partitioning of elements between these solid phases. Their studies indicated that for both oxides, 85-90% of

the surface sites are complexed by protons, but that δ -MnO₂ has approximately twenty times more sites per kg material than goethite. The high adsorption capacity of δ -MnO₂ for trace metals necessarily also implies that radioactive waste products such as ⁶⁰Co and certain actinides can be adsorbed strongly on δ -MnO₂. Although Fe oxides can outnumber Mn oxides by as much as twenty times (Hoffman and Eisenreich 1981; Means et al. 1978a), the high number of surface sites on δ -MnO₂ implies that both Mn and Fe oxides will play an important role in the mobility restriction of leached radioactive components from a waste disposal site. A literature review, by Means et al., (1978) indicates that there are strong binding sites for certain actinides on Fe and Mn oxides. Apparently, U and Th enrichment has been observed in deep-sea, Fe-rich Mn-nodules.

Means et al., (1978a,b) investigated the adsorption of radioactive waste products (⁶⁰Co and selected actinides) by Mn and Fe oxides in soils and sediments. Intermediate level radioactive waste had been delivered over a period of fifteen years to a number of different seepage pits and trenches at Oak Ridge National Laboratories. A reconnaissance sampling study revealed that soils, which had been exposed to the same contaminated groundwater in the areas surrounding the disposal sites contained dissimilar ⁶⁰Co concentrations, due to differences in soil composition. Means et al. (1978a,b) found that ⁶⁰Co, and various actinides, principally ²⁴⁴Cm, ²⁴¹Am and ²³⁸Pu, but also traces of ²²⁸Th, ²²⁴Ra, ²²⁶Ra, ^{239,240}Pu etc., were dominantly associated with Mn oxides. In none of their numerous analyses was there any strong indication that actinides, considered individually or as a group, were better correlated with Fe oxyhydroxides or insoluble organic material than with Mn oxides.

Although the actinides included in Means et al.'s study were primarily the short lived species ^{244}Cm ($t_{1/2} = 18$ yr.), ^{241}Am ($t_{1/2} = 470$ yr.) and ^{238}Pu ($t_{1/2} = 90$ yr.), the results apply also to the longer lived species which are the main constituents of radioactive waste after several thousand years of storage and decay (i.e. ^{245}Cm , $t_{1/2} = 11,000$ yr.); ^{243}Am , $t_{1/2} = 8000$ yr. and ^{239}Pu , $t_{1/2} = 24,300$ yr.).

The study mentioned above illustrates clearly the need for knowledge of adsorption strength and capacity of Mn oxides in order to understand and predict the fate of trace metals and actinides. The pH-dependent Implicit Langmuir function can provide the necessary information regarding the strength and extent of radioactive waste product association with $\delta\text{-MnO}_2$ for modeling purposes, especially since the Implicit Langmuir expression provides the binding energy for an 'empty' surface (Jenne, pers. comm. 1982).

In the planning of a radioactive waste disposal site, naturally occurring hydrous Mn and Fe oxides should be assessed, so that their immobilizing effects can be modeled. It should be investigated if circumstances in the soil are favourable for a stable MnO_2 phase. For instance, low pH and Eh should be avoided (Means et al. 1978a; Hoffmann and Eisenreich 1981) but the O_2 concentration should not be too high either, since actinides are more mobile in their oxidized forms (Means et al. 1978a). Certain complexing ligands may dissolve MnO_2 or alternatively strip actinides from MnO_2 . An example is EDTA, used for reactor spill cleanups (Means et al. 1978c), but naturally occurring humics could also exert such effects. The results of this study on MnO_2 again can provide the necessary information to estimate the extent of such phenomena.

Another factor that should be given attention is to ensure that the δ -MnO₂ present in soils is not likely to undergo alteration into another mineral form. Means et al., (1978a) mention that a high carbonate content coupled with a low Eh may promote alteration of Mn oxide to rhodochrosite (MnCO₃). This would mean loss of adsorption capacity. In the study presented here, it was shown how a combined effect of low pH, elevated temperature and certain K content could alter the mineralogy of δ -MnO₂ with loss of important adsorption capacity. Circumstances promoting the alteration of δ -MnO₂ into cryptomelane are very conceivable for radioactive waste disposal environments; groundwaters may be acid and contain salts, while temperatures will be high due to radioactive decay. In soils, δ -MnO₂ seems most common, but other forms of Mn oxides will also be present, likely with less adsorption capacity per unit oxide. This is suggested by the comparison study on the adsorption behaviour of a number of differently prepared δ -MnO₂ batches (Chapter 4).

Although many of the above factors need more study, the scope of MnO₂ for radioactive disposal technology seems promising. In Canada, disposal studies are concentrated on granites in the Canadian Shield as repositories. Weathering studies have shown that in such a situation one might want to focus on Fe oxides, since Mn oxides appear less stable during weathering (Cramer 1982). This, however, does not reduce the potential of δ -MnO₂ in other situations such as described for Oak Ridge. Also, consideration should be given to the use of MnO₂ as backfill material. Means et al. (1978a) propose that, once Mn nodules are harvested from the oceans for economic purposes (rich in

certain trace metals), these Mn and Fe rich materials will provide very feasible backfill material.

9.5 Environmental Health Studies

δ -MnO₂, prepared according to the neutral recipe, developed in Chapter 4, has very recently been used by Wallon (1982) as a model surface for the adsorption of enzymes, in an attempt to simulate the hypothesized inactivating affect that certain particulate chemical carcinogens can have on adsorbed enzymes. The study was carried out because solid nickel refining intermediates are implicated by epidemiological evidence in lung and nasal cancers in nickel workers (Cecutti and Nieboer 1981). The more insoluble nickel compounds, e.g. α -Ni₃S₂ and crystalline β -NiS appear to be the most effective carcinogens. It is suspected that these solids interact with critical enzymes, and hence interfere with nucleic acid synthesis. A model system to simulate this effect should ideally contain no Ni, to eliminate the effects of the Ni²⁺ ion which is mutagenic on its own. Initial results using materials and techniques developed in this study show that δ -MnO₂ can indeed serve as a suitable model surface to study the activity of enzymes and proteins in an adsorbed state.

9.6 Summary

δ -MnO₂ has applications in areas of environmental engineering due to the following aspects :

1. The δ -MnO₂ method is improved with the Implicit Langmuir adsorption model. This provides more accurate conditional stability constants for trace metal-organic interactions, which results in better predictive water quality and toxicity models.

2. The Implicit Langmuir function describes in a mathematically simple manner the adsorption process of Cu on $\delta\text{-MnO}_2$ and is likely to be a good model to describe adsorption of trace metals on hydrous oxides in general.
3. NTA is an environmentally important ligand and the conditional stability constants, measured with the improved MnO_2 method, provide a means of more accurately estimating the impact of NTA discharges on the aquatic environment.
4. From density calculations performed for the 'neutral' $\delta\text{-MnO}_2$ surface studied in this work, an assessment can be made of the surface area enhancing effect of hydrous Mn oxide coatings on silicate particles in natural waters and soils.
5. MnO_2 has a high affinity and sorption capacity for trace metals and actinides. Hence it may be an important factor in preventing or retarding migration of radioactive waste products from disposal sites.
6. The aging studies on $\delta\text{-MnO}_2$ provide information regarding the factors controlling the stability of $\delta\text{-MnO}_2$. This can be of importance for radioactive waste migration through soils.
7. $\delta\text{-MnO}_2$, prepared and characterized according to the methods developed in this study, can serve as a suitable model surface to study the effects of adsorption on the activity of enzymes and proteins.

CHAPTER 10

SUMMARY, CONCLUSIONS AND RECOMMENDATIONS
FOR FURTHER RESEARCH10.1 Context of Research

A very considerable amount of study has been, and is currently, directed towards more precisely predicting the fate of trace metals in natural waters. Knowledge of interactions between trace metals and dissolved and particulate material in natural aquatic systems is a necessity for making an accurate prognosis regarding water quality and toxicity of trace metals. The work presented in this thesis forms a contribution to such knowledge.

To study trace metal interactions in natural water systems, one has to be able to measure the extent and strength of such interactions and relationships, and to express these in measurable units. Stability constants assess the strength of trace metal ligand associations, while concentration and stoichiometry are a measure of the extent of these. Because ligands in natural waters possess mostly unknown, complex structures, conditional stability constants (CSC) and complexing capacity (CC), both only valid at the pH and ionic strength for which they were determined, replace stability constants and concentration.

10.2 The δ -MnO₂ Method

There are presently a large number of techniques available to measure CSC's and CC's. Amongst them are Anodic Stripping Voltam-

metry (ASV), Ion Exchange (IE) methods, the Ion Specific Electrode (ISE), Continuous Variation (CV), Potentiometric Titration (PT) and Dialysis (DI)-methods, Gel Filtration Chromatography (GFC) and the δ -MnO₂ method.

The δ -MnO₂ procedure has a definite advantage over the other methods, because of its capability to measure CSC's and CC's in filtered but unconcentrated natural water samples, at pH's varying from 6 to 9; most other methods can only be applied at low pH values and/or require concentrated samples. Therefore, the δ -MnO₂ method appears the most suitable method available to study trace metal-ligand associations in natural waters. Also, the δ -MnO₂ method has the potential of measuring both trace metal - ligand and trace metal - particulate matter associations in the same natural water sample (see Section 10.10).

Briefly, the δ -MnO₂ method, developed by van den Berg (1979) and van den Berg and Kramer (1979a,b), involves a titration, a resin and voltammetry to measure CSC's and CC's. The procedure was tested for Cu. Instead of measuring free trace metal (c.q. Cu²⁺) concentrations in a 0.45 μ M filtered natural water sample, a certain amount of δ -MnO₂ is added to the sample. This surface has been calibrated previously for Cu-uptake and acts as a weak ion exchange resin. After its addition, the solution is titrated with Cu, which causes the present (but unknown) organic material and the δ -MnO₂ to compete for the metal. After a certain equilibrium period (ie. 3/4 to 1 hr.), during which time the temperature and pH are kept constant, the resin is removed by means of a 0.45 μ M filtration. The filtrate is analysed

for Cu after acidification, by Differential Pulse Anodic Stripping Voltammetry (DPASV). Because the resin was calibrated for Cu uptake, prior to being used as a competing surface, the free Cu^{2+} concentration in solution, in equilibrium with the resin, can be calculated from the amount of Cu adsorbed on $\delta\text{-MnO}_2$. From the total amount of Cu added and the free Cu^{2+} concentration, the Cu-ligand concentration can be calculated from the mass balance for Cu. By plotting Cu^{2+} concentration vs. the ratio of $\text{Cu}^{2+}/\text{Cu-ligand}$, one obtains a straight line. From the slope of this line, the ligand concentration (i.e. the CC, assuming 1:1 complexation) can be calculated, while from the intercept and the slope, the CSC ($K'_{\text{Cu-L}}$) emerges.

It is obvious that this method will only yield reliable results if a number of conditions are met :

- (i) The $\delta\text{-MnO}_2$ surface must be characterized accurately for Cu uptake,
- (ii) Cu uptake on the $\delta\text{-MnO}_2$ surface should not change with time, i.e. aging of the surface should not alter its adsorption characteristics,
- (iii) The presence of unknown organic ligands in natural water samples should not influence the adsorption behaviour of the $\delta\text{-MnO}_2$ surface. In other words, organics and Cu-organic complexes should not adsorb on $\delta\text{-MnO}_2$.

Van den Berg (1979) proposes to characterize the adsorption behaviour of $\delta\text{-MnO}_2$ for Cu by a linearized Langmuir isotherm, and assumes that surface behaviour is unaltered for a period of at least two years. Van den Berg (1979) argues against adsorption of organics on $\delta\text{-MnO}_2$ on the basis that the CSC for Cu-glycine could be

reproduced accurately. Straight lines were obtained in the plots of Cu^{2+} vs. $\text{Cu}^{2+}/\text{Cu-L}$ for titrations of natural water samples. This is also used as an argument against adsorption. No direct investigation to ensure that any of the above conditions were met, was performed by van den Berg (1979).

However, preliminary experimental results in this work, and a thorough literature study, revealed that the $\delta\text{-MnO}_2$ method is subject to several problems :

- (i) A deviation was found from the linearized Langmuir isotherm at low surface coverages.
- (ii) The values for the adsorption parameters, Γ_{max} and B, as determined by van den Berg (1979) and van den Berg and Kramer (1979a,b) for Cu on $\delta\text{-MnO}_2$, could not be reproduced.
- (iii) Transmission Electron Microscopy (TEM) revealed that the morphology of $\delta\text{-MnO}_2$, prepared for this work, differed vastly from the appearance of van den Berg's $\delta\text{-MnO}_2$. The former consisted of very small round or hexagonal, uniform particles, while the latter consisted of fibrous material (likely cryptomelane).

The work described here was aimed at finding explanations for these discrepancies.

10.3 Structure, Preparation and Characterization of $\delta\text{-MnO}_2$

The structure and composition of naturally occurring- and laboratory produced- $\delta\text{-MnO}_2$ was investigated by means of an extensive literature review on natural and synthetic manganese IV oxides.

The natural formation and deposition of manganese oxides is

a complicated process, controlled by factors such as pH, temperature, O_2 availability, carbonate and manganese concentrations. Oxidation of Mn^{2+} to MnO_2 can occur along several pathways, but there is uncertainty in the literature regarding the relative importance of the various processes. Reduction of Mn^{7+} to MnO_2 is not an important natural process.

The fundamental structural unit in the tetravalent manganese oxides is the $(Mn^{IV}O_6)$ octahedron. These units can be linked by corner and edge sharing to result in a variety of chain, layer and tunnel structures. There is no uniform agreement in the literature on the exact structure of δ - MnO_2 , and whether the minerals known as δ - MnO_2 , birnessite, manganous manganite and vernadite are identical. Currently, most researchers are of the opinion that δ - MnO_2 consists of layers of pure MnO_2 , interspaced with layers containing Mn^{2+} , Mn^{3+} , H_2O , K^+ , Na^+ , Ca^{2+} and perhaps metal ions.

The preparation of δ - MnO_2 under laboratory circumstances appears to be influenced by the pH. A product, obtained under neutral pH conditions, may be more dispersive and hence possess a larger surface area. It seems likely that an explanation involving the formation of nuclei and their subsequent aggregation is of more importance than ionic strength effect, although these cannot be excluded on the basis of present knowledge.

δ - MnO_2 has been produced by numerous researchers. Basically, there are three methods to precipitate δ - MnO_2 :

- (i) A redox process, involving the simultaneous oxidation of Mn^{2+} and reduction of Mn^{7+} to Mn^{4+} .

- (ii) An oxidation process, involving the oxidation of Mn^{2+} to Mn^{4+} .
- (iii) A reduction process in which Mn^{7+} is reduced to Mn^{4+} .

Three different recipes, each involving one of the above mentioned processes, were used in this study to produce hydrous manganese oxide:

- (i) A 'neutral' MnO_2 surface was precipitated by the redox process at neutral pH.
- (ii) An 'alkaline' MnO_2 surface was fabricated via oxidation of Mn^{2+} at high pH.
- (iii) An 'acid' MnO_2 surface was produced at low pH by the reduction procedure.

Whether any or all of these recipes produces true δ - MnO_2 was investigated by characterizing the formed products on a number of points.

A positive identification of hydrous manganese oxide as δ - MnO_2 includes confirmation of characteristics such as oxygen number larger than 1.9 (after correction for K and H_2O content), a large adsorption capacity (around 0.25 mol Cu/mol MnO_2), an amorphous XRD pattern and a low pH_{zpc} . The morphology of δ - MnO_2 , as revealed by TEM, seems variable. If prepared with the neutral (redox) procedure, a distinct appearance of very small round or hexagonal particles results, while the acid (reduction) procedure produces δ - MnO_2 with a "flower-petal" appearance. The alkaline (oxidation) recipe does not produce δ - MnO_2 . This particular product has a lower oxidation number (1.6) than δ - MnO_2 and contains very little K and no easily removable H_2O . A large number of modifications of the neutral (redox) procedure did not have any noticeable effect on the TEM appearance of the

products, nor was there much effect on characteristics such as the oxidation number.

The literature review indicated that the conversion of $\delta\text{-MnO}_2$ to cryptomelane is possible through heat treatment. This implies that such a process may occur at a much slower rate at low temperatures. If such an aging process is capable of altering $\delta\text{-MnO}_2$ to cryptomelane, it is likely that adsorption parameters are also changed.

Heat treatment to simulate the aging process was applied to a number of $\delta\text{-MnO}_2$'s under various experimental conditions regarding pH and K content. The literature indicated that K content should be lower than 7 - 10% to convert $\delta\text{-MnO}_2$ to cryptomelane. To produce such a low K percentage in $\delta\text{-MnO}_2$, acid washing is necessary, which obscures the singular role of the pH in the conversion process. Heat treatment of $\delta\text{-MnO}_2$ samples at neutral pH's in this study did not significantly alter their appearance. However, identical treatment at low pH (which implies low K content) produced a conversion to several distinctly different shapes. Most abundant were large hexagonal shapes which are possibly Mn_2O_3 . Filaments also occurred in the heat treated samples and these are likely to be cryptomelane. Conversion of $\delta\text{-MnO}_2$ under acidic conditions upon heat treatment is a very rapid process and is complete in 35 minutes. A $\delta\text{-MnO}_2$ with high K content (> 10%) is protected from rapid conversion to cryptomelane by its high K content, which excludes cryptomelane stability. However, such samples are more filamentous in appearance after heat treatment. This indicates that there is a relationship between the time and the temperature of the aging process. Such a relationship could readily explain the filamentous MnO_2 sample inherited from van.

den Berg's research.

The characterization of $\delta\text{-MnO}_2$'s, prepared according to three procedures together with the study on aging behaviour, narrowed down the possible sources of differences with van den Berg's work considerably. From positive relationships obtained between adsorption capacity and H_2O - and K - content in the solid, and from amorphous XRD patterns, a number of conclusions regarding the $\delta\text{-MnO}_2$ structure could be drawn: Most likely, $\delta\text{-MnO}_2$ possesses a layer structure of perfect MnO_2 octahedra interspersed with layers containing a mixture of H_2O , OH^- , K^+ and H^+ ions. This may imply two adsorption sites for trace metals, a surface site and an interlayer site. The ratio of surface sites to interlayer sites can only be determined if these sites display different adsorption behaviour. As such, two distinct types could form an explanation for the observed deviation from linearity. Another explanation must be sought in the fact that the activity of the partaking surface groups is not constant during the adsorption process (see Section 10.4).

Adsorption behaviour for the various MnO_2 surfaces involved in this study displayed large differences in both adsorption strength and capacity. Clearly, the surfaces identified as true $\delta\text{-MnO}_2$ adsorbed the strongest and the most. The naturally aged cryptomelane sample from van den Berg's research displayed half of the adsorption capacity of a $\delta\text{-MnO}_2$ surface, with approximately equal strength. The heat induced aging process reduced the adsorption capacity of the $\delta\text{-MnO}_2$ surface drastically. Such effects can be attributed to a reduction of available surface area, apparent from TEM appearances.

10.4 Adsorption Theory

Adsorption behaviour of $\delta\text{-MnO}_2$ for trace metals (eg. Cu^{2+}) formed the central part of this work. Adsorption results that were fitted to a linearized Langmuir expression, deviated from linearity at low coverage of the surface. This may be caused by two distinct adsorption sites for Cu and a Double Langmuir expression should be able to predict this. Another explanation could be the fact that the activity of the adsorption sites on the $\delta\text{-MnO}_2$ surface is not constant during the adsorption process.

The literature was reviewed with respect to adsorption models generally developed for hydrous oxides. This provided the theoretical background needed to apply one or more of these models to the specific case of Cu- $\delta\text{-MnO}_2$ interactions. A literature review with respect to applications of adsorption models for $\delta\text{-MnO}_2$ revealed that only simple models, such as a Single Langmuir equation, had been applied.

The Implicit Langmuir model developed in this work attempts to create a link between general adsorption theory developed for hydrous oxides and the special case of adsorption of Cu on $\delta\text{-MnO}_2$. The model incorporates the non-constant activity of involved surface groups and various adsorption mechanisms. The Implicit Langmuir expression accounts for the influence of these factors on the overall bindings constant by taking into account the relative surface coverage at each adsorption point, and by estimating the pH dependency of the bindings constant.

The Implicit Langmuir model requires only adsorption measurements. No additional acidity constants for the surface groups, nor a calculation of surface charge, are necessary.

The main advantage of the Implicit Langmuir model over the Single Langmuir equation is that it is able to describe adsorption of trace metals on $\delta\text{-MnO}_2$ more accurately at low solution concentrations and low coverages of the $\delta\text{-MnO}_2$ surface. For use of $\delta\text{-MnO}_2$ as a tool in the determination of CSC's and CC's for natural waters, it is important that adsorption of Cu (and other metals) on $\delta\text{-MnO}_2$ is known precisely, since from this, free Cu^{2+} concentrations in solution are calculated. These, in turn, are involved in the calculation of conditional stability constants. The latter are usually derived at both the low ligand- and low- metal concentrations, characteristically found in natural waters. Since a low ligand concentration necessitates the use of only a small quantity of $\delta\text{-MnO}_2$ as a competing surface for the metal, which is also present in low (ie. trace) concentration, it is obvious that especially the area of low surface coverage of the $\delta\text{-MnO}_2$ surface needs to be modeled properly. The Implicit Langmuir model is capable of doing this. At the same time, the model is simple enough to be used with only the need for measurements of metal uptake by $\delta\text{-MnO}_2$ in the presence of unknown ligand, the Cu concentration remaining in solution, and the pH.

10.5 Adsorption of Organics on the $\delta\text{-MnO}_2$ Surface

The $\delta\text{-MnO}_2$ method can only be applied to determine CSC's and CC's of organic material, if that organic material does not adsorb on the $\delta\text{-MnO}_2$ surface. To calibrate the $\delta\text{-MnO}_2$ surface for Cu uptake at pH >6, glycine is often added to the solution to prevent Cu precipitation. It is therefore important that glycine does not adsorb on the $\delta\text{-MnO}_2$ surface. A study involving ^{14}C -labelled glycine indicated

that the adsorption of glycine onto δ -MnO₂ is negligible. Ligands such as NTA and aspartic acid do not adsorb onto δ -MnO₂ either, as demonstrated by ¹⁴C-labelled studies. No experiments were performed to investigate the adsorption of unknown natural organics on δ -MnO₂.

However, in a recent publication, van den Berg (1982) argues that humic and fulvic materials and δ -MnO₂ particles possess strongly negative charges at pH's > 4 and that repulsion between the two is favoured. The presence of organic material in seawater samples, after equilibration with δ -MnO₂ and subsequent removal of δ -MnO₂ and acidification, could be inferred from the presence of a certain peak in the DPASV voltammogram. This peak disappears in seawater samples that are equilibrated with δ -MnO₂ and acidified but not filtered. This implies that apparently-organic material in seawater (with and without Cu present) does not adsorb during equilibration with δ -MnO₂ at the pH of seawater (~8). At a pH of 1.8, however, organic material in seawater adsorbs strongly on the δ -MnO₂ surface in the presence of Cu.

Hence, it can be concluded that, providing the pH is well above acid values, organics do not adsorb onto the δ -MnO₂ surface. Results obtained with the δ -MnO₂ method can therefore be regarded as reliable in the pH range of natural waters (6 - 8.5).

10.6 Adsorption Behaviour of Various δ -MnO₂ Surfaces

The adsorption behaviour of the various δ -MnO₂ surfaces involved in this study, is compared qualitatively on several bases:

- (i) The three δ -MnO₂'s, precipitated according to the redox-, oxidation- and reduction-processes, are compared. The 'neutral' (redox) and 'acid' (reduction) surfaces behave very similarly,

which is surprising because their TEM appearance is very different. The 'alkaline' (oxidation) surface has a much lower adsorption capacity.

- (ii) The reproducibility of the 'neutral' surface is tested by adsorbing Cu onto three identically prepared 'neutral' δ -MnO₂ surfaces. It is concluded that reproducibility of the 'neutral' surface is poor.
- (iii) Isotherms obtained at identical pH values, in the presence and absence of glycine for the 'neutral' surfaces, do not compare satisfactorily. However, the fluctuations observed are similar to those observed for duplicate isotherms. It is, therefore, unlikely that the presence of glycine changes the adsorption behaviour of the 'neutral' surfaces. It was already mentioned that glycine does not adsorb in significant quantities on the δ -MnO₂ surface. However, the presence of glycine does have a negative effect on both Γ_{ads} and the Cu²⁺ concentration. This has consequences for the estimation of model parameters, because of the observed deviation from Langmuir linearity at the low end of the linearized isotherm.

10.7 Fitting of Adsorption Results to the Single-, Double- and Implicit Langmuir Models

The adsorption data are fitted to three different adsorption models of the Langmuir form.

According to the Single Langmuir model parameters, duplication of results is extremely poor. An observation was made that, although

the Single Langmuir model should be linearizable, the experimental data show a clear deviation from linearity at low coverage of the surface. This has important consequences for the Single Langmuir model parameters, which are usually estimated by linear regression, favouring the data at high surface coverage. A non-linear regression procedure improves this. However, it is inherent to the Langmuir model in general, that data at low surface coverage estimate the bindings energy, while data at high surface coverage estimate the maximum adsorption capacity. It is therefore necessary to obtain a large number of data points over the whole range of the isotherm in order to obtain reasonable estimates for the model parameters. The Single Langmuir model is only applicable for data obtained at the same pH and does not predict the observed deviation from linearity.

The Double Langmuir model assumes that there are two adsorption sites on the $\delta\text{-MnO}_2$ surface with a different affinity for Cu. Γ_{max} is divided into Γ_{m1} and Γ_{m2} , while bindings energy is also split into two components. This model does predict deviation from linearity, if the two components which make up the total bindings energy are noticeably different. However, this model is more specific and less flexible than the Single Langmuir model. Non-linear regression data did not show a particular pattern for the model parameters. Model fit was hard to obtain in a considerable number of cases, due to the fact that the data basically described different functions.

The Implicit Langmuir model predicts that the bindings energy of Cu on MnO_2 reduces in value with progressive coverage of the surface. The model also incorporates the pH in the overall value for the bindings

energy. This model is very flexible because it can accommodate adsorption data obtained for different pH values to estimate model parameters. Comparison of values for model parameters for the 'neutral' surfaces indicates very good agreement.

The three Langmuir shaped models were compared on five points. The Implicit Langmuir model is clearly the most suitable of the three, to describe adsorption of Cu onto δ -MnO₂. The main advantages of this model are that:

- (i) it is a very simple model, easy to understand and use,
- (ii) it incorporates the pH into the bindings energy, which makes the model very general,
- (iii) it corrects for changes in 'surface' charge, by taking the surface coverage into account for the estimation of the bindings energy,
- (iv) it predicts the amount of H⁺ that is released per amount of Cu²⁺ adsorbed,
- (v) it has a constant value for Γ_{\max} , which was found experimentally and,
- (vi) it predicts stronger binding at low coverage of the surface (which was observed experimentally) and a more or less constant bindings energy at higher Γ_{ads} (also observed).

10.8 Determination of Conditional Stability Constants for NTA and Certain Amino Acids with the Implicit Langmuir Model

The Single- and Implicit Langmuir models are compared for their ability to determine CSC's and total ligand concentrations (CC's) for NTA and glycine at $6 \leq \text{pH} \leq 8$.

The Single Langmuir model produces CSC's that are considerably

lower than literature values for both NTA and glycine. On the contrary, the CSC values obtained with the Implicit Langmuir model agree well with the range of CSC values for NTA and glycine obtained from the literature. However, CC values determined with the Implicit Langmuir model for NTA tend to be too low (5 - 12%) for which no explanation could be found.

Correction for both $\text{Cu}(\text{OH})^+$ and $\text{Cu}(\text{OH})_2^0$ formation has a large influence on CSC and CC results and should routinely be incorporated in the calculations.

The Implicit Langmuir model is very useful in determining the CSC's and CC's for high concentrations of relatively weak CuL and CuL_2 complex-forming ligands, such as the amino acids aspartic acid, glutamic acid and alanine. Although the individual values obtained for the CSC's and CC's are incorrect, their product, which controls Cu^{2+} concentration in solution, could be reproduced accurately.

The results for NTA and the amino acids provided a good validation of the Implicit Langmuir model and of the assumptions with which the expression was derived.

10.9 Applications of $\delta\text{-MnO}_2$ Research in the Field of Environmental Engineering

A number of areas in the field of environmental engineering can benefit from the studies on $\delta\text{-MnO}_2$ described in this thesis.

The $\delta\text{-MnO}_2$ method is improved with the Implicit Langmuir adsorption model. This provides more accurate CSC's for trace metal - organic interactions, which results in better predictive water quality and toxicity models.

The Implicit Langmuir function describes in a mathematically

simple manner, the adsorption process of Cu on δ -MnO₂ and is likely to be a good model to describe adsorption of trace metals on hydrous oxides in general. This is of importance for water quality models.

NTA is an environmentally important ligand and the CSC's, measured with the improved MnO₂ method, provide a means of more accurately estimating the impact of NTA discharges on the aquatic environment.

MnO₂ has a high affinity and adsorption capacity for trace metals and actinides. Hence, it may be an important factor in preventing or retarding migration of trace metals and/or radioactive waste products from disposal sites.

The aging studies on δ -MnO₂ provide information regarding the factors controlling the stability of δ -MnO₂. This can be of importance for waste migration through soils.

10.10 Specific Recommendations for Further Research

This study has developed a new adsorption model for Cu onto δ -MnO₂. A large number of other aspects of δ -MnO₂ were investigated in depth. It was shown that the δ -MnO₂ method, with these improvements, is now much more capable of producing reliable conditional stability constants for Cu-organic complexes.

However, a natural water sample usually contains an important particulate fraction, capable of binding trace metals. Applications of the δ -MnO₂ method have so far excluded this particular fraction. It is recommended here that the δ -MnO₂ method be used to assess all possible associations of trace metals in natural water samples.

More specifically, the following procedure is proposed to

assess the associations of trace metals (c.q. Cu) with dissolved and particulate matter in a complete (ie. unfiltered) natural water sample:

- (i) A natural water solution is titrated with Cu at the natural water pH in several steps. During titration, the solution contains Cu^{2+} , Cu-L, Cu-P, L and P. Samples are taken after a suitable equilibration period, after each Cu addition, and filtered through a 0.45 μm millipore filter.

These samples are divided into samples A and B.

- (ii) Sample A is acidified and used to determine the amount of dissolved Cu in the complete natural water solution:

$$\text{Cu}_{\text{diss}} = \text{Cu}^{2+} + \text{Cu-L} \quad (10.1)$$

while

$$\text{Cu-P} = \text{Cu}_t - \text{Cu}_{\text{diss}} \quad (10.2)$$

- (iii) Sample B is equilibrated with calibrated $\delta\text{-MnO}_2$ and further titrated, in several steps, with Cu, according to the normal $\delta\text{-MnO}_2$ procedure. With the results of this sub-titration,

$K'_{\text{Cu-L}}$ and L_t can be calculated for the dissolved organic material.

- (iv) The free Cu^{2+} concentration in the complete, natural water solution, prior to filtration, can now be calculated with the following mass balance equations:

$$L_t = L + \text{Cu-L} \quad \text{or} \quad L = L_t - \text{Cu-L} \quad (10.3)$$

$$\text{Cu}_{\text{diss}} = \text{Cu}^{2+} + \text{Cu-L} \quad \text{or} \quad \text{Cu-L} = \text{Cu}_{\text{diss}} - \text{Cu}^{2+} \quad (10.1)$$

$$L = L_t - \text{Cu-L} = L_t - \text{Cu}_{\text{diss}} + \text{Cu}^{2+} \quad (10.3)$$

$$K'_{\text{Cu-L}} = \frac{[\text{Cu-L}]}{[\text{Cu}^{2+}] \cdot [L]} \quad (10.4)$$

or

$$K'_{\text{Cu-L}} = \frac{[\text{Cu}_{\text{diss}} - \text{Cu}^{2+}]}{[\text{Cu}^{2+}] [\text{L}_t - \text{Cu}_{\text{diss}} + \text{Cu}^{2+}]} \quad (10.5)$$

$K'_{\text{Cu-L}}$ and L_t are known from (iii), Cu_{diss} is known from (ii) and hence (10.5) can be solved for Cu^{2+} .

(v) By repeating steps (i), (ii) and (iv), a number of values for Cu^{2+} concentrations and corresponding Cu-P concentrations can be determined.

(vi) By plotting Cu^{2+} vs. $\text{Cu}^{2+}/\text{Cu-P}$, P_t and $K'_{\text{Cu-P}}$ can be calculated from the slope and the intercept of the plot.

This procedure assesses trace metal interactions with both particulate and dissolved matter, by treating both fractions as ligands. This may prove very useful since it is known that many particulates occurring in natural waters are coated with organic material. Comparing $K'_{\text{Cu-L}}$ and $K'_{\text{Cu-P}}$ could provide useful information regarding the nature of the organics covering the particulate phase, as well as the extent of such a coverage.

REFERENCES

- Adamson, A.W. 1950. The kinetics of the manganous-permanganate reaction. *J. Am. Chem. Soc.*, 72, 293-303.
- Allen, H.E., M.L. Crosser and T.D. Brisbin. 1975. Metal speciation in aquatic environments, In International Joint Commission Workshop on toxicity to biota of metal forms in natural water, Duluth, Minnesota. W. Andrews, P.V. Hodson and D.E. Konasewich (eds.). 33-57
- Allen, H.E., W.R. Matson and K.H. Mancy. 1970. Trace metal characterization in aquatic environments by anodic stripping voltammetry. *J. Water Pollution Control Federation*, 42, 573-581.
- Anderson, B.J., E.A. Jenne and T.T. Chao. 1973. The sorption of silver by poorly crystallized manganese oxides. *Geochim. Cosmochim. Acta*, 37, 611-622.
- Anderson, M.A., J.F. Ferguson and J. Gavis. 1976. Arsenate adsorption on amorphous aluminum hydroxide. *J. Colloid & Interface Sci.*, 54, 391-399.
- Ardakani, M.S. and F.J. Stevenson. 1972. A modified ion-exchange technique for the determination of stability constants of metal-soil organic matter complexes. *Soil Sci. Soc. Amer. Proc.*, 36, 884-890.

- Baes, C.F. and R.E. Mesmer. 1976. The Hydrolysis of Cations. Wiley, New York, 489 pp.
- Balistrieri, L.S. and J.W. Murray. 1981. The surface chemistry of goethite (αFeOOH) in major ion seawater. *Am. J. Sci.*, 281, 788-806.
- Balistrieri, L.S. and J.W. Murray. 1982. The surface chemistry of $\delta\text{-MnO}_2$ in major ion seawater. *Geochim. Cosmochim. Acta*, 46, 1041-1052.
- Batley, G.E. and T.M. Florence. 1976. A novel scheme for the classification of heavy metal species in natural water. *Anal. Lett.*, 9, 379-388.
- Beck, M.T. 1970. Chemistry of Complex Equilibria. Van Nostrand Reinhold Company, New York. 86-89.
- Belcher, R. and A.J. Nutten. 1967. Quantitative Inorganic Analysis, Butterworths, London (2nd. ed.)
- Benjamin, M.M. and J.O. Leckie. 1981. Conceptual model for metal-ligand-surface interactions during adsorption. *Environm. Sci. and Technol.*, 15, 1050-1057.
- Benjamin, M.M. and J.O. Leckie. 1982. Effects of complexation by Cl , SO_4 and S_2O_3 on adsorption behaviour of Cd on oxide surfaces. *Environm. Sci. and Technol.*, 16, 162-170.
- Bilinski, H., R. Huston and W. Stumm. 1976. Determination of the stability constants of some hydroxo and carbonate complexes of Pb(II), Cu(II), Cd(II) and Zn(II) in dilute solutions by anodic stripping voltammetry and differential pulse polarography. *Anal. Chim. Acta*, 84, 157-164.
- Blaser, P., H. Flühler and J. Polomski. 1980a. Metal binding properties of leaf litter extracts: I. Discontinuous spectrophotometric titration with iron and copper. *Soil Sci. Soc. Am. J.*, 44, 709-716.

- Blaser, P., W. Landolt and H. Flüher. 1980b. Metal binding properties of leaf litter extracts: II. A bioassay technique. *Soil Sci. Soc. Am. J.*, 44, 717-720.
- Blutstein, H. and R. F. Shaw. 1981. Characterization of copper binding capacity in lakewater. *Environm. Sci. and Technol.*, 15, 1100-1102.
- Bourg, A. C. M. 1979. Effect of ligands at the solid solution interface upon the speciation of heavy metals in aquatic systems; *Int. Conf. Management and Control of Heavy Metals in the Environment*, London, Sept. 1979.
- Bourg, A. C. M. and R. H. Filby. 1974. Adsorption isotherms for the uptake of Zn^{2+} by clay minerals in a freshwater medium. *In J. Proc. Int. Conf. on Transport of Persistent Chemicals in Aquatic Ecosystems*, Ottawa, Canada.
- Bourg, A. C. M. and P. W. Schindler. 1978. Ternary surface complexes, I. Complex formation in the system silica-Cu(II)-ethylenediamine. *Chimia*, 32, 166-168.
- Bourg, A. C. M., S. Joss and P. W. Schindler. 1979. Ternary surface complexes. II. Complex formation in the system silica-Cu(II)-2,2'-bipyridil. *Chimia*, 33, 19-21.
- Bowden, J. W., A. M. Posner and J. R. Quirk. 1977. Ionic adsorption on variable charge mineral surfaces. Theoretical charge development and titration curves. *Austr. J. Soil Res.*, 15, 121-136.
- Bower, C. A. and J. O. Goertzen. 1959. Surface area of soils and clays by an equilibrium ethylene glycol method. *Soil Sci.*, 87, 288-292.
- Bradford, W. L. 1973. The determination of a stability constant for the aqueous complex $Zn(OH)_2^0$ using anodic stripping voltammetry. *Limnol. Oceanogr.*, 18, 757-762.
- Breeuwsma, A. and J. Lyklema. 1973. Physical and chemical adsorption of ions in the electrical double layer on hematite ($\alpha-Fe_2O_3$). *J. Coll. Interface Sci.*, 43, 437-448.

- Brezonik, P.L., P.A. Brauner and W. Stumm. 1976. Trace metal analysis by anodic stripping voltammetry: Effect of sorption by natural and model organic compounds. *Water Res.*, 10, 605-612.
- Bricker, O. 1965. Some stability relations in the system Mn - O₂ - H₂O at 25°C and one atmosphere total pressure. *Amer. Mineralogist.*, 50, 1296-1354.
- Brinkman, A.A.A.M. and J.M. Los. 1967. Pulse polarography III. Kinetic currents due to a preceding chemical reaction. *J. Electroanal. Chem.*, 14 269-284; Pulse polarography IV. Catalytic and purely rate-controlled currents. *J.E.C.* 14, 285-296.
- Brügge, D.G., J.R. Brown, G.M. Bancroft and W.S. Fyfe. 1980. Cation adsorption by hydrous manganese dioxide: A semiquantitative X-ray photoelectron spectroscopic (ESCA) study. *Chem. Geol.*, 28, 331-339.
- Brunauer, S., P.H. Emmett and E. Teller. 1938. Adsorption of gases in multi-molecular layers. *J. Am. Chem. Soc.*, 60, 309-319.
- Buffle, J., F.L. Greter and W. Haerdi. 1977. Measurement of complexation properties of humic and fulvic acids in natural waters with lead and copper ion-selective electrodes. *Anal. Chem.*, 49, 216-222.
- Burns, R.G. 1970. *Mineralogical Applications of Crystal Field Theory*. Cambridge University Press, 224 pp.
- Burns, R.G. 1976. The uptake of cobalt into ferromanganese (IV) oxides. *Geochim. Cosmochim. Acta*, 40, 95-102.
- Burns, R.G. and V.M. Burns. 1979. Marine Minerals, Chapter 1: Manganese Oxides. *In* Burns, R.G. (ed.) *Mineral. Soc. Amer. Short Course notes*, 6.
- Burns, R.G. and V.M. Burns. 1977. Marine Manganese Deposits, Chapter 7, G.P. Glasby (ed.), Elsevier, Amsterdam.

- Burns, V.M., R.G. Burns and W.K. Zwicker. 1975. Classification of natural manganese dioxide minerals, In : A. Kozawa and R.J. Brodd (eds.), Proc. Int. Symp. Manganese Dioxides, Electrochem. Soc., Cleveland, October 1975, 282-305.
- Buser, W. and P. Graf. 1955. Differentierung von Mangan(II)-manganite und δ -MnO₂ durch Oberflächenmessung nach Brunauer-Emmet-Teller. *Helv. Chim. Acta*, 38, 830-834.
- Buser, W., P. Graf and W. Feitknecht. 1954. Beitrag zur Kenntnis des Mangan(II)-manganite und des δ -MnO₂. *Helv. Chim. Acta*, 37, 2322-2333.
- Byström, A. and A.M. Byström. 1950. The crystal structure of hollandite, the related manganese oxide minerals and α -MnO₂. *Acta Cryst.*, 3, 146-154.
- Cahill, R.A. 1981. Geochemistry of recent Lake Michigan sediments. Champaign, Illinois State Geological Survey Division Circular 517.
- Campbell, P.G.C., M. Bisson, R. Gagné and A. Tessier. 1977. Critical evaluation of the copper (II) solubilization method for the determination of the complexation capacity of natural waters. *Anal. Chem.*, 49, 2358-2363.
- Catanzaro, E.J. 1976. Some relationships between exchangeable copper and lead and particulate matter in a sample of Hudson River water. *Environm. Sci. Technol.*, 10, 386-388.
- Cecutti, A. and E. Nieboer. 1981. Nickel metabolism and biochemistry and effects of nickel in animals and humans. In: Effects of nickel in the Canadian environment. N.R.C. of Canada. Publication # NRCC 18568, Ottawa. 193-260.
- Chao, T.T. and P.K. Theobald Jr. 1976. The significance of secondary iron and manganese oxides in geochemical exploration. *Econ. Geol.*, 71, 1560-1569.
- Chast, R.R.P. 1979. Settling behaviour of natural aquatic particulates. *Limnol. Oceanogr.*, 24, 417-426.

- Chau, Y.K., R. Gächter and K. Lum-Shue-Chan. 1974. Determination of the apparent complexing capacity of lake waters. *J. Fish. Res. Board Can.*, 31, 1515-1519.
- Chau, Y.K. and K. Lum-Shue-Chan. 1974. Determination of labile and strongly-bound metals in lake water. *Water Res.*, 8, 383-388.
- Chau, Y.K. and Shiomi, M.T. 1972. Complexing properties of nitrilotriacetic acid in the lake environment. *Water, Air and Soil Pollution*, 1, 149-164.
- Cheam, V. 1973. Chelation study of copper (II): Fulvic acid system. *Can. J. Soil Sci.*, 53, 377-382.
- Cheam, V. and D.S. Gamble. 1974. Metal-fulvic acid chelation equilibrium in aqueous NaNO_3 solution. Hg(II) , Cd(II) and Cu(II) fulvate complexes. *Can. J. Soil Sci.*, 54, 413-417.
- Chevillot, J.P. 1964. Relations between the formation, the structure and the properties of certain manganese dioxides. *J. Chim. Phys.*, 61, 748-750.
- Cole, W.F., A.D. Wadsley and A. Walkley. 1977. An X-ray diffraction study of manganese dioxide. *Trans. Electrochem. Soc.*, 92, 133-158.
- Copeland, L.C., F.S. Griffith and C.B. Schertzinger. 1947. Preparation of a dry cell depolarizer by air oxidation of manganous hydroxide. *Trans. Electrochem. Soc.*, 92, 127-132.
- Courpron, C. 1967. Determination des constantes de stabilité des complexes organometalliques des soils. *Annales Agronomiques*, 18, 623-638.
- Cramer, J.J. 1982. Effects of rock-water interaction on radionuclide transport. *In Techn. Rep. 201*, Atomic Energy of Canada Ltd., Pinawa, Manitoba.
- Davey, E.W., M.J. Morgan and S.J. Erickson. 1973. A biological measurement of the copper complexation capacity of seawater. *Limnol. Oceanogr.*, 18, 993-997.

- Davis, J.A. 1978. Adsorption of trace metals and complexing ligands at the oxide/water interface. Ph.D.thesis, Stanford Univ., Cal.
- Davis, J.A., R.O. James and J.O. Leckie. 1978. Surface ionization and complexation at the oxide/water interface. I. Computation of electrical double layer properties in simple electrolytes. *J. Colloid Interface Sci.*, 63, 480-499.
- Davis, J.A. and J.O. Leckie. 1978a. Surface ionization and complexation at the oxide/water interface. 2. Surface properties of amorphous iron oxyhydroxide and adsorption of metal ions. *J. Colloid Interface Sci.*, 67, 90-107.
- Davis, J.A. and J.O. Leckie. 1978b. Effect of adsorbed complexing ligands on trace metal uptake by hydrous oxides. *Environm. Sci. and Technol.*, 12, 1309-1315.
- Davis, J.A. and J.O. Leckie. 1979. Speciation of adsorbed ions at the oxide/water interface, *In: Chemical Modeling in Aqueous Systems*, ACS Symp. Ser., 93, E.A. Jenne (ed.), ACS, Washington D.C.
- Davis, J.A. and J.O. Leckie. 1980. Surface ionization and complexation at the oxide/water interface. 3. Adsorption of anions. *J. Colloid Interface Sci.*, 74, 32-43.
- Davis, R.A. Jr. 1973. Principles of Oceanography. Addison-Wesley Publ. Co., London, Ont.
- Dempsey, B.A. and Ph.C. Singer. 1980. The effect of calcium on the adsorption of zinc by $MnO_x(s)$ and $Fe(OH)_3(am)$. *In: Contaminants and Sediments*, R.A. Baker (ed.), Ann Arbor Science.
- Draper, N.R. and H. Smith. 1966. Applied Regression Analysis. John Wiley and Sons Inc., New York.

- Dugger, D.L., J.H. Stanton, B.N. Irby, B.L. McConnell, W.W. Cummings and R.W. Maatman. 1964. The exchange of twenty metal ions with the weakly acidic silanol groups of silica gel. *J. Phys. Chem.*, 68, 757-760.
- Dyal, R.S. and S.B. Hendricks. 1950. Total surface of clays in polar liquids as a characteristic index. *Soil Sci.*, 69, 421-432.
- Ernst, R., H.E. Allen and K.H. Mancy. 1975. Characterization of trace metal species and measurement of trace metal stability constants by electrochemical techniques. *Water Res.*, 9, 969-979.
- Figgis, B.N. 1966. *Introduction to Ligand Fields*. Interscience, New York.
- Figura, P. and B. McDuffie. 1979. Use of Chelex resin for determination of labile trace metal fractions in aqueous ligand media and comparison of the method with anodic stripping voltammetry. *Anal. Chem.*, 51, 120-125.
- Fleer, G.J. and J.N. de Wit. 1969. *Syllabus Kolloidchemie*. Dept. for Physical and Colloid Chemistry, Agricultural University, Wageningen, The Netherlands.
- Florence, T.M. 1977. Trace metal species in fresh waters. *Water Res.*, 11, 681-687.
- Folk, R.L. 1974. *Petrology of Sediments*, Univ. of Texas.
- Gabano, J.P., P. Etienne and J.F. Laurent. 1965. Etude des proprietes de surface du bioxyde de manganese. *Electrochim. Acta*, 10, 947-963.
- Gadde, R.R. and H.E. Laitinen. 1974. Studies of heavy metal adsorption by hydrous iron and manganese oxides. *Anal. Chem.*, 46, 2022-2026.
- Galindo, G. and H. Zumino. 1978. Some limiting factors of the ion exchange equilibrium method for determining apparent formation constants of mononuclear complexes. *Talanta*, 25, 447-450.

- Gaskill, A. Jr. 1978. Methods for the characterization of metal-humic interactions. M.Sc. thesis, Univ. of N. Carolina, Chapel Hill.
- Geering, H.R. and J.F. Hodgson. 1969. Micronutrient cation complexes in soil solution. III: Characterization of soil solution ligands and their complexes with Zn^{2+} and Cu^{2+} . Soil Sci. Soc. Am. Proc., 33, 54-59.
- Gerlach, R.W. and B.R. Kowalski. 1982. The generalized standard addition method: intermetallic interferences in anodic stripping voltammetry. Anal. Chim. Acta, 134, 119-127.
- Gillespie, P.A. and R.F. Vaccaro. 1978. A bacterial bioassay for measuring the copper-chelating capacity of seawater. Limnol. Oceanogr., 23, 543-548.
- Giovanoli, R. 1969. A simplified scheme for polymorphism in the manganese dioxides. Chimia, 23, 470-472.
- Giovanoli, R., E. Stähli and W. Feitknecht. 1970a. Über oxyhydroxide des vierwertigen Mangans mit Schichtengitter. 1. Mitteilung; Natriummangan (II, III) manganat (IV). Helv. Chim. Acta, 53, 209-220.
- Giovanoli, R., E. Stähli and W. Feitknecht. 1970b. Über hydroxide des vierwertigen Mangans mit Schichtengitter. 2. Mitteilung; Mangan (III) - Manganat (IV). Helv. Chim. Acta, 53, 453-464.
- Giovanoli, R., W. Feitknecht and F. Fischer. 1971. Über hydroxide des vierwertigen Mangans mit Schichtengitter. 3. Mitteilung; Reduction von Mangan (III) - Manganat (IV) mit Zimtalkohol. Helv. Chim. Acta, 54, 113-114.
- Giovanoli, R., P. Bürki, M. Giuffredi and W. Stumm. 1975. Layer structured manganese oxide hydroxides IV: The busserite group; structure stabilization by transition elements. Chimia, 29, 517-520.
- Gjessing, E.T. 1976. Physical and Chemical Characteristics of Aquatic Humics. Ann Arbor Sci. Inc., Michigan.

- Grahame, D.C. 1947. The electrical double layer and the theory of electrocapillarity. *Chem. Revs.*, 41, 441-501.
- Gran, G. 1952. Determination of the equivalence point in potentiometric titrations, part II. *The Analyst*, 77, 661-671.
- Gray, M.J. and M.A. Malati. 1979. a) Adsorption from aqueous solution by δ -manganese dioxide. I. Adsorption of the alkaline-earth cations. *J. Chem. Tech. Biotechnol.*, 29, 127-134.
b) Adsorption from aqueous solution by δ -manganese dioxide. II. Adsorption of some heavy metal cations. *J. Chem. Tech. Biotechnol.*, 29, 135-144.
- Gray, M.J., M.A. Malati and M.W. Raphael. 1978. The point of zero charge of manganese dioxides. *Electroanal. Chem.*, 89, 135-140.
- Green, J.B. and S.E. Manaban. 1977. Cupric ion binding by coal humic acids at pH's 1 - 3. *Can. J. Chem.*, 55, 3248-3254.
- Groenwegen, J.A. and W.M.H. Sachtler. 1972. The infrared spectrum of glycine chemisorbed by supported nickel. *J. Catalysis*, 27, 369-372.
- Guy, R.D. and C.L. Chakrabati. 1977. Analytical techniques for speciation of trace metals. *In: Int. Conf. on Heavy Metals in the Environment. Symp. Proc.* 1, 371pp, Toronto, 1975. 275-294.
- Guy, R.D. and C.L. Chakrabarti. 1976. Studies of metal organic interactions in model systems pertaining to natural waters. *Can. J. Chem.*, 54, 2600-2611.
- Guy, R.D., C.L. Chakrabarti and L.L. Schramm. 1975. The application of a simple chemical model of natural waters to metal fixation in particulate matter. *Can. J. Chem.*, 53, 661-669.
- Hanck, K.W. and J.W. Dillard. 1977. Determination of the complexing capacity of natural water by cobalt (III) complexation. *Anal. Chem.*, 49, 404-409.
- Harriss, R.C. and A.G. Troup. 1969. Chemistry and origin of freshwater ferromanganese concretions. *Limnol. Oceanogr.*, 20, 702-712.

- Healy, T.W. 1971. Selective adsorption of organics on inorganic surfaces. In: S.D. Faust and J.V. Hunter (Eds.), Organic Compounds in Aquatic Environments, Marcel Dekker, New York, 187-212.
- Healy, T.W. and D.W. Fuerstenau. 1965. The oxide-water interface. Interrelation of the zero point of charge and the heat of immersion. *J. Colloid Sci.*, 20, 376-386.
- Healy, T.W., A.P. Herring and D.W. Fuerstenau. 1966. The effect of crystal structure on the surface properties of a series of manganese dioxides. *J. Colloid Interface Sci.*, 21, 435-444.
- Hem, J.D. 1978. Redox processes at surfaces of manganese oxide and their effects on aqueous metal ions. *Chem. Geol.*, 21, 199-218.
- Hoffman, M.R. and S.J. Eisenreich. 1981. Development of a computer-generated equilibrium model for the variation of iron and manganese in the hypolimnion of Lake Mendota. *Environm. Sci. and Techn.*, 15, 339-344.
- Hohl, H. and W. Stumm. 1976. Interaction of Pb^{2+} with hydrous $\gamma-Al_2O_3$. *J. Coll. Int. Sci.*, 55, 281-288.
- Huang, C.P. and W. Stumm. 1973. Specific adsorption of cations on hydrous $\gamma-Al_2O_3$. *J. Coll. Int. Sci.*, 43, 409-420.
- Huang, C.P. and W. Stumm. 1972. The specific surface area of $\gamma-Al_2O_3$. *Surface Sci.*, 32, 287-296.
- Hunter, K.A. 1980. Microelectrophoretic properties of natural surface-active organic matter in coastal seawater. *Limnol. Oceanogr.*, 25, 807-822.
- James, R.O. and T.W. Healy. 1972. Adsorption of hydrolyzable ions at the oxide-water interface. I: Co(II) adsorption on SiO_2 and TiO_2 as model systems. II: Charge reversal of SiO_2 and TiO_2 colloids by adsorbed Co(II), La(III) and Th(IV) as model systems. III. A thermodynamic model of adsorption. *J. Coll. Int. Sci.* 40, 42-52, 53-64, 65-81.

- Jenne, E.A. 1968. Controls on Mn, Fe, Co, Ni, Cu and Zn concentrations in soils and water: The significant role of hydrous Mn and Fe oxides. *In: Trace Inorganics in Water*. R.F. Gould, (ed.), Advances in Chemistry Series (ACS), 73, 337-387.
- Jenne, E.A. 1982. Pers. comm.
- Jeffries, D.S. and W. Stumm. 1976. The metal adsorption chemistry of buserite. *Can. Mineral.*, 14, 16-22.
- Job, P. 1928. Recherches sur la formation de complexes minéraux en solution et sur leur stabilité. *Annales Chimia*, 9, 113-203.
- Jones, L.H.P. and A.A. Milne. 1956. Birnessite, a new manganese oxide mineral from Aberdeenshire, Scotland. *Min. Mag. & J. Mineral. Soc.*, 235, 283-288.
- Kessick, M.A. and J.J. Morgan. 1975. Mechanism of autoxidation of manganese in aqueous solution. *Environm. Sci. & Technol.*, 9, 157-159.
- Keyser, T.R., D.F.S. Matusch, C.A. Evans Jr. and R.W. Linton. 1978. Characterizing the surfaces of environmental particles. *Environm. Sci. & Technol.*, 12, 768-773.
- Koons, R.D., P.A. Helmke and M.L. Jackson. 1980. Association of trace elements with iron oxides during rock weathering. *Soil Sci. Soc. Am. J.*, 44, 155-159.
- Kopp, J.F. 1977. Current status of analytical methodology for trace metals. *In: Proc. Int. Conf. on Heavy Metals in the Environment*, Toronto, Ont., 1975, 261-275.
- Kruyt, H.R. 1952. *Colloid Science I*. Elsevier Pub. Co. Amsterdam.
- Kummert, R. and W. Stumm. 1980. The surface complexation of organic acids on hydrous γ - Al_2O_3 . *J. Coll. Int. Sci.*, 75, 373-385.
- Kunkel, R. and S.E. Manahan. 1973. Atomic absorption analysis of strong heavy-metal chelating agents in water and wastewater. *Anal. Chem.* 45, 1465-1468.

- Kurbatov, M.H., G.B. Wood and J.D. Kurbatov. 1951a. Application of the mass law to adsorption of divalent ions on hydrous ferric oxide. *J. Chem. Phys.*, 19, 258-259.
- Kurbatov, M.H., G.B. Wood and J.D. Kurbatov. 1951b. Isothermal adsorption of cobalt from dilute solutions. *J. Phys. Coll. Chem.*, 55, 1170-1182.
- Lal, D. The oceanic microcosm of particles. *Science*, 198, 997-1009.
- Laxen, D.P.H. and R.M. Harrison. 1981. Cleaning methods for polythene containers prior to the determination of trace metals in fresh water samples. *Anal. Chem.* 53, 345-350.
- Lazar, B., A. Katz and S. Ben-Yaakov. 1981. Copper complexing capacity of seawater: A critical appraisal of the direct ASV method. *Marine Chem.*, 10, 221-231.
- Leeuwen, H.P. van. 1977. Kinetic classification of metal complexes in electroanalytical speciation. Paper presented at EUCHEM Conf. on Electrode Measurements in Natural Waters, Lernum, Sweden, June 13-16, 1977.
- Leeuwen, H.P. van. 1979. Kinetic classification of metal complexes in electroanalytical speciation. *J. Electroanal. Chem.*, 99, 93-102.
- Leckie, J.O. and R.O. James. 1974. Control mechanisms for trace metals in natural waters. In: *Aqueous Environmental Chemistry of Metals*, A.J. Rubin (ed.), Ann Arbor Sci., Michigan.
- Lerman, A. and C.W. Childs. 1973. Metal-organic complexes in natural waters: Control of distribution by thermodynamic, kinetic and physical factors. In: *Trace Metals and Metal-Organic Interactions in Natural Waters*, P.C. Singer (ed.), Ann Arbor Sci., 237-263.
- Levine, S. and A.L. Smith. 1971. Theory of the differential capacity of the oxide/aqueous electrolyte interface. *Disc. Farad. Soc.*, 52, 290-301.

- Lingane, J.J. 1941. Interpretation of the polarographic waves of complex metal ions. *Chem.Rev.*, 29, 1-35.
- Loganathan, P. and R.G. Burau. 1973. Sorption of heavy metal ions by a hydrous manganese oxide. *Geochim.Cosmochim. Acta*, 37, 1277-1293.
- Loganathan, P., R.G. Burau and D.W. Fuerstenau. 1977. Influence of pH on the sorption of Co^{2+} , Zn^{2+} and Ca^{2+} by a hydrous manganese oxide. *Soil Sci.Soc.Am.J.*, 41, 57-62.
- Lyklema, J. 1968. The structure of the electrical double layer on porous surfaces. *J.Electroanal.Chem.*, 18, 341-348.
- Lyklema, J. 1976. Chemische en statistische thermodynamica van de adsorptie. Syllabus caputcollege; landbouw Hogeschool, Fysische en Kolloïdchemie, Wageningen.
- Lyklema, J. and H.J. Van der Hull. 1969. Specific surface areas by negative adsorption. *Proc. IUPAC Symp., Surface Area Determination*, 341-360.
- Malcolm, R.L., E.A. Jenne and P.W. McKinley. 1968. Conditional stability constants of a North Carolina soil fulvic acid with Co^{2+} and Fe^{3+} . *In: Proc.Symp. Organic Matter in Natural Waters*, D.W. Hood (ed.), Univ. of Alaska, 1968.
- Malotki, D.T. and M.A. Anderson. 1976. The adsorption of the potential determining arsenate anion on oxide surfaces. *Coll. and Interface Sci., IV, Hydrosols and Rheology*, 281-295.
- Manning, P.G. and S. Ramamoorthy. 1973. Equilibrium studies of metal-ion complexes of interest to natural waters - VII: Mixed-ligand complexes of Cu(II) involving fulvic acid as primary ligand. *J.Inorg.Nucl.Chem.*, 35, 1577-1581.
- Mantoura, R.F.C. and J.P. Riley. 1975. The use of gel filtration in the study of metal binding by humic acids and related compounds. *Anal.Chim.Acta*, 78, 193-200.

- Martell, A.E. and M. Calvin. 1952. Chemistry of Metal Chelate Compounds. Prentice Hall Inc., New York, 613pp.
- Massee, R. and F.J.M.J. Maessen. 1981. Losses of silver, arsenic, cadmium, selenium and zinc traces from distilled water and artificial seawater by sorption on various container surfaces. Anal. Chim. Acta, 127, 181-193.
- Matijević, E. 1967. Charge reversal of lyophobic colloids. In: Principles and Applications of Water Chemistry, S.D. Faust and J.V. Hunter (eds.), John Wiley & Sons, N.Y.
- Matijević, E., M.B. Abramson, K.F. Schulze and M. Kerka. 1960. Detection of metal ion hydrolysis by coagulation: II. Thorium. J. Phys. Chem., 64, 1157-1161.
- McBride, M.B. 1982. Adsorption characteristics of aluminum hydroxide and oxyhydroxides. Clays & Clay Minerals, 30, 21-28.
- McClure, D.S. 1957. The distribution of transition metal cations in spinels. J. Phys. Chem. Solids, 3, 311-317.
- McDuff, R.B. and F.M.M. Morel. 1973. Description and use of the chemical equilibrium program REDEQL 2. Techn. Rep. EQ-73-02, W.M. Keck Lab. of Environm. Eng. Sci. Caltech., Pasadena, Calif., 1973 (updated 1974, 1975).
- McLaren, R.G. and D.V. Crawford. 1973. Studies on soil copper - I. The specific adsorption of copper by soils. J. Soil Sci., 24, 443-452.
- McKenzie, R.M. 1970. The reaction of cobalt with manganese dioxide minerals. Austr. J. Soil Res., 8, 97-106.
- McKenzie, R.M. 1971. The synthesis of birnessite, cryptomelane and some other oxides and hydroxides of manganese. Min. Mag., 38, 493-502.
- McKenzie, R.M. 1972. The sorption of some heavy metals by the lower oxides of manganese. Geoderma, 8, 29-35.
- McKenzie, R.M. 1977. Manganese oxides and hydroxides. In: Minerals in Soil Environments, R.C. Dinauer (ed.), Soil Sci. Soc. Amer., Madison, Wisc., USA.

- McKenzie, R.M. 1979. Proton release during adsorption of heavy metal ions by a hydrous manganese dioxide. *Geochim. Cosmochim. Acta*, 43, 1855-1857.
- McMurdie, H.F. 1944. Microscopic and diffraction studies on dry cells and their raw materials. *Trans. Electrochem. Soc.*, 86, 313-326.
- Means, J.L., D.A. Crerar and J.L. Amster. 1977. Application of gel filtration chromatography to evaluation of organo-metallic interactions in natural waters. *Limnol. Oceanogr.*, 22, 957-965.
- Means, J.L., D.A. Crerar, M.P. Borcsik and J.O. Duguid. 1978a. Adsorption of Co and selected actinides by Mn and Fe oxides in soils and sediments. *Geochim. Cosmochim. Acta*, 42, 1763-1773.
- Means, J.L., D.A. Crerar, M.P. Borcsik and J.O. Duguid. 1978b. Radionuclide adsorption by manganese oxides and implications for radioactive waste disposal. *Nature*, 274, 44-47.
- Means, J.L., D.A. Crerar and J.O. Duguid. 1978c. Migration of radioactive wastes: Radionuclide mobilization by complexing agents. *Science*, 200, 1477-1481.
- Meeter, D.A. 1965. Non-linear least squares (GAUSHAUS), Univ. of Wisconsin Computer Sci.
- Morel, F.M.M., J.C. Westall, C.R.O' Melia and J.J. Morgan. 1975. Fate of trace metals in Los Angeles County wastewaters discharge. *Environm. Sci. and Technol.* 9, 756-761.
- Morgan, J.J. and W. Stumm. 1964. Colloid chemical properties of manganese dioxide. *J. Coll. Sci.* 19, 347-359.
- Morgan, J.J. and W. Stumm. 1965. Analytical chemistry of aqueous manganese. *J. Am. Water Works Assoc.*, 57 107-119.
- Mudroch, A. and T. Bistricki, 1981. Occurrence of manganese-rich microparticles in the eastern basin of Lake Erie. *Can. Mineralogist*, 19 435-440.

- Murray, D.J., T.W. Healy and D.W. Fuerstenau. 1968. The adsorption of aqueous metal on colloidal hydrous manganese oxide. *Adv. Chem.*, 79, 74-81.
- Murray, J.W. 1974. The surface chemistry of hydrous manganese dioxide. *J. Coll. Interface Sci.*, 46, 357-371.
- Murray, J.W. 1975a. The interaction of metal ions at the manganese dioxide-solution interface. *Geochim. Cosmochim. Acta*, 39, 505-519.
- Murray, J.W. 1975b. The interaction of cobalt with hydrous manganese dioxide. *Geochim. Cosmochim. Acta*, 39, 635-647.
- Murray, J.W. and J.G. Dillard. 1979. The oxidation of cobalt(II) adsorbed on manganese dioxide. *Geochim. Cosmochim. Acta*, 43, 781-787.
- Nakagawa, G., H. Wada and T. Hayakawa. 1975. Use of the copper(II) selective electrode for the determination of the stability constants of copper(II) complexes. *Bull. Chem. Soc. Japan*, 48, 424-427.
- Neihof, R.A. and G.I. Loeb. 1972. The surface charge of particulate matter in seawater. *Limnol. Oceanogr.*, 17, 7-16.
- Nissenbaum, A. and D.J. Swaine. 1976. Organic matter-metal interactions in recent sediments: The role of humic substances. *Geochim. Cosmochim. Acta*, 40, 809-816.
- Nriaga, J.O. (ed.). 1979 *Copper in the Environment*. Wiley. 522pp.
- Nordstrom, D.K. and 18 others. 1979. Comparison of computerized chemical models for equilibrium calculations in aqueous systems. *In: ACS Symp. Ser. on Chemical Modeling: Speciation, Sorption, Solubility and Kinetics in Aqueous Systems*. E.A. Jenne (ed.), 857-895.
- Otto, E., G.W. Vinal and E.H. Ostrander. 1944. Effect of digesting, autoclaving and neutralizing some battery manganese dioxides. *Trans. Electrochem. Soc.*, 86, 327-336.

- Orlov, D.S., I.A. Pivovarova and N.I. Gorbunov. 1973. Interaction of humic substances with minerals and the nature of their bond - a review. Soviet Soil Sci., translated from *Agrokhimiya*, 9, 140-153.
- Park, G.A. 1975. Adsorption in Marine Environment. In: *Chemical Oceanography*, J.P. Riley and G. Skirrow (eds.) VI, Academic Press, London.
- Perram, J.W. 1973. Structure of the double layer at the oxide/water interface. *J. Chem. Soc. Faraday Trans. II*, 7, 993-1003.
- Pita, F.W. and N.J. Hyne. 1975. The depositional environment of zinc, lead and cadmium in reservoir sediments. *Water Res.*, 9, 701-706.
- Polissar, M.J. 1935. The kinetics of the reaction between permanganate and manganous ions. *J. Phys. Chem.*, 39, 1057-1066.
- Posselt, H.S., F.J. Anderson and W.J. Weber. 1968a. Cation sorption on colloidal hydrous manganese dioxide. *Env. Sci. & Technol.*, 12, 1087-1093.
- Posselt, H.S., A.H. Reides and W.J. Weber, Jr. 1968b. Coagulation of colloidal manganese dioxide. *J. Am. Water Works Assoc.*, 60, 48-68.
- Potter, R.M. and G.R. Rossman. 1979. The tetravalent manganese oxides: identification, hydration and structural relationships by infrared spectroscopy. *Am. Mineralogist*, 64, 1199-1218.
- Ramamoorthy, S. and D.J. Kushner. 1975a. Heavy metal binding sites in river water. *Nature*, 256, 399-401.
- Ramamoorthy, S. and D.J. Kushner. 1975b. Heavy metal binding components of river water. *J. Fish. Res. Board Can.*, 30, 1755-1766.
- Ramamoorthy, S. and B.R. Rust. 1976. Mercury sorption and desorption characteristics of some Ottawa River sediments. *Can. J. Earth Sci.*, 13, 530-536.

- Rashid, M.A. 1974. Adsorption of metals on sedimentary and peat humic acids. *Chem. Geol.*, 13, 115-123.
- Raspor, B., P. Valenta, H.W. Nürnberg and M. Bramca. 1977. The chelation cadmium with NTA in seawater as a model for the typical behaviour of trace heavy metal chelates in natural waters. *Sci. of the Total Environment*, 9, 87-109.
- Reuter, J.H. and E.M. Perdue. 1977. Importance of heavy metal-organic interactions in natural waters. *Geochim. Cosmochim. Acta*, 41, 325-334.
- Riddick, Th.M. 1961. Zeta potential, new tool for water treatment. Part II. *Chem. Eng.*, 141-145.
- Ringbom, A. 1963. *Complexation in Analytical Chemistry*. Interscience, New York.
- Rossotti, F.J.C. and H. Rossotti. 1961. *The Determination of Stability Constants*. McGraw-Hill Inc., Toronto, 425pp.
- Rubio, J. and E. Matijević. 1979. Interactions of metal hydrous oxides with chelating agents. *J. Coll. Int. Sci.*, 68, 408-421.
- Saar, R.A. and J.H. Weber. 1980a. Lead (II) fulvic acid complexes. Conditional stability constants, solubility and implications for lead (II) mobility. *Env. Sci. & Technol.*, 14, 877-879.
- Saar, R.A. and J.H. Weber. 1980b. Lead (II) complexation by fulvic acid: How it differs from fulvic acid complexation of copper (II) and cadmium (II). *Geochim. Cosmochim. Acta*, 44, 1381-1382.
- Schindler, P.W., B. Fürst, R. Dick and P.U. Wolf. 1976. Ligand properties of surface silanol groups. 1. Surface complex formation with Fe^{3+} , Cu^{2+} , Cd^{2+} and Pb^{2+} . *J. Coll. Interface Sci.*, 55, 469-475.

- Schnitzer, M. 1971. Metal-organic matter interactions in soils and water. In: Organic Compounds in Aquatic Environment, S. Faust and J.V. Hunter (eds.), Marcel Dekker Inc., New York, 297-315.
- Schnitzer, M. and S.I.M. Skinner. 1963. Organo-metallic interactions in soils. 1 : Reactions between a number of metal ions and the organic matter of a podzol Bh horizon. Soil Sci., 96, 86-93.
- Schnitzer, M. and S.I.M. Skinner. 1966. Organo-metallic interactions in soils. 5 : Stability constants of Cu^{2+} -, Fe^{2+} -, and Zn^{2+} - fulvic acid complexes. Soil Sci., 102, 361-365.
- Schnitzer, M. and I. Hoffman. 1967. Thermogravimetric analysis of the salts and metal complexes of a soil fulvic acid. Geochim. Cosmochim. Acta, 31, 7-15.
- Schnitzer, M. and S.I.M. Skinner. 1967. Organo-metallic interactions in soils. 7 : Stability constants of Pb^{2+} -, Ni^{2+} -, Mn^{2+} -, Co^{2+} -, Ca^{2+} -, and Mg^{2+} - fulvic acid complexes. Soil Sci., 103, 247-252.
- Schnitzer, M. and E.H. Hansen. 1970. Organo-metallic interactions in soils: 8. An evaluation of methods for the determination of stability constants of metal-fulvic acid complexes. Soil Sci., 109, 333-340.
- Schnitzer, M. and S.U. Khan. 1972. Humic Substances in the Environment. Marcel Dekker Inc., New York, 327 pp.
- Schubert, J. 1948. Use of ion exchangers for the determination of physical-chemical properties of substances, particularly radiotracers. I.J. Phys. Coll. Chem., 52, 340-350.
- Shuman, M.S. 1978. Team looks at metal speciation. E.S.E. Notes, 14, Dept. of Env. Sci. & Eng., School of Pub. Health, Univ. of North Carolina, Chapel Hill.


- Shuman, M.S. and G.P. Woodward Jr. 1973. Chemical constants of metal complexes from a complexometric titration followed with anodic stripping voltammetry. *Anal. Chem.*, 45, 2032-2034.
- Shuman, M.S. and L.C. Michael. 1975. Ring-disk techniques for studying kinetics of metal complex formation and dissociation in natural waters. *Proc. Int. Conf. on Heavy Metals in the Environment, Toronto*, 227-248.
- Shuman, M.S. and G.P. Woodward Jr. 1976. Intermetallic compound formation between copper and zinc in mercury and its effects on anodic stripping voltammetry. *Anal. Chem.*, 48, 1979-1983.
- Shuman, M.S. and G.P. Woodward Jr. 1977. Stability constants of copper-organic chelates in aquatic samples. *Environm. Sci. & Technol.*, 11, 809-813.
- Shuman, M.S. and L.C. Michael. 1978. Application of the rotated disk electrode to measurement of copper complex dissociation rate constants in marine coastal samples. *Environm. Sci. & Technol.*, 12, 1069-1072.
- Sillen, L.G. 1961. The physical chemistry of seawater. In: *Pub. 67, Am. Assoc. Adv. Sci., M. Sears (ed.)*, 549-581.
- Sillen, L.G. and A.E. Martell. 1964. Stability constants of metal-ion complexes. *Spec. Pub. 17, Chem. Soc., London*.
- Smit, W., C.L.M. Holten, H.N. Stein, J.J.M. de Goeij and H.M.J. Theelen. 1978. A radiotracer determination of the adsorption of sodium ions in the compact part of the double layer of vitreous silica. *J. Coll. Interface Sci.*, 63, 120-128.
- Smit, W. and H.N. Stein. 1978. Note on the adsorption of sodium ions in the compact part of the electrical double layer of oxides. *J. Electroanal. Chem.*, 91, 393-394.

- Smith, R.G. Jr. 1978. Sources of copper and cadmium contamination in small biological samples. *Talanta*, 25, 1973-1975.
- Snodgrass, W.J. 1982. pers. comm.
- Stern, K.H. and E.S. Amis. 1959. Ionic size. *Chem. Rev.*, 59, 1-64.
- Stern, O. 1924. Zur theorie der elektrolytischen Doppelschicht. *z.f. Elektrochemie*, 30, 508-516.
- Stevenson, F.J. 1976. Stability constants of Cu^{2+} , Pb^{2+} , and Cd^{2+} complexes with humic acids. *Soil Sci. Soc. Am. J.*, 40, 665-672.
- Stevenson, F.J. 1977. Nature of divalent transition metal complexes of humic acids as revealed by a modified potentiometric titration method. *Soil Sci.*, 123, 10-17.
- Stevenson, F.J. and M.S. Ardakani. 1972. Organic matter reactions involving micronutrients in soils. *In: Micronutrients in Agriculture*. Soil Sci. Soc. Amer. Inc., Madison, Wis. E.J. Morveltdt, P.M. Giordano and W.L. Lindsay (eds.). 79-144.
- Storey, O.E., E. Steinhoff and E.R. Hoff. 1944. The anode problem in the electrodeposition of manganese dioxide. *Trans. Electrochem. Soc.*, 86, 337-343.
- Stroes, S. 1979. Trace metal interactions with dissolved organics and particulates in natural waters, with emphasis on zinc and copper. *In: Timetrends of water quality of softwater lakes due to long range atmospheric transport*. Prog. Rep. 1979, subm. to Office of Research Subventions, Inland Waters Directorate.
- Stroes, S. and S. Goudev. 1979. Zinc in natural waters. Unpub. Proj. Rep., McMaster Univ., Hamilton, Ont.
- Stroes, S. and K. Strijbis. 1977. Pulspolarografische en voltammetrische analyse van het Cd-EDTA systeem. Verslag doctoral onder Zoek (unpub.), Dept. of Physical and Colloid Chem., Agricultural Univ., Wageningen, The Netherlands.

- Stumm, W. 1977. Chemical interaction in particulate separation. *Environm. Sci. & Technol.*, 11, 1066-1070.
- Stumm, W., C.P. Huang and S.R. Jenkins. 1970. Specific chemical interaction affecting the stability of dispersed systems. *Croat. Chem. Acta*, 42, 223.
- Stumm, W. and J.J. Morgan. 1970. *Aquatic Chemistry*. Wiley Intersci., New York, 1st ed.
- Stumm, W. and R. Giovanelli. 1976. On the nature of particular manganese in simulated lake waters. *Chimia*, 30, 423-425.
- Stumm, W., H. Hohl, and F. Dalong. 1976. Interaction of metal ions with hydrous oxide surfaces. *Croat. Chem. Acta*, 48, 491-504.
- Stumm, W., R. Kummert and L. Sigg. 1980. A ligand exchange model for the adsorption of inorganic and organic ligands at hydrous oxide interfaces. *Croat. Chem. Acta*, 52, 291.
- Subramanian, K.S., C.L. Chakrabarti, J.E. Sûciras and I.S. Maines. 1978. Preservation of some trace metals in samples of natural waters. *Anal. Chem.*, 50, 444-448.
- Sugai, S.F. and M.L. Healy. 1978. Voltammetric studies of the organic association of copper and lead in two Canadian inlets. *Mar. Chem.*, 6, 291-308.
- Swallow, K.C., J.C. Westall, D.M. McKnight, N.M.L. Morel and F.M.M. Morel. 1978. Potentiometric determination of copper complexation by phytoplankton exudates. *Limnol. Oceanogr.*, 23, 538-542.
- Swisher, R.D., T.A. Tauli and E.J. Malec. 1973. Biodegradation of NTA metal complexes in river water. *In: Trace Metals and Metal-Organic Interactions in Natural Waters*, P.C. Singer (ed.), Ann Arbor Sci., 237-263.
- Takamatsu, T. and T. Yoshida. 1978. Determination of stability constants of metal-humic acid complexes by potentiometric titration and ion selective electrodes. *Soil Sci.*, 125, 377-386.

- Tan, K.H., R.A. Leonard, A.R. Bertrand and S.R. Wilkinson. 1971. The metal complexing capacity and the nature of the chelating ligands of water extract of poultry litter. *Soil Sci. Soc. Am. Proc.*, 35, 265-269.
- Tari, I. and T. Hirai. 1982. Effects of electrolytes upon potential-pH relation of electrolytic gamma manganese dioxide. *Electrochim. Acta*, 27, 235-238.
- Taylor, R.M., R.M. McKenzie and K. Norrish. 1964. The mineralogy and chemistry of manganese in some Australian soils. *Austr. J. Soil Res.*, 2, 235-248.
- Thomann, R.V. 1972. *Systems Analysis and Water Quality Management*. Environm. Res. & Appl. Inc., New York.
- Truitt, R.E. and J.H. Weber. 1981a. Determination of complexing capacity of fulvic acid for copper(II) and cadmium(II) by dialysis titration. *Anal. Chem.*, 53, 337-342.
- Truitt, R.E. and J.H. Weber. 1981b. Copper(II)- and cadmium(II)-binding abilities of some New Hampshire fresh waters determined by dialysis titration. *Environm. Sci. & Technol.*, 15, 1204-1208.
- Tschapek, M. and R.M. Torres Sanchez. 1978. The specific surface of Na⁺-humate on the basis of colion exclusion. *Geochim. Cosmochim. Acta*, 42, 1317-1320.
- Turner, S. and P.R. Buseck. 1979. Manganese oxide tunnel-structures and their intergrowths. *Science*, 203, 456-458.
- Turner, S. and P.R. Buseck. 1981. Todorokites: A new family of naturally occurring manganese oxides. *Science*, 212, 1024-1027.
- U.S. Dept. of Interior. 1968. Lake Erie Report. Great Lakes Region, Fed. Water Poll. Control Admin., 105pp.

- Van den Berg, C.M.G. 1975. Application of hydrous manganese IV oxide for the removal of heavy metals from water and waste. Unpub. Research Report.
- Van den Berg, C.M.G. 1979. Complexation of copper in natural waters. PhD. thesis, McMaster Univ., Hamilton, Ont.
- Van den Berg, C.M.G. 1982. Determination of copper complexation with natural organic ligands in seawater by equilibration with MnO_2 . I. Theory; II. Experimental procedures and application to surface seawater. *Marine Chemistry*, 11, 307-322; 323-342.
- Van den Berg, C.M.G. and J.R.Kramer. 1979a. Conditional stability constants for copper ions with ligands in natural waters, *In* Jenne, E.A. (ed.) *Speciation, Sorption, Solubility and Kinetics in Aqueous Systems*, ACS Symp. Series on Chemical Modeling. 115-132.
- Van den Berg, C.M.G. and J.R.Kramer. 1979b. Determination of complexing capacities and conditional stability constants for copper in natural waters, using MnO_2 . *Anal. Chim. Acta*, 106, 113-120.
- Von Glemser, O., G.Gattow and H.Meisler. 1961. Darstellung und Eigenschaften von Braunsteinen. I. (Die δ -Gruppe der Braunsteine). *Z.Anorg.Algem.Chem.*, 309, 1-20.
- Vuceta, J. and J.J.Morgan. 1978. Chemical modeling of trace metals in freshwaters: Role of complexation and adsorption. *Environm.Sci.& Technol.*, 12, 1302-1309.
- Vuceta, J. and J.J.Morgan. 1977. Hydrolysis of Cu(II). *Limnol.Oceanogr.*, 22, 742-746.
- Wadsley, A.D. 1950. A hydrous manganese oxide with exchange properties. *J.Am.Chem.Soc.*, 72, 1781-1784.
- Wallace, Jr.G.T., I.S.Fletcher and R.A.Duce. 1977. Filter washing, a simple means of reducing blank values and variability in trace metal environmental samples. *J.Environmental Health*, A 12, 493-506.

- Wallar, D.D. 1982. The adsorption of aldolase and human serum albumin on δ -manganese dioxide. B.Sc thesis, McMaster Univ., (Dept. of Biochem.), Hamilton, Ont.
- Westall, J.C., J.L. Zachary and F.M.M. Morel. 1976. MINEQL, a computer program for the calculation of chemical equilibrium composition of aqueous systems. Techn. Note #18, M.I.T., 91pp.
- Westall, J.C. and H. Hohl. 1980. A comparison of electrostatic models for the oxide/solution interface. Adv. Coll. Interface Sci., 12, 265-294.
- Willard, H.H., L.L. Merritt, Jr. and J.A. Dean. 1973. Instrumental Methods of Analysis. D. van Nostrand, Toronto.
- Wilson, D.E. 1974. Studies of the metal-ion binding characteristics of soluble, natural organic materials. Ph.D. thesis, Univ. of Alaska, College, Alaska. 70pp.
- Wilson, D.E. and P. Kinney. 1977. Effects of polymeric charge variations on the proton-metal ion equilibria of humic materials. Limnol. Oceanogr., 22, 281-288.
- Woods, D.R. 1976. Introduction to the Behaviour of Surfaces. McMaster Univ. notes, 2nd ed.
- Yates, D.E. and T.W. Healy. 1975. Mechanism of anion adsorption at the ferric and chromic oxide/water interface. J. Coll. Interface Sci., 52, 222-228.
- Yates, D.E., S. Levine and T.W. Healy. 1974. Site-binding model of the electrical double layer at the oxide/water interface. J. Chem. Soc. Faraday Trans. I, 70, 1807-1818.
- Zirino, A. and S. Yamamoto. 1972. A pH-dependent model for the chemical speciation of copper, zinc, cadmium and lead in seawater. Limnol. Oceanogr., 17, 661-671.
- Zunino, H., G. Galindo, P. Peirano and M. Aguilera. 1972a. Use of the resin exchange method for the determination of stability constants of metal-soil organic matter complexes. Soil Sci., 114, 229-233.
- 

- Zunino, H., P. Peirano, M. Aguilera and I. Escobar. 1972b.
Determination of maximum complexing ability of
water-soluble complexants. Soil Sci., 114, 414-416.
- Zunino, H., P. Peirano, M. Aguilera and E. B. Schalscha. 1975.
Measurement of metal-complexing ability of poly-
functional macromolecules: A discussion of the relat-
ionships between the metal-complexing properties of
extracted soil organic matter and soil genesis and
plant nutrition. Soil Sci., 119, 210-216.
- Zunino, H. and J. P. Martin. 1977. Metal-binding organic macro-
molecules in soil: 1. Hypothesis interpreting the
role of soil organic matter in the translocation
of metal ions from rocks to biological systems.
Soil Sci., 123, 65-76.

APPENDIX I

This Appendix contains additional information about experimental methods as well as about apparatus, chemicals and glassware used.

pH meters

- Horizon ecology Co. Model 5998-10
- Cole-Palmer DigipHase

pH electrodes

- Cole-Palmer sealed combination electrode with silver/silver chloride reference
- Sensorex sealed reference combination pH electrode

pH calibrations are done with BDH colourkey standard buffer solutions (pH 4, 7, 10)

Gas-purging

- Prepurified nitrogen (Canadian Liquid Air) is used to remove carbonates from the MnO_2 suspensions prior to the start of adsorption experiments. Traces of CO_2 are removed from the nitrogen by scrubbing the gas with Ascarite, interlayered with a drying agent.

Oxygen is removed from the subsamples prior to DPASV analysis by bubbling prepurified nitrogen through the solutions for about 5 minutes. Traces of CO_2 and O_2 are removed from the N_2 gas by again an Ascarite/drying agent column and 2 oxygen scrubbers in series: grains of a BTS catalyst and a vanadite solution (containing amalgamated zinc)

Magnetic Stirrers

- Corning magnetic stirrer
- Cole-Palmer 4 unit magnetic stirrer ('Magne-4')
- Teflon coated stirring bars

Thermostated waterbath

A large Pyrex dish is used as a waterbath. The temperature is kept constant via a thermostated reservoir with pump (Klinox MX110, Lauda). Water of constant temperature (25°C) is pumped through plastic tubing which is wrapped around the flasks in the Pyrex waterbath.

Filtration

Millipore 0.45 μm filterpaper, presoaked in 10% nitric acid (48 hr.), washed thoroughly with deionized H_2O and dried prior to usage on acid cleaned watchglasses under tissue paper in a 60-80°C oven.

Balances

- Mettler PI200 toploader
- Mettler type H16 capacity 80 gr.

Glassware and sample bottles; cleaning procedures

All glassware used is Pyrex. Cleaning procedures involve rinsing five times with distilled, deionized H_2O , 48 hr. soaking in 10% nitric acid (Laxen and Harrison 1981) and finally 10 times rinsing with distilled, deionized water. Cleaned glassware is dried upside down on tissuepaper in a 80-100°C oven. Subsamples are stored in Nalgene plastic bottles (30 mL) which receive the same treatment as glassware.

Pipettes and micropipets

Glasspipets are soaked in 10% nitric acid for 48 hours and rinsed copiously with deionized H₂O. Prior to use, glass pipets are rinsed 3x with the solution to be pipetted. Eppendorff micropipets (10-50-100, 200 and 500 μ L) are used for stepwise metal additions. Micropipet tips are rinsed with the solution to be pipetted prior to use.

Liquid Scintillation Counting

Bechman LS-230 (or 233) Liquid Scintillation System with 3 channels (^3H , ^{14}C , ^{14}C , ^3H). Amersham ACS Aqueous Counting Scintillant and Fisherbrand Scintillation vials are used for the liquid scintillation counting analyses.

Copper Measurements

Three techniques for Cu-measurements are used:

-A Princeton Applied Research Polarograph Model 74A is used in the Differential Pulse Anodic Stripping Voltammetry (DPASV) mode, with plating potential - 200 mV, plating time 2.5 minutes plus 0.5 minutes rest, scanning rates 5mV/sec and pulses with 0.5 sec. intervals. Initially it was found that the Hanging Mercury Drop (HMD) somehow possessed a memory which could not be erased even through extrusion and discarding of three Hg drops between analyses. An "empty scanning" procedure is therefore applied, which, implies that after each Cu-analysis, the HMD is kept at +100 mV for a few minutes, before the potential is removed. This procedure has improved the reproducibility of Cu analysis to within 1%, and has eliminated the positive memory effect of the HMD.

DPASV is used to measure Cu concentrations in the filtered, acidified subsamples, either at 25°C (waterthermostated cell) or at room temperature. Calibration of the polarograph is done via at least two standard additions of stocksolution Cu^{2+} to one or two of a set of subsamples, yielding one adsorption isotherm.

The reference Calomel electrode is connected with the solution to be analyzed, via a saltbridge containing 0.1 M KNO_3 , which is renewed for each set of measurements.

-Flame Atomic Absorption Spectrometry (Jarrell-Ash, Fisher Scientific).

Flame Atomic Absorption Spectrometry is used to measure Cu adsorbed on MnO_2 and retained by 0.45 μ filters, for mass-balance purposes. Filterpapers are reduced in oxalic acid to dissolve MnO_2 and free Cu. Standards are made up in exactly the same medium to avoid matrix effects from the oxalic acid.

-Copper Ion Sensing Electrodes (Model IS-146, International Crystal Field Laboratories) are used in a few instances to measure free Cu^{2+} concentrations directly and to compare them with REDEQL2 calculated concentrations. This could only be done at the relatively low pH of 6, due to the low levels of free Cu^{2+} at higher pH-values.

Chemicals

All chemicals used are Analar Grade (or better).

-Organic free H_2O

Distilled water, free of organics, is prepared for each adsorption

experiment and for stock suspensions. Distilled, deionized water is distilled in presence of 10 mL of an alkaline permanganate (0.1 M) solution in a glass distiller with a long column filled with small glass rings.

-Cu²⁺ stock solution

Stock solutions of 10^{-2} M Cu²⁺ are made up by dissolving pure Cu-turnings in small amounts of Aristar HNO₃, and diluting to the required volume with organic free H₂O.

-KNO₃ stock solution

A purified stock solution of 2M KNO₃ is made up with organic free H₂O and electrolytically purified over a mercury pool. KNO₃ is used as background electrolyte and in diluted form for the saltbridge in DPASV measurements.

-KCl saturated solution

A saturated KCl solution is made up with organic free H₂O and electrolytically purified over a mercury pool. KCl is used in the Calomel electrode and (in diluted form) in the saltbridge in DPASV measurements on occasions.

-Organic solutions

Organic stock solution (ACS Grade aminoacids, NTA) are made up in several concentrations, depending on the experimental requirements. The stock solutions are frequently renewed as a precaution, although bacterial growth was never observed in these solutions.

Acids and bases for pH corrections

Dilute and very dilute acid and base solutions are prepared from Aristar KNO_3 and Reagent Grade KOH for manual pH corrections, during adsorption experiments. Aristar KNO_3 is used for acidification of the subsamples. Oxalic acid is prepared in various concentrations (e.g. 0.25 - 0.5 M) for dissolution of MnO_2 on filterpapers.

 ^{14}C -labelled organics

^{14}C -labelled organics (aminoacids) are obtained from Amersham Inc. in low activities ($10 \mu \text{Ci/mL}$). ^{14}C -labelled NTA is obtained from the Canada Centre for Inland Waters, Burlington, Ontario (courtesy Dr. Y.K. Chau).

APPENDIX -II

Equilibrium acidity - and stability - constants for Cu and Glycine

(from Sillen and Martell 1964).

$$\frac{(\text{Cu-L}^+)}{(\text{Cu}^{2+})(\text{L}^-)} = 10^{8.61} \quad (\text{REDEQL2 uses } 10^{8.41} \text{ at } 25^\circ\text{C and } I = 0.01)$$

$$\frac{(\text{CuL}_2)}{(\text{Cu-L}^+)(\text{L}^-)} = 10^{7.10} \quad " \quad " \quad 10^{7.01} \quad " \quad " \quad " \quad "$$

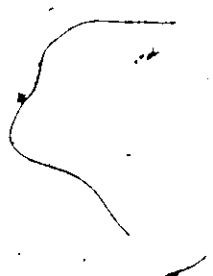
$$\frac{(\text{H}_2\text{L}^+)}{(\text{HL})(\text{H}^+)} = 10^{2.30} \quad " \quad " \quad 10^{2.32} \quad " \quad " \quad " \quad "$$

$$\frac{(\text{HL})}{(\text{H}^+)(\text{L}^-)} = 10^{9.70} \quad " \quad " \quad 10^{9.63} \quad " \quad " \quad " \quad "$$

$$\frac{(\text{CuOH}^+)}{(\text{Cu}^{2+})(\text{OH}^-)} = 10^{6.0}$$

$$\frac{(\text{Cu}(\text{OH})_2)}{(\text{Cu}^{2+})(\text{OH}^-)^2} = 10^{14.03}$$

APPENDIX III



Model 1 III made 050379

run 130979

pH 6.0

glycine --

linear regression

$\Gamma_{max} = 0.249$

$\log B = 6.06$

non-linear regression

Model 1 Single Langmuir Model

TSS = 0.1910890 E-01

RSS = 0.3998699 E-02

$\Gamma_{max} = 0.2334$

$B = 0.2512$

$\log B \pm 1\sigma = 6.40 \pm 0.15$

corr. $\Gamma_{max} - B = -0.5618$

8 d.o.f.

Model 2 Double Langmuir Model

TSS = 0.1910890 E-01

RSS = 0.1065669 E-02

$\Gamma_{m1} = 0.1262$

$\Gamma_{m2} = 0.1453$

$1/B_1 = 0.4199$

$1/B_2 = 0.4871$

corr. $\Gamma_{m1} - \Gamma_{m2} = -0.8491$

corr. $\Gamma_{m1} - B_1 = 0.9330$

corr. $\Gamma_{m1} - B_2 = 0.9051$

corr. $\Gamma_{m2} - B_1 = -0.8348$

corr. $\Gamma_{m2} - B_2 = -0.5604$

corr. $B_1 - B_2 = 0.8002$

6 d.o.f.

experimental adsorption data

observations 10

pcu²⁺ Γ_{ads}

6.67366 0.111

5.96059 0.151

5.48386 0.180

5.22265 0.195

5.04508 0.212

5.02027 0.246

4.82719 0.231

4.77490 0.236

4.73722 0.253

4.61961 0.236

Model 3 Implicit Langmuir Model

TSS = 0.3293699

RSS = 0.5242644 E-01

$\Gamma_{max} = 0.2425$

$x = -4.782$

$n = 1.852$

corr. $\Gamma_{max} - x = -0.6816$

corr. $\Gamma_{max} - n = 0.6236$

corr. $x - n = -0.9933$

92 d.o.f.

Model 1 III made 050379

run 130979

pH 6.5

glycine --

linear regression

$\Gamma_{max} = 0.284$

$\log B = 6.50$

non-linear regression

Model 1 Single Langmuir Model

TSS = 0.5232899 E-02

RSS = 0.1244255 E-02

$\Gamma_{max} = 0.2737$

$B = 0.3201$

$\log B \pm 1\sigma = 6.50 \pm 0.11$

corr. $\Gamma_{max} - B = -0.8516$

7 d.o.f.

Model 2 Double Langmuir Model

TSS = 0.5232899 E-02

RSS = 0.1244256 E-02

$\Gamma_{m1} = 0.1403$

$\Gamma_{m2} = 0.1334$

$1/B_1 = 0.3123$

$1/B_2 = 0.3122$

corr. $\Gamma_{m1} - \Gamma_{m2} = -1.0000$

corr. $\Gamma_{m1} - B_1 = -0.1552$

corr. $\Gamma_{m1} - B_2 = +0.1552$

corr. $\Gamma_{m2} - B_1 = +0.1552$

corr. $\Gamma_{m2} - B_2 = -0.1552$

corr. $B_1 - B_2 = -1.0000$

7 d.o.f.

experimental adsorption data

observations 9

pcu²⁺ Γ_{ads}

6.01682 0.193

5.91906 0.203

5.88498 0.228

5.81320 0.234

5.72554 0.240

5.74028 0.253

5.61400 0.253

5.45047 0.258

5.38036 0.270

Model 3 Implicit Langmuir Model

see run 130979

MnO₂ III made 050379

run 170979
pH 7.0
glycine 50µM

linear regression

$\Gamma_{max} = 0.241$
 $\log B = 8.13$

non-linear regression

Model 1 Single Langmuir Model

TSS = 0.3853450 E-01
RSS = 0.2325477 E-02

$\Gamma_{max} = 0.2281 \pm 0.2450$
 $B = 9.2939 E+09 \ 0.4265 E+09$

$\log B \pm 1\sigma = 8.45 \pm 0.11$
corr. $\Gamma_{max} - B = -0.4929$

7 d.o.f.

Model 2 Double Langmuir Model

TSS = 0.3853450 E-01
RSS = 0.5753601 E-01

$\Gamma_{m1} = 0.1698 \ 0.2193$
 $\Gamma_{m2} = 0.1169 \ 0.1836$

$1/B_1 = 0.1602 E-08 \ 0.2928 E-08$
 $1/B_2 = 0.1636 E-06 \ 0.5332 E-06$

corr. $\Gamma_{m1} - \Gamma_{m2} = 0.0764$
corr. $\Gamma_{m1} - B_1 = 0.8860$

corr. $\Gamma_{m1} - B_2 = 0.8374$
corr. $\Gamma_{m2} - B_1 = -0.0055$

corr. $\Gamma_{m2} - B_2 = 0.5876$
corr. $B_1 - B_2 = 0.6927$

5 d.o.f.

experimental adsorption data

observations 9
pCu²⁺ Γ_{ads}

pCu ²⁺	Γ_{ads}
9.33208	0.0454
8.56981	0.0954
8.21635	0.1505
7.45887	0.1818
7.10159	0.1963
6.90937	0.2187
6.76895	0.2277
6.66870	0.2444
6.42750	0.2450

MnO₂ III made 050379

run 240979
pH 7.0
glycine 50µM

linear regression

$\Gamma_{max} = 0.256$
 $\log B = 7.80$

non-linear regression

Model 1 Single Langmuir Model

TSS = 0.2708875 E-02
RSS = 0.1182595 E-03

$\Gamma_{max} = 0.2512 \pm 0.2598$
 $B = 0.7268 E+08 \ 0.6925 E+08$

$\log B \pm 1\sigma = 7.86 \pm 0.05$
corr. $\Gamma_{max} - B = -0.9013$

6 d.o.f.

Model 2 Double Langmuir Model

TSS = 0.2708875 E-02
RSS = 0.4296025 E-03

$\Gamma_{m1} = 0.1636 \ 0.4988$
 $\Gamma_{m2} = 0.1177 \ 0.3649$

$1/B_1 = 0.1847 E-08 \ 0.3572 E-07$
 $1/B_2 = 0.1047 E-06 \ 0.6766 E-06$

corr. $\Gamma_{m1} - \Gamma_{m2} = -0.9803$
corr. $\Gamma_{m1} - B_1 = 0.9957$

corr. $\Gamma_{m1} - B_2 = 0.9894$
corr. $\Gamma_{m2} - B_1 = -0.9965$

corr. $\Gamma_{m2} - B_2 = -0.9601$
corr. $B_1 - B_2 = 0.9731$

4 d.o.f.

experimental adsorption data

observations 8
pCu²⁺ Γ_{ads}

pCu ²⁺	Γ_{ads}
7.44806	0.184
7.37202	0.193
7.25019	0.200
7.11323	0.205
7.05468	0.217
6.92167	0.223
6.82094	0.233
6.67502	0.240

Model 3 Implicit Langmuir Model

see run 130979

MnO₂ III made 050379

run 170979

pH 7.5

glycine 50 µM

linear regression

$\Gamma_{max} = 0.261$

$\log B = 9.20$

non-linear regression

Model 1 Single Langmuir Model

TSS = 0.4824922 E-01

RSS = 0.8545564 E-02

$\Gamma_{max} = 0.2349 \pm 0.2630$

$B = 0.3651 E+10 \pm 0.4262 E+10$

$\log B \pm 1\sigma = 9.56 \pm 0.04$

corr. $\Gamma_{max} - B = -0.1515$

7 d.o.f.

Model 2 Double Langmuir Model

TSS = 0.4824923 E-01

RSS = 0.3416710 E-02

$\Gamma_{m1} = 0.08681 \pm 0.1937$

$\Gamma_{m2} = 0.1777 \pm 0.2724$

$1/B_1 = 0.1829 E-10 \pm 0.9053 E-10$

$1/B_2 = 0.1878 E-08 \pm 0.5900 E-08$

corr. $\Gamma_{m1} - \Gamma_{m2} = -0.8469$

corr. $\Gamma_{m1} - B_1 = 0.9112$

corr. $\Gamma_{m1} - B_2 = 0.8127$

corr. $\Gamma_{m2} - B_1 = -0.8195$

corr. $\Gamma_{m2} - B_2 = -0.4435$

corr. $B_1 - B_2 = 0.6590$

5 d.o.f.

Experimental adsorption data

observations 9

pCu²⁺ Γ_{ads}

9.80521 0.0450

10.33606 0.0708

9.97551 0.0983

9.58419 0.1289

8.95628 0.1613

8.44430 0.1935

8.05324 0.2250

7.87203 0.2431

7.63601 0.2603

MnO₂ III made 050379

run 081079

pH 7.5

glycine 50 µM

linear regression

$\Gamma_{max} = 0.284$

$\log B = 8.90$

non-linear regression

Model 1 Single Langmuir Model

TSS = 0.1138176 E-01

RSS = 0.2179924 E-02

$\Gamma_{max} = 0.2660 \pm 0.2864$

$B = 0.7443 E+09 \pm 0.1074 E+10$

$\log B \pm 1\sigma = 8.87 \pm 0.10$

corr. $\Gamma_{max} - B = -0.7921$

6 d.o.f.

Model 2 Double Langmuir Model

RSS = no convergence after

$\Gamma_{m1} = 50$ iterations; output

$\Gamma_{m2} =$ file exceeded.

$1/B_1 =$

$1/B_2 =$

corr. $\Gamma_{m1} - \Gamma_{m2} =$

corr. $\Gamma_{m1} - B_1 =$

corr. $\Gamma_{m1} - B_2 =$

corr. $\Gamma_{m2} - B_1 =$

corr. $\Gamma_{m2} - B_2 =$

corr. $B_1 - B_2 =$

d.o.f.

Experimental adsorption data

observations 10

pCu²⁺ Γ_{ads}

8.69897 0.1736

8.57187 0.1833

8.42251 0.1928

8.28067 0.2026

8.05306 0.2072

7.92154 0.2184

7.84710 0.2346

7.82160 0.2584

7.63601 0.2718

7.47743 0.2681

Model 3 Implicit Langmuir Model

sec run 130979

MnO₂ III made 050379

run 240979

pH 7.5

glycine 50 µM

linear regression

$\Gamma_{max} = 0.284$

$\log B = 8.67$

non-linear regression

Model 1 Single Langmuir Model

TSS = 0.1407289 E-01

RSS = 0.8949246 E-02

$\Gamma_{max} = 0.2492 \pm 0.2744$

$B = 0.6690 E+10 \pm 0.7405 E+10$

$\log B \pm 1\sigma = 9.83 \pm 0.02$

corr. $\Gamma_{max} - B = -0.0404$

7 d.o.f.

Model 2 Double Langmuir Model

TSS = 0.1407289 E-01

RSS = 0.6938512 E-03

$\Gamma_{m1} = 0.1774 \pm 0.2097$

$\Gamma_{m2} = 0.2109 \pm 0.094$

$1/B_1 = 0.1996 E-21 \pm 0.8599 E-10$

$1/B_2 = 0.2436 E-07 \pm 0.6112 E-07$

corr. $\Gamma_{m1} - \Gamma_{m2} = 0.5294$

corr. $\Gamma_{m1} - B_1 = 0.7872$

corr. $\Gamma_{m1} - B_2 = 0.8323$

corr. $\Gamma_{m2} - B_1 = 0.3994$

corr. $\Gamma_{m2} - B_2 = 0.8969$

corr. $B_1 - B_2 = 0.6425$

5 d.o.f.

experimental adsorption data

observations 9

pcu²⁺

Γ_{ads}

9.55284 0.181

8.67778 0.186

8.41229 0.209

8.16877 0.216

8.07676 0.231

7.95782 0.246

7.74400 0.256

7.73072 0.289

7.43180 0.300

MnO₂ III made 050379

run 111079

pH 7.8

glycine 50 µM

linear regression

$\Gamma_{max} = 0.219$

$\log B = 10.12$

non-linear regression

Model 1 Single Langmuir Model

TSS = 0.1775822 E-01

RSS = 0.4407577 E-02

$\Gamma_{max} = 0.2016 \pm 0.1828$

$B = 0.2057 E+11 \pm 0.2104 E+11$

$\log B \pm 1\sigma = 10.31 \pm 0.005$

corr. $\Gamma_{max} - B = -0.0354$

8 d.o.f.

Model 2 Double Langmuir Model

TSS = no convergence after

RSS = 50 iterations, output

$\Gamma_{m1} =$ file exceeded.

$\Gamma_{m2} =$

$1/B_1 =$

$1/B_2 =$

corr. $\Gamma_{m1} - \Gamma_{m2} =$

corr. $\Gamma_{m1} - B_1 =$

corr. $\Gamma_{m1} - B_2 =$

corr. $\Gamma_{m2} - B_1 =$

corr. $\Gamma_{m2} - B_2 =$

corr. $B_1 - B_2 =$

d.o.f.

experimental adsorption data

observations 10

pcu²⁺

Γ_{ads}

9.99140 0.0896

10.54516 0.103

10.34486 0.116

10.08302 0.131

9.79022 0.147

9.47405 0.163

9.16165 0.181

9.00139 0.190

9.06596 0.208

8.74654 0.217

Model 3 Implicit Langmuir Model

see run 130979

NO₂ III made 050379

run 270979

pH 8.0

glycine 50 µM

linear regression

$\Gamma_{max} = 0.226$
 $\log B = 10.37$

non-linear regression

Model 1 Single Langmuir Model

TSS = 0.1904403 E-01
RSS = 0.8870613 E-03
 $\Gamma_{max} = 0.2106$ 0.2192
B = 0.3647 E+11 0.3668 E+11
0.3626 E+11

$\log B \pm 1\sigma = 10.56 \pm 0.001$
corr. $\Gamma_{max} - B = -0.0216$

8 d.o.f.

Model 2 Double Langmuir Model

TSS = 0.190440 E-01
RSS = 0.2904591 E-04
 $\Gamma_{m1} = 0.1683$ 0.1806
0.1560
 $\Gamma_{m2} = 0.1607$ 0.2834
0.03809
 $1/B_1 = 0.1562$ E-10 0.1852 E-10
0.1272 E-10
 $1/B_2 = 0.1756$ E-08 0.4212 E-08
-0.7001 E-09

corr. $\Gamma_{m1} - \Gamma_{m2} = 0.7766$
corr. $\Gamma_{m1} - B_1 = 0.2459$
corr. $\Gamma_{m1} - B_2 = 0.8738$
corr. $\Gamma_{m2} - B_1 = 0.8620$
corr. $\Gamma_{m2} - B_2 = 0.9831$
corr. $B_1 - B_2 = 0.7668$

6 d.o.f.

experimental adsorption data

observations 10

pCu ²⁺	Γ_{ads}
10.75172	0.0905
10.64125	0.103
10.48031	0.116
10.32905	0.132
10.07569	0.148
9.81969	0.166
9.47396	0.184
9.38793	0.196
9.17809	0.207
9.00464	0.224

Model 3 Implicit Langmuir Model

see run 130979

NO₂ III made 050379

run 270979

pH 8.5

glycine 50 µM

linear regression

$\Gamma_{max} = 0.226$
 $\log B = 11.02$

non-linear regression

Model 1 Single Langmuir Model

TSS = no convergence after
RSS = 50 iterations; output
 $\Gamma_{max} =$ file exceeded.
B =

$\log B \pm 1\sigma =$
corr. $\Gamma_{max} - B =$

d.o.f.

Model 2 Double Langmuir Model

TSS = no convergence after
RSS = 50 iterations; output
 $\Gamma_{m1} =$ file exceeded.
 $\Gamma_{m2} =$
 $1/B_1 =$
 $1/B_2 =$

corr. $\Gamma_{m1} - \Gamma_{m2} =$
corr. $\Gamma_{m1} - B_1 =$
corr. $\Gamma_{m1} - B_2 =$
corr. $\Gamma_{m2} - B_1 =$
corr. $\Gamma_{m2} - B_2 =$
corr. $B_1 - B_2 =$

d.o.f.

experimental adsorption data

observations 10

pCu ²⁺	Γ_{ads}
11.46218	0.056
11.42251	0.068
11.26043	0.0818
11.14935	0.0967
11.06803	0.1125
10.88406	0.1319
10.65679	0.1523
10.59414	0.1651
10.39233	0.1784
10.21746	0.1977

Model 3 Implicit Langmuir Model

see run 130979

EXPNO2 III made 050379

run 160381 (new data)

pH 6.5

glycine 50 µM

linear regression

$\Gamma_{max} = 0.239$
 $\log B = 7.87$

non-linear regression

Model 1 Single Langmuir Model

TSS = 0.5117174 E-01
RSS = 0.2494626 E-02
 $\Gamma_{max} = 0.2136$ 0.1919
 $B = 0.2719$ E+09 0.3685 E+09
 $\log B \pm 1\sigma = 8.43 \pm 0.14$
corr. $\Gamma_{max} - B = -0.4161$

7 d.o.f.

Model 2 Double Langmuir Model

TSS = 0.5117174 E-01
RSS = 0.3521941 E-03
 $\Gamma_{m1} = 0.1610$ 0.2078
 $\Gamma_{m2} = 0.1836$ -0.1323
 $1/B_1 = 0.2199$ E-06 0.3479 E-06
 $1/B_2 = 0.8147$ E-06 0.3908 E-05

corr. $\Gamma_{m1} - \Gamma_{m2} = 0.8014$
corr. $\Gamma_{m1} - B_1 = 0.9324$
corr. $\Gamma_{m1} - B_2 = 0.9018$
corr. $\Gamma_{m2} - B_1 = 0.7336$
corr. $\Gamma_{m2} - B_2 = 0.3784$
corr. $B_1 - B_2 = 0.8301$

5 d.o.f.

Experimental adsorption data

observations 9

PCu²⁺

Γ_{ads}

9.17298 0.02510
8.99576 0.05311
8.89483 0.06866
8.52847 0.08572
8.46542 0.10500
6.96495 0.17820
6.72520 0.19335
5.36027 0.22591
6.18535 0.24125

Model 3 Implicit Langmuir Model

TSS = 0.1382992
RSS = 0.3700523 E-01
 $\Gamma_{max} = 0.2271$ 0.2322
 $B = -3.963$ -1.305
 $n = 1.754$ 2.066
corr. $\Gamma_{max} - x = -0.6889$
corr. $\Gamma_{max} - n = 0.5963$
corr. $x - n = -0.9876$

22 d.o.f.

EXPNO2 III made 050379

run 160381 (new data)

pH 7.5

glycine 50 µM

linear regression

$\Gamma_{max} = 0.238$
 $\log B = 9.60$

non-linear regression

Model 1 Single Langmuir Model

TSS = 0.4875052 E-01
RSS = 0.2207999 E-02
 $\Gamma_{max} = 0.2132$ 0.2331
 $B = 0.7727$ E+10 0.8111 E+10
 $\log B \pm 1\sigma = 9.60 \pm 0.01$
corr. $\Gamma_{max} - B = -0.0494$

6 d.o.f.

Model 2 Double Langmuir Model

TSS = 0.4875052 E-01
RSS = 0.1721413 E-03
 $\Gamma_{m1} = 0.1554$ 0.1950
 $\Gamma_{m2} = 0.1302$ 0.2077
 $1/B_1 = 0.6924$ E-10 0.9925 E-10
 $1/B_2 = 0.5962$ E-08 -0.5140 E-08

corr. $\Gamma_{m1} - \Gamma_{m2} = 0.0318$
corr. $\Gamma_{m1} - B_1 = 0.8607$
corr. $\Gamma_{m1} - B_2 = 0.9076$
corr. $\Gamma_{m2} - B_1 = 0.5805$
corr. $\Gamma_{m2} - B_2 = 0.8865$
corr. $B_1 - B_2 = 0.3374$

5 d.o.f.

Experimental adsorption data

observations 8

PCu²⁺

Γ_{ads}

10.68981 0.02571
10.65879 0.04054
10.49673 0.05700
10.19239 0.07529
9.12084 0.1557
8.82917 0.1767
8.24002 0.2170
7.99581 0.2373

Model 3 Implicit Langmuir Model

see run 160381

Run 2 III made 050379

run 160381 (new data)

pH 8.5

glycine 50 µM

linear regression

$\Gamma_{max} = 0.209$

$\log B = 11.42$

non-linear regression

Model 1 Single Langmuir Model

TSS = no convergence after

RSS = 50 iterations.

$\Gamma_{max} =$

$B =$

$\log B \pm 1\sigma =$

corr. $\Gamma_{max} - B =$

d.o.f.

Model 2 Double Langmuir Model

TSS =

RSS = no convergence after

$\Gamma_{m1} =$ 50 iterations; output

$\Gamma_{m2} =$ file exceeded.

$1/B_1 =$

$1/B_2 =$

corr. $\Gamma_{m1} - \Gamma_{m2} =$

corr. $\Gamma_{m1} - B_1 =$

corr. $\Gamma_{m1} - B_2 =$

corr. $\Gamma_{m2} - B_1 =$

corr. $\Gamma_{m2} - B_2 =$

corr. $B_1 - B_2 =$

d.o.f.

experimental adsorption data

observations 9

pCu²⁺ Γ_{ads}

12.28696 0.02474

12.21189 0.03824

12.14981 0.05302

12.01457 0.06942

11.71181 0.08764

10.82994 0.14556

10.56910 0.16532

10.25866 0.18694

10.01135 0.20670

Model 3 Implicit Langmuir Model

see run 160381

Run 2 VIB. made 220180

run 210380

pH 6.0

glycine --

linear regression

$\Gamma_{max} = 0.255$

$\log B = 6.02$

non-linear regression

Model 1 Single Langmuir Model

TSS = 0.1404222 E-01

RSS = 0.2900273 E-02

$\Gamma_{max} = 0.2411$ 0.2596

$B = 0.2100$ E+07 0.7160 E+06

$\log B \pm 1\sigma = 6.32 \pm 0.14$

corr. $\Gamma_{max} - B = -0.5785$

d.o.f.

Model 2 Double Langmuir Model

TSS = 0.1404222 E-01

RSS = 0.9381167 E-03

$\Gamma_{m1} = 0.1463$ 0.2749

$\Gamma_{m2} = 0.1273$ 0.2232

$1/B_1 = 0.7111$ E-07 0.4452 E-06

$1/B_2 = 0.7248$ E-05 0.2688 E-04

corr. $\Gamma_{m1} - \Gamma_{m2} = 0.7955$

corr. $\Gamma_{m1} - B_1 = 0.9552$

corr. $\Gamma_{m1} - B_2 = 0.9309$

corr. $\Gamma_{m2} - B_1 = -0.8124$

corr. $\Gamma_{m2} - B_2 = -0.5360$

corr. $B_1 - B_2 = 0.9500$

d.o.f.

experimental adsorption data

observations 9

pCu²⁺ Γ_{ads}

6.38300 0.132

5.71399 0.172

5.31358 0.199

5.09253 0.211

4.91027 0.219

4.85310 0.246

4.68725 0.256

4.75671 0.259

4.58843 0.236

Model 3 Implicit Langmuir Model

TSS = 0.2522523 E+00

RSS = 0.86884262 E-01

$\Gamma_{max} = 0.2543$ 0.2657

$B = -4.828$ -5.673

$n = 1.874$ 2.001

corr. $\Gamma_{max} - x = -0.5600$

corr. $\Gamma_{max} - n = 0.4565$

corr. $x - n = -0.9847$

94 d.o.f.

Mo. Vib made 220180

run 210380
 pH 6.0
 glycine 50 pH

linear regression

$\Gamma_{max} = 0.210$
 $\log B = 7.09$

non-linear regression

Model 1. Single Langmuir Model

TSS = 0.3937875 E-02
 RSS = 0.1642187 E-02

$\Gamma_{max} = 0.2185$ 0.2376
 0.1995

$B = 0.4455$ E+07 0.8369 E+07
 0.5410 E+06

$\log B \pm 1\sigma = 6.95 \pm 0.19$
 corr. $\Gamma_{max} - B = -0.7417$

5 d.o.f.

Model 2 Double Langmuir Model

TSS =
 RSS = no convergence after
 $\Gamma_{m1} =$ 50 iterations; output
 $\Gamma_{m2} =$ file exceeded.

$1/B_1 =$
 $1/B_2 =$

corr. $\Gamma_{m1} - \Gamma_{m2} =$
 corr. $\Gamma_{m1} - B_1 =$
 corr. $\Gamma_{m1} - B_2 =$
 corr. $\Gamma_{m2} - B_1 =$
 corr. $\Gamma_{m2} - B_2 =$
 corr. $B_1 - B_2 =$

d.o.f.

experimental adsorption data

observations 8

PCu ²⁺	Γ_{ads}
6.23247	0.163
5.82218	0.180
5.62838	0.195
5.44358	0.202
5.31453	0.200
5.27860	0.242
5.16172	0.219
5.04547	0.196

Mo. Vib made 220180

run 210580
 pH 6.0
 glycine

linear regression

$\Gamma_{max} = 0.293$
 $\log B = 6.20$

non-linear regression

Model 1. Single Langmuir Model

TSS = 0.2454622 E-01
 RSS = 0.1711398 E-02

$\Gamma_{max} = 0.2842$ 0.2992
 0.2692

$B = 0.2278$ E+07 0.3133 E+07
 0.4403 E+07

$\log B \pm 1\sigma = 6.36 \pm 0.06$
 corr. $\Gamma_{max} - B = -0.6042$

7 d.o.f.

Model 2 Double Langmuir Model

TSS = 0.2454622 E-01
 RSS = 0.5695154 E-03
 $\Gamma_{m1} = 0.1523$ 0.3319
 $\Gamma_{m2} = 0.1535$ 0.3327
 $1/B_1 = 0.9131$ E-07 0.4172 E-06
 $1/B_2 = 0.2485$ E-05 0.2345 E-06
 0.7795 E-05

corr. $\Gamma_{m1} - \Gamma_{m2} = -0.0002$
 corr. $\Gamma_{m1} - B_1 = 0.9715$
 corr. $\Gamma_{m1} - B_2 = 0.9515$
 corr. $\Gamma_{m2} - B_1 = -0.9755$
 corr. $\Gamma_{m2} - B_2 = -0.9046$
 corr. $B_1 - B_2 = 0.8830$

5 d.o.f.

experimental adsorption data

observations 9

PCu ²⁺	Γ_{ads}
6.55129	0.170
6.05306	0.181
5.58054	0.222
5.28575	0.242
5.15002	0.279
4.99055	0.283
4.82623	0.273
4.78537	0.286
4.71128	0.286

Model 3 Implicit Langmuir Model

see run 210380

experimental adsorption data

observations 9

PCu ²⁺	Γ_{ads}
7.15627	0.130
6.31114	0.164
5.89041	0.180
5.67026	0.198
5.48628	0.208
5.37941	0.216
5.23502	0.209
5.18021	0.216
5.23756	0.288

MMO₂ VIB made 220180

run 290580

pH 6.0

glycine 50 μ M

linear regression

$\Gamma_{max} = 0.218$

$\log B = 6.93$

non-linear regression

Model 1 Single Langmuir Model

TSS = 0.1477200 E-01

RSS = 0.7054348 E-02

$\Gamma_{max} = 0.2193 \pm 0.2450$

$B = 0.1553 E+08 - 0.2865 E+07$

$\log B \pm 1\sigma = 7.19 \pm 0.26$

corr. $\Gamma_{max} - B = -0.4601$

7 d.o.f.

Model 2 Double Langmuir Model

TSS =

RSS := no convergence after

$\Gamma_{m1} = 50$ iterations: output

$\Gamma_{m2} =$ file exceeded.

$1/B_1 =$

$1/B_2 =$

corr. $\Gamma_{m1} - \Gamma_{m2} =$

corr. $\Gamma_{m1} - B_1 =$

corr. $\Gamma_{m1} - B_2 =$

corr. $\Gamma_{m2} - B_1 =$

corr. $\Gamma_{m2} - B_2 =$

corr. $B_1 - B_2 =$

d.o.f.

experimental adsorption data

observations 9

PCu ²⁺	Γ_{ads}
6.99140	0.128
6.35067	0.167
5.92154	0.191
5.69379	0.203
5.52695	0.220
5.40705	0.226
5.31114	0.240
5.25367	0.245
5.20964	0.263

MMO₂ VIB made 220180

run 290580 A

pH 6.0

glycine 50 μ M

linear regression

$\Gamma_{max} = 0.263$

$\log B = 6.41$

non-linear regression

Model 1 Single Langmuir Model

TSS = 0.1426756 E-01

RSS = 0.3019361 E-02

$\Gamma_{max} = 0.2304 \pm 0.2552$

$B = 0.8051 E+07 - 0.1345 E+08$

$\log B \pm 1\sigma = 6.91 \pm 0.15$

corr. $\Gamma_{max} - B = -0.5766$

7 d.o.f.

Model 2 Double Langmuir Model

TSS =

RSS = no convergence after

$\Gamma_{m1} = 50$ iterations: output

$\Gamma_{m2} =$ file exceeded.

$1/B_1 =$

$1/B_2 =$

corr. $\Gamma_{m1} - \Gamma_{m2} =$

corr. $\Gamma_{m1} - B_1 =$

corr. $\Gamma_{m1} - B_2 =$

corr. $\Gamma_{m2} - B_1 =$

corr. $\Gamma_{m2} - B_2 =$

corr. $B_1 - B_2 =$

d.o.f.

Model 3 Implicit Langmuir Model

see run 210380

Model 3 Implicit Langmuir Model

see run 210380

MnO₂ VIB / made 220180
 run 150580
 pH 6.0
 glycine --
 linear regression
 $\Gamma_{\max} = 0.262$
 $\log B = 5.80$
 non-linear regression

Model 1 Single Langmuir Model
 TSS = 0.1364422 E-01
 RSS = 0.1938569 E-02
 $\Gamma_{\max} = 0.2418 \pm 0.2588$
 $B = 0.1357 E+07 \pm 0.6422 E+06$
 $\log B \pm 1\sigma = 6.13 \pm 0.11$
 corr. $\Gamma_{\max} - B = -0.6578$
 7 d.o.f.

Model 2 Double Langmuir Model
 TSS = no convergence after
 RSS = 50 iterations; output
 $\Gamma_{m1} =$
 $\Gamma_{m2} =$ file exceeded.
 $1/B_1 =$
 $1/B_2 =$
 $\text{corr. } \Gamma_{m1} - \Gamma_{m2} =$
 $\text{corr. } \Gamma_{m1} - B_1 =$
 $\text{corr. } \Gamma_{m1} - B_2 =$
 $\text{corr. } \Gamma_{m2} - B_1 =$
 $\text{corr. } \Gamma_{m2} - B_2 =$
 $\text{corr. } B_1 - B_2 =$
 d.o.f.

experimental adsorption data
 observations 9
 pCu²⁺ Γ_{ads}
 6.20831 0.128
 5.67081 0.168
 5.32203 0.198
 5.05022 0.197
 4.93360 0.233
 4.83660 0.231
 4.73302 0.236
 4.69463 0.248
 4.63506 0.256

Model 3 Implicit Langmuir Model
 see run 210380

MnO₂ VIB / made 220180
 run 150580
 pH 6.0, 40 μM Cu total
 glycine titration with glycine
 linear regression
 $\Gamma_{\max} = 0.280$
 $\log B = 5.99$
 non-linear regression

Model 1 Single Langmuir Model
 TSS = 0.7478000 E-02
 RSS = 0.5541747 E-03
 $\Gamma_{\max} = 0.2817 \pm 0.2958$
 $B = 0.3400 E+06 \pm 0.1195 E+07$
 $\log B \pm 1\sigma = 5.97 \pm 0.06$
 corr. $\Gamma_{\max} - B = 0.9588$
 7 d.o.f.

Model 2 Double Langmuir Model
 TSS = 0.7478000 E-02
 RSS = 0.5541747 E-03
 $\Gamma_{m1} = 0.1441 \pm 0.8973 E+05$
 $\Gamma_{m2} = 0.1377 \pm 0.8973 E+05$
 $1/B_1 = 0.1064 E-05 \pm 0.1978 E+01$
 $1/B_2 = 0.1064 E-05 \pm 0.2070 E+01$
 $\text{corr. } \Gamma_{m1} - \Gamma_{m2} = 1.0000$
 $\text{corr. } \Gamma_{m1} - B_1 = 0.4553$
 $\text{corr. } \Gamma_{m1} - B_2 = -0.4553$
 $\text{corr. } \Gamma_{m2} - B_1 = -0.5857$
 $\text{corr. } \Gamma_{m2} - B_2 = 0.4553$
 $\text{corr. } B_1 - B_2 = -1.0000$
 d.o.f.

experimental adsorption data
 observations 9
 pCu²⁺ Γ_{ads}
 4.69347 0.270
 4.80824 0.258
 4.92526 0.250
 5.18635 0.257
 5.36635 0.233
 5.42193 0.214
 5.52724 0.214
 5.59654 0.189
 5.65916 0.188

Model 3 Implicit Langmuir Model
 see run 210380

experimental adsorption data

observations 9

pcu ²⁺	Γ_{ads}
7.49935	0.132
6.58922	0.177
6.04153	0.206
5.81906	0.228
5.60945	0.244
5.53971	0.269
5.40225	0.277
5.34058	0.284
5.26521	0.292

Model 3 Implicit Langmuir Model

see run 210380

run 120680 made 220180

run 120680

pH 6.0

glycine 50 μ M

linear regression

$\Gamma_{max} = 0.299$
 $\log B = 6.52$

non-linear regression

Model 1 Single Langmuir Model

TSS = 0.2351000 E-01
 RSS = 0.7435397 E-02
 $\Gamma_{max} = 0.2600$ 0.2866
 $B = .0.2001$ E+08 0.4007 E+08
 $\log B \pm 1\sigma = 7.30 \pm 0.22$
 corr. $\Gamma_{max} - B = -0.4514$

7 d.o.f.

Model 2 Double Langmuir Model

TSS = 0.2351000 E-01
 RSS = 0.1458608 E-03
 $\Gamma_{m1} = 0.1580$ 0.1873
 $\Gamma_{m2} = 0.2143$ 0.2704
 $1/B_1 = 0.9147$ E-08 0.3149 E-08
 $1/B_2 = 0.3821$ E-05 0.6790 E-05

corr. $\Gamma_{m1} - \Gamma_{m2} = 0.5060$
 corr. $\Gamma_{m1} - B_1 = 0.4293$
 corr. $\Gamma_{m1} - B_2 = 0.3266$
 corr. $\Gamma_{m2} - B_1 = 0.3679$
 corr. $\Gamma_{m2} - B_2 = 0.8947$
 corr. $B_1 - B_2 = 0.6473$

5 d.o.f.

experimental adsorption data

observations

pcu ²⁺	Γ_{ads}
6.85699	0.132
6.15304	0.183
5.61607	0.224
5.34814	0.252
5.12604	0.274
4.98481	0.283
4.92162	0.318
4.80981	0.305
4.71507	0.301

Model 3 Implicit Langmuir Model

see run 210380

run 120680 made 220180

run 120680

pH 6.0

glycine

linear regression

$\Gamma_{max} = 0.315$
 $\log B = 6.15$

non-linear regression

Model 1 Single Langmuir Model

TSS = 0.3095422 E-01
 RSS = 0.5361672 E-02
 $\Gamma_{max} = 0.2919$ 0.3168
 $B = 0.3353$ E+07 0.5683 E+07
 $\log B \pm 1\sigma = 6.53 \pm 0.15$
 corr. $\Gamma_{max} - B = -0.5426$

7 d.o.f.

Model 2 Double Langmuir Model

TSS = 0.3095422 E-01
 RSS = 0.1620081 E-03
 $\Gamma_{m1} = 0.1741$ 0.2204
 $\Gamma_{m2} = 0.1765$ 0.2116
 $1/B_1 = 0.5043$ E-07 0.1069 E-06
 $1/B_2 = 0.5485$ E-05 0.6052 E-04

corr. $\Gamma_{m1} - \Gamma_{m2} = -0.5460$
 corr. $\Gamma_{m1} - B_1 = 0.8931$
 corr. $\Gamma_{m1} - B_2 = 0.9785$
 corr. $\Gamma_{m2} - B_1 = -0.5465$
 corr. $\Gamma_{m2} - B_2 = -0.0808$
 corr. $B_1 - B_2 = 0.7365$

5 d.o.f.

MnO₂ Vib made 220180

run 210380
pH 7.0
glycine 50 µM

linear regression

$\Gamma_{max} = 0.210$
 $\log B = 7.09$
non-linear regression

Model 1 Single Langmuir Model

TSS = 0.4402622 E-01
RSS = 0.4567468 E-02
 $\Gamma_{max} = 0.2444$ 0.2659
B = 0.6404 E+09 0.1108 E+10
 $\log B \pm 1\sigma = 8.81 \pm 0.16$
corr. $\Gamma_{max} - B = -0.4038$

7 d.o.f.

Model 2 Double Langmuir Model

TSS = 0.4402622 E-01
RSS = 0.4640118 E-03
 $\Gamma_{m1} = 0.1552$ 0.2093
 $\Gamma_{m2} = 0.1355$ 0.1745
 $1/B_1 = 0.6251$ E-09 0.1037 E-06
 $1/B_2 = 0.6749$ E-07 0.2188 E-09
corr. $\Gamma_{m1} - \Gamma_{m2} = -0.3668$
corr. $\Gamma_{m1} - B_1 = 0.6506$
corr. $\Gamma_{m1} - B_2 = 0.6540$
corr. $\Gamma_{m2} - B_1 = -0.3662$
corr. $\Gamma_{m2} - B_2 = 0.1393$
corr. $B_1 - B_2 = 0.6880$

5 d.o.f.

Experimental adsorption data

observations	g	PCu ₂ ⁺	Γ_{ads}
9.39137	0.055		
9.01359	0.114		
7.98763	0.171		
7.44773	0.204		
7.25678	0.229		
6.97710	0.241		
6.90679	0.257		
6.78823	0.268		
6.58832	0.266		

Model 1 Single Langmuir Model

TSS = 0.1522022 E-01
RSS = 0.1745042 E-02
 $\Gamma_{max} = 0.2157$ 0.2287
B = 0.3181 E+11 0.3213 E+11
 $\log B \pm 1\sigma = 10.50 \pm 0.002$
corr. $\Gamma_{max} - B = -0.0216$

7 d.o.f.

Model 2 Double Langmuir Model

TSS = 0.1522022 E-01
RSS = 0.311775 E-04
 $\Gamma_{m1} = 0.1510$ 0.1368
 $\Gamma_{m2} = 0.1240$ 0.1393
 $1/B_1 = 0.1020$ E-10 0.1274 E-10
 $1/B_2 = 0.926$ E-09 0.1252 E-03
corr. $\Gamma_{m1} - \Gamma_{m2} = 0.1029$
corr. $\Gamma_{m1} - B_1 = 0.9403$
corr. $\Gamma_{m1} - B_2 = 0.8849$
corr. $\Gamma_{m2} - B_1 = -0.0155$
corr. $\Gamma_{m2} - B_2 = 0.5312$
corr. $B_1 - B_2 = 0.7674$

5 d.o.f.

MnO₂ Vib made 220180

run 210380
pH 8.0
glycine 50 µM

linear regression

$\Gamma_{max} = 0.239$
 $\log B = 10.19$
non-linear regression

Model 1 Single Langmuir Model

TSS = 0.1522022 E-01
RSS = 0.1745042 E-02
 $\Gamma_{max} = 0.2157$ 0.2287
B = 0.3181 E+11 0.3213 E+11
 $\log B \pm 1\sigma = 10.50 \pm 0.002$
corr. $\Gamma_{max} - B = -0.0216$

7 d.o.f.

Model 2 Double Langmuir Model

TSS = 0.1522022 E-01
RSS = 0.311775 E-04
 $\Gamma_{m1} = 0.1510$ 0.1368
 $\Gamma_{m2} = 0.1240$ 0.1393
 $1/B_1 = 0.1020$ E-10 0.1274 E-10
 $1/B_2 = 0.926$ E-09 0.1252 E-03
corr. $\Gamma_{m1} - \Gamma_{m2} = 0.1029$
corr. $\Gamma_{m1} - B_1 = 0.9403$
corr. $\Gamma_{m1} - B_2 = 0.8849$
corr. $\Gamma_{m2} - B_1 = -0.0155$
corr. $\Gamma_{m2} - B_2 = 0.5312$
corr. $B_1 - B_2 = 0.7674$

5 d.o.f.

Experimental adsorption data

observations	g	PCu ₂ ⁺	Γ_{ads}
10.62057	0.109		
10.46438	0.123		
10.17164	0.138		
9.98767	0.154		
9.69914	0.169		
9.42830	0.184		
9.22840	0.204		
8.99509	0.218		
8.75002	0.236		

Model 3 Implicit Langmuir Model

see run 210380

MNO₂ XVC made 220181

run 210481
pH 6.0

glycine --

linear regression

$\Gamma_{max} = 0.193$
 $\log B = 6.88$

non-linear regression

Model 1 Single Langmuir Model

TSS = 0.2108212 E-01
RSS = 0.1566143 E-02

$\Gamma_{max} = 0.1502$ 0.1707

$B = 0.2791$ E+08 0.5111 E+08

$\log B \pm 1\sigma = 7.45 \pm 0.18$

corr. $\Gamma_{max} - B = -0.4512$

5 d.o.f.

Model 2 Double Langmuir Model

TSS = 0.2100212 E-01

RSS = 0.8422360 E-04

$\Gamma_{m1} = 0.1065$ 0.1254

$\Gamma_{m2} = 0.1837$ 0.1837

$1/B_1 = 0.1191$ 0.05445

$1/B_2 = 0.1628$ E-07 0.2338 E-07

corr. $\Gamma_{m1} - \Gamma_{m2} = 0.4087$

corr. $\Gamma_{m1} - B_1 = 0.7921$

corr. $\Gamma_{m1} - B_2 = 0.7712$

corr. $\Gamma_{m2} - B_1 = 0.2775$

corr. $\Gamma_{m2} - B_2 = 0.8779$

corr. $B_1 - B_2 = 0.5727$

3 d.o.f.

experimental adsorption data

observations : 7

PCu²⁺ Γ_{ads}

8.50169 0.0220

7.98548 0.0355

7.78861 0.0573

6.73255 0.1028

5.95657 0.1351

5.69461 0.1459

5.29470 0.1759

Model 3 Implicit Langmuir Model

TSS = 0.4554451

RSS = 0.1290204

$\Gamma_{max} = 0.1988$ 0.2140

$b = -3.119$ -2.213

$n = 1.655$ 1.781

$n = 1.655$ 1.529

corr. $\Gamma_{max} - x = -0.3836$

corr. $\Gamma_{max} - n = 0.2610$

corr. $x - n = -0.9648$

109 d.o.f.

MNO₂ XVC made 220181

run 210481

pH 7.0

glycine --

linear regression

$\Gamma_{max} = 0.251$

$\log B = 7.68$

non-linear regression

Model 1 Single Langmuir Model

TSS = 0.2653584 E-01

RSS = 0.9683631 E-03

$\Gamma_{max} = 0.2475$ 0.2886

$B = 0.5509$ E+08 0.7946 E+08

$\log B \pm 1\sigma = 7.74 \pm 0.10$

corr. $\Gamma_{max} - B = -0.8706$

5 d.o.f.

Model 2 Double Langmuir Model

TSS = 0.2663584 E-01

RSS = 0.9683632 E-03

$\Gamma_{m1} = 0.1157$ \pm 0.7487 E+06

$\Gamma_{m2} = 0.1317$ \pm 0.7487 E+06

$1/B_1 = 0.1814$ E-07 \pm 0.4376 E-02

$1/B_2 = 0.1814$ E-07 \pm 0.3845 E-02

corr. $\Gamma_{m1} - \Gamma_{m2} = -1.0000$

corr. $\Gamma_{m1} - B_1 = 0.0970$

corr. $\Gamma_{m1} - B_2 = -0.0974$

corr. $\Gamma_{m2} - B_1 = -0.1343$

corr. $\Gamma_{m2} - B_2 = 0.0974$

corr. $B_1 - B_2 = -1.0000$

d.o.f.

experimental adsorption data

observations 7

PCu²⁺ Γ_{ads}

8.58110 0.0312

8.16610 0.0485

8.00211 0.0774

8.03411 0.1031

7.62611 0.1488

7.23917 0.1908

7.08420 0.1972

Model 3 Implicit Langmuir Model

see run 210481

MNO₂ XVC made 220181

run 080481
pH 8.0

Aspartic acid 80 pH
linear regression

$\Gamma_{max} = 0.238$
 $\log B = 10.19$

non-linear regression

Model 1 Single Langmuir Model

TSS = .
RSS = no convergence after
 $\Gamma_{max} = 50$ iterations
B =

$\log B \pm 1\sigma =$
corr. $\Gamma_{max} - B =$

d.o.f.

Model 2 Double Langmuir Model

TSS = 0.2930710 E-01
RSS = 0.9635654 E-04

$\Gamma_{m1} = 0.1326$ 0.1595
 $\Gamma_{m2} = 0.3245$ 0.7129

$1/B_1 = 0.1321$ E-10 0.1896 E-10
 $1/B_2 = 0.1542$ E-08 0.4613 E-08

corr. $\Gamma_{m1} - \Gamma_{m2} = 0.8365$
corr. $\Gamma_{m1} - B_1 = 0.8947$
corr. $\Gamma_{m1} - B_2 = 0.8978$
corr. $\Gamma_{m2} - B_1 = 0.6717$
corr. $\Gamma_{m2} - B_2 = 0.9915$
corr. $B_1 - B_2 = 0.7377$

5 d.o.f.

MNO₂ XVC made 220181

run 080481
pH 8.0

Alanine 80 pH

linear regression

$\Gamma_{max} = 0.245$
 $\log B = 10.20$

non-linear regression

Model 1 Single Langmuir Model

TSS = 0.3507970 E-01
RSS = 0.3688454 E-02
 $\Gamma_{max} = 0.2176$ output file
B = 0.3307 B+11 exceeded, 95%

$\log B \pm 1\sigma = 10.52$ confidence
corr. $\Gamma_{max} - B =$ limits and
correlation

7 d.o.f. lost

Model 2 Double Langmuir Model

TSS = 0.3507970 E-01
RSS = 0.2264883 E-03

$\Gamma_{m1} = 0.1447$ 0.1669
 $\Gamma_{m2} = 0.2262$ 0.4024

$1/B_1 = 0.8122$ E-11 0.1172 E-10
 $1/B_2 = 0.1611$ E-08 0.4107 E-08

corr. $\Gamma_{m1} - \Gamma_{m2} = 0.6426$
corr. $\Gamma_{m1} - B_1 = 0.7840$
corr. $\Gamma_{m1} - B_2 = 0.8041$
corr. $\Gamma_{m2} - B_1 = 0.4266$
corr. $\Gamma_{m2} - B_2 = 0.9677$
corr. $B_1 - B_2 = 0.5640$

5 d.o.f.

experimental adsorption data

observations 9

pCu²⁺ Γ_{ads}

11.43950 0.0497
11.01472 0.0766
10.18616 0.1325
9.88257 0.1608
9.45900 0.1830
9.31171 0.1956
9.19636 0.2118
9.03936 0.2263
8.88826 0.2439

Model 3 Implicit Langmuir Model

see run 210481

experimental adsorption data

observations 9

pCu²⁺ Γ_{ads}

11.11403 0.0515
10.76043 0.0783
10.01175 0.1286
9.81279 0.1494
9.63761 0.1758
9.48325 0.1826
9.37038 0.1952
9.27331 0.2122
9.16207 0.2319

Model 3 Implicit Langmuir Model

see run 210481

experimental adsorption data
observations 9

pcu ²⁺	Γ_{ads}
7.49201	0.0260
7.45198	0.0559
7.38987	0.0883
7.05988	0.1218
6.79336	0.1501
6.31901	0.1873
5.98019	0.2113
5.74253	0.2363
5.49936	0.2515

Model 3 Implicit Langmuir Model

see run 210481

run 010381
pH 6.0
glycine 50 μ M

linear regression
 $\Gamma_{max} = 0.258$
 $\log B = 6.88$

non-linear regression
Model 1 Single Langmuir Model
TSS = 0.5177722 E-01
RSS = 0.2167156 E-02

$\Gamma_{max} = 0.2469$ 0.2701
D = 0.9332 E+07 0.1283 E+08
 $\log B \pm 1\sigma = 6.97 \pm 0.08$
corr. $\Gamma_{max} - B = -0.6586$
7 d.o.f.

Model 2 Double Langmuir Model

TSS = no convergence after
RSS = 50 iterations; output,
 $\Gamma_{m1} =$ file exceeded.
 $\Gamma_{m2} =$
1/B₁ =
1/B₂ =
corr. $\Gamma_{m1} - \Gamma_{m2} =$
corr. $\Gamma_{m1} - B_1 =$
corr. $\Gamma_{m1} - B_2 =$
corr. $\Gamma_{m2} - B_1 =$
corr. $\Gamma_{m2} - B_2 =$
corr. B₁ - B₂ =
d.o.f.

experimental adsorption data
observations 8

pcu ²⁺	Γ_{ads}
10.18296	0.0774
9.45198	0.1319
9.16493	0.1582
8.80348	0.1765
8.69932	0.1900
8.52160	0.1956
8.42807	0.2147
8.29301	0.2326

Model 3 Implicit Langmuir Model

see run 210481

run 080481
pH 8.0
Glutamic acid 80 μ M

linear regression
 $\Gamma_{max} = 0.237$
 $\log B = 9.44$

non-linear regression
Model 1 Single Langmuir Model
TSS = 0.1714437 E-01
RSS = 0.1716230 E-02

$\Gamma_{max} = 0.2161$ 0.2307
B = 0.5077 E+10 0.5415 E+10
 $\log B \pm 1\sigma = 9.71 \pm 0.01$
corr. $\Gamma_{max} - B = -0.1129$
6 d.o.f.

Model 2 Double Langmuir Model

TSS = 0.7714437 E-01
RSS = 0.1113165 E-03
 $\Gamma_{m1} = 0.1582$ 0.1810
 $\Gamma_{m2} = 0.5545$ 3.275
1/B₁ = 0.7324 E-10 0.1055 E-09
1/B₂ = 0.3206 E-07 -0.1578 E-06
corr. $\Gamma_{m1} - \Gamma_{m2} = 0.8195$
corr. $\Gamma_{m1} - B_1 = 0.8463$
corr. $\Gamma_{m1} - B_2 = 0.8431$
corr. $\Gamma_{m2} - B_1 = 0.6035$
corr. $\Gamma_{m2} - B_2 = 0.9989$
corr. B₁ - B₂ = 0.6270
4 d.o.f.

experimental adsorption data

observations 9

pcu ²⁺	Γ_{ads}
11.18689	0.0141
11.27507	0.0296
10.96855	0.0463
10.72379	0.0643
10.50063	0.0840
10.26758	0.1057
10.09623	0.1302
9.81164	0.1568
9.46138	0.1850

MnO₂ XVC made 220181

run 010381

pH 8.0

glycine 50 μ M

linear regression

$\Gamma_{max} = 0.205$
 $\log B = 10.38$

non-linear regression

Model 1 Single Langmuir Model

TSS = 0.2736092 E-01
 RSS = 0.3156840 E-03
 $\Gamma_{max} = 0.2060 \pm 0.2147$
 $B = 0.2176 E+11 \pm 0.2163 E+11$
 $\log B \pm 1\sigma = 10.34 \pm 0.601$
 corr. $\Gamma_{max} - B = -0.0439$

7 d.o.f.

Model 2 Double Langmuir Model

TSS =
 RSS = 1 no convergence after
 $\Gamma_{m1} = 50$ iterations; output
 $\Gamma_{m2} =$ file exceeded.
 $1/B_1 =$
 $1/B_2 =$

corr. $\Gamma_{m1} - \Gamma_{m2} =$
 corr. $\Gamma_{m1} - B_1 =$
 corr. $\Gamma_{m1} - B_2 =$
 corr. $\Gamma_{m2} - B_1 =$
 corr. $\Gamma_{m2} - B_2 =$
 corr. $B_1 - B_2 =$
 d.o.f.

see run 210481

Model 3 Implicit Langmuir Model

experimental adsorption data

observations 9

pcu ²⁺	Γ_{ads}
9.17444	0.0139
8.90985	0.0289
9.02415	0.0458
9.05222	0.0643
8.93592	0.0843
8.67393	0.1059
8.54115	0.1306
8.33840	0.1565
7.93537	0.1871

MnO₂ XVC made 220181

run 010381

pH 7.0

glycine 50 μ M

linear regression

$\Gamma_{max} = 0.221$
 $\log B = 8.69$

non-linear regression

Model 1 Single Langmuir Model

TSS = 0.2818326 E-01
 RSS = 0.3399648 E-02
 $\Gamma_{max} = 0.2572 \pm 0.3483$
 $B = 0.2862 E+09 \pm 0.4869 E+09$
 $\log B \pm 1\sigma = 8.46 \pm 0.15$
 corr. $\Gamma_{max} - B = -0.9107$

7 d.o.f.

Model 2 Double Langmuir Model

TSS = 0.2818326 E-01
 RSS = 0.3399649 E-02
 $\Gamma_{m1} = 0.1799 \pm 0.6433 E+23$
 $\Gamma_{m2} = 0.07723 \pm 0.6433 E+23$
 $1/B_1 = 0.3489 E-08 \pm 0.4997 E+11$
 $1/B_2 = 0.3449 E-08 \pm 0.5215 E+09$

corr. $\Gamma_{m1} - \Gamma_{m2} = -1.0000$
 corr. $\Gamma_{m1} - B_1 = -0.9989$
 corr. $\Gamma_{m1} - B_2 = -1.0424$
 corr. $\Gamma_{m2} - B_1 = 1.0002$
 corr. $\Gamma_{m2} - B_2 = 1.0424$
 corr. $B_1 - B_2 = 1.0425$

5 d.o.f.

see run 210481

Model 3 Implicit Langmuir Model

MNO₂ XVC made 220181

run 240781

pH 6.0

glycine 50 µM

linear regression

$\Gamma_{max} = 0.155$

$\log B = 7.23$

non-linear regression

Model 1 Single Langmuir Model

TSS = 0.1628420 E-01

RSS = 0.1341537 E-02

$\Gamma_{max} = 0.1371$ 0.1524

B = 0.5551 E+08 0.9485 E+08

$\log B \pm 1\sigma = 7.74 \pm 0.15$

corr. $\Gamma_{max} - B = -0.4778$

6 d.o.f.

Model 2 Double Langmuir Model

TSS = 0.1628420 E-01

RSS = 0.1107019 E-03

$\Gamma_{m1} = 0.09543$ 0.1144

$\Gamma_{m2} = 0.1115$ 0.1871

$1/B_1 = 0.7441$ E-08 0.1131 E-07

$1/B_2 = 0.1420$ E-05 0.3858 E-05

corr. $\Gamma_{m1} - \Gamma_{m2} = 0.4872$

corr. $\Gamma_{m1} - B_1 = 0.8237$

corr. $\Gamma_{m1} - B_2 = 0.7626$

corr. $\Gamma_{m2} - B_1 = 0.3664$

corr. $\Gamma_{m2} - B_2 = 0.9131$

corr. $B_1 - B_2 = 0.6023$

4 d.o.f.

experimental adsorption data

observations 8

pCu²⁺ Γ_{ads}

8.47965 0.0218

8.29654 0.0458

7.69424 0.0717

6.92422 0.0978

6.34557 0.1199

6.16195 0.1315

5.96342 0.1438

5.75867 0.1560

MNO₂ XVC made 220181

run 280681

pH 7.0

glycine

linear regression

$\Gamma_{max} = 0.225$

$\log B = 8.00$

non-linear regression

Model 1 Single Langmuir Model

TSS = 0.2528508 E-01

RSS = 0.1570558 E-02

$\Gamma_{max} = 0.2188$ 0.2525

B = 0.9590 E+08 0.1435 E+09

$\log B \pm 1\sigma = 7.98 \pm 0.11$

corr. $\Gamma_{max} - B = 0.8169$

6 d.o.f.

Model 2 Double Langmuir Model

TSS = 0.2528503 E-01

RSS = 0.4360203 E-03

$\Gamma_{m1} = 0.04790$ 0.1130

$\Gamma_{m2} = 0.2041$ 0.2517

$1/B_1 = 0.7813$ E-09 0.2438 E-08

$1/B_2 = 0.2759$ E-07 0.6130 E-07

corr. $\Gamma_{m1} - \Gamma_{m2} = -0.5558$

corr. $\Gamma_{m1} - B_1 = 0.9283$

corr. $\Gamma_{m1} - B_2 = 0.1112$

corr. $\Gamma_{m2} - B_1 = -0.6017$

corr. $\Gamma_{m2} - B_2 = -0.1984$

corr. $B_1 - B_2 = 0.7851$

4 d.o.f.

experimental adsorption data

observations 0

pCu²⁺ Γ_{ads}

9.00309 0.0421

8.56809 0.0582

8.33910 0.0762

7.98610 0.0962

7.79611 0.1193

7.60312 0.1462

7.19417 0.1767

7.00722 0.2155

Model 3 Implicit Langmuir Model

see run 210481

run 280681
 pH 7.0
 glycine 50 µM

linear regression
 $\Gamma_{max} = 0.218$
 $\log B = 8.64$

non-linear regression
 Model 1 Single Langmuir Model
 TSS = 0.3141446 E-01
 RSS = 0.3062675 E-02
 $\Gamma_{max} = 0.1902$ 0.2120
 $B = 0.1221$ E+10 0.1673 E+10
 $\log B \pm 1\sigma = 9.09 \pm 0.08$
 corr. $\Gamma_{max} - B = -0.2831$

6 d.o.f.

Model 2 Double Langmuir Model
 TSS = 0.3141446 E-01
 RSS = 0.1681846 E-03
 $\Gamma_{m1} = 0.1204$ 0.1486
 $\Gamma_{m2} = 0.1178$ 0.1421
 $1/B_1 = 0.2184$ E-09 0.3587 E-09
 $1/B_2 = 0.2283$ E-07 0.7815 E-10
 corr. $\Gamma_{m1} - \Gamma_{m2} = -0.1962$
 corr. $\Gamma_{m1} - B_1 = 0.8645$
 corr. $\Gamma_{m1} - B_2 = 0.8699$
 corr. $\Gamma_{m2} - B_1 = -0.4039$
 corr. $\Gamma_{m2} - B_2 = 0.0527$
 corr. $B_1 - B_2 = 0.7843$

4 d.o.f.

run 210681
 pH 6.0
 Aspartic acid 48 µM

linear regression
 $\Gamma_{max} = 0.173$
 $\log B = 7.55$

non-linear regression
 Model 1 Single Langmuir Model
 TSS = 0.1814283 E-01
 RSS = 0.5194353 E-03
 $\Gamma_{max} = 0.1609$ 0.1711
 $B = 0.6653$ E+08 0.9121 E+08
 $\log B \pm 1\sigma = 7.82 \pm 0.08$
 corr. $\Gamma_{max} - B = -0.5660$

6 d.o.f.

Model 2 Double Langmuir Model
 TSS = 0.1814283 E-01
 RSS = 0.6919083 E-04
 $\Gamma_{m1} = 0.1339$ 0.1543
 $\Gamma_{m2} = 0.07902$ 0.1134
 $1/B_1 = 0.9668$ E-08 0.1303 E-07
 $1/B_2 = 0.9647$ E-06 0.2727 E-05
 corr. $\Gamma_{m1} - \Gamma_{m2} = 0.0704$
 corr. $\Gamma_{m1} - B_1 = 0.8702$
 corr. $\Gamma_{m1} - B_2 = 0.8612$
 corr. $\Gamma_{m2} - B_1 = 0.4971$
 corr. $\Gamma_{m2} - B_2 = 0.9488$
 corr. $B_1 - B_2 = 0.6810$

4 d.o.f.

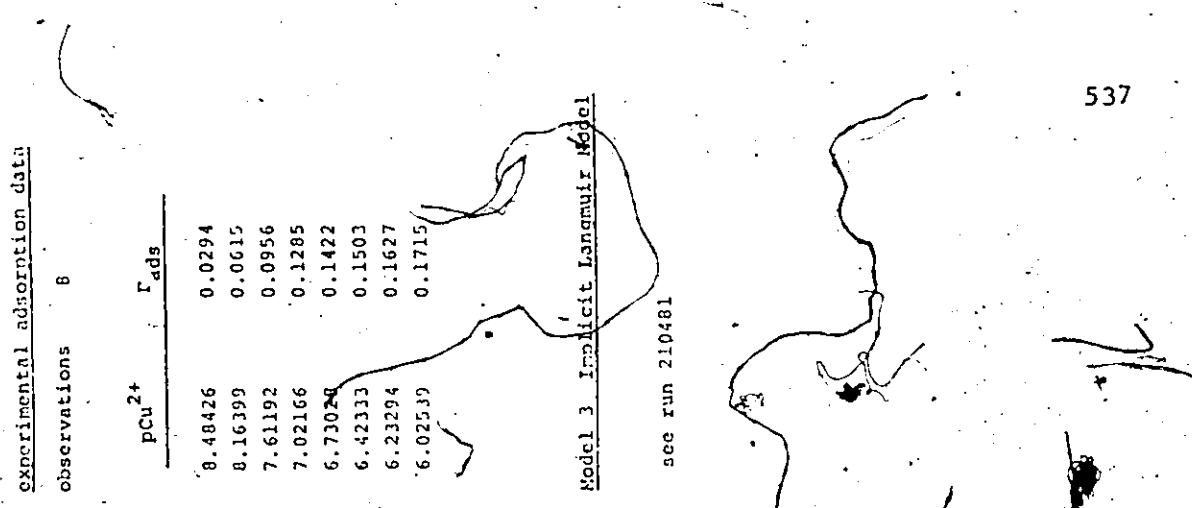
run 220181
 pH 6.0
 Aspartic acid 48 µM

linear regression
 $\Gamma_{max} = 0.173$
 $\log B = 7.55$

non-linear regression
 Model 1 Single Langmuir Model
 TSS = 0.1814283 E-01
 RSS = 0.5194353 E-03
 $\Gamma_{max} = 0.1609$ 0.1711
 $B = 0.6653$ E+08 0.9121 E+08
 $\log B \pm 1\sigma = 7.82 \pm 0.08$
 corr. $\Gamma_{max} - B = -0.5660$

6 d.o.f.

Model 3 Implicit Langmuir Model
 see run 210481



MnO₂ XVC made 220181

ruh 210681
pH 6.0
glycine

linear regression

Γ_{max} = 0.206
log B = 7.20

non-linear regression

Model 1 Single Langmuir Model

TSS = 0.2355 E-01
RSS = 0.7736 E-03
 Γ_{max} = 0.1911 0.2082
B = 0.2085 E+08 0.2806 E+08
log B ± 1σ = 7.32 ± 0.07
corr. Γ_{max} - B = -0.7042

46 d.o.f.

Model 2 Double Langmuir Model

TSS = 0.2355274 E-01
RSS = 0.78273723-04
 Γ_{m1} = 0.1252 0.1601
 Γ_{m2} = 0.1072 0.1356
1/B₁ = 0.1994 E-07 0.3044 E-07
1/B₂ = 0.6142 E-06 0.1425 E-05
corr. Γ_{m1} - Γ_{m2} = -0.3235
corr. Γ_{m1} - B₁ = 0.9371
corr. Γ_{m1} - B₂ = 0.8874
corr. Γ_{m2} - B₁ = -0.4332
corr. Γ_{m2} - B₂ = 0.1179
corr. B₁ - B₂ = 0.7520

4 d.o.f.

experimental adsorption data

observations 8

pcu²⁺ Γ_{ads}

8.21954 0.0297
7.79653 0.0624
7.46354 0.0802
7.22854 0.1002
7.02854 0.1229
6.57555 0.1476
6.21056 0.1748
5.80359 0.2009

Model 3 Implicit Langmuir Model

see run 210481

MnO₂ XVC made 220181

ruh 210681
pH 6.0
glycine 50 μM

linear regression

Γ_{max} = 0.150
log B = 7.96

non-linear regression

Model 1 Single Langmuir Model

TSS = 0.5808 E-02
RSS = 0.1707 E-03
 Γ_{max} = 0.1475 0.1732
B = 0.1018 E+09 0.1563 E+09
log B ± 1σ = 8.01 ± 0.12
corr. Γ_{max} - B = -0.7948

2 d.o.f.

Model 2 Double Langmuir Model

TSS = 0.5807687 E-02
RSS = 0.1707419 E-03
 Γ_{m1} = 0.1475
 Γ_{m2} = 0.3867 E-09
1/B₁ = 0.9816 E-08
1/B₂ = 0.2576 E-04
corr. Γ_{m1} - Γ_{m2} = -0.6912
corr. Γ_{m1} - B₁ = 0.9492
corr. Γ_{m1} - B₂ = -0.3502
corr. Γ_{m2} - B₁ = -0.5325
corr. Γ_{m2} - B₂ = 0.9142
corr. B₁ - B₂ = -0.1840

no d.o.f.'s

experimental adsorption data

observations 4

pcu²⁺ Γ_{ads}

8.46055 0.0291
8.27254 0.0610
7.73028 0.0954
7.10104 0.1312

Model 3 Implicit Langmuir Model

see run 210481

run 070480 made 230180
 pH 6.0
 glycine 50 µM

pcu ²⁺	Γ _{ads}
5.84924	0.058
5.62949	0.072
5.52331	0.076
5.41039	0.074
5.30963	0.074
5.20344	0.0713
5.11475	0.0760
5.01701	0.0793
4.97179	0.0900

linear regression
 Γ_{max} = 0.089
 log B = 5.92

non-linear regression

Model 1 Single Langmuir Model
 TSS = 0.5589300 E-03
 RSS = 0.2826195 E-03
 Γ_{max} = 0.0620 0.08920
 B = 0.2365 E+07 0.4632 E+07

log B ± 1σ = 6.38 ± 0.11
 corr. Γ_{max} - B = -0.9336

7 d.o.f.

run 070480 made 230180
 pH 6.0
 glycine 50 µM

pcu ²⁺	Γ _{ads}
5.40176	0.0828
5.16058	0.1031
5.02196	0.1007
4.93794	0.1101
4.85496	0.1184
4.76379	0.1209
4.62003	0.1329
4.59047	0.1278
4.56416	0.1485

linear regression
 Γ_{max} = 0.089
 log B = 5.92

non-linear regression

Model 2 Double Langmuir Model
 TSS = 0.2601084 E-01
 RSS = 0.6381659 E-02
 Γ_{max} = 0.1613 0.1864
 b = -5.563 -6.249
 n = 1.770 1.862

corr. Γ_{max} - x = -0.4851
 corr. Γ_{max} - n = 0.1671
 corr. x - n = -0.9433

31 d.o.f.

run 070480 made 230180
 pH 6.0
 glycine 50 µM

pcu ²⁺	Γ _{ads}
5.84924	0.058
5.62949	0.072
5.52331	0.076
5.41039	0.074
5.30963	0.074
5.20344	0.0713
5.11475	0.0760
5.01701	0.0793
4.97179	0.0900

linear regression
 Γ_{max} = 0.161
 log B = 5.33

non-linear regression

Model 3 Implicit Langmuir Model
 TSS = 0.2601084 E-01
 RSS = 0.6381659 E-02
 Γ_{max} = 0.1613 0.1864
 b = -5.563 -6.249
 n = 1.770 1.862

corr. Γ_{max} - x = -0.4851
 corr. Γ_{max} - n = 0.1671
 corr. x - n = -0.9433

31 d.o.f.

run 070480 made 230180
 pH 6.0
 glycine 50 µM

pcu ²⁺	Γ _{ads}
5.84924	0.058
5.62949	0.072
5.52331	0.076
5.41039	0.074
5.30963	0.074
5.20344	0.0713
5.11475	0.0760
5.01701	0.0793
4.97179	0.0900

linear regression
 Γ_{max} = 0.161
 log B = 5.33

non-linear regression

Model 1 Single Langmuir Model
 TSS = 0.1048 E-02
 RSS = 0.4079490 E-03
 Γ_{max} = 0.1548 0.1716
 B = 0.2509 E+06 0.3658 E+06

log B ± 1σ = 5.40 ± 0.10
 corr. Γ_{max} - B = -0.9166

7 d.o.f.

run 070480 made 230180
 pH 6.0
 glycine 50 µM

pcu ²⁺	Γ _{ads}
5.84924	0.058
5.62949	0.072
5.52331	0.076
5.41039	0.074
5.30963	0.074
5.20344	0.0713
5.11475	0.0760
5.01701	0.0793
4.97179	0.0900

linear regression
 Γ_{max} = 0.161
 log B = 5.33

non-linear regression

Model 2 Double Langmuir Model
 TSS = 0.2601084 E-01
 RSS = 0.6381659 E-02
 Γ_{max} = 0.1613 0.1864
 b = -5.563 -6.249
 n = 1.770 1.862

corr. Γ_{max} - x = -0.4851
 corr. Γ_{max} - n = 0.1671
 corr. x - n = -0.9433

31 d.o.f.

Model 3 Implicit Langmuir Model
 see run 070480

Model 2 Double Langmuir Model
 TSS = 0.2601084 E-01
 RSS = 0.6381659 E-02
 Γ_{max} = 0.1613 0.1864
 b = -5.563 -6.249
 n = 1.770 1.862

corr. Γ_{max} - x = -0.4851
 corr. Γ_{max} - n = 0.1671
 corr. x - n = -0.9433

31 d.o.f.

Model 1 Single Langmuir Model
 TSS = 0.5589300 E-03
 RSS = 0.2826195 E-03
 Γ_{max} = 0.0620 0.08920
 B = 0.2365 E+07 0.4632 E+07

log B ± 1σ = 6.38 ± 0.11
 corr. Γ_{max} - B = -0.9336

7 d.o.f.

Model 3 Implicit Langmuir Model
 TSS = 0.2601084 E-01
 RSS = 0.6381659 E-02
 Γ_{max} = 0.1613 0.1864
 b = -5.563 -6.249
 n = 1.770 1.862

corr. Γ_{max} - x = -0.4851
 corr. Γ_{max} - n = 0.1671
 corr. x - n = -0.9433

31 d.o.f.

experimental adsorption data

run 070480
 pH 8.0
 glycine 50 µM

pcu ²⁺	r _{ads}
8.95273	0.063
8.79751	0.078
8.65876	0.095
8.54121	0.098
8.56273	0.121
8.40682	0.121
8.29286	0.130
8.17809	0.143

run 070480
 pH 8.0
 glycine 50 µM

linear regression
 $r_{max} = 0.189$
 $\log B = 8.66$

non-linear regression
 Model 1 Single Langmuir Model
 $TSS = 0.5212875 E-02$
 $RSS = 0.3498126 E-03$
 $r_{max} = 0.1862 \pm 0.2133$
 $B = 0.4663 E+09 \pm 0.6190 E+09$
 $\log B \pm 1\sigma = 8.67 \pm 0.07$
 $corr. r_{max} - B = -0.9284$

6 d.o.f.
 Model 2 Double Langmuir Model
 $TSS = 0.5212875 E-02$
 $RSS = 0.3498401 E-03$
 $r_{m1} = 0.1878 \pm 0.4650$
 $r_{m2} = 0.9183 E-08 \pm 0.2929 E+04$
 $1/B_1 = 0.2134 E-08 \pm 0.6205 E-03$
 $1/B_2 = 0.4560 E-04 \pm 0.1180 E+08$
 $corr. r_{m1} - r_{m2} = -0.7673$
 $corr. r_{m1} - B_1 = 0.9884$
 $corr. r_{m1} - B_2 = 0.0580$
 $corr. r_{m2} - B_1 = -0.7369$
 $corr. r_{m2} - B_2 = 0.5845$
 $corr. B_1 - B_2 = 0.0687$
 d.o.f.

Model 3 Implicit Langmuir Model

see run 070480

experimental adsorption data

run 070480
 pH 7.0
 glycine 150 µM

pcu ²⁺	r _{ads}
7.63507	0.0345
7.12674	0.0563
6.79237	0.0739
6.65521	0.0835
6.58220	0.1088
6.36452	0.102
6.23302	0.124
6.13665	0.136

run 070480
 pH 7.0
 glycine 150 µM

linear regression
 $r_{max} = 0.153$
 $\log B = 7.14$

non-linear regression
 Model 1 Single Langmuir Model
 $TSS = 0.8286715 E-02$
 $RSS = 0.6177425 E-03$
 $r_{max} = 0.1515 \pm 0.1795$
 $B = 0.7128 E+07 \pm 0.1134 E+08$
 $\log B \pm 1\sigma = 6.85 \pm 0.13$
 $corr. r_{max} - B = -0.9072$

6 d.o.f.
 Model 2 Double Langmuir Model
 $TSS = 0.8286715 E-02$
 $RSS = 0.3820721 E-03$
 $r_{m1} = 0.04758 \pm 0.8334$
 $r_{m2} = 0.1528 \pm 0.2718$
 $1/B_1 = 0.1623 E-07 \pm 0.8130 E-07$
 $1/B_2 = 0.5610 E-06 \pm 0.3003 E-05$
 $corr. r_{m1} - r_{m2} = 0.4959$
 $corr. r_{m1} - B_1 = 0.9596$
 $corr. r_{m1} - B_2 = 0.9526$
 $corr. r_{m2} - B_1 = 0.3606$
 $corr. r_{m2} - B_2 = 0.7308$
 $corr. B_1 - B_2 = 0.8668$
 d.o.f.

Model 3 Implicit Langmuir Model

see run 070480

MoO₂ VIIIB made 230180

run 020480

pH 6.0

glycine

linear regression

$\Gamma_{max} = 0.243$

$\log B = 5.94$

non-linear regression

Model 1 Single Langmuir Model

TSS = 0.627556 E-02

RSS = 0.1933739 E-02

$\Gamma_{max} = 0.2227 \pm 0.2375$

$B = 0.2625 \pm 0.07 \pm 0.4302 \pm 0.07$

$\log B \pm 1\sigma = 6.42 \pm 0.14$

corr. $\Gamma_{max} - B = -0.5793$

7 d.o.f.

Model 2 Double Langmuir Model

TSS =

RSS =

$\Gamma_{m1} =$ no convergence after

$\Gamma_{m2} =$ 50 iterations; error

$1/B_1 =$ file exceeded.

$1/B_2 =$

corr. $\Gamma_{m1} - \Gamma_{m2} =$

corr. $\Gamma_{m1} - B_1 =$

corr. $\Gamma_{m1} - B_2 =$

corr. $\Gamma_{m2} - B_1 =$

corr. $\Gamma_{m2} - B_2 =$

corr. $B_1 - B_2 =$

d.o.f.

experimental adsorption data

observations 9

pCu²⁺ Γ_{ads}

6.30803 0.139

5.97687 0.173

5.82084 0.194

5.13650 0.198

4.99516 0.204

4.87739 0.213

4.78252 0.233

4.72319 0.241

4.62958 0.230

Model 3 Implicit Langmuir Model

TSS = 0.7333026

RSS = 0.5530088 E-01

$\Gamma_{max} = 0.2502 \pm 0.2742$

$x = -1.969 \pm 1.003$

$n = 1.439 \pm 1.624$

corr. $\Gamma_{max} - x = -0.5012$

corr. $\Gamma_{max} - n = 0.401$

corr. $x - n = -0.9869$

33 d.o.f.

MoO₂ VIIIB made 230180

run 020480

pH 6.0

glycine 50 μ M

linear regression

$\Gamma_{max} = 0.397$

$\log B = 6.14$

non-linear regression

Model 1 Single Langmuir Model

TSS = 0.4310200 E-01

RSS = 0.8261159 E-02

$\Gamma_{max} = 0.3732 \pm 0.4490$

$B = 0.1677 \pm 0.07 \pm 0.2960 \pm 0.07$

$\log B \pm 1\sigma = 6.22 \pm 0.17$

corr. $\Gamma_{max} - B = -0.9009$

7 d.o.f.

Model 2 Double Langmuir Model

TSS = 0.4310200 E-01

RSS = 0.6612670 E-03

$\Gamma_{m1} = 0.1460 \pm 0.3130$

$\Gamma_{m2} = 0.9540 \pm 0.2211$

$1/B_1 = 0.0191 \pm 0.07 \pm 0.1010 \pm 0.06$

$1/B_2 = 0.1115 \pm 0.04 \pm 0.5700 \pm 0.04$

corr. $\Gamma_{m1} - \Gamma_{m2} = 0.8720$

corr. $\Gamma_{m1} - B_1 = 0.9237$

corr. $\Gamma_{m1} - B_2 = 0.9048$

corr. $\Gamma_{m2} - B_1 = 0.7435$

corr. $\Gamma_{m2} - B_2 = 0.9971$

corr. $B_1 - B_2 = 0.7700$

d.o.f.

experimental adsorption data

observations 9

pCu²⁺ Γ_{ads}

6.82974 0.137

6.39364 0.179

6.00349 0.202

5.92592 0.230

5.77288 0.248

5.65326 0.273

5.55909 0.310

5.52564 0.340

5.41873 0.352

Model 3 Implicit Langmuir Model

see run 020480

NO. V114b made 230180

run 020480

pH 7.0

glycine 50 µM

linear regression

$\Gamma_{max} = 0.293$
 $\log B = 7.70$

non-linear regression

Model 1 Single Langmuir Model

TSS = 0.448900 E-01
RSS = 0.8156408 E-02
 $\Gamma_{max} = 0.2469$ 0.2796
B = 0.1878 E+09 0.3800 E-09
 $\log B \pm 1\sigma = 8.27 \pm 0.22$
corr. $\Gamma_{max} - B = -0.5603$

7 d.o.f.

Model 2 Double Langmuir Model

TSS = 0.000000 E-01
RSS = 0.2487902 E-02
 $\Gamma_{m1} = 0.1629$ 0.1955
 $\Gamma_{m2} = 0.6311$ 2.510
 $1/B_1 = 0.1688$ E-08 0.2672 E-08
 $1/B_2 = 0.1025$ E-05 0.5057 E-05
corr. $\Gamma_{m1} - \Gamma_{m2} = 0.8107$
corr. $\Gamma_{m1} - B_1 = 0.7893$
corr. $\Gamma_{m1} - B_2 = 0.8455$
corr. $\Gamma_{m2} - B_1 = 0.5999$
corr. $\Gamma_{m2} - B_2 = 0.9976$
corr. $B_1 - B_2 = 0.6304$

5 d.o.f.

experimental adsorption data

observations 9

PCu²⁺

Γ_{ads}

8.93855 0.057
8.30682 0.119
7.55236 0.166
7.28476 0.186
7.09221 0.204
6.87935 0.231
6.81814 0.252
6.66549 0.262
6.57768 0.295

NO. V114b made 230180

run 020480

pH 8.0

glycine 50 µM

linear regression

$\Gamma_{max} = 0.234$
 $\log B = 9.17$

non-linear regression

Model 1 Single Langmuir Model

TSS = 0.1156889 E-01
RSS = 0.1318310 E-02
 $\Gamma_{max} = 0.2139$ 0.2246
B = 0.1136 E+11 0.1163 E+11
 $\log B \pm 1\sigma = 10.06 \pm 0.005$
corr. $\Gamma_{max} - B = -0.0479$

7 d.o.f.

Model 2 Double Langmuir Model

TSS = 0.1156889 E-01
RSS = 0.3442030 E-04
 $\Gamma_{m1} = 0.1594$ 0.1716
 $\Gamma_{m2} = 0.09845$ 0.1136
 $1/B_1 = 0.2795$ E-10 0.4489 E-10
 $1/B_2 = 0.1448$ E-09 0.2395 E-09
corr. $\Gamma_{m1} - \Gamma_{m2} = -0.8148$
corr. $\Gamma_{m1} - B_1 = 0.9469$
corr. $\Gamma_{m1} - B_2 = 0.9304$
corr. $\Gamma_{m2} - B_1 = -0.8267$
corr. $\Gamma_{m2} - B_2 = -0.5656$
corr. $B_1 - B_2 = 0.8303$

5 d.o.f.

experimental adsorption data

observations 9

PCu²⁺

Γ_{ads}

10.13787 0.113
9.77989 0.140
9.35340 0.163
9.19044 0.174
9.03787 0.187
8.82548 0.194
8.67020 0.210
8.43021 0.219
8.19527 0.230

Model 3 Implicit Langmuir Model

see run 020480

NO. XXV-A code 250581

run 280581
pH 6.0
glycine 50 μ M

linear regression

r_{max} = 0.038
 $\log B$ = 5.64

non-linear regression

Model 1 Single Langmuir Model

TSS = 0.4057488 E-03
RSS = 0.1202007 E-03
 r_{max} = 0.03204 0.3687
B = 0.1596 E+07 0.3318 E+07
 $\log B \pm 1\sigma$ = 6.20 \pm 0.23
corr. r_{max} - B = -0.6210
6 d.o.f.

Model 2 Double Langmuir Model

TSS = no convergence after
RSS = 50 iterations; output
 r_{m1} = file exceeded.
 r_{m2} =
1/B₁ =
1/B₂ =

corr. r_{m1} - r_{m2} =
corr. r_{m1} - B₁ =
corr. r_{m1} - B₂ =
corr. r_{m2} - B₁ =
corr. r_{m2} - B₂ =
corr. B₁ - B₂ =
d.o.f.

Experimental adsorption data

observations 8

PCU²⁺ r_{ads}

6.47756 0.0141
5.81059 0.0224
5.44065 0.0243
5.03983 0.0238
4.90793 0.0262
4.31602 0.0340
4.71215 0.0340
4.60632 0.0371

Model 3 Implicit Langmuir Model

TSS = 0.1974548 E-02
RSS = 0.4591682 E-03
 r_{max} = 0.03652 0.04284
b = -0.3559 E+01 -2.465
n = 1.519 1.650
corr. r_{max} - x = -0.6982
corr. r_{max} - n = 0.5502
corr. x - n = -0.0760
d.o.f.

NO. XXV-A code 280581

run 280581
pH 6.0
glycine 50 μ M

linear regression

r_{max} = 0.039
 $\log B$ = 5.64

non-linear regression

Model 1 Single Langmuir Model

TSS = 0.6693556 E-03
RSS = 0.1436630 E-03
 r_{max} = 0.03996 0.05276
B = 0.1703 E+06 0.7181 E+06
 $\log B \pm 1\sigma$ = 5.57 \pm 0.20
corr. r_{max} - B = -0.9109
7 d.o.f.

Model 2 Double Langmuir Model

TSS =
RSS = no convergence after
 r_{m1} = 50 iterations; output
 r_{m2} = file exceeded.
1/B₁ =
1/B₂ =

corr. r_{m1} - r_{m2} =
corr. r_{m1} - B₁ =
corr. r_{m1} - B₂ =
corr. r_{m2} - B₁ =
corr. r_{m2} - B₂ =
corr. B₁ - B₂ =
d.o.f.

Experimental adsorption data

observations 9

PCU²⁺ r_{ads}

6.77726 0.0112
6.12373 0.0126
5.83247 0.0112
5.69059 0.0181
5.42208 0.0226
5.29751 0.0209
5.11913 0.0287
5.02829 0.0345
4.93492 0.0335

Model 3 Implicit Langmuir Model

see run 280581

MnO₂ XXVA made 250581

run 280581
pH 7.0
glycine 50 µM

linear regression

Γ_{max} = 0.032
log B = 7.43

non-linear regression

Model 1 Single Langmuir Model

TSS = 0.2665143 E-03
RSS = 0.1834643 E-03

Γ_{max} = 0.02380 0.02951
B = 0.1486 E+09 0.2698 E+09
log B ± 1σ = 8.17 ± 0.18

corr. Γ_{max} - B = -0.3357
5 d.o.f.

Model 2 Double Langmuir Model

TSS = no convergence after
RSS = 50 iterations; output file exceeded.

Γ_{m1} =
 Γ_{m2} =
1/B₁ =
1/B₂ =

corr. Γ_{m1} - Γ_{m2} =
corr. Γ_{m1} - B₁ =
corr. Γ_{m1} - B₂ =
corr. Γ_{m2} - B₁ =
corr. Γ_{m2} - B₂ =
corr. B₁ - B₂ =
d.o.f.

experimental adsorption data

observations 7

pCu²⁺ Γ_{ads}

8.41016 0.0142
7.68561 0.0153
7.30882 0.0146
7.13140 0.0165
6.97770 0.0209
6.75279 0.0299
6.60365 0.0284

Model 3 Implicit Langmuir Model

see run 280581

MnO₂ XXVA made 250581

run 280581
pH 8.0
glycine 50 µM

linear regression

Γ_{max} = 0.029
log B = 9.01

non-linear regression

Model 1 Single Langmuir Model

TSS = 0.1670300 E-03
RSS = 0.1944179 E-05

Γ_{max} = 0.02890 0.03015
B = 0.1069 E+10 0.1087 E+10
log B ± 1σ = 9.03 ± 0.004

corr. Γ_{max} - B = -0.1306
4 d.o.f.

Model 2 Double Langmuir Model

TSS = 0.1670300 E-03
RSS = 0.2201817 E-01

Γ_{m1} = 0.1472 2.385
 Γ_{m2} = 0.1685 E-08 0.6541 E+04
1/B₁ = 0.1175 E-08 0.2180 E-07
1/B₂ = 0.3812 E-04 -0.3981 E+09

corr. Γ_{m1} - Γ_{m2} = -0.1917
corr. Γ_{m1} - B₁ = 0.9591
corr. Γ_{m1} - B₂ = 0.9480
corr. Γ_{m2} - B₁ = -0.3083
corr. Γ_{m2} - B₂ = 0.3226
corr. B₁ - B₂ = 0.7120
d.o.f.

experimental adsorption data

observations 6

pCu²⁺ Γ_{ads}

9.45710 0.0076
9.22001 0.0111
9.05329 0.0148
8.87285 0.0175
8.67480 0.0187
8.40352 0.0239

Model 3 Implicit Langmuir Model

see run 280581

Model 13 made 1977 or 1978

run 240781

pH 6.0

glycine

linear regression

$\Gamma_{max} = 0.148$

$\log B = 5.93$

non-linear regression

Model 1 Single Langmuir Model

TSS = 0.1367937 E-01

RSS = 0.4656187 E-03

$\Gamma_{max} = 0.1542 \pm 0.1314$

$B = 0.6595 E+06 \pm 0.8640 E+06$

$\log B \pm 1\sigma = 5.82 \pm 0.10$

corr. $\Gamma_{max} - B = -0.9111$

7 d.o.f.

Model 2 Double Langmuir Model

TSS = 0.1367937 E-01

RSS = 0.3582017 E+00

$\Gamma_{m1} = 0.1503 \pm 0.3196 E+02$

$\Gamma_{m2} = 0.1471 \pm 0.3191 E+02$

$1/B_1 = 0.9340 E-18 \pm 0.3022 E-05$

$1/B_2 = 0.6183 E-07 \pm 0.1179 E-04$

corr. $\Gamma_{m1} - \Gamma_{m2} = -1.0000$

corr. $\Gamma_{m1} - B_1 = 0.9868$

corr. $\Gamma_{m1} - B_2 = 0.9830$

corr. $\Gamma_{m2} - B_1 = 0.9675$

corr. $\Gamma_{m2} - B_2 = -0.9319$

corr. $B_1 - B_2 = 9.9426$

5 d.o.f.

Model 13 made 1977 or 1978

run 190781

pH 6.0

glycine

linear regression

$\Gamma_{max} = 0.159$

$\log B = 6.09$

non-linear regression

Model 1 Single Langmuir Model

TSS = 0.1291236 E-01

RSS = 0.8416209 E-03

$\Gamma_{max} = 0.1708 \pm 0.2126$

$B = 0.9186 E+06 \pm 0.1527 E+07$

$\log B \pm 1\sigma = 5.96 \pm 0.14$

corr. $\Gamma_{max} - B = -0.9238$

6 d.o.f.

Model 2 Double Langmuir Model

TSS = 0.2965672 E-02

RSS = 0.1709 E-02

$\Gamma_{m1} = -4.016 \pm 3.483$

$\Gamma_{m2} = 1.694 \pm 1.668$

$1/B_1 = -0.6871$

$1/B_2 = 0.4513$

corr. $\Gamma_{m1} - \Gamma_{m2} = -0.9325$

corr. $\Gamma_{m1} - B_1 = 30$

corr. $\Gamma_{m1} - B_2 = 30$

corr. $\Gamma_{m2} - B_1 = 30$

corr. $\Gamma_{m2} - B_2 = 30$

corr. $B_1 - B_2 = 30$

30 d.o.f.

Model 13 made 1977 or 1978

run 190781

pH 6.0

glycine

linear regression

$\Gamma_{max} = 0.159$

$\log B = 6.09$

non-linear regression

Model 1 Single Langmuir Model

TSS = 0.1291236 E-01

RSS = 0.8416209 E-03

$\Gamma_{max} = 0.1708 \pm 0.2126$

$B = 0.9186 E+06 \pm 0.1527 E+07$

$\log B \pm 1\sigma = 5.96 \pm 0.14$

corr. $\Gamma_{max} - B = -0.9238$

6 d.o.f.

Model 2 Double Langmuir Model

TSS = 0.2965672 E-02

RSS = 0.1709 E-02

$\Gamma_{m1} = -4.016 \pm 3.483$

$\Gamma_{m2} = 1.694 \pm 1.668$

$1/B_1 = -0.6871$

$1/B_2 = 0.4513$

corr. $\Gamma_{m1} - \Gamma_{m2} = 30$

corr. $\Gamma_{m1} - B_1 = 30$

corr. $\Gamma_{m1} - B_2 = 30$

corr. $\Gamma_{m2} - B_1 = 30$

corr. $\Gamma_{m2} - B_2 = 30$

corr. $B_1 - B_2 = 30$

30 d.o.f.

Model 13 made 1977 or 1978

run 190781

pH 6.0

glycine

linear regression

$\Gamma_{max} = 0.159$

$\log B = 6.09$

non-linear regression

Model 1 Single Langmuir Model

TSS = 0.1291236 E-01

RSS = 0.8416209 E-03

$\Gamma_{max} = 0.1708 \pm 0.2126$

$B = 0.9186 E+06 \pm 0.1527 E+07$

$\log B \pm 1\sigma = 5.96 \pm 0.14$

corr. $\Gamma_{max} - B = -0.9238$

6 d.o.f.

Model 2 Double Langmuir Model

TSS = 0.2965672 E-02

RSS = 0.1709 E-02

$\Gamma_{m1} = -4.016 \pm 3.483$

$\Gamma_{m2} = 1.694 \pm 1.668$

$1/B_1 = -0.6871$

$1/B_2 = 0.4513$

corr. $\Gamma_{m1} - \Gamma_{m2} = 30$

corr. $\Gamma_{m1} - B_1 = 30$

corr. $\Gamma_{m1} - B_2 = 30$

corr. $\Gamma_{m2} - B_1 = 30$

corr. $\Gamma_{m2} - B_2 = 30$

corr. $B_1 - B_2 = 30$

30 d.o.f.

MMO₂ 13 made 1977 of 1978

run 190781
pH 7.0
glycine 50 μM

linear regression
F_{max} = 0.144
log B = 7.58

non-linear regression
Model 1 Single Langmuir Model
TSS = 0.9585435 E-02
RSS = 0.4052163 E-03
F_{max} = 0.1443 0.1686
B = 0.3500 E+08 0.5142 E+08
log B ± 1σ = 7.54 ± 0.10
corr. F_{max} - B = -0.9121

6 d.o.f.
Model 2 Double Langmuir Model
TSS = 0.9585435 E-02
RSS = 0.4632242 E-04
F_{m1} = 0.05008 0.09967
F_{m2} = 0.144 0.6942
1/B₁ = 0.5606 E-08 0.1444 E-07
1/B₂ = 0.2715 E-06 0.5747 E-06
corr. F_{m1} - F_{m2} = 0.4697
corr. F_{m1} - B₁ = 0.9705
corr. F_{m1} - B₂ = 0.9324
corr. F_{m2} - B₁ = 0.7809
corr. F_{m2} - B₂ = 0.9886
corr. B₁ - B₂ = 0.8565

4 d.o.f.

MMO₂ 13 made 1977 of 1978

run 190781
pH 8.0
glycine 50 μM

linear regression
F_{max} = 0.147
log B = 9.25

non-linear regression
Model 1 Single Langmuir Model
TSS = 0.9961020 E-02
RSS = 0.2969183 E-03
F_{max} = 0.1457 0.1557
B = 0.1721 E+10 0.1862 E+10
log B ± 1σ = 9.24 ± 0.02
corr. F_{max} - B = -0.3804

6 d.o.f.
Model 2 Double Langmuir Model
TSS = 0.9961020 E-02
RSS = 0.3135902 E-04
F_{m1} = 0.06928 0.1170
F_{m2} = 1.257 26.54
1/B₁ = 0.1644 E-09 0.3623 E-09
1/B₂ = 0.4782 E-07 0.9768 E-06
corr. F_{m1} - F_{m2} = 0.410
corr. F_{m1} - B₁ = 0.9744
corr. F_{m1} - B₂ = 0.9452
corr. F_{m2} - B₁ = 0.8737
corr. F_{m2} - B₂ = 0.9999
corr. B₁ - B₂ = 0.8784

4 d.o.f.

experimental adsorption data
observations 8

PCu²⁺ Γ_{ads}
10.07995 0.0206
9.93603 0.0324
9.66737 0.0437
9.44638 0.0555
9.05211 0.0780
8.93426 0.0929
8.76104 0.1073
8.61297 0.1268

experimental adsorption data
observations 8

PCu²⁺ Γ_{ads}
8.41818 0.0203
8.28277 0.0319
7.98767 0.0430
7.73993 0.0545
7.35074 0.0767
7.26048 0.0910
7.10006 0.1068
6.93866 0.1236

MMO₂ 13 made 1977 of 1978

run 190781
pH 8.0
glycine 50 μM

linear regression
F_{max} = 0.147
log B = 9.25

non-linear regression
Model 1 Single Langmuir Model
TSS = 0.9961020 E-02
RSS = 0.2969183 E-03
F_{max} = 0.1457 0.1557
B = 0.1721 E+10 0.1862 E+10
log B ± 1σ = 9.24 ± 0.02
corr. F_{max} - B = -0.3804

6 d.o.f.
Model 2 Double Langmuir Model
TSS = 0.9961020 E-02
RSS = 0.3135902 E-04
F_{m1} = 0.06928 0.1170
F_{m2} = 1.257 26.54
1/B₁ = 0.1644 E-09 0.3623 E-09
1/B₂ = 0.4782 E-07 0.9768 E-06
corr. F_{m1} - F_{m2} = 0.410
corr. F_{m1} - B₁ = 0.9744
corr. F_{m1} - B₂ = 0.9452
corr. F_{m2} - B₁ = 0.8737
corr. F_{m2} - B₂ = 0.9999
corr. B₁ - B₂ = 0.8784

4 d.o.f.

experimental adsorption data
observations 8

PCu²⁺ Γ_{ads}
10.07995 0.0206
9.93603 0.0324
9.66737 0.0437
9.44638 0.0555
9.05211 0.0780
8.93426 0.0929
8.76104 0.1073
8.61297 0.1268

APPENDIX IV

Figure 7.9 Duplicate isotherms at pH 7.0, in the presence of 50 μ M glycine, for MnO_2 , III

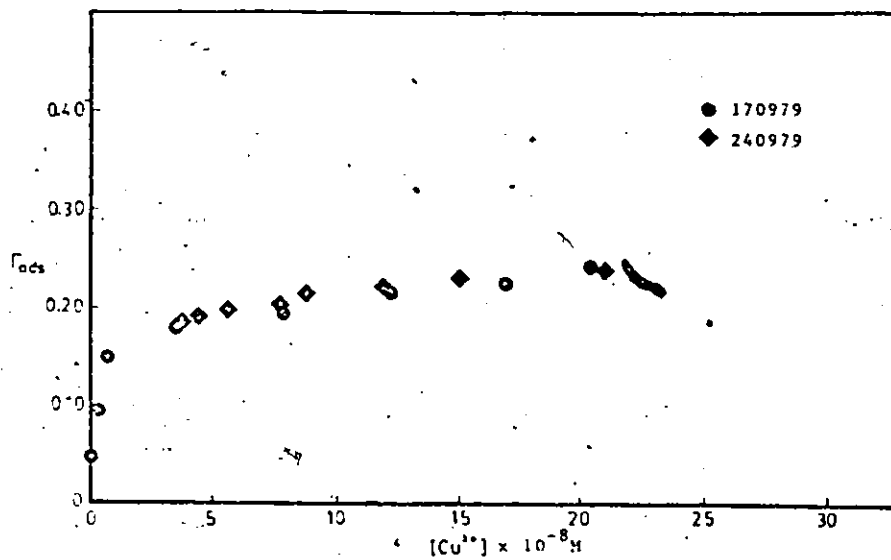


Figure 7.11 Duplicate isotherms at pH 8.5, in the presence of 50 μ M glycine, for MnO_2 , III

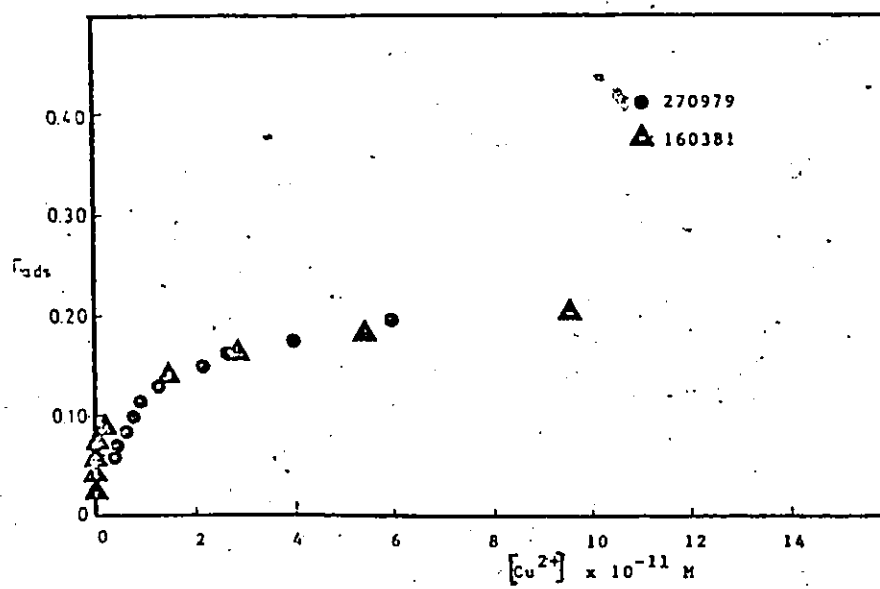


Figure 7.14 Duplicate isotherms in the absence of glycine at pH 6.0, for MnO₂ XVe (220181)

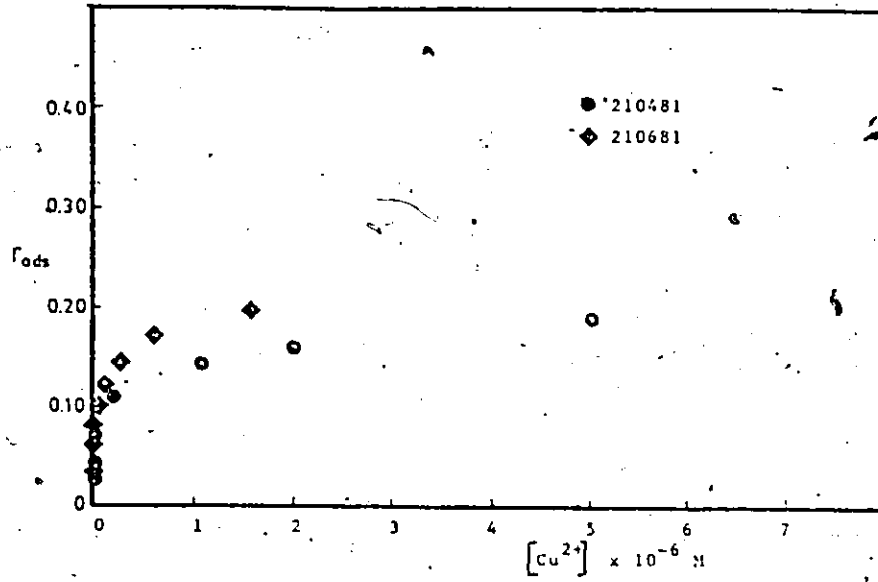


Figure 7.15 Duplicate isotherms in the absence of glycine at pH 7.0 for MnO₂ XVe (220181)

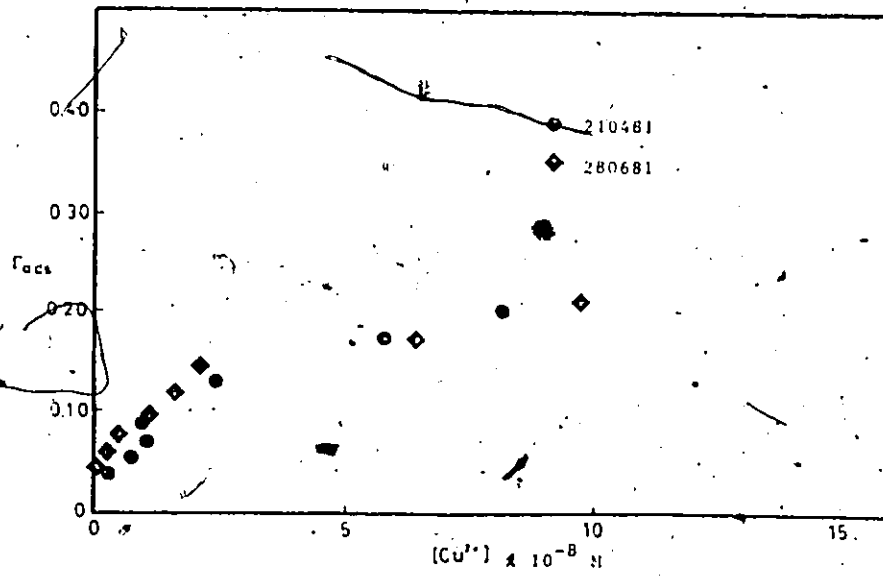


Figure 7.13 Duplicate isotherms in the presence of glycine at pH 6.0, for MnO₂ Vib (220180)

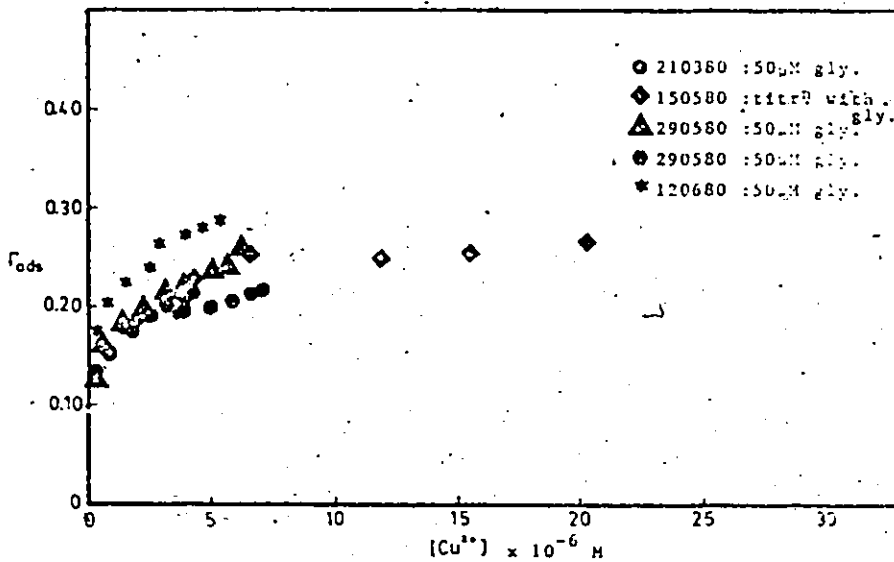


Figure 7.16 Duplicate isotherms in the presence of 50 μM glycine at pH 6.0, for SnO₂ XVe (220181)

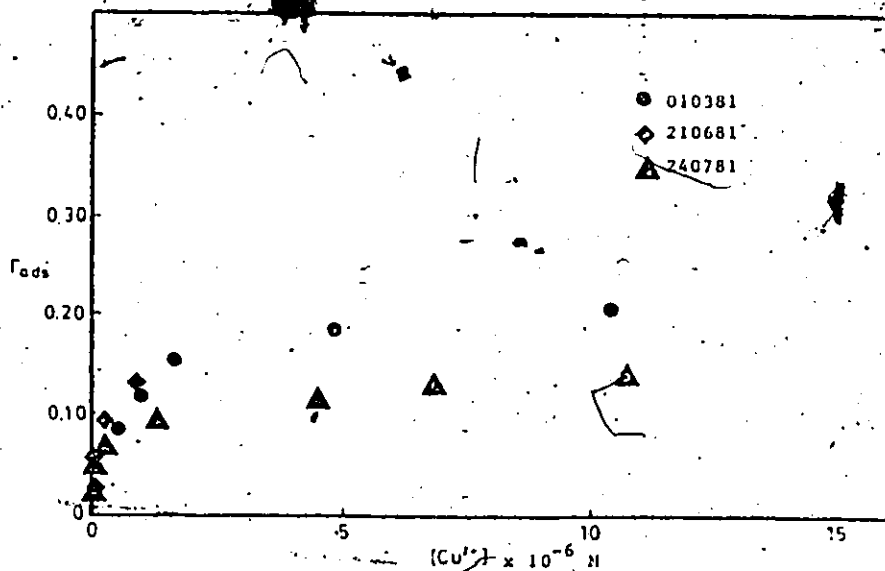


Figure 7.17 Duplicate isotherms in the presence of 50 μ M glycine at pH 7.0, for MnO_2 Xvc (220181)

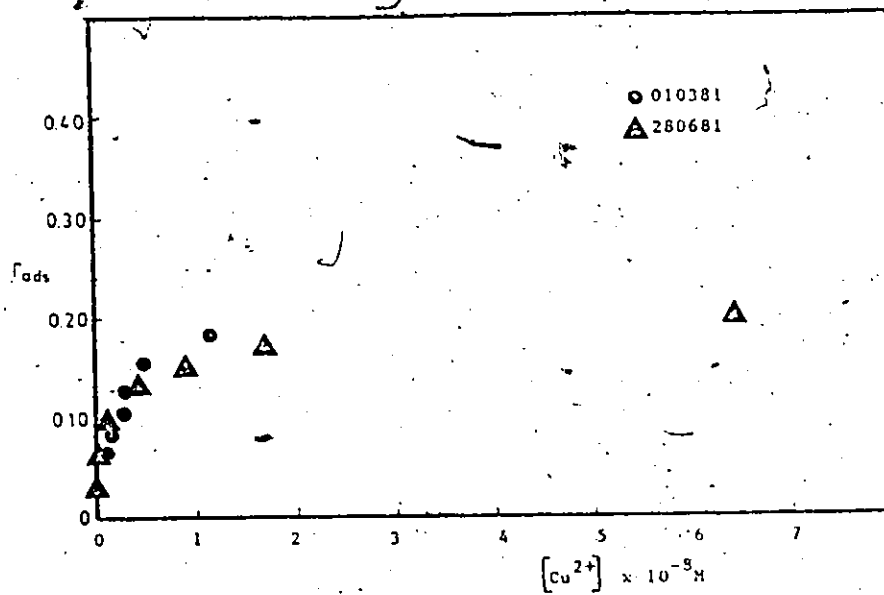


Figure 7.20 Comparison of isotherms in the presence, and absence, of 50 μ M glycine at pH 6.0, for MnO_2 Vib (220180)

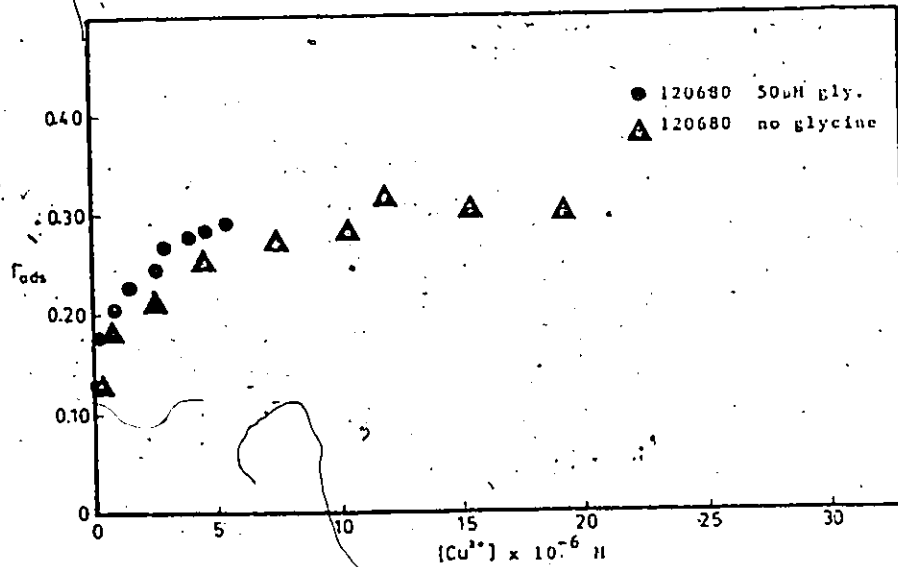


Figure 7.23. Comparison of isotherms in the presence, and absence, of 50 μ M glycine at pH 6.0, for MnO₂ VIb (220180)

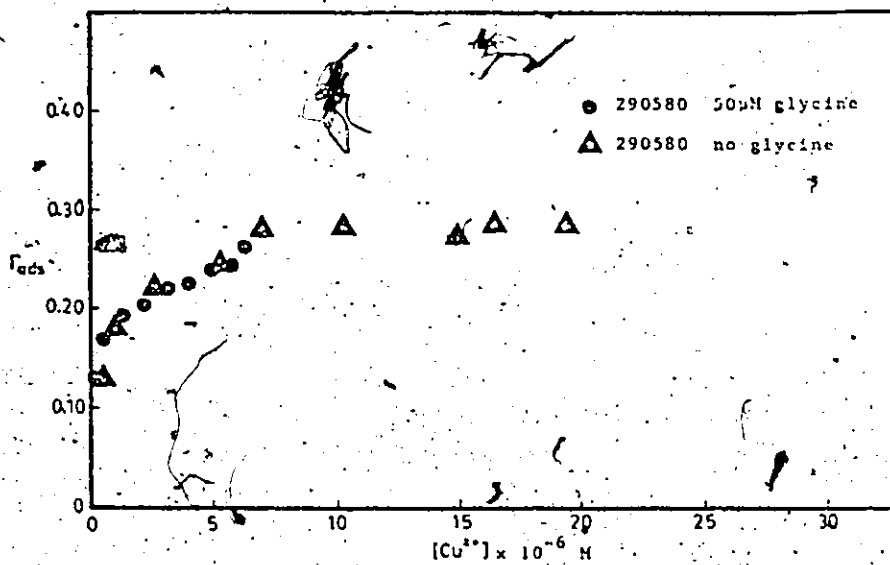


Figure 7.24. Comparison of isotherms in the presence, and absence, of 50 μ M glycine at pH 6.0, for MnO₂ Vc (220181)

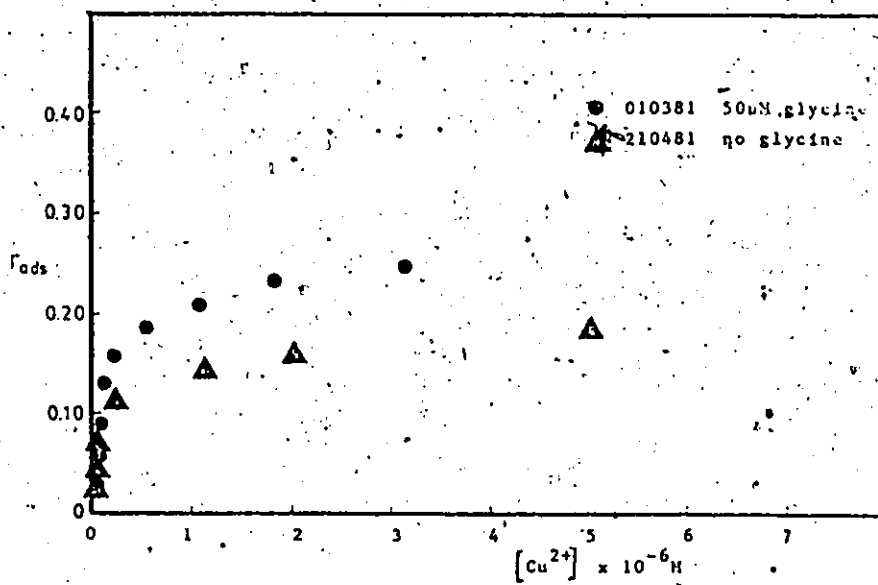


Figure 7.26 Comparison of isotherms in the presence, and absence, of 50 μ M glycine at pH 7.0, for MnO₂ Xvc (220181)

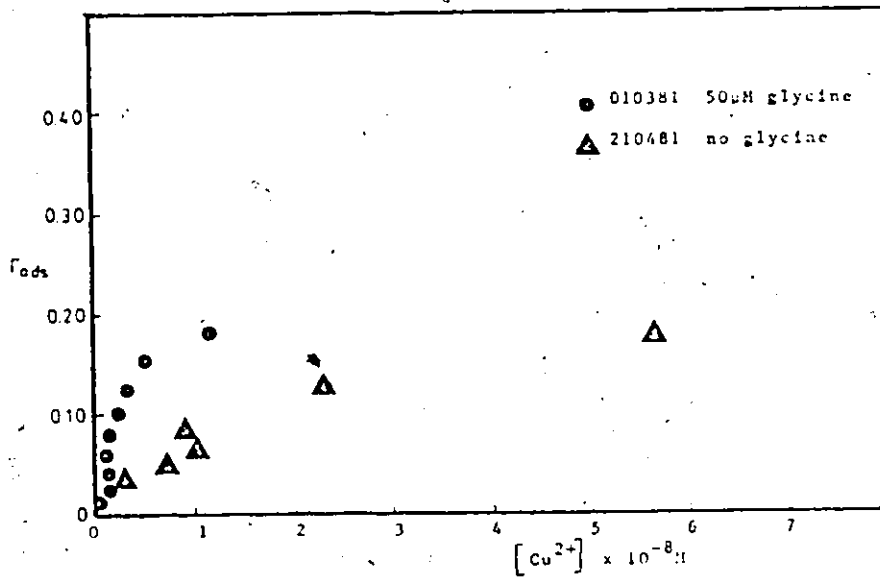


Figure 7.29 Comparison of isotherms for a naturally, and an artificially, aged 'neutral' MnO₂ at pH 6.0, in the presence of 50 μ glycine

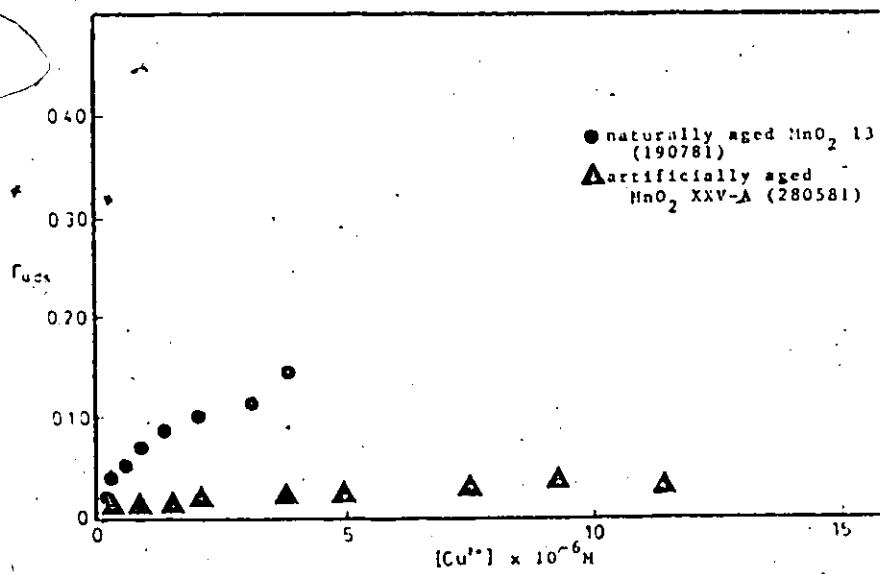


Figure 7.29 Comparison of isotherms for a naturally, and artificially, aged 'neutral' MnO_2 at pH 7.0, in the presence of 50 M glycine

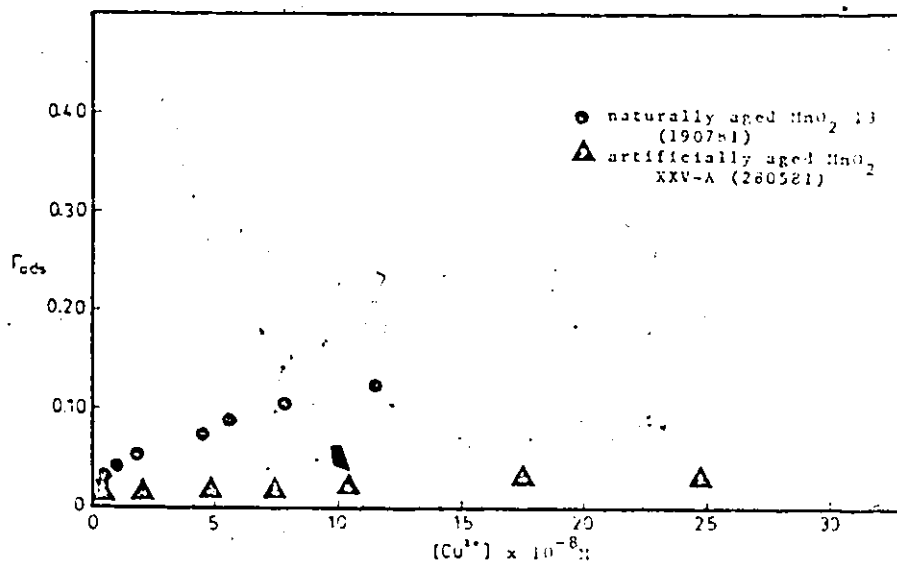


Figure 7.30 Comparison of isotherms for artificially, and naturally, aged 'neutral' MnO_2 at pH 5.0, in the presence of 50 M glycine

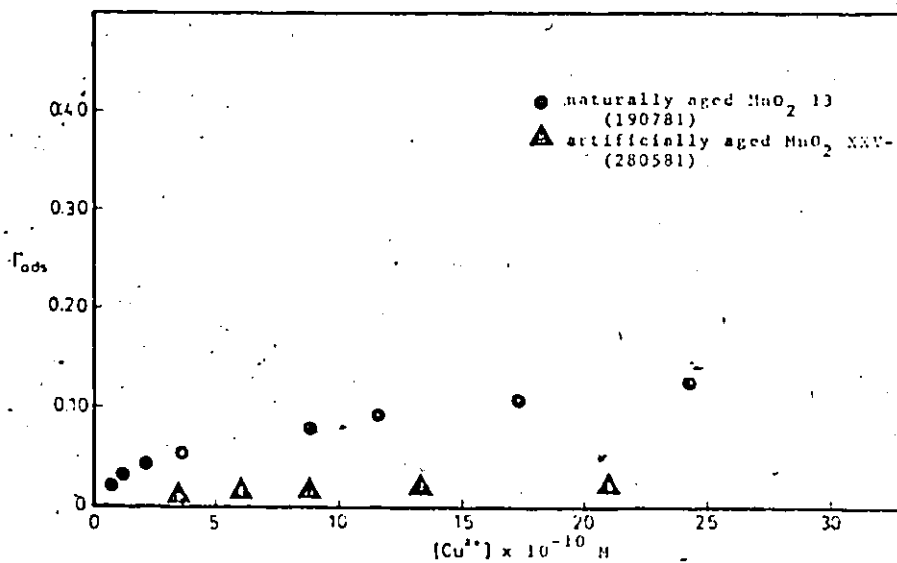
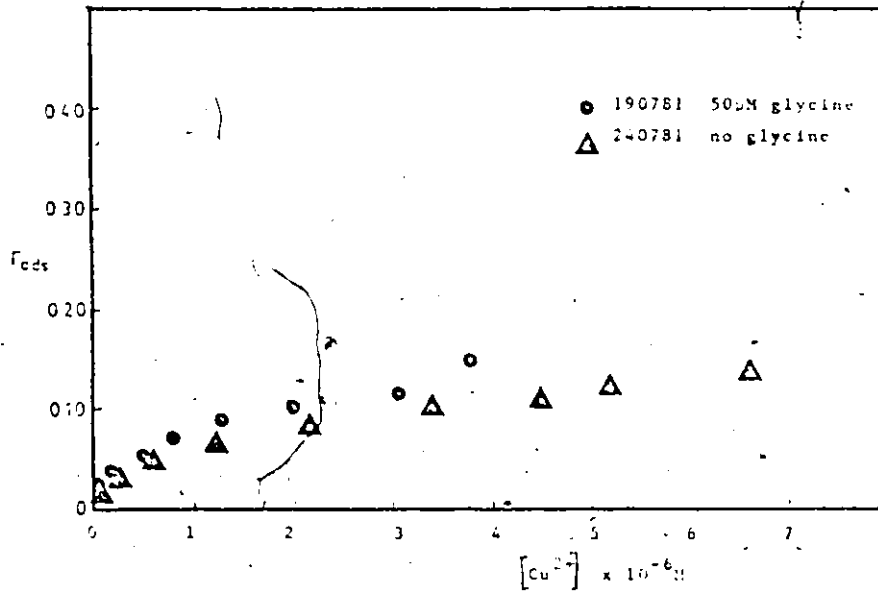


Figure 7.31 Comparison of isotherms in the presence, and absence, of 50 μ M glycine at pH 6.0, for MnO_2 . 13



APPENDIX V


```

90 IF (TYPE.EQ.M) GO TO 70
91 NP = ILOW, LUP
92 WRITE(6,729) I, (C(I, J), J=LOW, I)
93 DO 71 J=I, ILOW, LUP
94 WRITE(6,721) I, (C(I, J), J=LOW, I)
95 CONTINUE
96 IF (LOW2.NE.95) GO TO 97
97 NP = ILOW, LUP
98 WRITE(6,725) I, (C(I, J), J=LOW, LUP)
99 CONTINUE
100 WRITE(6,721) I, (C(I, J), J=LOW, LUP)
101 LUP = LUP + 10
102 NP = NP - 1
103 GO TO 10
500 FORMAT(7F16.9I12)
501 FORMAT(10L12.4)
502 FORMAT(10F13.1X, F7.4, 9F12.4)
503 FORMAT(10F13.1X, E10.4, 9E12.4)
504 CONTINUE
505 RETURN
506 END

```

```

PROGRAM TSI (INPUT, OUTPUT, IAPES, INPUT, IAPES, OUTPUT)
NON-LINEAR LEAST SQUARES FIT FOR CU ADSORPTION ONTO MN02
IONIC STRENGTH IS 0.01. T IS 25 C
--USE MODEL IN WHICH THE BINDING CONSTANT CHANGES WITH PH AND AMOUNT ADS.
--USING NEWTONS METHOD IN SUBROUTINE AS READ IN AS PCU AND PH AND CONVERTED LATER
CU AND H CONCENTRATIONS ARE READ IN AS PCU AND PH AND CONVERTED LATER
DATA NOT CORRECTED FOR CLASS ADSORPTION
DIMENSION TH(3),DIFF(3),SIGMS(3),Y(200),SCRAT(1000)
COMMON X(200),H(200),Y085(200)
EXTERNAL MODEL
DATA APROR,MP,MOB,MIT/1,3,42,50/
DATA F,AM,FNU/1,0,10,0/
DATA OEFF(1),DIFF(2),DIFF(3)/0,0,1,0,0,1,0,0,1/
DATA E,AL,AL2,AL3,AL4,AL5,AL6,AL7,AL8,AL9/
DATA S,AL1,AL2,AL3,AL4,AL5,AL6,AL7,AL8,AL9/
DATA TH(1),TH(2),TH(3)/0,300,1,5,1,0E-5/
DO 66 I=1,200
  READ(5,*)MOB(I),X(II),H(II)
  FURHA(1)=1.0-5*I
  WRITE(6,27) Y(II),H(II)
  FORM(1)=F(10,5)
  Y085(II) = Y(II)
  CONTINUE
CALL UMHAUS(MPROB,MODEL,MOB,Y,MP,TH,DIFF,SIGMS,EPS1,EPS2,MIT,FLAM,
2FMU,SCRAT)
STOP
END

```

--COMMON BLOCKS--

11300 //

--ENTRY POINTS--

33 INPUT#

TSI

--EXTERNALS--

INPCI, MNUPPV, MODEL, OUTCI, STOP, UMHAUS

---STATEMENT LABELS---

.26 F 2030

2030

.27 F 2050

2050

.66 IO 08

08

30 TAPES0

548 TAPES0

--VARIABLE MAP--

```

DIFF 2
E 2
FNU 2
INPUT# 1

```

```

EPS1 3
FLAM 3
H 3
INPCI 3
MIP 3

```

```

3469 3
3568 3
3108 //
2628 3

```

200

EXTERNAL, 200

```

SUBROUTINE MODELIMPROR,TH,F,NOB,MP)
DIMENSION TH(3),F(200)
COMMON X(200),H(200),Y00S(200)
DO 77 I=1,COH
C=10**(-X(I))
P=YABS*(H(I))
DO 100 J=1,NV
TH(J)=EXP(I-YABS/TH(I))
C1=YABS*(H(I))
C2=YABS*(H(I))
F00SP=YABS*(H(I))
IF I=3(YABS-YABS).LE.0.00001 GO TO 101
YABS=YABS
CONTINUE
F(I)=YABS
77 CONTINUE
WRITE(6,28)
FORMAT(1X,/)
RETURN
END

```

--COMMON BLOCKS--

11303 //

--EXTERNALS--

--STATEMENT LABELS--

25 F 106D .77 D 67B .101 60B 63B

--VARIABLE MAP--

AA	EXP	ITOX	OUTCI	TAPE6	KTOYS
135H					INTRINSIC
126R					B.E.F.
135I					132B //
127R	EXTERNAL				310B //
0H					100B ENTRY
0B					0B
130R					EXTERNAL:
0B					0B //
131D					EXTERNAL: 200
					234B //
					620B //
					200

```

ABS
EXP
H
H
MODEL
MP
OUTCI
TAPE6
YABS
Y00S

```

APPENDIX VI

Figure A-1 Calibration of Cu^{2+} electrode in deaerated organic-free H_2O , $\text{pH} = 6.0 \pm 0.01$, $l = 0.01 \text{M KNO}_3$

